AFSWC-TWC-TDR-62-64

SWC
TDR
62-64

A GUIDE FOR THE DESIGN OF SHOCK ISOLATION SYSTEMS FOR UNDERGROUND PROTECTIVE STRUCTURES

TECHNICAL DOCUMENTARY REPORT NUMBER AFSWC-TDR-62-64

December 1962

Research Directorate
AIR FORCE SPECIAL WEAPONS CENTER
Air Force Systems Command
Kirtland Air Force Base
New Mexico

Project Number 1080, Task Number 10803

This research has been sponsored by the
Defense Atomic Support Agency under WEB No. 13.004

(Prepared under Contract AF 29(601)-4551
by The Ralph M. Parsons Company, Los
Angeles, California)

HEADQUARTERS
AIR FORCE SPECIAL WEAPONS CENTER
Air Force Systems Command
Kirtland Air Force Base
New Mexico

FOREWORD

While the general subject of shock isolation has received considerable attention during recent years, the designer of isolation systems for use in underground protective structures is confronted with many special and difficult problems. In particular, the lack of an adequate description of the shock to which the systems are exposed has not only prevented the use of powerful analytical techniques, but has also reduced confidence in the ability of the systems to perform as intended. This and similar problems have indicated a pressing need for a summary of the state-of-the-art in those fields directly related to isolation systems for underground protective structures application and for the development of broad design principles to assist the designer in achieving greater reliability.

Early in 1961, after many discussions with facility engineers, the Research Directorate, Air Force Special Weapons Center, selected The Ralph M. Parsons Company as prime contractor, to review the state-of-the-art of all major factors relating to the analysis and design of shock isolation systems for hardened facilities. Contributing substantially to this effort were the Stanford Research Institute and the Armour Research Foundation of The Illinois Institute of Technology.

The parameters significantly influencing the selection and analysis of shock isolation systems for protective underground structures are so numerous and complex that reduction of the design to a routine procedure is virtually impossible. For this reason the Design Guide stresses an understanding, qualitative where necessary, of the basic phenomena. Areas where extra caution must be exercised are pointed out and suggestions are made regarding possible methods of approach. In some areas definite recommendations can be and are given; in others the designer may be left with little more than an enhanced appreciation for the magnitude of the problem confronting him. Such is the state-of-the-art.

While far from being a complete work on the subject in its present form, it is hoped nonetheless that the Design Guide will be of assistance to the facility engineer in improving the economy and reliability of isolation system designs. The comments and suggestions of all users of the Design Guide are earnestly solicited.

The Ralph M. Parsons Company gratefully acknowledges the invaluable assistance rendered by its consultants and subcontractors. Professor L. S. Jacobsen, Stanford University, Professor C. E. Crede, California Institute of Technology, and Mr. S. Wilson, Shannon and Wilson, Inc. assisted in formulating the objectives of the project and reviewed portions of the preliminary draft. In addition, the Design Guide has drawn freely on Professor Crede's numerous publications in the field of shock tolerances and shock test theory. Dr. G. N. Bycroft and Mr. F. Sauer of the Stanford Research Institute and Mr. B. Juskie of the Armour Research Foundation contributed generously to the material on nonlinear systems analysis, ground shock data and shock tolerances respectively. Dr. S. T. Epure, Mr. J. Dastur, and Mr. R. Frankian of The Ralph M. Parsons Company prepared the sections on systems analysis and ground shock prediction methods. Mr. H. R. Saffell coordinated the activities and made substantial contributions to the study.

Technical direction was given the study at the Stanford Research Institute by Dr. E. G. Chilton and at the Armour Research Foundation by Dr. E. Sevin. Dr. M. S. Agbabian, Technical Director, Systems Engineering Division, managed the program for The Ralph M. Parsons Company.

The support and helpful suggestions of the staff at the Air Force Special Weapons Center are greatly appreciated. Special thanks is due Dr. George Young, formerly of the Research Directorate, AFSWC, whose recognition of the problem prompted the preparation of the Design Guide, and to Lt. Douglas Merkle, AFSWC, Project Officer, who not only monitored the work but also prepared the material on human shock tolerances and critically reviewed the section on systems analysis.

ABSTRACT

This report reviews the major considerations relating to the design of Shock Isolation Systems for use in underground protective structures, emphasizing in particular those areas where special guidance is needed by the facility engineer. The motion of the ground due to nuclear blast, the interaction of the ground motion with buried structures, and the tolerances of typical facility equipment to shock are described and employed to establish the input and output requirements for isolation systems. Analytical methods for determining the dynamic responses of both linear and nonlinear isolation systems are summarized and, for several of the more commonly used configurations, the equations are reduced to simple form. The report suggests the use of the shock response spectrum in a unified approach to the specification of attenuation requirements, equipment shock tolerances, and shock test machine selection.

PUBLICATION REVIEW

This report has been reviewed and is approved.

DONALD I. PRICKETT
Colonel USAF
Director, Research Directorate

JOHN J. DISHUCK
Colonel USAF
DCS/Plans & Operations

TABLE OF CONTENTS

Note: A detailed Table of Contents for each section precedes the section

SECTION 1.0 INTRODUCTION

TABLE OF CONTENTS

1.1 Purpose of the Design Guide

An essential element in the design of underground structures for protection from nuclear blast is the provision of reliable shock isolation systems for personnel and equipment. The levels of shock to which the systems may be exposed at many sites are very high, with ground accelerations measured in hundreds of g's and ground displacements in feet. Very few accessories are capable of withstanding shocks of this magnitude without serious damage while the peak shock which can be tolerated by the unsupported human being falls far short of these figures. Yet the unimpaired functioning of both personnel and equipment immediately following attack must be preserved if the facility is to fulfill its intended mission.

In the design of early facilities of low hardness level, the magnitudes of the expected ground motions were relatively small. As a consequence, the attenuation requirements which were dictated by the survival tolerances of the enclosed equipment or personnel could be met with little difficulty. As the hardness level of new facilities increased, confidence in the details of the predicted ground shock was reduced and economic considerations discouraged the arbitrary acceptance of very large margins of safety. Further, more severe attenuation requirements, demands for larger load capacity and greater flexibility in load arrangement resulted in isolator designs of greater sophistication. These critical criteria generally impose an additional need for a more refined definition of the input shocks. Thus the basic concepts of shock isolation design were subjected to a more searching inspection.

In a broad sense, the problems confronting the designer of shock isolation systems for underground protective structures are no different from those encountered in the design of shock resistant packaging, earthquake resistant buildings, gust resistant aircraft, or other apparatus which accept an energy impulse and convert it to a more tolerable form. In all these cases, the principal complication is introduced by the fact that the exact description of the impulse in time is rarely unique. The designer must deal with the typifying characteristics of the shock and must design his system to be relatively insensitive to its less predictable features.

Insufficient data have been accumulated to date on ground shock resulting from a high-yield nuclear blast, to provide a basis for any but the most general of observations about the shock waveform. Indeed, the differences in soil structure between the test and the actual site in all known cases are so great that it is doubtful if experiment can ever be expected to yield design data directly. The nonlinearity of the phenomena precludes direct extrapolation. The correlation of low-yield data with theory and subsequent extrapolation of the theory to higher yields at other sites is handicapped by the many simplifications necessarily employed in theoretical treatments. These simplifications could easily obscure the existence of phenomena of significant influence on the time history of the ground motion.

The designer of shock isolation systems for underground protective structures is provided very little information on even the general characteristics of the wave to which his system may be subjected. Thus, many techniques employed by designers in other fields are not available to him.

Other special problems also face the isolation system designer. In many other engineering applications, components which must survive rigorous environments are either designed specially for the purpose or are selected on the basis of the results of exhaustive tests. A large percentage of equipment installed in underground facilities, however, comprises off-the-shelf items intended for stationary industrial use. While in some instances the shock tolerance of the equipment is high, more often it has never been determined under controlled conditions. When the equipment has been tested, the results are rarely in a useful form for the underground facilities designer. Since economy dictates the continued use of industrial equipment wherever possible, the isolation system designer is faced with the questions of whether the equipment will withstand the shock without attenuation and, if not, what must be the output of the isolation system to ensure equipment survival.

Despite a lack of information concerning the nature of the input shock or of the output necessary to ensure survival of the isolated equipment, the designer is charged with the responsibility for devising an energy conversion system with the required transfer characteristics and for predicting the peak displacement of the system relative to the surrounding structure. Notwithstanding these areas of ignorance, it is evident that the designer can achieve a highly reliable system by: (a) selecting a type of system which responds only to gross characteristics of the input shock, (b) assuming an input waveform which is most disadvantageous to his system, (c) fixing the output at an extremely low frequency and acceleration, and (d) increasing the clearance between the supported mass and the structure to a value well above that estimated to be required. The economic penalty for compounding margins of safety in this manner, however, is usually prohibitive, not only with respect to the isolation system components but also for the increased volume of the underground structure housing the system.

Even though generous clearance (rattlespace) has been shown to be the least expensive technique for adequate shock isolation, the engineering principle of minimizing unoccupied structural volumes, the almost inevitable growth of the suspended weight due to equipment or mission updating with center of gravity shift due to such additions, and the deterioration of system performance due to aging and wear all act to decrease the margin of safety afforded by extra clearance.

To these special technical problems is added the usual contractual necessity of completing the design in a minimum of time. The final design of most facilities of this nature is accomplished in a matter of months. Considering the significant number of isolation systems contained in a single facility, it is evident that design approaches must

be clearly defined and analytical procedures reduced to the simplest form consistent with the required accuracy if design time limitations are to be met with consistency.

This Design Guide is intended to assist the facility engineer in solving these difficult design problems by critcially examining the input shock for parameters of significance to the performance of isolation systems, by reviewing the standards for the survival tolerances of equipment and relating them to isolation system characteristics and by summarizing techniques by which the dynamic response of the systems themselves may be analyzed. Where the state-of-the-art precludes the formulation of explicit design procedures, emphasis has been placed on current concepts of the underlying phenomena with the hope of providing the designer with some basis for judgement.

A complete description of the technical problems relating to the design of isolation systems for underground protective structures must draw equally from the fields of soil mechanics, rigid body dynamics, equipment damage mechanisms, and shock testing equipment and techniques. Each of these subjects is treated in the Design Guide from the viewpoint of the isolation system designer. The Design Guide is of equal importance to the specialist in acquainting him with the demands of isolation system design on his field of interest and in directing his attention to those areas wherein further research is needed.

1.2 Basis for Design Approach

The transmission of ground pressure waves from a nuclear explosion occurring at the surface of the ground is shown schematically in Figure 1.2-1 and diagramatically in Figure 1.2-2. In the process of explosion, the tremendous quantity of energy released by a nuclear weapon vaporizes the weapon casing, thus creating a small ball of metal vapor plasma at intense pressure. As the ball expands, it compresses the surrounding atmosphere generating an air blast wave which recedes rapidly from the source. For a surface burst, pressure is transmitted to the ground both by the direct impingement of the metal-vapor ball and by the passage of the air blast wave across the surface.

The large number of parameters influencing the manner in which the shock is generated and transmitted through the ground to the isolation system precludes, from a practical point of view, a determination of an exact shape for the shock waveform. Ground shock waveforms have been measured at test sites but the size of the weapon, formation of the soil, and orientation of the instrumentation in all tests differed significantly from those conditions expected at any known underground protective installation. In view of the meagerness of the data and the nonlinearity of the phenomenon, the usefullness of test results in predicting the detailed characteristics of the waveform at an actual site is severely limited.

In current design it is customary to estimate the strength of the shock wave expected at an underground protective structure by computing, from simple force-velocity relationships, the peak ground motion resulting from given pressure loadings and to represent the shock by means of its response spectrum. The response spectrum is the distribution of peak responses to the ground shock, of a series of single-degree-of-freedom oscillators as a function of the natural frequencies of the oscillators. Thus, the response spectrum is not so much a description of the shock as it is a measure of the effect of the shock. As computed by accepted practices for a given site, the response spectrum is the envelope of the peak responses to all waves which might be expected at that location rather than the effect of a single shock wave.

There are two inherent characteristics of the response spectrum which deserve special mention. First, since the response spectrum contains no information on phasing of the peak responses at the various frequencies, it is not possible to deduce from it the time history of the shock which produced it. An infinite number of shocks can produce identical response spectra. Second, since the peak response of even a single-degree-of-freedom oscillator is dependent on the shape of the disturbing impulse, the act of constructing a response spectrum from weapons effects data implies some knowledge of the shock waveform. This latter point is of particular significance when it is noted that current practice suggests the use of a velocity amplification factor of 1.5-2.0 which is a value based on test data obtained under atypical conditions. Yet it is easily shown that small variations from the waveforms measured at

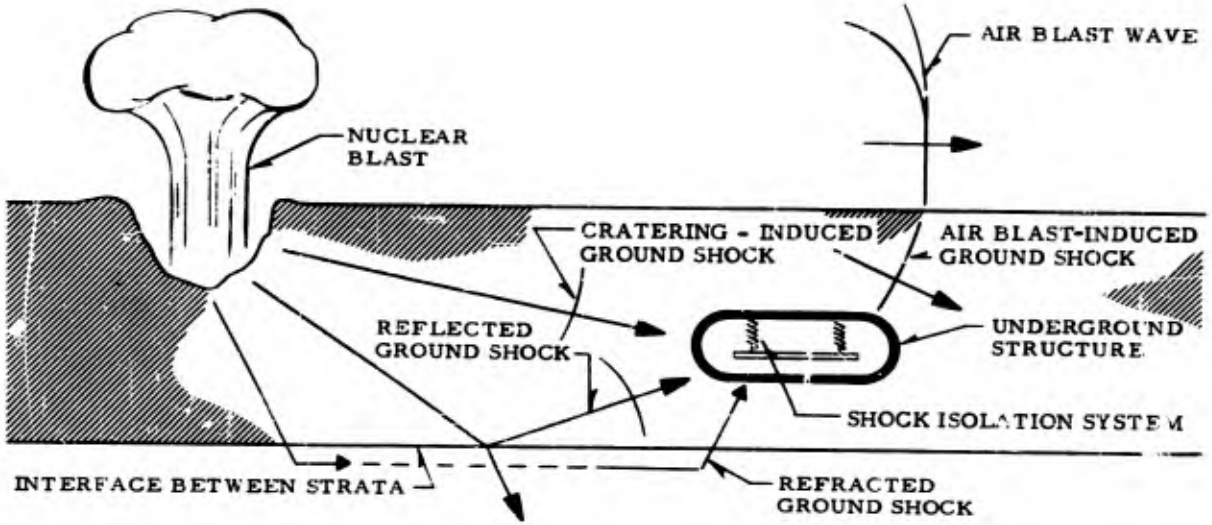

Figure 1.2-1 Transmission of Ground Waves Resulting from Nuclear Explosion

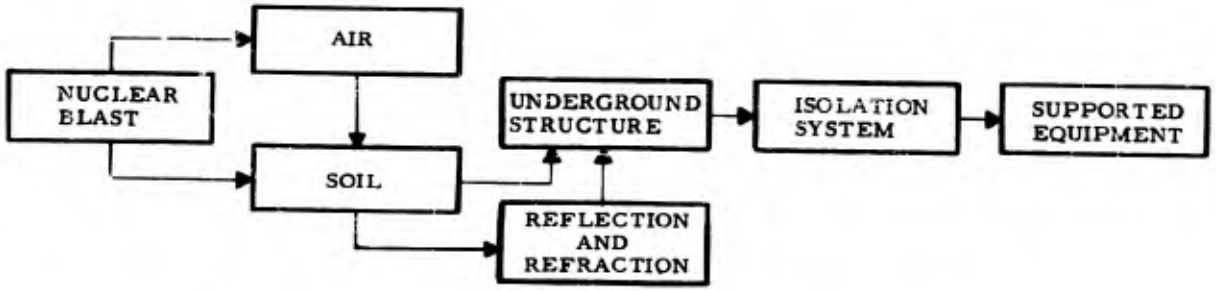

Figure .2-2 Diagram of Ground Wave Transmission

the test sites can produce sizeable increases in the linear velocity amplification factors.

Despite the limited information concerning the nature of the shock revealed by the response spectrum, the concept of applying the response spectrum to the solution of problems of shock isolation and structural dynamics has been a useful one. If the designer assumes tacitly or otherwise that the velocity amplification factor incorporated in the spectrum will not be exceeded at the actual site, then, by definition, the peak responses of single-degree-of-freedom, undamped linear systems are established. Further, although the response spectrum contains no phasing information, the upper limit of responses of coupled linear systems can be calculated by the method of modal superposition. While in some instances this method must yield highly conservative results, the high degree of reliability demanded of these facility components, coupled with the lack of detailed information on the shock, does not make this degree of conservatism undesirable.

The acceptance of an arbitrary velocity amplification factor irrespective of site or orientation of the facility from the blast does not appear to be justified in view of existing analyses of test data. It appears that under some combinations of site and weapon parameters, the waveform of the ground shock contains a strong low-frequency oscillatory component. Since the response spectrum is particularly sensitive to oscillatory inputs, an amplification factor should not be assigned until a careful inspection of the probable ground wave patterns at the point of interest has been made.

Further, the dynamic response of nonlinear systems cannot be determined from the information contained in the spectrum alone, nor can the upper bounds of the responses be established. To evaluate the dynamic behavior of this large class of systems the input must be defined in time.

As a consequence of the above statements, it is evident that the shock isolation system designer must possess at least a qualitative understanding of ground shock phenomena in order to be on guard for those characteristics to which his system is particularly sensitive and to appreciate the assumptions implicit in the information supplied him by the soils engineer. The Design Guide therefore begins with a description of these phenomena and a discussion of the propagation of pressure waves within the ground, their reflections and refractions at interfaces separating strata of different properties, and the phasing of their arrival times at points variously oriented with the explosion.

The waveform of the ground shock at the point of interest is simply the resultant of the waveforms of the constituent waves and their phasing. The physical phenomena governing their summation may be nonlinear. Nevertheless, if the time histories of the initial disturbances, their distortions due to transmission and reflection, their arrival times, and local soil properties were defined in reasonable detail, the amplification

factor and other shock parameters of importance to the isolation system designer could be calculated directly. Unfortunately, neither experimental data nor theory are available to define the waveform in such detail.

In an effort to establish a better basis for evaluating the amplification factor of the shock spectrum at a particular site and to provide the designer of nonlinear systems with some indication of the gross features of the input waveform, the Design Guide approaches the problem of ground shock prediction by an empirical procedure based on these steps:

- Establish general characteristics of isolation systems for the application in order to define those input parameters significant to system response.
- Examine all available test data for recurrent waveform patterns.
- Review prediction methods in an attempt to find a correlation between waveform shape, weapon parameters, and site conditions.

With regard to the generalization of isolation system characteristics, the only feature which might be considered to be common without seriously restricting the usefulness of the Design Guide is that of natural frequency. In almost all shock isolation systems, for use in underground protective structures, the natural frequency will vary between about 0.5 cps and 5 cps. Thus, the high-frequency components of the input shock are of little interest and can be deleted from the input waveform with no appreciable loss of accuracy in the computed system response.

With the stipulation that only low-frequency components are of interest, all available free-field ground motion records have been examin for the purpose of identifying recurrent waveform patterns. Particular attention was given to the possibility of the occurrence of oscillatory phenomena. The data were from tests of low-yield weapons at sites where the soil formations were not typical of any known facility location. The only data existing in sufficient quantity were for vertical motions near the surface of the ground. The possible danger of extrapolating these waveforms to weapon yields larger by orders of magnitude and soils vastly different in composition and stratification is recognized. It was hoped, nonetheless, that characteristics would be revealed which could be related to known fundamental parameters describing the motion of the ground, and that the parameters could then be extended to other environments. This approach implies, of course, that no important phenomena occur at higher levels or at other sites which could not be observed in existing data.

Two distinctly different types of low-frequency waveforms were identified and are presented in the Design Guide. Type I, shown in Figure 2.3.1 , page 2-26 , is an impulse with a very short velocity rise time followed by a relatively slow decay. This waveform is of the same general shape as that predicted from simple theory for the response of the ground to the air-blast pressure.

Type II, shown in Figure 2.3.3 , page 2-27, is an oscillatory wave. While the magnitudes of all Type II waves found in the records are much lower than those of the Type I wave, their frequencies range from 3 cps to 5 cps. The number of cycles for this type is sufficiently large to be of genuine concern to the isolation system designer. The Type II waveform has the general appearance of the response of a lightly damped linear system in resonance with a damped sinusoidal disturbance.

The mechanism by which the Type II wave is produced cannot be traced with the data available. It is probable that it is associated with reflection phenomena in some manner and, as such, appears to be of concern only at those sites where the soil is markedly stratified. Until a better definition is available, however, the strong influence of the Type II waveform on the dynamic response of low-frequency systems clearly indicates the importance of providing for the possibility of its occurrence in all designs.

The Design Guide describes the investigation which lead to the identification of the two types of waveforms and presents nondimensionalized response spectra of waveforms composed of various ratios of Type I to Type II.

Methods for predicting the significant parameters of the Type I waveform for a given weapon and site condition are fairly well established and are summarized in Section 2.0. Velocity rise time, positive velocity phase duration, and peak velocity generally serve to define the Type I waveform in sufficient detail to provide the isolation system designer with the information he needs.

Until the origin of the Type II waveform has been clearly established, however, the possibility of quantitatively fixing such parameters as peak velocity, damping, and frequency appears to be remote. If it is postulated that the Type II waveform can occur only in a reflection field, the phasing of the direct and reflected waves may be approximated by computing the times of arrival of each wave at the point of interest. By itself, however, this information is of little value to the isolation system designer.

The discussion of the Type II waveform in the Design Guide is highly qualitative in view of the preceding paragraphs. The existence of the Type II waveform as a phenomenon which may occur at other than the tests sites is accepted. It is assumed that somehow it is the result of

reflected waves, possibly through their interaction with the directly transmitted waves. It is further assumed, without validation, that the strength of the Type II component will be greatest in the regions where the reflected waves are strongest. On this basis, the reflection and refraction of elastic waves in layered media are examined and zones of influence established for various site conditions. It is shown that in a region lying above a layer of higher seismic velocity, the contribution of the reflected and refracted waves to the total ground motion increases with distance from the source. Thus, although the strength of the total shock is attenuated with distance, the response of a linear system in or near resonance with the Type II waveform may reach a peak at some intermediate location.

The designer cannot be given specific instructions for locating the point of maximum linear response or for determining the magnitude of the peak response. He is urged, however, to examine carefully the soil formations and facility orientation at each site of interest and is given broad guide lines to assist him in estimating the importance of the Type II waveform to his particular problem.

The ground motions discussed previously are those in the free-field, away from local disturbances. However, the shock isolation system is located within a cavity in the soil or within a partially or fully buried structure. The cavity or structure defracts the incident free-field waves, distorts the local flow, and produces motions different from those in the undisturbed regions. In addition the normal modes of oscillation of the structure itself are excited by the shock, further modifying the waveform of the motion at the points of attachment of the shock isolation system.

The principal concern of the isolation system designer, when considering the effect of soil-structure interaction, is the possibility that the low-frequency components of the free-field ground motion will be altered appreciably. Here again, few experimental data or theoretical studies can be applied directly to the designer's problem and he must rely heavily on broad interpretations of available works combined with knowledgeable conservatism. Section 2.0 of the Design Guide concludes by presenting a few of the results of interaction studies and notes those configurations where special precautions appear to be required.

Section 3.0 is devoted principally to the formal processes of developing the equations of motion for shock isolation systems and of solving the equations in general form for several of the most frequently employed suspension configurations. In the development of the equations for linear systems it is assumed that the shock is defined by its response spectrum. For nonlinear systems equations, the ground motion must be known in time. Much of the material presented here is available in standard works on dynamics or in publications relating to the special problems of response to ground shock. These data have been assembled in the Design Guide and applied to specific problems to assist in expediting the analysis procedures required of the designer.

Two topics treated here in some detail are of special importance to the isolation system designer. First, the equations of motion for the popular pendulum suspension system are derived rigorously for the two- and three-degree-of-freedom cases. The large effect of nonlinear coupling on horizontal oscillation for configurations of certain geometries is demonstrated and a criterion presented for determining system properties necessary to minimize this effect. Second, a series of design charts are presented for calculating the peak response of single-degree-of-freedom bilinear systems to shocks composed of combinations of the Type I and Type II waveforms. The system parameters and input waveforms are defined in nondimensional form so as to permit the use of the charts in a wide variety of applications.

It is obvious that the sole purpose of shock mounting equipment in an underground protective structure is to prevent it from becoming damaged to the extent that it cannot fulfill its intended function. Yet the damage-producing elements of shock are not clearly identified nor is it expected that they would be the same for all types of equipment. If the damage to a component can be related to stress, then the peak absolute acceleration to which the component is exposed can be employed as its criterion of damage. However, the dynamic properties of equipment can rarely be represented as one single-degree-of-freedom system. Instead they comprise a large number of such systems each with its own natural frequency. To describe a shock which the equipment will survive, it is necessary to define the acceleration of the shock at the frequency of each element; i.e., the response spectrum of the shock.

It should be further noted that if the equipment contains nonlinear or coupled linear elements, even the response spectrum is no longer a valid criterion of damage. This follows from the fact that the peak acceleration of elements of this type is dependent on parameters described only by the waveform of the shock. It is rarely possible during design to determine the dynamic characteristics of the exact piece of equipment to be installed in the facility. Indeed, the make and model number of the specific item is usually not known until the facility design has been completed. Yet early in design the designer is faced with the problems of deciding whether or not shock isolation is necessary and, if so, of determining the degree of attenuation required.

A logical solution would be to determine by test the survivability of equipment to a shock with a waveform identical to that expected in service from the ground shock or from the isolation system. This approach is not possible however in view of the lack of information on the ground shock waveform, the fact that the design must be completed before the particular equipment item is selected, and the inability of most test machines to reproduce waveforms with sufficient accuracy. For these reasons, the acceptance of the response spectrum as a criterion of damage potential appears to be a more practical choice. It is pointed out that despite its theoretical limitations, this criterion is not without experimental foundation. With the acceptance of this criterion

of damage potential, a direct quantitative comparison can be made between the test machine output and the service environment. While the problem of obtaining test data of a specific item which has yet to be selected still remains, shock tolerance data for general classes of equipment can be correlated much more readily by means of the shock spectrum than by waveform.

In Section 4.0, shock tolerance data on equipment typical of that installed in underground facilities have been assembled and correlated with the response spectrum of the test shock. The tabulations are far from complete and the equipment categories have been selected more on the basis of availability of data than of importance to the designer. Nevertheless, the compilation should serve as a demonstration of a rational approach to the problem and a step toward providing the designer with quantitative information prior to test. The response spectra given in Section 4.0 for test machines can also be used as a basis for the selection of a machine to reproduce a given damage potential.

If the designer decides that his equipment must be shock isolated, he must ensure that the response spectrum of the isolated system is lower, for all frequencies, than that of a shock the equipment has survived. In effect, this implies that he know the response of the isolation system before the system constants are selected. In the Design Guide a procedure is described whereby the waveform of the motion of the isolated system is approximated and readily converted to a spectrum. By a short iterative routine, the required frequency and attenuation of the isolation system are then established.

Many suspension systems in underground protected structures are intended to support personnel. For each case, the "mode of failure" must be defined before attenuation requirements can be determined. For example, if personnel are permitted to move about freely and are not prepared for the shock, the mode of failure may be loss of balance. In other instances, where personnel are strapped in seats, the mode of failure may be injury due to the direct acceleration of the seat.

Data on the shock and vibration tolerances of human beings for different modes of failure are presented in the Design Guide. In those modes where the man is well supported and subjected to high accelerations, the data are fairly plentiful. Where simple loss of balance is the criterion of failure however, little information is available.

The influence of practical operational considerations on the design of shock isolation systems and on the selection of their components is reviewed in Section 5.0. Factors modifying coupling and resonance characteristics, the signficance of system restoring time, and means for reducing the possible effects of uncertain features of the shock are pointed out and discussed. The Section concludes with a demonstration of a design procedure drawing on the approaches presented in the earlier Sections.

It is hoped that the Design Guide will serve to encourage the shock isolation system designer to view his system in a broad perspective and to instill in him an appreciation for the many uncertainties obscuring both the nature of the input and the requirements of the output. Since the transient characteristics of his system cannot be explicitly defined, he must remain constantly abreast of the accomplishments in the related fields and must concentrate his attention on systems whose broad stability characteristics render them less sensitive to perturbations of the estimated environment. In any event, the high reliability demanded of those systems, and the impossibility of conducting full-scale proof tests of the complete system, emphasize the essential need for thoroughness and conservatism in design.

SECTION 2.0 SHOCK PREDICTION METHODS

TABLE OF CONTENTS

2.1 Introduction

Methods for predicting characteristics of the shock waveform important to the response of shock isolation systems are studied in this Section. Phenomena governing the generation of waves in the ground by nuclear blast are described, their methods of transmission, reflection and refraction within real, layered soils are reviewed, experimental data are examined for recurrent waveform patterns, and existing methods for estimating certain waveform parameters are summarized. A wavefront diagram is suggested as a basis for determining the early characteristics of the ground shock.

In general, the discussions of ground shock phenomena are of a qualitative nature being directed primarily toward the immediate needs of the shock isolation system designer. Theoretical treatment has been avoided and the results are presented only where they apply directly to this specific problem.

The design procedures, developed in this Section, are based on the best information available at this time. It is evident that they should be frequently reviewed in the light of future experiment and theory.

2.2 Factors Influencing the Character of the Ground Motion

2.2.1 Air Blast- and Cratering-Induced Phenomena

Ground motion from a nuclear surface burst may be generated by two distinct processes: (a) the direct conversion of hydrodynamic energy into mechanical energy due to the impact of the vapors of the bomb materials directly on the ground and (b) the pressure loading on the ground surface due to the rapidly growing fireball or air shock wave.

Although total energies transferred to the air and to the weapon materials during the explosion of the weapon are comparable, the pressures generated by the compression of the air near the weapon initially are several orders of magnitude less than the pressures created by the vaporization of the weapon materials. Assuming a hydrodynamic model, Brode and Bjork (Reference 2.1) calculate the stresses and early motions associated with the explosion of a two megaton weapon on the surface of a medium composed of a "tuff" rock. Their results show that, for all points lying in the ground within a right circular cone of a 70 degree half angle with the apex at the point of detonation, the principal pressure in the ground shock wave is the result of the weapon vapor loading.

The pressures developed in the ground by the impact of the weapon vapors are sometimes called "direct induced" or "direct transmitted" pressures. Perhaps a more descriptive term would be "cratering induced" since, unless the burst occurs close enough to the ground surface to create a crater, this source of direct impact energy will be absent. For air bursts, in which the fireball does not touch the ground, the ground motions are principally "air-blast induced". For buried bursts, there is little air overpressure and the ground motions are almost entirely cratering induced.

At any point on the surface of the ground outside the fireball, the pressure behind the spherically expanding air-blast wave reaches a peak at the instant the wave reaches the point and it then decays exponentially as the wave passes on (Figure 2.2.1, page 2-5). Also, the peak pressure (P_o) immediately behind the wave decreases as the wave moves further from the source, thus retarding the wave until eventually it is slowed to acoustic velocity. Curves showing the relationship of overpressure versus distance from source, impulse, wave arrival time, et cetera, have been prepared by Brode (Reference 2.2). These curves are for weapons of various yields and assume that the temperature of the air into which the wave is advancing is uniform and the viscous effects at the ground surface are neglected. Some of the most frequently used curves are replotted here as Figures 2.2.2 to 2.2.5 (pages 2-6 - 2-9).

The most significant deviation of the actual from the ideal air blast shock front is the possible development of a higher velocity

shock front, or "precursor", near the ground surface. While all of the details concerning the formation of the precursor are not clear, it is believed to be the result of the formation of a high-temperature layer of air, or air-dust mixture, near the ground surface by energy radiated from the weapon at the instant of detonation (Reference 2.3). Since the air-blast wave velocity is dependent on the temperature of the medium into which it is advancing, and the medium near the surface may be warmer, the wave near the surface may arrive first at a given point. The effect of the earlier arrival of the wave at the surface may have a significant influence on the waveform of the air-blast induced ground shock within the first 100 feet below the surface. At lower depths, however, it is not expected to be of importance.

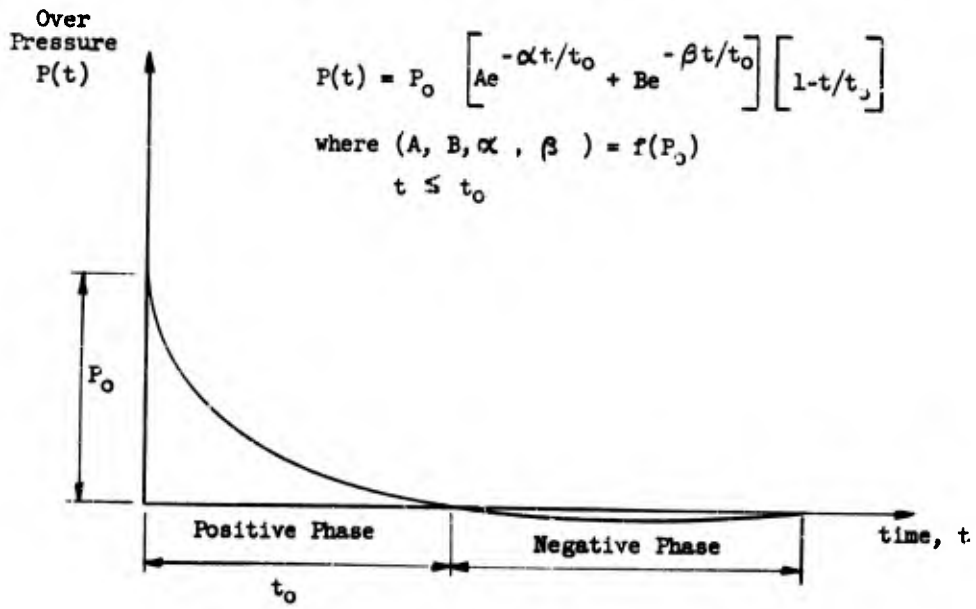

Figure 2.2.1 Idealized Overpressure Decay

If the temperature of the air into which the air-blast shock wave is advancing is uniform, the velocity of the wave is a function only of the peak pressure behind it. Thus, the velocity of the air-blast shock wave in this medium becomes progressively less with distance from ground zero.

The composition of most soils is highly nonuniform. Therefore the seismic velocity throughout the ground will vary both with depth and range, the vertical variation usually being the greater due to layering of the soil. As a result, a disturbance generated in a surface layer may be quickly transmitted to a lower layer of higher seismic velocity

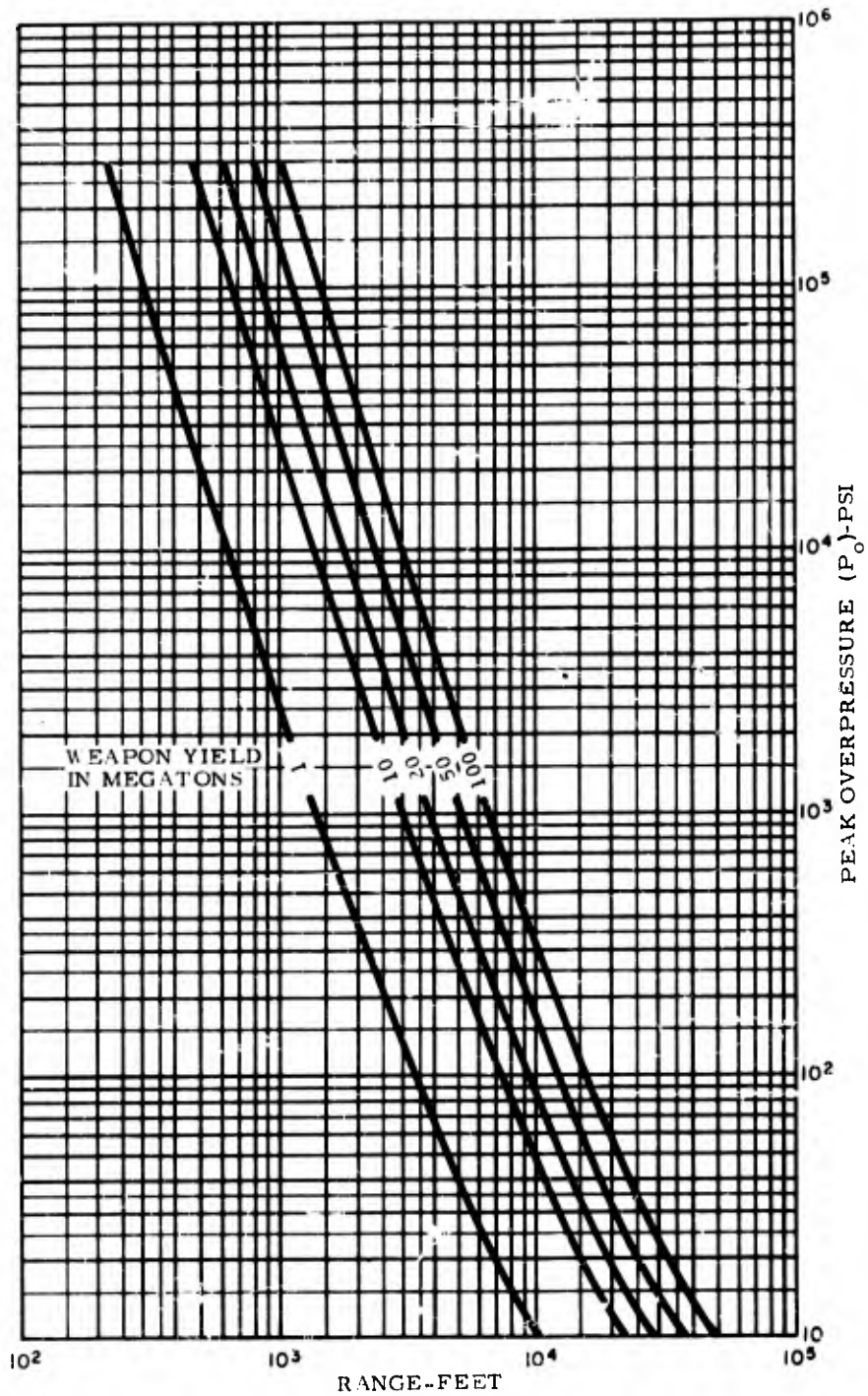

Figure 2.2.2 Peak Overpressure vs. Range

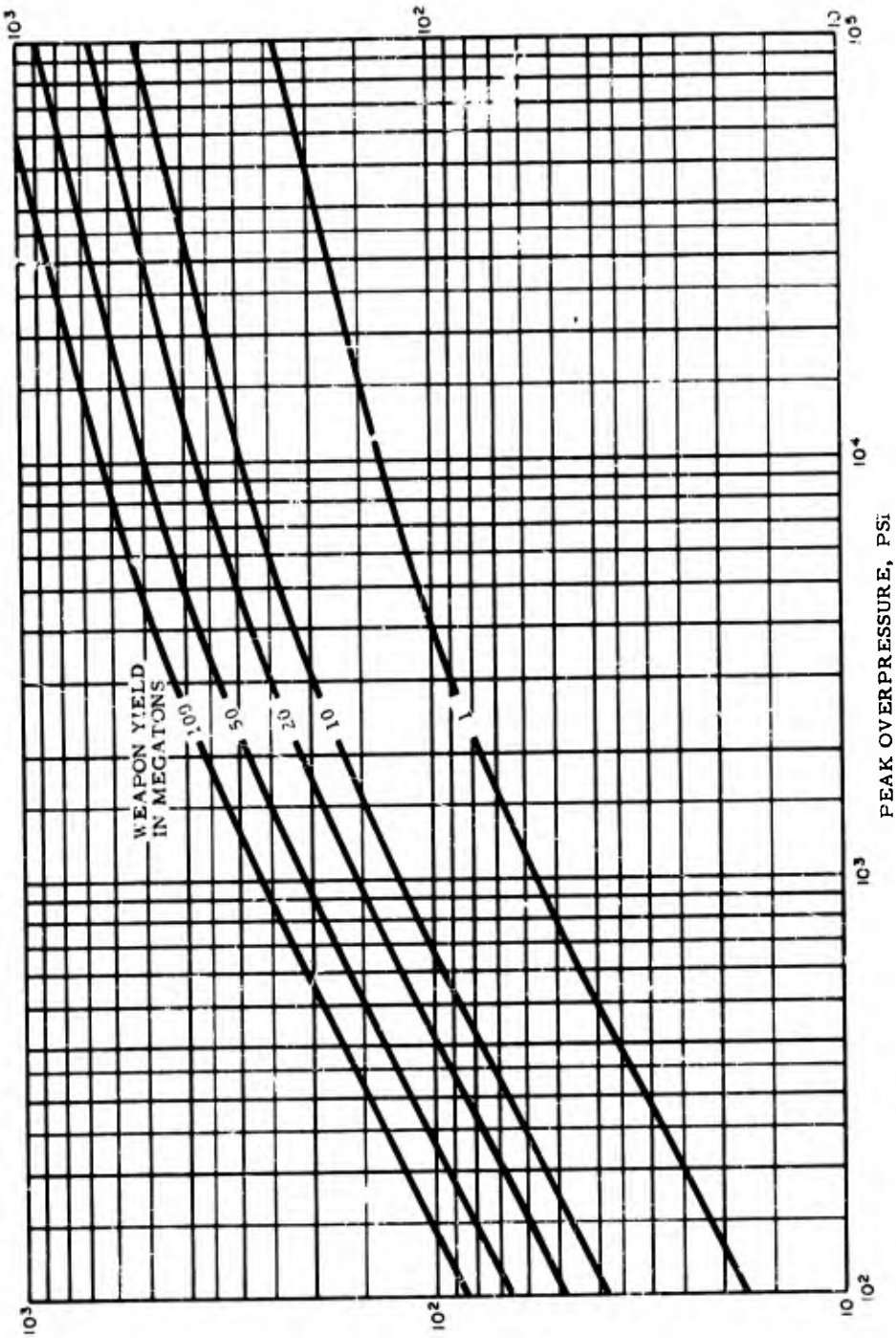

Figure 2.2.3 Impulse vs. Peak Overpressure

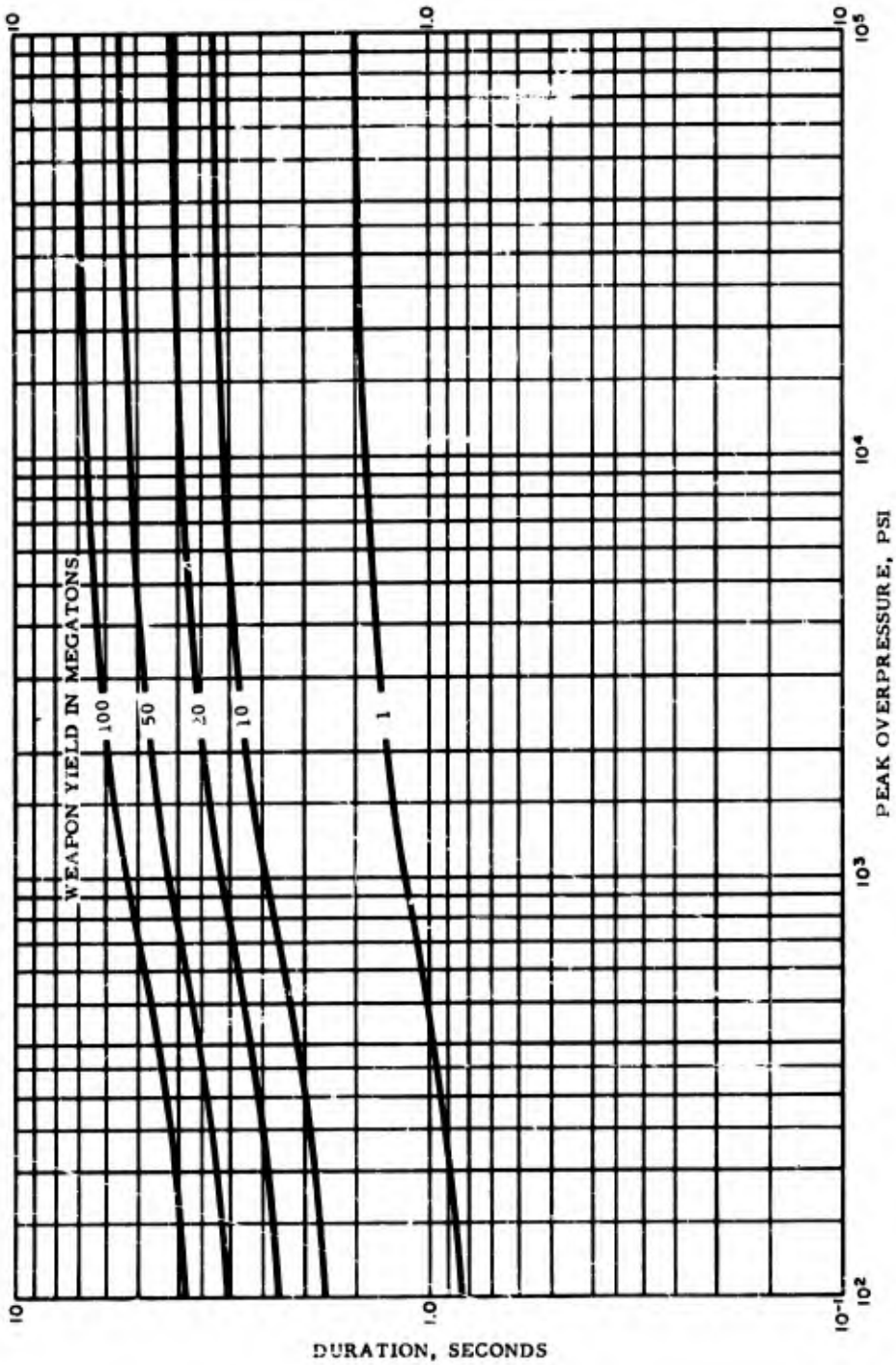

Figure 2.2.4 Positive Phase Duration (to) vs. Peak Overpressure

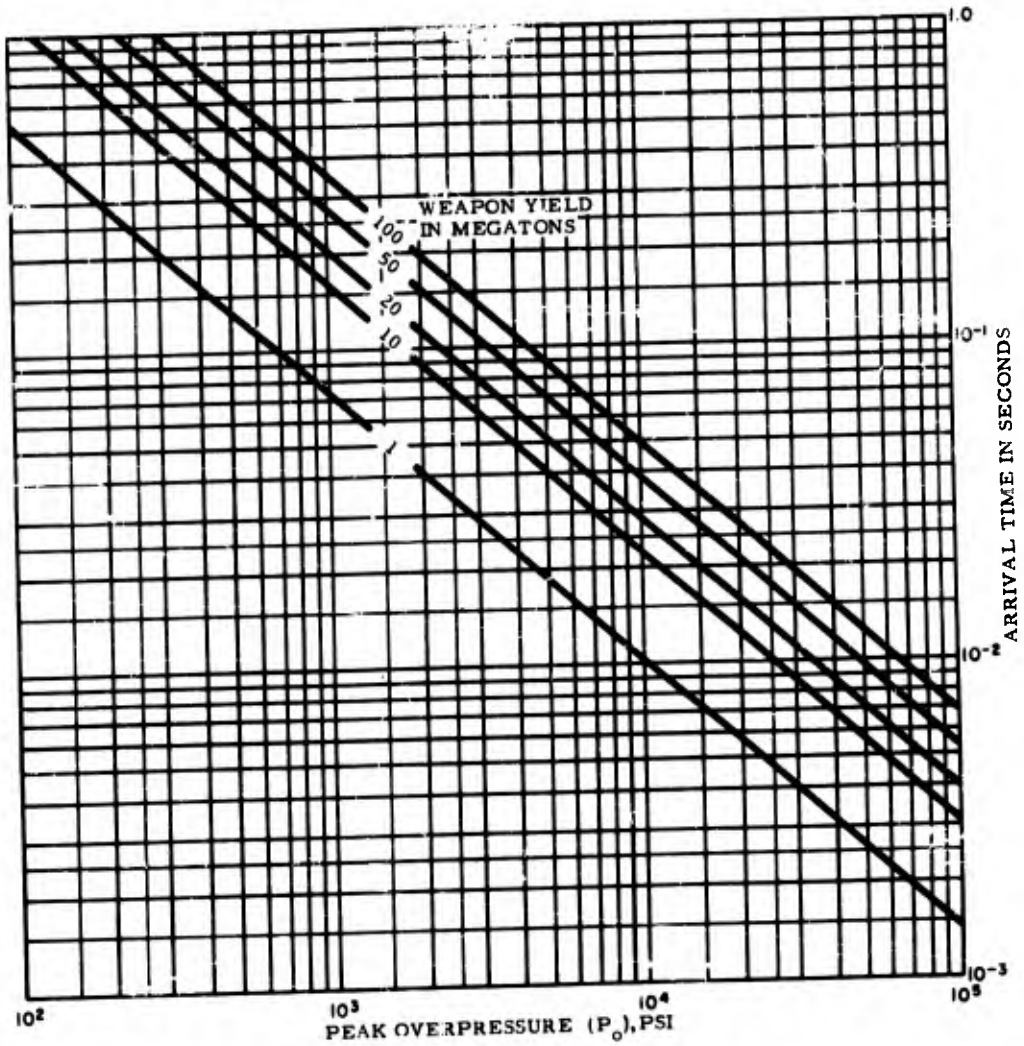

Figure 2.2.5 Arrival Time from Ground Zero *vs.* Peak Overpressure

where it will race ahead of the wave in the surface layer. Further, refractions from the higher velocity wave will be transmitted back into the surface layer, reaching a given point at the surface prior to the arrival of the wave transmitted directly through the surface layer from the source.

The phasing of the arrival times of the air-blast shock waves and the ground waves is divided into three regimes. If the air-blast shock wave arrives at a given distance from the source prior to the arrival of any wave transmitted through the ground, the condition is said to be "superseismic". This case is shown in Figure 2.2.7-1 (page 2-11), and can only occur if the velocity of the air-blast shock wave at that point exceeds the seismic velocity of the soil and if no reflections or refractions from lower layers have outdistanced the shock wave. The inclination of the air-blast induced shock from the ground surface for the superseismic case is shown in Figure 2.2.8.

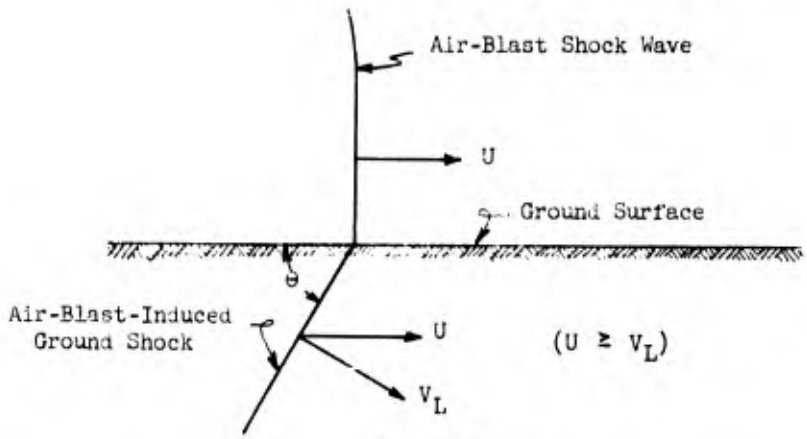

Figure 2.2.8

Inclination of Air-Blast-Induced Ground Shock

The angle θ is a function of the air-blast shock wave velocity U, and the seismic velocity V_L and can be expressed

$$\theta = \sin^{-1} \frac{V_L}{U}$$

In Figures 2.2.7-2 and 2.2.7-3 the initial motion of the ground is the result of a ground-transmitted wave rather than the direct effect of the air-blast pressure. In Figure 2.2.7-2 the local seismic velocity exceeds the air-blast wave velocity thus causing the ground shock to "outrun" the air wave. In Figure 2.2.7-3 the ground is set in motion initially by a refracted wave from a lower layer of high seismic velocity. Both of these cases are called the "subseismic" condition. The intermediate

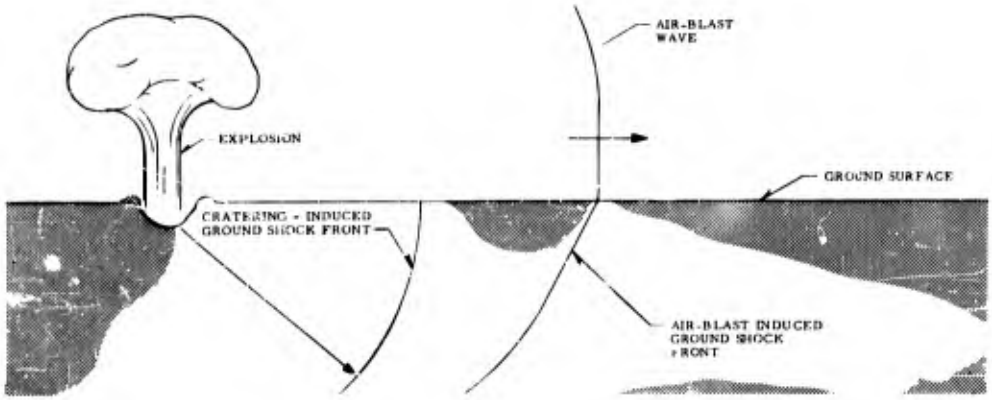

(7-1) Superseismic Regime

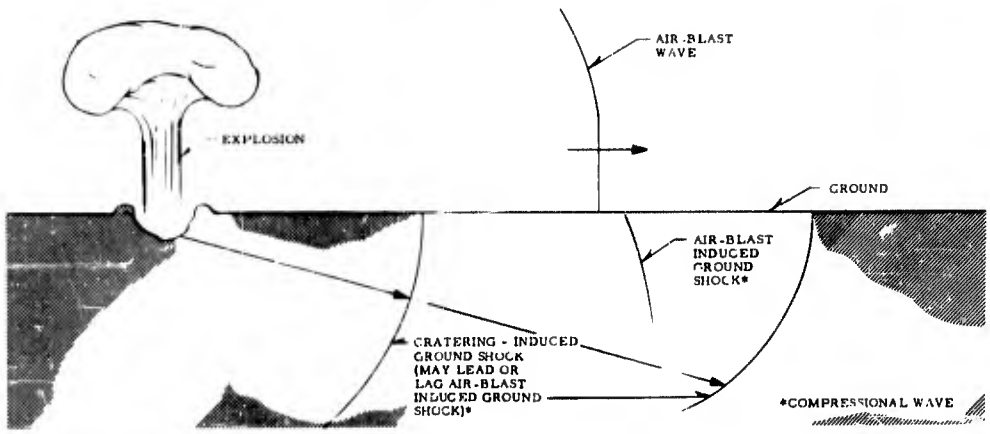

(7-2) Subseismic Regime - Outrunning

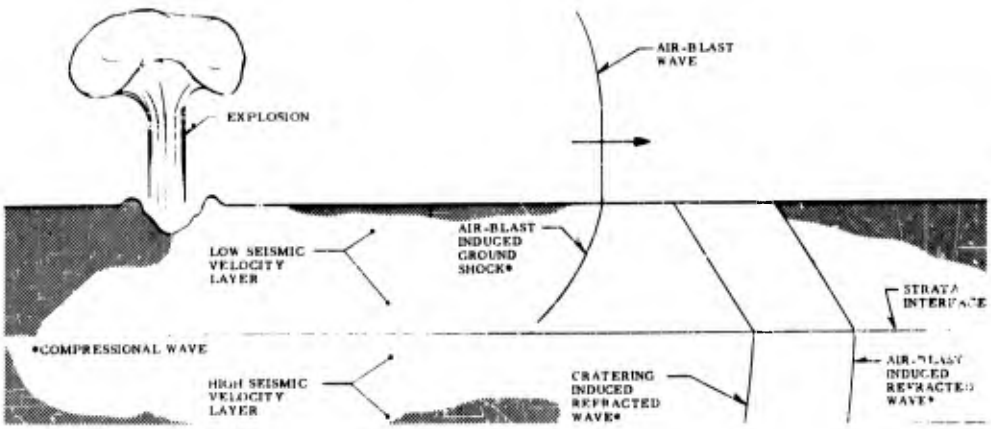

(7-3) Subseismic Regime - Refracting

Figure 2.2.7 Ground Shock Wave Propagation Regimes

condition where the air-blast wave and the ground shock arrive at a point nearly simultaneously is known as the "transseismic" case.

It can be seen from Figures 2.2.7 that the initial horizontal component of the motion of a particle due to nuclear blast is always away from the source while the initial vertical component may be either up or down. For the superseismic case, the initial motion will be down. For the subseismic and transseismic cases, the direction of the initial motion will depend on the position of the point in question with respect to the source, on the degree of layering and on the character of the material.

Since the waveform of the motion of a particle is the direct result of the waveforms of the constituent shocks, the details of phasing between the peaks of the outrunning refracted waves, the direct cratering-induced waves, and the air-blast induced waves all will affect the determination of the maximum pressure at the point of interest. At shallow depths, the rise time of the air-blast induced wave is very small. Thus, the phasing of the waves in the superseismic case will rarely affect the peak pressure, although later portions of the pressure-time history will be influenced. As the depth of the point of interest is increased, the wave arrival regime tends to become subseismic setting up a condition conducive to the coincidence and the resulting amplification of peak pressures. For a given overpressure, the larger the yield of the weapon, the greater the probability of the wave arrival regime being subseismic.

In Figure 2.2.8 , the velocity of propagation of the air-blast wave as a function of peak overpressure is compared with the seismic velocities of soil and rock.

2.2.2 Transmission of Elastic Waves

In the absence of body forces, and where the soil may be approximated as a homogeneous, isotropic, elastic solid subject to only small strains, energy is transmitted as either longitudinal or shear elastic body waves (Reference 2.4). In addition to such body waves there may be two types of surface waves, the Rayleigh and the Love waves. Each of these four waves propagate at different velocities, depending upon the elastic constants of the medium. Virtually all elastic analyses consider points of interest at a great distance from the source and consider the wave fronts to be plane waves, that is, having no curvature.

The motions of the particles of the medium for the longitudinal wave, also called dilatational, compressional, or (in earthquake studies) the primary wave, are parallel to the direction of propagation, like those of sound in air. The velocity of propagation of longitudinal waves in an elastic medium is

$$V_L = \left[\frac{E}{\rho} \frac{(1-\mu)}{(1+\mu)(1-2\mu)} \right]^{1/2}$$

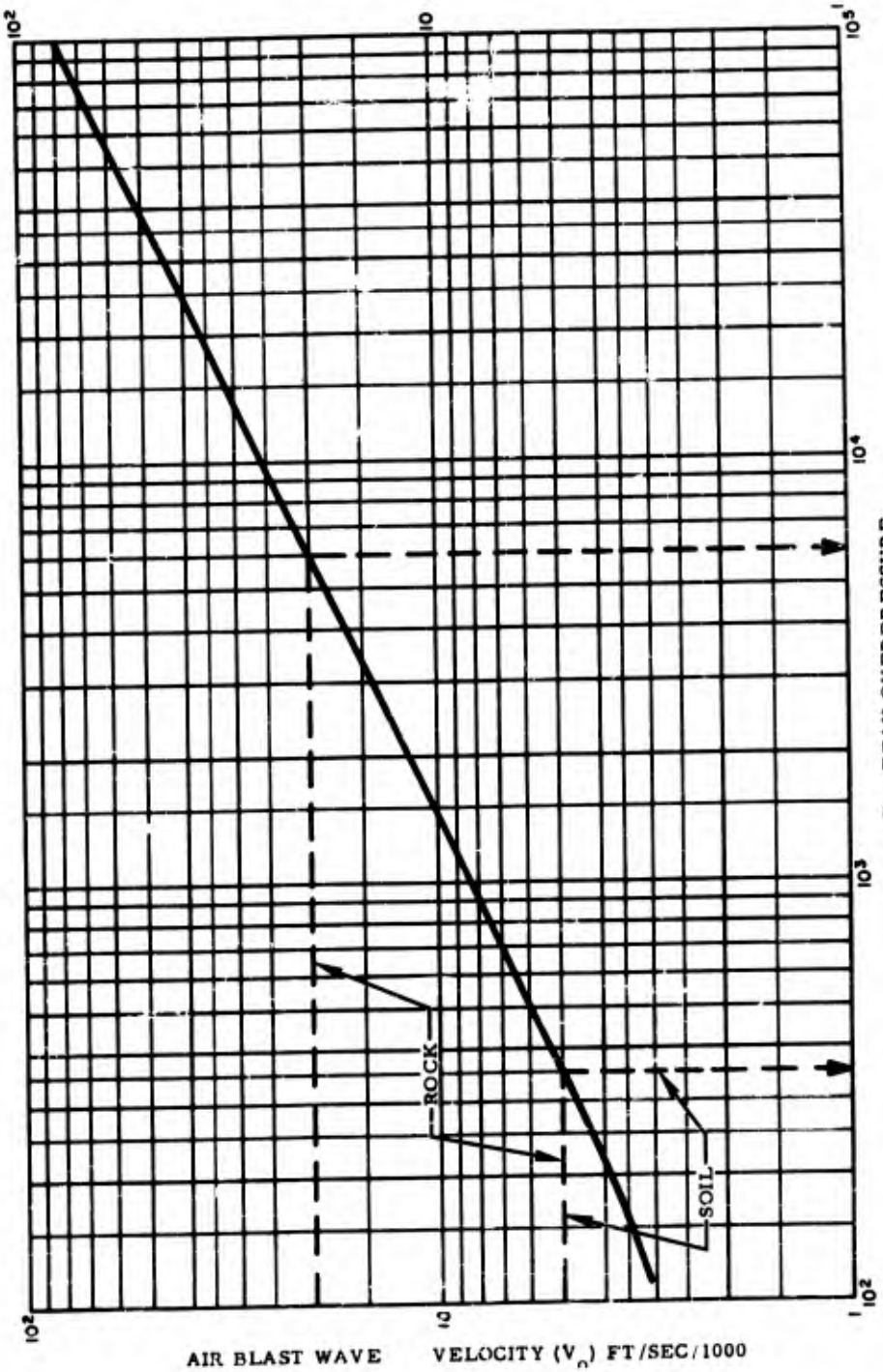

igure 2.2.8 Airblast Wave Velocity vs. Peak Overpressure

where

E = Young's modulus

ρ = Density

μ = Poisson's ratio

The motions of particles of the medium for the shear wave, also called the transverse, or in earthquake terminology the secondary wave, are perpendicular to the direction of propagation, like waves of a vibrating string. The velocity of propagation of shear waves is

$$V_S = \left[\frac{E}{\rho} \quad \frac{1}{2(1 + \mu)} \right]^{1/2}$$

Comparison of the equations for the velocity of propagation of the two body waves shows that the velocity of longitudinal waves (V_L) is always greater that that of shear waves (V_S) according to the ratio

$$\frac{V_L}{V_S} = \left(\frac{1 - \mu}{1/2 - \mu} \right)^{1/2}$$

At the free surface of a semi-infinite elastic solid a group of surface waves, one of which is called the Rayleigh wave, can be developed. The particle motion of the Rayleigh wave is a combination of longitudinal and transverse vibration giving rise to an elliptical motion of the particles. The major axis of this ellipse is perpendicular to the surface and to the direction of propagation. For the special case when Poisson's ratio is 0.25, typical value for rock, the velocity of propagation of the Rayleigh wave is approximately 0.92 V_S (References 2.5 and 2.6).

Love waves are shear waves which travel at the lower boundary of thin surface layers. The velocity of their propagation depends upon the wave length, and varies between that of shear waves in the surface layer and shear waves in the underlying layer.

For the case where Poisson's ratio equals 0.25, the velocities of the longitudinal, shear, and Rayleigh waves (V_R) have the following ratio:

$$V_L : V_S : V_R = 1 : 0.577 : 0.531$$

As a result, at least three separate wave fronts would pass a given point somewhat removed from the source. According to elastic theory (Reference 2.6)Rayleigh waves are capable of producing very high stresses in a surface zone below which the stresses attenuate rapidly with depth. The surface zone may be defined as having a depth below the surface of approximately one quarter of the range from the source. If the velocity

of the air-blast induced wave is near or equal to the velocity of the Rayleigh wave, elastic theory also indicates that the resulting ground motions will be very large. However two practical considerations appear to diminish the importance of Rayleigh waves in ground shock problems. First, at the high stresses predicted by elastic theory, the theory becomes invalid due to plastic deformation of the real soil. Second, since the velocity of the air-blast induced wave changes rapidly with range, the velocities of the two waves will be the same only for a very short period of time. While the effect of the Rayleigh wave may be of significance at point of coincidence of velocities, the short duration of the quasi-resonance condition will result in much lower motions than those predicted by theory (Ref. 2.35)

No solutions or test records are available indicating that the Love wave is of major significance. Howell (Reference 2.4) reports that, in the records of underground explosions, Love waves (and body shear waves also) are conspicuously weak. He notes that this is not surprising if it is considered that the energy is initiated by a radial pressure around the charge, which sends out a compressional pulse through the ground but produces relatively little shear. However, it must be assumed that a surface burst would produce shear forces in the area of the crater, and that shear waves will be generated from the air-blast shock front as it travels over the ground surface. As will be discussed later, shear waves can also be produced when longitudinal waves are reflected or refracted from a layer with different elastic properties.

It has been found from seismological studies (Reference 24)that the amplitude of ground motion decreases with distance from the source, due to:

- radial spreading of the energy
- absorption, within each medium, of energy from the pulse because of the nonlinear properties of the medium
- the length of the seismic pulse (especially in surface waves)
- the division of the original pulse due to part of the energy being reflected at each boundary encountered and part being transmitted to the new medium.

In the case of body waves generated near the earth's surface, the energy is distributed over a hemisphere whose area is proportional to the square of the distance from the source. In general, absorption by the ground is an exponential function of distance so that for any body wave

$$E'' = \frac{E'}{R^2 e^{aR}}$$

where E" is the energy per unit area in the waves at a distance R
E' is the total energy at unit distance

R is the range in feet
a is the coefficient of absorption

Typical values determined from small explosions for the coefficient of absorption for longitudinal waves in the weathered layer (0 to 50 feet typically) is 0.062 per meter, and 0.00033 when refracted through a near-surface rock layer. The results of measurements from earthquakes also indicate values of a equal to 0.062 per meter.

Generally, high-frequency vibrations travel at a different velocity from low-frequency vibrations. The coefficient of absorption also generally increases with freqency. In some cases with surface waves, a has been noted to increase with the square of the frequency. The result is a rapid loss of high-frequency energy in seismic waves as distance from the source increases. At large distances, the principal wavelengths of the observed motions are generally greater than near the source.

When a wave front strikes the interface separating two layers of different elastic properties, the energy of the incident wave is divided between four new waves. Part of this energy is reflected as a shear wave and longitudinal wave, and part transmitted into the new layer as a refracted shear and longitudinal wave.

The basic principles controlling the propagation, reflection, and refraction of elastic waves are similar to those controlling light waves. According to Snell's Law, the angles made by the rays or paths along which elastic waves are propagated (Figure 2.2. 9, page 2-17), are governed by the following equation:

$$\sin a : \sin b : \sin c : \sin d = V_{L1} : V_{L2} : V_{s1} : V_{s2}$$

For a ray in a lower velocity layer V_{L1}, striking the boundary of a higher velocity layer V_{L2}, there is a certain critical angle of incidence a' for which the angle of refraction b is 90 degrees and the refracted wave is parallel to the boundary. According to Snell's Law this critical angle of incidence a' is equal to

$$\sin a' = \frac{V_{L1}}{V_{L2}}$$

For any angle of incidence greater than a', there can be no refracted ray in the second layer and, therefore, no transmission into that layer. Thus, for incident angles greater than the critical angle there is total reflection. Similar relationships may also be derived from Snell's Law for critical angles when shear waves are the incident waves (Reference 2.4).

The equations representing the division of energy between the various reflected and refracted waves derived by Knott have been solved by Muskat and Meres (Reference 2.7) for various angles of incidence, and velocity and density ratios. These results show that the energy carried by the reflections are relatively unimportant (11-15% of the

total of the incident wave) at angles of incidence less than the critical angle (that is, more normal to the boundary), whereas only the reflected longitudinal energy is important at angles greater than the critical angle of incidence.

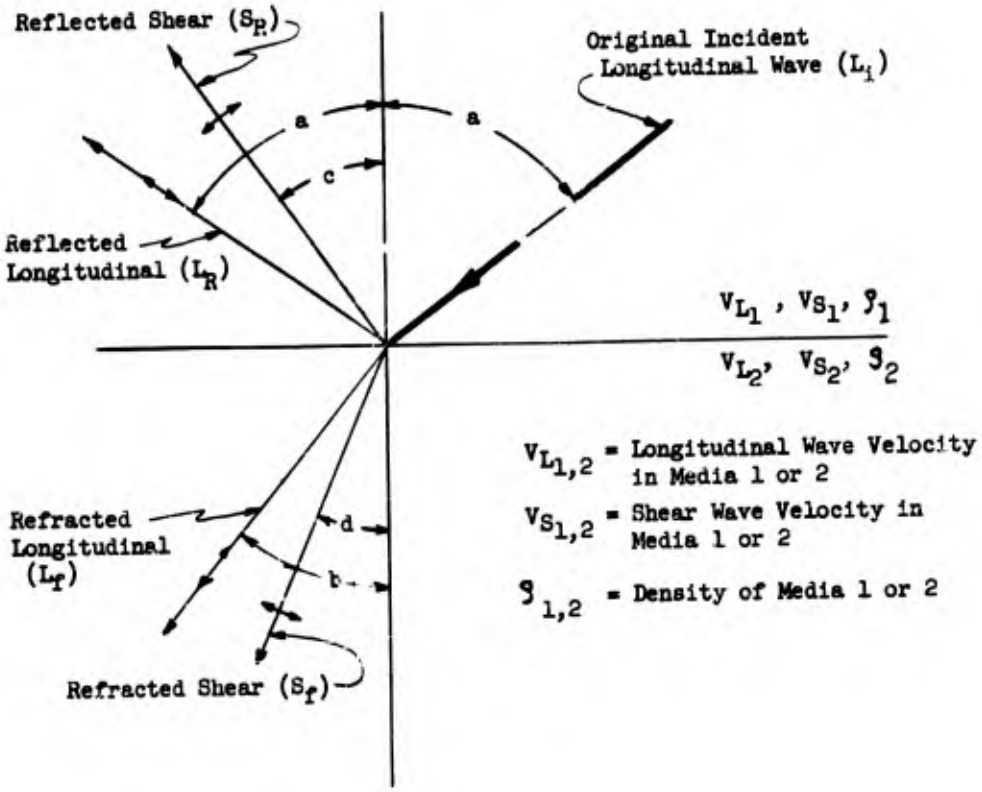

Figure 2.2.9

Relation Between Reflected and Refracted Wave Rays at the Boundary of two Elastic Media

In both cases the energy carried by the generated shear waves is small (0.12%). When the angle of incidence is less than the critical value, the ratio of the energy carried by the refracted longitudinal wave to the energy in the incident wave increases from between 0.8 to 0.9 for ratios of V_{L2}/V_{L1} less than one; to unity when V_{L2} equals V_{L1}; then decreases by 10 to 25 per cent as V_{L2} approaches twice V_{L1}. As the ratio of the densities ρ_2 / ρ_1 increases from one to 1.3, the energy carried by the refracted longitudinal wave decreases, but only nominally.

For practical purposes it can be assumed that, for an angle of incidence less than the critical angle, all the energy carried by an incident longitudinal wave will be transferred to the refracted longitudinal wave, while for incident angles greater than the critical angle, all the energy will be transferred to the reflected longitudinal wave. This appears to be reasonable regardless of density or velocity ratio, within the practical limits of predictability of the soil properties.

By the application of Huygens principle it is possible to construct a wave front diagram such as that shown on Figure 2.2.10. Huygens' principle states that each point on an advancing wave front in an isotropic, homogeneous medium may be considered the source of a new spherical wave. The wave front at any time is tangent to the envelop of these new spherical waves. The diagram of Figure 2.2.10 shows the position of the first arrival of each wave emanating from a single point source. The upper plot on Figure 2.2.10 shows a time-travel graph of the waves as the first arrivals would be picked up by geophones at the surface; as for example, during a refraction seismic survey.

Also shown in Figure 2.2.10 is an air-blast arrival time curve for a 20-megaton weapon with ground zero at the shot point (Reference 2.2). Most details of the construction of the wave front diagram are given in the Figure. Lines labeled abc and ade on the wave front diagram represent the points where the times of arrival from the underlying layer and from the surrounding layer are the same. The slopes of lines ab and fd represent the critical angles of incidence between layer 1 and 2 and between layer 2 and 3, respectively. Additional details on the construction of wave front diagrams may be found in papers by Leet (Reference 2.8) and Thornburgh (Reference 2.9).

Several characteristics of particular interest can be illustrated by means of the wave front diagram. The upward component of the velocity of the waves refracted from lower layers is clearly evident. The range at which the transition from the superseismic to the subseismic cases occurs can be found from the wave front arrival-time diagram by sliding the origin of the refracted wave arrival-time curve along the air-blast wave arrival-time curve until the two intersect at a minimum ground range. It may be noted that the tangent to the air-blast wave arrival curve at point a' (Figure 2.2.10) is parallel to the refracted wave arrival curve. For the site and weapon conditions considered in the Figure it may be seen that an air-blast induced wave generated at a range of 6,000 feet will reach the 8,000-foot range at about the same time as the air-blast wave itself. This marks the transeismic region. Nearer the source the air-blast wave will be superseismic while further from the source it will be subseismic.

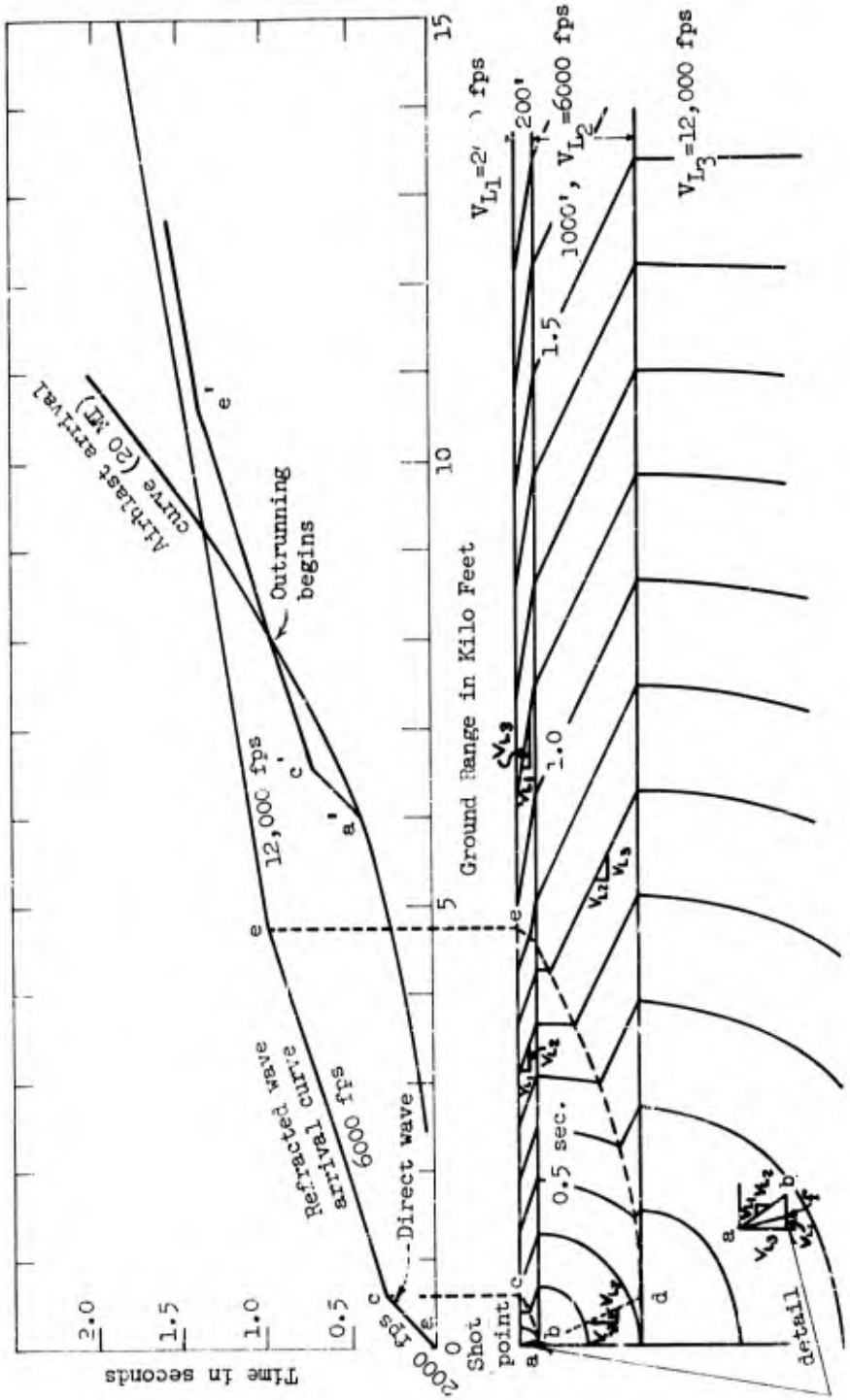

Figure 2.2.10 Refracted Wave Front Diagram

The wavefront diagram can also be used to confirm that outrunning will occur at shorter ranges in the deeper, higher velocity layers. By constructing an arrival-time curve for the depth of interest, the wave-arrival relationships discussed above for conditions at the surface can be established for the new depth.

Although, with the proper choice of wave velocities, first arrival times can be found directly by using the wavefront diagram, the distribution of energy from the traveling airblast shock front cannot. If the incident angle between two layers is less than the critical incident angle, it can be assumed that all the energy is transmitted by refraction to the adjacent new layer. At larger incident angles the energy is reflected back into the upper layer. According to Fermat's principle, the path along which energy will radiate from a point source is the minimum time path. This concept will be applied more fully in subsequent paragraphs.

2.2.3 Influence of Nonlinear, Nonelastic Properties

Virtually all of the present theoretical studies of waves in layered media assume that each layer is isotropic, homogeneous and elastic, and that the contact boundaries between layers are sharp and non-dispersive. In fact no discussion has been found dealing with the reflection and refraction phenomena in nonlinear, inelastic media. The assumption of an isotropic medium would appear valid for igneous rock since the rock is mostly crystalline, and commonly, the crystals are oriented randomly. For sedimentary rocks and stratified soil this would seldom be a valid assumption. Because of the mode of their geological formation, it is expected that they exhibit a greater rigidity parallel to the bedding than transverse to the bedding. This is often demonstrated by comparisons of the higher, nearly horizontal velocities computed from refraction seismic surveys with the vertical velocities obtained in uphole surveys at the same sites. Ratios of horizontal to vertical velocities of two are not uncommon. The full significance of the non-isotropic characteristics of an aeolotropic material on wave phenomena is not clear. Ewing, Jardetzky and Press (Reference 2.10) state that there is no sharp distinction between the longitudinal and shear waves if a disturbance is propagated in an aeolotropic medium, further, an explosion in such a medium will produce both longitudinal and shear waves. The ground wave pattern in an aeolotropic material would also differ from that of an isotropic medium. Although it has not been verified, it may be possible to transform the scales, when constructing the wavefront diagram, to correct for the aeolotropic effect in a way similar to the use of transformed flow nets in ground water seepage problems when the coefficients of permeability differ in two directions.

When there is a continuous increase of seismic velocity with depth, as there often is with real sites, refraction will still occur, but reflection will not. Reflection requires a discontinuity. Even where there are virtually step increases in velocity on a macro

scale, the details of gradational change and weathering at the contact boundaries have a great influence on the ability to reflect energy. The question of whether or not elastic theory can predict all of the phenomena of significance is of real concern. Although many observed phenomena can be explained by elastic and near-elastic assumptions (Sauer, Reference 2.11) the level of the stress in many practical problems makes it difficult to accept these elastic assumptions for soils and near surface rock. However, saturation of the soil and the confinement of overlying material, as well as precompaction by prior attack, may make the assumption valid within reasonable depths below the surface for special cases.

Figure 2.2.11, page 2-22 illustrates a typical stress-strain curve for a granular soil, such as a sand, subjected to a unidirectional confined compression test. The total deformation developed by dynamic loading is made up of both elastic and plastic strains. The elastic motion is due to simple compression of the mineral grains and the fluid in the voids. The plastic portion is that due to slippage of grains and would require a loss of fluid for a saturated soil.

At very low stresses, the deflections produced in the material are almost entirely elastic. When the level of the stress becomes high enough to cause slippage of grains relative to one another, the strains are nonrecoverable or plastic. The stress increase required to develop plastic motions is probably a moderate per cent of the effective confining pressure existing on the element under consideration. In a fragmental material, such as soil, as the grains are moved into a denser position by the applied compressive forces, the elastic modulus increases in magnitude. The limiting value of the modulus, at very high stress levels, probably is that of the mineral composing the grains. Once the stress level has risen to the point where significant grain slippage occurs, the tangent modulus of deformation decreases and remains low until the voids are essentially filled. The tangent modulus then increases again to a value equal to or greater than the initial elastic modulus. Upon unloading it is probable that the recovered strain follows the highest elastic modulus.

The original relative density of the sand and the initial confining pressure have a great effect on the location of the inflection points of the stress-strain curve. It was observed at the Nevada Test Site that measureable plastic deformation did not occur at less than 40 psi overpressure (Perret, Reference 2.12). The degree of saturation should also have an important effect, since, for a saturated soil when there is insufficient time for any significant drainage to occur, the water will carry practically all of the applied load. This effect might smooth out the stress-strain curve for an increase in initial density, initial confining pressure, and saturation. A similar phenomenon also apparently exists for clays, based on the information reported by Wilson (Reference 2.13). However, for clays, the modulus and shape of the curve are more strongly influenced by past compressions than for sands. Repeated loading

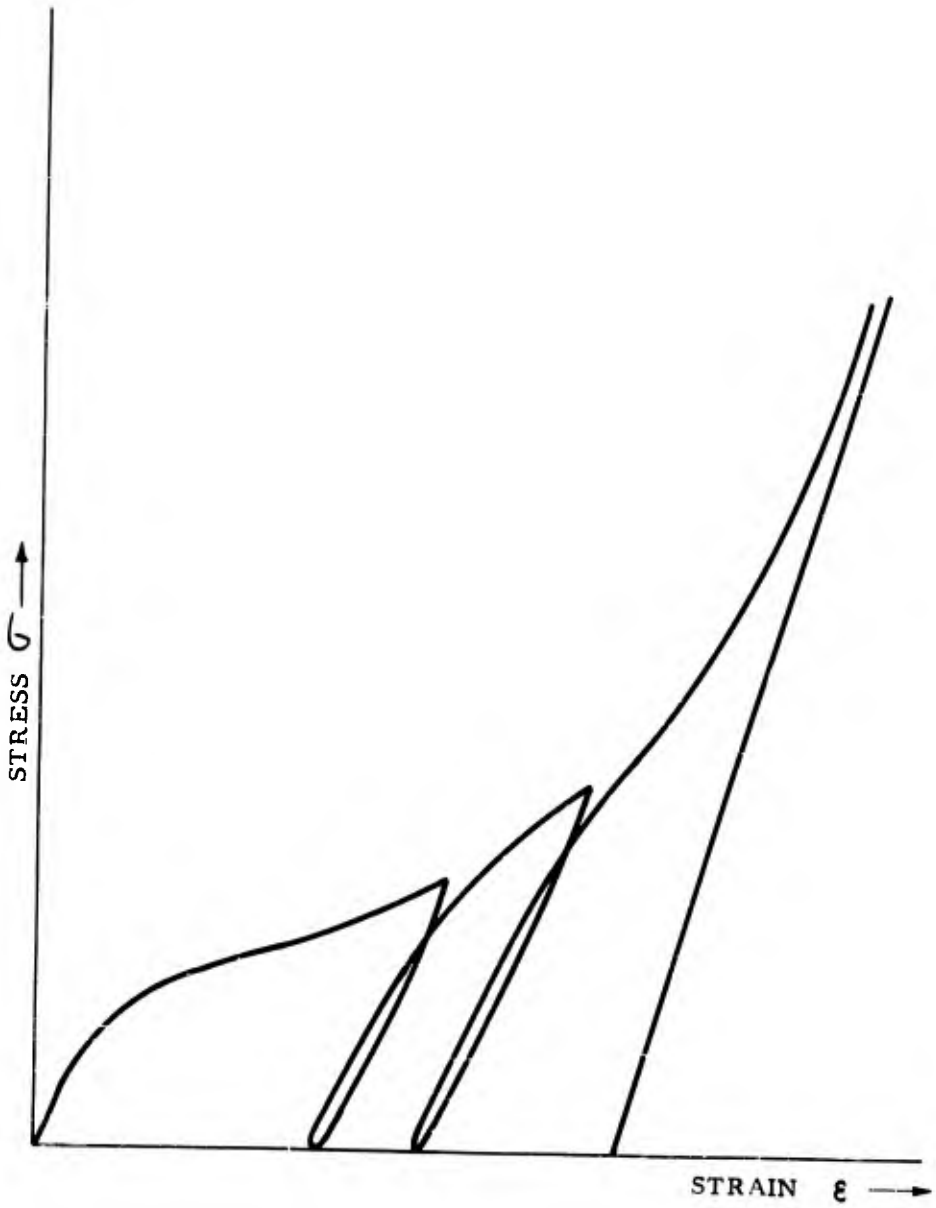

"TYPICAL CONFINED COMPRESSION STRESS-STRAIN CURVE"

Figure 2.2.11

and unloading compacts the material causing it eventually to behave more nearly linearly. This may have real significance in a study of particle velocity waveforms at sites exposed to multiple attack.

2.3 Synthesized Waveforms

None of the available methods for predicting the strength of ground shocks in real, layered soils, due to nuclear blast, yield waveform shapes. In addition, the results of existing theoretical treatments do not enable the calculation of the waveforms. Considerable work has been done on the nature of the pulses generated by the air blast and the bomb vapors and on their distortion by passage through homogeneous media. These studies have revealed the gross characteristics of basic waveforms which can be correlated with experimental data obtained under nearly ideal conditions. However, records of actual blasts have frequently shown an oscillatory component superimposed on the simple shape predicted by theory. In a few cases the simple pulse was completely masked by the oscillation. Since the response of an isolation system to an oscillation is particularly severe if the frequencies are near resonance, the presence of the oscillation is of considerable concern to the isolation system designer. For example, Newmark and Hansen (Reference 2.14) define the simple pulse and oscillatory waves as "systematic" and "random" pulses and note that the peak relative velocity amplification could be as high as 5 for undamped systems in layered media.

These considerations prompted the review of all available data of the ground motions resulting from nuclear blasts with the view toward identifying recurrent waveform patterns. If characteristic waveforms could be found and correlated with weapon and site conditions, it was hoped that existing methods could be employed to predict the significant wave dimensions. The available records of actual tests are not extensive and the sites and weapons were not typical of those expected at any known underground facility. However, all sites were layered, so that conditions were favorable for the production of complex wave patterns.

Isolators, by their very nature, have a low natural frequency compared to the frequencies in the input, and consequently the characteristics of the low frequencies in the input waveform are by far the more pertinent, i.e., if the isolator isolates the low frequency content in the input it will certainly isolate the higher frequencies. Only vertical motions have been considered.

An examination of the ground acceleration records showed erratic behavior with no common features except perhaps the sharp spike of acceleration caused by the leading edge of the air shock wave. However, if these records are integrated to give the ground velocity, some common characteristics become apparent. In fact, two separate mechanisms may be seen to be operating. First, there is the ground motion arising when the air blast is superseismic and, second, there is the motion when the air blast is subseismic.

When the air blast is superseismic the vertical ground motion is comparatively simple and is well known. The ground velocity undergoes a rapid jump which decays to zero and oscillates once or twice about zero with a small amplitude. A wave shape, designated Type I, has been developed to represent the essential features of the superseismic case. When the ground motion outruns the air blast, the motion is far more complicated, involving the various refractions and reflections through the complex terrain between the point of detonation and that of observation. However, the records show a strong tendency for the ground velocity in this case to exhibit an oscillation of two to three cycles. This has been represented by a Type II waveform. If the air blast is superseismic, then the first type of ground motion appears alone, but otherwise both forms appear superimposed in various ways.

The data used to develop the Type I waveform are based primarily on the measurements made during Operation Tumbler (Reference 2.15) and in the high pressure region on Shot Priscilla (Reference 2.16, 2.17). Ground motions, where the air blast was nonideal, (i.e., there were precursor waveforms) were not used in the analysis. Figure 2.3.1, page 2-26, shows the final form of the Type I waveform together with its displacement curve. The first part of the velocity curve between normalized times 0 and 1.0 is a smoothed average of the composite data shown in Figure 2.3.2 , page 2-26. The individual data points show many departures from the Type I waveform but these are essentially reflections of part of the Type II waveform. The tail of the Type I waveform (after normalized time 1) is very ill-defined in the records. The duration of the tail was based on work by the Sandia Corporation on Priscilla which indicated that the tail had approximately twice the duration of the first part of the wave. The amplitude of the tail was arranged somewhat arbitrarily to give a residual displacement of approximately half the maximum displacement.

The Type II waveform is shown in Figure 2. 3.3, page 2-27. This was developed by comparing the outrunning Tumbler data, from which the Type I ground motion had been subtracted, with the data for Koa 12 (reference 2.18). For Koa the Type I motion had been filtered out by the ground. The relative amplitudes of the various peaks were averaged over these data as were the relative time durations of the cycles. More weight was given to the Koa data, since the yield for this shot was in the megaton range. After the first tentative curve had been constructed it was integrated to give the displacement and adjustments were made in the latter portions of the velocity curve so that the residual displacement would be zero; this was done for no better reason than that there is no suitable information available for this case.

The normalized plot was checked by redrawing the assumed motion on the original velocity-time plots. Some of these plots for shots Koa and Cactus are shown in Figures 2.3.4 through 2.3. 7, (Reference 2. 18) . In some cases, the normalized curve fits the

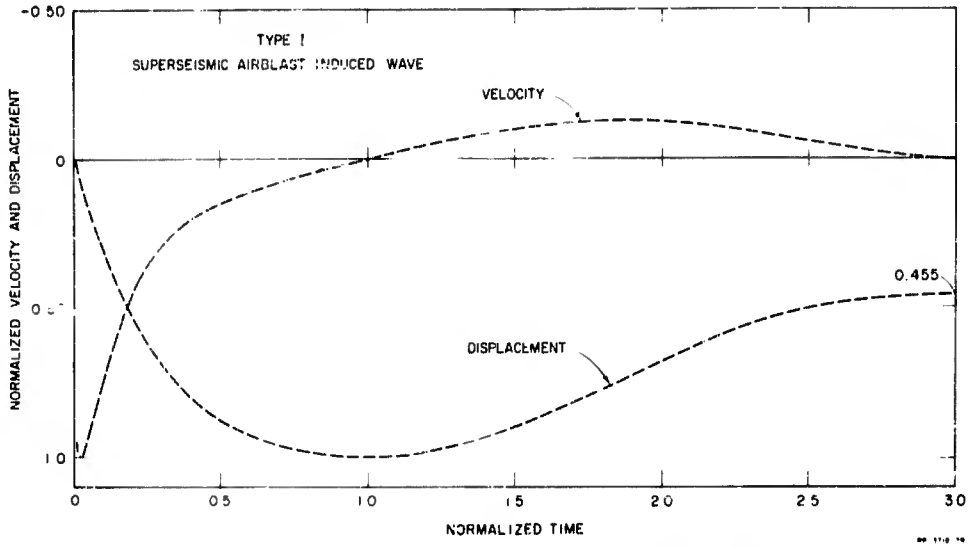

Figure 2.3.1: Type I Vertical Velocity Waveform and its Displacement

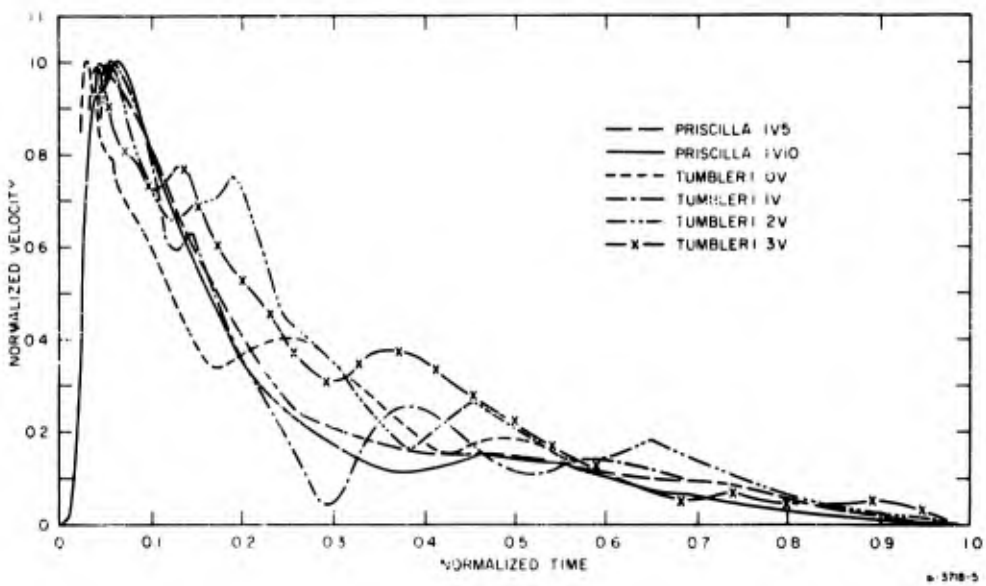

Figure 2.3.2: Data Used to Establish Type I Waveform

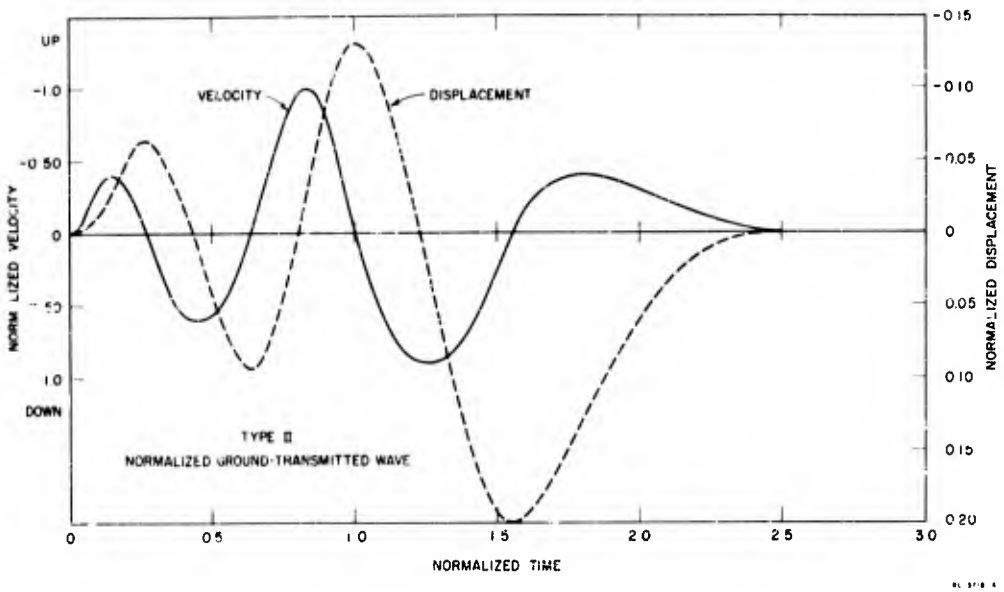

Figure 2.3.3: Type II Vertical Velocity Waveform and its Displacement

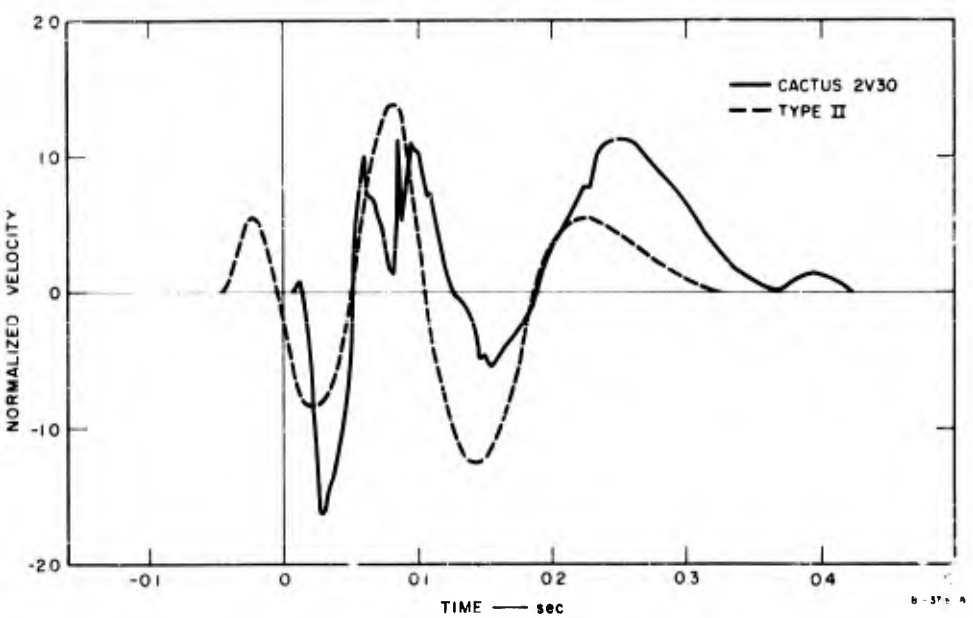

Figure 2.3.4: Comparison of the Type II Vertical Velocity Waveform with Data from Shot Cactus, Gage 2V30 (Ground Range = 650 ft; Depth = 30 ft.)

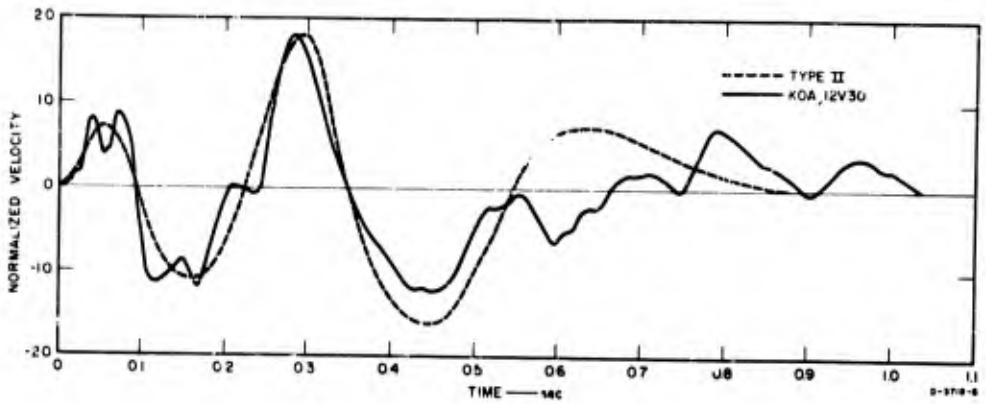

Figure 2.3.5: Comparison of the Type II Vertical Velocity Waveform with Data from Shot Koa, Gage 12V30 (Ground Range = 3,144 ft; Depth = 30 ft.)

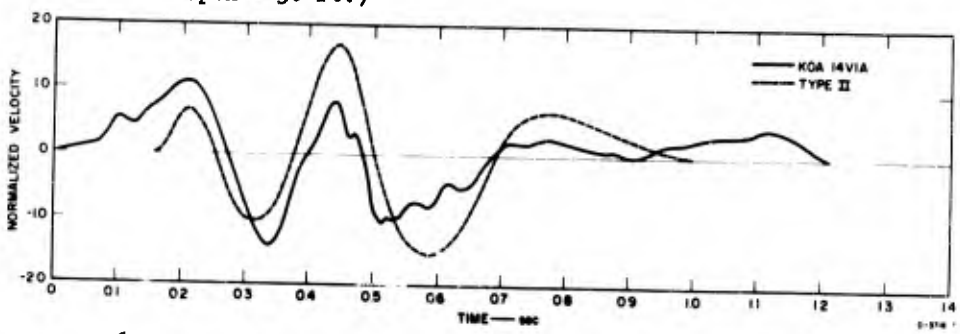

Figure 2.3.6: Comparison of the Type II Vertical Velocity Waveform with Data from Shot Koa, Gage 14V1A (Ground Range = 4,700 ft; Depth = 1 ft.)

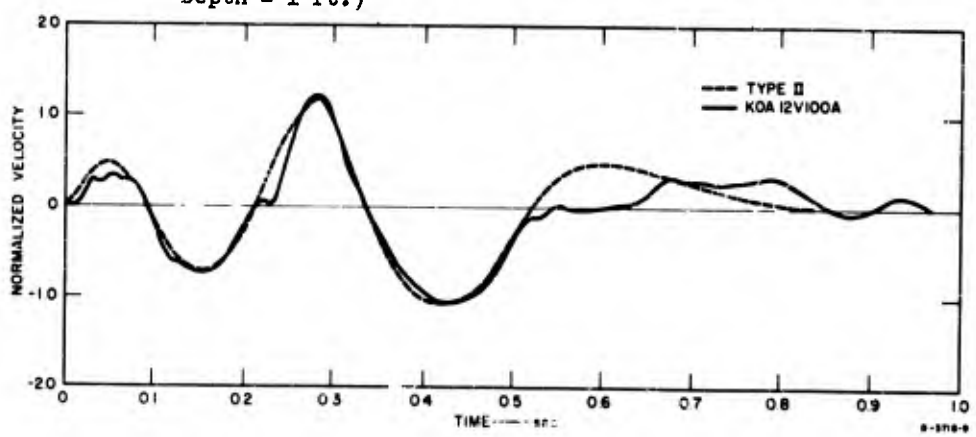

Figure 2.3.7: Comparison of the Type II Vertical Velocity Waveform with Data from Shot Koa, Gage 12V100A (Ground Range = 3,144 ft; Depth = 100 ft.)

data very well; in others, the fit is not so good, but the normalized curve still has the general shape of the measured motions. Detailed examination of these plots shows that the waveform is indeed changing as the ground range increases. It appears that the first cycle becomes a lower frequency relative to the remaining cycles as ground range increases. The time and amplitude parameters which define the particle velocity waveform have been normalized based on the data observed in the test records. Different ratios would be expected at other sites, overpressures, and weapon yields, although the generic forms may remain the same as Types I and II.

In one dimensional theory the ground wave is propagated at a velocity corresponding to the tangent modulus at the stress (Sauer, Reference 2.11). As a result, the initial stresses outrun the larger stresses and the wavefront spreads out in time. This effect is very significant in summing the stresses to determine the maximum stress occurring at a point. At practical depths, summing the stresses may result in a different ratio of velocity rise-time to total duration than is shown by the Type I waveform. The observations from the Nevada Test Site playa dry silts indicated that the peak stresses traveled at a velocity of between one-half to two-thirds of the seismic velocity (Sauer, Reference 2.11; and Wilson, Reference 2.13). Of course, this ratio would vary with the type of material and the other factors discussed previously. A plot of the observed difference in first motion velocity (seismic velocity) and the velocity computed from the arrival time of the peak stress at Frenchman Flat is presented in Figure 2.3.8 , page 2-30 . A general type I waveform may be described by three times and two amplitudes, as follows:

- time to peak positive particle velocity
- time to end of positive phase particle velocity
- time to end of negative phase particle velocity
- amplitude of peak positive velocity
- amplitude of peak negative velocity

The Type II waveform is more difficult to define in a simple manner. Parameters of significance to the response of isolation systems are:

- number of cycles
- period of each cycle
- peak velocity of each cycle

The mechanism by which the Type II wave is produced is not clearly understood, however, it is evident that the assignment of principal proportions on the basis of the observed waves is necessary. Current prediction methods cannot be expected to yield much more than the peak velocity of the first loop, its rise time, and the phasing of the Type I and Type II arrival times. Since the two test sites where the field records were taken are rather unique geologically, descriptions of the site conditions are given below.

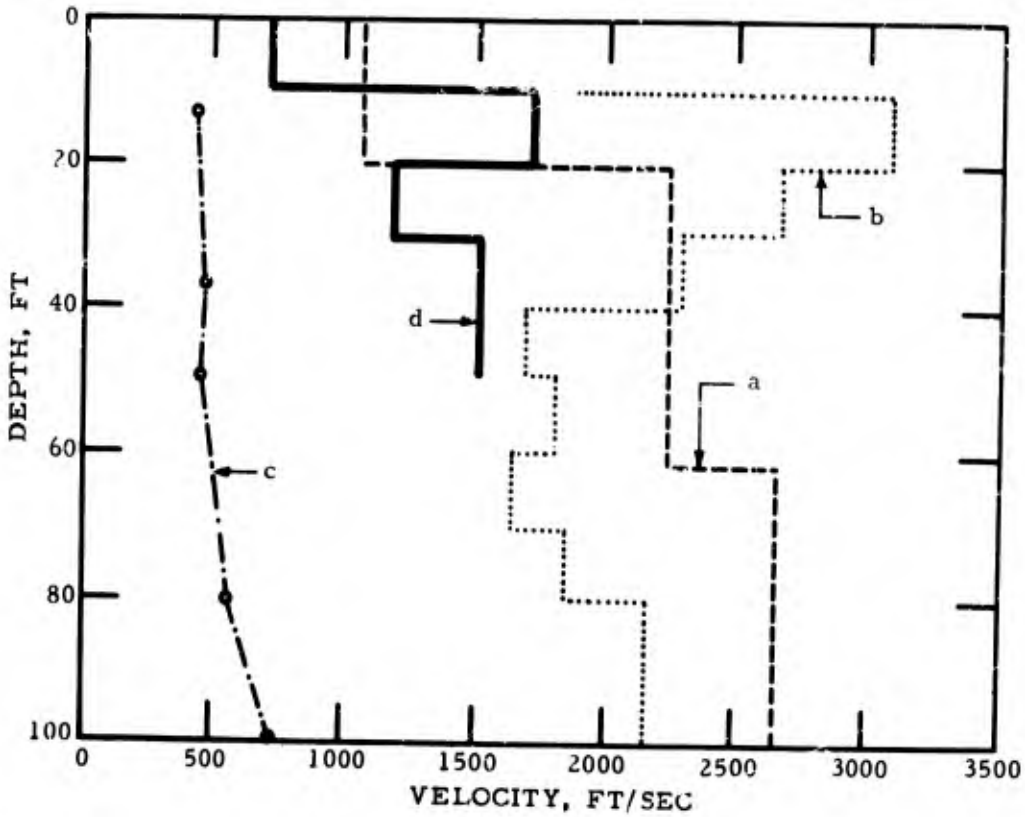

Figure 2.3.8: Longitudinal Wave Velocity vs. Depth
Frenchman Flat, Computed from

(a) Seismic refraction survey
(b) Vertical seismic survey
(c) Static modulus of deformation at 100 psi
(d) Arrival time of wave of high stress

(From Reference 2-11)

The first 200 feet of the Frenchman Flat area of the Nevada Test Site is composed of nonsaturated, inorganic clayey silt deposit, formed as a playa under desert type processes of erosion and deposition. Below 200 feet lies the original lake bed and at this depth the soil becomes a sand-gravel aggregate. At a depth of 650 feet, a basement rock is encountered. Seismic surveys of Frenchman Flat confirm the relative homogeneous nature of the site and indicate that the seismic velocities vary from 1000 to 3500 feet per second above 650 feet, increasing to 10,000 feet per second below 650 feet (Wilson reference 2.13). A detail plot of the seismic velocity profile is presented on Figure 2.3.8.

The Eniwetok Proving Grounds (site of shot Koa) are coral atolls composed of a heterogeneous mixture of gravel, sand and silt-size broken coral and shell fragments, interbedded by cemented zones. At a depth of about two miles this is underlain by an igneous basement. The seismic velocity in the dry, loose layer above the water table varies from 800 feet per second at the surface to 4000 feet per second near the water level. A cemented zone several feet thick is usually encountered at the water level. Below the water table, and extending to a depth of about 2500 feet is a heterogeneous layer with an average velocity about 800 feet per second. The seismic velocity then increases for the next 5000 to 10,000 feet to 11,000 feet per second. The underlying formation, presumed to be the igneous basement, has a velocity of 17,000 feet per second (Sauer, reference 2.11).

Other test records are also available in the published literature. A separate tabulation of all unclassified Weapon Test Reports relating to full-scale free field ground shock measurements and structural motions in regions of surface overpressure greater than 20 psi is given at the end of this section.

2.4 Theoretical Analyses

The theoretical studies discussed here are limited to those which are believed to be the most useful in predicting the Type I and Type II waveform parameters listed in the preceding paragraphs. Because of the complexity of the wave patterns at real sites, most of the mathematical models employed in the studies of interest are for the one-dimensional case. As a result, the representation of the air blast-induced wave is valid only as the wave approaches the overhead position. Another limitation of the existing theoretical works is their neglect of variations in the compression modulus with depth. The change in compression modulus, almost always an increase, can be due to layering of materials with different compressive properties and to confining pressure on otherwise homogeneous materials. Layering would be the major cause at sites where the profile is composed primarily of competent rock, since very large confining pressure changes are required to significantly change the compressive modulus of rock (Grine and Fowles, reference 2.19). The increase in confining pressure would correspond to the increase in depth below the surface.

For soils, layering would also be important. Included here is the effect of the presence of a water table, since the degree of saturation has a large influence on the dynamic compressibility of soils. Granular soils show a significant increase in compression modulus with increasing confining pressure, even though the volume change may be small. The compression modulus for very fine grained soils such as clay, are dependent to a large extent upon the past history of compressions. The compression modulus of all soils depends upon the pressure increment change in relation to the existing confining pressure. That is, a change of stress of 100 psi would be very significant for a surface soil where the confining pressure approaches zero. At a depth of 100 feet or so, where the confining pressure is high, that pressure change would cause only a slight rearrangement of the soil structure. As a result, even though layering were not present at a site, it is probable that the compressive modulus corresponding to the first dynamic stresses will increase with depth. As will be seen, the theoretical analyses presently available consider that one stress-strain curve applies to all depths.

2.4.1 Analyses of a Half-Space Geometry

Although most analyses consider wave propagation only in one dimension, three of those reviewed treated the more general problem of a half-space. An analysis by Brode and Bjork (reference 2.1) considers the stresses and early motions associated with the cratering of rock from a 2 megaton surface burst based on a hydrodynamic model of a "tuff". Although this analysis does not consider plasticity and viscosity beyond the limits of classical hydrodynamic theory, the profile of peak pressures and the shape of the pressure-time curve are useful in predicting conditions close to the crater in crater-induced ground shock problems. Some of the results of this method will be given later and compared with those of a prediction method developed by Newmark. The other half-space analysis, published by Sackman (reference 2.20), considers the plane strain solution for the stress distribution produced by the passage of a constant velocity pressure wave across the surface of a viscoelastic medium. This analysis considers only the superseismic case. The results have been evaluated by Baron and Parnes (reference 2.21) at a point 500 feet deep and where the surface air-pressure equals 2000 psi. The medium is rock with a compressional wave velocity of 10,000 feet per second. The authors point out that much work remains to be done on the experimental determination of the appropriate viscoelastic constants which are needed in the analysis, since such information is not available at the present time.

Based on Sackman's analysis, the stresses computed for the medium with assumed viscoelastic properties are compared to the stresses computed for similar points in a linear-elastic material. The results

show that the first arrival stresses are less for the viscoelastic model, but rise to values slightly greater, then attenuate slower than those for the linear-elastic model. Newmark (Reference 2.22) used a graphical quasi-static, half-space solution to determine the attenuation with depth of the vertical stress due to the moving air pressure loading. Based upon Boussinesq's elastic theory, the stress distribution includes the influence of a moving air blast load of variable intensity and duration. The pressure-depth curves were computed for a site with a uniform seismic velocity in which layering was not considered. An expression for attenuation was obtained by allowing the seismic velocity to approach infinity. This was applied to the attenuation of vertical particle velocities with depth. The expression and its use will be given in the paragraphs on "Prediction Methods".

2.4.2 One-Dimensional Analyses

The applicable closed form expressions for the peak vertical particle velocity and peak vertical stress which have been derived by one-dimensional theory, using various linear stress-strain curves, are presented in Figures 2.4.1 through 2.4.5 , pages 2-34, 2-37, and 2-38 . Plots of vertical stress and particle velocity versus depth for various assumed conditions are presented on Figures 2.4.6 and 2.4. 7 , pages 2-40,44, respectively.

2.4.2.1 Elastic Media

Figure 2.4.1 presents the relationships for a linear-elastic material. With this assumption there is no attenuation of particle velocity or stress with depth. For a homogeneous medium, the shape of the wave form due to the air-blast loading is identical with the decay curve of the air pressure. The wave front moves at the seismic velocity of the medium at all pressures. These assumptions clearly represent the conservative case with respect to the amplitude of the particle velocity at depth, since there is no attenuating mechanism. However, a comparison of the particle velocities computed by this assumption and certain nonelastic assumptions, discussed subsequently using different stress-strain curves, indicate that the near surface particle velocities are higher using nonelastic assumptions.

Plots of the peak vertical stress and particle velocity versus depth are shown on Figures 2.4.6 and 2.4.7 , respectively. The values used in the computation were:

P_o = 300 psi at t = 0

ρ = 4.04 slugs/ft^3

V_L = 5,960 fps

E = 1 x 10^6 psi

W = 20 megatons

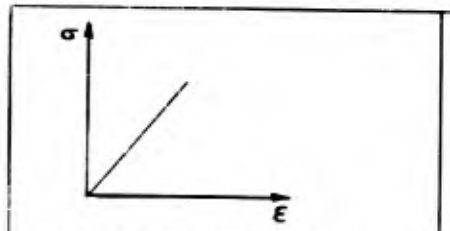

Figure 2.4.1: Elastic Media

$z = V_L t$

$\dot{z} = V_L$

$\sigma_z = P_o$

$\dot{u} = \frac{P_o V_L}{E} = \epsilon V_L$

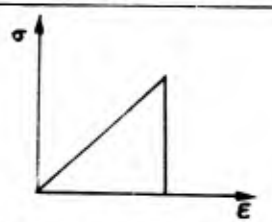

Figure 2.4.2: Linear, Non-Recovering Media (Reference 2-23)

$z = V_L t$

$\dot{z} = V_L$

$\sigma_z = \frac{I(t)}{t} = \frac{I(t)}{z_s} V_L$

$\dot{u} = \frac{I(t)}{\rho V_L t}$

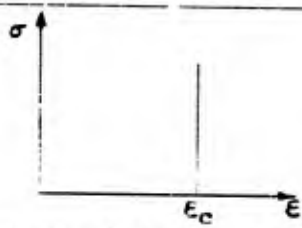

Figure 2.4.3: Ideal Locking Media (Reference 2-24)

$z = \left[\frac{2}{\rho \epsilon_c} \int_o^t I(t)\, dt\right]^{\frac{1}{2}}$

$\dot{z} = \left[I(t)\ 2\rho\epsilon_c \int_o^t I(t)\, dt\right]^{-\frac{1}{2}}$

$\sigma_z = \left[\frac{1}{\rho \epsilon_c}\ \frac{I(t)}{z}\right]^2$

$\dot{u} = \frac{I(t)}{\rho z}$

$I(t)$ = impulse of air blast pressure
E = compression modulus
$\dot{u}$ = particle velocity
z = displacement of wavefront
$\dot{z}$ = velocity of wavefront
V_L = seismic velocity of media
ϵ = strain in medium
ρ = density of medium
σ_z = stress in medium at wavefront

2.4.2.2 Linear Non-Recovering Media

Figure 2.4.2 presents the relationships for a linear, non-recovering medium. It may be noted that the compaction front moves with a constant velocity equal to the seismic velocity of the material. The peak vertical stress is equal to the average pressure of the impulse to the time of interest. When the majority of the impulse has passed, the attenuation of the vertical stress and particle velocity at the wave front are inversely proportional to depth. At any time, the velocity gradient behind the shock front with respect to depth is zero, that is, the material behind the shock front moves as a rigid body.

The fact that the stress and particle velocity are attenuated with depth and approach zero in this one-dimensional analysis makes the general behavior of this medium considerably different from that of the elastic material. As the rate of surface pressure decay decreases, such as at low overpressures and large yields, the differences in peak particle velocities in the two materials at depths less than several hundreds of feet, will not be appreciable; although the shape of the particle velocity wave form will differ as will the amount of total deflection. Plots of vertical stress and particle velocity versus depth are shown on Figures 2.4.6 and 2.4.7 , respectively. The values used in the computation were:

P_o = 300 psi

ρ = 4.04 slugs/ft^3

V_L = 5,960 fps

E = 1 x 10^6 psi

W = 20 megatons

2.4.2.3 Partially Locking Media

The condition of no return upon unloading is a special case of the more general problem of partially locking or partially reversible media. Salvadori, Skalak and Weidlinger (Reference 2.23) have presented a solution for the general case. Although the expressions of interest cannot be stated in closed form, requiring the solution of several simultaneous equations, the same conclusions can be drawn as for the special case of no return motion. A numerical solution for an overpressure of 100 psi with the return seismic velocity twice that of the loading velocity indicates a slightly smaller degree of attenuation of the stress and particle velocity with time and depth compared to the material with no recovery.

2.4.2.4 Ideal Locking Media

Figure 2.4.3 presents the relationships for ideal locking media, that is, materials which offer no resistance until a critical strain is reached and then compact to a rigid state. The dependence of the peak vertical stress and peak particle velocity on the impulse can be noted. The long-time attenuation of the peak vertical stress varies inversely with the square of the depth, and increases with the square of the impulse. According to Miles(Reference 2.25) for a step impulse the stress varies inversely as the three-halves power of the time. From the shape of the stress-strain curve, it would appear that this analysis is applicable to dry, loose sand but not to saturated soils or rocks.

Plots of vertical stress and particle velocity are shown in Figures 2.4.6 and 2.4.7 , respectively. The values used for the computation were:

P_o = 300 psi

ε_c = .02

ρ = 4.04 slugs/ft^3

W = 20 megatons

A comparison of the attenuation of stress with depth for ideal locking media with ε_c equal to 0.12 and 0.10 is given by Reference 2.24. This comparison shows that at the high initial pressure levels near ground zero the influence of varying ε_c is small at depths below 200 to 500 feet. As would be expected, the material with the larger ε_c had the greater attenuation with depth.

2.4.2.5 Linear-Locking Media

Figure 2.4.4 presents the expressions for vertical stresses and particle velocities of a material with linear-locking stress-strain characteristics. The irrecoverable strain equals $\varepsilon_c - \varepsilon_o$ for stresses equal to or greater than σ_o.

When the applied pressure is greater than P_c, the velocity of the compaction front (z) is greater than V_L. While the compaction front is superseismic the vertical stress varies as the square of z , and the particle velocity as the first power of z. At a time t_s, the vertical stress becomes equal to P_c and the compaction front has the velocity V_L. The time t_s may be evaluated from the expression equating the integral of the surface pressure-time curve to the integral of the surface impulse-time curve between the limits of zero and t_s. The time t_s may also be evaluated from a plot of z_s versus time at the point where z is equal to V_L.

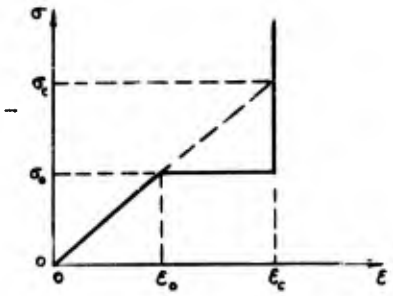

Stress-Strain Diagram for Linear Locking Medium

At time t_s, $\frac{\dot{z}}{V_L} = 1$; t_s may be determined from equation: $\bar{F} = \bar{\bar{F}}\sqrt{\frac{\sigma_c}{\sigma_o}}$

At time t_e motion of compaction front relative to medium ahead ceases

t_e may be found from equation: $t_e - t_s = \bar{F} - \frac{z_s}{V_L}$

Case A: $\frac{\dot{z}}{V_L} > 1$	Case B: $\frac{\dot{z}}{V_L} < 1$	Case C - Elastic Precursor
$z = V_L \left(\frac{\varepsilon_o}{\varepsilon_c}\right)^{1/2} \frac{T}{\bar{F}}$	$z = \frac{(1-\varepsilon_o)}{\left[\frac{\varepsilon_c}{\varepsilon_o} - 1\right]^{1/2}} V_L \left\{\frac{T}{\bar{F}} - \left[\frac{z_s}{V_L} + (t-t_s)\right]^2\right\}^{1/2} + \varepsilon_o V_L (t-t_s) + \varepsilon_o z_s$	
$\dot{z} = V_L \left(\frac{\varepsilon_o}{\varepsilon_c}\right)^{1/2} \frac{T}{\bar{F}}$	$\dot{z} = \frac{(1-\varepsilon_o)}{\left[\frac{\varepsilon_c}{\varepsilon_o} - 1\right]^{1/2}} V_L \frac{\left\{\bar{F} - \left[\frac{z_s}{V_L} + (t-t_s)\right]\right\}}{\left\{\frac{T}{\bar{F}} - \left[\frac{z_s}{V_L} + (t-t_s)\right]\right\}} + \varepsilon_o V_L$	$\dot{z} = V_L$
$\sigma_z = \sigma_c \left(\frac{\dot{z}}{V_L}\right)^2$	$\sigma_z = \sigma_o \left[1 + \left(\frac{\dot{z}}{V_L} - \varepsilon_o\right)^2 \frac{\left(\frac{\varepsilon_c}{\varepsilon_o} - 1\right)}{(1-\varepsilon_o)^2}\right]$	$\sigma_z = \sigma_o$
$\dot{u} = \varepsilon_c \dot{z}$	$\dot{u} = \varepsilon_o \dot{z} \frac{\left(\frac{\varepsilon_c}{\varepsilon_o} - 1\right)}{(1-\varepsilon_o)} + \varepsilon_o V_L \frac{1-\varepsilon_c}{1-\varepsilon_o}$	$u = \varepsilon_o V_L$

$$\bar{F} = \frac{\int_0^t P_o(t)\,dt}{\sigma_o}$$

$$\bar{\bar{F}} = \left[\frac{2}{\sigma_o} \iint_0^t P_o(t)\,dt\,dt\right]^{1/2}$$

t = Time

t_e = Time at which Relative Motion of Compaction Wave Front Ceases

t_s = Time at which $\frac{\dot{z}}{V_L} = 1$

$\dot{u}$ = Particle velocity at wave front

V_L = Seismic velocity

ε_c, ε_o = Unit strains from stress-strain diagram

σ_c, σ_o = Stresses from stress-strain diagram

σ_z = Stress at wave front

$P_o(t)$ = Overpressure - time relation

$\dot{z}$ = Wave front velocity

Figure 2.4.4: Vertical Stress and Particle Velocities in Linear-Locking Media

The compaction front moves at less than the seismic velocity when $t > t_s$ and the motion relative to the motion of the medium ahead ceases at time t_e. When t is equal to t_s an elastic wave is generated which travels at a velocity V_L with a constant stress σ_o. At all depths greater than that of the compaction front at time t_s, the linear-locking wave outruns the compaction front. The elastic precursor stress is not attenuated with depth, but follows the behavior of the one-dimensional linear-elastic case. At times greater than t_e, the entire locked mass moves at the particle velocity of the precursor at the limiting depth of the compaction front at time t_e.

The solution for a pulse, which starts as a subsonic front at $t = 0$, is obtained from the expressions shown by setting $t_s = z_s = 0$. In the event $\varepsilon_c = \varepsilon_o$, a compaction front moving supersesmically exists when $P_o > \sigma_o$; but if $P_o < \sigma_o$, only elastic waves will be propagated.

Plots of vertical stress and particle velocity are shown on Figures 2.4.6 and 2.4.7, respectively. The values used for the computations were:

P_o = 300 psi

ε_c = .02

ρ = 4.04 slugs/ft^3

E = 1 x 10^6 psi

W = 20 megatons

2.4.2.6 Bilinear (Deadband) Media

A one-dimensional analysis of a wave propagating in a material with a bilinear stress-strain characteristic (Figure 2.4.5) was made by Skalak (Reference 2.23).

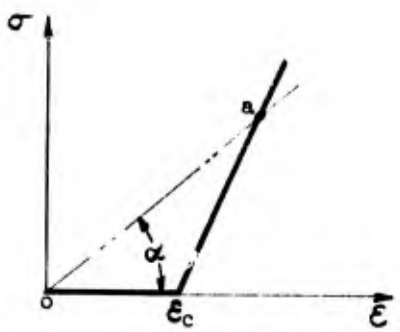

Figure 2.4.5
Stress-Strain Diagram for Plastic-Elastic Media

The results are not included here because the equations require numerical solution, but the velocity of the wave front was found to be a function of the angle α where 'a' designates the stress at the point of interest. With a decaying air pressure on the surface of the medium, the stress, and therefore the wave velocity, was continuously changing.

2.4.2.7 Comparison of Predicted Attenuations

A comparison of the curves of vertical stress for ideal locking media and plastic-elastic media shows a smaller percentage attenuation for the plastic-elastic case to depths of about 1000 feet but greater attenuations at greater depths.

Despite the differences in attenuation predicted by the various mathematical treatments, a comparison of the vertical stress and particle velocities (Figures 2.4.6 and 2.4.7) estimated by all of the one-dimensional analyses show there is no major differences between the results obtained for the first 100 feet of depth. Another interesting comparison can be made between the vertical stresses obtained by one-dimensional analyses and those suggested by Newmark for the propagation of waves generated in an elastic half space by a moving air blast loading (Reference 2.22). Newmark's equation is

$$\frac{\sigma_z}{\sigma_s} = \frac{\dot{u}_z}{u_s} = \frac{1}{1 + \frac{y}{L}}$$

where σ_s and u_s are the surface values and for overpressures less than 500 psi L is given by

$$L = 300 \text{ (ft)} \left[\frac{100 \text{ (psi)}}{P_o} \right]^{.6} W(\text{Mt})^{1/3}$$

Considering the same case as used previously, i.e., W = 20 Mt and P_o = 300 psi, the spatial attenuation calculated by above equations is also shown in these Figures. It would appear, even from this very rough comparison, that a significant error might be introduced by ignoring the attenuation from spatial dispersion at the high overpressures. When spatial attenuation is added to that from other causes, it is probable that the total attenuation of peak stress and particle velocity would be much higher than predicted by any of the theory. This, in fact, appears to be in general agreement with the results of field tests (Reference 2.12).

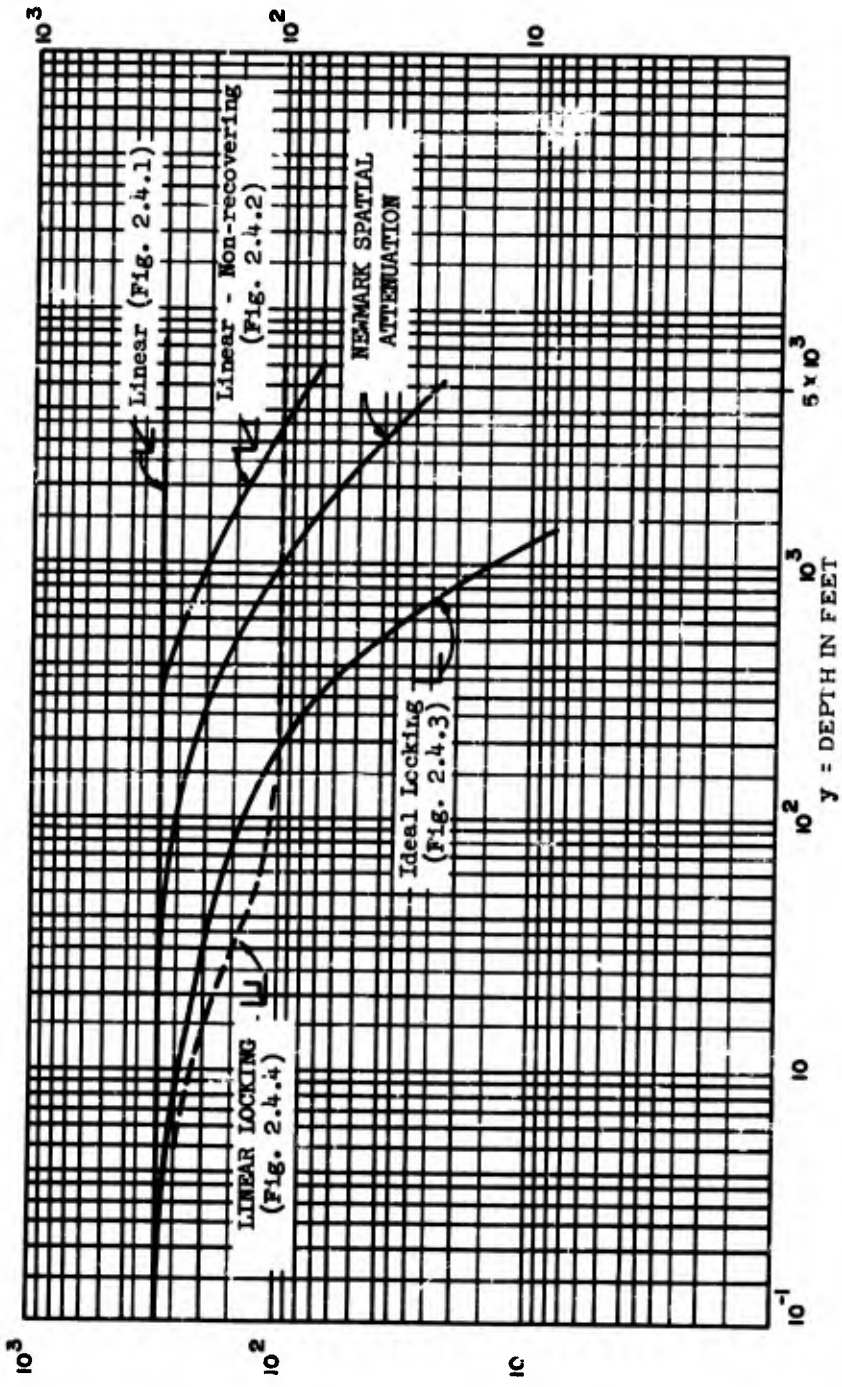

Figure 2.4.6: Comparison of Predicted Attenuations of Peak Vertical Stress with Depth.

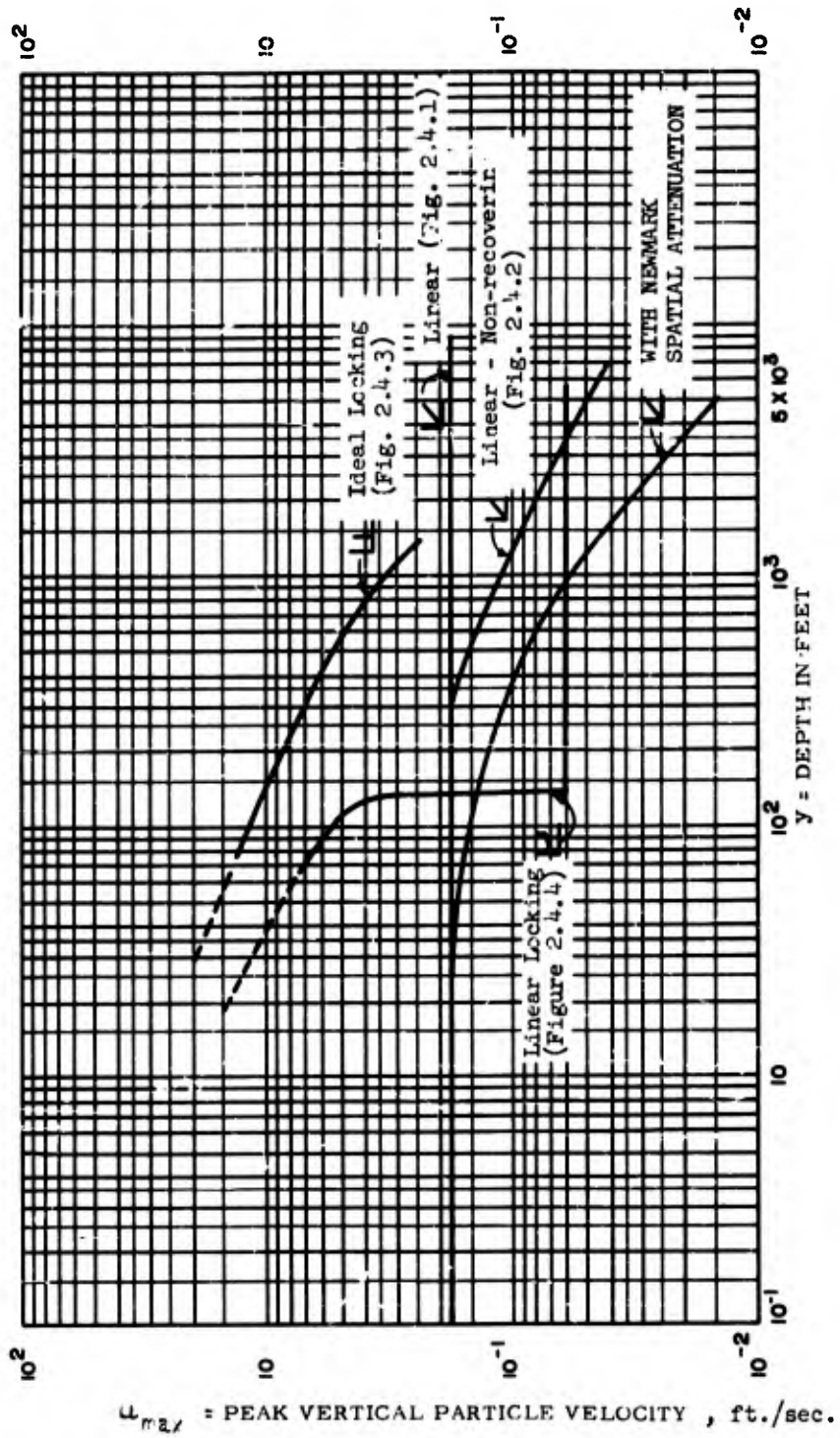

Figure 2.4.7: Comparison of Predicted Attenuation of Peak Vertical Particle Velocity with Depth

Initial conditions: yield = 2[illegible] megatons
P_o = 300 psi
for soil parameters see text.

2.5 Prediction Methods

It was seen in the preceding paragraphs that most theories of ground motion are directed more toward obtaining an indication of the peak values of displacement, velocity, and acceleration than toward defining the details of the wave form. Indeed, it is evident that while the assumption of a highly idealized material characteristic may permit the approximation of the gross behavior of the material under shock, the lesser characteristics of the time-history of the motion at an actual site will be considerably different.

Most prediction methods have been formulated by modifying simple theory to match experimental data. This, coupled with the complexity of recorded wave forms, has in general limited the use of the methods to the estimation of peak values. Yet the sensitivity of the response of dynamic systems to wave form characteristics is well known and, in at least one prediction method, correction factors are applied to the response spectrum to account for complex wave forms occurring under certain local site conditions (Reference 2.14).

By combining the Type I and Type II wave forms in proportions dependent upon particular weapon and site conditions, however, not only will the response spectrum of the composite wave form be more representative of the final conditions, but a time-history is obtained for use in the solution of those isolation system response problems where the spectrum information is insufficient. It remains, however, to determine whether existing prediction methods can be used to estimate the magnitudes of the significant parameters describing the two synthesized wave forms. For this reason, the three principal prediction methods are reviewed and their results compared with theory.

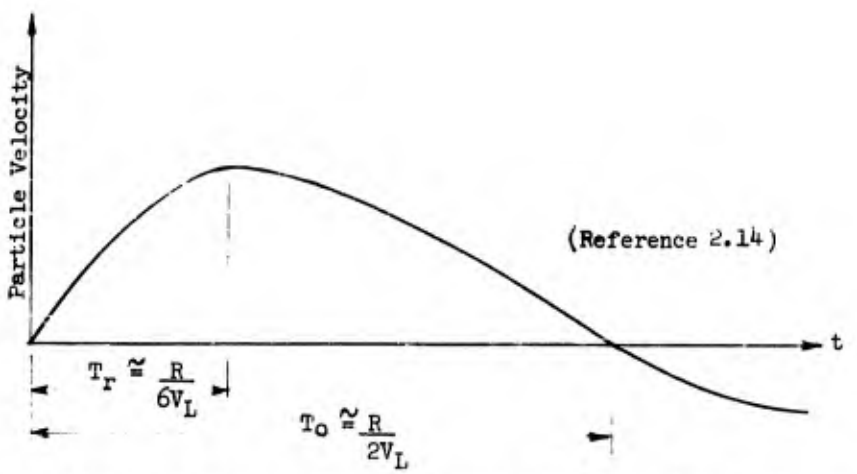

Figure 2.5.1 Initial Portion of Velocity-Time Curve for Completely Buried Shot in Rock

2.5.1 Newmark Prediction Methods

2.5.1.1 Cratering Induced Waves

Newmark (Reference 2.14) has formulated relationships for the peak particle velocity, displacement, and acceleration for cratering induced ground shock. These relationships are restricted to surface bursts in granite and to ranges where the air-blast overpressure is between 100 and 600 psi. The method is based on one-dimensional elastic theory, with scaling criteria obtained from measurements from buried bursts of high explosives and small nuclear weapons (References 2.26).

The assumed velocity wave shape is shown in Figure 2.5.1 and the equations in Figure 2.5.2 . Peak displacement was found by assuming the wave shape to be parabolic and integrating, giving

$$u_{max} = \frac{2}{3} \frac{R}{V_L} \dot{u}_{max}$$

To obtain peak acceleration, it was assumed that the initial acceleration was twice the average acceleration during the velocity rise time t_r. Then

$$\ddot{u}_{max} = \frac{12\, V_L\, \dot{u}_{max}}{R}$$

In a layered system, Newmark suggests using an average seismic velocity $\overline{V}_L$ to the point of interest, when estimating velocities and accelerations, but not displacements. The term $\overline{V}_L$ = range/earliest arrival time from a refracted wave. For slant ranges, Newmark recommends that the computed values be considered as horizontal components. The vertical components of displacement and strain should be taken at one-half these values. The vertical components of velocity and acceleration should be taken at full value.

In view of the limitations placed on the use of the expressions by Newmark, it is interesting to compare his results with the values developed by Brode's hydrodynamic analyses. At a depth of 800 feet directly below ground zero, Brode's analysis (Reference 2.1) gives a vertical peak pressure of approximately 900 x 10^4 psf for a 2 megaton burst. (In comparing this value for a two-megaton burst with the corresponding depth from, presumably, a one-megaton burst reported in Brode, Reference 2.2), the pressures are identical. If the particle velocity from Newmark's equation is computed for the same point, using a seismic velocity of 6000 feet per second for the tuff rock, it is found to have a value of 17 fps. Converting this particle velocity to a corresponding peak stress, by the use of one-dimensional elastic theory

$$\sigma = \frac{\dot{u}\rho}{V_L}$$

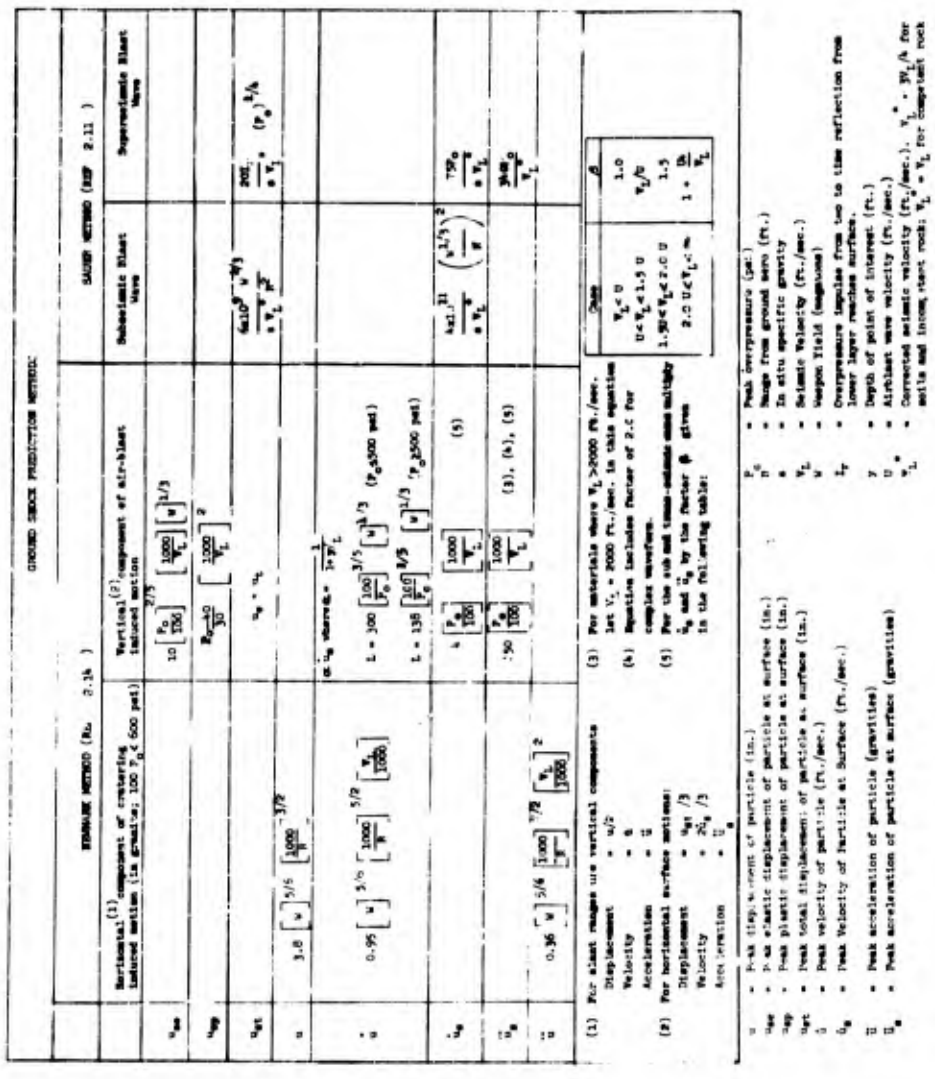

Figure 2.5.2: Summary of Ground Shock Prediction Methods

and assuming $E = \rho V_L^2$ where $\rho = 5$ slugs/ft^3, it is found that the stress has a value of 45×10^4 psf, which is lower by a factor of 20.

It should be noted that the hydrodynamic analysis does not consider viscosity or other dissipative losses beyond valid hydrodynamic assumptions, while Newmark's values are based upon field measurements for low yield weapons. It would appear, from a plot of the pressures versus range developed by the hydrodynamic analysis, that the pressure attenuates as the inverse cube of the range in the very high pressure region, and as the inverse three-halves power of the range below a pressure of about 40 kilobars (14.7 x 1000 x 40 psi). Thus, at large ranges the hydrodynamic analysis will predict stresses much larger than those predicted by Newmark's analyses, since the particle velocity in Newmark's expression attenuates as the inverse 2.5 power of the range. However, the values measured during the Rainier buried shots appear to agree reasonably well with predictions made by Newmark's equations. The Rainier shots were in a volcanic tuff similar to the material used in the hydrodynamic analysis.

The shape of the pressure-time curves developed by the hydrodynamic analysis and the velocity-time curves described by Newmark are similar. Both peak near the middle third of the total duration. This, of course, differs from what would be expected near the surface for a superseismic air-blast induced wave.

2.5.1.2 Air-Blast Induced Waves

Figure 2.5.2 also presents the expressions suggested by Newmark for air-blast induced ground motion. These expressions were derived using one-dimensional elastic theory and selecting coefficients which would match the Nevada Test Site data. In computing displacement, Newmark approximates the air-blast pressure loading by a triangular shaped pulse with the same impulse as the actual air pressure-time curve. The duration (t_1) of the assumed pulse then is

$$t_1 = 0.40 \left[\frac{100}{P_o}\right]^{3/5} \left[W\right]^{1/3}$$

where

t_1 = pulse duration, sec

P_o = air-blast peak overpressure, psi

W = weapon yield, megatons

For a site of uniform seismic velocity, the elastic displacement corresponds to the total deflection of a column of material, of length $t_1 V_L$, subjected to an average pressure $P_o/2$. The maximum transient

elastic vertical displacement, in layered or nonhomogeneous media, is computed for several positions of shock. The computations consider the values of V_L for each layer and sum of the instantaneous values of strain so determined. The maximum displacement is the value recorded for the elastic displacement at the surface. In both cases, the elastic modulus for soils with a density of about 115 lb. per cu. ft. and $\mu = 0.25$ is approximately

$$E = 9\, V_L^2 = 25 \times 10^3 \left(\frac{V_L}{10^3} \right)^2$$

where

E = Young's modulus, psi

9 = Mass density, slugs/ft^3

V_L = Seismic velocity, ft/sec

μ = Poisson's ratio

At a point below the ground surface, the maximum elastic displacement is equal to the total displacements of all the material below the point considered. In calculating elastic displacement, Newmark recommends no change with depth be made in peak stress, rise time, or duration.

Newmark considers the permanent, or plastic, vertical displacement to be negligible below depths of about 100 feet. He suggests that it be assumed to vary linearly between the surface and this depth. The seismic velocity in this region can be taken as the average value. It should be noted again that the data on which these methods are based were obtained from the Nevada Test Site. It is usually found that at layered sites the seismic velocity of the material at great depth controls the maximum displacement. Since the triangular pressure pulse is steep fronted, the maximum pressures arrive early in the deep layers.

At the interface of the two layers, Newmark suggests the use of transmission and reflection factors derived for the one-dimensional case. If the interface is fairly sharp, an estimate can be made from the following relationship

$$\sigma_r = \frac{1 - \Psi}{1 + \Psi} \sigma_i$$

$$\sigma_t = \frac{2}{1 + \Psi} \sigma_i$$

where σ_r = incident stress, σ_i = reflected stress, σ_t = transmitted stress, and

$$\Psi = \text{ratio of impedances of two media} = \frac{E_1 V_{L2}}{E_2 V_{L1}}$$

Newmark defines the transeismic and subseismic conditions as the outrunning of the air-blast wave only by air-blast induced ground waves or their reflections or refractions. That is, in his prediction method, all transeismic and subseismic phenomena are treated as special cases of the air-blast induced waves. Thus, the values for particle velocity and acceleration given in Figure 2.5.2 for air-blast induced ground motion should be increased by the following factors to account for outrunning:

Condition	Multiplier
$V_L < U$	1.0
$U < V_L < 1.5\ U$	V_L/U
$1.5\ U < V_L < 2\ U$	1.5
$2\ U < V_L$	$1 + U/V_L$

Newmark recommends that the displacement not be modified. It is noted that this multiplies the uncorrected velocity and acceleration value by a factor having a maximum value of 1.5, at a seismic velocity such that the air-blast front velocity is nearly equal to the Rayleigh wave velocity (Section 2.2.2). V_L should be taken as the seismic velocity in the layer of interest. However, Newmark suggests that if the seismic velocity of a deeper layer gives a higher value of acceleration or velocity, its seismic velocity should be used for the upper layers when obtaining the multiplying factor for the upper layer. The basis for this can be seen from the refracted wave front diagram, Figure 2.2.10. The arrival of the refracted wave from the deeper layers appears to an observer in the upper layer to have the velocity of the deeper layer.

As mentioned before, the expression for the attenuation of peak stress with depth, which is also used for the attenuation of vertical particle velocity with depth, was derived by Newmark using Boussinesq's theory of stress distribution for an elastic half-space with a partially loaded surface. Westergaard's theory of stress distribution for the same problem except with the assumption that the elastic medium is reinforced with a series of membranes infinitely rigid in a lateral direction but infinitely flexible vertically, would give stresses approximately two-thirds of those from the Boussinesq theory. The physical significance of the membranes is that during loading lateral deformation of the soil is prevented. In soil mechanics, Westergaard's theory is generally used as being more applicable to a stratified subsurface profile. It may also be more applicable to this problem as well. Of course, this would indicate an even larger attenuation with

depth of peak stress and particle velocity, due to spatial dispersion, than is indicated by Newmark's expression.

2.5.2 Sauer Prediction Method

The prediction procedure developed by Sauer (Reference 2.11) is semi-empirical in nature and is based upon a correlation of field measurements at the Nevada Test Site and the Pacific Proving Grounds using "near elastic" scaling. These equations predict peak values at the surface which may then be attenuated for depth by the use of curves suitably scaled for weapon yield. With these expressions it is possible to predict ground motions in both the superseismic and the subseismic regions. The applicable expressions appear on Figure 2.5.2. The limits associated with each expression indicate the spread of measured data. Sauer suggests using a refraction wave front diagram to determine if the point of interest is in the superseismic or subseismic region.

For alluvial soils and incompetent rocks V_L should be taken as the velocity of propagation of waves of high stress. For soils where this is not known, Sauer suggests using a value of three-quarters of the seismic velocity which is based on data from the Nevada Test Site. For competent rock, V_L should be taken equal to the seismic velocity. In computing the reflection characteristics of local disturbances, only those reflecting layers which exhibit marked changes of physical properties as well as changes in seismic velocity should be included.

Sauer restricts the correlations to ground motions in the overburden, i.e., the first layer, or to ground motion in substrata if the scaled depth of the overburden is a small fraction of the pressure pulse length. In the latter case, it is necessary to neglect the presence of the overburden. For intermediate depths of overburden, Sauer suggests that a conservative estimate of vertical ground motion may be made as follows: compute the motion assuming that the second layer extends to the surface; compute the motion at the interface based on the properties of the overburden and apply the appropriate elastic reflection factors for the motion in the second layer; choose the larger of the two values for the motion at the interface and let it attenuate at the rate corresponding to the properties of the second layer.

Unfortunately this method breaks down and greatly overestimates the vertical velocity and stress as the scaled depth becomes smaller and the ratio of seismic velocities becomes larger. For these cases it is necessary to compute the reflection history in detail. There is no formal way to determine the shape of the velocity-time wave form given. Sauer does suggest that the pulse duration would equal the overpressure duration, or approximately the time for a reflection to return to the surface, whichever is smaller.

2.5.3 Wilson Prediction Method

A procedure for predicting the peak displacement in the superseismic region was developed by Wilson (Reference 2-13). Basically this is a graphic procedure similar to the one described for Newmark's air-blast induced layered case with some important modifications. In brief, Wilson's modifications to the Newmark procedure are:

- The initial wave front, or pulse pressure, travels downward at a velocity equal to the vertical seismic velocity while the peak pressure travels downward at a velocity equal to between one-half and three-quarters of the vertical seismic velocity. This is dependent on the type of material and the evaluator's judgment regarding the slope of the stress-strain curve at the particular stress.

- The peak stress is attenuated approximately in accordance with Newmark's expression for the attenuation of particle velocity with depth.

- The vertical compression of a soil layer which is made up of both elastic and inelastic components at any depth, is attained simultaneously with the application of load. As the vertical stress decays, the elastic portion of the compression recovers in proportion to the decay of the pressure curve.

- The percent of the total strain of a layer that is elastic and the percent which is inelastic is estimated for the particular material from laboratory tests. Wilson & Sibley, Reference 2.13, give a description and discussion of these soil tests.

- The procedure is carried to a depth where a material with a seismic velocity of 10,000 fps or greater is encountered. The displacement below this depth is computed by Sauer's expression for displacement using the value of the attenuated stress ΔP_o. The displacement-time curve for the point of interest is then determined by summing the compressions of the various layers below versus time. By considering the inclination of the superseismic wave front (Figure 2.2.6) at the point of interest and assuming that the only compression is that normal to the wave front, the horizontal component of the motion is obtained. This assumes that the horizontal motion is in-phase with the vertical movement with respect to time and depth. This method usually results in horizontal displacements which may vary from 1/10 to 1/2 of the vertical displacements.

After a comprehensive investigation of the soil at the Nevada Test Site, this procedure was checked with results from Shot Priscilla and good agreement was obtained (Reference 2-27).

2.5.4 Discussion of Prediction Methods

The prediction methods just reviewed are all based on experimental data obtained at two general areas, the Nevada Test Site and the Eniwetok Proving Grounds. Newmark's method is one-dimensional theory corrected to match the data; Sauer's method consists of empirical equations based directly on the data, and Wilson's method is a refinement of Newmark's displacement equations. Each method presents equations for estimating the ground motion for different "cases" of ground wave configuration. For example, Newmark divides the ground motion into two basic classifications, air-blast induced and cratering induced. The air-blast induced ground motions are then divided into the superseismic case and the transeismic-subseismic case, both of which may be corrected for layering. The peak cratering-induced ground motions may also be computed for homogeneous and layered media. Newmark then notes that the wave form of all motions may be "random" or "systematic" and suggests amplification factors for the "random" pulses.

On the other hand, Sauer's equations consider all motions as falling into the superseismic or the subseismic categories while Wilson's method attempts only to predict superseismic air-blast induced ground displacement.

In Section 2.2.1, various means by which energy from a nuclear blast may be transmitted to a point in the ground were described. Summarizing, they are:

- Direct effect of air-blast induced ground wave
- Outrunning of air-blast induced ground wave
- Reflected or refracted air-blast induced ground wave
- Direct effect of cratering-induced ground wave
- Reflected or refracted cratering-induced ground wave.

Any or all of these waves may impinge on a soil particle as a result of a single surface burst, the wave form, phasing, and direction of each wave being dependent on the weapon and site conditions.

Further, the "waves" mentioned above refer to the compressive waves, yet as noted in Section 2.2.2 there is a second body wave, i.e., the shear wave, and such surface phenomena as Love and Rayleigh waves which may also be present. Certainly then, if all these waves may be generated by a burst at a site of interest, and if the time history of the composite wave action at a point is of importance, it would be most desirable if the existing ground motion prediction methods could be employed to account for each component wave form.

It is of interest then to review the various categories of ground motions used in the prediction methods with a view toward isolating the independent effect of each source of ground motion listed above.

The wave form of the ground motion generated only by the direct effect of the pressure of the air-blast wave on the surface, with no precursor or outrunning, is generally agreed to be similar to the Type I wave form. Both Newmark's and Sauer's methods can be used to predict most of the significant parameters defining in reasonable detail the ground motion from this source both at the ground surface and at some depth.

The general shape of the wave form of the ground motion generated only by the direct effect of the cratering-induced ground motion has been reported by Newmark to be as shown in Figure 2.5.1. This form was observed in tests of confined bursts so that no air-blast wave was present. This case has not been treated by Sauer.

In layered media, Newmark uses separate methods to account for the effects on air-blast and on cratering-induced motions. In the air-blast induced case he further distinguishes between the superseismic and the trans/subseismic regions. This latter distinction appears to be unnecessary in view of the fact that the difference between the air-blast induced superseismic wave in a layered medium and the air-blast induced trans/subseismic wave is simply a matter of the phasing of the direct and reflected components.

For cratering-induced waves in layered media, Newmark suggests the use of an "equivalent seismic velocity" to correct the equations for homogeneous media.

Newmark then notes that "ordinarily the input for ground motion consists of two parts, a systematic portion on top of which is superimposed a series of random oscillations" and suggests the following adjustments be made to the values computed as indicated above.

	Recommended Amplification Factor		
	Displacement	Velocity	Acceleration
Air-Blast Induced:			
Superseismic, homogeneous media	1.0	1.5	1.0
Transeismic, homogeneous media	1.0	1.5	2.0
All conditions, layered media	1.0	1.5	2.0
Cratering-Induced:			
All cases	1.0	1.5	2.0

If all of the ground waves generated by a nuclear blast are classified as suggested previously in the Design Guide, it is believed that not only is a clearer picture of the phenomena revealed but also the effect of these phenomena on a shock isolation system can be better related to a given site. Moreover, the wave form of the shock is described permitting a direct solution of the equations of motion of nonlinear shock isolation systems.

Specifically, it is suggested that it be assumed that all cratering- and air-blast-induced waves (including precursors) have regular, smooth wave forms (similar to Type I), disregarding high frequency oscillations outside the range of interest to the isolation system designer. It is further suggested that all reflection and refraction waves be assumed to be oscillatory (similar to Type II), with a frequency in the order of magnitude of that of the isolation system. It is then suggested that by combining the two wave forms in a manner consistent with the Nevada site and weapon conditions, the resulting amplification factors as indicated by the response spectrum of the composite wave form will match closely the amplification factors given by Newmark.

In comparing the two approaches, it is essential to distinguish clearly between free-field ground motion and the displacements, velocities and accelerations indicated by the response spectrum of the motion. Only ground motion parameters can be applied to Type I and Type II synthesized wave forms.

In discussing the superseismic air-blast induced wave, Newmark suggests it be considered as "highly damped" with a "systematic" pulse and producing peak spectral responses of 1.0, 1.5, and 2.0 for relative displacement, velocity, and absolute acceleration respectively. It should be noted, however, that the equation for surface acceleration shown in Figure 2.5.2 already contains the factor 2.0 and should not be increased further. These values correspond closely to the spectral responses which would be expected from a simple pulse similar to Type I (see Figure 3.7.5(b) Case 1 for the velocity response spectrum of Type I wave form).

For the direct cratering-induced motion, Newmark again suggests amplification factors of 1.0, 1.5, and 2.0 and here again the pulse is regular (Figure 2.5.1) so that with proportions selected to match the weapon and site conditions, the Type I wave form might again be used. Note that in this case Newmark's equations for acceleration (Figure 2.5.2) do not contain an amplification factor.

However, Newmark recommends the use of the same factors for cratering-induced motion in layered media. This would seem to imply either that reflections and refractions arising from cratering-induced waves introduce no significant distortions in the wave form or that no appreciable reflections or refractions from this source were measured at the test site.

It is suggested then that the "systematic" pulses discussed by Newmark are generated by unreflected air-blast and/or cratering-induced waves and that the "random" [illegible] of the pulses is the result of reflections and/or refractions. The physical mechanisms by which reflections or refractions might produce oscillatory waves have not been investigated here. Oscillations have been observed in the data reviewed in this study, however, both for the superseismic and subseismic cases. In all cases where the oscillation was detected, reflections and refractions from lower layers of higher seismic velocity were possible.

The simple observance of these phenomena in the limited data available does not constitute proof of the explanation offered. In the absence of systematic experimental evaluations, more realistic theoretical analyses are needed.

However the approach may offer a method by which both the shock wave form and the response spectrum can be related more directly to the conditions at a particular site. While the estimation of the magnitudes of each of the wave form parameters remains largely dependent on existing prediction methods, this information combined with basic wave form shapes would not only provide a more detailed description of the shock but would also be in a form of greater usefulness to the isolation system designer.

2.6 Wave Form Parameter Prediction Procedures

2.6.1 Significance of Wave Form Characteristics

To illustrate the significance of various factors contributing to the shape of a typical ground shock wave form, three examples will be discussed. In the first two examples, wave forms are hypothesized, and their principal features are related to possible site and weapon characteristics. The third example consists of a simplified step-by-step procedure which might be employed to establish a rough outline of a wave form for given weapon and site conditions.

Consider first the vertical velocity wave form shown in Figure 2.6.1. It is evident that an actual record of a ground shock will contain a large number of high frequency components not shown in the Figure. But since the isolation system designer is concerned primarily with the low-frequency characteristics, and to reveal more clearly the basic characteristics of the shock, the wave form may be considered as having been "smoothed out".

The initial oscillation between points a and b is due to the outrunning of the ground wave by the air-blast wave (i.e., the air-blast wave is subseismic), due to refractions, pulses generated directly by the cratering stresses, or pulses arriving from remote air-blast pressures. The local air-blast induced motion is indicated by the abrupt "velocity jump" at cd. The blip between d and e could represent a double peak in the air-blast wave or a relatively weak reflection returning from a deeper high velocity layer. Between e and h the pressure peak has passed and the slope of the curve is influenced by the decay rate of the air-blast wave, the elastic rebound of the soil, the continued motion in the deeper zones as the pressure pulse continues into the ground, and any reflections or refractions impinging on the point during this period of time.

The time phasing (t_p) between the arrival of the outrunning ground ion and the velocity jump at point c can be estimated from a refraction front diagram such as that shown in Figure 2.2.10. The duration of the main pulse (t_o) is closely related to the positive phase duration of the air-blast pressure wave unless strong additional reflections from deeper layers arrive before the positive phase terminates.

The area under curve a-f is equal to the maximum absolute transient displacement and the area of curve a-h is equal to the permanent or plastic displacement of the point considered. In an actual trace, however, the positive velocity portion of the curve is usually difficult to define accurately due to the relatively small velocities in this region and the presence of many higher frequency components. Further, no known prediction methods make it possible to calculate the positive velocity region f-h. In constructing a curve, then, the expected plastic deformation is estimated and the f-h section of the curve adjusted accordingly.

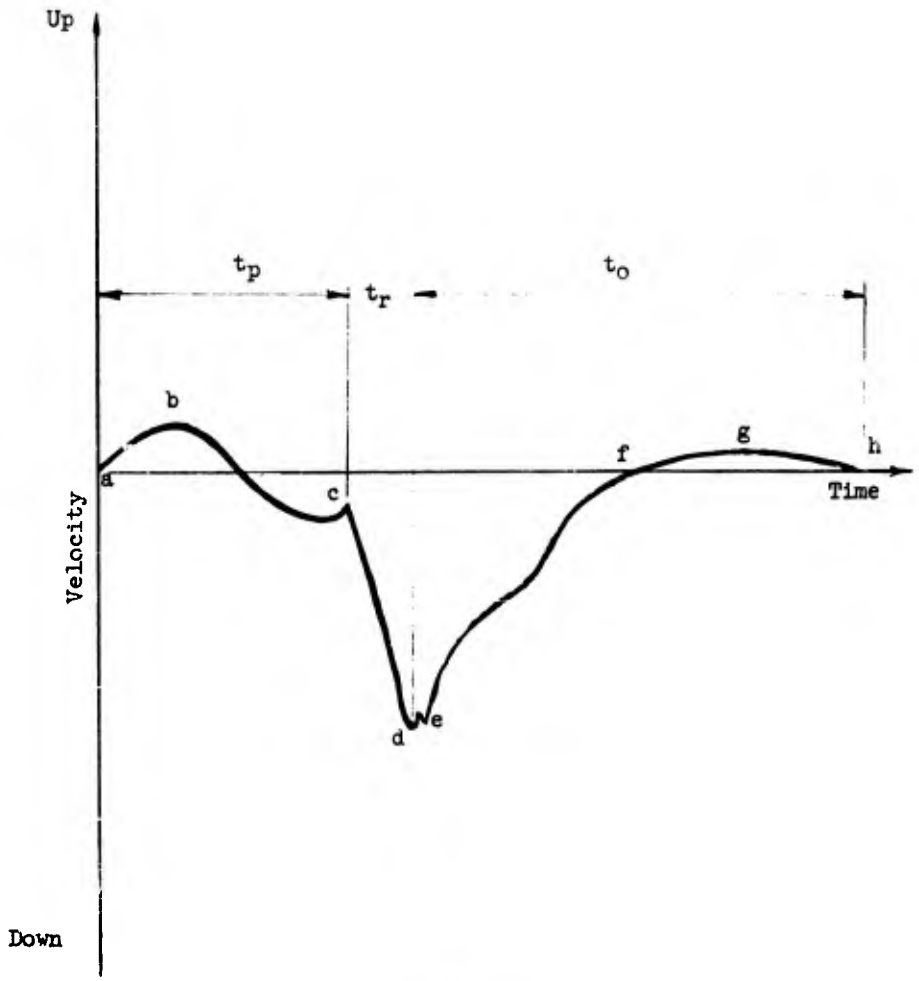

Figure 2.6.1

Example of Vertical Particle Wave Form

The velocity-jump rise time, t_r, is dependent on the depth of the point in question, the abruptness of the air-blast wave shock front and the elastic and dissipative properties of the soil. In any case it would not be greater than that computed considering only spatial dispersion of stress and the stress-velocity relationships of one-dimensional theory.

The amplitudes and durations of the positive and negative velocity peaks and the number of oscillations between a and c present the most difficult estimate to make. If the result of reflections or refractions, the oscillations may be of the general form of the Type II wave and may extend well beyond point c, being of a period near that of the incident wave which produced them. Only a gross estimate of the peak values of the oscillatory wave parameters can be determined.

Several general observations on the location of the site with repect to ground zero and on the soil properties can be deduced from the shape of the wave form. It is probable, for example, that the site was near the surface since the permanent displacement of the soil was large. The increasing modulus of the soil with depth due to added initial confinement will tend to reduce the plastic deformation. Further, it is unlikely that the soil was saturated since large permanent displacements would not be expected below a permanent water table.

The classic form of the velocity jump, together with knowledge of a shallow depth confirm the opinion that the air-blast wave was not preceded by a precursor. An inclination of the precursor would have otherwise appeared between points c and d.

Had the point of interest been closer to the crater, at least in the superseismic region, and at a depth such that it lay below a line extending down from the crater at an angle of about 20 degrees from the horizontal, the velocity wave form would have been entirely dissimilar, appearing more like that shown in Figure 2.5.1. At deep, close-in sites, the cratering-induced wave form would undoubtedly be the only important one. As the point of interest moves away from the source and to shallower depths, the air-blast induced wave (Type I) increases in strength, first lagging the cratering-induced wave, then leading it.

Consider as a second example, the site represented by the wave front diagram shown in Figure 2.2.10. At ranges smaller than about 3000 feet from a 20-megaton burst (2-3000 psi region), the wave form of the shock would be expected to be similar to that shown in Figure 2.5.1 and its parameters could be estimated roughly by the use of Newmark's equations for cratering-induced motions. The earth for a considerable distance away from the crater (at least several crater radii from the burst point) would be stressed so highly that the rules of reflection and refraction in an elastic material would not be valid.

At very great ranges, probably beyond 10,000 feet or more (100 psi region), depending primarily upon the ability of the earth material to transmit the motions, the Type II wave form may have larger amplitudes than the Type I wave form. At these ranges the air-blast pressure would be low, and the energy transmitted through the deeper, high-velocity layers and returned to the point of interest may be of primary significance.

In the intermediate range there would be a shift in the relative importance of the two types of waves from the predominance close to the burst of the single pulse Type I wave form, typical of the air-blast induced wave form and the somewhat modified cratering-induced wave form, to the Type II wave form at the larger ranges.

2.6.2 Wave Form Prediction Procedure

The prediction methods available for estimating the magnitude of those parameters defining the wave form of the vertical motion of a particle are shown in Figure 2.6.2. The environments in which the experimental data forming the bases of these methods have been obtained are described in detail by the original investigators and have been summarized earlier in this Section. In general, these environments are much less severe than those of existing or proposed military facilities; nonetheless, in lieu of strong theoretical support, they form the only basis available for engineering design. In extrapolating these procedures to new environments, the designer is cautioned to exercise good engineering judgement biased heavily toward conservatism.

For the most part, the prediction equations recommended here are those proposed by Newmark. In many cases, methods suggested by others yield essentially the same results for conditions at the Test Site. In general, however, Newmark's equations, based on one-dimensional theory, are more comprehensive and are simpler to use.

The single exception is in the case of predicting the peak downward displacement of the Type II wave form for which the method derived by Sauer from field test data appears to be more applicable.

Some parameters needed to define the Type II wave form are not treated by any known prediction method. Of particular importance are the frequency and the ratios of the peak velocities for each oscillation. Thus, in defining this wave form it has been necessary to fix certain proportions on the basis of the range throughout which they varied in the experimental records. These proportions are shown in Figure 2.3.3 where the only additional parameters needed to define the wave are peak velocity of the largest loop and total duration.

The equations presented in Figure 2.6.2(a) and (b) for calculating the parameters of the air-blast induced and cratering-induced velocity wave forms (Type I) have been taken from Newmark. The procedure is

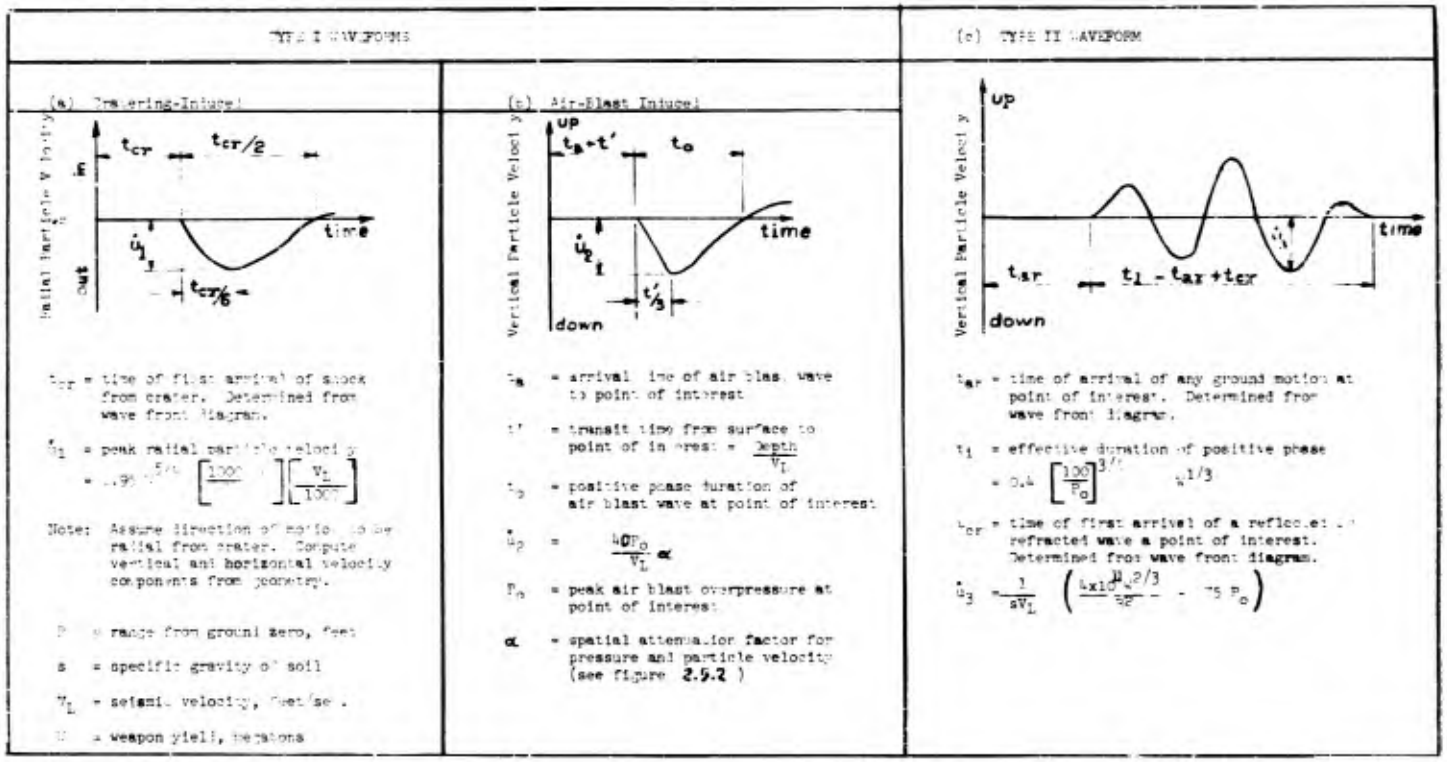

Figure 2.6.2: Tabulation of Waveform Parameter Calculation Procedure

straightforward and the exact shape of the wave at intermediate points is of no great significance to the isolation system designer.

In defining the Type II wave form (Figure 2.6.2(c)) Sauer's expressions for peak particle velocities have been used to obtain $\dot{u}_3$, while the number of cycles, their general shape, and their peak velocities relative to $\dot{u}_3$ have been fixed. The duration of the Type II wave form has been assumed to be equal to the total period of time the air-blast induced or cratering-induced waves impinge on the point of interest.

A typical plot of Sauer's equations showing peak velocity versus range is presented in Figure 2.6.3. Near ground zero the air-blast wave is superseismic so the superseismic equations apply (curve (a)). At greater ranges, the air-blast wave slows and wave pattern becomes subseismic (curve (b)). In the transeismic region, Sauer suggests that the two curves be connected by a straight horizontal line although he notes that the observed records show a slight reflex curve in this region.

It may be noted that the peak velocities observed by Sauer were always greater at a given range for the subseismic case than for the superseismic case. This, and the site conditions, suggest that the subseismic wave form consisted of a combination of Type I and Type II curves, superimposed at an undetermined phase relationship. If the velocities of the superseismic and subseismic curves are substracted and plotted, the result is curve (c) to the left of point (d). Curve (c) does not necessarily represent the peak velocities of the Type II wave form since the phasing of the two waves in the subseismic case is not known.

Although there is considerable scatter in the data from the Nevada Test Site, there are indications that the subseismic curve would peak and then decay as the range approached ground zero. This trend has been indicated in Figure 2.6.3 by adding the section of curve (c) to the left of point (d) and adjusting it to match the transeismic reflex curve connecting (a) and (b).

The general shape of curve (c) as a representation of the velocity-range relationship of a Type II wave form appears to be consistent with other known factors. For example, at short ranges, the angle of incidence of the air-blast and cratering-induced waves reflecting from a lower layer of higher seismic velocity is large and little reflection would be expected. As the range is increased, the reflections become stronger but the greater length of the path of the wave and reflections increases the dissipation. At some critical range, the strength of the reflections would reach a maximum and then, as the range is increased further, would decay.

As mentioned above, the phasing of the Type I and Type II waves in the subseismic region is not known. In fact, a unique phase relationship cannot exist since the velocity of the air-blast which produces the

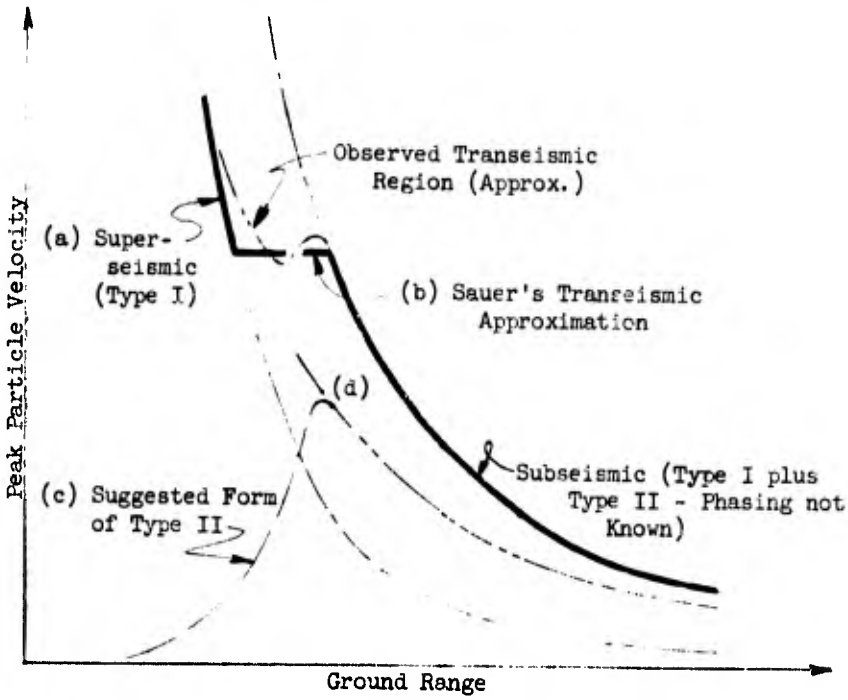

Figure 2.6.3

Typical Velocity-Ground Range Curve

Type I wave is decreasing significantly with range while the velocity of the Type II wave will, if anything, increase slightly with range. One would expect the changing phase relationship to produce oscillations in the subseismic velocity range but if they existed at the Test Site they were so small they were masked by the scatter of data or the recording stations were not spaced closely enough to identify them. The possibility still remains that the assumption of the subseismic curve (b) as a combination of the two types of wave forms may not be a valid one.

In lieu of a better indication of the phenomena, it is suggested here that Sauer's subseismic equations be considered to predict the peak velocity that can be generated by any combination of the Type I and Type II wave forms. Thus at a given range, by subtracting algebraically the peak velocity of the superseismic case from that of the subseismic case, the peak velocity of the Type II wave form ($\dot{u}_3$ of Figure 2.6.2) can be found directly.

For use in some applications this approximation might be overly optimistic. In the design of shock isolation systems, however, this optimism in the strength of the input will probably be more than offset by the usual practice of neglecting the internal friction of materials, the drag force exerted by the atmosphere, et cetera. It should be noted that small damping forces can reduce appreciably the response of a system to a shock of oscillatory wave form such as that of the Type II.

It must be constantly borne in mind that all prediction methods are based ultimately on tests conducted at two specific sites whose geological formations are not typical of those at any known underground installation. Further, insufficient data were obtained to permit an explanation of many of the observed phenomena even at the test site conditions. In each of the many reports presenting the test data and attempting to formulate some general rules-of-thumb, the authors repeatedly point out the limited conditions under which the data were obtained and urge the utmost caution in applying the results elsewhere. Nonetheless, these empirical methods are the only bases on which the isolation system designer can estimate the strength of the shock input.

As a design procedure, therefore, it is recommended that the magnitude of each parameter of the Type I and Type II wave forms be established as a range of possible values rather than as a single number. The breadth of the range will depend on the extent and accuracy of the geological information available on the site, the complexity of the soil formations, and the proportions of the Type I to the Type II wave form expected at the point of interest.

Thus a family of composite wave forms is constructed to represent the ground motion rather than a single wave. The envelope of their response spectra can then be employed in the design of linear isolation systems. It must be remembered, however, that all high-frequency components have been deleted from the synthesized wave forms so that the

response spectra are valid only in the low-frequency range.

This procedure is discussed in greater detail in Section 5.0, Isolation System Design.

2.7 Soil-Structure Interaction

The designer of shock isolation systems requires knowledge of the shock input to equipment items of interest at various locations within the hardened facility. This input results from the primary structural response of the facility to the blast-induced ground (and/or air) shock loading, and will be referred to as the structure-shock environment. Specification of this environment, in turn, requires knowledge of the free-field shock environment (i.e., the motion of the ground in the absence of the structure) and pertinent dynamical properties of the structure. Determination of the response of a structure embedded in a medium such as soil or rock to the free-field environment is complicated due to the dependence of the ground-transmitted forces on the relative motion of the medium and structure. For this reason, the response problem is referred to as one of structure-medium interaction. Other complicating factors include the little understood dynamical properties of real media, and the physics of load interaction through detonation of high yield nuclear weapons.

During the last few years, a number of analytical, and some experimental, studies of the structure-medium interaction problem have been undertaken. Among these, the work of Robinson (References 2.28, 2.29), Baron, Bleich and Wiedlinger (Reference 2.30), Pao (Reference 2.31), Soldate and Hook (Reference 2.32), and Morrison (Reference 2.33) should be noted. No attempt is made here to generally review the studies as these reports are all readily available. Suffice it to say that the analytical difficulties are enormous and, as a result, none of the studies cited has so far produced an adequate description of the structure-shock environment. It should be noted, also, that most studies to date have been directed toward the structural design problem, the structural shock environment being of secondary concern.

It is intuitively clear that the structure shock environment will differ from the free-field environment inasmuch as the dynamical properties of the structure can be expected to differ substantially from those of the medium it replaces. The nature of this difference is not so easy to anticipate. One of the first analytical solutions to a related problem was that of the response of a rigid silo-like inclusion in an elastic medium acted on by a harmonic disturbance. This solution showed that the inclusion tended to follow the motion of the medium for excitations of long wave length compared to the diameter of the silo, and was not responsive to excitations of short wave length. In terms of frequency, the structure thus was shown to attenuate the high-frequency components of the free-field shock environment.

This result is plausible and, for lack of better information, has been extended to actual design situations by assuming that the structure shock environment can be characterized by a shock spectrum which is some fractional multiple of the free-field spectrum over the entire frequency range of interest. This constant multiplier, in terms of which is

embodied the entire structure-medium problem, in the past has been included among the system design criteria. That is to say, no computational scheme for its determination is known. Obviously, there is question as to the legitimacy of such an approach.

The complex stress pattern produced by the impingement of a wave of irregular form on a cavity or structure within a real soil has necessitated many simplifications in treating the problem analytically. The mathematical model frequently studied consists of a two-dimensional cylindrical cavity, lined or unlined, in an elastic medium and engulfed by a plane shock wave with a step pressure distribution in time. In view of the previous discussions in this Section on the nature of the ground wave, the inhomogeneities of the media at most sites, and the inelastic behavior of many soils, the gross differences in the mathematical methods and the actual conditions are readily apparent.

Some studies have indicated a significant amplification of the free-field motion at certain locations on the surface of a cavity or lining throughout specific frequency ranges. For example, Baron (Reference 2.30) in presenting amplifications of responses due to zero rise-time shock waves, suggests his factors be used in design "particularly for installations in which the shock mounted equipment has high frequency components". On the other hand, Reference 2.34 notes that on the basis of a limited study of responses to waves of finite rise time, the trend indicates "an attenuation of the high frequency end of the free-field spectrum while in many instances the low frequency end is amplified".

Very few studies consider the soil as an elastic-plastic medium and thus neglect a significant damping factor. While rock may be considered to respond elastically at moderate pressures, most actual installations in rock are surrounded by a layer of frangible material to minimize damage due to spalling. In these cases an attenuation of high frequencies could also be expected.

Despite the work done to date in this difficult field, the designer is afforded little guidance in evaluating the effect of soil/structure interaction. Until such time as more applicable information becomes available, therefore, it is recommended that he assume that the free-field motion applies to the shell lining. For unlined cavities in rock, Baron's results (Reference 2.30) should be reviewed before a final decision is made. It must be remembered, however, that the wave front used in Baron's analysis had a zero rise time. For the case of a pressure wave with a finite rise time, the intensity of the high frequency portions of the spectrum would be substantially decreased.

In those cases where the isolation system is attached not to the shell lining but to a secondary structure, the designer is cautioned to determine the response of the secondary structure at the point of attachment.

Section 2 - Notations

a = coefficient of absorption; overpressure decay coefficient
e = 2.718
E = Young's Modulus, psi
E' = energy at unit distance
E'' = energy at distance R
$I(t)$ = total impulse of air-blast wave, psi-sec.
I_r = impulse of air-blast wave from t = 0 to time reflection reaches surface, psi-sec.
L = attenuation coefficient
$P(t)$ = air-blast pressure-time function, psi
P_o = peak air-blast overpressure, psi
R = range from ground zero, feet
s = in situ specific gravity
t = time, sec
t_a = arrival time of air-blast wave, sec
t_{ar} = arrival time of ground motion, sec
t_{cr} = arrival time of first ground motion, sec
t_c = time at which relative motion of compaction front ceases, sec
t_e = duration of equivalent air-blast pressure pulse, sec
t_p = duration of positive phase of air-blast pressure, sec
t_s = time at which $z/V_L = 1$
t' = transit time of wave from surface to depth of interest, sec
u = peak displacement of particle, in.
u_{se} = peak elastic displacement of particle at surface, in.
u_{sp} = peak plastic displacement of particle at surface, in.
u_{st} = peak total displacement of particle at surface, in.
$\dot{u}$ = peak particle velocity, fps
$\dot{u}_s$ = peak velocity of particle at surface, fps
$\dot{u}_{1r}$ = peak radial velocity of cratering-induced Type I wave form, fps
$\dot{u}_v$ = peak vertical velocity of air-blast induced Type I wave form, fps
$\dot{u}_{II}$ = peak vertical velocity of Type II wave form, fps
U = air-blast wave velocity, fps
$\ddot{u}$ = peak acceleration of particle, gravities
$\ddot{u}_s$ = peak acceleration of particle at surface, gravities
V_L = seismic (compression wave) velocity, fps
V_L^* = corrected seismic (compression wave) velocity, fps
V_R = Rayleigh wave velocity, fps
V_S = shear wave velocity, fps
W = weapon yield, megatons
y = depth below surface, feet
z = displacement of ground shock wave front, feet
$\dot{z}$ = velocity of ground shock wave front, fps

α = attenuation factor
ε = unit strain
ε_c = maximum plastic unit strain
ε_o = maximum elastic unit strain
ψ = angle of inclination of air-blast induced ground shock front
μ = Poisson's ratio
γ' = mass density, lb-sec^2/ft^4
σ = stress, psi
σ_c = stress at strain ε_c, psi
σ_o = stress at strain ε_o, psi
Ψ = ratio of impedances of two contacting media

SECTION 2.0 REFERENCES

2.1 Brode, H. L., and Bjork, R. L.
Cratering from a Megaton Surface Burst
Shock, Vibration, and Associated Environments
Bulletin 29, Part III, Department of Defense.
July 1961

2.2 Brode, H. L.
Weapons Effects for Protective Design
The RAND Corporation, P-1951. March 1960

2.3 Brode, H. L.
Nuclear Weapons Phenomena Pertinent to Protective Design
The RAND Corporation, Research Memo RM-1938.
July 1957 (C)

2.4 Howell, B. F. Jr.
Introduction to Geophysics
McGraw-Hill Book Company, Inc., New York. 1959

2.5 Nettleton, L. L.
Geophysics Prospecting for Oil
McGraw-Hill Book Company, Inc., New York. 1940

2.6 Baron, W. L., and Lecht, C.
Elastic Rayleigh Wave Effects Due to Nuclear Blasts
Journal Engineering Mechanics Division, Proceedings
ASCE. October 1961

2.7 Muskat, M., and Meres, M. W.
Reflection and Transmission Coefficients for Plane Waves
In Elastic Media
Geophysics, Volume 5, pp. 115-148. 1940

2.8 Leet, L. D.
Earth Waves
Harvard Monographs in Applied Science No. 2,
Harvard University Press. 1950

2.9 Thornburgh, H. R.
Wave-Front Diagram in Seismic Interpretation
Bulletin, American Association of Geology, Volume 14.
1930

2.10 Ewing, W. M., Jardetzky, W. S., and Press, F.
Elastic Waves in Layered Media
McGraw-Hill Book Company, Inc., New York. 1957

2.11 Sauer, F. M.
Ground Motions Produced by Aboveground Nuclear Explosions
Air Force Special Weapons Center SWC-TN-59-71.
April 1959 (S)

2.12 Perret, W. R.
Ground Motion Studies at High Incident Overpressure
Sandia Corp. WT-1405, Operation Plumbbob - Project 1.5.
1960

2.13 Wilson, S. D., and Sibley, E. A.
Ground Displacements Resulting from Air Blast Loading
Preprint of Paper Presented at Houston Convention,
ASCE. February 1962

2.14 Newmark, N. M., et al.
Protective Construction Review Guide- Hardening
Volume I, Department of Defense. June 1961

2.15 Salmon, V., and Horing, S. R.
Earth Acceleration vs. Time and Distance
Operation Tumbler, Project 1.7, WT-517, Stanford
Research Institute. February 1953 (C)

2.16 Swift, L. M., Sacks, D. C., and Sauer, F. M.
Ground Acceleration, Stress, and Strain at High Incident
Overpressures
Operation Plumbbob, Project 1.4, WT-1404, Stanford
Research Institute. May 1960 (C)

2.17 Wistor, J. W., and Perrett, W. R.
Ground Motion Studies at High Incident Overpressure
Operation Plumbbob, Project 1.5, WT-1405, Sandia
Corp. October 1957 (C)

2.18 Swift, L. M., and Sacks, D. C.
Ground Motion Produced by Nuclear Detonations
Operation Hardtack, Project 1.8, ITR-1613, Stanford
Research Institute. August 1958 (S)

2.19 Grine, D. R., and Fowles, G. H.
The Attenuation of Shock Waves in Solid Materials with
Seismic Application
Colorado School of Mines Quarterly, Volume 54, No. 3
1959

2.20 Sackman, J. L.
A Study of the Effect of a Progressing Surface Pressure in a Viscoelastic Half-Space
The MITRE Corporation. February 1961

2.21 Baron, M. L., and Parnes, R.
A Study of the Effect of a Progressing Surface Pressure in a Viscoelastic Half-Space
The MITRE Corporation. February 1961

2.22 Newmark, N. M., and Hall, W. J.
Preliminary Design Methods for Underground Protective Structures
Air Force Special Weapons Center, AF Contract No. AF 29(601)-1171. December 1959 (S)

2.23 Salvadori, M. G., Skalak, R, Weidlinger, P.
Waves and Shocks in Locking and Dissipative Media
Journal Engineering Mechanics Division, Proceedings ASCE. April 1960

2.24 Baron, M. L., Bleich, H. H., Weidlinger, P.
Theoretical Studies on Ground Shock Phenomena
The MITRE Corporation. October 1960

2.25 Miles, J. W.
The Propagation of an Impulse into a Viscous Locking Medium
Journal of Applied Mechanics. March 1961

2.26 Anon
An Engineering Manual on the Design of Underground Installations in Rock
U. S. Bureau of Mines. March 1957 (C)

2.27 Wilson, S. D., and Hammer, M. J.
Subsurface Investigations and Ground Motion Studies at Nevada Test Site
Shannon and Wilson, AF Contract No. AF 04(647)-650, January 1961 (S); Addendum I, April 1961 (S)

2.28 Robinson, R. R.
Investigation of Silo and Tunnel Linings
Final Report, Contract No. AF 29(601)-2596 for AFSWC, Kirtland AFB, New Mexico. Armour Research Foundation, Chicago, Illinois. December 1961 (C)

2.29 Robinson, R. R.
Investigation of Silo and Tunnel Linings
Armour Research Foundation, Chicago, Illinois, Contract AF 29(601)-2596, AFSWC-TDR-62-1, March 1962.

2.30 Baron, M. L., Bleich, H. H., Weidlinger, P.
Theoretical Studies on Ground Shock Phenomena
Final Report for the MITRE Corporation, Paul Weidlinger Consulting Engineers, New York. October 1960

2.31 Pao, H. Y.
Dynamical Stress Concentration In an Elastic Plate
Presented at West Coast Conference, ASME. August 1961

2.32 Soldate, A. M., Hook, J. F.
A Theoretical Study of Structure-Medium Interaction
National Engineering Science Co., Final Report, Contract No. AF 29(601)-2838 for AFSWC, Kirtland AFB, New Mexico. November 1960

2.33 Morrison, T. G.
A Simplified Theory of Interaction of Shell Structures with Soil
Shock and Vibration Bulletin No. 29. July 1961

2.34 Unpublished Communication from the Armour Research Foundation dated June 1962

2.35 Miles, J. W.,
On the Response of an Elastic Half Space to a Moving Blast Wave, EM 8-21, Space Technology Laboratories, November 1958.

APPENDIX 2-A

UNCLASSIFIED WEAPON TEST REPORTS RELATED TO FREE-FIELD GROUND SHOCK

TEST OPERATION	W.T. NO.	DATE	TITLE	ORG.
JANGLE 1.1	388	10/52	Ground Acceleration Measurements	NOL
JANGLE 1.2a-2	385	8/52	Transient Ground Mechanical Effects From HE and Nuclear Explosions	BRL
JANGLE 1.2b	364	7/52	Close-in Ground Measurements	AFSWP/ Sandia
JANGLE 1.5a	382	7/52	Transient Ground Displacement Measurement	NOL
JANGLE 1.5b	326	7/52	Detection of Time of Arrival of First Earth Motion	DT
JANGLE 1.6	353	7/52	Earth Displacements (Shear Shafts)	CCE
JANGLE 1.7	357	8/52	Ground Acceleration (Shock Pins)	MIT
JANGLE 1(8)a-1	327	10/52	Seismic Refraction Studies for Nye County, Nev.	UGC
JANGLE 1.9	358	7/52	Theoretical Studies of Underground Shock Wave	UCRL
JANGLE 1(9)a	380	8/52	Ground Acceleration, Ground & Air Pressures for Underground Tests	SRI
JANGLE 1.9-1	328	7/52	Application of the Kirkwood-Brinkley Method to the Theory of Underground Explosions	RAND
JANGLE 1.9-2	378	7/52	Notes on Surface and Underground Bursts	RAND
JANGLE 1.9-3	350	7/52	Predictions for Underground Test	SRI
JANGLE 1(9)-1	377	7/52	Scaled HE Tests	SRI
JANGLE 3.29	336	7/52	Engineer Soil Mechanics Test	NCE
BUSTER-JANGLE 10.10a	302	7/52	Attenuation of Earth Pressures Induced by Air Blast	Sandia

TEST OPERATION	W.T. NO.	DATE	TITLE	ORG.
JANGLE V	365	9/52	HE Tests	AFSWP
JANGLE V	366	10/52	Blast & Shock Measurement I	AFSWP
JANGLE V	367	9/52	Blast & Shock Measurement II	AFSWP
JANGLE V	368	9/52	Blast & Shock Measurement III	AFSWP
JANGLE V	369	8/52	UG Explosion Theory	AFSWP
TUMBLER 1.7	517	4/53	Earth Acceleration vs. Time and Distance	SRI
TUMBLER 19.1	503	10/52	Earth Stresses and Earth Strains	Sandia
UPSHOT-K 1.4	716	4/55	Free-Field Measurements of Earth Stress, Strain, and Ground Motion	Sandia
TEAPOT 1.7	1106	3/58	Underground Explosion Effects	SRI/ONR
PLUMBBOB 1.4	1404	5/60	Ground Acceleration, Stress and Strain at High Incident Overpressure	SRI
PLUMBBOB 1.5	1405	7/60	Ground Motion Studies at High Incident Overpressure	Sandia
PLUMBBOB 1.9	1487	8/59	Spectra of Ground Shocks Produced by Nuclear Detonations	AFBMD
PLUMBBOB 3.8	1427	11/59	Soil Survey and Backfill Control in Frenchman Flat	WSS
PLUMBBOB 26.4a	1528	4/60	Surface Motion from an Underground Detonation	SRI
PLUMBBOB 26.4b	1529	8/61	Subsurface Motions from a Confined Underground Detonation (Part I)	Sandia
PLUMBBOB 26.4d	1530	11/58	Surface Motions from an Underground Explosion	USC/USGS
PLUMBBOB 26.4e	1531	4/59	Subsurface Accelerations and Strains from an Underground Detonation (Part II)	ERDL/BRL
PLUMBBOB 26.4f	1532	7/58	Photographic Analysis of Earth Motion, Shot RAINIER	EG & G

TEST OPERATION	W.T. NO.	DATE	TITLE	ORG.
PLUMBBOB N/N	1499	10/53	Preliminary Summary Report of Strong Motion Measurements from a Confined Underground Nuclear Detonation	Sandia/ UCRL
HARDTACK II 26.1	1702	10/61	Earth Motion Measurements	SRI
HARDTACK II 26.1	1740	8/60	Postshot Disturbances and Surface Motions - Operation Hardtack II	
HARDTACK II 26.2 & 26.10	ITR 1703	8/59	Surface and Subsurface Strong Motion Measurements	Sandia
HARDTACK II 26.3	ITR 1704	1/60	Ground Motion Measurements	ERDL
HARDTACK II 26.4	1741	7/61	Surface Motions from a Series of Underground Nuclear Tests	USC & GS
HARDTACK II 26.5	ITR 1706	6/59	Earth Motion Studies	EG & G
HARDTACK II 26.6	1707	N/D	Physical Studies of Medium	USGS
HARDTACK II 26.8	ITR 1709	8/59	Preliminary Report on Medium Studies	
HARDTACK II 26.11	1712	W/D	Permanent Displacement Studies	USC & GS
HARDTACK II 26.0	ITR 1711	6/60	Summary of Strong Motion Measurements, Underground Nuclear Detonations	

SECTION 3.0 ISOLATION SYSTEM ANALYSIS

TABLE OF CONTENTS

3.1 Introduction

General methods of analyzing the behavior of dynamic systems have been treated thoroughly in the literature and while in some cases detailed procedures may be complicated, the basic theory is easily developed from first principles. In the design of systems for underground protected structures, one of the major problems arises from the lack of time in which to select the most appropriate procedure, to set up the problem in proper form, and to perform the required algebra.

This Section is included in the Design Guide to review the more useful methods of analyzing the dynamic response of isolation systems, to discuss briefly the underlying theory and to work out solutions for the general cases most frequently used. It is hoped in this way the job of the isolation system designer will be expedited.

Shock isolation systems fall under the general category of "systems with constraints", i.e., mass particles of isolation systems are not free, but must adhere to paths and boundaries prescribed by the nature of the imposed constraints. In general, they can be further partitioned into two broad classifications, namely:

- Multidirectional, single-mass systems (Figure 3.1.1)
- Multimass, unidirectional systems (Figure 3.1.2)

The general case is a combination of these classifications (Figure 3.1.3). In all three cases, the masses may be rigid or flexible.

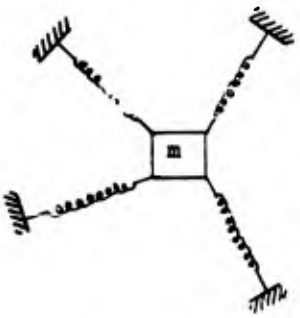

Figure 3.1.1
Multidirectional Single Mass System

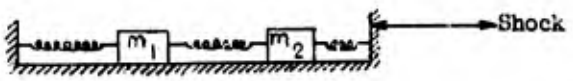

Figure 3.1.2
Multimass, Unidirectional System

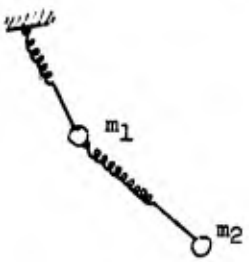

Figure 3.1.3
Multimass, Multidirectional General System

Another method of classifying the entire range of shock isolation systems is based on the nature of the mathematical representation of the system, as follows:

- Linear Systems - systems whose physical behavior can be represented, within engineering approximations, by linear ordinary differential equations with constant coefficients.
- Rheolinear Systems - systems whose behavior can be approximated by linear ordinary differential equations with coefficients.
- Nonlinear Systems - systems that require the use of nonlinear ordinary differential equations for an accurate representation of their behavior.

The properties of an isolation system which characterize it as linear, rheolinear, or nonlinear are determined by the isolator elements themselves; the general configuration of the entire system; and the approximations acceptable in establishing the mathematical model for the physical system. The various classifications discussed above are listed in Figure 3.1.4.

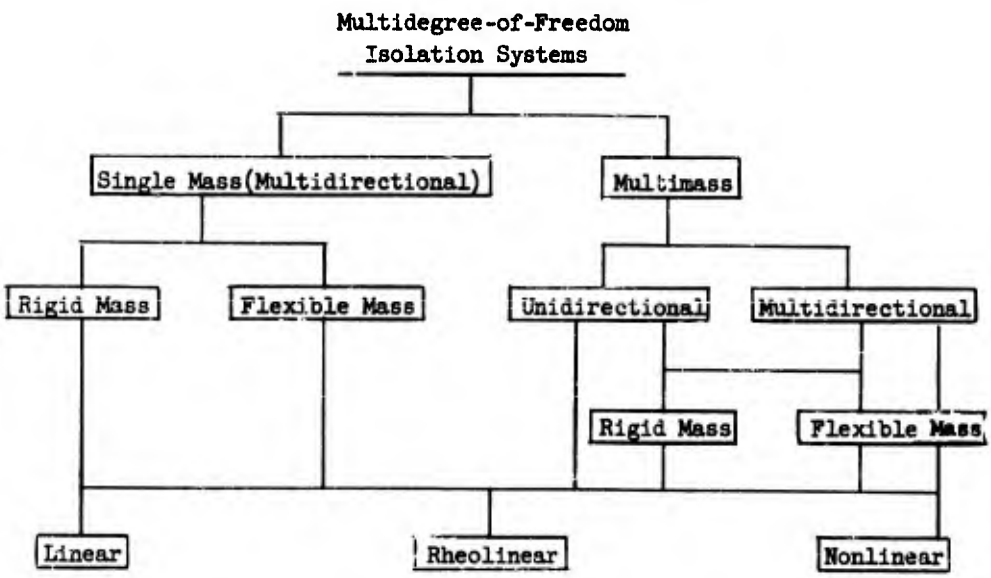

Figure 3.1.4

The response of any dynamic system to a defined shock can be theoretically determined once the equations of motion, explicitly expressing all significant forces and accelerations, have been written. The principal problem, of course, lies in adequately defining the shock input and in ensuring that the mathematical equations are sufficiently complete to describe the physical system, within the desired accuracy. Section 3.0 of the Design Guide is primarily concerned with the mechanics of setting up the equations of motion for several systems typical of those frequently employed in underground protective structures. The methods advocated require that the input be given as a shock spectrum in the analysis of linear and rheolinear systems, or as a time history for nonlinear systems. In all cases considered, the flexibility of the suspended mass has been neglected and the body is assumed to be rigid. The properties of dynamic systems have been defined and are presented in matrix form. The general equations of motion for linear and nonlinear systems are then presented.

Six examples of multidegree-of-freedom, rigid mass undamped, linear shock isolation systems have been defined and solved. Equations of motion for the same six examples have been set up, including pendulum motion in one plane, for the rheolinear classification. The cases studied include isolator elements with and without shear stiffness components, and with symmetrical and unsymmetrical supporting systems. The designer may use the results of these examples directly by substituting his coefficients in the final matrix equations and completing the solution. It is evident that the solution of the completely coupled, six-degree-of-freedom case becomes very tedious. It is anticipated that the designer will use a digital computer in these instances, and for this reason several equations can be applied to any simple case by ignoring the unwanted terms.

Three particular aspects of the design of nonlinear systems have also been considered in this section. Many nonlinear isolation systems can be uncoupled and reduced to several independent single-degree-of-freedom systems. Further, force-displacement characteristics of many nonlinear isolators can be approximated by two straight lines. Yet the solution of even the bilinear system problem becomes time consuming if the response to several inputs of complex wave form are to be determined. In this section, the peak response of a wide variety of nonlinear elements to a broad family of synthesized wave forms has been computed by electric analog and plotted so that the resonse can be found directly. Further the optimum system dimensions can be determined for given input and output requirements. In using these curves it must be remembered that the maximum responses were obtained for a specific group of wave-form combinations. However, the range of parameters was sufficiently broad to encompass most practical cases and the curves should be of value in selecting an isolator of nearly optimum proportions. The dimensions so obtained can then be used in a formal analysis to obtain the response to the actual shock.

The effects of nonlinear coupling in the popular pendulum type suspension system are also emphasized in this section. The results of a computer solution of the two-degree-of-freedom case indicate that amplifications of angular displacements by factors greater than three above that predicted by the linearized solutions are possible. The importance of including the nonlinear coupling terms in the analysis of all pendulum type suspension systems is clearly evident.

In a subsequent subsection, rheolinear equations of motion are set up for the six-degree-of-freedom pendulum system. The simplification has been made that the pendulum motion is planar so that care must be exercised in selecting the coordinate system in order that the horizontal shock occurs in the pendulum plane. If the restoring force due to the isolator in the pendulum arm is not linear, the nonlinear characteristic can be introduced into the equations.

3.2 Multidirectional Rigid-Mass Systems

3.2.1 Dynamic Behavior of a Rigid Body

A rigid body is a system of mass particles in which the distances between the various mass points of the body always remain constant. In general, six independent coordinates are required to define uniquely the position and orientation of a rigid body in space. Three translational coordinates specify the position of any point in the body and three additional angular coordinates fix the angular orientation of the body with respect to the point. A rigid body is thus said to possess six degrees of freedom.

The equations describing the motion of a rigid body in space are developed from Newton's second and third laws for translation of a single mass point (References 3.1, 3.2).

Translational motion of a rigid body is governed by the equation

$$\vec{F} = m\ddot{\vec{S}} \tag{1}$$

where $\vec{F}$ = resultant of all external forces acting on the body

m = total mass of the body

$\ddot{\vec{S}}$ = acceleration of the center of mass in a fixed coordinate system.

Rotational motion of a rigid body is governed by the equations

$$\vec{M}_O = \dot{\vec{H}}_O$$

and

$$\vec{M}_C = \dot{\vec{H}}_C \tag{2}$$

where $\vec{M}_O$ = moment of the resultant of all external forces acting on the body about any fixed point, O.

$\dot{\vec{H}}_O$ = time rate of change of the moment of momentum of the mass center about the fixed point, O.

$\vec{M}_C$ = moment of the resultant of all external forces acting on the body, about the mass center.

$\dot{\vec{H}}_C$ = time rate of change of the moment of momentum of the mass about the mass center.

For a rigid body moving with respect to a fixed coordinate system x y z, having a second moving coordinate system x_1 y_1 z_1 located with its origin at the mass center and axes fixed in the body coincident with its principal inertia axes, the equation

$$\vec{M}_C = \dot{\vec{H}}_C$$

reduces to Euler's equations. (Figure 3.2.1.)

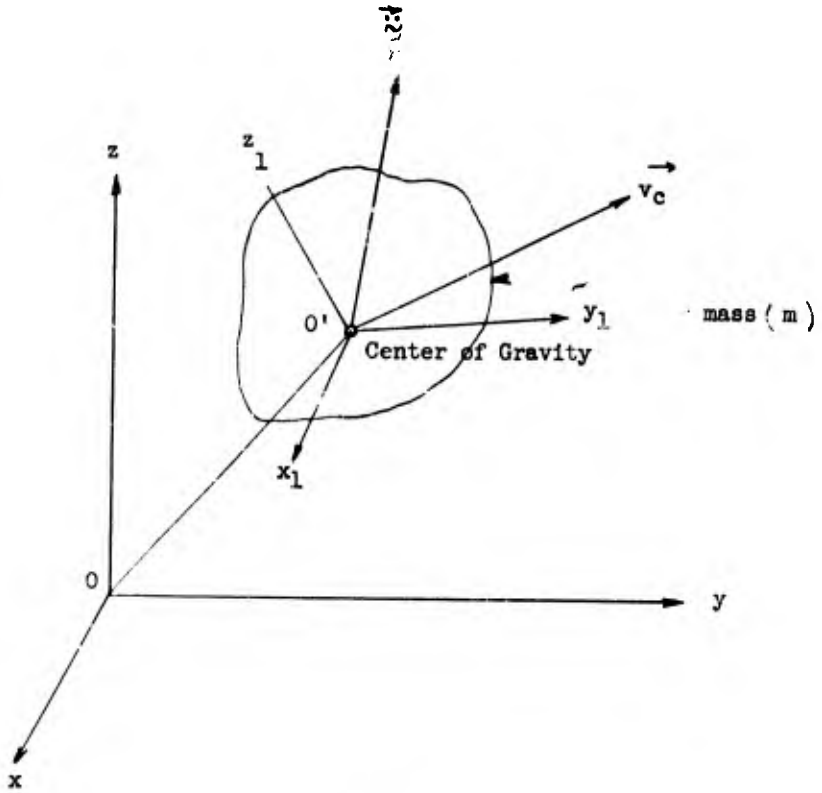

Figure 3.2.1
Rigid Body in 3-Dimensional Space

$$
\begin{aligned}
M_{x_1} &= (I_{xx})_1 \ddot{\phi}_{x_1} + \left[(I_{zz})_1 - (I_{yy})_1\right] \dot{\phi}_{y_1} \dot{\phi}_{z_1} \\
M_{y_1} &= (I_{yy})_1 \ddot{\phi}_{y_1} + \left[(I_{xx})_1 - (I_{zz})_1\right] \dot{\phi}_{x_1} \dot{\phi}_{z_1} \qquad (3) \\
M_{z_1} &= (I_{zz})_1 \ddot{\phi}_{z_1} + \left[(I_{yy})_1 - (I_{xx})_1\right] \dot{\phi}_{x_1} \dot{\phi}_{y_1}
\end{aligned}
$$

If the angular velocities are small in comparison with the angular accelerations, Euler's equations may be approximated:

$$
\begin{aligned}
M_{x_1} &= (I_{xx})_1 \ddot{\phi}_{x_1} \\
M_{y_1} &= (I_{yy})_1 \ddot{\phi}_{y_1} \\
M_{z_1} &= (I_{zz})_1 \ddot{\phi}_{z_1}
\end{aligned} \tag{4}
$$

where all quantities are expressed in terms of the moving coordinate system (x_1, y_1, z_1). If the displacements of the body also are small, the fixed coordinate system can be taken coincident with the moving coordinate system, so that the equations for translation and rotation can be expressed in the same coordinates.

In matrix form, the equations of motion for a rigid body undergoing small relative displacements are:

$$
\begin{aligned}
\{F\} &= m \{\ddot{S}\} \\
\{M\} &= [I] \{\ddot{\phi}\}
\end{aligned} \tag{5}
$$

where

$$
\{F\} = \begin{Bmatrix} F_x \\ F_y \\ F_z \end{Bmatrix}
$$

$$
\{S\} = \begin{Bmatrix} \ddot{X} \\ \ddot{Y} \\ \ddot{Z} \end{Bmatrix}
$$

$$
\{M\} = \begin{Bmatrix} M_{x_1} \\ M_{y_1} \\ M_{z_1} \end{Bmatrix}
$$

$$
[I] = \begin{bmatrix} (I_{xx})_1 & 0 & 0 \\ 0 & (I_{yy})_1 & 0 \\ 0 & 0 & (I_{zz})_1 \end{bmatrix}
$$

$$\{\ddot{\phi}\} = \begin{bmatrix} \ddot{\phi}_{x_1} \\ \ddot{\phi}_{y_1} \\ \ddot{\phi}_{z_1} \end{bmatrix}$$

3.2.2 The Stiffness Matrix of an Isolator

The stiffness matrix of an isolator may be defined by its typical element c_{ij} which represents the restoring force in the isolator in direction i due to a unit deformation of the isolator in direction j. Consider any general isolator located in a Cartesian system of reference (x,y,z); then, provided the isolator is a linear isolator governed by Hooke's Law, i.e., displacements in any direction are proportional to the restoring forces, the components of the restoring forces acting on the isolator, in directions x, y, and z due to deformations δ_x, δ_y, and δ_z are given by equation (6).

$$\begin{aligned} F_x &= c_{xx}\,\delta_x + c_{xy}\,\delta_y + c_{xz}\,\delta_z \\ F_y &= c_{yx}\,\delta_x + c_{yy}\,\delta_y + c_{yz}\,\delta_z \\ F_z &= c_{zx}\,\delta_x + c_{zy}\,\delta_y + c_{zz}\,\delta_z \end{aligned} \tag{6}$$

In matrix form, $\{F\} = [c]\{\delta\}$, where $[c]$ is the stiffness matrix of the isolator and is given by

$$[c] = \begin{bmatrix} c_{xx} & c_{xy} & c_{xz} \\ c_{yx} & c_{yy} & c_{yz} \\ c_{zx} & c_{zy} & c_{zz} \end{bmatrix}$$

Denoting x, y, and z by using the numerical notations 1, 2, and 3 respectively,

$$[c] = \begin{bmatrix} c_{11} & c_{12} & c_{13} \\ c_{21} & c_{22} & c_{23} \\ c_{31} & c_{32} & c_{33} \end{bmatrix} \tag{7}$$

In general, an isolator has three principal directions: the axial direction, and the two orthogonal lateral directions perpendicular to the axial direction. The stiffnesses corresponding to these principal directions are respectively referred to as the "axial stiffness" and the

"lateral stiffness". These so-called "principal stiffnesses" of the isolator completely define its elastic properties. However, to obtain the stiffness matrix of an isolator, the additional parameters, i.e., the inclinations of the principal axes of the isolator to the related Cartesian reference system, are required. If the principal axial directions of the isolator are parallel to the Cartesian reference system, the elements c_{ij} $(i \neq j)$ of the stiffness matrix $[c]$ all vanish and the stiffness matrix reduces to:

$$[c] = \begin{bmatrix} c_{xx} & 0 & 0 \\ 0 & c_{yy} & 0 \\ 0 & 0 & c_{zz} \end{bmatrix}$$

where c_{xx}, c_{yy}, and c_{zz} are the three principal stiffnesses of the isolator. This implies the shear stresses are zero on the principal stress planes of a structural element.

It often happens in practice that an isolator does not have all of its three orthogonal principal directions coincident with the Cartesian system of reference. It then becomes necessary to evaluate a new stiffness matrix of the isolator, with all its shear components, in terms of the three principal stiffnesses with the angles of inclination defining the location of the isolator principal axes with respect to the reference system.

For the sake of illustration, consider an isolator with principal stiffnesses c_{xx}, c_{yy}, and c_{zz} located such that the axial direction defining c_{xx} is inclined at an angle θ to the x axis of the reference system, and lying in the xy plane. The 'z' axis of the reference system is parallel to the principal direction of the isolator defining stiffness c_{zz}. The above system can be reduced to an equivalent system consisting of three isolators, possessing axial stiffnesses only, and located such that each isolator coincides with the corresponding principal direction of the original isolator (Figure 3.2.2, page 3-12).

Since linearity of the isolator has been assumed, a superposition of the three unidirectional isolators is valid. Then, considering an isolator with axial stiffness only, inclined at an angle of θ to the x-axis (positive direction as shown) and lying in the xy plane, a linear transformation is obtained as follows:

$$F = \delta_x \cos\theta \, c_{xx}$$

and

$$F_x = F \cos\theta = c_{ll} \, \delta_x$$

$$\therefore \delta_x \cos\theta \, c_{xx} \cos\theta = c_{ll} \, \delta_x$$

$$\therefore c_{ll} = c_{xx} \cos^2\theta \qquad (8)$$

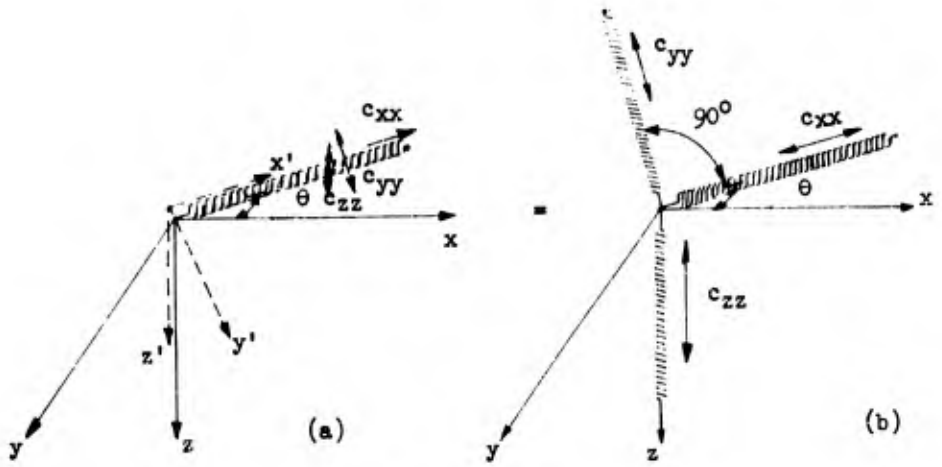

Figure 3.2.2
Isolator in xy Plane - Principal Directions
Not Coincident with Reference Axes

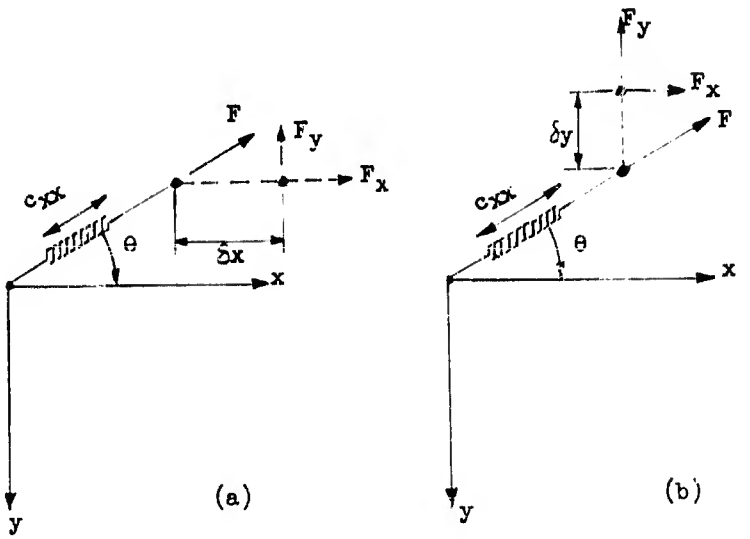

Figure 3.2.3
Uni-Axial Isolator in xy Plane

$$F_y = F \sin\theta = -c_{21}\,\delta_x$$

$$\delta_x \cos\theta\, c_{xx} \sin\theta = -c_{21}\,\delta_x$$

$$\therefore \quad c_{21} = -\frac{1}{2} c_{xx} \sin 2\theta \tag{9}$$

$$F = -\delta_y \sin\theta\, c_{xx}$$

$$F_y = F \sin\theta = -c_{22}\,\delta_y$$

$$-\delta_y \sin\theta\, c_{xx} \sin\theta = -c_{22}\,\delta_y$$

$$\therefore \quad c_{22} = c_{xx} \sin^2\theta \tag{10}$$

$$F_x = F \cos\theta = c_{12}\,\delta_y$$

$$-\delta_y \sin\theta\, c_{xx} \cos\theta = c_{12}\,\delta_y$$

$$\therefore \quad c_{12} = -\frac{1}{2} c_{xx} \sin 2\theta \tag{11}$$

Hence the stiffness matrix for an isolator with an axial stiffness c_{xx} and inclined at θ to the x axis, as previously explained, is given by:

$$[c]_x = \begin{bmatrix} c_{xx}\cos^2\theta & -\frac{1}{2} c_{xx}\sin 2\theta & 0 \\ -\frac{1}{2} c_{xx}\sin 2\theta & c_{xx}\sin^2\theta & 0 \\ 0 & 0 & 0 \end{bmatrix}_x \tag{12a}$$

The isolator with axial stiffness c_{yy} has an angle of inclination equal to $90 + \theta$. Hence, making the necessary substitutions

$$[c]_y = \begin{bmatrix} c_{yy}\sin^2\theta & \frac{1}{2} c_{yy}\sin 2\theta & 0 \\ \frac{1}{2} c_{yy}\sin 2\theta & c_{yy}\cos^2\theta & 0 \\ 0 & 0 & 0 \end{bmatrix}_y \tag{12b}$$

The complete stiffness matrix for the isolator with principal stiffnesses c_{xx}, c_{yy}, and c_{zz} for an angle of inclination θ is then

given by a summation of equations (12a) and (12b) and including c_{zz} as follows:

$$[c]_\theta = \begin{bmatrix} c_{xx}\cos^2\theta + c_{yy}\sin^2\theta & \frac{1}{2}\sin 2\theta\,(c_{yy} - c_{xx}) & 0 \\ \frac{1}{2}\sin 2\theta\,(c_{yy} - c_{xx}) & c_{xx}\sin^2\theta + c_{yy}\cos^2\theta & 0 \\ 0 & 0 & c_{zz} \end{bmatrix}_\theta \qquad (13)$$

If c_{xx} and c_{yy} are thought of as principal stresses, c_{11} and c_{22} as normal stresses on a plane whose normal is inclined at an angle θ to the principal plane of c_{xx}, and c_{12} and c_{21} as the complementary shear stresses, then it is apparent that the above linear transformation is exactly equivalent to the Mohr's circle transformations in examples of plane stress.

The problem may also be approached by linear transformations associated with rotating the reference system about one of its axes. Thus, if x, y, z are the coordinates of a point in any Cartesian system of reference, the coordinates of this same point x^*, y^*, z^* in a new reference system obtained by a rotation θ of the reference system about the original z axis are given by the relationship

$$\begin{bmatrix} x^* \\ y^* \\ z^* \end{bmatrix} = \begin{bmatrix} \cos\theta & \sin\theta & 0 \\ -\sin\theta & \cos\theta & 0 \\ 0 & 0 & 1 \end{bmatrix} \begin{bmatrix} x \\ y \\ z \end{bmatrix}$$

or

$$\left\{\bar{X}^*\right\}_z = \left[D\right]_z \left\{\bar{X}\right\} \qquad (14a)$$

A similar transformation for a rotation ϕ about the y axis yields:

$$\begin{bmatrix} x^* \\ y^* \\ z^* \end{bmatrix}_y = \begin{bmatrix} \cos\phi & 0 & -\sin\phi \\ 0 & 1 & 0 \\ \sin\phi & 0 & \cos\phi \end{bmatrix} \begin{bmatrix} x \\ y \\ z \end{bmatrix}$$

or

$$\left\{\bar{X}^*\right\}_y = \left[D\right]_y \left\{\bar{X}\right\} \qquad (14b)$$

If the transformation about the y axis is performed after the transformation about the z axis, then

$$\left\{\bar{X}^*\right\}_{zy} = \left[D\right]_y \left[D\right]_z \left\{\bar{X}\right\} = \left[D\right] \left\{\bar{X}\right\} \qquad (14c)$$

where
$$[D] = [D]_y [D]_z = \begin{bmatrix} \cos\phi\cos\theta & \cos\phi\sin\theta & -\sin\phi \\ -\sin\theta & \cos\theta & 0 \\ \sin\phi\cos\theta & \sin\phi\sin\theta & \cos\phi \end{bmatrix} \quad (15)$$

It may be noted that $[D]$ is orthogonal, i.e., $[D]^T = [D]^{-1}$. Then in general, the transformations for forces and displacement may be obtained thus:

$$\{F^*\} = \{F\}_{yz} = [D]\{F\}$$

and
$$\{\delta^*\} = \{\delta\}_{yz} = [D]\{\delta\}$$

However, from equation (6), $\{F\} = [C]\{\delta\}$

$$\therefore [D]\{F\} = [D][C]\{\delta\}$$
$$\therefore [D]\{F\} = [D][C][D]^{-1}[D]\{\delta\}$$
$$\therefore \{F^*\} = [D][C][D]^{-1}\{\delta^*\}$$
$$\therefore [C^*] = [D][C][D]^{-1} \quad (16)$$

because $\{F^*\} = [C^*]\{\delta^*\}$ from equation 6.

The above transformation gives the stiffness matrix of any isolator in a three-dimensional space. Thus, if $[C]$ is the principal stiffness matrix, then $[C]_{yz}$ is equal to:

$$\begin{bmatrix} (c_{xx}\cos^2\theta + c_{22}\sin^2\theta)\cos^2\phi + c_{zz}\sin^2\phi & \frac{\sin2\theta}{2}(c_{yy} - c_{xx})\cos\phi & (c_{xx}\cos^2\phi + c_{yy}\sin^2\phi - c_{zz})\ \frac{\sin2\phi}{2} \\ \frac{\sin2\theta}{2}(c_{yy} - c_{xx})\cos\phi & c_{xx}\sin^2\theta + c_{yy}\cos^2\theta & \frac{\sin2\theta}{2}(c_{yy} - c_{xx})\sin\phi \\ (c_{xx}\cos^2\phi + c_{yy}\sin^2\phi - c_{zz}\sin2\phi & \frac{\sin2\theta}{2}(c_{yy} - c_{xx})\sin\phi & (c_{xx}\cos^2\theta + c_{yy}\sin^2\theta)\sin^2\phi + c_{zz}\cos^2\phi \end{bmatrix} \quad (17)$$

It may be noted here, that for linear isolators, the stiffness matrix is always symmetrical.

3.2.3 First Moment of the Stiffness Matrix

The first moment of the stiffness matrix of an isolator is a matrix which can be defined by its typical element b_{ij} which represents the resultant restoring force in the isolator, in direction i, due to a unit rotation of the isolated mass about an axis through the mass centroid in direction j. Further, since $c_{ij} = c_{ji}$, b_{ij} also represents the resultant moment of the restoring forces in the isolator about an axis through the mass centroid in direction j, due to a unit displacement of the mass centroid in direction i. Then using the Cartesian coordinate system as shown in Figure 3.2.4 for an isolator whose point of attachment is distant (r_1, r_2, r_3) from the centroid of the suspended mass, the [b] matrix is given by the vectorial relationship

$\vec{b} = \vec{c} \times \vec{r}$, that is:

$$\begin{aligned} b_{11} &= r_2c_{13}-r_3c_{12} & b_{12} &= r_3c_{11}-r_1c_{13} & b_{13} &= r_1c_{12}-r_2c_{11} \\ b_{21} &= r_2c_{23}-r_3c_{22} & b_{22} &= r_3c_{21}-r_1c_{23} & b_{23} &= r_1c_{22}-r_2c_{21} \\ b_{31} &= r_2c_{33}-r_3c_{32} & b_{32} &= r_3c_{31}-r_1c_{33} & b_{33} &= r_1c_{32}-r_2c_{31} \end{aligned} \qquad (18)$$

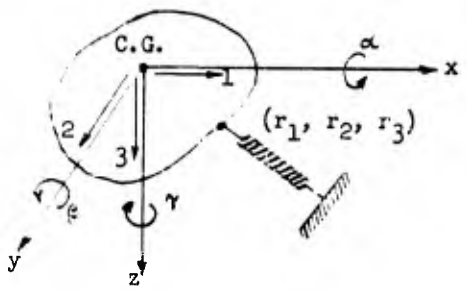

Figure 3.2.4
Coordinates of Isolator Attachment Point

For a linear isolator, the components of the restoring forces acting on the isolator in directions x, y, and z due to angular rotations δ_α δ_β and δ_γ at the mass centroid are as follows:

$$F_x = b_{11}\delta_\alpha + b_{12}\delta_\beta + b_{13}\delta_\gamma$$
$$F_y = b_{21}\delta_\alpha + b_{22}\delta_\beta + b_{23}\delta_\gamma \qquad (19)$$
$$F_z = b_{31}\delta_\alpha + b_{32}\delta_\beta + b_{33}\delta_\gamma$$

In matrix form $\{F\} = [b]\{\phi\}$ where $[b]$ is the first moment of the stiffness matrix of the isolator and is given by:

$$[b] = \begin{bmatrix} b_{11} & b_{12} & b_{13} \\ b_{21} & b_{22} & b_{23} \\ b_{31} & b_{32} & b_{33} \end{bmatrix} \qquad (20)$$

The components of the restoring moments of the isolator in directions α β and γ due to displacement δ_x, δ_y, and δ_z of the centroid of the mass are as follows:

$$M_x = b_{11}\delta_x + b_{21}\delta_y + b_{31}\delta_z$$
$$M_y = b_{12}\delta_x + b_{22}\delta_y + b_{32}\delta_z \qquad (21)$$
$$M_z = b_{13}\delta_x + b_{23}\delta_y + b_{33}\delta_z$$

In matrix form, $\{M\} = [b]^t\{s\}$ where $[b]^t$ is the transpose of the first moment of the stiffness matrix $[b]$. Since the first moment of the stiffness matrix is not necessarily symmetrical, $[b]$ is not necessarily equal to $[b]^t$. It is clearly seen that the $[b]$ matrix for a given isolator is completely defined by its related stiffness matrix $[c]$; and the location of the point of attachment of the isolator with respect to the centroid of the suspended mass, as defined by r_1, r_2, and r_3.

3.2.4 Second Moment of the Stiffness Matrix

The second moment of the stiffness matrix of an isolator is a matrix which can be defined by its typical element e_{ij} which represents the resultant moment of the restoring forces in the isolator about an axis through the mass centroid in direction i, due to a unit rotation of the isolated mass about an axis through the mass centroid in direction j. Then using the same Cartesian coordinate system as before, for an isolator whose point of attachment is distant (r_1, r_2, r_3) from the centroid of the suspended mass, it can be shown that

$$e_{11} = r_2b_{31} - r_3b_{21} \quad e_{12} = r_2b_{32} - r_3b_{22} \quad e_{13} = r_2b_{33} - r_3b_{23}$$
$$e_{21} = r_3b_{11} - r_1b_{31} \quad e_{22} = r_3b_{12} - r_1b_{32} \quad e_{23} = r_3b_{13} - r_1b_{33} \qquad (22)$$
$$e_{31} = r_1b_{21} - r_2b_{11} \quad e_{32} = r_1b_{22} - r_2b_{12} \quad e_{33} = r_1b_{23} - r_2b_{13}$$

For a linear isolator, the components of the moments of the restoring forces of the isolator in directions α, β, and γ produced by angular rotations δ_α, δ_β, and δ_γ are as follows:

$$\begin{aligned} M_x &= e_{11}\delta_\alpha + e_{12}\delta_\beta + e_{13}\delta_\gamma \\ M_y &= e_{21}\delta_\alpha + e_{22}\delta_\beta + e_{23}\delta_\gamma \\ M_z &= e_{31}\delta_\alpha + e_{32}\delta_\beta + e_{33}\delta_\gamma \end{aligned} \tag{23}$$

In the matrix form $\{M\} = [e]\{\phi\}$ where $[e]$ is the second moment of the stiffness matrix of the isolator and is given by

$$[e] = \begin{bmatrix} e_{11} & e_{12} & e_{13} \\ e_{21} & e_{22} & e_{23} \\ e_{31} & e_{32} & e_{33} \end{bmatrix} \tag{24}$$

The $[e]$ matrix is completely defined by its related stiffness matrix $[c]$ and the coordinates (r_1, r_2, r_3) of its point of attachment. It may be noted here that, for a group of isolators acting on the same mass,

$$[C] = \sum [c] \; ; \; [B] = \sum [b] \text{ and } [E] = \sum [e]$$

3.2.5 Restoring Force System Due to Isolators

From the definitions of a stiffness matrix, the first moment of a stiffness matrix, and the second moment of a stiffness matrix of an isolator, the total restoring force system due to a group of isolators acting on a rigid body whose centroid is displaced by the coordinates x, y, and z and rotated by angles α, β, and γ, is given by a resultant restoring force and a resultant restoring moment due to all the isolators, as follows:

$$\begin{bmatrix} F_x \\ F_y \\ F_z \end{bmatrix} = \begin{bmatrix} c_{11} & c_{12} & c_{13} \\ c_{21} & c_{22} & c_{23} \\ c_{31} & c_{32} & c_{33} \end{bmatrix} \begin{bmatrix} x \\ y \\ z \end{bmatrix} + \begin{bmatrix} b_{11} & b_{12} & b_{13} \\ b_{21} & b_{22} & b_{23} \\ b_{31} & b_{32} & b_{33} \end{bmatrix} \begin{bmatrix} \alpha \\ \beta \\ \gamma \end{bmatrix}$$

$$\begin{bmatrix} M_x \\ M_y \\ M_z \end{bmatrix} = \begin{bmatrix} b_{11} & b_{21} & b_{31} \\ b_{12} & b_{22} & b_{32} \\ b_{13} & b_{23} & b_{33} \end{bmatrix} \begin{bmatrix} x \\ y \\ z \end{bmatrix} + \begin{bmatrix} e_{11} & e_{12} & e_{13} \\ e_{21} & e_{22} & e_{23} \\ e_{31} & e_{32} & e_{33} \end{bmatrix} \begin{bmatrix} \alpha \\ \beta \\ \gamma \end{bmatrix}$$

or

$$\begin{aligned} \{F\} &= [C]\{S\} + [B]\{\phi\} \\ \{M\} &= [B]^t\{S\} + [E]\{\phi\} \end{aligned} \tag{25}$$

where $[C]$, $[B]$ and $[E]$ are evaluated as previously discussed. These equations are general and apply to any isolating system irrespective of its orientation provided the correct values of the components of the stiffness matrix are considered.

A few special cases, commonly encountered, are illustrated below, assuming the isolators to have axial stiffnesses only.

Springs in x direction:

$$[c]_x = \begin{bmatrix} c_{11} & 0 & 0 \\ 0 & 0 & 0 \\ 0 & 0 & 0 \end{bmatrix}_x$$

$$[b]_x = \begin{bmatrix} 0 & b_{12} & b_{13} \\ 0 & 0 & 0 \\ 0 & 0 & 0 \end{bmatrix}_x \qquad (b_{12}) = r_3 c_{11};\ (b_{13})_x = -r_2 c_{11}$$

$$[e]_x = \begin{bmatrix} 0 & 0 & 0 \\ 0 & e_{22} & e_{23} \\ 0 & e_{32} & e_{33} \end{bmatrix}_x \qquad (e_{22})_x = r_3 b_{12};\ (e_{23})_x = r_3 b_{13}$$
$$(e_{32})_x = -r_2 b_{12};\ (e_{33})_x = -r_2 b_{13}$$

Springs in y direction:

$$[c]_y = \begin{bmatrix} 0 & 0 & 0 \\ 0 & c_{22} & 0 \\ 0 & 0 & 0 \end{bmatrix}_y$$

$$[b]_y = \begin{bmatrix} 0 & 0 & 0 \\ b_{21} & 0 & b_{23} \\ 0 & 0 & 0 \end{bmatrix}_y \qquad (b_{21})_y = -r_3 c_{22};\ (b_{23})_y = r_1 c_{22}$$

$$[e]_y \qquad \begin{bmatrix} e_{11} & 0 & e_{13} \\ 0 & 0 & 0 \\ e_{31} & 0 & e_{33} \end{bmatrix}_y \qquad (e_{11})_y = -r_3 b_{21};\ (e_{13})_y = -r_3 b_{23}$$
$$(e_{31})_y = r_1 b_{21};\ (e_{33})_y = r_1 b_{23}$$

Springs in z direction:

$$[c]_z = \begin{bmatrix} 0 & 0 & 0 \\ 0 & 0 & 0 \\ 0 & 0 & c_{33} \end{bmatrix}_z$$

$$[b]_z = \begin{bmatrix} 0 & 0 & 0 \\ 0 & 0 & 0 \\ b_{31} & b_{32} & 0 \end{bmatrix}_z \qquad (b_{31})_z = r_2 c_{33};\ (b_{32})_z = -r_1 c_{33}$$

$$[e]_z = \begin{bmatrix} e_{11} & e_{12} & 0 \\ e_{21} & e_{22} & 0 \\ 0 & 0 & 0 \end{bmatrix}_z \qquad (e_{11})_z = r_2 b_{31};\ (e_{12})_z = r_2 b_{32}$$
$$(e_{21})_z = -r_1 b_{31};\ (e_{22})_z = -r_1 b_{32}$$

As a consequence there results:

$$[C] = \sum [c] = \begin{bmatrix} c_{11} & 0 & 0 \\ 0 & c_{22} & 0 \\ 0 & 0 & c_{33} \end{bmatrix} \qquad \begin{aligned} c_{11} &= \sum (c_{11})_x = K_x \\ c_{22} &= \sum (c_{22})_y = K_y \\ c_{33} &= \sum (c_{33})_z = K_z \end{aligned}$$

$$[B] = \sum [b] = \begin{bmatrix} 0 & B_{12} & B_{13} \\ B_{21} & 0 & B_{23} \\ B_{31} & B_{32} & 0 \end{bmatrix} \qquad \begin{aligned} B_{12} &= \sum (b_{12})_x,\ B_{13} = \sum (b_{13})_x \\ B_{21} &= \sum (b_{21})_y,\ B_{23} = \sum (b_{23})_y \\ B_{31} &= \sum (b_{31})_z,\ B_{32} = \sum (b_{32})_z \end{aligned}$$

$$[E] = \sum [e] = \begin{bmatrix} E_{11} & E_{12} & E_{13} \\ E_{21} & E_{22} & E_{23} \\ E_{31} & E_{32} & E_{33} \end{bmatrix} \qquad \begin{aligned} E_{11} &= \sum (e_{11})_y + \sum (e_{11})_z,\ E_{12} = \sum (e_{12})_z,\ E_{13} = \sum (e_{13})_y \\ E_{21} &= \sum (e_{21})_z,\ E_{22} = \sum (e_{22})_x + \sum (e_{22})_z,\ E_{23} = \sum (e_{23})_x \\ E_{31} &= \sum (e_{31})_y,\ E_{32} = \sum (e_{32})_x,\ E_{33} = \sum (e_{33})_x + \sum (e_{33})_y \end{aligned}$$

Then the total restoring force system due to all isolators becomes:

$$F_x = K_x\ x + \beta \sum (b_{12})_x + \gamma \sum (b_{13})_x$$
$$F_y = K_y\ y + \alpha \sum (b_{21})_y + \gamma \sum (b_{23})_y$$
$$F_z = K_z\ z + \alpha \sum (b_{31})_z + \beta \sum (b_{32})_z$$

$$M_x = y \sum (b_{21})_y + z \sum (b_{31})_z + \alpha \left(\sum (e_{11})_y + \sum (e_{11})_z\right) + \beta \sum (e_{12})_z + \gamma \sum (e_{13})_y$$
$$M_y = x \sum (b_{12})_x + z \sum (b_{32})_z + \alpha \sum (e_{21})_z + \beta \left(\sum (e_{22})_x + \sum (e_{22})_z\right) + \gamma \sum (e_{23})_x$$
$$M_z = x \sum (b_{13})_x + y \sum (b_{23})_y + \alpha \sum (e_{31})_y + \beta \sum (e_{32})_x + \gamma \left(\sum (e_{33})_x + \sum (e_{33})_y\right)$$

In particular, if the isolators are arranged in a symmetrical manner about the centroid of the mass system in each of the three coordinate directions, all points of attachment being co-planar with the centroid in a plane parallel to one of the reference planes, then:

$$F_x = K_x X$$
$$F_y = K_y Y$$
$$F_z = K_z Z$$
$$M_x = \alpha \sum (e_{11})_z$$
$$M_y = \beta \sum (e_{22})_z$$
$$M_z = \gamma \left\{ \sum (e_{33})_x + \sum (e_{33})_y \right\}$$

3.2.6 The Equations of Motion of Multidegree-of-Freedom Isolation Systems

The behavior of any isolated system can be regarded in general as that of a free body acted upon by the restoring forces developed by the isolators. The motion of such a general system can be conveniently defined by an instantaneous displacement of its centroid together with an instantaneous rotation of the entire system about its centroid, as compatible with the imposed constraints. Such a system possesses six-degrees-of-freedom, and can be defined by three generalized linear displacements and three generalized angular displacements.

Because of the physical characteristics of the isolators, it may be assumed that the system performs small oscillations about a stable position of equilibrium. The motion of the centroid of the system may be referred to an inertial reference system , whereas the motion of the system about its centroid may be referred to a moving reference system parallel to the former. The positive sense of both these reference systems is oriented counterclockwise and directed downward. The two systems of reference may be connected by various kinematic devices, such as in the pendulum, discussed later in the text.

The support to which the entire mechanical system is connected by the isolators is subjected to a transient impact of short duration. As a result, additional forces and moments are developed in the constraints. The isolated body may be assumed to be rigid without any loss of generality and for the purpose of setting up a mathematical model to describe as closely as possible the behavior of the physical system and its performance under shock. Then the general equations of motion of such a system are obtained by equating the inertia forces to the sum of the restoring forces that are due to the isolators and the gravity field (if any), and the constraint forces developed by the isolators due to the transient shock applied to the base.

The evaluation of these various forces is made by summarizing previous results as follows:

The Restoring Forces: Assuming no motion of the isolator supports, the forces acting at the center of mass and the moments about the center of mass due to the isolated system are given by equation (25) as follows:

$$\{F\} = [C]\{\bar{S}\} + [B]\{\tilde{\phi}\}$$

$$\{M\} = [B]^t\{\bar{S}\} + [E]\{\tilde{\phi}\}$$

The Forces of Constraint are developed by the isolators because of the shock transmitted to the system. The shock may be described by the associated displacement of the base $[S_o]$, and the rotation of the base $[\phi_o]$. Assuming no motion of the body, the forces of constraint due to motions of the isolated system supports may then be expressed similar to the restoring forces, as follows:

$$\{F_o\} = [C]\{\tilde{S}_o\} + [B]\{\tilde{\phi}_o\}$$

$$\{M_o\} = [B]^t\{\tilde{S}_o\} + [E]\{\tilde{\phi}_o\}$$

The Inertia Forces System as given by equation (5), is as follows:

$$\text{Dynamic Force} = [m]\{\ddot{\bar{S}}\}$$

$$\text{Dynamic Moment} = [I]\{\ddot{\tilde{\phi}}\}$$

The Equations of Motion are then obtained by the algebraic summation of the dynamic forces, the restoring forces, and the forces of constraint, and equating the sum to zero. Another set of equations is obtained by equating the sum of the moments due to these same forces to zero, as follows:

$$\begin{aligned} [m]\{\ddot{\tilde{s}}\} + [C]\{\tilde{s} - \tilde{s}_o\} + [B]\{\tilde{\phi} - \tilde{\phi}_o\} &= 0 \\ [I]\{\ddot{\tilde{\phi}}\} + [B]^t\{\tilde{s} - \tilde{s}_o\} + [E]\{\tilde{\phi} - \tilde{\phi}_o\} &= 0 \end{aligned} \tag{26}$$

Since the response spectrum of the shock is in terms of relative displacement, it is convenient to transform the above equations to relative coordinates by the relationship:

$$\begin{aligned} \vec{s} &= \vec{\tilde{s}} - \vec{\tilde{s}}_c \\ \vec{\phi} &= \vec{\tilde{\phi}} - \vec{\tilde{\phi}}_o \end{aligned}$$

The equations of motion in relative coordinates are

$$\begin{aligned} [m]\{\ddot{s}\} + [C]\{s\} + [B]\{\phi\} &= -[m]\{\ddot{s}_o\} \\ [I]\{\ddot{\phi}\} + [B]^t\{s\} + [B]\{\phi\} &= -[I]\{\ddot{\phi}_o\} \end{aligned} \tag{27}$$

The sign $\sim$ on the terms of the right hand side of the equations has been omitted for clarity and simplicity, without any loss of generality.

The above discussion pertains to small displacement theory only. If large displacements are anticipated, care must be taken in representing the configuration of the system and to incorporate any additionally required parameters in the equations of motion. Typical cases, where additional constraints may lead to large displacements, are the pendulum and the double pendulum. Additional equations and/or forces must be provided in such cases to more accurately describe the modified configuration. Moreover, since the orientation of the principal directions of the stiffness matrix will also be appreciably altered by large displacements, the stiffness matrix together with its first and second moments must be recalculated for the new condition.

3.2.7 Uncoupling Requirements for Multidegree-of-Freedom Systems

As already discussed, many shock isolated masses may be treated dynamically as simple rigid bodies supported in a gravity field by elastic constraints. When disturbed from rest, the resulting motion of the rigid body at any instant may be resolved into a translation of its centroid and a rotation about an instantaneous axis passing through its centroid. The vectors describing the translation and rotation will vary in time, both with respect to their magnitude and direction. The

equations of motion of this system, in matrix form are given by equation (27) as follows:

$$[m]\{\ddot{S}\} + [c]\{S\} + [B]\{\phi\} = -[m]\{\ddot{S}_o\}$$

$$[I]\{\ddot{\phi}\} + [B]^t\{S\} + [E]\{\phi\} = -[I]\{\ddot{\phi}_o\}$$

It is apparent from the above equations that the translational motion and the rotational motion are not independent, but are coupled.

The translation and the rotation may be made independent of one another, resulting in an uncoupled dynamic system, if the first moment of the stiffness matrix $[B]$ is zero. The equations of motion are then reduced to the form:

$$[m]\{\ddot{S}\} + [C]\{S\} = -[m]\{\ddot{S}_o\}$$

$$[I]\{\ddot{\phi}\} + [E]\{\phi\} = -[I]\{\ddot{\phi}_o\}$$

The condition $[B] = 0$ infers that the centroid of the stiffness matrix coincides with the centroid of the suspended mass.

The motions of the isolated mass in translation as well as rotation, although now decoupled, are still not completely independent since the components of $\vec{S}$, as well as the components of $\vec{\phi}$, are interrelated. To further simplify the motion of the system by making all of its coordinates independent of one another, it is necessary that the $[C]$, $[E]$, and $[I]$ matrices be diagonal, i.e:

$$[C] = \begin{bmatrix} \Sigma c_{11} & 0 & 0 \\ 0 & \Sigma c_{22} & 0 \\ 0 & 0 & \Sigma c_{33} \end{bmatrix}$$

$$[E] = \begin{bmatrix} \Sigma e_{11} & 0 & 0 \\ 0 & \Sigma e_{22} & 0 \\ 0 & 0 & \Sigma e_{33} \end{bmatrix}$$

$$[I] = \begin{bmatrix} I_{xx} & 0 & 0 \\ 0 & I_{yy} & 0 \\ 0 & 0 & I_{zz} \end{bmatrix}$$

The above conditions infer that the group of isolators have no shear components, and that the mass distribution is such that the resulting products of inertia vanish. The latter is valid if the reference axes are taken coincident with the principal axes of the suspended mass. The equations of motion now reduce to six independent equations:

$$m\ddot{x} + \Sigma c_{11} x = -m\ddot{x}_o \qquad I_{xx}\alpha + \Sigma e_{11}\ddot{\alpha} = -I_{xx}\ddot{\alpha}_o$$

$$m\ddot{y} + \Sigma c_{22} y = -m\ddot{y}_c \qquad I_{yy}\beta + \Sigma e_{22}\ddot{\beta} = -I_{yy}\ddot{\beta}_o$$

$$m\ddot{z} + \Sigma c_{33} z = -m\ddot{z}_o \qquad I_{zz}\gamma + \Sigma e_{33}\ddot{\gamma} = -I_{zz}\ddot{\gamma}_o$$

The design of a system satisfying the above conditions will be called a balanced design.

Summarizing the above results, the conditions for a balanced design are:

1. The centroid of the isolator system must coincide with the centroid of the suspended mass; i.e., the resultant restoring force from all the isolators must pass through the mass centroid.

2. The arrangement of mass about the center of gravity of the system must be such that the related products of inertia vanish; i.e., the reference system must be coincident with the principal axes of the suspended mass.

3. The isolators must be so arranged that the principal axes of the stiffness matrix are parallel to the principal axes of the suspended mass.

The physical significance of uncoupling may be illustrated by means of Figures 3.2.5 through 3.2.7.

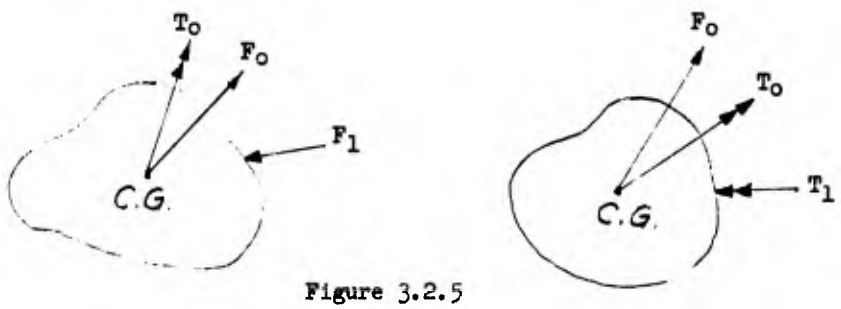

Figure 3.2.5

Restoring Forces on an Isolated Mass

In general, a force F_1 applied through the center of gravity of a constrained rigid body results in a resultant restoring force F_o through the center of gravity, not necessarily colinear with F_1, and a resultant moment T_o about the center of gravity. Likewise, an externally applied moment T_1 will produce a resultant restoring moment T_o, not necessarily in the same direction as T_1, and a resultant restoring force F_o through the center of gravity. (Figure 3.2.5.)

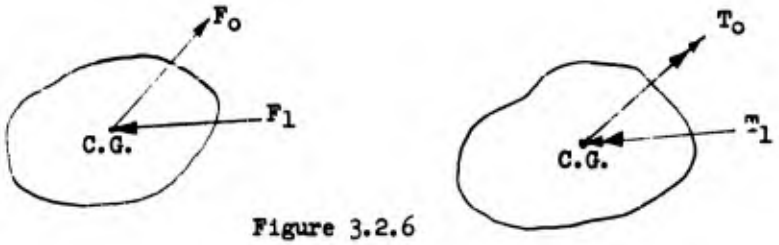

Figure 3.2.6

Restoring Forces on a Partially Uncoupled Isolated Mass

The first stage of uncoupling attempts to locate the isolators so that F_o results in a restoring force F_1, not necessarily colinear with F_o, but no restoring moment T_1. Likewise, T_o results in a restoring moment T_1, not necessarily in the same direction as T_o, but no restoring force F_1 (Figure 3.2.6).

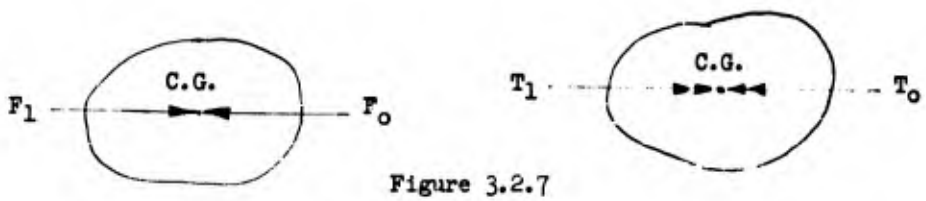

Figure 3.2.7

Restoring Forces on a Completely Uncoupled Isolated Mass

The second stage of uncoupling attempts to locate the isolators so that F_o results in a colinear resultant restoring force F_1, and no restoring moment; likewise T_o results in a resultant restoring moment T_1 colinear with T_o but no resultant restoring force. (Figure 3.2.7.)

The practical advantages of an uncoupled system are many. Of particular importance to the facility designer is the fact that, since the rotational component of ground shock is usually ignored in the

present state-of-the-art, an uncoupled isolation system will move only in translation, thus minimizing the rattlespace, providing a uniform acceleration at every point on the suspended mass, and simplifying tremendously the dynamic analysis. The latter advantage is of no little importance since the more complex analysis procedures are not only subject to greater numerical error, but also imply a greater knowledge of the system and the nature of the ground shock.

In actual applications, the design specifications may be such that only part or none of the above requirements can be satisfied because of particular or specific conditions imposed. In the differential equations of motion for such a case there will appear certain quantities, termed "eccentricities", representing the measure of the departure of the motion of the system from the ideal conditions as represented by a balanced design. If these eccentricities are small, compared with the principal geometric parameters defining the system, they may be ignored, thus leading to an approximate balanced design. However, if the eccentricities are significant, they must be conserved in the equations of motion, leading to a partially or totally coupled dynamic system. For a coupled system, the necessary rattlespaces to allow the mass to move freely under shock are usually far larger than those for uncoupled systems in which all the six degrees of freedom act independently.

3.3 Multimass Undirectional Systems

3.3.1 Dynamic Behavior of a Multimass System

A general multimass system consists of a number of rigid masses constrained in their motions relative to one another, by means of elements possessing stiffnesses, elastic or otherwise, linear or nonlinear. Each rigid mass of the multimass system theoretically commands a maximum of six degrees-of-freedom. Hence a system with 'n' rigid masses can enjoy a maximum of '6n' degrees-of-freedom. However, as often occurs in practice, the individual masses may be constrained, so that they are limited to less than six degrees-of-freedom each. A particular limiting case is considered in Section 3.3, in which all the masses are constrained to move in one and the same direction only; this is the "multimass unidirectional" case, where a system with 'n' masses possesses 'n' degrees-of-freedom. The 'n' coordinates defining the degrees-of-freedom of the system are the 'n' independent translations of the 'n' masses, as shown in Figure 3.3.1.

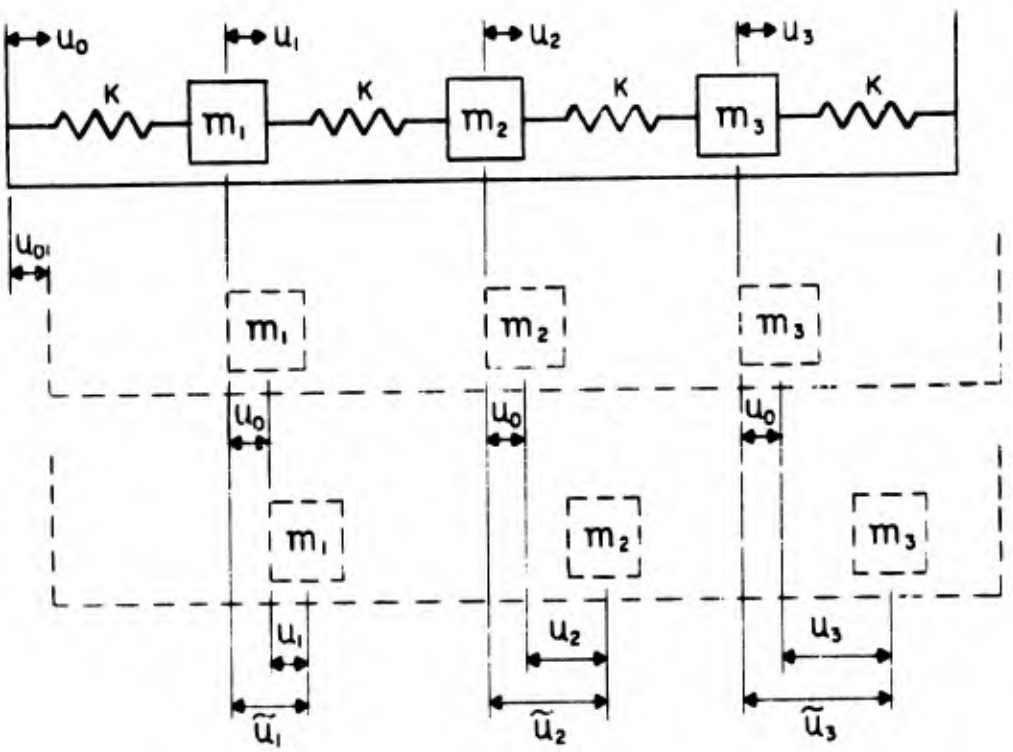

Figure No. 3.3.1

Multimass Undirectional System

3.3.2 Equations of Motion of Multimass Systems

A multimass system is governed by the same basic equations of motion as a single rigid body. The equations are set up considering each mass separately and applying to each the forces of constraint generated by the shock input, as well as by the disturbances transmitted by the adjoining masses coupled to it. The following example illustrates the procedure involved.

Considering each mass separately, the equations of motion in absolute coordinates are:

$$m_1 \ddot{\tilde{u}}_1 + K \dot{\tilde{u}}_1 - K u_o + K \tilde{u}_1 - K \tilde{u}_2 = 0$$

$$m_2 \ddot{\tilde{u}}_2 + K \dot{\tilde{u}}_2 - K \dot{\tilde{u}}_1 + K \tilde{u}_2 - K \tilde{u}_3 = 0$$

$$m_3 \ddot{\tilde{u}}_3 + K \dot{\tilde{u}}_3 - K \dot{\tilde{u}}_2 + K \tilde{u}_3 - K u_o = 0$$

Substituting:

$$\tilde{u}_1 = u_o + u_1$$

$$\tilde{u}_2 = u_o + u_2$$

$$\tilde{u}_3 = u_o + u_3$$

the equations are:

$$m_1 (\ddot{u}_1 + \ddot{u}_o) + 2K (\dot{\tilde{u}}_1 - u_o) - K (\tilde{u}_2 - u_o) = 0$$

$$m_2 (\ddot{u}_2 + \ddot{u}_o) - K (\dot{\tilde{u}}_1 - u_o) + 2K (\tilde{u}_2 - u_o) - K (\tilde{u}_3 - u_o) = 0$$

$$m_3 (\ddot{u}_3 + \ddot{u}_o) - K (\dot{\tilde{u}}_2 - u_o) + 2K (\tilde{u}_3 - u_o) = 0$$

The above equations in relative coordinates reduce to:

$$\begin{aligned} m_1\ddot{u}_1 + 2K u_1 - K u_2 &= -m_1\ddot{u}_o \\ m_2\ddot{u}_2 - K u_1 + 2K u_2 - K u_3 &= -m_2\ddot{u}_o \\ m_3\ddot{u}_3 - K u_2 + 2K u_3 &= -m_3\ddot{u}_o \end{aligned} \qquad (28)$$

In matrix form

$$[m]\{\ddot{u}\} + [K]\{u\} = -[m]\{\ddot{u}_o\}$$

This is the same form as a multidirectional system and has the same type of solution as will be shown later. Hence, no particular distinction need be made between multidirectional and multimass systems, except for the slightly modified approach in setting up the equations of motion.

3.4 Forced Response of a Single-Degree-of-Freedom Linear System

3.4.1 Undamped System

The single-degree-of-freedom system has been treated here, not so much as an example of practical interest, but as a step towards the treatment of a multidegree of freedom system. Voluminous literature (References 3.3-3.11) exists on the treatment of single-degree-of-freedom linear systems for those interested in the fundamentals of the subject. Considering the spring-mass system of Figure 3.4.1, the equation of motion is given as

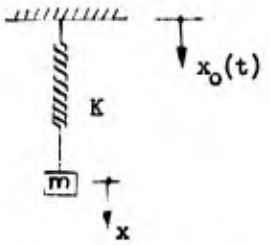

Figure 3.4.1
Undamped Single-Degree-of-Freedom
Linear System

$$m \ddot{\tilde{x}} + K \tilde{x} = K \tilde{x}_o (t)$$

where $\sim$ signifies absolute coordinates. However, since $\tilde{x} = x + x_o$, the equation of motion in relative coordinates is

$$m \ddot{x} + K x = - m \ddot{x}_o (t)$$

or

$$\ddot{x} + \frac{K}{m} x = \ddot{x}_o (t) \qquad (29)$$

Substituting $\omega_n^2 = \frac{K}{m}$ = natural frequency of the system, the solution of the above differential equation is

$$x = \frac{1}{\omega_n} \int_o^t \ddot{x}_o (\tau) \sin \omega_n (t - \tau) \lambda \tau$$

However, since the shock input is defined by a response spectrum, by definition, $|x_{max}|$ = response spectrum relative displacement corresponding to frequency ω_n = the required rattlespace = $|D_n|$.

The method of Laplace Transformation has been introduced later in the text, for solving multidegree-of-freedom systems. Hence it is deemed appropriate to compare the solution obtained above with the solution obtained by using Laplace Transformation. As was obtained previously (equation 29),

$$\ddot{x} + \omega_n^2 x = - \ddot{x}_o$$

The conversion of this equation from the time domain (t) to the complex frequency domain (s) is accomplished by the Laplace Transform

$$s \int_o^\infty e^{-st} dt$$

where $s^2 = -\omega^2$. This is necessary since the shock input is usually defined by a response spectrum which is a function of the frequency ω, and not of t. Therefore, in Laplace form, assuming initial velocity and displacement to be zero (Reference 3.3),

$$s^2 \bar{x} + \omega_n^2 \bar{x} = -\mathcal{L}\, \ddot{x}_o$$

where $\mathcal{L}\, \ddot{x}_o$ is the Laplace Transform of $\ddot{x}_o$.

$$\therefore \quad \bar{x} = -\frac{1}{s^2 + \omega_n^2}\, \mathcal{L}\, \ddot{x}_o$$

$$\therefore \quad x = \mathcal{L}^{-1}\left(-\frac{1}{s^2 + \omega_n^2}\, \mathcal{L}\, \ddot{x}_o\right)$$

But $|x_{max}| = |D_n|$

$$\therefore \left|\mathcal{L}^{-1} \frac{1}{s^2 + \omega_n^2}\, \mathcal{L}\, \ddot{x}_o\right| = |D_n| \qquad (30)$$

That is, the inverse Laplace transformation of $-\frac{1}{s^2 + \omega_n^2}\, \mathcal{L}\, \ddot{x}_o$ represents the maximum displacement of mass m for a natural frequency ω_n. The result will be used later in dealing with multidegree-of-freedom systems.

3.4.2 Damped System

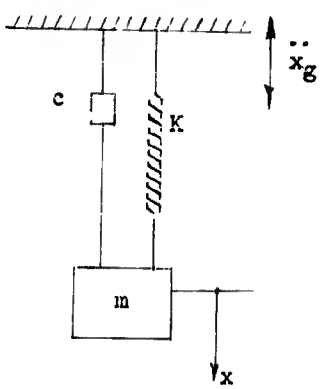

Figure 3.4.2
Damped Single-Degree-of-Freedom
Linear System

The equation of motion for a damped linear system as shown in Figure 3.4.2, is given in relative coordinates (Reference 3.4).

$$m\ddot{x} + c\dot{x} + Kx = -m\ddot{x}_o$$

where c is the coefficient of damping.

Let $\frac{c}{m} = 2n$, $\frac{K}{m} = \omega_n^2$

then

$$\ddot{x} + 2n\dot{x} + \omega_n^2 x = -\ddot{x}_o \tag{31}$$

Or, introducing the concept of critical damping, i.e., damping at which $n = \omega_n$, the above equation reduces to

$$\ddot{x} + 2\delta\omega_n\dot{x} + \omega_n^2 x = -\ddot{x}_o \tag{31a}$$

where

$$\delta = \frac{c}{c_{cr}} \text{ and } c_{cr} = \text{critical damping} = 2\sqrt{Km.}$$

Applying the Laplace transformation as before, the equation of motion for the damped case reduces to

$$(s^2 + 2\delta\omega_n s + \omega_n^2)\bar{x} = -\mathcal{L}\ddot{x}_o$$

The roots of the characteristic equation

$$s^2 + 2\delta\omega_n s + \omega_n^2 = 0$$

are

$$s = a \pm ib$$

where $a = -\delta\omega_n$

$$b = 2\omega_n\sqrt{1-\delta^2}$$

$$\therefore \left[(s - a - ib)(s - a + ib)\right]\bar{x} = -\mathcal{L}\ddot{x}_o$$

or

$$\left[(s-a)^2 + b^2\right]\bar{x} = -\mathcal{L}\ddot{x}_o$$

$$\therefore \bar{x} = \frac{-\mathcal{L}\ddot{x}_o}{(s-a)^2 + b^2}$$

$$x = \mathcal{L}^{-1}\frac{-\mathcal{L}x_o}{\left[(s-a)^2 + b^2\right]} \tag{32}$$

Here $|x|_{max}$ is given by a response spectrum at a damped frequency b^2 and damping represented by the quantity 'a'. It may be noted that when damping is not present the above result reduces to

$$x = \frac{\mathcal{L}^{-1}\left[-\ddot{x}_o\right]}{s^2 + \omega_n^2}$$

which is the same as equation (30).

3.5 Forced Response of Multi-Degree-of-Freedom Linear Systems

3.5.1 Dynamic Stability

A dynamic system, moving under the action of applied forces, is described by a set of differential equations. The solution of these differential equations explicitly defines the motion of the system as a function of time. Small disturbing influences applied to the system may cause it to deviate only slightly from the previous condition of motion, or they may cause it to depart further from this condition of motion. If the deviation is slight, the system is said to be dynamically stable. If the motion continues to increase with time, the system is said to be dynamically unstable. A system is considered dynamically stable only if it is stable for all kinds of disturbances that it is likely to experience.

In case of linear systems, i.e. systems capable of being defined by a set of linear ordinary differential equations, it is not necessary to determine the actual motion of the system in order to determine its stability. The stability criteria for linear systems, as defined by the Routh-Hurwitz stability criteria in Appendix 3.9E is a function of the physical parameters of the system, such as the linear dimensions, the mass and moment of inertia, and the stiffness of the various elements of the system. However, for nonlinear systems, the stability is dependent on the input to the system as well as discussed in paragraph 3.6.2.2.J.

3.5.2 Damping

In order to have better agreement with actual physical conditions, analytical discussions of dynamical problems lead to the consideration of damping forces. Damping forces arise from several different sources, but may be classified into two main groups; a) the internal or structural damping forces, which are an inherent part of the system, and b) the applied damping forces, i.e. artificially created damping forces, in conformity with the requirements of the system. As shown in 3.4.1, the Laplace Method used in the test can easily be modified to consider damping as long as the equations of motion remain linear. In that case, however, since the usual spectrum is based on the response of undamped or lightly damped systems, the spectrum must be modified to incorporate damping. Fung (Reference 3.12, page 225) states that the difference in the peak responses of an undamped system, and one containing 6% to 7% of critical damping is small and can be neglected in most practical cases. This is not strictly true, since the amount of shock spectrum modification due to damping will depend on the type of shock waveform being considered. Indications exist, although not yet rigorously verified that the shock spectrum due to a type II waveform, as discussed in Section 2.0, could be appreciably effected by damping.

3.5.3 Methods of Analysis

Two methods are presented for solving the matrix equations describing the motion of multidegree-of-freedom linearly elastic, undamped systems to an impulsive motion of the base. The Normal Mode (Modal) Method and the Laplace Method are formulated in general terms and illustrated by means of the same numerical example. The results yielded by the two methods are identical, the only difference being in mathematical representation.

3.5.3.1 Normal Mode Method

In reference 3.13 Young considers an undamped linear system with n degrees of freedom subjected to a shock. The equations of motion in absolute coordinates are:

$$[m]\{\ddot{u}_a\} + [K]\{u_a\} = [K]\{u_o\} \qquad (33)$$

where the n equations of motion are expressed in a single matrix equation. Here

$[m]$ = mass or inertia matrix
$\{\ddot{u}_a\}$ = absolute acceleration matrix
$\{u_a\}$ = absolute displacement matrix
$[K]$ = stiffness matrix
$\{u_o\}$ is the column matrix of ground motion displacement.

Since the rattlespace is defined in relative coordinates, it is necessary to convert Equation (33) accordingly. Hence, by performing the transformation $u = u_a - u_o$, where u represents the relative displacement of the masses, the matrix equation of motion in relative coordinates is

$$[m]\{\ddot{u}\} + [K]\{u\} = [-m]\{\ddot{u}_o\} \qquad (34)$$

where,

$\{\ddot{u}_o\}$ is the column matrix of ground motion acceleration
$\{u\}$ is the relative displacement column matrix
$\{\ddot{u}\}$ is the relative acceleration column matrix

Using the concept of normal coordinate q and the modal matrix $[\phi]$, as in reference 3.13 we have the relationship $\{u\} = [\phi]\{q\}$; and the matrix equation of motion in relative coordinates is

$$[m][\phi]\{\ddot{q}\} + [K][\phi]\{q\} = -[m]\{\ddot{u}_o\} \qquad (35)$$

where,

$\{\ddot{q}\}$ is the acceleration matrix in normal coordinates
$[\phi]$ is the modal matrix
$\{q\}$ is the (n by 1) displacement matrix in normal coordinates

Equation (35) can be modified as follows:

$$\{\ddot{q}\} + [\phi]^{-1}[m]^{-1}[K]\,[\phi]\,\{q\} = -\,[\phi]^{-1}\{\ddot{u}_o\}$$

but $[\phi]^{-1}\,[m]^{-1}\,[K]\,[\phi] = [\omega_n{}^2]$ = the diagonal frequency matrix

$$\therefore \quad \{\ddot{q}\} + [\omega_n{}^2]\,\{q\} = -[\phi]^{-1}\{\ddot{u}_o\} \qquad (36)$$

Considering for the sake of illustration a three-degree-of-freedom system,

$$\text{Let } [\phi]^{-1} = \begin{bmatrix} \phi'_{11} & \phi'_{12} & \phi'_{13} \\ \phi'_{21} & \phi'_{22} & \phi'_{23} \\ \phi'_{31} & \phi'_{32} & \phi'_{33} \end{bmatrix} = \begin{bmatrix} \{\gamma_1\} \\ \{\gamma_2\} \\ \{\gamma_3\} \end{bmatrix}$$

$$\text{where } \{\gamma_1\} = \{\phi'_{11} \quad \phi'_{12} \quad \phi'_{13}\}$$
$$\{\gamma_2\} = \{\phi'_{21} \quad \phi'_{22} \quad \phi'_{23}\}$$
$$\{\gamma_3\} = \{\phi'_{31} \quad \phi'_{32} \quad \phi'_{33}\}$$

The solution of Equation (36) is given by

$$q_n = \{\phi'_{n1} \quad \phi'_{n2} \quad \phi'_{n3}\} \begin{bmatrix} -\frac{1}{\omega_n}\int_o^t \ddot{u}_{1_o}(\tau)\sin\omega_n(t-\tau)\,d\tau \\ -\frac{1}{\omega_n}\int_o^t \ddot{u}_{2_o}(\tau)\sin\omega_n(t-\tau)\,d\tau \\ -\frac{1}{\omega_n}\int_o^t \ddot{u}_{3_o}(\tau)\sin\omega_n(t-\tau)\,d\tau \end{bmatrix}_{n=1,2,3}$$

To solve the above equation and obtain the response in time, the time-history of the shock must be known. Using the shock response spectrum, only the peak absolute response $|q_n|_{max}$ can be estimated by

$$|q_n|_{max} = \{\phi'_{n1} \quad \phi'_{n2} \quad \phi'_{n3}\} \begin{bmatrix} D_{n1} \\ D_{n2} \\ D_{n3} \end{bmatrix} = \{\gamma_n\} \{D_n\}$$

where D_{ij} is the peak displacement indicated by the given shock spectrum, in direction j, at the mode frequency ω_i.

$$\therefore \quad \{q\}_{max} = \left\{ \{\gamma_1\} \{D_1\} \{\gamma_2\} \{D_2\} \{\gamma_3\} \{D_3\} \right\} \qquad (37)$$

then $$\{u\}_{max} = [\phi] \{q\}_{max}$$

$$= [\phi] \left\{ \{\gamma_1\} \{D_1\} \{\gamma_2\} \{D_2\} \{\gamma_3\} \{D_3\} \right\} \qquad (38)$$

The above equation for maximum response assumes the peak displacements in all the directions occurs at the same time, i.e. phasing is ignored.

A special case arises when the shock input is the same in all directions, as in the example worked out later (Figure 3.5.1), in which case

say $D_{i1} = D_{i2} = D_{i3} = D_{ii}$

$$(q_1)_{max} = (\phi'_{11} + \phi'_{12} + \phi'_{13}) \quad (D_{11})$$

$$(q_2)_{max} = (\phi'_{21} + \phi'_{22} + \phi'_{23}) \quad (D_{22})$$

$$(q_3)_{max} = (\phi'_{31} + \phi'_{32} + \phi'_{33}) \quad (D_{33})$$

substituting $\phi'_{11} + \phi'_{12} + \phi'_{13} = \gamma_{11}$

$$\phi'_{21} + \phi'_{22} + \phi'_{23} = \gamma_{22}$$

$$\phi'_{31} + \phi'_{32} + \phi'_{33} = \gamma_{33}$$

Equation (37) becomes:

$$\begin{bmatrix} q_1 \\ q_2 \\ q_3 \end{bmatrix}_{max} = \begin{bmatrix} \gamma_{11} & 0 & 0 \\ 0 & \gamma_{22} & 0 \\ 0 & 0 & \gamma_{33} \end{bmatrix} \begin{bmatrix} D_{11} \\ D_{22} \\ D_{33} \end{bmatrix}$$

or $$\{q\}_{max} = [\gamma] \{D\}$$

$$\text{then } \{u\}_{max} = [\phi][\gamma]\{D\} \qquad (39)$$

where $[\gamma]$ is commonly referred to as the modal participation factor matrix (Reference 3.13). Each dimensionless element of $[\gamma]$ represents the magnitude of the contribution of the mode it governs, toward the entire motion.

γ_{nn} is given by the formula (reference 3.13).

$$\gamma_{nn} = \frac{\sum_{i=1}^{n} m_i \phi_{in}}{\sum_{i=1}^{n} \phi_{in} m_i \phi_{in}}$$

For example, calculate the response to a ground shock response spectrum of the undamped three-degree-of-freedom system shown (Figure 3.5.1).

$m_1 = m$
$m_2 = 2m$
$m_3 = 3m$

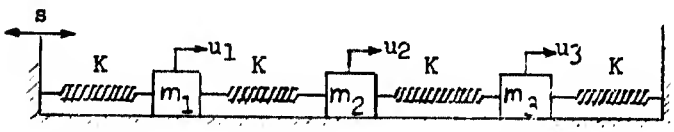

Figure 3.5.1
Multimass, Undirectional System

Step No. 1: Calculate the three natural frequencies corresponding to the three principal modes of vibration.

The equations of motion in relative coordinates will be

$$m_1 \ddot{u}_1 + 2Ku_1 - Ku_2 = 0$$

$$m_2 \ddot{u}_2 - Ku_1 + 2Ku_2 - Ku_3 = 0$$

$$m_3 \ddot{u}_3 - Ku_2 + 2Ku_3 = 0$$

If we let $u_i = A_i \sin(\omega_i t + \theta)$, the above equations can be rewritten as follows

$$\begin{bmatrix} 2K - m_1\omega_i^2 & -K & 0 \\ -K & 2K - m_2\omega_i^2 & -K \\ 0 & -K & 2K - m_3\omega_i^2 \end{bmatrix} \begin{bmatrix} A_1 \\ A_2 \\ A_3 \end{bmatrix} = \begin{bmatrix} 0 \\ 0 \\ 0 \end{bmatrix} \qquad (40)$$

The above equation has a nontrivial solution only if the determinant of the three-by-three frequency matrix is zero. Substituting the values of mass, and denoting $p^2 = \frac{K}{m}$, the determinant is given by

$$\omega^6 - \frac{11}{3} p^2 \omega^4 + \frac{10}{3} p^4 \omega^2 - \frac{2}{3} p^6 = 0$$

The solution of this polynomial is:

$$\omega_1^2 = 0.279\, p^2$$
$$\omega_2^2 = p^2$$
$$\omega_3^2 = 2.387\, p^2$$

These are the three natural frequencies of vibration of the system.

Step No. 2: Calculate the modal matrix of the system. Substituting the first frequency ($\omega_1^2 = 0.279\, p^2$) in Equation (40), we get

$$\phi_{11} = \frac{A_1}{A_1} = 1.0; \quad \phi_{21} = \frac{A_2}{A_1} = 1.7208; \quad \phi_{31} = \frac{A_3}{A_1} = 1.4805$$

Similarly for $\omega_2^2 = p^2$ and $\omega_3^2 = 2.387\, p^2$, we get

$$\phi_{11} = \frac{A_1}{A_1} = 1.0; \quad \phi_{21} = \frac{A_2}{A_1} = 1.00; \quad \phi_{31} = \frac{A_3}{A_1} = 1.0$$
$$\phi_{11} = \frac{A_1}{A_1} = 1.0; \quad \phi_{21} = \frac{A_2}{A_1} = 0.3874; \quad \phi_{31} = \frac{A_3}{A_1} = 0.0751$$

Hence the modal matrix is given by

$$[\phi] = \begin{bmatrix} \phi_{11} & \phi_{12} & \phi_{13} \\ \phi_{21} & \phi_{22} & \phi_{23} \\ \phi_{31} & \phi_{32} & \phi_{33} \end{bmatrix} = \begin{bmatrix} 1.0 & 1.0 & 1.0 \\ 1.7208 & 1.0 & -0.3874 \\ 1.4805 & -1.0 & 0.0751 \end{bmatrix}$$

Step No. 3: Calculate the modal participation factor γ . This is given by the expression

$$\gamma_{nn} = \frac{\sum_{i=1}^{n} m_i \phi_{in}}{\sum_{i=1}^{n} \phi_{in} m_i \phi_{in}}$$

Hence

$$\gamma_{11} = \frac{(m)(1) + (2m)(1.7208) + (3m)(1.4805)}{(m)(1)^2 + (2m)(1.7208)^2 + (3m)(1.4805)^2} = 0.66$$

$$\gamma_{22} = \frac{(m)(1) + (2m)(1) + (3m)(-1)}{(m)(1)^2 + (2m)(1)^2 + (3m)(-1)^2} = 0.0$$

$$\gamma_{33} = \frac{(m)(1) + (2m)(-0.3874) + (3m)(0.0751)}{(m)(1)^2 + (2m)(-0.3874)^2 + (3m)(0.0751)^2} = 0.345$$

Hence

$$[\gamma] = \begin{bmatrix} 0.66 & 0 & 0 \\ 0 & 0 & 0 \\ 0 & 0 & 0.345 \end{bmatrix}$$

Step No. 4: Calculate the response of the system to the given shock. From Equation (39)

$$\{u_{max}\} = [\phi]\,[\gamma]\,\{D_n\}$$

$$\therefore \begin{bmatrix} u_1 \\ u_2 \\ u_3 \end{bmatrix} = \begin{bmatrix} 1 & 1 & 1 \\ 1.7208 & 1 & -0.3874 \\ 1.4805 & -1 & 0.0751 \end{bmatrix} \begin{bmatrix} 0.66 & 0 & 0 \\ 0 & 0 & 0 \\ 0 & 0 & 0.345 \end{bmatrix} \begin{bmatrix} D_1 \\ D_2 \\ D_3 \end{bmatrix}$$

Since D_1, D_2, and D_3 are the undamped relative displacements, as given by the response spectrum for frequencies ω_1, ω_2, and ω_3, respectively, u_1, u_2, and u_3 are obtained.

3.5.3.2 Laplace Method

Referring to equation (36), the motion is given by the matrix equation

$$\{\ddot{q}\} + [\omega_n^2]\{q\} = -[\phi]^{-1}\{\ddot{u}_o\}$$

The conversion of this equation from the time domain 't' to the complex frequency domain 's' is accomplished by the Laplace Transform,

$$s \int_o^\infty e^{-st}\, dt \qquad \text{where } s^2 = -\omega^2$$

The new equation for initial conditions, $t(o) = q(o) = \dot{q}(o)$ is

$$-[\omega^2]\{\bar{q}\} + [\omega_n^2]\{\bar{q}\} = -[\phi]^{-1}\mathcal{L}\{\ddot{u}_o\}$$

$$\text{or } \{\bar{q}\} = -\left(-[\omega^2] + [\omega_n^2]\right)^{-1}[\phi]^{-1}\mathcal{L}\{\ddot{u}_o\}$$

This is no longer a differential equation but an algebraic equation in matrix form.

$$\text{Then } \{\bar{u}\} = [\phi]\{\bar{q}\} = -[\phi]\left(-[\omega^2] + [\omega_n^2]\right)^{-1}[\phi]^{-1}\mathcal{L}\{\ddot{u}_o\}$$

$$\therefore \{u\} = -[\phi]\mathcal{L}^{-1}\left\{\left(-[\omega^2] + [\omega_n^2]\right)^{-1}[\phi]^{-1}\mathcal{L}\{\ddot{u}_o\}\right\}$$

This is essentially the same result as obtained previously by the Modal Method, since the quantity $\mathcal{L}^{-1}\left\{\left(-[\omega^2] + [\omega_n^2]\right)^{-1}\mathcal{L}\{\ddot{u}_o\}\right\}$ is the spectral representation of the shock input. The Laplace Method is extended to more complicated cases later in this section.

To demonstrate the use of the Laplace Method, solve the same numerical example as before. The equations of motion in relative coordinates are:

$$[m]\{\ddot{u}\} + [K]\{u\} = -[m]\{\ddot{u}_o\}$$

Converting, in Laplace form, to the complex frequency domain $s = j\omega$ the equations become:

$$\begin{aligned}
s^2\bar{U}_1 + 2p^2\bar{U}_1 - p^2\bar{U}_2 &= -s^2\bar{U}_o \\
2s^2\bar{U}_2 - p^2\bar{U}_1 + 2p^2\bar{U}_2 - p^2\bar{U}_3 &= -2s^2\bar{U}_o \\
3s^2\bar{U}_3 - p^2\bar{U}_2 + 2p^2\bar{U}_3 &= -3s^2\bar{U}_o
\end{aligned}$$

In matrix form:

$$\begin{bmatrix} s^2+2p^2 & -p^2 & 0 \\ -p^2 & 2s^2+2p^2 & -p^2 \\ 0 & -p^2 & 3s^2+2p^2 \end{bmatrix} \begin{bmatrix} \bar{U}_1 \\ \bar{U}_2 \\ \bar{U}_3 \end{bmatrix} = - \begin{bmatrix} s^2\bar{U}_o \\ 2s^2\bar{U}_o \\ 3s^2\bar{U}_o \end{bmatrix}$$

or

$$[W] \quad [\bar{U}] \quad = \quad -[\bar{U}_o] \tag{41}$$

Where $[W]$ is the frequency matrix. The determinant of $[W]$ equated to zero gives a sixth order polynomial in s, the solution of which yields

$$-s_1^2 = -(j\omega_1)^2 = \omega_1^2 = 0.279p^2$$

$$-s_2^2 = -(j\omega_2)^2 = \omega_2^2 = p^2$$

$$-s_3^2 = -(j\omega_3)^2 = \omega_3^2 = 2.387p^2$$

The solution of the problem is given by

$$[\bar{U}] = -[W]^{-1} [\bar{U}_o] \tag{42}$$

Inverting the frequency matrix $[W]$

$$[W]^{-1} = \frac{1}{6(s^2+0.279p^2)(s^2+p^2)(s^2+2.387p^2)} \begin{bmatrix} 6s^4+10s^2p^2+3p^4 & 3s^2p^2+2p^4 & p^4 \\ 3s^2p^2+2p^4 & 3s^4+8s^2p^2+4p^4 & s^2p^2+2p^4 \\ p^4 & s^2p^2+2p^4 & 2s^4+6s^2p^2+3p^4 \end{bmatrix}$$

Substituting the value of $[W]^{-1}$ and expanding the equations, there remains the following set:

$$\bar{U}_1 = -\frac{6s^4+16s^2p^2+10p^4}{6(s^2+0.279p^2)(s^2+p^2)(s^2+2.387p^2)} s^2\bar{U}_o$$

$$\bar{U}_2 = -\frac{6s^4+22s^2p^2+16p^4}{6(s^2+0.279p^2)(s^2+p^2)(s^2+2.387p^2)} s^2\bar{U}_o$$

$$\bar{U}_3 = -\frac{6s^4+20s^2p^2+14p^4}{6(s^2+0.279p^2)(s^2+p^2)(s^2+2.387p^2)} s^2\bar{U}_o$$

Expanding the above into partial fractions:

$$\bar{U}_1 = -\left[\frac{0.66}{(s^2+0.279p^2)} + \frac{0}{(s^2+p^2)} + \frac{0.345}{(s^2+2.387p^2)}\right] s^2\bar{U}_o$$

$$\bar{U}_2 = -\left[\frac{1.135}{(s^2+0.279p^2} + \frac{0}{(s^2+p^2)} - \frac{0.132}{(s^2+2.387p^2)}\right] s^2\bar{U}_o$$

$$\bar{U}_3 = -\left[\frac{0.972}{(s^2+0.279p^2} + \frac{0}{(s^2+p^2} + \frac{0.027}{(s^2+2.387p^2)}\right] s^2\bar{U}_o$$

In matrix form

$$\begin{bmatrix}\bar{U}_1\\ \bar{U}_2\\ \bar{U}_3\end{bmatrix} = -\begin{bmatrix}0.66 & 0 & 0.345\\ 1.135 & 0 & -0.132\\ 0.972 & 0 & 0.027\end{bmatrix}\begin{bmatrix}\frac{s^2\bar{U}_o}{s^2+0.279p^2}\\ \frac{s^2\bar{U}_o}{s^2+p^2}\\ \frac{s^2\bar{U}_o}{s^2+2.387p^2}\end{bmatrix}$$

Converting to normalized form, the result previously obtained

$$\begin{bmatrix}\bar{U}_1\\ \bar{U}_2\\ \bar{U}_3\end{bmatrix} = -\begin{bmatrix}1.00 & 1.00 & 1.00\\ 1.721 & 1.00 & -0.387\\ 1.481 & -1.00 & 0.0751\end{bmatrix}\begin{bmatrix}0.66 & 0 & 0\\ 0 & 0 & 0\\ 0 & 0 & 0.345\end{bmatrix}\begin{bmatrix}\frac{s^2\bar{U}_o}{s^2+o.279p^2}\\ \frac{s^2\bar{U}_o}{s^2+p^2}\\ \frac{s^2\bar{U}_o}{s^2+2.387p^2}\end{bmatrix}$$

Hence there is obtained directly:

$$\begin{bmatrix}1.00 & 1.00 & 1.00\\ 1.721 & 1.00 & -0.387\\ 1.481 & -1.00 & 0.0751\end{bmatrix} = \text{the modal matrix}$$

$$\begin{bmatrix}0.66 & 0 & 0\\ 0 & 0 & 0\\ 0 & 0 & 0.345\end{bmatrix} = \text{the modal participation factor}$$

Now, in place of $\frac{s^2\overline{U}_o}{s^2+0.279p^2}$, substitute the maximum relative displacement of shock spectrum for $\omega^2 = 0.279p^2$. Similarly for $s^2\overline{U}_o/s^2+p^2$, substitute the maximum relative displacement corresponding to $\omega^2 = p^2$ and for $s^2\overline{U}_o/s^2+2.385p^2$ that due to $\omega^2 = 2.385p^2$

Next, solve the matrix equation for U_1, U_2, and U_3, giving the required displacements in relative coordinates, i.e., the rattle space.

3.5.3.3 Comparison of Normal Mode and Laplace Methods

The Modal Method, as formulated by Young, is applicable only to systems with unidirectional inputs, whereas the Laplace method is a general method applicable to both multimass and multidirectional systems. Furthermore, the Laplace method has greater adaptability for use on an electronic digital computer, thus lending itself to greater speed and accuracy in computation. Hence, for the purposes of this Design Guide, the Laplace method has been used and is strongly recommended. The basic approximation for both methods lies in the maximax (see Reference 3.13 for definition) evaluation of the response, which is based on a conservative assumption that the maximum contribution of each participating mode occurs at the same instant of time. This disregard for the existence of phasing of the modal peaks, gives an upper bound of the estimated peak response of the system.

3.5.4 Procedure to calculate the peak response of a linearly isolated, nonpendulous mass using a response spectrum.

Step No. 1: Determine the location of the center of gravity of the mass to be isolated. Determine the principal axes of the mass, that is, the set of three orthogonal axes about which the product of inertia terms such as I_{xy}, are all zero.

Step No. 2: With these principal axes as the reference system, set up the equations of dynamic equilibrium, using formulas for the [B] and [E] matrices as previously discussed.

Step No. 3: As a first approximation, ignoring the possible eccentricities, compute the isolator stiffnesses necessary so that the suspended mass conforms approximately to rattlespace, acceleration, velocity or frequency requirements for the system. It may be noted that, by ignoring eccentricities, the equations are reduced to six single-degree-of-freedom equations for this first approximation. Hence, the response spectrum can be used directly to make a reasonable estimate of the spring stiffnesses.

Step No. 4: Using the numerical values of the spring stiffnesses obtained in Step 3, and considering all the eccentricity terms, convert the six equations to the Laplace form. A matrix formulation of these equations gives a 6-by-6 frequency matrix, multiplied by a 6-by-1 column

matrix of the six unknown response parameters, on the left-hand side of the matrix equation; and a 6-by-1 column matrix consisting of the shock input in the six coordinate directions of the system, on the right-hand side of the matrix equation.

Step No. 5: Evaluate the determinant of the 6-by-6 frequency matrix formed from the six equations of Step 4. The expanded determinant will be a sixth order polynomial in s^2. The six roots of this polynomial equated to zero give the six natural frequencies of the system, it being remembered that $s^2 = -\omega^2$.

Step No. 6: Check the polynomial of Step 5 for dynamic stability by the Routh-Hurwitz stability criterion as discussed in Appendix 3-E.

Step No. 7: Evaluate the six natural frequencies of the system, as described in Step 5. For small eccentricities, these will not be appreciably different from the frequencies obtained by ignoring the eccentricities.

Step No. 8: Invert the frequency matrix of Step 4. The inverted matrix will have its elements in the form of a division of a fifth order polynomial in s^2, by the sixth order determinant polynomial obtained in Step 5.

Step No. 9: Convert each of the elements of the inverted frequency matrix of Step 8 into six partial fractions, each partial fraction corresponding to one of the six natural frequencies determined in Step 7.

Step No. 10: The result of Step 9 can be rewritten in the form of six 6-by-6 matrices, each corresponding to one of the six natural frequencies of Step 7. These are now treated as single-degree-of-freedom systems, each mode corresponding to its respective frequency. These can now be referred to the response spectrum, and the sum of the six components, due to the six modes, for shock inputs in all the six directions give the necessary response of the system. The simple addition of the peak responses in each of the modes is called the maximax principle. Since the response spectrum contains no information on the phasing of the responses, it is not possible to determine the phasing of the oscillations in each mode. The maximax principle implies that all peak responses occur simultaneously thus yielding the most severe condition possible.

3.5.5 Examples for Response of Suspended Elements to Shock

All problems dealing with the response of shock isolated systems to impulsive shock loads involve three main investigations, viz: given an element to be shock isolated for a shock of given intensity (represented either by the time-history of the shock or by its response spectrum):

- What isolator stiffnesses are required for the system to conform with the imposed rattlespace, velocity, or acceleration criteria?

- What will be the maximum displacements, velocities, or accelerations of the elements of the given system, with isolators of given stiffness, under the action of other possible shocks?

- Is the system stable under the action of all possible shocks?

Depending on the nature of the particular problem, one or all of the above three investigations may be necessary. The examples considered have been separated into the following classifications:

- Platforms suspended by linear isolators so that their centers of symmetry are coincident with the centers of gravity of the platforms. Nonlinear coupling due to pendulum action is assumed to be negligible.

- Platforms suspended by linear isolators so that their centers of symmetry are eccentric with respect to the centers of gravity of the platforms. Nonlinear coupling due to pendulum action is assumed to be negligible.

- Platforms suspended by linear isolators, whose centers of symmetry are coincident with the centers of gravity of the platforms. Nonlinear coupling due to pendulum action is accounted for.

- Platforms suspended by linear isolators, whose centers of symmetry are not coincident with the centers of gravity of the platforms. Nonlinear coupling due to pendulum action is accounted for.

For each of the above cases, three general types of the more commonly encountered isolator arrangements have been considered.

3.5.5.1 Linear Isolators, No Eccentricities, Nonlinear Coupling Due to Pendulum Action Ignored (Case A)

Three different arrangements of linear isolators have been considered for this case; but for all three arrangements, the center of symmetry of the isolators is coincident with the center of gravity of the platform. Furthermore, the reference system has been chosen to coincide with the three principal axes of the platform, so that the cross moments of inertia terms such as I_{ij} are all zero. As will be shown, for this case, the six modes of vibration are completely decoupled, i.e., they are independent of one another, thus making the

system equivalent to six single-degree-of-freedom systems. The peak responses can therefore be obtained directly from the response spectrum. Hence, for the solution of these problems, there is no necessity to go into either the Laplace Method or the Normal Mode Method. However, to familiarize the reader with the generality of the procedure, as few deviations as are practicable have been made in solving these problems by the Laplace Method.

3.5.5.1.1 Example A-1: Isolators parallel to a single principal axis.

The isolation system is as shown in the Figure 3.5.2.

Let K_a = axial stiffness of each isolator

K = lateral stiffness of each isolator, assumed to be identical in all lateral directions

W = total weight of the isolated mass

then

$$I_{xx} = \frac{W}{3g}B^2 \; ; \; I_{yy} = \frac{W}{3g}L^2 \; ; \; I_{zz} = \frac{W}{3g}\,(B^2+L^2)$$

$$I_{xy} = I_{yz} = I_{zx} = 0$$

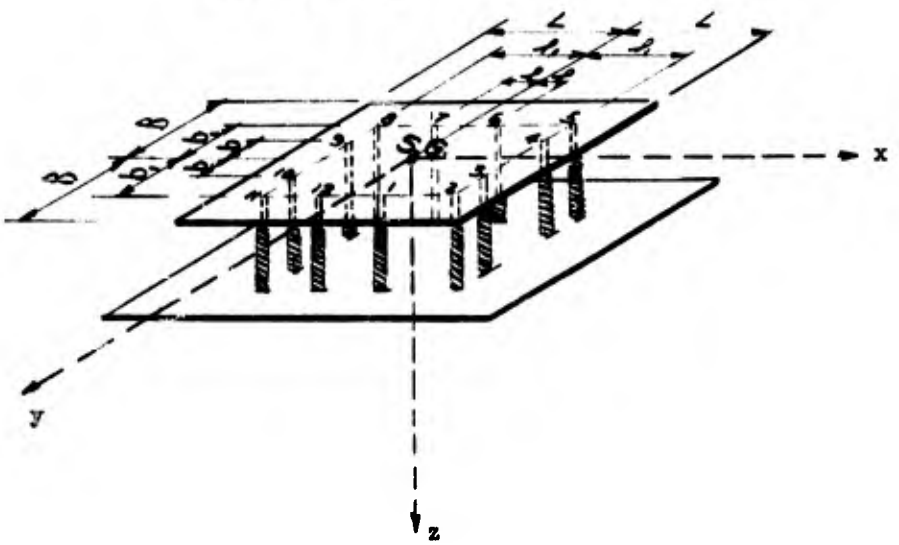

Figure 3.5.2
Linear System With Isolators Parallel to Principal Axis

The equations of motion in matrix form are:

$$[m]\{\ddot{s}\} + [c]\{s\} + [B]\{\phi\} = -[m]\{\ddot{s}_o\}$$
$$[I]\{\ddot{\phi}\} + [B]^t\{s\} + [E]\{\phi\} = -[I]\{\ddot{\phi}_o\}$$

In this example,

$$[m] = \begin{bmatrix} \frac{W}{g} & o & o \\ o & \frac{W}{g} & o \\ o & o & \frac{W}{g} \end{bmatrix} \qquad [I] = \begin{bmatrix} \frac{W}{3g}B^2 & o & o \\ o & \frac{W}{3g}L^2 & o \\ o & o & \frac{W}{3g}(L^2+B^2) \end{bmatrix}$$

There are no shear components of the isolator stiffnesses since there are no inclined springs. Therefore,

$$[c] = \begin{bmatrix} c_{11} & o & o \\ o & c_{22} & o \\ o & o & c_{33} \end{bmatrix}$$

The first moments of the stiffnesses are:

$b_{11}=r_2c_{13}-r_3c_{13}=0$ $b_{12}=r_3c_{11}-r_1c_{13}=0$ $b_{13}=r_1c_{12}-r_2c_{11}=-r_2c_{11}$

$b_{21}=r_2c_{23}-r_3c_{22}=0$ $b_{22}=r_3c_{21}-r_1c_{23}=0$ $b_{23}=r_1c_{22}-r_2c_{21}=r_1c_{22}$

$b_{31}=r_2c_{33}-r_3c_{32}=r_2c_{33}$ $b_{32}=r_3c_{31}-r_1c_{33}=-r_1c_{33}$ $b_{33}=r_1c_{32}-r_2c_{31}=0$

Then the matrix of the first moments is

$$[b] = \begin{bmatrix} o & o & b_{13} \\ o & o & b_{23} \\ b_{31} & b_{32} & o \end{bmatrix}$$

The second moments of the stiffnesses are:

$e_{11}=r_2b_{31}-r_3b_{21}=r_2b_{31}$ $e_{12}=r_2b_{32}-r_3b_{22}=r_2b_{32}$ $e_{13}=r_2b_{33}-r_3b_{23}=0$

$e_{21}=r_3b_{11}-r_1b_{31}=-r_1b_{31}$ $e_{22}=r_3b_{12}-r_1b_{32}=r_1b_{32}$ $e_{23}=r_3b_{13}-r_1b_{33}=0$

$e_{31}=r_1b_{21}-r_2b_{11}=0$ $e_{32}=r_1b_{22}-r_2b_{12}=0$ $e_{33}=r_1b_{23}-r_2b_{13}$

and the second moment matrix becomes

$$[e] = \begin{bmatrix} e_{11} & e_{12} & 0 \\ e_{21} & e_{22} & 0 \\ 0 & 0 & e_{33} \end{bmatrix}$$

The above values have been tabulated on page 3-50; and the matrices [C], [B] and [E] formed by the summations of these values for all the twelve isolators have been evaluated.

The equations of motion in explicit matrix form are then given as follows:

$$\begin{bmatrix} \frac{W}{g} & 0 & 0 \\ 0 & \frac{W}{g} & 0 \\ 0 & 0 & \frac{W}{g} \end{bmatrix} \begin{bmatrix} \ddot{x} \\ \ddot{y} \\ \ddot{z} \end{bmatrix} + \begin{bmatrix} 12K_f & 0 & 0 \\ 0 & 12K_f & 0 \\ 0 & 0 & 12K_a \end{bmatrix} \begin{bmatrix} x \\ y \\ z \end{bmatrix} = - \begin{bmatrix} \frac{W}{g} & 0 & 0 \\ 0 & \frac{W}{g} & 0 \\ 0 & 0 & \frac{W}{g} \end{bmatrix} \begin{bmatrix} \ddot{x}_o \\ \ddot{y}_o \\ \ddot{z}_o \end{bmatrix}$$

$$\begin{bmatrix} \frac{W}{3g}B^2 & 0 & 0 \\ 0 & \frac{W}{3g}L^2 & 0 \\ 0 & 0 & \frac{W}{3g}(L^2+B^2) \end{bmatrix} \begin{bmatrix} \ddot{\alpha} \\ \ddot{\beta} \\ \ddot{\gamma} \end{bmatrix} + \begin{bmatrix} (8b_1^2+4b^2)K_a & 0 & 0 \\ 0 & (8f_1^2+4f^2)K_a & 0 \\ 0 & 0 & (8b_1^2+4b^2)K_f \\ & & (8f_1^2+4f^2)K_f \end{bmatrix} \begin{bmatrix} \alpha \\ \beta \\ \gamma \end{bmatrix} = 0$$

It will be noted that for all cases, the right hand side of the second matrix equation is zero, since the ground acceleration is given for the x, y, and z directions only, it being assumed that the shock has no rotational components.

In this case, since the two equations are completely decoupled, we need consider the first equation only. Thus, after dividing throughout by $\frac{W}{g}$, we obtain the equation in Laplace form as follows:

$$\begin{bmatrix} s^2+12\frac{gK_f}{W} & 0 & 0 \\ 0 & s^2+12\frac{gK_f}{W} & 0 \\ 0 & 0 & s^2+12\frac{gK_a}{W} \end{bmatrix} \begin{bmatrix} \bar{x} \\ \bar{y} \\ \bar{z} \end{bmatrix} = - \begin{bmatrix} s^2\bar{x}_o \\ s^2\bar{y}_o \\ s^2\bar{z}_o \end{bmatrix}$$

Isolator Number	r_1	r_2	r_3	c_{11}	c_{22}	c_{33}	$b_{13} = r_2 c_{11}$	$b_{23} = r_1 c_{22}$	$b_{31} = r_2 c_{33}$	$b_{32} = r_1 c_{33}$	$e_{11} = r_2 b_{31}$	$e_{12} = r_2 b_{32}$	$e_{21} = r_1 b_{31}$	$e_{22} = r_1 b_{32}$	$e_{33} = r_2 b_{13} = r_1 b_{23}$
1	ℓ	b_1	0	K_ℓ	K_ℓ	K_a	$-b_1 K_\ell$	ℓK_ℓ	$b_1 K_a$	$-\ell K_a$	$b_1^2 K_a$	$-b_1 \ell K_a$	$-b_1 \ell K_a$	$\ell^2 K_a$	$\ell^2 K_\ell + b_1^2 K_\ell$
2	$-\ell_1$	b_1	0	K_ℓ	K_ℓ	K_a	$-b_1 K_\ell$	$\ell_1 K_\ell$	$b_1 K_a$	$-\ell_1 K_a$	$b_1^2 K_a$	$-b_1 \ell_1 K_a$	$-b_1 \ell_1 K_a$	$\ell_1^2 K_a$	$\ell_1^2 K_\ell + b_1^2 K_\ell$
3	$-\ell_1$	b	0	K_ℓ	K_ℓ	K_a	$-b K_\ell$	$\ell_1 K_\ell$	$b K_a$	$-\ell_1 K_a$	$b^2 K_a$	$-b \ell_1 K_a$	$-b \ell_1 K_a$	$\ell_1^2 K_a$	$\ell_1^2 K_\ell + b^2 K_\ell$
4	$-\ell_1$	$-b$	0	K_ℓ	K_ℓ	K_a	$b K_\ell$	$\ell_1 K_\ell$	$-b K_a$	$-\ell_1 K_a$	$b^2 K_a$	$b \ell_1 K_a$	$b \ell_1 K_a$	$\ell_1^2 K_a$	$\ell_1^2 K_\ell + b^2 K_\ell$
5	$-\ell_1$	$-b_1$	0	K_ℓ	K_ℓ	K_a	$b_1 K_\ell$	$\ell_1 K_\ell$	$-b_1 K_a$	$-\ell_1 K_a$	$b_1^2 K_a$	$b_1 \ell_1 K_a$	$b_1 \ell_1 K_a$	$\ell_1^2 K_a$	$\ell_1^2 K_\ell + b_1^2 K_\ell$
6	ℓ	$-b_1$	0	K_ℓ	K_ℓ	K_a	$b_1 K_\ell$	ℓK_ℓ	$-b_1 K_a$	$-\ell K_a$	$b_1^2 K_a$	$b_1 \ell K_a$	$b_1 \ell K_a$	$\ell^2 K_a$	$\ell^2 K_\ell + b_1^2 K_\ell$
7	$-\ell$	b_1	0	K_ℓ	K_ℓ	K_a	$b_1 K_\ell$	$-\ell K_\ell$	$-b_1 K_a$	ℓK_a	$b_1^2 K_a$	$-b_1 \ell K_a$	$-b_1 \ell K_a$	$\ell^2 K_a$	$\ell^2 K_\ell + b_1^2 K_\ell$
8	$-\ell_1$	$-b_1$	0	K_ℓ	K_ℓ	K_a	$b_1 K_\ell$	$-\ell_1 K_\ell$	$-b_1 K_a$	$\ell_1 K_a$	$b_1^2 K_a$	$-b_1 \ell_1 K_a$	$-b_1 \ell_1 K_a$	$\ell_1^2 K_a$	$\ell_1^2 K_\ell + b_1^2 K_\ell$
9	$-\ell_1$	$-b$	0	K_ℓ	K_ℓ	K_a	$b K_\ell$	$-\ell_1 K_\ell$	$-b K_a$	$\ell_1 K_a$	$b^2 K_a$	$-b \ell_1 K_a$	$-b \ell_1 K_a$	$\ell_1^2 K_a$	$\ell_1^2 K_\ell + b^2 K_\ell$
10	$-\ell_1$	b	0	K_ℓ	K_ℓ	K_a	$-b K_\ell$	$-\ell_1 K_\ell$	$b K_a$	$\ell_1 K_a$	$b^2 K_a$	$b \ell_1 K_a$	$b \ell_1 K_a$	$\ell_1^2 K_a$	$\ell_1^2 K_\ell + b^2 K_\ell$
11	$-\ell_1$	b_1	0	K_ℓ	K_ℓ	K_a	$-b K_\ell$	$-\ell_1 K_1$	$b_1 K_a$	$\ell_1 K_a$	$b_1^2 K_a$	$b_1 \ell_1 K_a$	$b_1 \ell_1 K_a$	$\ell_1^2 K_a$	$\ell_1^2 K_\ell + b_1^2 K_\ell$
12	$-\ell$	b_1	0	K_ℓ	K_ℓ	K_a	$-b_1 K_\ell$	$-\ell K_\ell$	$b_1 K_a$	ℓK_a	$b_1^2 K_a$	$b_1 \ell K_a$	$b_1 \ell K_a$	$\ell^2 K_a$	$\ell^2 K_\ell + b_1^2 K_\ell$
		$\sum =$		$12 K_\ell$	$12 K_\ell$	$12 K_a$	0	0	0	0	$(8b_1^2 + 4b^2) K_a$	0	0	$(8\ell_1^2 + 4\ell^2) K_a$	$\{(8b_1^2 + 4b^2) + (8\ell_1^2 + 4\ell^2) K_\ell\}$

$$\therefore [C] = \begin{bmatrix} 12K_\ell & 0 & 0 \\ 0 & 12K_\ell & 0 \\ 0 & 0 & 12K_a \end{bmatrix} \qquad \therefore [B] = 0 \qquad \therefore [E] = \begin{bmatrix} (8b_1^2 + 4b^2)K_a & 0 & 0 \\ 0 & (8\ell_1^2 + 4\ell^2)K_a & 0 \\ 0 & 0 & \{(8b_1^2 + 4b^2)K_\ell + (8\ell_1^2 + 4\ell^2)K_\ell\} \end{bmatrix}$$

$$\therefore \quad \begin{bmatrix} \bar{x} \\ \bar{y} \\ \bar{z} \end{bmatrix} = - \begin{bmatrix} \frac{1}{s^2+12\frac{g}{w}K_\ell} & o & o \\ o & \frac{1}{s^2+12\frac{g}{w}K_\ell} & o \\ o & o & \frac{1}{s^2+12\frac{g}{w}K_a} \end{bmatrix} \begin{bmatrix} s^2\bar{x}_o \\ s^2\bar{y}_o \\ s^2\bar{z}_o \end{bmatrix}$$

or

$$\begin{bmatrix} \bar{x} \\ \bar{y} \\ \bar{z} \end{bmatrix} = \begin{bmatrix} 1 & o & o \\ o & 1 & o \\ o & o & 1 \end{bmatrix} \begin{bmatrix} s^2 \frac{\bar{x}_o}{s^2+12\frac{g}{w}K_\ell} \\ s^2 \frac{\bar{y}_o}{s^2+12\frac{g}{w}K_\ell} \\ s^2 \frac{\bar{z}_o}{s^2+12\frac{g}{w}K_a} \end{bmatrix}$$

Where $\bar{x}$, $\bar{y}$ and $\bar{z}$ are the displacements of the platform in directions x, y and z respectively. These may be specified as the maximum permissible rattlespace, in which case the above equation can be used to determine K_ℓ and K_a. Thus,

$$\omega_x^2 = \frac{12\,g}{W} K \;, \quad \omega_y^2 = \frac{12\,g}{W} K \;, \quad \omega_z^2 = \frac{12\,g}{W} K_a$$

ω_x, ω_y and ω_z may be obtained from the response spectrum, corresponding to the relative displacements $\bar{x}$, $\bar{y}$ and $\bar{z}$.

Then $$K_\ell = \frac{W}{g} \frac{\omega x^2}{12}$$

or $$K_\ell = \frac{W}{g} \frac{\omega y^2}{12}$$

and $$K_a = \frac{W}{g} \frac{\omega z^2}{12}$$

The higher value of k_ℓ is chosen if displacements are critical, and lower value if accelerations are critical.

3.5.5.1.2 Example A-2: Isolators inclined to principal axes.

The arrangement of isolators is as shown in Figure 3.5.3, the main feature being the use of isolators inclined to the reference system. These isolators contribute a form of shear stiffness, in addition to the axial and lateral stiffnesses.

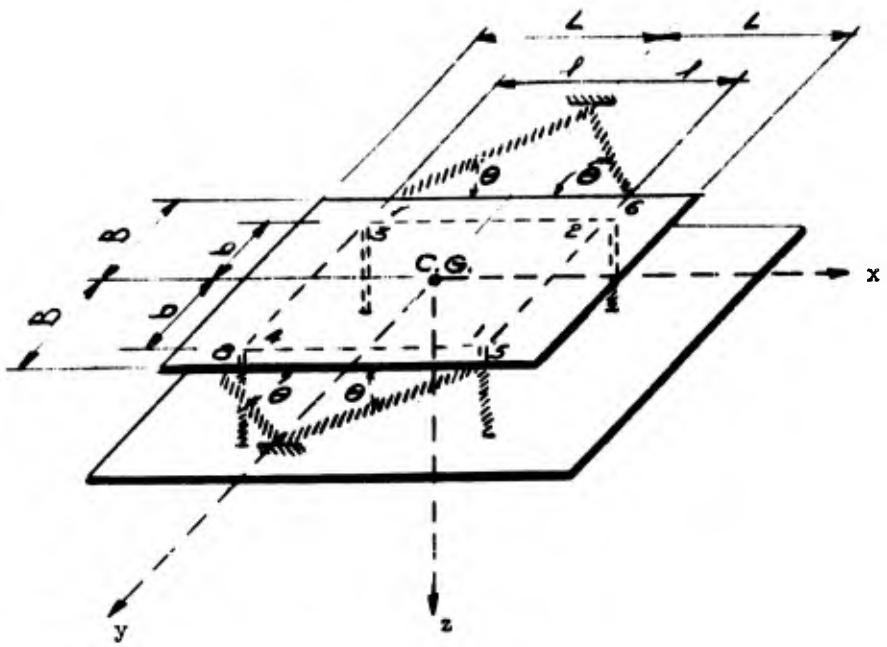

Figure 3.5.3
Linear System With Isolators Inclined to Principal Axes

Let K_{av} = axial stiffness of each vertical isolator
$K_{\ell v}$ = lateral stiffness of each vertical isolator
K_{ah} = axial stiffness of each horizontal isolator
$K_{\ell h}$ = laterial stiffness of each horizontal isolator

The moments of inertia and [c], [b] , and [e] matrices for the vertical isolators are similar to those encountered in Example A-1.

However, the principal directions of the horizontal, inclined isolators do not coincide with the reference axes. For example, isolator No. 5 has its longitudinal axis inclined at an angle of $(180^o - \theta)$ to the positive direction of the x-axis, whereas isolator No. 8 is inclined at an angle θ^o. Designating [c] as the stiffness matrix of an isolator in its principal directions by

$$[c] = \begin{bmatrix} c_{11} & o & o \\ o & c_{22} & o \\ o & o & c_{33} \end{bmatrix}$$

and $[c]_{\theta_o}$ as the stiffness matrix of the same isolator in a direction making an angle θ with the principal direction 1, then

$$[c]_{\theta_o} = \begin{bmatrix} (c_{11})_{\theta_o} & (c_{12})_{\theta_o} & 0 \\ (c_{21})_{\theta_o} & (c_{22})_{\theta_o} & 0 \\ 0 & 0 & (c_{33})_{\theta_o} \end{bmatrix}$$

Where, by the equivalent of Mohr's diagram,

$$(c_{11})_{\theta_o} = (\cos^2\theta_o)\ c_{11} + (\sin^2\theta_o)\ c_{22}$$

$$(c_{22})_{\theta_o} = (\cos^2\theta_o)\ c_{22} + (\sin^2\theta_o)\ c_{11}$$

$$(c_{33})_{\theta_o} = c_{33}$$

$$(c_{21})_{\theta_o} = (c_{12})_{\theta_o} = -\frac{\sin 2\theta_o}{2}\ c_{11} + \frac{\sin 2\theta_o}{2}\ c_{22}$$

In this case, for isolator No. 5, $\theta_o = 180^o + \theta$

for isolator No. 6, $\theta_o = 180^o - \theta$

for isolator No. 7, $\theta_o = +\theta$

and for isolator No. 8, $\theta_o = -\theta$

These values have been tabulated on pages 3-55 thru 3-57 . Knowing these values, the [b] and [e] values may be obtained for each of the isolators as in the previous example, as shown on the referenced pages. The summation matrices [C] , [B] , and [E] have likewise been evaluated.

Hence, the equations of motion in matrix form are:

$$\begin{bmatrix} \frac{W}{g} & 0 & 0 \\ 0 & \frac{W}{g} & 0 \\ 0 & 0 & \frac{W}{g} \end{bmatrix} \begin{bmatrix} \ddot{x} \\ \ddot{y} \\ \ddot{z} \end{bmatrix} + \begin{bmatrix} 4\left[K_{\ell v}+K_{\ell h}\sin^2\theta+K_{ah}\cos^2\theta\right] & & \\ & 4\left[K_{\ell v}+K_{ah}\sin^2\theta+K_{\ell h}\cos^2\theta\right] & \\ & & 4\left[K_{av}+K_{\ell h}\right] \end{bmatrix} \begin{bmatrix} x \\ y \\ z \end{bmatrix} = - \begin{bmatrix} \frac{W}{g} & 0 & 0 \\ 0 & \frac{W}{g} & 0 \\ 0 & 0 & \frac{W}{g} \end{bmatrix} \begin{bmatrix} \ddot{x}_o \\ \ddot{y}_o \\ \ddot{z}_o \end{bmatrix}$$

$$\begin{bmatrix} \frac{W}{3g}B^2 & 0 & 0 \\ 0 & \frac{W}{3g}L^2 & 0 \\ 0 & 0 & \frac{W}{3g}L^2+B^2 \end{bmatrix} \begin{bmatrix} \ddot{\alpha} \\ \ddot{\beta} \\ \ddot{\gamma} \end{bmatrix} + \begin{bmatrix} 4\left[b^2K_{av}+B^2K_{\ell h}\right] & 0 & 0 \\ 0 & 4k^2\left[K_{av}+K_{\ell h}\right] & 0 \\ 0 & 0 & 4\left[K_{\ell v}(\ell^2+b^2) \right. \\ & & \left. +K_{ah}(\ell\sin\theta+B\cos\theta)^2 \right. \\ & & \left. +K_{\ell h}(\ell\cos\theta-B\sin\theta)^2\right] \end{bmatrix} \begin{bmatrix} \alpha \\ \beta \\ \gamma \end{bmatrix} = 0$$

The equations are then decoupled. Applying the usual Laplace transformations, we obtain

$$\begin{bmatrix} s^2+\frac{4g}{W}\left[K_{\ell v}+K_{\ell h}\sin^2\theta+K_{ah}\cos^2\theta\right] & 0 & 0 \\ 0 & s^2+\frac{4g}{W}\left[K_{\ell v}+K_{ah}\sin^2\theta+K_{\ell h}\cos^2\theta\right] & 0 \\ 0 & 0 & \frac{4g}{W}\left[K_{av}+K_{\ell h}\right] \end{bmatrix} \begin{bmatrix} \bar{x} \\ \bar{y} \\ \bar{z} \end{bmatrix} = - \begin{bmatrix} s^2\bar{x}_o \\ s^2\bar{y}_o \\ s^2\bar{z}_o \end{bmatrix}$$

or

$$\begin{bmatrix} \bar{x} \\ \bar{y} \\ \bar{z} \end{bmatrix} = \begin{bmatrix} 1 & 0 & 0 \\ 0 & 1 & 0 \\ 0 & 0 & 1 \end{bmatrix} \begin{bmatrix} -\dfrac{s^2\bar{x}_o}{s^2+\frac{4g}{W}\left[K_{\ell v}+K_{\ell h}\sin^2\theta+K_{ah}\cos^2\theta\right]} \\ -\dfrac{s^2\bar{y}_o}{s^2+\frac{4g}{W}\left[K_{\ell v}+K_{ah}\sin^2\theta+K_{\ell h}\cos^2\theta\right]} \\ -\dfrac{s^2\bar{z}_o}{s^2+\frac{4g}{W}\left[K_{av}+K_{\ell h}\right]} \end{bmatrix}$$

Then as before,

$$\omega_x^2 = \frac{4g}{W}\left[K_{\ell v}+K_{\ell h}\sin^2\theta + K_{ah}\cos^2\theta\right]$$

$$\omega_y^2 = \frac{4g}{W}\left[K_{\ell v}+K_{ah}\sin^2\theta + K_{\ell h}\cos^2\theta\right]$$

$$\omega_z^2 = \frac{4g}{W}\left[K_{av}+K_{\ell h}\right]$$

ω_x, ω_y, and ω_z are obtained from the response spectrum corresponding to the displacements $\bar{x}$, $\bar{y}$, $\bar{z}$, and the spring stiffnesses $K_{\ell h}$, K_{ah}, K_{av}, K_{hv}, chosen to satisfy the performance requirements of the system.

Isolator Number	$b_{13} = (r_1c_{12} - r_2c_{11})$	$b_{23} = r_1c_{22} - r_2c_{21}$	$b_{31} = r_2c_{33}$	$b_{32} = -r_1c_{33}$
1	$-bK_{\ell v}$	$\ell K_{\ell v}$	bK_{av}	$-\ell K_{av}$
2	$bK_{\ell v}$	$\ell K_{\ell v}$	$-bK_{av}$	$-\ell K_{av}$
3	$bK_{\ell v}$	$-\ell K_{\ell v}$	$-bK_{av}$	ℓK_{av}
4	$-bK_{\ell v}$	$-\ell K_{\ell v}$	bK_{av}	ℓK_{av}
5	$\ell\left[K_{\ell h}\frac{\sin 2\theta}{2} - K_{ah}\frac{\sin 2\theta}{2}\right]$ $-B\left[K_{\ell h}\sin^2\theta + K_{ah}\cos^2\theta\right]$	$\ell\left[K_{ah}\sin^2\theta + K_{\ell h}\cos^2\theta\right]$ $-B\left[K_{\ell h}\frac{\sin 2\theta}{2} - K_{ah}\frac{\sin 2\theta}{2}\right]$	$BK_{\ell h}$	$-\ell K_{1h}$
6	$\ell\left[-K_{\ell h}\frac{\sin 2\theta}{2} + K_{ah}\frac{\sin 2\theta}{2}\right]$ $+B\left[K_{\ell h}\sin^2\theta + K_{ah}\cos^2\theta\right]$	$\ell\left[K_{ah}\sin^2\theta + K_{\ell h}\cos^2\theta\right]$ $+B\left[-K_{\ell h}\frac{\sin 2\theta}{2} + K_{ah}\frac{\sin 2\theta}{2}\right]$	$-BK_{\ell h}$	ℓK_{1h}
7	$-\ell\left[K_{\ell h}\frac{\sin 2\theta}{2} - K_{ah}\frac{\sin 2\theta}{2}\right]$ $+B\left[K_{\ell h}\sin^2\theta + K_{ah}\cos^2\theta\right]$	$-\ell\left[K_{ah}\sin^2\theta + K_{\ell h}\cos^2\theta\right]$ $+B\left[K_{\ell h}\frac{\sin 2\theta}{2} - K_{ah}\frac{\sin 2\theta}{2}\right]$	$-BK_{\ell h}$	ℓK_{1h}
8	$-\ell\left[-K_{\ell h}\frac{\sin 2\theta}{2} + K_{ah}\frac{\sin 2\theta}{2}\right]$ $-B\left[K_{\ell h}\sin^2\theta + K_{ah}\cos^2\theta\right]$	$-\ell\left[K_{ah}\sin^2\theta + K_{\ell h}\cos^2\theta\right]$ $-B\left[-K_{\ell h}\frac{\sin 2\theta}{2} + K_{ah}\frac{\sin 2\theta}{2}\right]$	$BK_{\ell h}$	ℓK_{1h}
Σ =	0	0	0	0

$$\therefore \quad [B] = 0$$

Isolator Number	r_1	r_2	r_3	c_{11}	c_{22}	c_{33}	c_{12}	c_{21}	$c_{13}=c_{31}$	$c_{32}=c_{23}$
1	ℓ	b	o	$K_{\ell v}$	$K_{\ell v}$	K_{av}	o	o	o	o
2	ℓ	-b	o	$K_{\ell v}$	$K_{\ell v}$	K_{av}	o	o	o	o
3	$-\ell$	-b	o	$K_{\ell v}$	$K_{\ell v}$	K_{av}	o	o	o	o
4	$-\ell$	b	o	$K_{\ell v}$	$K_{\ell v}$	K_{av}	o	o	o	o
5	ℓ	B	o	$(K_{\ell h}\sin^2\varphi + K_{ah}\cos^2\varphi)$	$(K_{ah}\sin^2\varphi + K_{\ell h}\cos^2\varphi)$	$K_{\ell h}$	$\left(\frac{K_{\ell h}}{2}\sin 2\varphi - \frac{K_{ah}}{2}\sin 2\varphi\right)$	$\left(\frac{K_{\ell h}}{2}\sin 2\varphi - \frac{K_{ah}}{2}\sin 2\varphi\right)$	o	o
6	ℓ	-B	o	$(K_{\ell h}\sin^2\varphi + K_{ah}\cos^2\varphi)$	$(K_{ah}\sin^2\varphi + K_{\ell h}\cos^2\varphi)$	$K_{\ell h}$	$\left(\frac{K_{\ell h}}{2}\sin 2\varphi + \frac{K_{ah}}{2}\sin 2\varphi\right)$	$-\left(\frac{K_{\ell h}}{2}\sin 2\varphi + \frac{K_{ah}}{2}\sin 2\varphi\right)$	o	o
7	$-\ell$	-B	o	$(K_{\ell h}\sin^2\varphi + K_{ah}\cos^2\varphi)$	$(K_{ah}\sin^2\varphi + K_{\ell h}\cos^2\varphi)$	$K_{\ell h}$	$\left(\frac{K_{\ell h}}{2}\sin 2\varphi - \frac{K_{ah}}{2}\sin 2\varphi\right)$	$\left(\frac{K_{\ell h}}{2}\sin 2\varphi - \frac{K_{ah}}{2}\sin 2\varphi\right)$	o	o
8	$-\ell$	B	o	$(K_{\ell h}\sin^2\varphi + K_{ah}\cos^2\varphi)$	$(K_{ah}\sin^2\varphi + K_{\ell h}\cos^2\varphi)$	$K_{\ell h}$	$\left(\frac{K_{\ell h}}{2}\sin 2\varphi + \frac{K_{ah}}{2}\sin 2\varphi\right)$	$-\left(\frac{K_{\ell h}}{2}\sin 2\varphi + \frac{K_{ah}}{2}\sin 2\varphi\right)$	o	o

$\sum$: $c_{11}=(4K_{\ell v}+4K_{\ell h}\sin^2\varphi+4K_{ah}\cos^2\varphi)$; $c_{22}=4K_{\ell v}+4K_{ah}\sin^2\varphi+4K_{\ell h}\cos^2\varphi)$; $c_{33}=4(K_{av}+K_{\ell h})$; $c_{12}=0$; $c_{21}=0$; $c_{13}=0$; $c_{31}=0$; $c_{32}=0$; $c_{23}=0$

$$[c]=\begin{bmatrix} 4\left[K_{\ell v}+K_{\ell h}\sin^2\varphi+K_{ah}\cos^2\varphi\right] & 0 & 0 \\ 0 & 4\left[K_{\ell v}+K_{ah}\sin^2\varphi+K_{\ell h}\cos^2\varphi\right] & 0 \\ 0 & 0 & 4\left[K_{av}+K_{\ell h}\right] \end{bmatrix}$$

Isolator Number	$e_{11} = r_2 b_{31}$	$e_{12} = r_2 b_{32}$	$e_{21} = -r_1 b_{31}$	$e_{22} = -r_1 b_{32}$	$e_{33} = (r_1 b_{23} - r_2 b_{13})$
1	$b^2 K_{av}$	$-b\ell K_{av}$	$-b\ell K_{av}$	$\ell^2 K_{av}$	$\ell^2 K_{\ell v} + b^2 K_{\ell v}$
2	$b^2 K_{av}$	$b\ell K_{av}$	$b\ell K_{av}$	$\ell^2 K_{av}$	$\ell^2 K_{\ell v} + b^2 K_{\ell v}$
3	$b^2 K_{av}$	$-b\ell K_{av}$	$-b\ell K_{av}$	$\ell^2 K_{av}$	$\ell^2 K_{\ell v} + b^2 K_{\ell v}$
4	$b^2 K_{av}$	$b\ell K_{av}$	$b\ell K_{av}$	$\ell^2 K_{av}$	$\ell^2 K_{\ell v} + b^2 K_{\ell v}$
5	$B^2 K_{\ell h}$	$-B\ell K_{\ell h}$	$-B\ell K_{\ell h}$	$\ell^2 K_{\ell h}$	$K_{ah}(\ell \sin\theta + B\cos\theta)^2 + K_{\ell h}(\ell\cos\theta - B\sin\theta)^2$
6	$B^2 K_{\ell h}$	$+B\ell K_{\ell h}$	$B\ell K_{\ell h}$	$\ell^2 K_{\ell h}$	$K_{ah}(\ell \sin\theta + B\cos\theta)^2 + K_{\ell h}(\ell\cos\theta - B\sin\theta)^2$
7	$B^2 K_{\ell h}$	$-B\ell K_{\ell h}$	$-B\ell K_{\ell h}$	$\ell^2 K_{\ell h}$	$K_{ah}(\ell \sin\theta + B\cos\theta)^2 + K_{\ell h}(\ell\cos\theta - B\sin\theta)^2$
8	$B^2 K_{\ell h}$	$+B\ell K_{\ell h}$	$B\ell K_{\ell h}$	$\ell^2 K_{\ell h}$	$K_{ah}(\ell \sin\theta + B\cos\theta)^2 + K_{\ell h}(\ell\cos\theta - B\sin\theta)^2$
$\sum$ =	$(4b^2 K_{av} + 4B^2 K_{\ell h})$	0	0	$4\ell^2(K_{av}+K_{\ell h})$	$4\left[K_{\ell v}(\ell^2+b^2) + K_{ah}(\ell\sin\theta + B\cos\theta)^2 + K_{\ell h}(\ell\cos\theta - B\sin\theta)^2\right]$

$$\therefore [E] = \begin{bmatrix} (4b^2 K_{av} + 4B^2 K_{\ell h}) & 0 & 0 \\ 0 & 4\ell^2(K_{av}+K_{\ell h}) & 0 \\ 0 & 0 & 4\left[K_{\ell v}(\ell^2+b^2) + K_{ah}(\ell\sin\theta + B\cos\theta)^2 + K_{\ell h}(\ell\cos\theta - B\sin\theta)^2\right] \end{bmatrix}$$

3.5.5.1.3 Example A-3: Isolators parallel to all three principal axes.

For the third example of Case A, consider a system consisting of isolators in the x, y, and z directions as shown in the Figure 3.5.4. The center of gravity of the platform coincides with the center of symmetry of the isolator system.

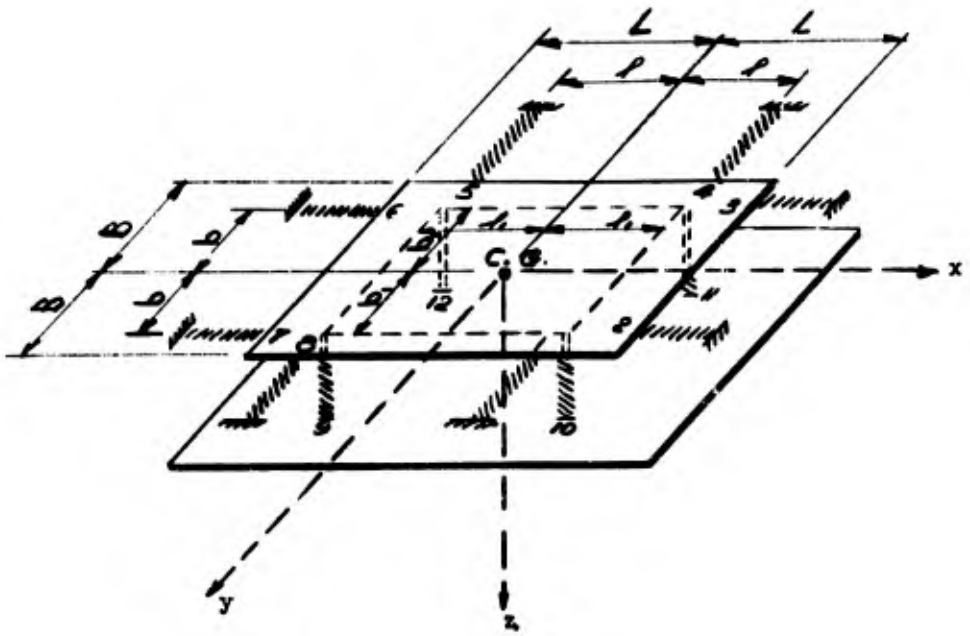

Figure 3.5.4
Linear System with Isolators Parallel to All Three Principal Axes

Let K_{1a} = axial stiffness of each isolator parallel to x axis

$K_{1\ell}$ = lateral stiffness of each isolator parallel to x axis

K_{2a} = axial stiffness of each isolator parallel to y axis

$K_{2\ell}$ = lateral stiffness of each isolator parallel to y axis

K_{3a} = axial stiffness of each isolator parallel to z axis

$K_{3\ell}$ = lateral stiffness of each isolator parallel to z axis

The table on page 3-59 following the pattern of the two previous examples is self-explanatory.

Isolator Number	r_1	r_2	r_3	c_{11}	c_{22}	c_{33}	b_{13} $=-r_2c_{11}$	b_{23} $=r_1c_{22}$	b_{31} $=r_2c_{33}$	b_{32} $=-r_1c_{33}$	e_{11} $=r_2b_{31}$	e_{22} $-r_1b_{32}$	e_{33} $=r_1b_{23}-r_2b_{13}$	e_{12} $=r_2b_{32}$	e_{21} $=-r_1b_{31}$
1	ℓ	B	o	$K_{2\ell}$	K_{2a}	$K_{2\ell}$	$-BK_{2\ell}$	ℓK_{2a}	$BK_{2\ell}$	$-\ell K_{2\ell}$	$B^2K_{2\ell}$	$\ell^2K_{2\ell}$	$\ell^2K_{2a}+B^2K_{2\ell}$	$-B\ell K_{2\ell}$	$-B\ell K_{2\ell}$
2	L	b	o	K_{1a}	$K_{1\ell}$	$K_{1\ell}$	$-bK_{1a}$	$LK_{1\ell}$	$bK_{1\ell}$	$-LK_{1\ell}$	$b^2K_{1\ell}$	$L^2K_{1\ell}$	$L^2K_{1\ell}+b^2K_{1a}$	$-bLK_{1\ell}$	$-bLK_{1\ell}$
3	L	-b	o	K_{1a}	$K_{1\ell}$	$K_{1\ell}$	bK_{1a}	$LK_{1\ell}$	$-bK_{1\ell}$	$-LK_{1\ell}$	$b^2K_{1\ell}$	$L^2K_{1\ell}$	$L^2K_{1\ell}+b^2K_{1a}$	$bLK_{1\ell}$	$bLK_{1\ell}$
4	ℓ	-B	o	$K_{2\ell}$	K_{2a}	$K_{2\ell}$	$BK_{2\ell}$	ℓK_{2a}	$-BK_{2\ell}$	$-\ell K_{2\ell}$	$B^2K_{2\ell}$	$\ell^2K_{2\ell}$	$\ell^2K_{2a}+B^2K_{2\ell}$	$B\ell K_{2\ell}$	$B\ell K_{2\ell}$
5	$-\ell$	-B	c	$K_{2\ell}$	K_{2a}	$K_{2\ell}$	$BK_{2\ell}$	$-\ell K_{2a}$	$-BK_{2\ell}$	$+\ell K_{2\ell}$	$B^2K_{2\ell}$	$\ell^2K_{2\ell}$	$\ell^2K_{2a}+B^2K_{2\ell}$	$-B\ell K_{2\ell}$	$-B\ell K_{2\ell}$
6	-L	-b	o	K_{1a}	$K_{1\ell}$	$K_{1\ell}$	bK_{1a}	$-LK_{1\ell}$	$-bK_{1\ell}$	$+LK_{1\ell}$	$b^2K_{1\ell}$	$L^2K_{1\ell}$	$L^2K_{1\ell}+b^2K_{1a}$	$-bLK_{1\ell}$	$bLK_{1\ell}$
7	-L	b	o	K_{1a}	$K_{1\ell}$	$K_{1\ell}$	$-bK_{1a}$	$-LK_{1\ell}$	$bK_{1\ell}$	$LK_{1\ell}$	$b^2K_{1\ell}$	$L^2K_{1\ell}$	$L^2K_{1\ell}+b^2K_{1a}$	$bLK_{1\ell}$	$bLK_{1\ell}$
8	$-\ell$	B	o	$K_{2\ell}$	K_{2a}	$K_{2\ell}$	$-BK_{2\ell}$	$-\ell K_{2a}$	$BK_{2\ell}$	$\ell K_{2\ell}$	$B^2K_{2\ell}$	$\ell^2K_{2\ell}$	$\ell^2K_{2a}+B^2K_{2\ell}$	$B\ell K_{2\ell}$	$B\ell K_{2\ell}$
9	ℓ_1	b_1	o	$K_{3\ell}$	$K_{3\ell}$	K_{3a}	$-b_1K_{3\ell}$	$\ell_1K_{3\ell}$	b_1K_{3a}	$-\ell_1K_{3a}$	$b_1^2K_{3a}$	$\ell_1^2K_{3a}$	$\ell_1^2K_{3\ell}+b_1^2K_{3\ell}$	$-b_1\ell_1K_{3a}$	$-B_1\ell_1K_{3a}$
10	ℓ_1	$-b_1$	o	$K_{3\ell}$	$K_{3\ell}$	K_{3a}	$b_1K_{3\ell}$	$\ell_1K_{3\ell}$	$-b_1K_{3a}$	$-\ell_1K_{3a}$	$b_1^2K_{3a}$	$\ell_1^2K_{3a}$	$\ell_1^2K_{3\ell}+b_1^2K_{3\ell}$	$b_1\ell_1K_{3a}$	$b_1\ell_1K_{3a}$
11	$-\ell_1$	$-b_1$	o	$K_{3\ell}$	$K_{3\ell}$	K_{3a}	$b_1K_{3\ell}$	$-\ell_1K_{3\ell}$	$-b_1K_{3a}$	ℓ_1K_{3a}	$b_1^2K_{3a}$	$\ell_1^2K_{3a}$	$\ell_1^2K_{3\ell}+b_1^2K_{3\ell}$	$-b_1\ell_1K_{3a}$	$-b_1\ell_1K_{3a}$
12	$-\ell_1$	b_1	o	$K_{3\ell}$	$K_{3\ell}$	K_{3a}	$-b_1K_{3\ell}$	$-\ell_1K_{3\ell}$	b_1K_{3a}	ℓ_1K_{3a}	$b_1^2K_{3a}$	$\ell_1^2K_{3a}$	$\ell_1^2K_{3\ell}+b_1^2K_{3\ell}$	$b_1\ell_1K_{3a}$	$b_1\ell_1K_{3a}$

$\sum$: $c_{11}=4(K_{1a}+K_{2\ell}+K_{3\ell})$; $c_{22}=4(K_{3a}+K_{1\ell}+K_{3\ell})$; $c_{33}=4(K_{1\ell}+K_{2\ell}+K_{3a})$; $b_{13}=0$; $b_{23}=0$; $b_{31}=0$; $b_{32}=0$; $e_{11}=4(B^2K_{2\ell}+b^2K_{1\ell}+b_1^2K_{3a})$; $e_{22}=4(\ell^2K_{2\ell}+L^2K_{1\ell}+\ell_1^2K_{3a})$; $e_{33}=4\{(\ell^2K_{2a}+L^2K_{1\ell})+(B^2K_{2\ell}+b^2K_{1a})+(\ell_1^2+b_1^2)K_{3\ell}\}$; $e_{12}=0$; $e_{21}=0$

$$[c] = \begin{bmatrix} 4(K_{1a}+K_{2\ell}+K_{3\ell}) & o & o \\ o & 4(K_{2a}+K_{1\ell}+K_{3\ell}) & o \\ o & o & 4(K_{1\ell}+K_{2\ell}+K_{3a}) \end{bmatrix}; \quad [e] = \begin{bmatrix} 4(B^2K_{2\ell}+b^2K_{1\ell}+b_1^2K_{3a}) & o & o \\ o & 4(\ell^2K_{2\ell}+L^2K_{1\ell}+\ell_1^2K_{3a}) & o \\ o & o & 4\{(\ell^2K_{2a}+L^2K_{1\ell}+B^2K_{2\ell}+b^2K_{1a})+(\ell_1^2+b_1^2)K_{3\ell}\} \end{bmatrix}$$

$$[B] = o$$

The equations of motion are:

$$\begin{bmatrix} \frac{W}{g} & 0 & 0 \\ 0 & \frac{W}{g} & 0 \\ 0 & 0 & \frac{W}{g} \end{bmatrix} \begin{bmatrix} \ddot{x} \\ \ddot{y} \\ \ddot{z} \end{bmatrix} + \begin{bmatrix} 4(K_{1a}+K_{2\ell}+K_{3\ell}) & 0 & 0 \\ 0 & 4(K_{1\ell}+K_{2a}+K_{3\ell}) & 0 \\ 0 & 0 & 4(K_{1\ell}+K_{2\ell}+K_{3a}) \end{bmatrix} \begin{bmatrix} x \\ y \\ z \end{bmatrix} = - \begin{bmatrix} \frac{W}{g} & 0 & 0 \\ 0 & \frac{W}{g} & 0 \\ 0 & 0 & \frac{W}{g} \end{bmatrix} \begin{bmatrix} \ddot{x}_o \\ \ddot{y}_o \\ \ddot{z}_o \end{bmatrix}$$

$$\begin{bmatrix} \frac{W}{3g}B^2 & 0 & 0 \\ 0 & \frac{W}{3g}L^2 & 0 \\ 0 & 0 & \frac{W}{3g}(L^2+B^2) \end{bmatrix} \begin{bmatrix} \ddot{\alpha} \\ \ddot{\beta} \\ \ddot{\gamma} \end{bmatrix} + \begin{bmatrix} 4(B^2K_{2\ell}+b^2K_{1\ell}+b_1^2K_{3a}) & 0 & 0 \\ 0 & 4(\ell^2K_{2\ell}+L^2K_{1\ell}+\ell_1^2K_{3a}) & 0 \\ 0 & 0 & \begin{matrix} 4(\ell^2K_{2a}+L^2K_{1\ell}+B^2K_{2\ell} \\ +b^2K_{1a})+4(\ell_1^2+b_1^2)K_{3\ell} \end{matrix} \end{bmatrix} \begin{bmatrix} \alpha \\ \beta \\ \gamma \end{bmatrix} = 0$$

Again, these are decoupled, and in Laplace form may be written

$$\begin{bmatrix} s^2+4(K_{1a}+K_{2\ell}+K_{3\ell})\frac{g}{W} & 0 & 0 \\ 0 & s^2+4(K_{1\ell}+K_{2a}+K_{3\ell})\frac{g}{W} & 0 \\ 0 & 0 & s^2+4(K_{1\ell}+K_{2\ell}+K_{3a})\frac{g}{W} \end{bmatrix} \begin{bmatrix} \bar{x} \\ \bar{y} \\ \bar{z} \end{bmatrix} = - \begin{bmatrix} s^2\bar{x}_o \\ s^2\bar{y}_o \\ s^2\bar{z}_o \end{bmatrix}$$

$$\begin{bmatrix} \bar{x} \\ \bar{y} \\ \bar{z} \end{bmatrix} = - \begin{bmatrix} 1 & 0 & 0 \\ 0 & 1 & 0 \\ 0 & 0 & 1 \end{bmatrix} \begin{bmatrix} \frac{s^2\bar{x}_o}{s^2+\frac{4g}{W}(K_{1a}+K_{2\ell}+K_{3\ell})} \\ \frac{s^2\bar{y}_o}{s^2+\frac{4g}{W}(K_{1\ell}+K_{2a}+K_{3\ell})} \\ \frac{s^2\bar{z}_o}{s^2+\frac{4g}{W}(K_{1\ell}+K_{2\ell}+K_{3a})} \end{bmatrix}$$

Then,

$$\omega_x^2 = \frac{4g}{W}(K_{1a}+K_{2\ell}+K_{3\ell})$$

$$\omega_y^2 = \frac{4g}{W}(K_{1\ell}+K_{2a}+K_{3\ell})$$

$$\omega_z^2 = \frac{4g}{W}(K_{1\ell}+K_{2\ell}+K_{3a})$$

ω_x, ω_y, and ω_z are obtained from the response spectrum, corresponding to the displacements $\bar{x}$, $\bar{y}$, and $\bar{z}$, and the stiffnesses K_{1a}, $K_{1\ell}$, K_{2a}, $K_{2\ell}$, K_{3a}, $K_{3\ell}$ determined. Several combinations of the above six stiffnesses are possible, the final selection being dependent on practical considerations.

3.5.5.2 Linear Isolators, Eccentrically Placed, Nonlinear Coupling Due to Pendulum Action Ignored (Case B)

The same three arrangements of linear isolators as for Case A have been considered. However, in Case B the center of symmetry of the isolators is not coincident with the center of gravity of the suspended mass. Hence, the first moment of the stiffness matrix of the isolators, as given by matrix [B], will be non-zero. As a result, the translational displacements of the platform, as given by coordinates x, y and z, are no longer independent of the rotational displacements, as given by α, β and γ, and there exists a coupling between the rotational and translational coordinates of the system. Problems of this type reduce to the solution of six simultaneous linear differential equations of the second order.

Example B-1 has been solved numerically, and the effects of small and large eccentricities on the frequencies of the natural modes of vibration of the system are discussed. The problem of equal frequencies for two different modes is also considered.

3.5.5.2.1 Example B-1: Isolators parallel to a single principal axis.

The isolation system is as shown in Figure 3.5.5, page 3-62.

Let K_a = the axial stiffness of each isolator

$K_{\ell x}$ = the lateral stiffness of each isolator in the direction of the x axis

$K_{\ell y}$ = the lateral stiffness of each isolator in the direction of the y axis

Since none of the isolators are inclined with reference to the x, y, and z coordinates, there are no shear components for the stiffness matrix and thus for each isolator:

$$[c] = \begin{bmatrix} c_{11} & 0 & 0 \\ 0 & c_{22} & 0 \\ 0 & 0 & c_{33} \end{bmatrix}$$

The values of the [C], [B] and [E] matrices obtained by the standard formulas are derived on the following pages.

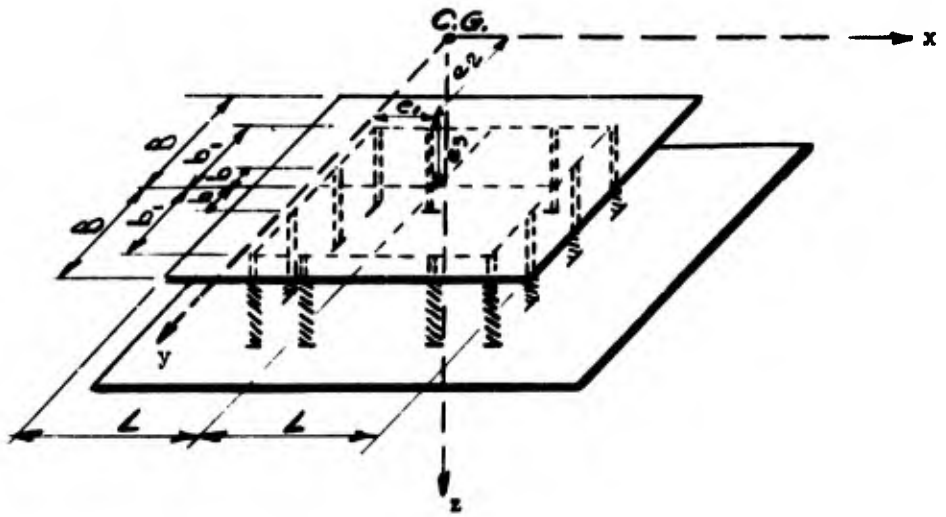

Figure 3.5.5
Linear System With Eccentricities and
Isolators Parallel to a Principal Axis

The six equations of motion in explicit matrix form are given as follows:

$$\begin{bmatrix} m & o & o \\ o & m & o \\ o & o & m \end{bmatrix}\begin{bmatrix} \ddot{x} \\ \ddot{y} \\ \ddot{z} \end{bmatrix} + \begin{bmatrix} 12K_{fx} & o & o \\ o & 12K_{fy} & o \\ o & o & 12K_a \end{bmatrix}\begin{bmatrix} x \\ y \\ z \end{bmatrix} + \begin{bmatrix} o & 12e_3K_{fx} & -12e_2K_{fx} \\ -12e_3K_{fy} & o & 12e_1K_{fy} \\ 12e_2K_a & -12e_1K_a & o \end{bmatrix}\begin{bmatrix} \alpha \\ \beta \\ \gamma \end{bmatrix} = -\begin{bmatrix} m & o & o \\ o & m & o \\ o & o & m \end{bmatrix}\begin{bmatrix} \ddot{x}_o \\ \ddot{y}_o \\ \ddot{z}_o \end{bmatrix}$$

$$\begin{bmatrix} mk_{xx}^2 & -mk_{xy}^2 & -mk_{xz}^2 \\ -mk_{yx}^2 & mk_{yy}^2 & -mk_{yz}^2 \\ -mk_{zx}^2 & -mk_{zy}^2 & mk_{zz}^2 \end{bmatrix}\begin{bmatrix} \ddot{\alpha} \\ \ddot{\beta} \\ \ddot{\gamma} \end{bmatrix} + \begin{bmatrix} o & 12e_3K_{fx} & -12e_2K_{fx} \\ -12e_3K_{fy} & o & 12e_1K_{fy} \\ 12e_2K_a & -12e_1K_a & o \end{bmatrix}\begin{bmatrix} x \\ y \\ z \end{bmatrix} + \begin{bmatrix} 4K_a(b^2+2b_1^2+3e_2^2) & -12e_1e_2K_a & -12e_1e_3K_{fy} \\ +12e_3^2K_{fy} & & \\ -12e_1e_2K_a & 4K_a(\ell^2+2\ell_1^2+3e_1^2) & -12e_2e_3K_{fx} \\ & +12e_3^2K_{fx} & \\ -12e_1e_3K_{fy} & -12e_2e_3K_{fx} & \{4K_{fx}(b^2+2b_1^2+3e_2^2) \\ & & +4K_{fy}(\ell^2+2\ell_1^2+3e_1^2)\} \end{bmatrix}\begin{bmatrix} \alpha \\ \beta \\ \gamma \end{bmatrix} = 0$$

Isolator Number	b_{12} $=(r_3c_{11})$	b_{21} $=(-r_3c_{22})$	b_{23} $=(r_1c_{22})$	b_{32} $=(-r_1c_{33})$	b_{13} $=(-r_2c_{11})$	b_{31} $=(r_2c_{33})$	b_{11}, b_{22}, b_{33}
1	$e_3K_{\ell x}$	$-e_3K_{\ell y}$	$(\ell+e_1)K_{\ell y}$	$-(\ell+e_1)K_a$	$-(b_1+e_2)K_{\ell x}$	$(b_1+e_2)K_a$	0
2	$e_3K_{\ell x}$	$-e_3K_{\ell y}$	$(\ell_1+e_1)K_{\ell y}$	$-(\ell_1+e_1)K_a$	$-(b_1+e_2)K_{\ell x}$	$(b_1+e_2)K_a$	0
3	$e_3K_{\ell x}$	$-e_3K_{\ell y}$	$(\ell_1+e_1)K_{\ell y}$	$-(\ell_1+e_1)K_a$	$-(b+e_2)K_{\ell x}$	$(b+e_2)K_a$	0
4	$e_3K_{\ell x}$	$-e_3K_{\ell y}$	$(\ell_1+e_1)K_{\ell y}$	$-(\ell_1+e_1)K_a$	$-(e_2-b)K_{\ell x}$	$(e_2-b)K_a$	0
5	$e_3K_{\ell x}$	$-e_3K_{\ell y}$	$(\ell_1+e_1)K_{\ell y}$	$-(\ell_1+e_1)K_a$	$-(e_2-b_1)K_{\ell x}$	$(e_2-b_1)K_a$	0
6	$e_3K_{\ell x}$	$-e_3K_{\ell y}$	$(\ell+e_1)K_{\ell y}$	$-(\ell+e_1)K_a$	$-(e_2-b_1)K_{\ell x}$	$(e_2-b_1)K_a$	0
7	$e_3K_{\ell x}$	$-e_3K_{\ell y}$	$(e_1-\ell_1)K_{\ell y}$	$-(e_1-\ell)K_a$	$-(e_2-b_1)K_{\ell x}$	$(e_2-b_1)K_a$	0
8	$e_3K_{\ell x}$	$-e_3K_{\ell y}$	$(e_1-\ell_1)K_{\ell y}$	$-(e_1-\ell_1)K_a$	$-(e_2-b_1)K_{\ell x}$	$(e_2-b_1)K_a$	0
9	$e_3K_{\ell x}$	$-e_3K_{\ell y}$	$(e_1-\ell_1)K_{\ell y}$	$-(e_1-\ell_1)K_a$	$-(e_2-b)K_{\ell x}$	$(e_2-b)K_a$	0
10	$e_3K_{\ell x}$	$-e_3K_{\ell y}$	$(e_1-\ell_1)K_{\ell y}$	$-(e_1-\ell_1)K_a$	$-(b+e_2)K_{\ell x}$	$(b+e_2)K_a$	0
11	$e_3K_{\ell x}$	$-e_3K_{\ell y}$	$(e_1-\ell_1)K_{\ell y}$	$-(e_1-\ell_1)K_a$	$-(b_1+e_2)K_{\ell x}$	$(b_1+2)K_a$	0
12	$e_3K_{\ell x}$	$-e_3K_{\ell y}$	$(e_1-\ell)K_{\ell y}$	$-(e_1-\ell)K_a$	$-(b_1+e_2)K_{\ell x}$	$(b_1+e_2)K_a$	0
$\sum$	$+(12e_3K_{\ell x})$	$-(12e_3K_{\ell y})$	$+(12e_1K_{\ell y})$	$-(12e_1K_a)$	$-(12e_2K_{\ell x})$	$+(12e_2K_a)$	0

$$\therefore \quad [B] = \begin{bmatrix} 0 & 12e_3K_{\ell x} & -12e_2K_{\ell x} \\ -12e_3K_{\ell y} & 0 & 12e_1K_{\ell y} \\ 12e_2K_a & -12e_1K_a & 0 \end{bmatrix}$$

Isolator Number	Axial Orientation	r_1	r_2	r_3	c_{11}	c_{22}	c_{33}	c_{12}, c_{21}, c_{13}, c_{31}, c_{23}, c_{32}
1	Parallel to z axis	$\ell+e_1$	b_1+e_2	e_3	$K_{\ell x}$	$K_{\ell y}$	K_a	o
2	Parallel to z axis	ℓ_1+e_1	b_1+e_2	e_3	$K_{\ell x}$	$K_{\ell y}$	K_a	o
3	Parallel to z axis	ℓ_1+e_1	$b+e_2$	e_3	$K_{\ell x}$	$K_{\ell y}$	K_a	o
4	Parallel to z axis	ℓ_1+e_1	e_2-b	e_3	$K_{\ell x}$	$K_{\ell y}$	K_a	o
5	Parallel to z axis	ℓ_1+e_1	e_2-b_1	e_3	$K_{\ell x}$	$K_{\ell y}$	K_a	o
6	Parallel to z axis	$\ell+e_1$	e_2-b_1	e_3	$K_{\ell x}$	$K_{\ell y}$	K_a	o
7	Parallel to z axis	$e_1-\ell$	e_2-b_1	e_3	$K_{\ell x}$	$K_{\ell y}$	K_a	o
8	Parallel to z axis	$e_1-\ell_1$	e_2-b_1	e_3	$K_{\ell x}$	$K_{\ell y}$	K_a	o
9	Parallel to z axis	$e_1-\ell_1$	e_2-b	e_3	$K_{\ell x}$	$K_{\ell y}$	K_a	o
10	Parallel to z axis	$e_1-\ell_1$	$b+e_2$	e_3	$K_{\ell x}$	$K_{\ell y}$	K_a	o
11	Parallel to z axis	$e_1-\ell_1$	b_1+e_2	e_3	$K_{\ell x}$	$K_{\ell y}$	K_a	o
12	Parallel to z axis	$e_1-\ell$	b_1+e_2	e_3	$K_{\ell x}$	$K_{\ell y}$	K_a	o

$\sum$: $c_{11}=12K_{\ell x}$; $c_{22}=12K_{\ell y}$; $c_{33}=12K_a$; $c_{12}=o$; $c_{21}=o$; $c_{13}=0$; $c_{31}=o$; $c_{23}=o$; $c_{32}=o$

$$[c] = \begin{bmatrix} 12K_{\ell x} & o & o \\ o & 12K_{\ell y} & o \\ o & o & 12K_a \end{bmatrix}$$

ISOLATOR NUMBER	e_{11} $=(r_2 b_{31} - r_3 b_{21})$	e_{12} $=(r_2 b_{32})$	e_{13} $=-(r_3 b_{23})$	e_{21} $=-(r_1 b_{31})$	e_{22} $=(r_3 b_{12} - r_1 b_{32})$	e_{23} $=(r_3 b_{13})$	e_{31} $=(r_1 b_{21})$	e_{32} $=-(r_2 b_{12})$	e_{33} $=(r_1 b_{23} - r_2 b_{13})$
1	$(b_1+e_2)^2 K_a + e_3^2 K_{\ell Y}$	$-(b_1+e_2)(\ell+e_1)K_a$	$-e_3(\ell+e_1)K_{\ell Y}$	$-(\ell+e_1)(b_1+e_2)K_a$	$e_3^2 K_{\ell X}+(\ell+e_1)^2 K_a$	$-e_3(b_1+e_2)K_{\ell X}$	$-e_3(\ell+e_1)K_{\ell Y}$	$-e_3(b_1+e_2)K_{\ell X}$	$(\ell+e_1)^2 K_{\ell Y}+(b_1+e_2)^2 K_{\ell X}$
2	$(b_1+e_2)^2 K_a + e_3^2 K_{\ell Y}$	$-(b_1+e_2)(\ell_1+e_1)K_a$	$-e_3(\ell_1+e_1)K_{\ell Y}$	$-(\ell_1+e_1)(b_1+e_2)K_a$	$e_3^2 K_{\ell X}+(\ell_1+e_1)^2 K_a$	$-e_3(b_1+e_2)K_{\ell X}$	$-e_3(\ell_1+e_1)K_{\ell Y}$	$-e_3(b_1+e_2)K_{\ell X}$	$(\ell_1+e_1)^2 K_{\ell Y}+(b_1+e_2)^2 K_{\ell X}$
3	$(b+e_2)^2 K_a + e_3^2 K_{\ell Y}$	$-(b+e_2)(\ell_1+e_1)K_a$	$-e_3(\ell_1+e_1)K_{\ell Y}$	$-(\ell_1+e_1)(b_1+e_2)K_a$	$e_3^2 K_{\ell X}+(\ell_1+e_1)^2 K_a$	$-e_3(b+e_2)K_{\ell X}$	$-e_3(\ell_1+e_1)K_{\ell Y}$	$-e_3(b+e_2)K_{\ell X}$	$(\ell_1+e_1)^2 K_{\ell Y}+(b+e_2)^2 K_{\ell X}$
4	$(e_2-b)^2 K_a + e_3^2 K_{\ell Y}$	$-(e_2-b)(\ell_1+e_1)K_a$	$-e_3(\ell_1+e_1)K_{\ell Y}$	$-(\ell_1+e_1)(e_2-b)K_a$	$e_3^2 K_{\ell X}+(\ell_1+e_1)^2 K_a$	$-e_3(e_2-b)K_{\ell X}$	$-e_3(\ell_1+e_1)K_{\ell Y}$	$-e_3(e_2-b)K_{\ell X}$	$(\ell_1+e_1)^2 K_{\ell Y}+(e_2-b)^2 K_{\ell X}$
5	$(e_2-b_1)^2 K_a + e_3^2 K_{\ell Y}$	$-(e_2-b_1)(\ell_1+e_1)K_a$	$-e_3(\ell_1+e_1)K_{\ell Y}$	$-(\ell_1+e_1)(e_2-b_1)K_a$	$e_3^2 K_{\ell X}+(\ell_1+e_1)^2 K_a$	$-e_3(e_2-b_1)K_{\ell X}$	$-e_3(\ell_1+e_1)K_{\ell Y}$	$-e_3(e_2-b_1)K_{\ell X}$	$(\ell+e_1)^2 K_{\ell Y}+(e_2-b_1)^2 K_{\ell X}$
6	$(e_2-b_1)^2 K_a + e_3^2 K_{\ell Y}$	$-(e_2-b_1)(\ell+e_1)K_a$	$-e_3(\ell+e_1)K_{\ell Y}$	$-(\ell+e_1)(e_2-b_1)K_a$	$e_3^2 K_{\ell X}+(\ell+e_1)^2 K_a$	$-e_3(e_2-b_1)K_{\ell X}$	$-e_3(\ell+e_1)K_{\ell Y}$	$-e_3(e_2-b_1)K_{\ell X}$	$(\ell+e_1)^2 K_{\ell Y}+(e_2-b_1)^2 K_{\ell X}$
7	$(e_2-b_1)^2 K_a + e_3^2 K_{\ell Y}$	$-(e_2-b_1)(e_1-\ell)K_a$	$-e_3(e_1-\ell)K_{\ell Y}$	$-(e_1-\ell)(e_2-b_1)K_a$	$e_3^2 K_{\ell X}+(e_1-\ell)^2 K_a$	$-e_3(e_2-b_1)K_{\ell X}$	$-e_3(e_1-\ell)K_{\ell Y}$	$-e_3(e_2-b_1)K_{\ell X}$	$(e_1-\ell)^2 K_{\ell Y}+(e_2-b_1)^2 K_{\ell X}$
8	$(e_2-b_1)^2 K_a + e_3^2 K_{\ell Y}$	$-(e_2-b_1)(e_1-\ell_1)K_a$	$-e_3(e_1-\ell_1)K_{\ell Y}$	$-(e_1-\ell_1)(e_2-b_1)K_a$	$e_3^2 K_{\ell X}+(e_1-\ell_1)^2 K_a$	$-e_3(e_2-b_1)K_{\ell X}$	$-e_3(e_1-\ell_1)K_{\ell Y}$	$-e_3(e_2-b_1)K_{\ell X}$	$(e_1-\ell_1)^2 K_{\ell Y}+(e_2-b_1)^2 K_{\ell X}$
9	$(e_2-b)^2 K_a + e_3^2 K_{\ell Y}$	$-(e_2-b)(e_1-\ell_1)K_a$	$-e_3(e_1-\ell_1)K_{\ell Y}$	$-(e_1-\ell)(e_2-b_1)K_a$	$e_3^2 K_{\ell X}+(e_1-\ell_1)^2 K_a$	$-e_3(e_2-b)K_{\ell X}$	$-e_3(e_1-\ell_1)K_{\ell Y}$	$-e_3(e_2-b)K_{\ell X}$	$(e_1-\ell_1)^2 K_{\ell Y}+(e_2-b)^2 K_{\ell X}$
10	$(b+e_2)^2 K_a + e_3^2 K_{\ell Y}$	$-(b+e_2)(e_1-\ell_1)K_a$	$-e_3(e_1-\ell_1)K_{\ell Y}$	$-(e_1-\ell_1)(b+e_2)K_a$	$e_3^2 K_{\ell X}+(e_1-\ell_1)^2 K_a$	$-e_3(b+e_2)K_{\ell X}$	$-e_3(e_1-\ell_1)K_{\ell Y}$	$-e_3(b+e_2)K_{\ell X}$	$(e_1-\ell_1)^2 K_{\ell Y}+(b+e_2)^2 K_{\ell X}$
11	$(b_1+e_2)^2 K_a + e_3^2 K_{\ell Y}$	$-(b_1+e_2)(e_1-\ell_1)K_a$	$-e_3(e_1-\ell_1)K_{\ell Y}$	$-(e_1-\ell_1)(b_1+e_2)K_a$	$e_3^2 K_{\ell X}+(e_1-\ell_1)^2 K_a$	$-e_3(b_1+e_2)K_{\ell X}$	$-e_3(e_1-\ell_1)K_{\ell Y}$	$-e_3(b_1+e_2)K_{\ell X}$	$(e_1-\ell_1)^2 K_{\ell Y}+(b_1+e_2)^2 K_{\ell X}$
12	$(b_1+e_2)^2 K_a + e_3^2 K_{\ell Y}$	$-(b_1-e_2)(e_1-\ell)K_a$	$-e_3(e_1-\ell)K_{\ell Y}$	$-(e_1-\ell)(b_1+e_2)K_a$	$e_3^2 K_{\ell X}+(e_1-\ell)^2 K_a$	$-e_3(b_1+e_2)K_{\ell X}$	$-e_3(e_1-\ell)K_{\ell Y}$	$-e_3(b_1+e_2)K_{\ell X}$	$(e_1-\ell)^2 K_{\ell Y}+(b_1+e_2)^2 K_{\ell X}$

$\sum =$ $e_{11} = 12 e_3^2 K_{\ell Y} + 4 K_a \left[b^2 + 2 b_1^2 + 3 e_2^2 \right]$; $e_{12} = -12 e_1 e_2 K_a$; $e_{13} = -12 e_1 e_3 K_{\ell Y}$; $e_{21} = -12 e_1 e_2 K_a$; $e_{22} = 12 e_3^2 K_{\ell X} + 4 K_a \left[\ell^2 + 2 \ell_1^2 + 3 e_1^2 \right]$;

$e_{23} = -12 e_2 e_3 K_{\ell X}$; $e_{31} = -12 e_1 e_3 K_{\ell Y}$; $e_{32} = -12 e_2 e_3 K_{\ell X}$; $e_{33} = 4 K_{\ell X} (b^2 + 2 b_1^2 + 3 e_2^2) + 4 K_{\ell Y} (\ell^2 + 2 \ell_1^2 + 3 e_1^2)$

$$\therefore [E] = \begin{bmatrix} 4K_a\left[b^2+2b_1^2+3e_2^2\right]+12e_3^2K_{\ell Y} & -12 e_1 e_2 K_a & -12 e_1 e_3 K_{\ell Y} \\ -12 e_1 e_2 K_a & 4K_a\left[\ell^2+2\ell_1^2+3e_1^2\right]+12e_3^2K_{\ell X} & -12 e_2 e_3 K_{\ell X} \\ -12 e_1 e_3 K_{\ell Y} & -12 e_2 e_3 K_{\ell X} & 4K_{\ell X}(b^2+2b_1^2+3e_2^2)+4K_{\ell Y}(\ell^2+2\ell_1^2+3e_1^2) \end{bmatrix}$$

Dividing throughout by m, making the following substitutions:

$$\omega_x^2 = \frac{12}{m} K_{fx}$$

$$\omega_y^2 = \frac{12}{m} K_{fy}$$

$$\omega_z^2 = \frac{12}{m} K_a$$

and converting to the Laplace form, the six equations in matrix form can be written as follows:

$$\begin{bmatrix}
s^2+\omega_x^2 & 0 & 0 & 0 & e_3\omega_x^2 & -e_2\omega_x^2 \\
0 & s^2+\omega_y^2 & 0 & -e_3\omega_y^2 & 0 & e_1\omega_y^2 \\
0 & 0 & s^2+\omega_z^2 & e_2\omega_z^2 & -e_1\omega_z^2 & 0 \\
0 & -e_3\omega_y^2 & e_2\omega_z^2 & \begin{matrix}\vartheta_{xx}^2 s^2+e_3^2\omega_y^2 \\ +\omega_z^2(b^2+2b_1^2+3e_2^2)(\frac{1}{3})\end{matrix} & -\vartheta_{xy}^2 s^2-e_1e_2\omega_z^2 & -\vartheta_{xz}^2 s^2-e_1e_3\omega_y^2 \\
e_3\omega_x^2 & 0 & -e_1\omega_z^2 & -\vartheta_{yx}^2 s^2-e_1e_2\omega_z^2 & \begin{matrix}\vartheta_{yy}^2 s^2+e_3^2\omega_x^2 \\ +\frac{1}{3}\omega_z^2(l^2+2l_1^2+3e_1^2)\end{matrix} & -\vartheta_{yz}^2 s^2-e_1e_3\omega_x^2 \\
-e_2\omega_x^2 & e_1\omega_y^2 & 0 & -\vartheta_{zx}^2 s^2-e_1e_3\omega_y^2 & -\vartheta_{yz}^2 s^2-e_2e_3\omega_x^2 & \begin{matrix}\vartheta_{zz}^2 s^2 \\ +\frac{1}{3}(\omega_x^2)(b^2+2b_1^2+3e_2^2) \\ +\frac{1}{3}(\omega_y^2)(l^2+2l_1^2+3e_1^2)\end{matrix}
\end{bmatrix}
\begin{bmatrix} \bar{x} \\ \bar{y} \\ \bar{z} \\ \bar{\alpha} \\ \bar{\beta} \\ \bar{\gamma} \end{bmatrix}
=
\begin{bmatrix} -s\bar{x}_o \\ -s\bar{y}_o \\ -s\bar{z}_o \\ 0 \\ 0 \\ 0 \end{bmatrix}$$

Or concisely $$\left[\Delta\right]\left[\bar{X}\right] = -\left[\bar{Y}_o\right]$$

Then $$\left[\bar{X}\right] = -\left[\Delta\right]^{-1}\left[\bar{X}_o\right]$$

3.5.5.2.2 Example B-2: Isolators inclined to principal axes.

The isolation system is as shown in Figure 3.5.6.

Let K_{av} = axial stiffness of each vertical isolator

$K_{\ell v}$ = lateral stiffness of each vertical isolator

K_{ah} = axial stiffness of each horizontal isolator

$K_{\ell h}$ = lateral stiffness of each horizontal isolator

The isolator stiffnesses are the same as for Example A-2, however, the values ℓ_1, ℓ_2 and ℓ_3, must be modified to include the eccentricities. Hence, the [B] and [E] matrices are not similar to the corresponding [B] and [E] matrices of Example A-2, although the [C] matrix is similar. The evaluation of the [C] , [B] and [E] matrices for this configuration is shown on the following pages.

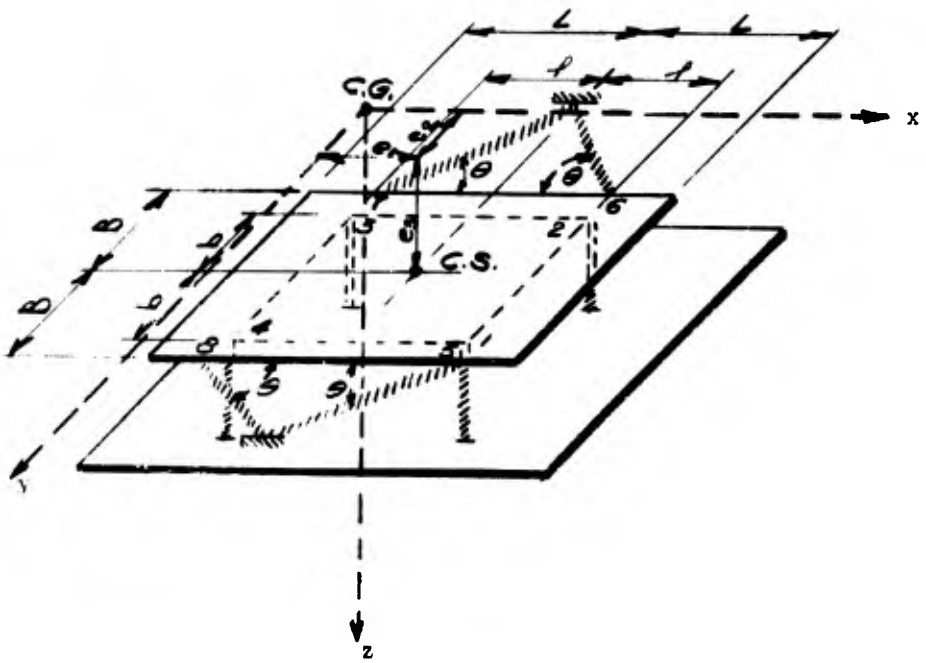

Figure 3.5.6
Linear System With Eccentricities
and Isolators Inclined to Principal Axes

Isolator Number	Axial Orientation	r_1	r_2	r_3	c_{11}	c_{22}	c_{33}	c_{12}	c_{21}	c_{31}, c_{13} c_{23}, c_{32}
1	Parallel to z axis	$\ell+e_1$	$b+e_2$	e_3	$K_{\ell v}$	$K_{\ell v}$	K_{av}	0	0	0
2	Parallel to z axis	$\ell+e_1$	e_2-b	e_3	$K_{\ell v}$	$K_{\ell v}$	K_{av}	0	0	0
3	Parallel to z axis	$e_1-\ell$	e_2-b	e_3	$K_{\ell v}$	$K_{\ell v}$	K_{av}	0	0	0
4	Parallel to z axis	$e_1-\ell$	$b+e_2$	e_3	$K_{\ell v}$	$K_{\ell v}$	K_{av}	0	0	0
5	$(180+\theta)^\circ$ to x axis	$\ell+e_1$	$B+e_2$	e_3	$K_{\ell h}\sin^2\theta + K_{ah}\cos^2\theta$	$K_{ah}\sin^2\theta + K_{\ell h}\cos^2\theta$	$K_{\ell h}$	$K_{\ell h}\frac{\sin 2\theta}{2} - K_{ah}\frac{\sin 2\theta}{2}$	$K_{\ell h}\frac{\sin 2\theta}{2} - K_{ah}\frac{\sin 2\theta}{2}$	0
6	$(180-\theta)^\circ$ to x axis	$\ell+e_1$	e_2-B	e_3	$K_{\ell h}\sin^2\theta + K_{ah}\cos^2\theta$	$K_{ah}\sin^2\theta + K_{\ell h}\cos^2\theta$	$K_{\ell h}$	$-K_{\ell h}\frac{\sin 2\theta}{2} + K_{ah}\frac{\sin 2\theta}{2}$	$-K_{\ell h}\frac{\sin 2\theta}{2} + K_{ah}\frac{\sin 2\theta}{2}$	0
7	$+\theta$ to x axis	$e_1-\ell$	e_2-B	e_3	$K_{\ell h}\sin^2\theta + K_{ah}\cos^2\theta$	$K_{ah}\sin^2\theta + K_{\ell h}\cos^2\theta$	$K_{\ell h}$	$K_{\ell h}\frac{\sin 2\theta}{2} - K_{ah}\frac{\sin 2\theta}{2}$	$K_{\ell h}\frac{\sin 2\theta}{2} - K_{ah}\frac{\sin 2\theta}{2}$	0
8	$-\theta^\circ$ to x axis	$e_1-\ell$	$B+e_2$	e_3	$K_{\ell h}\sin^2\theta + K_{ah}\cos^2\theta$	$K_{ah}\sin^2\theta + K_{\ell h}\cos^2\theta$	$K_{\ell h}$	$-K_{\ell h}\frac{\sin 2\theta}{2} + K_{ah}\frac{\sin 2\theta}{2}$	$-K_{\ell h}\frac{\sin 2\theta}{2} + K_{ah}\frac{\sin 2\theta}{2}$	0

$$\sum = \quad c_{11}=4K_{\ell v}+4(K_{\ell h}\sin^2\theta+K_{ah}\cos^2\theta);\ c_{22}=4(K_{ah}\sin^2\theta+K_{\ell h}\cos^2\theta)+4K_{\ell v};\ c_{33}=4(K_{\ell h}+K_{av});$$

$$c_{12}=0;\ c_{21}=0;\ c_{31}=0;\ c_{13}=0;\ c_{23}=0;\ c_{32}=0$$

$$[c] = \begin{bmatrix} 4(K_{\ell v}+K_{\ell h}\sin^2\theta+K_{ah}\cos^2\theta) & 0 & 0 \\ 0 & 4(K_{\ell v}+K_{ah}\sin^2\theta+K_{\ell h}\cos^2\theta) & 0 \\ 0 & 0 & 4(K_{\ell h}+K_{av}) \end{bmatrix}$$

Isolator Number	b_{11} $=-(r_3c_{12})$	b_{22} $=(r_3c_{21})$	b_{33}	b_{12} $=(r_3c_{11})$	b_{21} $=-(r_3c_{22})$	b_{13} $=(r_1c_{12}-r_2c_{11})$	b_{31} $=(r_2c_{33})$	b_{32} $=(-r_1c_{33})$	b_{23} $=(r_1c_{22}-r_2c_{21})$
1	o	o	o	e_3K_{fv}	$-e_3K_{fv}$	$-(b+e_2)K_{fv}$	$(b+e_2)K_{av}$	$-(f+e_1)K_{av}$	$(f+e_1)K_{fv}$
2	o	o	o	e_3K_{fv}	$-e_3K_{fv}$	$-(e_2-b)K_{fv}$	$(e_2-b)K_{av}$	$-(f+e_1)K_{av}$	$(f+e_1)K_{fv}$
3	o	o	o	e_3K_{fv}	$-e_3K_{fv}$	$-(e_2-b)K_{fv}$	$(e_2-b)K_{av}$	$-(e_1-f)K_{av}$	$(e_1-f)K_{fv}$
4	o	o	o	e_3K_{fv}	$-e_3K_{fv}$	$-(b+e_2)K_{fv}$	$(b+e_2)K_{av}$	$-(e_1-f)K_{av}$	$(e_1-f)K_{fv}$
5	$-e_3\frac{\sin2\theta}{2}(K_{fh}-K_{ah})$	$e_3\frac{\sin2\theta}{2}(K_{fh}-K_{ah})$	o	$e_3\left[K_{fh}\sin^2\theta+K_{ah}\cos^2\theta\right]$	$-e_3\left[K_{ah}\sin^2\theta+K_{fh}\cos^2\theta\right]$	$-(B+e_2)(K_{fh}\sin^2\theta+K_{ah}\cos^2\theta)+(f+e_1)(\frac{\sin2\theta}{2})(K_{fh}-K_{ah})$	$(B+e_2)K_{fh}$	$-(f+e_1)K_{fh}$	$(f+e_1)(K_{ah}\sin\theta+K_{fh}\cos\theta)-(B+e_2)(\frac{\sin2\theta}{2})(K_{fh}-K_{ah})$
6	$e_3\frac{\sin2\theta}{2}(K_{fh}-K_{ah})$	$-e_3\frac{\sin2\theta}{2}(K_{fh}-K_{ah})$	o	$e_3\left[K_{fh}\sin^2\theta+K_{ah}\cos^2\theta\right]$	$-e_3\left[K_{ah}\sin^2\theta+K_{fh}\cos^2\theta\right]$	$-(e_2-B)(K_{fh}\sin^2\theta+K_{ah}\cos^2\theta)+(f-e_1)(\frac{\sin2\theta}{2})(K_{fh}-K_{ah})$	$(e_2-B)K_{fh}$	$-(f+e_1)K_{fh}$	$(f+e_1)(K_{ah}\sin\theta+K_{fh}\cos\theta)-(e_2-B)(\frac{\sin2\theta}{2})(K_{fh}-K_{ah})$
7	$-e_3\frac{\sin2\theta}{2}(K_{fh}-K_{ah})$	$e_3\frac{\sin2\theta}{2}(K_{fh}-K_{ah})$	o	$e_3\left[K_{fh}\sin^2\theta+K_{ah}\cos^2\theta\right]$	$-e_3\left[K_{ah}\sin^2\theta+K_{fh}\cos^2\theta\right]$	$-(e_2-B)(K_{fh}\sin^2\theta+K_{ah}\cos^2\theta)+(e_1-f)(\frac{\sin2\theta}{2})(K_{fh}-K_{ah})$	$(e_2-B)K_{fh}$	$-(e_1-f)K_{fh}$	$(e_1-f)(K_{ah}\sin\theta+K_{fh}\cos\theta)-(e_2-B)(\frac{\sin2\theta}{2})(K_{fh}-K_{ah})$
8	$e_3\frac{\sin2\theta}{2}(K_{fh}-K_{ah})$	$-e_3\frac{\sin2\theta}{2}(K_{fh}-K_{ah})$	o	$e_3\left[K_{fh}\sin^2\theta+K_{ah}\cos^2\theta\right]$	$-e_3\left[K_{ah}\sin^2\theta+K_{fh}\cos^2\theta\right]$	$-(B+e_2)(K_{fh}\sin^2\theta+K_{ah}\cos^2\theta)+(e_1-f)(\frac{\sin2\theta}{2})(K_{fh}-K_{ah})$	$(B+e_2)K_{fh}$	$-(e_1-f)K_{fh}$	$(e_1-f)(K_{ah}\sin\theta+K_{fh}\cos\theta)-(B+e_2)(\frac{\sin2\theta}{2})(K_{fh}-K_{ah})$

$\sum$: $b_{11}=0$; $b_{22}=0$; $b_{33}=0$; $b_{12}=4e_3\left[K_{fh}\sin^2\theta+K_{ah}\cos^2\theta+K_{fv}\right]$; $b_{21}=-4e_3\left[K_{ah}\sin^2\theta+K_{fh}\cos^2\theta+K_{fv}\right]$; $b_{13}=-4e_2\left[K_{fh}\sin^2\theta+K_{ah}\cos^2\theta+K_{fv}\right]$; $b_{31}=4e_2\left[K_{fh}+K_{av}\right]$;

$b_{32}=-4e_1\left[K_{fh}+K_{av}\right]$; $b_{23}=4e_1\left[K_{ah}\sin^2\theta+K_{fh}\cos^2\theta+K_{fv}\right]$

$$\therefore [B] = \begin{bmatrix} o & 4e_3(K_{fv}+K_{fh}\sin^2\theta+K_{ah}\cos^2\theta) & -4e_2(K_{fv}+K_{fh}\sin^2\theta+K_{ah}\cos^2\theta) \\ -4e_3(K_{fv}+K_{ah}\sin^2\theta+K_{fh}\cos^2\theta) & o & 4e_1(K_{fv}+K_{ah}\sin^2\theta+K_{fh}\cos^2\theta) \\ 4e_2(K_{av}+K_{fh}) & -4e_1(K_{av}+K_{fh}) & o \end{bmatrix}$$

Isolator Number	e_{21} $(r_3b_{11}-r_1b_{31})$	e_{13} $(-r_3b_{23})$	e_{31} $(r_1b_{21}-r_2b_{11})$	e_{23} (r_3b_{13})	e_{32} $(r_1b_{22}-r_2b_{12})$
1	$-(\ell+e_1)(b+e_2)K_{av}$	$-e_3(\ell+e_1)K_{fv}$	$-(\ell+e_1)e_3K_{fv}$	$-e_3(b+e_2)K_{fv}$	$-(b+e_2)e_3K_{fv}$
2	$-(\ell+e_1)(e_2-b)K_{av}$	$-e_3(\ell+e_1)K_{fv}$	$-(\ell+e_1)e_3K_{fv}$	$-e_3(e_2-b)K_{fv}$	$-(e_2-b)e_3K_{fv}$
3	$-(e_1-\ell)(e_2-b)K_{av}$	$-e_3(e_1-\ell)K_{fv}$	$-(e_1-\ell)e_3K_{fv}$	$-e_3(e_2-b)K_{fv}$	$-(e_2-b)e_3K_{fv}$
4	$-(e_1-\ell)(b+e_2)K_{av}$	$-e_3(e_1-\ell)K_{fv}$	$-(e_1-\ell)e_3K_{fv}$	$-e_3(b+e_2)K_{fv}$	$-(b+e_2)e_3K_{fv}$
5	$\left[e_3^2(-\frac{\sin2\theta}{2})(K_{fh}-K_{ah})\right.$ $\left.-(\ell+e_1)(B+e_2)K_{fh}\right]$	$-e_3\left[(\ell+e_1)(K_{ah}\sin^2\theta+K_{fh}\cos^2\theta)\right.$ $\left.+(B+e_2)(-\frac{\sin2\theta}{2})(K_{fh}-K_{ah})\right]$	$-(\ell+e_1)e_3(K_{ah}\sin^2\theta+K_{fh}\cos^2\theta)$ $-(B+e_2)e_3(-\frac{\sin2\theta}{2})(K_{fh}-K_{ah})$	$e_3(\ell+e_1)(\frac{\sin2\theta}{2})(K_{fh}-K_{ah})$ $-e_3(B+e_2)(K_{fh}\sin^2\theta+K_{ah}\cos^2\theta)$	$(\ell+e_1)e_3(\frac{\sin2\theta}{2})(K_{fh}-K_{ah})$ $-(B+e_2)e_3(K_{fh}\sin^2\theta+K_{ah}\cos^2\theta)$
6	$\left[-e_3^2(-\frac{\sin2\theta}{2})(K_{fh}-K_{ah})\right.$ $\left.-(\ell+e_1)(e_2-B)K_{fh}\right]$	$-e_3\left[(\ell+e_1)(K_{ah}\sin^2\theta+K_{fh}\cos^2\theta)\right.$ $\left.+(e_2-B)(\frac{\sin2\theta}{2})(K_{fh}-K_{ah})\right]$	$-(\ell+e_1)e_3(K_{ah}\sin^2\theta+K_{fh}\cos^2\theta)$ $-(e_2-B)e_3(\frac{\sin2\theta}{2})K_{fh}-K_{ah})$	$e_3(\ell+e_1)(-\frac{\sin2\theta}{2})(K_{fh}-K_{ah})$ $-e_3(e_2-B)(K_{fh}\sin^2\theta+K_{ah}\cos^2\theta)$	$(\ell+e_1)e_3(-\frac{\sin2\theta}{2})(K_{fh}-K_{ah})$ $-(e_2-B)e_3(K_{fh}\sin^2\theta+K_{ah}\cos^2\theta)$
7	$\left[e_3^2(-\frac{\sin2\theta}{2})(K_{fh}-K_{ah})\right.$ $\left.-(e_1-\ell)(e_2-B)K_{fh}\right]$	$-e_3\left[(e_1-\ell)(K_{ah}\sin^2\theta+K_{fh}\cos^2\theta)\right.$ $\left.+(e_2-B)(-\frac{\sin2\theta}{2})(K_{fh}-K_{ah})\right]$	$-(e_1-\ell)e_3(K_{ah}\sin^2\theta+K_{fh}\cos^2\theta)$ $-(e_2-B)e_3(-\frac{\sin2\theta}{2})(K_{fh}-K_{ah})$	$e_3(e_1-\ell)(\frac{\sin2\theta}{2})(K_{fh}-K_{ah})$ $-e_3(e_2-B)(K_{fh}\sin^2\theta+K_{ah}\cos^2\theta)$	$(e_1-\ell)e_3(\frac{\sin2\theta}{2})(K_{fh}-K_{ah})$ $-(e_2-B)e_3(K_{fh}\sin^2\theta+K_{ah}\cos^2\theta)$
8	$\left[e_3^2(-\frac{\sin2\theta}{2})(K_{fh}-K_{ah})\right.$ $\left.-(e_1-\ell)(B+e_2)K_{fh}\right]$	$-e_3\left[(e_1-\ell)(K_{ah}\sin^2\theta+K_{fh}\cos^2\theta)\right.$ $\left.+(B+e_2)(\frac{\sin2\theta}{2})(K_{fh}-K_{ah})\right]$	$-(B+e_2)e_3(\frac{\sin2\theta}{2})(K_{fh}-K_{ah})$	$-e_3(B+e_2)(K_{fh}\sin^2\theta+K_{ah}\cos^2\theta)$	$-(B+e_2)e_3(K_{fh}\sin^2\theta+K_{ah}\cos^2\theta)$

3-70(a)

$$[E]=\begin{bmatrix}
\left[4b^2K_{av}+4B^2K_{fh}+4e_2^2(K_{av}+K_{fh})\right. & (-4e_1e_2K_{av}-4e_1e_2K_{fh}) & \left[-4e_1e_3K_{fv}-4e_1e_3(K_{ah}\sin^2\theta+K_{fh}\cos^2\theta)\right. \\
\left.+4e_3^2K_{fv}+4e_3^2(K_{ah}\sin^2\theta+K_{fh}\cos^2\theta)\right] & & \\
(-4e_1e_2K_{av}-4e_1e_2K_{fh}) & \left[4\ell^2(K_{av}+K_{fh})+4e_1^2(K_{av}+K_{fh})\right. & \left[-4e_2e_3K_{fv}-4e_2e_3(K_{fh}\sin^2\theta+K_{ah}\cos^2\theta)\right] \\
 & \left.+4e_3^2K_{fv}+4e_3^2(K_{fh}\sin^2\theta+K_{ah}\cos^2\theta)\right] & \\
\left[-4e_1e_3K_{fv}-4e_1e_3(K_{ah}\sin^2\theta+K_{fh}\cos^2\theta)\right] & \left[-4e_2e_3K_{fv}-4e_2e_3(K_{fh}\sin^2\theta+K_{ah}\cos^2\theta)\right] & \left[4(\ell^2+e_1^2)(K_{ah}\sin^2\theta+K_{fh}\cos^2\theta)\right. \\
 & & +4(B^2+e_2^2)(K_{fh}\sin^2\theta+K_{ah}\cos^2\theta) \\
 & & +4(\ell^2+e_1^2)K_{fv}+4(b^2+e_2^2)K_{fv} \\
 & & \left.+8Be(-\frac{\sin2\theta}{2})(K_{fh}-K_{ah})\right]
\end{bmatrix}$$

Isolator Number	e_{11} $(r_2b_{11} - r_3b_{21})$	e_{22} $(r_3b_{12} - r_1b_{32})$	e_{33} $(r_1b_{23} - r_2b_{13})$	e_{12} $(r_2b_{32} - r_3b_{22})$
1	$(b+e_2)^2K_{av}+e_3^2K_{\ell v}$	$e_3^2K_{\ell v}+(\ell+e_1)^2K_{av}$	$(\ell+e_1)^2K_{\ell v}+(b+e_2)^2K_{\ell v}$	$-(b+e_2)(\ell+e_1)K_{av}$
2	$(e_2-b)^2K_{av}+e_3^2K_{\ell v}$	$e_3^2K_{\ell v}+(\ell+e_1)^2K_{av}$	$(\ell+e_1)^2K_{\ell v}+(e_2-b)^2K_{\ell v}$	$-(e_2-b)(\ell+e_1)K_{av}$
3	$(e_2-b)^2K_{av}+e_3^2K_{\ell v}$	$e_3^2K_{\ell v}+(e_1-\ell)^2K_{av}$	$(e_1-\ell)^2K_{\ell v}+(e_2-b)^2K_{\ell v}$	$-(e_2-b)(e_1-\ell)K_{av}$
4	$(b+e_2)^2K_{av}+e_3^2K_{\ell v}$	$e_3^2K_{\ell v}+(e_1-\ell)^2K_{av}$	$(e_1-\ell)^2K_{\ell v}+(b+e_2)^2K_{\ell v}$	$-(b+e_2)(e_1-\ell)K_{av}$
5	$(B+e_2)^2K_{\ell h}+e_3^2$ $(K_{ah}\sin^2\theta+K_{\ell h}\cos^2\theta)$	$e_3^2\{K_{\ell h}\sin^2\theta+K_{ah}\cos^2\theta\}$ $+(\ell+e_1)^2K_{\ell h}$	$(\ell+e_1)\{(\ell+e_1)(K_{ah}\sin^2\theta+K_{\ell h}\cos^2\theta)-(b+e_2)$ $(\frac{\sin2\theta}{2})(K_{\ell h}-K_{ah})\}+(b+e_2)\{(\ell+e_1)$ $(\frac{\sin2\theta}{2})(K_{\ell h}-K_{ah})-(b+e_2)(K_{\ell h}\sin^2\theta$ $+K_{ah}\cos^2\theta)\}$	$-(B+e_2)(\ell+e_1)K_{\ell h}$ $-e_3^2(\frac{\sin2\theta}{2})(K_{\ell h}-K_{ah})$
6	$(e_2-B)^2K_{\ell h}+e_3^2$ $(K_{ah}\sin^2\theta+K_{\ell h}\cos^2\theta)$	$e_3^2(K_{\ell h}\sin^2\theta+K_{ah}\sin^2\theta)$ $+(\ell+e_1)^2K_{\ell h}$	$(\ell+e_1)\{(\ell+e_1)(K_{ah}\sin^2\theta+K_{\ell h}\cos^2\theta)-(e_2-B)$ $(\frac{\sin2\theta}{2})(K_{\ell h}-K_{ah})\}+(e_2-B)\{(\ell+e_1)$ $(\frac{\sin2\theta}{2})(K_{\ell h}-K_{ah})-(e_2-B)(K_{\ell h}\sin^2\theta$ $+K_{ah}\cos^2\theta)\}$	$-(e_2-B)(\ell+e_1)K_{\ell h}$ $-e_3^2(\frac{\sin2\theta}{2})(K_{\ell h}-K_{ah})$
7	$(e_2-B)^2K_{\ell h}+e_3^2$ $(K_{ah}\sin^2\theta+K_{\ell h}\cos^2\theta)$	$e_3^2(K_{\ell h}\sin^2\theta+K_{ah}\cos^2\theta)$ $+(e_1-\ell)^2K_{\ell h}$	$(e_1-\ell)\{(e_1-\ell)(K_{ah}\sin^2\theta+K_{\ell h}\cos^2\theta)-(e_2-B)$ $(\frac{\sin2\theta}{2})(K_{\ell h}-K_{ah})\}+(e_2-B)\{(e_1-\ell)$ $(\frac{\sin2\theta}{2})(K_{\ell h}-K_{ah})-(e_2-B)(K_{\ell h}\sin^2\theta$ $+K_{ah}\cos^2\theta)\}$	$-(e_2-B)(e_1-\ell)K_{\ell h}$ $-e_3^2(\frac{\sin2\theta}{2})(K_{\ell h}-K_{ah})$
8	$(B+e_2)^2K_{\ell h}+e_3^2$ $(K_{ah}\sin^2\theta+K_{\ell h}\cos^2\theta)$	$e_3^2(K_{\ell h}\sin^2\theta+K_{ah}\cos^2\theta)$ $+(e_1-\ell)^2K_{\ell h}$	$(e_1-\ell)\{(e_1-\ell)(K_{ah}\sin^2\theta+K_{\ell h}\cos^2\theta)-(B+e_2)$ $(\frac{\sin2\theta}{2})(K_{\ell h}-K_{ah})-(B+e_2)(e_1-\ell)$ $(\frac{\sin2\theta}{2})(K_{\ell h}-K_{ah})\}+(B+e_2)\{K_{\ell h}\sin^2\theta$ $+K_{ah}\cos^2\theta)\}$	$-(B+e_2)(e_1-\ell)K_{\ell h}$ $-e_3^2(\frac{\sin2\theta}{2})(K_{\ell h}-K_{ah})$

The six equations of motion in matrix form are:

$$\begin{bmatrix} m & o & o \\ o & m & o \\ o & o & m \end{bmatrix} \begin{bmatrix} \ddot{x} \\ \ddot{y} \\ \ddot{z} \end{bmatrix} + \begin{bmatrix} 4(K_{1a}+K_{2\ell}+K_{3\ell}) & o & o \\ o & 4(K_{1\ell}+K_{2a}+K_{3\ell}) & o \\ o & o & 4(K_{1\ell}+K_{2\ell}+K_{3a}) \end{bmatrix} \begin{bmatrix} x \\ y \\ z \end{bmatrix} +$$

$$\begin{bmatrix} o & 4e_3(K_{1a}+K_{2\ell}+K_{3\ell}) & -4e_2(K_{1a}+K_{2\ell}+K_{3\ell}) \\ -4e_3(K_{1\ell}+K_{2a}+K_{3\ell}) & o & +4e_1(K_{1\ell}+K_{2a}+K_{3\ell}) \\ 4e_2(K_{1\ell}+K_{2\ell}+K_{3a}) & -4e_1(K_{1\ell}+K_{2\ell}+K_{3a}) & o \end{bmatrix} \begin{bmatrix} \alpha \\ \beta \\ \gamma \end{bmatrix} = - \begin{bmatrix} m & o & o \\ o & m & o \\ o & o & m \end{bmatrix} \begin{bmatrix} \ddot{x}_o \\ \ddot{y}_o \\ \ddot{z}_o \end{bmatrix}$$

and

$$\begin{bmatrix} m\mathfrak{g}_{xx}^2 & -m\mathfrak{g}_{xy}^2 & -m\mathfrak{g}_{xz}^2 \\ -m\mathfrak{g}_{yx}^2 & m\mathfrak{g}_{yy}^2 & -m\mathfrak{g}_{yz}^2 \\ -m\mathfrak{g}_{zx}^2 & -m\mathfrak{g}_{zy}^2 & m\mathfrak{g}_{zz}^2 \end{bmatrix} \begin{bmatrix} \ddot{\alpha} \\ \ddot{\beta} \\ \ddot{\gamma} \end{bmatrix} + \begin{bmatrix} o & -4e_3(K_{1\ell}+K_{2a}+K_{3\ell}) & 4e_2(K_{1\ell}+K_{2\ell}+K_{3a}) \\ 4e_3(K_{1a}+K_{2\ell}+K_{3\ell}) & o & -4e_1(K_{1\ell}+K_{2\ell}+K_{3a}) \\ -4e_2(K_{1a}+K_{2\ell}+K_{3\ell}) & 4e_1(K_{1\ell}+K_{2a}+K_{3\ell}) & o \end{bmatrix} \begin{bmatrix} x \\ y \\ z \end{bmatrix}$$

$$\begin{bmatrix} \{4(B^2K_{2\ell}+b^2K_{1\ell}+b_1^2K_{3a}) & & \\ +4e_2^2(K_{2\ell}+K_{1\ell}+K_{3a}) & -4e_1e_2(K_{2\ell}+K_{1\ell}+K_{3a}) & -4e_1e_3(K_{1\ell}+K_{2a}+K_{3\ell}) \\ +4e_3^2(K_{2a}+K_{1\ell}+K_{3\ell})\} & & \\ & \{4(\ell^2K_{2\ell}+L^2K_{1\ell}+\ell_1^2K_{3a}) & \\ -4e_1e_2(K_{1\ell}+K_{2\ell}+K_{3a}) & +4e_1^2(K_{1\ell}+K_{2\ell}+K_{3a}) & -4e_2e_3(K_{1a}+K_{2\ell}+K_{3\ell}) \\ & +4e_3^2(K_{1a}+K_{2\ell}+K_{3\ell})\} & \\ & & 4\{\ell^2K_{2a}+L^2K_{1\ell}+\ell_1^2K_{3\ell}+B^2K_{2\ell} \\ -4e_1e_3(K_{1\ell}+K_{2a}+K_{3\ell}) & -4e_2e_3(K_{1a}+K_{2\ell}+K_{3\ell}) & +b^2K_{1a}+b_1^2K_{3\ell}\} \\ & & +4e_1^2(K_{1\ell}+K_{2a}+K_{3\ell})+4e_2^2(K_{1a}+K_{2\ell}+K_{3\ell}) \end{bmatrix} \begin{bmatrix} \alpha \\ \beta \\ \gamma \end{bmatrix} = o$$

Dividing throughout by m, making the following substitutions

$$\omega_x^2 = \frac{4}{m}(K_{1a}+K_{2\ell}+K_{3\ell})$$

$$\omega_y^2 = \frac{4}{m}(K_{1\ell}+K_{2a}+K_{3\ell})$$

$$\omega_z^2 = \frac{4}{m}(K_{1\ell}+K_{2\ell}+K_{3a})$$

and converting to the Laplace form, the above equations may be rewritten in matrix form as follows:

$$\begin{bmatrix} s^2+\omega_x^2 & 0 & 0 & 0 & e_3\omega_x^2 & -e_2\omega_x^2 \\ 0 & s^2+\omega_y^2 & 0 & -e_3\omega_y^2 & 0 & e_1\omega_y^2 \\ 0 & 0 & s^2+\omega_z^2 & e_2\omega_z^2 & -e_1\omega_z^2 & 0 \\ 0 & -e_3\omega_y^2 & e_2\omega_z^2 & \left\{\rho_{xx}^2 s^2+e_3^2\omega_y^2+e_2^2\omega_z^2 \right. & -(\rho_{xy}^2 s^2+e_1e_2\omega_z^2) & -(\rho_{xz}^2 s^2+e_1e_3\omega_y^2) \\ & & & \left. +4\frac{b^2}{m} K_{av}+4\frac{B^2}{m} K_{\rho h}\right\} & & \\ e_3\omega_x^2 & 0 & -e_1\omega_x^2 & -(\rho_{yx}^2 s^2+e_1e_2\omega_z^2) & \left\{\rho_{yy}^2 s^2+e_3^2\omega_x^2 \right. & -(\rho_{yz}^2 s^2+e_2e_3\omega_x^2) \\ & & & & \left. +e_1^2\omega_z^2+\ell^2\omega_z^2\right\} & \\ -e_2\omega_x^2 & e_1\omega_y^2 & 0 & -(\rho_{zx}^2 s^2+e_1e_3\omega_y^2) & -(\rho_{zy}^2 s^2+e_2e_3\omega_x^2) & \left\{\rho_{zz}^2 s^2+e_1^2\omega_y^2+e_2^2\omega_x^2 \right. \\ & & & & & \left. +\ell^2\omega_y^2+B^2\omega_x^2 \right. \\ & & & & & \left. +8\frac{B\ell}{m}(K_{\rho h}-K_{ah})(-\frac{\sin 2\theta}{2})\right\} \end{bmatrix} \begin{bmatrix} \bar{x} \\ \bar{y} \\ \bar{z} \\ \bar{\alpha} \\ \bar{\beta} \\ \bar{\gamma} \end{bmatrix} = - \begin{bmatrix} s^2\bar{x}_o \\ s^2\bar{y}_o \\ s^2\bar{z}_o \\ 0 \\ 0 \\ 0 \end{bmatrix}$$

Or, as before, $[\Delta]\{\bar{X}\} = -\{\bar{X}_o\}$

Then, $\{\bar{X}\} = -[\Delta]^{-1}\{\bar{X}_o\}$

3.5.5.2.3 Example B-3: Isolators parallel to all three principal axes.

The isolation system is as shown in Figure 3.5.7, page 3-73

Let K_{1a} = axial stiffness of each isolator parallel to the x axis

K_1 = lateral stiffness of each isolator parallel to the x axis

K_{2a} = axial stiffness of each isolator parallel to the y axis

K_2 = lateral stiffness of each isolator parallel to the y axis

K_{3a} = axial stiffness of each isolator parallel to the z axis

K_3 = lateral stiffness of each isolator parallel to the z axis

Since none of the isolators are inclined with reference to the x, y, and z coordinates, there are no shear components for the stiffness matrix.

$$\therefore \quad [c] = \begin{bmatrix} c_{11} & 0 & 0 \\ 0 & c_{22} & 0 \\ 0 & 0 & c_{33} \end{bmatrix}$$

The values of the $[C]$, $[B]$ and $[E]$ matrices obtained by the standard formulas, are derived on the following pages.

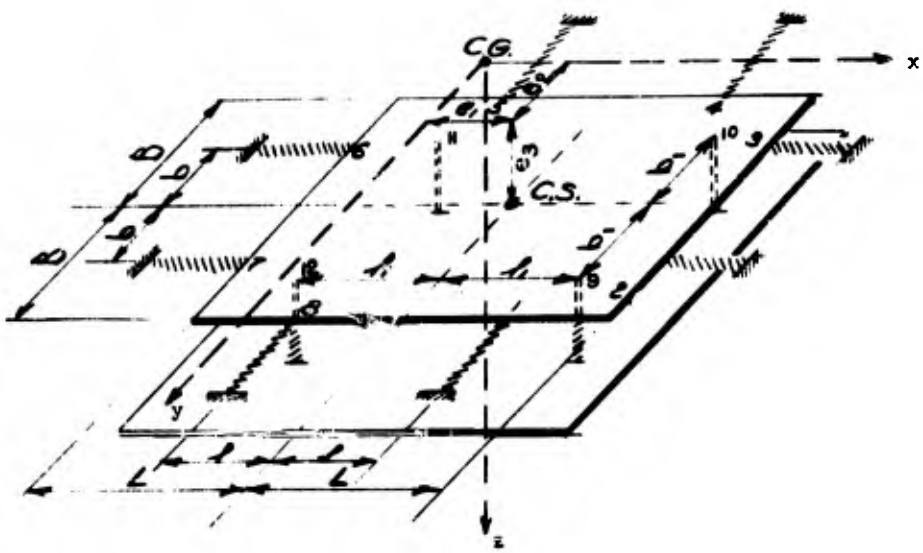

Figure 3.5.7
Linear System With Eccentricities and Isolators
Parallel to all Three Principal Axes

Isolator Number	Axial Orientation	r_1	r_2	r_3	c_{11}	c_{22}	c_{33}	c_{12}, c_{21}, c_{23}, c_{32}, c_{13}, c_{31}
1	Parallel to y Axis	$\ell + e_1$	$B + e_2$	e_3	$K_{2\ell}$	K_{2a}	$K_{2\ell}$	0
4	Parallel to y Axis	$\ell + e_1$	$e_2 - B$	e_3	$K_{2\ell}$	K_{2a}	$K_{2\ell}$	0
5	Parallel to y Axis	$e_1 - \ell$	$e_2 - B$	e_3	$K_{2\ell}$	K_{2a}	$K_{2\ell}$	0
8	Parallel to y Axis	$e_1 - \ell$	$B + e_2$	e_3	$K_{2\ell}$	K_{2a}	$K_{2\ell}$	0
2	Parallel to x Axis	$L + e_1$	$b + e_2$	e_3	K_{1a}	$K_{1\ell}$	$K_{1\ell}$	0
3	Parallel to x Axis	$L + e_1$	$e_2 - b$	e_3	K_{1a}	$K_{1\ell}$	$K_{1\ell}$	0
6	Parallel to x Axis	$e_1 - L$	$e_2 - b$	e_3	K_{1a}	$K_{1\ell}$	$K_{1\ell}$	0
7	Parallel to x Axis	$e_1 - L$	$b + e_2$	e_3	K_{1a}	$K_{1\ell}$	$K_{1\ell}$	0
9	Parallel to z Axis	$\ell_1 + e_1$	$b_1 + e_2$	e_3	$K_{3\ell}$	$K_{3\ell}$	K_{3a}	
10	Parallel to z Axis	$\ell_1 + e_1$	$e_2 - b_1$	e_3	$K_{3\ell}$	$K_{3\ell}$	K_{3a}	0
11	Parallel to z Axis	$e_1 - \ell_1$	$e_2 - b_1$	e_3	$K_{3\ell}$	$K_{3\ell}$	K_{3a}	0
12	Parallel to z Axis	$e_1 - \ell_1$	$b_1 + e_2$	e_3	$K_{3\ell}$	$K_{3\ell}$	K_{3a}	0
				$\sum = 4(K_{1a}+K_{2\ell}+K_{3\ell})$	$4(K_{1\ell}+K_{2a}+K_{3\ell})$		$4(K_{1\ell}+K_{2\ell}+K_{3a})$	

$$\therefore [C] = \begin{bmatrix} 4(K_{1a}+K_{2\ell}+K_{3\ell}) & 0 & 0 \\ 0 & 4(K_{1\ell}+K_{2a}+K_{3\ell}) & 0 \\ 0 & 0 & 4(K_{1\ell}+K_{2\ell}+K_{3a}) \end{bmatrix}$$

Isolator Number	b_{12} $=(r_3c_{11})$	b_{21} $= -(r_3c_{22})$	b_{13} $= -(r_2c_{11})$	b_{31} $=(r_2c_{33})$	b_{23} $=(r_1c_{22})$	b_{32} $= -(r_1c_{33})$	b_{11}, b_{22}, b_{33}
1	$e_3K_{2\ell}$	$-e_3K_{2a}$	$-(B+e_2)K_{2\ell}$	$(B+e_2)K_{2\ell}$	$(\ell+e_1)K_{2a}$	$-(\ell+e_1)K_{2\ell}$	0
4	$e_3K_{2\ell}$	$-e_3K_{2a}$	$-(e_2-B)K_{2\ell}$	$(e_2-B)K_{2\ell}$	$(\ell+e_1)K_{2a}$	$-(\ell+e_1)K_{2\ell}$	0
5	$e_3K_{2\ell}$	$-e_3K_{2a}$	$-(e_2-B)K_{2\ell}$	$(e_2-B)K_{2\ell}$	$(e_1-\ell)K_{2a}$	$-(e_1-\ell)K_{2\ell}$	0
8	$e_3K_{2\ell}$	$-e_3K_{2a}$	$-(B+e_2)K_{2\ell}$	$(B+e_2)K_{2\ell}$	$(e_1-\ell)K_{2a}$	$-(e_1-\ell)K_{2\ell}$	0
2	e_3K_{1a}	$-e_3K_{1\ell}$	$-(b+e_2)K_{1a}$	$(b+e_2)K_{1\ell}$	$(L+e_1)K_{1\ell}$	$-(L+e_1)K_{1\ell}$	0
3	e_3K_{1a}	$-e_3K_{1\ell}$	$-(e_2-b)K_{1a}$	$(e_2-b)K_{1\ell}$	$(L+e_1)K_{1\ell}$	$-(L+e_1)K_{1\ell}$	0
6	e_3K_{1a}	$-e_3K_{1\ell}$	$-(e_2-b)K_{1a}$	$(e_2-b)K_{1\ell}$	$(e_1-L)K_{1\ell}$	$-(e_1-L)K_{1\ell}$	0
7	e_3K_{1a}	$-e_3K_{1\ell}$	$-(b+e_2)K_{1a}$	$(b+e_2)K_{1\ell}$	$(e_1-L)K_{1\ell}$	$-(e_1-L)K_{1\ell}$	0
9	$e_3K_{3\ell}$	$-e_3K_{3\ell}$	$-(b_1+e_2)K_{3\ell}$	$(b_1+e_2)K_{3a}$	$(\ell_1+e_1)K_{3\ell}$	$-(\ell_1+e_1)K_{3a}$	0
10	$e_3K_{3\ell}$	$-e_3K_{3\ell}$	$-(e_2-b_1)K_{3\ell}$	$(e_2-b_1)K_{3a}$	$(\ell_1+e_1)K_{3\ell}$	$-(\ell_1+e_1)K_{3a}$	0
11	$e_3K_{3\ell}$	$-e_3K_{3\ell}$	$-(e_2-b_1)K_{3\ell}$	$(e_2-b_1)K_{3a}$	$(e_1-\ell_1)K_{3\ell}$	$-(e_1-\ell_1)K_{3a}$	0
12	$e_3K_{3\ell}$	$-e_3K_{3\ell}$	$-(b_1+e_2)K_{3\ell}$	$(b_1+e_2)K_{3a}$	$(e_1-\ell_1)K_{3\ell}$	$-(e_1-\ell_1)K_{3a}$	0

$\sum$: $b_{12}=4e_3(K_{1a}+K_{2\ell}+K_{3\ell})$; $b_{21}= -4e_3(K_{1\ell}+K_{2a}+K_{3\ell})$; $b_{13}= -4e_2(K_{1a}+K_{2\ell}+K_{3\ell})$; $b_{31}=4e_2(K_{1\ell}+K_{2\ell}+K_{3a})$;

$b_{23}=4e_1(K_{1\ell}+K_{2a}+K_{3\ell})$; $b_{32}= -4e_1(K_{1\ell}+K_{2\ell}+K_{3a})$

$$\therefore \quad [B] = \begin{bmatrix} 0 & 4e_3(K_{1a}+K_{2\ell}+K_{3\ell}) & -4e_2(K_{1a}+K_{2\ell}+K_{3\ell}) \\ -4e_3(K_{1\ell}+K_{2a}+K_{3\ell}) & 0 & 4e_1(K_{1\ell}+K_{2a}+K_{3\ell}) \\ 4e_2(K_{1\ell}+K_{2\ell}+K_{3a}) & -4e_1(K_{1\ell}+K_{2\ell}+K_{3a}) & 0 \end{bmatrix}$$

Isolator Number	e_{11} $=(r_2b_{31}-r_3b_{21})$	e_{12} $=(r_3b_{32})$	e_{13} $=-(r_3b_{23})$	e_{21} $=-(r_1b_{31})$	e_{22} $=(r_3b_{12}-r_1b_{32})$	e_{23} $=(r_1b_{13})$	e_{31} $=(r_1b_{21})$	e_{32} $=-(r_2b_{12})$	e_{33} $=(r_1b_{23}-r_2b_{13})$
1	$(B+e_2)^2K_{2f}$ $+e_3^2K_{2a}$	$-(B+e_2)(J+e_1)K_{2f}$	$-e_3(J+e_1)K_{2a}$	$-(J+e_1)(B+e_2)K_{2f}$	$e_3^2K_{2f}$ $+(J+e_1)^2K_{2f}$	$-e_3(B+e_2)K_{2f}$	$-e_3(J+e_1)K_{2a}$	$-e_3(B+e_2)K_{2f}$	$(J+e_1)^2K_{2a}$ $+(B+e_2)^2K_{2f}$
4	$(e_2-B)^2K_{2f}$ $+e_3^2K_{2a}$	$-(e_2-B)(J+e_1)K_{2f}$	$-e_3(J+e_1)K_{2a}$	$-(J+e_1)(e_2-B)K_{2f}$	$e_3^2K_{2f}$ $+(J+e_1)^2K_{2f}$	$-e_3(e_2-B)K_{2f}$	$-e_3(J+e_1)K_{2a}$	$-e_3(e_2-B)K_{2f}$	$(J+e_1)^2K_{2a}$ $+(e_2-B)^2K_{2f}$
5	$(e_2-B)^2K_{2f}$ $+e_3^2K_{2a}$	$-(e_2-B)(e_1-J)K_{2f}$	$-e_3(e_1-J)K_{2a}$	$-(e_1-J)(e_2-B)K_{2f}$	$e_3^2K_{2f}$ $+(e_1-J)^2K_{2f}$	$-e_3(e_2-B)K_{2f}$	$-e_3(e_1-J)K_{2a}$	$-e_3(e_2-B)K_{2f}$	$(e_1-J)^2K_{2a}$ $+(e_2-B)^2K_{2f}$
8	$(B+e_2)^2K_{2f}$ $+e_3^2K_{2a}$	$-(B+e_2)(e_1-J)K_{2f}$	$-e_3(e_1-J)K_{2a}$	$-(e_1-J)(B+e_2)K_{2f}$	$e_3^2K_{2f}$ $+(e_1-J)^2K_{2f}$	$-e_3(B+e_2)K_{2f}$	$-e_3(e_1-J)K_{2a}$	$-e_3(B+e_2)K_{2f}$	$(e_1-J)^2K_{2a}$ $+(B+e_2)^2K_{2f}$
2	$(b+e_2)^2K_{1f}$ $+e_3^2K_{1f}$	$-(b+e_2)(L+e_1)K_{1f}$	$-e_3(L+e_1)K_{1f}$	$-(L+e_1)(b+e_2)K_{1f}$	$e_3^2K_{1a}$ $+(L+e_1)^2K_{1f}$	$-e_3(b+e_2)K_{1a}$	$-e_3(L+e_1)K_{1f}$	$-e_3(b+e_2)K_{1a}$	$(L+e_1)^2K_{1f}$ $+(b+e_2)^2K_{1a}$
3	$(e_2-b)^2K_{1f}$ $+e_3^2K_{1f}$	$-(e_2-b)(L+e_1)K_{1f}$	$-e_3(L+e_1)K_{1f}$	$-(L+e_1)(e_2-b)K_{1f}$	$e_3^2K_{1a}$ $+(L+e_1)^2K_{1f}$	$-e_3(e_2-b)K_{1a}$	$-e_3(L+e_1)K_{1f}$	$-e_3(e_2-b)K_{1a}$	$(L+e_1)^2K_{1f}$ $+(e_2-b)^2K_{1a}$
6	$(e_2-b)^2K_{1f}$ $+e_3^2K_{1f}$	$-(e_2-b)(e_1-L)K_{1f}$	$-e_3(e_1-L)K_{1f}$	$-(e_1-L)(e_2-b)K_{1f}$	$e_3^2K_{1a}$ $-(e_1-L)^2K_{1f}$	$-e_3(e_2-b)K_{1a}$	$-e_3(e_1-L)K_{1f}$	$-e_3(e_2-b)K_{1a}$	$(e_1-L)^2K_{1f}$ $+(e_2-b)^2K_{1a}$
7	$(b+e_2)^2K_{1f}$ $+e_3^2K_{1f}$	$-(b+e_2)(e_1-L)K_{1f}$	$-e_3(e_1-L)K_{1f}$	$-(e_1-L)(b+e_2)K_{1f}$	$e_3^2K_{1a}$ $+(e_1-L)^2K_{1f}$	$-e_3(b+e_2)_{1a}$	$-e_3(e_1-L)K_{1f}$	$-e_3(b+e_2)K_{1a}$	$(e_1-L)^2K_{1f}$ $+(b+e_2)^2K_{1a}$
9	$(b_1+e_2)^2K_{3a}$ $+e_3^2K_{3f}$	$-(b_1+e_2)(J_1+e_1)K_{3a}$	$-e_3(J_1+e_1)K_{3f}$	$-(J_1+e_1)(b_1+e_2)K_{3a}$	$e_3^2K_{3f}$ $+(J_1+e_1)^2K_{3a}$	$-e_3(b_1+e_2)K_{3f}$	$-e_3(J_1+e_1)K_{3f}$	$-e_3(b_1+e_2)K_{3f}$	$(J_1+e_1)^2K_{3a}$ $+(b_1+e_2)^2K_{3f}$
10	$(e_2-b_1)^2K_{3a}$ $+e_3^2K_{3f}$	$-(e_2-b_1)(J_1+e_1)K_{3a}$	$-e_3(J_1+e_1)K_{3f}$	$-(J_1+e_1)(e_2-b_1)K_{3a}$	$e_3^2K_{3f}$ $+(J_1+e_1)^2K_{3a}$	$-e_3(e_2-b_1)K_{3f}$	$-e_3(J_1+e_1)K_{3f}$	$-e_3(e_2-b_1)K_{3f}$	$(J_1+e_1)^2K_{3f}$ $+(e_2-b_1)^2K_{3f}$
11	$(e_2-b_1)^2K_{3a}$ $+e_3^2K_{3f}$	$-(e_2-b_1)(e_1-J_1)K_{3a}$	$-e_3(e_1-J_1)K_{3f}$	$-(e_1-J_1)(e_2-b_1)K_{3a}$	$e_3^2K_{3f}$ $+(e_1-J_1)^2K_{3a}$	$-e_3(e_2-b_1)K_{3f}$	$-e_3(e_1-J_1)K_{3f}$	$-e_3(e_2-b_1)K_{3f}$	$(e_1-J_1)^2K_{3f}$ $+(e_2-b_1)^2K_{3f}$
12	$(e_2+b_1)^2K_{3a}$ $+e_3^2K_{3f}$	$-(b_1+e_2)(e_1-J_1)K_{3a}$	$-e_3(e_1-J_1)K_{3f}$	$-(e_1-J_1)(b_1+e_2)K_{3a}$	$e_3^2K_{3f}$ $+(e_1-J_1)^2K_{3a}$	$-e_3(b_1+e_2)K_{3f}$	$-e_3(e_1-J_1)K_{3f}$	$-e_3(b_1+e_2)K_{3f}$	$(e_1-J_1)^2K_{3f}$ $+(b_1+e_2)^2K_{3f}$

$$\therefore \quad [\Sigma] = \begin{bmatrix} \{4(B^2K_{2f}+b^2K_{1f}+b_1^2K_{3a}) & +4e_1e_2(K_{2f}+K_{1f}+K_{3a}) & -4e_1e_3(K_{1f}-K_{2a}+K_{3f}) \\ -4e_2^2(K_{2f}+K_{1f}+K_{3a})+4e_3^2(K_{2a}+K_{1f}+K_{3f})\} & & \\ -4e_1e_2(K_{1f}+K_{2f}+K_{3a}) & \{4(J^2K_{2f}+L^2K_{1f}+J_1^2K_{3a}) & -4e_2e_3(K_{1a}+K_{2f}+K_{3f}) \\ & +4e_1^2(K_{1f}+K_{2f}+K_{3a})-4e_3^2(K_{1a}+K_{2f}+K_{3f})\} & \\ -4e_1e_3(K_{1f}-K_{2a}+K_{3f}) & -4e_2e_3(K_{1a}+K_{2f}+K_{3f}) & -\{J^2K_{2a}+L^2K_{1f}+J_1^2K_{3f} \\ & & +B^2K_{2f}+b^2K_{1a}+b_1^2K_{3f}\} \\ & & +4e_1^2(K_{1f}+K_{2a}+K_{3f}) \\ & & +4e_2^2(K_{1a}+K_{2f}+K_{3f})] \end{bmatrix}$$

The six equations of motion in matrix form are:

$$\begin{bmatrix} m & o & o \\ o & m & o \\ o & o & m \end{bmatrix} \begin{bmatrix} \ddot{x} \\ \ddot{y} \\ \ddot{z} \end{bmatrix} + \begin{bmatrix} 4(K_{\ell v}+K_{\ell h}\sin^2\theta+K_{ah}\cos^2\theta) & o & o \\ o & 4(K_{\ell v}+K_{ah}\sin^2\theta+K_{\ell h}\cos^2\theta) & o \\ o & o & 4(K_{\ell h}+K_{ah}) \end{bmatrix} \begin{bmatrix} x \\ y \\ z \end{bmatrix} +$$

$$\begin{bmatrix} o & 4e_3(K_{\ell v}+K_{\ell h}\sin^2\theta+K_{ah}\cos^2\theta) & -4e_2(K_{\ell v}+K_{\ell h}\sin^2\theta+K_{ah}\cos^2\theta) \\ -4e_3(K_{\ell v}+K_{ah}\sin^2\theta+K_{\ell h}\cos^2\theta) & o & +4e_1(K_{\ell v}+K_{\ell h}\sin^2\theta+K_{ah}\cos^2\theta) \\ 4e_2(K_{av}+K_{\ell h}) & -4e_1(K_{av}+K_{\ell h}) & o \end{bmatrix} \begin{bmatrix} \alpha \\ \beta \\ \gamma \end{bmatrix} = - \begin{bmatrix} m & o & o \\ o & m & o \\ o & o & m \end{bmatrix} \begin{bmatrix} \ddot{x}_o \\ \ddot{y}_o \\ \ddot{z}_o \end{bmatrix}$$

and

$$\begin{bmatrix} m\rho_{xx}^2 & -m\rho_{xy}^2 & -m\rho_{xz}^2 \\ -m\rho_{yx}^2 & m\rho_{yy}^2 & -m\rho_{yz}^2 \\ -m\rho_{zx}^2 & -m\rho_{zy}^2 & m\rho_{zz}^2 \end{bmatrix} \begin{bmatrix} \ddot{\alpha} \\ \ddot{\beta} \\ \ddot{\gamma} \end{bmatrix} + \begin{bmatrix} o & -4e_3(K_{\ell v}+K_{ah}\sin^2\theta+K_{\ell h}\cos^2\theta) & 4e_2(K_{av}+K_{\ell h}) \\ 4e_3(K_{\ell v}+K_{\ell h}\sin^2\theta+K_{ah}\cos^2\theta) & o & -4e_1(K_{av}+K_{\ell h}) \\ -4e_2(K_{\ell v}+K_{\ell h}\sin^2\theta+K_{ah}\cos^2\theta) & 4e_1(K_{\ell v}+K_{\ell h}\sin^2\theta+K_{ah}\cos^2\theta) & o \end{bmatrix} \begin{bmatrix} x \\ y \\ z \end{bmatrix} +$$

$$\begin{bmatrix} 4b^2K_{av}+4B^2K_{\ell h}+4e_3^2K_{\ell v} \\ +4e_3^2(K_{ah}\sin^2\theta+K_{\ell h}\cos^2\theta) \\ +4e_2^2(K_{av}+K_{\ell h}) \end{bmatrix} \quad \begin{matrix} -4e_1e_2(K_{av}+K_{\ell h}) \\ \end{matrix} \quad \begin{matrix} -4e_1e_3(K_{\ell v}+K_{ah}\sin^2\theta+K_{\ell h}\cos^2\theta) \\ \end{matrix}$$

$$\begin{matrix} -4e_1e_2(K_{av}+K_{\ell h}) \\ \end{matrix} \quad \begin{bmatrix} 4\ell^2(K_{av}+K_{\ell h})+4e_1^2(K_{av}+K_{\ell h}) \\ +4e_3^2(K_{\ell h}\sin^2\theta+K_{ah}\cos^2\theta) \\ +4e_3^2K_{\ell v} \end{bmatrix} \quad \begin{matrix} -4e_2e_3(K_{\ell v}+K_{\ell h}\sin^2\theta+K_{ah}\cos^2\theta) \\ \end{matrix}$$

$$\begin{matrix} -4e_1e_3(K_{\ell v}+K_{ah}\sin^2\theta+ \\ K_{\ell h}\cos^2\theta) \\ \end{matrix} \quad \begin{matrix} -4e_2e_3(K_{\ell v}+K_{\ell h}\sin^2\theta+K_{ah}\cos^2\theta) \\ \end{matrix} \quad \begin{bmatrix} 4(\ell^2+e_1^2)(K_{ah}\sin^2\theta+K_{\ell h}\cos^2\theta+K_{\ell v}) \\ +4(b^2+e_2^2)(K_{\ell h}\sin^2\theta+K_{ah}\cos^2\theta) \\ +4(B^2+e_2^2)K_{\ell v} \\ +8B(K_{\ell h}-K_{ah})(-\frac{\sin 2\theta}{2}) \end{bmatrix}$$

$$\begin{bmatrix} \alpha \\ \beta \\ \gamma \end{bmatrix} = 0$$

Dividing through by m, making the following substitutions,

$$\omega_x^2 = \frac{4}{m}(K_{\ell v}+K_{\ell h}\sin^2\theta+K_{ah}\cos^2\theta)$$

$$\omega_y^2 = \frac{4}{m}(K_{\ell v}+K_{ah}\sin^2\theta+K_{\ell h}\cos^2\theta)$$

$$\omega_z^2 = \frac{4}{m}(K_{\ell h}+K_{av})$$

and converting to the Laplace form, the six equations can be rewritten in matrix form, as follows:

$$\begin{bmatrix} s^2+\omega_x^2 & 0 & 0 & 0 & e_3\omega_x^2 & -e_2\omega_x^2 \\ 0 & s^2+\omega_y^2 & 0 & -e_3\omega_y^2 & 0 & e_1\omega_y^2 \\ 0 & 0 & s^2+\omega_z^2 & e_2\omega_z^2 & -e_1\omega_z^2 & 0 \\ 0 & -e_3\omega_y^2 & e_2\omega_z^2 & \frac{4}{m}(B^2K_{2\ell}+b^2K_{1\ell}+b_1^2K_{3\ell}) & -(\rho_{xy}^2 s^2+e_1e_2\omega_z^2) & -(\rho_{xz}^2 s^2+e_1e_3\omega_y^2) \\ & & & +e_2^2\omega_z^2+e_3^2\omega_y^2+\rho_{xx}^2 s^2 & & \\ e_3\omega_x^2 & 0 & -e_1\omega_z^2 & -(\rho_{yx}^2 s^2+e_1e_2\omega_z^2) & \frac{4}{m}(\ell^2K_{2\ell}+L^2K_{1\ell}+\ell_1^2K_{3\ell}) & -(\rho_{yz}^2 s^2+e_2e_3\omega_x^2) \\ & & & & +e_1^2\omega_z^2+e_3^2\omega_x^2+\rho_{yy}^2 s^2 & \\ -e_2\omega_x^2 & e_1\omega_y^2 & 0 & -(\rho_{zx}^2 s^2+e_1e_3\omega_y^2) & -(\rho_{yz}^2 s^2+e_2e_3\omega_x^2) & \frac{4}{m}(\ell^2K_{2a}+L^2K_{1\ell}+\ell_1^2K_{3\ell} \\ & & & & & +B^2K_{2\ell}+b^2K_{1a}+b_1^2K_{3\ell}) \\ & & & & & +e_1^2\omega_y^2+e_2^2\omega_x^2+\rho_{zz}^2 s^2 \end{bmatrix} \begin{bmatrix} \bar{x} \\ \bar{y} \\ \bar{z} \\ \bar{\alpha} \\ \bar{\beta} \\ \bar{\gamma} \end{bmatrix} = \begin{bmatrix} -s^2\bar{x}_o \\ -s^2\bar{y}_o \\ -s^2\bar{z}_o \\ 0 \\ 0 \\ 0 \end{bmatrix}$$

That is, $[\Delta][\bar{X}] = -[\bar{X}_o]$

Therefore, $[\bar{X}] = -[\Delta]^{-1}[\bar{X}_o]$

3.5.5.3 Numerical Solution to Example B-1

Example B-1 has been selected to illustrate the numerical solution.

Step No. 1: Given:

W = 60,000 lbs		m = 1865 slugs	
L = 12 Ft.		Platform Thickness =	1.5 Ft.
B = 6 Ft.			
H = 12 Ft.		e_1 = -0.5 Ft.	
b = 4 Ft.		e_2 = -1.0 Ft.	
b^1 = 5 Ft.		e_3 = 1.5 Ft.	
ℓ = 8 Ft.		ρ_{xx}^2 = 67 Ft.^{2}	
ℓ^1 = 10 Ft.		ρ_{yy}^2 = 21.5 Ft.^{2}	
$\rho_{xy}^2 = \rho_{xz}^2 = \rho_{yz}^2 = 0$		ρ_{zz}^2 = 75 Ft.^{2}	

Note: Reference axes are the principal axes located at the C.G. of the suspended mass.

Step No. 2: Using the equations derived in Example B-1, substituting the numerical values given above and converting to the Laplace, Matrix Form, the equations of motion are:

$$\begin{bmatrix} (s^2+\omega_x^2) & 0 & 0 & 0 & e_3\omega_x^2 & -e_2\omega_x^2 \\ 0 & (s^2+\omega_y^2) & 0 & -e_3\omega_y^2 & 0 & e_1\omega_y^2 \\ 0 & 0 & (s^2+\omega_z^2) & e_2\omega_z^2 & -e_1\omega_z^2 & 0 \\ 0 & -e_3\omega_y^2 & e_2\omega_z^2 & (67s^2+23\omega_z^2 & -e_1e_2\omega_z^2 & -e_1e_3\omega_y^2 \\ & & & +e_3^2\omega_y^2) & & \\ e_3\omega_x^2 & 0 & -e_1\omega_z^2 & -e_1e_2\omega_z^2 & (21.5s^2+88.25\omega_z^2 & -e_2e_3\omega_x^2 \\ & & & & +e_3^2\omega_x^2) & \\ -e_2\omega_x^2 & e_1\omega_y^2 & 0 & -e_1e_3\omega_y^2 & -e_2e_3\omega_x^2 & (75s^2+25\omega_x^2 \\ & & & & & +88.25\omega_y^2) \end{bmatrix} \begin{bmatrix} \bar{x} \\ \bar{y} \\ \bar{z} \\ \bar{\alpha} \\ \bar{\beta} \\ \bar{\gamma} \end{bmatrix} = - \begin{bmatrix} s^2\bar{x}_o \\ s^2\bar{y}_o \\ s^2\bar{z}_o \\ 0 \\ 0 \\ 0 \end{bmatrix}$$

Step No. 3: Neglecting the eccentricity terms, as a first approximation,

$$\bar{x} = -\frac{s^2\bar{x}_o}{s^2+\omega_x^2} = \text{approximate rattlespace in the x - direction}$$

$$\bar{y} = -\frac{s^2\bar{y}_o}{s^2+\omega_y^2} = \text{approximate rattlespace in the y - direction}$$

$$\bar{z} = -\frac{s^2\bar{z}_o}{s^2+\omega_z^2} = \text{approximate rattlespace in the z - direction}$$

Assuming in this problem, that the response spectrum shows $\omega_x^2 = 60\ \text{sec}^{-2}$, $\omega_y^2 = 40\ \text{sec}^{-2}$, $\omega_z^2 = 25\ \text{sec}^{-2}$, for the approximate rattlespace requirements of the system.

Step Nos. 4 & 5: Considering all the eccentricity terms, and substituting numerical values of ω_x^2, ω_y^2 and ω_z^2 from Step 3, the frequency determinant is as follows

$$D(s^2) = \begin{bmatrix} s^2+60 & 0 & 0 & 0 & 90 & 60 \\ 0 & s^2+40 & 0 & -60 & 0 & -20 \\ 0 & 0 & s^2+25 & -25 & 12.5 & 0 \\ 0 & -60 & -25 & (67s^2+665) & -12.5 & 30 \\ 90 & 0 & 12.5 & -12.5 & (21.5s^2+2341.25) & 90 \\ 60 & -20 & 0 & 30 & 90 & (75s^2+4910) \end{bmatrix}$$

Evaluating on an electronic digital computer as explained in Appendix 3.E.

$$D(s^2) = 108,0375s^{12}+33,414,607.5s^{10}+3,921,548,184.0s^8 +222,739,502,100s^6+6,352,141,605,000s^4 +82,968,840,900,000s^2+351,384,000,000,000 = 0$$

Step No. 6: Rewrite the polynomial of Step 5 so that the leading coefficient is unity.

Then: $s^{12} + 309.28712s^{10} + 36298.0278s^8 + 2061686.93s^6 + 58,795,711s^4 + 767,963,354s^2 + 3252426240 = 0$

$\therefore$ $a_0 = 1$
$a_1 = 309.28712$
$a_2 = 36298.0278$
$a_3 = 2061686.93$
$a_4 = 58795711$
$a_5 = 767963354$
$a_6 = 3252426240$

All a's are positive i.e. condition (i) of the Routh-Hurwitz (Appendix 3.E) stability criterion is satisfied.

$$a_5\left[a_1a_2a_3a_4-a_1^2a_4-a_3^2a_4+2a_1a_4a_5+a_2a_3a_5-a_1a_2^2a_5+a_5^2\right]$$
$$= (10)^{29}\ (8.257319) \qquad \text{L.H.S.}$$

$$a_6\left[a_1a_2a_3^2-2a_1^2a_2a_5-a_1^2a_3a_4+a_1^3a_6+3a_1a_3a_5-a_3^3\right]$$
$$= (10)^{27}\ (7.983165) \qquad \text{R.H.S.}$$

$\therefore$ L.H.S. > R.H.S.

This satisfies the second Routh-Hurwitz stability criterion. Hence, the system is stable.

Step No. 7: $D(s^2) = 0$ can be written as follows:

$$s^{12} + 309.28712s^{10} + 36298.0278s^{8} + 2061686.93s^{6} + 58795711s^{4} + 767963354s^{2} + 3252426240 = 0$$

The solution of the above polynomial yields

$$s_1^2 = -\omega_1^2 = -52.96 \quad \text{sec}^{-2}$$
$$s_2^2 = -\omega_2^2 = -40.56 \quad \text{sec}^{-2}$$
$$s_3^2 = -\omega_3^2 = -25.37 \quad \text{sec}^{-2}$$
$$s_4^2 = -\omega_4^2 = -7.72 \quad \text{sec}^{-2}$$
$$s_5^2 = -\omega_5^2 = -116.1 \quad \text{sec}^{-2}$$
$$s_6^2 = -\omega_6^2 = -66.6 \quad \text{sec}^{-2}$$

Step No. 8: Using an electronic digital computer, and the method suggested in Appendix 3.A, the frequency matrix of Step 4, is inverted as is shown on page 3-82.

Step No. 9: Again, using an electronic digital computer and the formulae derived in Appendix 3.C, the inverted frequency matrix is converted to the partial fraction form as shown on page 3-84.

Step No. 10: The equation form as obtained in Step 9 is now referred to the response spectrum for the six frequencies in question, and x, y, z, α, β, γ, due to the total effect evaluated.

3.5.6 Effect of Small Eccentricities on the Natural Frequencies of an Isolated System

A six-degree-of-freedom isolated mass has six modes of vibration, each mode having its own natural frequency. If the center of symmetry of the isolators is coincident with the center of gravity of the isolated mass, the six modes of vibration are the six reference coordinates of the system, namely, the three orthogonal translational modes, and the three orthogonal rotational modes. The frequencies corresponding to these natural modes can be obtained very easily by standard one-degree-of-freedom methods. However, if the center of symmetry of the isolators is eccentric with respect to the center of

$$[\Delta]^{-1} =$$

gravity of the isolated mass, the modes are no longer pure translations and pure rotations, but are a combination of any or all of the six coordinates of the system. For small eccentricities, each of these modes will have one predominant coordinate and the frequency of vibration of each mode will be approximately of the same magnitude as the natural frequency of the system, in the direction of the predominant coordinate, when the eccentricities are neglected. This has been illustrated by considering the numerical solution of Example B-1 (3.5.5.3).

The equations of motion, for zero eccentricity are

$$\ddot{x}+\omega_x^2 x = -\ddot{x}_o \; ; \qquad \ddot{y}+\omega_y^2 y = -\ddot{y}_o \; ; \qquad z+\omega_z^2 z = -\ddot{z}_o \; ;$$

$$\rho_{xx}^2\ddot{\alpha}+\omega_z^2\left\{\frac{1}{3}(b^2+2b_1^2)\right\}\alpha = -\rho_{xx}^2\ddot{\alpha}_o \; ; \quad \rho_{yy}^2\ddot{\beta}+\omega_z^2\left\{\frac{1}{3}(l^2+2l_1^2)\right\}\beta = -\rho_{yy}^2\ddot{\theta}_o \; ;$$

$$\text{and} \quad \rho_{zz}^2\gamma+\left[\omega_x^2\left\{\frac{1}{3}(b^2+2b_1^2)\right\}+\omega_y^2\left\{\frac{1}{3}(l^2+2l_1^2)\right\}\right]\gamma = -\rho_{zz}^2\ddot{\nu}_o$$

taking $\omega_x^2 = 60 \text{ sec}^{-2}$; $\omega_y^2 = 40 \text{ sec}^{-2}$; $\omega_z^2 = 29 \text{ sec}^{-2}$

$\omega_1^2 = \omega_x^2 = 60 \text{ sec}^{-2}$ $\qquad \omega_4^2 = \omega_\alpha^2 = 8.21 \text{ sec}^{-2}$

$\omega_2^2 = \omega_y^2 = 40 \text{ sec}^{-2}$ $\qquad \omega_5^2 = \omega_\beta^2 = 102.31 \text{ sec}^{-2}$

$\omega_3^2 = \omega_z^2 = 25 \text{ sec}^{-2}$ $\qquad \omega_6^2 = \omega_\gamma^2 = 64.53 \text{ sec}^{-2}$

The following table shows the effect of various eccentricities on the six natural frequencies. The frequencies where derived by equating the frequency matrix of the six coupled equations to zero, and solving for its roots, as mentioned in Step 7, paragraph 3.5.5.3.

		Case 1	Case 2	Case 3	Case 4	Case 5
Eccentricity	e_1	0	0	0	-0.5'	-0.5'
	e_2	0	0	-1.0'	0	-1.0'
	e_3	0	1.5'	0	0	1.5'
ω_1^2		60 sec^{-2}	51.37	55.25	60.0	52.96
ω_2^2		40 sec^{-2}	43.01	40.0	39.8	40.57
ω_3^2		25 sec^{-2}	25.0	25.548	24.905	25.37
ω_4^2		8.21 sec^{-2}	7.872	8.0324	8.21	7.72
ω_5^2		102.31 sec^{-2}	115.905	102.31	102.75	116.08
ω_6^2		64.53 sec^{-2}	64.53	70.085	64.8345	66.59

$$
\begin{bmatrix} \bar{x} \\ \bar{y} \\ \bar{z} \\ \bar{\phi} \\ \bar{\theta} \\ \bar{\psi} \end{bmatrix}
=
\begin{bmatrix}
0.8798 & 0.0155 & -0.0298 & 0.0005 & -0.0593 & -0.0455 \\
0.0155 & 1.7755 & 0.3153 & 0.1333 & -0.0042 & 0.0158 \\
-0.0298 & 0.3153 & 0.2047 & 0.1344 & 0.0016 & 0.0025 \\
0.0005 & 0.1333 & 0.1344 & 0.0953 & -0.0002 & -0.0003 \\
-0.0593 & -0.0042 & 0.0016 & -0.0002 & 0.0042 & 0.0033 \\
-0.0455 & 0.0158 & 0.0025 & -0.0003 & 0.0033 & 0.0014
\end{bmatrix}
\begin{bmatrix} -\frac{s^2 x_0}{s^2+52.96} \\ -\frac{s^2 y_0}{s^2+52.96} \\ -\frac{s^2 z_0}{s^2+52.96} \\ 0 \\ 0 \\ 0 \end{bmatrix}
+
\begin{bmatrix}
-0.0071 & 0.0035 & 0.0004 & -0.0001 & 0.0006 & 0.0003 \\
0.0035 & -0.0756 & -0.0161 & -0.0063 & -0.0007 & -0.0010 \\
0.0004 & -0.0161 & -0.0103 & -0.0066 & 0.0000 & -0.0001 \\
-0.0001 & -0.0063 & -0.0066 & -0.0047 & 0.0000 & 0.0000 \\
0.0006 & -0.0001 & 0.0000 & 0.0000 & 0.0000 & 0.0000 \\
0.0003 & -0.0010 & -0.0001 & 0.0000 & 0.0000 & 0.0000
\end{bmatrix}
\begin{bmatrix} -\frac{s^2 x_0}{s^2+40.56} \\ -\frac{s^2 y_0}{s^2+40.56} \\ -\frac{s^2 z_0}{s^2+40.56} \\ 0 \\ 0 \\ 0 \end{bmatrix}
$$

$$
+
\begin{bmatrix}
0.0143 & -0.0101 & 0.0206 & -0.0002 & -0.0012 & -0.0006 \\
-0.0101 & 0.1450 & -0.1052 & -0.0285 & 0.0010 & 0.0023 \\
0.0206 & -0.1052 & 0.9390 & -0.0382 & -0.0078 & -0.0004 \\
-0.0002 & -0.0285 & -0.0382 & -0.0127 & 0.0002 & -0.0001 \\
-0.0012 & 0.0010 & -0.0078 & 0.0002 & 0.0001 & 0.0000 \\
-0.0006 & 0.0023 & -0.0004 & -0.0001 & 0.0000 & 0.0001
\end{bmatrix}
\begin{bmatrix} -\frac{s^2 x_0}{s^2+45.37} \\ -\frac{s^2 y_0}{s^2+45.37} \\ -\frac{s^2 z_0}{s^2+45.37} \\ 0 \\ 0 \\ 0 \end{bmatrix}
+
\begin{bmatrix}
-0.0005 & 0.0003 & 0.0001 & 0.0000 & 0.0000 & 0.0000 \\
0.0003 & 0.0457 & 0.0398 & 0.0278 & -0.0001 & 0.0000 \\
0.0001 & 0.0398 & 0.0311 & 0.0215 & -0.0001 & 0.0000 \\
0.0000 & 0.0278 & 0.0215 & 0.0148 & 0.0000 & 0.0000 \\
0.0000 & -0.0001 & -0.0001 & 0.0000 & 0.0000 & 0.0000 \\
0.0000 & 0.0000 & 0.0000 & 0.0000 & 0.0000 & 0.0000
\end{bmatrix}
\begin{bmatrix} -\frac{s^2 x_0}{s^2+[illegible].72} \\ -\frac{s^2 y_0}{s^2+[illegible].72} \\ -\frac{s^2 z_0}{s^2+[illegible].72} \\ 0 \\ 0 \\ 0 \end{bmatrix}
$$

$$
+
\begin{bmatrix}
0.1166 & -0.0018 & 0.0001 & 0.0000 & 0.0676 & 0.0033 \\
-0.0018 & 0.0903 & 0.0505 & 0.0333 & -0.0005 & 0.0003 \\
0.0001 & 0.0505 & 0.0394 & 0.0265 & 0.0055 & 0.0003 \\
0.0000 & 0.0333 & 0.0265 & 0.0183 & -0.0001 & 0.0000 \\
0.0676 & -0.0005 & 0.0055 & -0.0001 & 0.0410 & 0.0000 \\
0.0033 & 0.0003 & 0.0003 & 0.0000 & 0.0026 & 0.0001
\end{bmatrix}
\begin{bmatrix} -\frac{s^2 x_0}{s^2+116.1} \\ -\frac{s^2 y_0}{s^2+116.1} \\ -\frac{s^2 z_0}{s^2+116.1} \\ 0 \\ 0 \\ 0 \end{bmatrix}
+
\begin{bmatrix}
-0.0031 & -0.0075 & -0.0004 & -0.0002 & -0.0077 & 0.0425 \\
-0.0075 & -0.9599 & -0.2843 & -0.1596 & 0.0040 & -0.0175 \\
-0.0004 & -0.2843 & -0.2040 & -0.1376 & 0.0007 & -0.0024 \\
-0.0002 & -0.1596 & -0.1376 & -0.0961 & 0.0002 & 0.0003 \\
-0.0077 & 0.0040 & 0.0007 & 0.0002 & 0.0012 & -0.0053 \\
0.0425 & -0.0175 & -0.0024 & 0.0003 & -0.0053 & 0.0117
\end{bmatrix}
\begin{bmatrix} -\frac{s^2 x_0}{s^2+66.6} \\ -\frac{s^2 y_0}{s^2+66.6} \\ -\frac{s^2 z_0}{s^2+66.6} \\ 0 \\ 0 \\ 0 \end{bmatrix}
$$

3.6 Nonlinear Systems

3.6.1 General

It has been said that all nature behaves in a nonlinear manner. Certainly if the shock isolation system designer were to closely inspect the characteristics of the elements he employs, he would find nonlinearities inherent in all of them. The resistance to Coulomb friction and to the turbulent flow of fluids, the stiffness of elastomers, and the discontinuities of backlash, saturation, and preload are just a few of the many nonlinearities with which the designer is familiar. Many nonlinearities however, are not so well appreciated. For example, even in the common wire spring, the stiffness is dependent on displacement and on the rate of loading. It is somewhat surprising then that a very accurate indication of the dynamic response of many physical systems can be obtained by representing their forces and accelerations by linear differential equations. The obvious conclusion is therefore drawn that in many cases the effect of the nonlinearities is slight.

The behavior of nonlinear systems however cannot be regarded categorically as being "just a little different" from that of linear ones. While the response of some nonlinear systems is simply a distortion of the response of its related linear counterpart, other phenomena may occur which are strictly due to the nonlinearity and for which no parallel in linear systems exists. Further, these fundamentally different and often unexpected responses in nonlinear systems may result in peak accelerations and displacements far exceeding those predicted by a "linearized" solution. Whether or not the designer purposely selects a nonlinear system to take advantage of some desirable characteristic, the many nonlinearities inherent in practical isolation systems make it essential that he be aware of the basic characteristics of these systems and of the extent to which linear approximations can be expected to yield dependable results.

In this subsection the fundamental differences between linear and nonlinear systems are discussed, phenomena associated with the behavior of nonlinear systems reviewed, and methods for solving certain nonlinear equations described. Particular emphasis is given to those systems whose restoring force can be approximated by a bilinear stiffness and to the effects of nonlinear coupling in the popular pendulum support system.

3.6.2 Unique Characteristics of Nonlinear Systems

3.6.2.1 Linear versus Nonlinear Systems

In physical terms, nonlinear systems are systems whose behavior is governed by nonlinear ordinary differential equations, usually of the form

$$\ddot{x}_i = F.\ (x_1,\ x_2 \ldots \dot{x}_n;\ \dot{x}_1,\ \dot{x}_2 \ldots \dot{x}_n;\ a_1,\ a_2 \ldots a_n;\ t) \qquad (43)$$

where t is the independent time variable
x_i are the dependent displacement variables
$\dot{x}_i$ are the corresponding velocities
a_i are the system parameters.

The functions F_i are sums of individual terms each of which, in a very general sense, is a force per unit mass. The physical meaning of nonlinearity is that a plot of such an individual force term at any instant, plotted as a function of displacement (or velocity) on which it depends, does not result in a straight line.

The coefficients of the dependent variable (usually the displacement coordinate of the system) of the nonlinear equations of motion of dynamic systems contain the characteristic parameters of the configuration, such as masses, isolator stiffness, and dissipation factors, and in general depend explicitly on the time variable and/or on the dependent variable of the system. If the time variable occurs explicitly in the coefficients of the differential equations, the system is said to be "rheonomic", whereas if it does not appear explicitly, the system is said to be "skleronomic". Furthermore, systems represented by equations containing only coordinates or coordinates and time are called "holonomic" systems. However, if these equations also contain the rate of change of coordinates, they are said to represent "nonholonomic" systems.

Linear systems consider constant masses, such as spring forces proportional to deflections, damping forces proportional to velocities and the geometry of constraints, such that their behavior can be described by ordinary linear differential equations with constant coefficients. The deviation of nonlinear systems from this general pattern of linear systems has its source in either or both of two conditions. First, the restoring forces may be nonlinear, as when they are not directly proportional to the displacement. Or second, the kinetic forces of constraint may be nonlinear, as in the case of a pendulum configuration undergoing large displacements. The former is dependent on the physical properties of the isolators, the latter on the geometry of the system. These nonlinearities are reflected in the governing differential equations of motion, in three forms as follows:

- The differential equations are linear in the dependent variable, but the coefficients are functions of time (rheolinear equations).
- The differential equations are not linear, in that the displacement (dependent variable) and/or its derivatives appear at powers higher than the first, but their coefficients remain independent of time (nonlinear equations).
- The differential equations are not linear in the sense of the statement above, and further, the coefficients are functions of time (rheo-nonlinear).

Nonlinear systems may have any number of degrees-of-freedom, which may be coupled kinematically, dynamically, or by a combination of the two. However, unlike the linear systems, the coupling cannot be transferred from one to the other type by a change of the system coordinates or reference system.

3.6.2.2 General Character of Nonlinear Systems

Nonlinear systems have patterns of behavior which differ basically from those of linear systems. It is important that these unique characteristics of nonlinear systems be brought to the attention of the designer as a check against his intuitive reasoning, based on concepts formed by experience with linear systems. The characteristics defining the behavior of nonlinear systems fall into two classifications: first there are phenomena which have counterparts in the related linear systems but which are distorted in some manner because of the nonlinearity, and second, there are phenomena that are strictly due to the nonlinearity and for which no parallel exists in linear systems. It may be mentioned that the "related linear system" is usually the one whose differential equations of motion are obtained by ignoring the nonlinear terms from the equations under study.

The more important general characteristics of nonlinear systems are described, as follows:

Invalidity of the Principle of Superposition

The principle of superposition does not apply to nonlinear systems. Unlike linear systems, the knowledge of two particular solutions of, say, a second order nonlinear differential equation of a nonlinear system does not lead to a general solution in the form of a sum of the two known particular solutions. Hence, very few nonlinear differential equations are known for which a general solution has been found. As a rule, only a particular solution can be found, and even then only in an approximate manner. This fact is of particular significance in investigating the transient behavior of a nonlinear system excited by pulses.

Quasiperiodic Response

Unlike that of a linear system, the response of nonlinear systems to harmonic inputs is neither harmonic nor at the same frequency as the input. The difference between the frequency of the true nonlinear oscillation and that of the exciting forces is called "detuning". The oscillations of a nonlinear system are not harmonic but always contain harmonics of various orders. Hence the response of nonlinear systems in the time domain appears distorted (creep phenomenon) and is characterized by an almost periodic behavior and also by quasiharmonic oscillations having a shape close to a harmonic wave form.

Entrainment

If a periodic force of frequency ω is applied to an oscillating system of frequency ω_o, there results the well known phenomenon of "beats"; i.e., an oscillating motion of periodically modulated amplitudes. As the difference between the two frequencies decreases the beat frequency also decreases. In linear systems the beat frequency decreases indefinitely as $|\omega - \omega_o| \to 0$. However, for nonlinear systems, it has been found by experiment that the oscillatory frequency ω_o falls in synchronism or is "entrained" by the externally applied frequency ω, within a certain band of frequencies. This phenomenon is called entrainment of frequency and the band of frequencies in which entrainment occurs is called the zone of entrainment. If and when detuning is sufficiently small, the beats disappear and the motion becomes periodic with the same frequency as that of the exciting forces.

Autonomous and Nonautonomous Systems

Free vibrations of nonlinear systems are termed as "autonomous" whereas forced vibrations are termed "nonautonomous". Because the principle of superposition does not apply for nonlinear systems, free and forced vibrations cannot be treated separately. The two are interrelated. The character of a forced nonlinear oscillation can change completely if free oscillations are superimposed on it.

Amplitude-Frequency Relationship

In all nonlinear oscillations there exists a fixed relationship between the amplitude of the response and the frequency of the system. In other words, the frequency of a nonlinear system is a function, not only of the physical properties of the system but also of the input to the system.

Tilting-Discontinuity-Creep

The response of a nonlinear system is, at best, described in terms of four parameters, i.e., amplitude of the input; amplitude of the response; ratio of input period to the natural period; and the damping ratio. An inspection of various plots of the above parameters reveals a distortion of the response curve in the frequency domain (also called the transmissibility curve) called "tilting effect" as well as a distortion of the response wave form in the time domain (shape of the oscillations) called the "creep effect", together with the appearance of various regions of instability in both domains due to the "jump resonance" phenomenon. (Figure 3.6.1, page 3.89).

Auto-Oscillations

In externally excited oscillations, a periodic excitation in the form of a force or displacement is available independent of the

motion of the system. The excitation delivers energy necessary for the motion. The frequency of resulting motion is determined by the frequency of excitation. In many nonlinear systems the two frequencies may coincide.

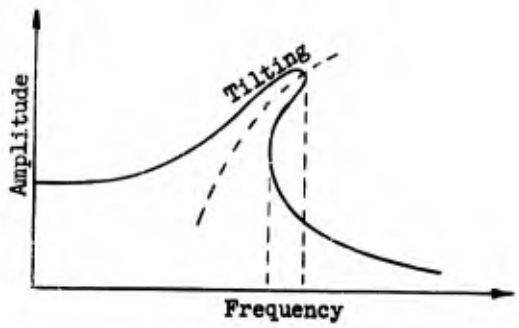

Figure 3.6.1 Tilting Effect of Response Spectrum for Nonlinear System

However, in the case of internally excited oscillations (auto-oscillations) there is a constant source of internal energy available. Once in motion, the driving force is released by the motion of the system itself. The resulting motion of a nonlinear system has approximately the frequency corresponding to the natural frequency of the system, if the internal source of energy is not very large compared with the spring and inertia forces. Essentially the character of a self-excited motion is that of a forced motion with negative damping. The damping force becomes a driving force instead of a restoring force and performs positive work on the system.

Subharmonic Resonance

In linear systems, large amplitudes may be excited by impure disturbances at a frequency which is a multiple of the fundamental frequency of the input. Large amplitude oscillations never occur at submultiples of the fundamental frequency of the input. Nonlinear systems, however, may be excited at submultiples of the fundamental frequency. This phenomenon is called "subharmonic resonance" or "frequency demultiplication" and implies that a harmonic input of frequency f excites an oscillation with frequency f/n where n is an integer. It occurs in nonlinear systems (regardless of whether the nonlinearity appears in the isolator or in the damper) because:

- it is not possible to separate the free vibrations from the forced oscillations.
- there exists a fixed relationship between amplitude and frequency of motion.

the response is not harmonic but always contains various harmonics of higher order. Subharmonic resonance occurs not only in self-excited nonlinear vibrations but also in forced nonlinear vibrations with little or no damping, in which case, the nonlinearities are usually caused by the isolators.

Jump Resonance

A nonlinear system behaves differently for different inputs. This dependence of the system behavior on the actual input is evidenced by the phenomenon of "jump resonance". If the ratio of output to input is plotted as a function of the frequency and the input held constant, there will result a distorted curve. As the frequency is increased from zero, the response will follow the curve up to a certain frequency, when an incremental increase in frequency will result in a discontinuous jump in the response. Thereafter, further increase in the frequency leads to values of the response along the curve. The same phenomenon occurs when the frequency is decreased. However, the jump magnitude is different and occurs at different critical frequencies than in the previous case. The over-all curve exhibits a jump resonance which depends not only on the instantaneous value of the input but also on the past history of the system.

Stability and Pseudostability

Linear systems are either stable or unstable without qualification. But the behavior of nonlinear systems does not show a clear demarcation between stable and unstable conditions. In nonlinear systems when a periodic solution is unstable, the amplitude of motion may grow indefinitely or until some bound has been reached. In certain cases the amplitude may not grow, but the motion may become erratic. As a consequence, when dealing with nonlinear systems the meaning of stability must be clearly defined.

In certain nonlinear systems the amplitude of the output may increase until it reaches a condition of steady oscillation at constant amplitude and period, although the wave may not be harmonic. This intermediate unstable condition (pseudostable) is defined by the so-called "limit cycles" for nonlinear systems. Unlike in linear theory, the occurrence of limit cycles depends only on the parameters of the system and not on the initial conditions. The stability of nonlinear systems depends on the input level and initial conditions of the system. Whereas, for linear elements, the amplification factor is independent of the input amplitude and initial conditions, for nonlinear elements the amplification factor is a function of the input amplitude as well as of the initial conditions.

Evaluation of Nonlinearities

The performance of nonlinear elements of a mechanical system

may be evaluated by the rate of change of the nonlinear characteristics. All nonlinearities may be classified as:

- Fast (nonremovable) nonlinearities for which the mode of operation of the system changes rapidly compared with the response time of the system. Mathematically, such nonlinearities can be expressed in the general form

$$\dot{x}_i = f_i(x_1, x_2, \ldots x_n; a_1, a_2, \ldots a_n; t)$$

where f_i are nonlinear functions of $\dot{x}_i$. The nonlinearities being strong, the behavior changes rapidly with time.

- Slow (removable) nonlinearities for which the behavior of the system remains linear over a time interval which is long compared with the response time of the system. Mathematically, such nonlinearities can be expressed in the general form

$$\dot{x}_i = f_i(x_1, x_2, \ldots x_n; t) + \lambda_i g_i(x_1, x_2, \ldots x_n; t) \qquad (44)$$

where f_i are linear functions of $\dot{x}_i$, whereas g_i are not. The quantities λ_i are constants, usually small in absolute magnitude, so that higher powers of λ_i may be ignored when compared with λ_i. Such nonlinearities, being small, permit the system to be assumed linear over a longer period of time. Such systems are called "quasilinear". Phenomena existing in linear systems are only slightly changed for the equivalent quasilinear systems. A majority of physical systems can be described by quasilinear behavior. The describing function method of analyzing the behavior of nonlinear systems is an attempt to approximate fast nonlinearities by slow nonlinearities within tolerable limits.

In view of the foregoing discussion, the mathematical expression for these two classes of nonlinearities is:

$$(\operatorname{sgn} \dot{x})\, 2\, \delta\omega_o \sum f(x, \dot{x})\, \dot{x} + \omega_o^2\, g(x)$$

representing the generalized Van der Pol type of nonlinearities (for example the pneumatic isolator) and

$$2\, \delta\omega_o\, p_1(x)\, \dot{x} + \omega_o^2\, p_2(x)\, x$$

representing the generalized Hill type of nonlinear elements (for example the pendulum suspension system). Here δ is the damping ratio, ω_o is the natural frequency of the associated linear element, $f(x,\dot{x})$ and $g(x)$, respectively, are algebraic functions in x and $\dot{x}$, whereas $p_1(x)$ and $p_2(x)$ are periodic functions in x.

A further subdivision depending on the expressions associated with the algebraic polynominals $f(x,\dot{x})$ and $g(x)$, and with the

trigonometric polynominals $p_1(x)$ and $p_2(x)$ is as follows:

For the Van der Pol type of nonlinear element, nonlinear springs with characteristics of the general form

$$2\,\delta\omega_o\,\dot{x} + \omega_o^2\,(x \pm c\,x^n)$$

can be described. These would include springs with curved characteristics, either hardening or softening (Figure 3.6.2(a), page 3-93), straight line characteristics such as bilinear, preload, and backlash (Figure 3.6.2 c, d, e, and f). Nonlinear dampers of the generalized form

$$(\operatorname{sgn}\dot{x})\,2\,\delta\omega_o\,g(\dot{x}) + \omega_o^2\,x$$

include dampers of the dry friction, viscous, and nonviscous types.

Similarly for the Hill type of nonlinear element, the Mathieu harmonic ripple of the general form

$$p_1(x) = \lambda \pm 2\gamma\cos 2x \qquad (45)$$

represents a harmonic oscillation of the restoring force of the system about a mean value λ (Figure 3.6.3(a), page 3-94); the Meissner rectangular ripple of the general form

$$p_2(x) = \lambda \pm \gamma \qquad (46)$$

represents a restoring force varying discontinuously but periodically about a mean value λ with an amplitude $|\gamma|$ (Figure 3.6.3(b)).

3.6.2.3 Single-Degree-of-Freedom Nonlinear Systems

At present there is no single, generally applicable method, theory, or body of knowledge regarding the solution of nonlinear problems. The methods used to find the solution of nonlinear differential equations vary widely with the problem under consideration. A large majority of nonlinear differential equations do not admit of closed form or exact solutions. Methods presented so far have serious limitations such as lack of accuracy, lengthy calculations, and limited areas of application. Most of the mathematical work done so far deals with qualitative results. The basic methods for finding approximate solutions of nonlinear differential equations at present can be broadly grouped under three major classes:

- Classical analytical methods
- Averaging methods using describing functions
- Topological methods, essentially graphical

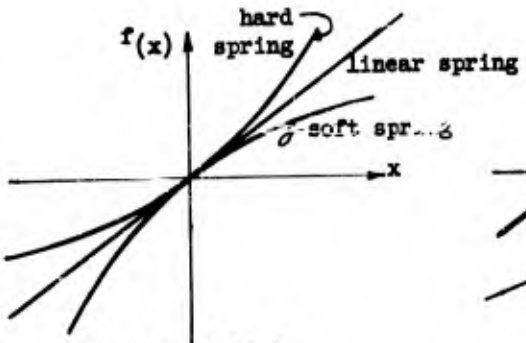

Figure 3.6.2(a)
Nonlinear Springs with Curved Characteristics

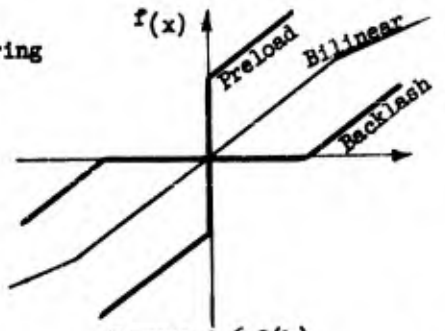

Figure 3.6.2(b)
Nonlinear Springs with Straight Line Characteristics

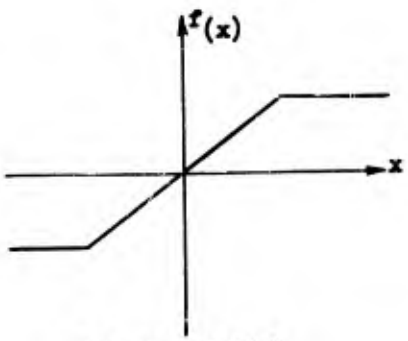

Figure 3.6.2(c)
Saturation

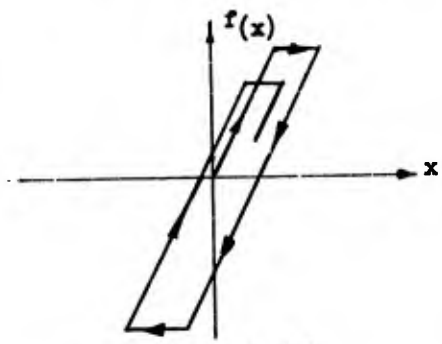

Figure 3.6.2(d)
Saturation with Hysteresis

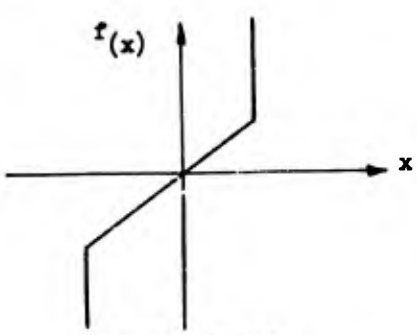

Figure 3.6.2(e)
Locking

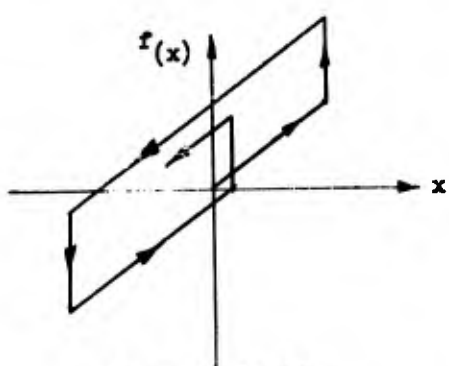

Figure 3.6.2(f)
Locking with Hysteresis

Figure 3.6.2: Nonlinear Spring Characteristics

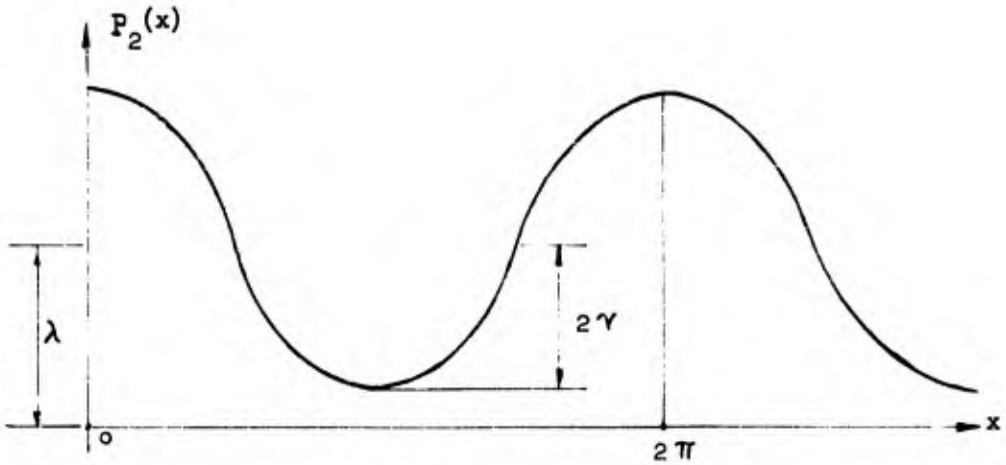

Figure 3.6.3(a)

Mathieu Harmonic Ripple

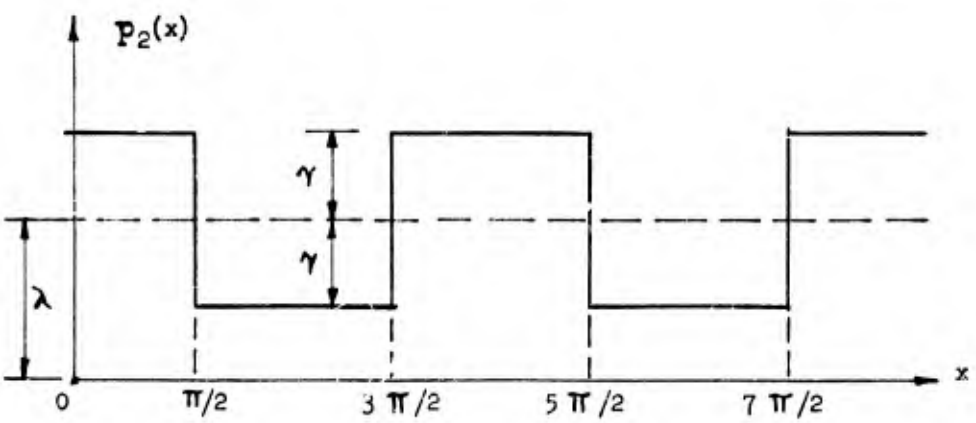

Figure 3.6.3(b)

Meissner Rectangular Ripple

All the above methods consider only quasilinear systems whereby only small nonlinearities are considered. The methods for quantitative results for unrestricted nonlinear systems exist only on a mathematical basis and yield results which are not of a general and deal with the existence, uniqueness, and stability of periodic solutions. The results obtained concern only particular problems and do not cover classes of problems. Their validity is more or less doubtful.

The classical analytical methods referred to are:

- The "iteration method" which assumes as a first approximation the solution of the linear system by discarding the nonlinear terms, followed by a repeated iteration in order to obtain approximations of higher order. The solution obtained by iteration assumes the convergence of its representative series. Although the simplest for computational work, the validity of the iteration method is often questionable.

- The "perturbation method" which uses the basic idea of constructing solutions for an unknown problem by means of solutions of known simpler problems which lie close to the unknown case. The difficulties in this procedure consist of the occurrence of singular solutions leading to algebraically inextricable computations. The accuracy of the perturbation method depends on the number of terms assumed in the series expansion of the variable quantity considered in the nonlinear differential equation.

- The "variation of parameters method" assumes solutions which have the appearance of simple harmonic functions, but of amplitudes and frequencies which vary slowly as a function of time. The secondary differential equations may be solved either by approximation or by the perturbation method. The accuracy of this method depends on the number of terms retained in the series expansion of the variable quantity.

All three analytical methods are applicable to autonomous as well as nonautonomous systems. For practical applications, all three methods are of limited usefulness to designers since the computations are lengthy and the results depend on the assumptions and the degree of accuracy implied by neglecting certain terms in the solutions.

The averaging methods are:

- The Krylov-Bogoliubov method which evaluates the nonlinear elements incorporated in a system by an equivalent linearization process over a certain period. This method has been linked to the Routh-Hurwitz criterion of stability.

- The Ritz-Gallerkin method which approximates, in the mean, the entire nonlinear differential equation representing a nonlinear system. This method has led to the describing function method based on the first harmonic component of the averaging series. The describing function approximates the problem by assuming that the input is sinusoidal and that the only significant frequency component of the input is that component at the input frequency.

- The Ljapunov method of equivalent approximation of a nonlinear configuration based on variational methods leading to a stability criterion, whose accuracy depends on the number of terms considered in the averaging series.

The topological methods are based on the geometrical aspect of the behavior of nonlinear configurations leading to graphic constructions. The methods use solutions, or integral curves in the phase-space, leading to construction of individual curves. The three basic methods in this group are:

- The Isocline
- The Lienard
- The Meissner

Whereas the first two are applicable to autonomous systems only, the Meissner method may be applied to nonautonomous systems as well. The phase-plane methods are generally applicable to only second order systems, but may be employed to obtain approximations of the responses of higher order systems.

The phase-plane and the describing function methods, being of most usefulness in practical application, will be discussed in greater detail.

3.6.2.3.1 The Phase-Plane Method

Except for a few special cases, use of the phase-plane method is restricted to the study of transient motion of simple systems characterized by such nonlinearities as backlash and saturation. Fundamentally, the method consists of graphically plotting the output velocity $\dot{x}$ versus the output displacement x. The initial conditions fix a point in the phase plane. If the $x - \dot{x}$ trajectory starting from the initial point eventually reaches a steady-state condition, the system is stable.

The applicability of the phase-plane method as a procedure leading to the solution of typical problems arising in isolation system design is:

- Only signal-dependent nonlinearities can be considered; that is, the method is restricted to skleronomic systems.

- The method can be applied only to second order systems. Unless higher order systems can be reduced to second order, no methods of general applicability have yet been developed to determine their response by this method.

- In general, the method can be applied only to autonomous systems. Response to step- and ramp-functions can be obtained but the procedures for analyzing the response of systems to inputs typical of those experienced in ground shock have not been developed.

- The complications of constructing phase-plane diagrams increase rapidly with the number of degrees of freedom.

3.6.2.3.2 The Describing Function Method

The range of applicability of this method is restricted to nonlinear systems with a single nonlinear element. If there are several nonlinear elements, they must be lumped together. Further, no time variation of the parameters of the nonlinear element is considered. The basic assumption in the describing function method is that both the input and the output are sinusoidal, thus inferring that the higher harmonics are insignificant. For this reason, the describing function method is often termed a sinusoidal analysis. The describing function method is appropriate for the determination of both the existence of sustained oscillations and the approximate amplitude and frequency but it does not describe the wave form. Although the greater part of mathematical work in nonlinear mechanics has been concerned with the establishment of the existence of limit cycles in practical applications, it is desirable, more often, to determine the performance of a nonlinear system which is known to be stable.

The describing function, as a ratio between the fundamental component of the output to the input amplitude, is in general a function of input amplitude and frequency. If this function is single valued, the describing function is real and does not depend on the phase. If multiple valued, the describing function is complex and therefore will depend on the phase. Furthermore, if the system exhibits a change in the energy storage, the describing function will depend on the frequency. In special cases where the describing function is real and independent of frequency, the amplitude of the nonlinear device varies only with the amplitude of the input and this variation can be interpreted as a motion of the poles along the root loci. Consequently the describing function analysis indicates the transient response only insofar as it demonstrates approximately the relative stability and band width. The describing analysis is not readily applicable to the study of the response of nonlinear systems to random input functions.

The describing function analysis replaces the rapidly moving poles and zeros by critical frequencies which move slowly. The equivalence is valid only at a point on the imaginary axis, i.e., at the sinusoidal frequency. The poles and zeros move with the change in amplitude of the signal input of the nonlinear device. Stability can be evaluated as a function of the signal level by letting the test point on the imaginary axis (i.e., the test frequency) vary from zero to infinity. The accuracy of the approximation of rapidly moving poles and zeros by slowly moving critical frequencies is reduced by neglecting all harmonic components except the fundamental in the output of the nonlinear device. The validity of the approximation depends directly on the harmonic distortion of the output and the extent of the low-pass filtering in the linear components between the output and input terminals of the nonlinear device.

The difficulty arising in the describing function analysis is of computational nature associated with the determination of the describing function for a wide range of amplitudes and frequencies. Furthermore, there is no simple method for evaluating the accuracy of the describing function analysis of a nonlinear system, and therefore no definite assurance that the results obtained with a describing function are approximately correct. However, by incorporating a second term in the series of the result of the describing function analysis containing only the first term, the results of the describing function analysis can be partially corrected and an idea of the accuracy to be expected determined. In that case, the answer will be given to a second approximation which, however, infers more elaborate calculations. Nevertheless, it cannot be inferred that in the absence of an indication of accuracy, the accuracy of the describing function is poor. The accuracy achieved in a great number of cases reported in the literature is rather startling. This results from the fact that, in a wide variety of systems, the errors introduced by the approximation of the describing function method are small compared to the probable errors in the description of the nonlinear element characteristics. In the great majority of cases the describing function method offers a rough measure of the effect of certain nonlinearities and a quick method for evaluating the effects of additional linear or nonlinear components introduced within a mechanical loop.

Summarizing the above discussion, for second order systems the three groups of methods explained above give about the same result. For higher order systems the describing function method is more useful but limited to sinusoidal input. In general, none of the above methods give full results.

3.7 Response of Single-Degree-of-Freedom, Bilinear and Hysteretic Systems to Typical Ground Shock Wave Forms

3.7.1 Introduction

It is evident from the preceding paragraphs that the analytical solution of problems involving the response of nonlinear systems to shocks of complex wave forms can be exceedingly difficult. Yet nonlinear isolators and suspension methods form a large area of practical interest to the isolation system designer. For those systems containing large nonlinearities, or many coupled degrees-of-freedom, or where there is question as to the stability of the system, the designer has little recourse but to program the equations for solution by electronic computer.

The nonlinearities of many systems however can be approximated by a simple bilinear or hysteretic characteristic. Such problems, while simple in concept, still require considerable time to analyze formally. However, because of their apparent simplicity, there is frequently a reluctance to resort to a computer solution. To assist the designer, not only in estimating the response of such systems but also in selecting optimum components, the responses of a large number of simple nonlinear systems to various combinations of the Types I and II wave forms, synthesized in Section 2.0, were determined on the Stanford Research Institute analog computer. It should be emphasized that since the Type I and Type II wave forms were synthesized on the basis of records of vertical motions, the applicability of these results to horizontal ground motions remains to be determined. The 34 shock inputs used in the study are shown in Figure 3.7.5(a), page 3-109. Inputs 1 - 29 were composed of various proportions of the Type I and Type II wave forms while inputs 30 - 34 were obtained from test records. Undamped, linear response spectra for inputs 1 - 29 are given in Figure 3.7.5(b), page 3-110.

3.7.2 Isolator Characteristics and Equations of Motion

The isolators investigated had bilinear and hysteretic stiffness characteristics and dissipation. Figures 3.7.1 and 3.7.2, page 3-100, show the stiffness characteristics with restoring force as a function of displacement. These characteristics cover the essential nature of a large number of real isolators. The bilinear stiffness characteristic can be used to approximate fairly closely stiffness characteristics which are actually curved, including "hardening" and "softening" systems and preloaded systems. The hysteretic stiffness characteristic includes pneumatic systems, solid friction and plastic yielding. In the bilinear and hysteretic cases viscous damping only was included. Hydraulic or velocity-square damping and Coulomb or friction damping were considered only for a linear spring.

3.7.2.1 Bilinear Stiffness Characteristic with Viscous Damping (Case A)

The equation of motion of an isolator with a bilinear stiffness (Figure 3.7.1) characteristic and viscous damping, after dividing through by the mass, is:

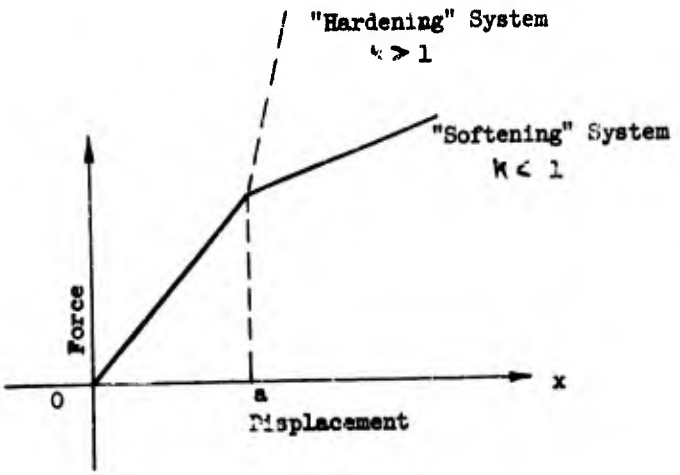

Figure 3.7.1

Bilinear Stiffness Characteristic

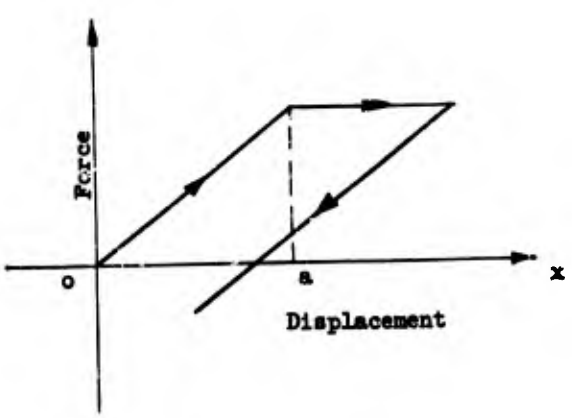

Figure 3.7.2

Hysteretic Stiffness Characteristic

$$\ddot{x} + 2\lambda\omega\dot{x} + \omega^2 \begin{bmatrix} x, & x < a \\ a + k(x - a), & x > a \end{bmatrix} = -\dot{v} \qquad (47)$$

where

x = relative displacement between isolator platform and ground

λ = coefficient of viscous damping referred to the first part of the stiffness characteristic

ω = natural angular frequency of the isolated mass, oscillating on the first part of the characteristic (rad/sec)

a = the relative displacement at which the elastic stiffness characteristic changes slope

v = input velocity

k = ratio of the square of the angular frequencies corresponding to the final and initial values of stiffness

t = time.

The above equation is written only for positive x. The characteristic is assumed to be symmetric about the origin. The third term in equation (47) represents the stiffness characteristic shown in Figure 3.7.1. Depending on whether the displacement x is less or greater than the displacement a, this term represents one or the other of the two straight lines making up the stiffness characteristic.

Equation (47) contains five independent parameters, λ, ω, a, k, v, and may be nondimensionalized by the following change of variables. Put,

$$X = x/a \qquad (48)$$

$$T = tp \qquad (49)$$

$$V = \frac{v}{ap} \qquad (50)$$

$$\Omega = \frac{\omega}{p} \qquad (51)$$

where

$$p = \frac{2\pi}{t_o} \qquad (52)$$

and t_o is the duration of the input wave, the equation of motion becomes

$$\frac{d^2X}{dT^2} + 2\lambda\Omega\frac{dX}{dT} + \Omega^2\begin{bmatrix} X & , & X < 1 \\ 1 + k(X - 1) & , & X > 1 \end{bmatrix} = -\frac{dV}{dT} \qquad (53)$$

The equation is now nondimensionalized and one parameter has been eliminated leaving λ, Ω, k, and V. One further variable is introduced to complete the nondimensionalization. The acceleration Z experienced by the isolated body is given by the sum of the dissipative and elastic terms,

$$Z = 2\lambda\omega\dot{x} + \omega^2\begin{bmatrix} x & , & x < a \\ a + k(x - a) & , & x > a \end{bmatrix} \qquad (54)$$

Define a new symbol,

$$G = 2\lambda\Omega\frac{dX}{dT} + \Omega^2\begin{bmatrix} X & , & X < 1 \\ 1 + k(X - 1) & , & X > 1 \end{bmatrix} \qquad (55)$$

then

$$Z = ap^2G. \qquad (56)$$

All the results are presented in terms of these nondimensionalized variables λ, Ω, k, X, V, G and to convert them to dimensional variables, equations (48), (49), (50), (51), (52), (56) are used. The maximum values of X, V, G are denoted by X_m, V_m, G_m.

3.7.2.2 Hysteretic Stiffness Characteristic With Viscous Damping (Case B)

The equation of motion and all nomenclature for the hysteretic stiffness characteristic (Figure 3.7.2) with viscous damping are identical to the bilinear case for k = 0 except that when the relative velocity changes sign the characteristic returns down a path parallel to the initial path through the origin. This situation may be written formally as

$$\begin{aligned} \ddot{x} + 2\lambda\omega\dot{x} + \omega^2(x - u) &= \dot{v}, \quad |x - u| \le a \\ \ddot{x} + 2\lambda\omega\dot{x} + \omega^2 a\,\operatorname{sgn}\dot{x} &= \dot{v}, \quad |x - u| > a \end{aligned} \qquad (57)$$

where u is the algebraic sum of all previous "yield" displacements up to the time considered, and where the sign of the yield displacement is that of the velocity at that time. As the nondimensionalization and

nomenclature are identical to the bilinear case they are not repeated. Equations (48), (49), (50), (51), (52), (56) apply as in the bilinear case.

3.7.2.3 Linear Spring and Coulomb Friction (Case C)

The case where the isolated body is connected in series by a spring to a friction damper which then slides on the moving base is the same as the hysteretic case (B) when $\lambda = 0$. However, if the isolated body is connected directly by a spring to the base and the friction damper is also connected in parallel between the body and the base, the situation is different.

The equation of motion in this case is

$$\ddot{x} + \omega^2 c \operatorname{sgn} \dot{x} + \omega^2 x = \dot{v} \tag{58}$$

where the notation is as before with c in place of a. The acceleration corresponding to the friction force is given by $\omega^2 c$. The nondimensionalization proceeds as in Case A and equations (48), (49), (50), (51), (52), (56) apply as before with c in in place of a.

3.7.2.4 Linear Spring with Square-Law Damping (Case D)

A damping term proportional to the square of the velocity is to be expected in certain hydraulic systems.

The equation of motion is given by,

$$\ddot{x} + C(\dot{x})^2 \operatorname{sgn} \dot{x} + \omega^2 x = \dot{v} \tag{59}$$

where C is the square-law damping coefficient. To nondimensionalize this equation it is necessary to introduce a characteristic length. This may be done by defining,

$$e = \frac{v_m}{p} \tag{60}$$

where v_m is the maximum value of v. If the same procedure is followed as in Case A using the value e in place of a, the equation of motion becomes

$$\frac{d^2X}{dT^2} + H\left(\frac{dX}{dT}\right)^2 \operatorname{sgn} \frac{dX}{dT} + \Omega^2 X = \frac{dV}{dT} \tag{61}$$

where $H = Ce$ and is the nondimensional damping coefficient. It is to be noted that in this case the value of the nondimensionalized variable V_m has the value of unity. Equations (48), (49), (50), (51), (52), (56) apply as before with e in place of a.

3.7.2.5 Linear Spring with Viscous Damping (Case E)

This case is covered by Case A when $X_m \leq 1$ and is shown in the results by $X_m = 1$.

3.7.2.6 Viscous Damping Only (No Stiffness) (Case F)

This degenerate case is of interest because it illustrates the importance of damping and has the equation of motion given by

$$\ddot{x} + \mu \dot{x} = \dot{v} \tag{62}$$

where μ is the viscous damping coefficient. As before, put $e = v_m/p$ and obtain

$$\frac{d^2X}{dT^2} + L \frac{dX}{dT} = \frac{dV}{dT} \tag{63}$$

where $L = \mu/p$ and is the nondimensional damping coefficient. Again the value of V_m is unity, and equations (48), (49), (50), (51), (52), (56) apply with e in place of a.

3.7.2.7 Square-Law Damping Only (Case G)

In equation (61) set $\Omega = 0$ and Case D degenerates to that of Case G.

3.7.2.8 Coulomb Damping Only (Case H)

The equation of motion is,

$$\ddot{x} + F \operatorname{sgn} \dot{x} = \dot{v} \tag{64}$$

where F is the acceleration corresponding to the Coulomb friction force. As before, introduce $e = v_m/p$ and obtain

$$\frac{d^2X}{dT^2} + M \operatorname{sgn} \frac{dX}{dT} = \frac{dV}{dT} \tag{65}$$

where $M = G_m = F/pv_m$, the value of V_m is unity and equations (48), (49), (50), (51), (52), (56) apply with e in place of a.

3.7.3 Presentation and Optimization of Results

3.7.3.1 Range of Parameter Values

Values for k in equation (47) of 0, 0.2, 0.5, 1.0 and 2.0 were chosen. These include three softening systems and one hardening system as well as the linear case. Values of λ = 0, 0.1, 0.2

were selected as reasonable. Generally eight to ten values of the nondimensional angular frequency Ω were used from zero up to a value where the system was no longer isolating, i.e., when the isolated body experienced an acceleration greater than the acceleration associated with the input velocity. The values of the nondimensional maximum input velocity V_m used were such that the resulting nondimensional maximum relative displacement X_m took a series of values between 1 and 5. These values span the more relevant part of the stiffness characteristic. For large values of X_m of course, the initial part of the stiffness characteristic is of little importance and the case degenerates to that of a linear preloaded isolator.

3.7.3.2 Presentation of Results

In this work only the "maximax" values are presented, i.e., for one isolator specified by particular values of Ω, k, λ, and V_m, only the largest values of G and X occurring from the different inputs are tabulated and are called G_m and X_m. Depending on the particular values of Ω, k, λ, and V_m, this largest value may come from any of the different inputs. In general for a given isolator the largest values of G and X will come from the same input shape, but this is not always true.

Initially V_m and G_m were plotted against X_m to give the values of V_m and G_m at values of X_m = 1, 2, 3, 4, 5. From these a set of curves is constructed showing for every particular value of k and λ, the values V_m and G_m at X_m = 1, 2, 3, 4, 5 as a function of Ω. Given particular ground motion parameters and isolator parameters v_m, p, ω, λ, k, a, these graphs together with equations (48), (49), (50), (51), (52), and (56) determine the maximax acceleration experienced by the body together with the maximax "rattlespace".

3.7.3.3 Optimization

1. Minimum "Rattlespace" for Specified Acceleration

The most common design problem is that of minimizing the "rattlespace" when the maximum acceleration of the isolated body is specified. This problem cannot be solved from the V_m, G_m -versus- Ω curves directly because of the nondimensionalization which eliminates the value of a which is the displacement at which the break point occurs. Thus the question becomes one of determining real variables such as a rather than nondimensionalized ones. This may be approached in the following fashion.

Let z_m = specified maximum acceleration the body is to experience

x_m = maximum "rattlespace" which is to be minimized, (66)

Then from equations (48), (50), and (56) we have

$$x_m = \left(\frac{v_m}{p}\right)\left(\frac{X_m}{V_m}\right) \tag{67}$$

Introduce a new variable

$$\sigma = \frac{z_m}{v_m p} = \frac{G_m}{V_m} \tag{68}$$

Now, z_m, v_m, p are specified, and thus σ is specified and the value we are endeavoring to minimize, x_m, is a product of a fixed specified value v_m/p and the factor X_m/V_m. The problem now is to minimize X_m/V_m for specified values of G_m/V_m, i.e., σ. This was done by preparing a plot of G_m against V_m for X_m = 1, 2, 3, 4, 5 for each set of values of λ, k. Corresponding values of V_m and G_m have the same values of X_m and Ω. Figure 3.7.4 shows a plot of this form.

Radial lines from zero are drawn for a set of values of $\sigma = G_m/V_m$. A second and final plot is made from the first one of (X_m/V_m) versus V_m for the various values of σ. From these curves the value of V_m giving the smallest value of X_m/V_m and hence of x_m for a particular σ may be determined. The value of a is found by rewriting equation (50) in the form

$$a = v_m / V_m p$$

and, by referring to the relevant V_m - versus - Ω curves, Ω may be established. Arcs of hyperbolas are drawn to separate the linear region ($X_m < 1$) from the nonlinear region.

In the case of the linear spring with square-law damping it is noted that the parameter σ degenerates to $\sigma' \equiv G_m$.

2. Minimum Acceleration for Specified "Rattlespace"

The question of minimum acceleration for specified rattlespace is effectively the same as the question of minimum rattlespace for specified acceleration, and it may be answered from the same optimization curves. If a certain maximum displacement, x_m, is specified, then this means that the value X_m/V_m is specified. If a horizontal line is drawn through this specified value of X_m/V_m, then the lowest value of σ giving a curve which will meet this horizontal line represents the lowest acceleration which may be obtained for the specified x_m and the other particular parameters. As before, the value of V_m arising at the meeting of the X_m/V_m line and the σ curve determines the parameters a, Ω, and hence ω.

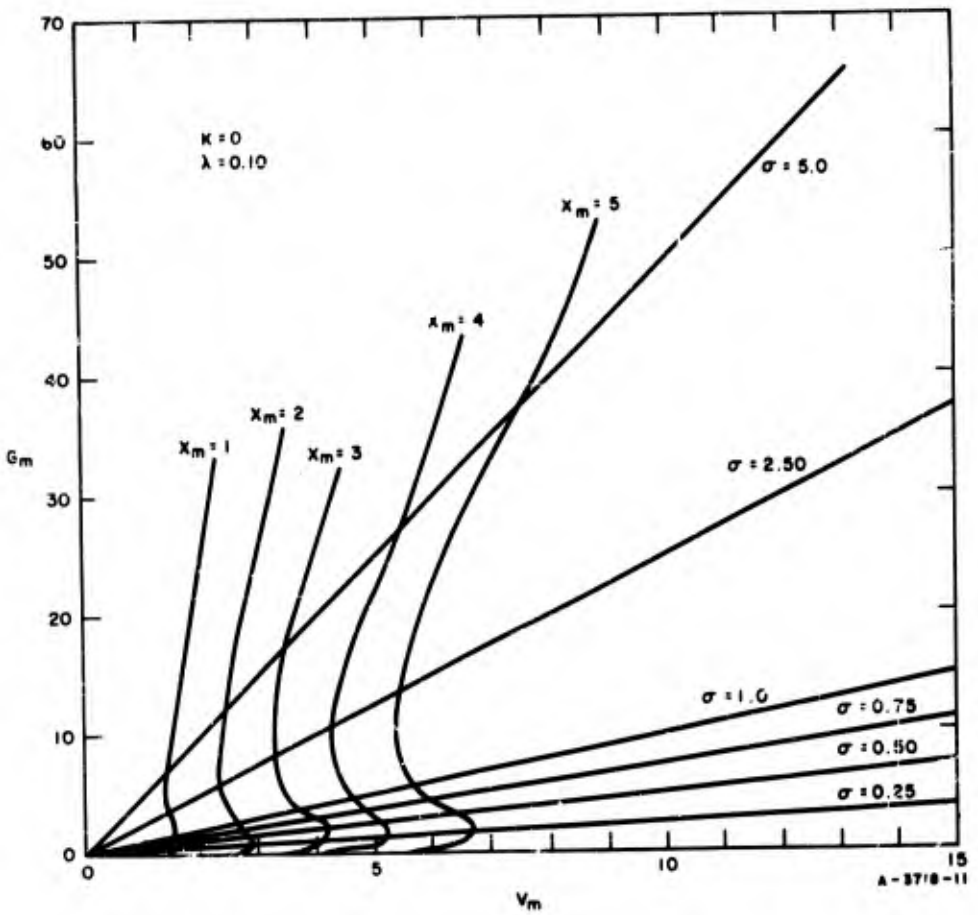

Figure 3.7.4
Typical Plot for Construction of
Optimization Curves

It is to be noted that whereas one can always design for any specified body acceleration no matter how small, it is not necessarily possible to do this for the relative displacement without incurring accelerations greater than those existing in the input.

3.7.4 Results

The results are given in graphical form in Figures 3.7.5 through 3.7.26 in this subsection, as functions of the nondimensional variables discussed in Section 3.7.2. In general, there are three graphs associated with each set of parameters. These graphs show the relation between Ω^2/G_m and Ω, V_m and Ω, and (X_m/V_m) and V_m for various values of subsidiary parameters, e.g., X_m, H, σ, etc. The value Ω^2/G_m is plotted instead of G_m because of the large range of values taken by G_m.

3.7.4.1 Undamped Linear Spectra

Figure 3.7.5(b), page 3-110, gives the undamped spectra of the family of the 29 input shapes * in terms of $\Omega X_m/V_m$ against Ω. The term $\Omega X_m/V_m$ which equals $\omega x_m/v_m$ is a pseudo velocity and is the standard way of presenting spectra of ground motion.

The numbers 1 through 29 identify the spectra of the various velocity input wave forms outlined in Figure 3.7.5(a), page 3-109. As is to be expected, the spectra are all different and it is well to note again that in what follows only the maximax value of the response of a particular isolator to the family of inputs is tabulated. The response of a particular isolator to any particular input wave form will often be considerably less. Figure 3.7.6, page 3-111, shows the envelope and the mean value of the spectra of the family of input wave forms. The shape of the envelope is very similar to that assumed in the T_1, T_2 spectra. The ratio of the envelope of the individual spectra to the mean value (approximately 2:1) gives an idea of the dispersion of the maximum values in the undamped case.

3.7.4.2 Viscous-Damped Bilinear Characteristic

Figures 3.7.7 to 3.7.19, pages 3-114 through 3-126, show the responses of the various bilinear isolators considered, together with the optimization curves. For each pair of values of damping coefficient λ and nonlinearity factor k there are three sets of curves. The first set of curves shows the nondimensional velocity input, V_m, as a function of the nondimensional frequency Ω for various values of the maximum nondimensional relative displacement X_m. The second set shows the nondimensional maximax acceleration of the isolated body in terms of Ω^2/G_m as a function of Ω for various values of X_m.

* These 29 input shapes plus five actual velocity curves make up the total of 34 inputs.

Amplitude Ratio		Duration Ratio		Phasing
	Type I:Type II		Type I:Type II	
A_1	2:1	A_2	2:1	A_3 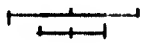
B_1	1:1	B_2	1:1	B_3 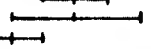
C_1	1:2	C_2	1:2	C_3 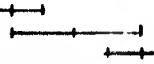

Shape No.	Combination	Shape No.	Combination	Shape No.	Combination
1	Type I	13	B_1 A_2 C_3	25	C_1 B_2 C_3
2	A_1 A_2 A_3	14	B_1 B_2 A_3	26	C_1 C_2 A_3
3	B_3	15	B_3	27	B_3
4	C_3	16	C_3	28	C_3
5	A_1 B_2 A_3	17	B_1 C_2 A_3	29	Type II
6	B_3	18	B_3	30	Tumbler 3V
7	C_3	19	C_3	31	Tumbler IV
8	A_1 C_2 A_3	20	C_1 A_2 A_3	32	Cactus 3V30
9	B_3	21	B_3	33	Tumbler 2-2V
10	C_3	22	C_3	34	Koa 12V30
11	B_1 A_2 A_3	23	C_1 B_2 A_3		
12	B_3	24	B_3		

In type B_3 and C_3 the shorter duration type is always centered on the beginning or end, respectively, of the longer duration one. Thus, in A_2B_3 Type II starts first and is half over before Type I begins (see shapes 3, 12, or 21 on Figure 3.7.28). In C_2B_3, on the other hand, Type I starts first and is half over before Type II begins (see shapes 9, 18, or 27 on Figure 3.7.28).

Figure 3.7.5(a)
Key to Wave Shape Combinations

The third set gives the factor (X_m/V_m) which is proportional to the actual relative displacement, x_m, as a function of V_m for various values of σ. It is noted from equation (55) that when $\lambda = 0$ and $X_m > 1$ the variable G_m is given simply by

$$G_m = \Omega^2 \left[1 + k(X_m - 1)\right] \tag{69}$$

and, as this is a simple relation, it has not been plotted.

When $\lambda \neq 0$ the value of G_m is the sum of two terms as shown by equation (55). If Ω is very small then the second term in Ω^2 is negligible compared to the first term in Ω and we have

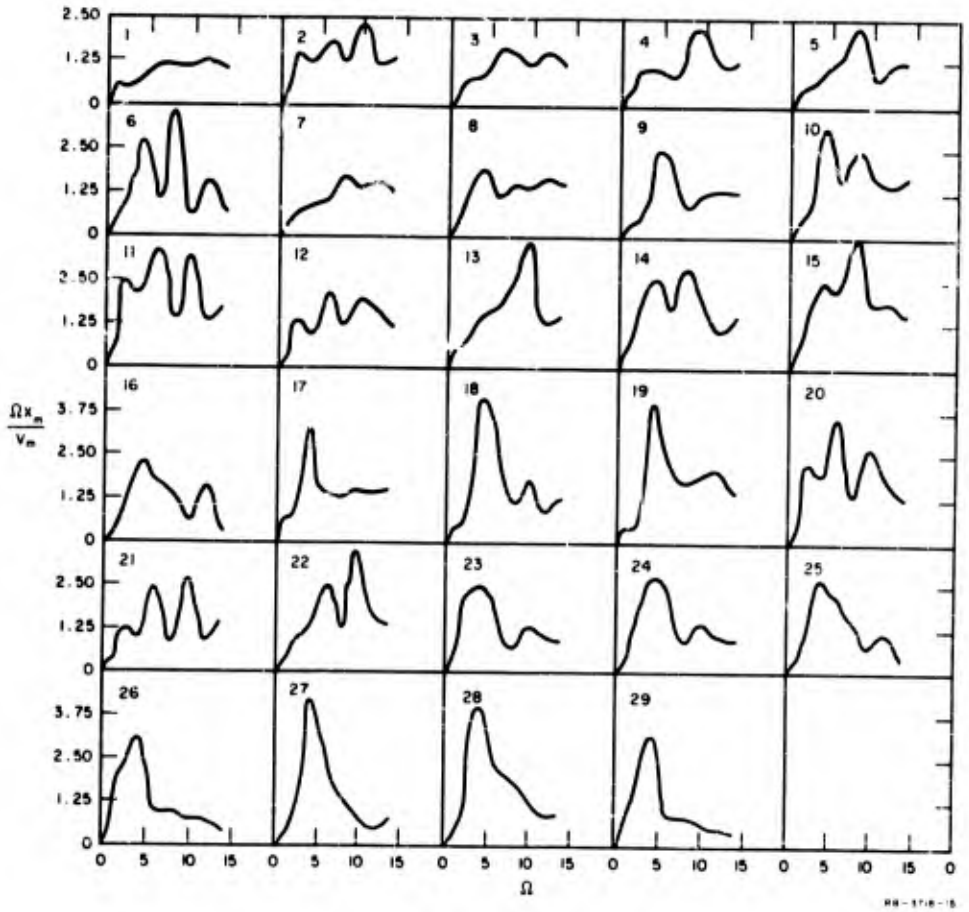

Figure 3.7.5(b) Undamped Spectra of the Family of Input Velocity Waveforms

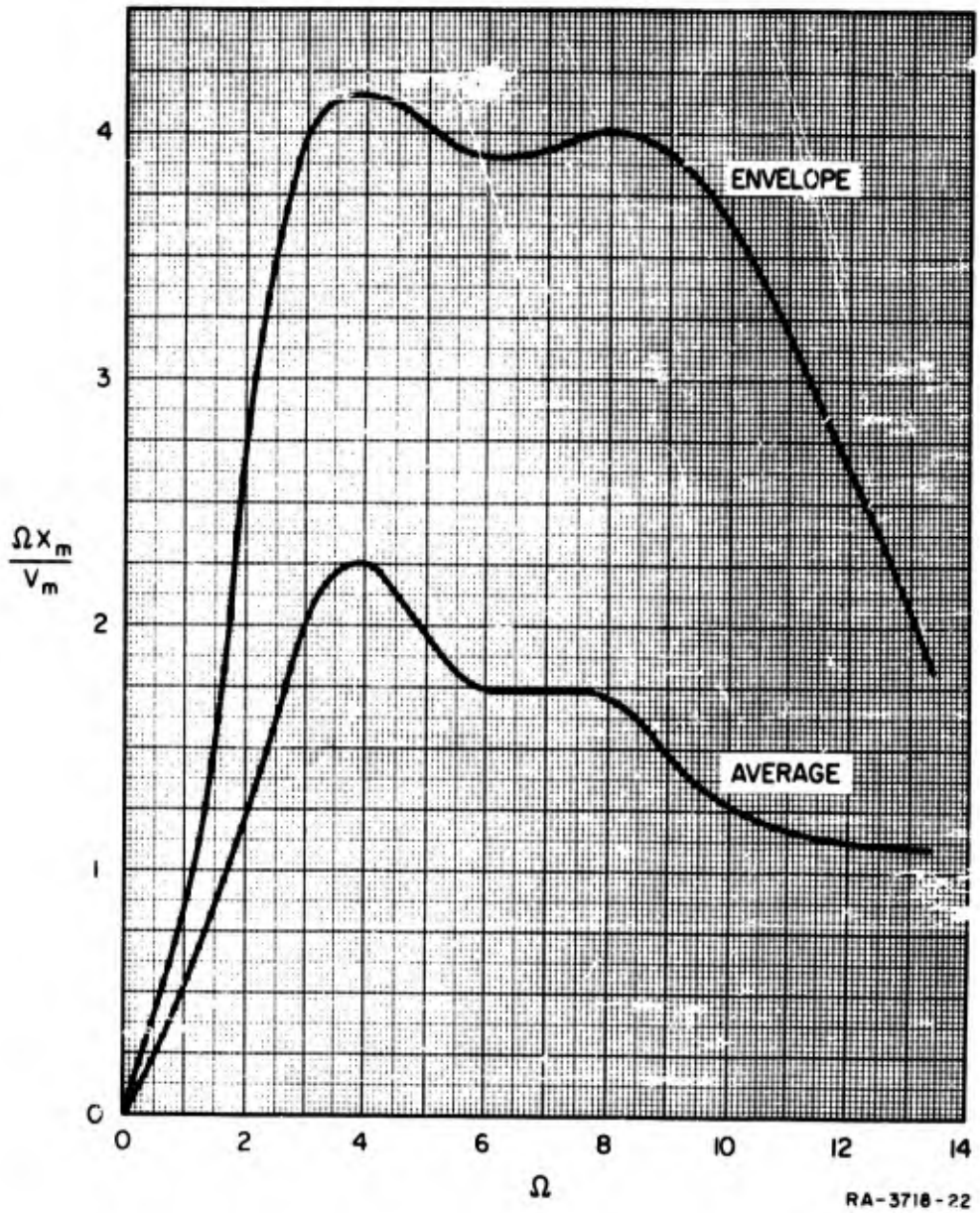

Figure 3.7.6 Envelope and Average Unlamped Spectra of the Input Velocity Waveforms

$$\frac{\Omega^2}{G_m} \approx \frac{\Omega}{2 \lambda V_m}$$

Thus the initial parts of the Ω^2/G_m curves are straight lines through the origin. However, when Ω is large, the second term predominates and Ω^2/G_m tends to a constant value of $1/[1 + k(X_m - 1)]$. When there is no damping, G reaches its maximum value when X does. However, because of phasing this is not true when damping is present.

Figures 3.7.7, 3.7.11, 3.7.14, and 3.7.17 show the undamped case $\lambda = 0$. The V_m - versus - Ω curves for the various values of X_m indicate a quasiresonance taking place at certain values of Ω. This is indicated by a minimum point in the V_m-versus- Ω curves, i.e., the point which requires less input to give the same displacement. In Figure 3.7.7 this situation is seen in the linear case, i.e., $X_m = 1$ at the value $\Omega = 3.25$. As the amplitude increases, i.e., X_m increases, the natural period decreases. Therefore the quasiresonant point moves to the right. Also, a second such point rapidly appears with increasing X_m.

Changing the nonlinearity parameter, k, from a "softening" system given by $k = 0$ to a "hardening" system given by $k = 2.0$ has little effect on the essential character and amplitude of these responses. The main effect is to change the direction in which the quasiresonant point moves. In a "hardening" system the natural frequency increases with increasing amplitude and consequently the resonant point moves to the left.

The relatively small effect of the parameter k is best seen by a study of the optimization curves. For the same values of λ and σ these curves all start at the same point on the hyperbola dividing the linear region ($X_m \leq 1$) from the nonlinear region ($X_m > 1$); and apart from trivial fluctuations they show a roughly horizontal trend, especially for lower values of σ. Thus the nonlinear cases do not give any significant decrease in rattlespace for a specified σ over that of the linear situation.

It is interesting to note that in many cases in Figures 3.7.7, 3.7.11, 3.7.14, and 3.7.17, designing for a larger acceleration actually demands a greater relative displacement. To obtain such an acceleration means approaching the quasiresonant condition with the attendant large displacement. Naturally, in this situation one would design for a lower maximum acceleration than specified to obtain the attendant lower relative displacement.

Figures 3.7.8, 3.7.12, 3.7.15, and 3.7.18 show the effect of the addition of 10% damping to the first part of the stiffness characteristic. The addition of damping smoothes out the fluctuations in the amplitude response curves, increases the V_m necessary to give a particular X_m, and hence lowers the optimization curves. Once again the difference

between the various k values is not significant for the smaller values of σ . For the value σ = 7.5 it is noticed that the value k = 0 has a very distinct advantage over the value k = 2.0. When k = 2, as before, we have the situation where a smaller design acceleration can be obtained together with a smaller rattlespace.

Figures 3.7.9, 3.7.13, 3.7.16, and 3.7.19 show the effect of a further increase in damping, i.e., λ = 0.2. As before, the relative displacements are further lowered, but again the effect of the nonlinearity parameter k is not great except for the higher values of σ Figure 3.7.10 shows the case k = 0 with 50% damping. A further reduction in relative displacement is noted. These observations all point to the importance of damping in the system and the insignificance of the various nonlinear stiffness characteristics considered.

3.7.4.3 Viscous-Damped Hysteretic Characteristic

A hysteretic characteristic involves a substantial dissipation of energy; and, considering the effect of dissipation in the bilinear case, it is not surprising that the same effects are noted here. Figures 3.7.20 through 3.7.22, pages 3-127 - 3-129, show the response and optimization curves for various values of viscous damping. A comparison of V_m-versus- Ω curves for the bilinear k = 0, λ = 0, and the hysteretic case λ = 0 show the effect of the hysteretic damping, i.e., a much larger value of V_m is necessary to give the same relative displacements. This is more obvious in the optimization curve shown in Figure 3.7.20. As V_m and X_m tend to infinity, the hysteretic case approaches that of simple Coulomb friction with no springs. The results for Coulomb friction, from a separate computation, are plotted on the far right of Figure 3.7.20; and it is seen that as V_m gets large, the hysteretic case is indeed approaching that of Coulomb friction. The addition of viscous damping as shown in Figures 3.7.21 and 3.7.22 further decreases the maximum relative displacement.

3.7.4.4 Linear Spring with Coulomb Friction

Figure 3.7.23, page 3-130, shows the response and optimization curves for a linear spring with a Coulomb-friction damper in parallel. The G_m curves can be shown to have the simple relation

$$G_m = \Omega^2 (1 + X_m) \qquad (70)$$

and they have not been plotted. The ratio of the maximum spring force to the friction force equals X_m as may be seen from equation (70). Thus as X_m becomes large, the situation tends to that of an undamped linear spring. This tendency may be seen in Figure 3.7.23 where, as X_m increases, the shapes of the V_m-versus- Ω curves tend towards that of the undamped linear case. The optimization curves in Figure 3.7.23 show again that the higher the friction, the less is the relative displacement for the same acceleration. This is true except for the

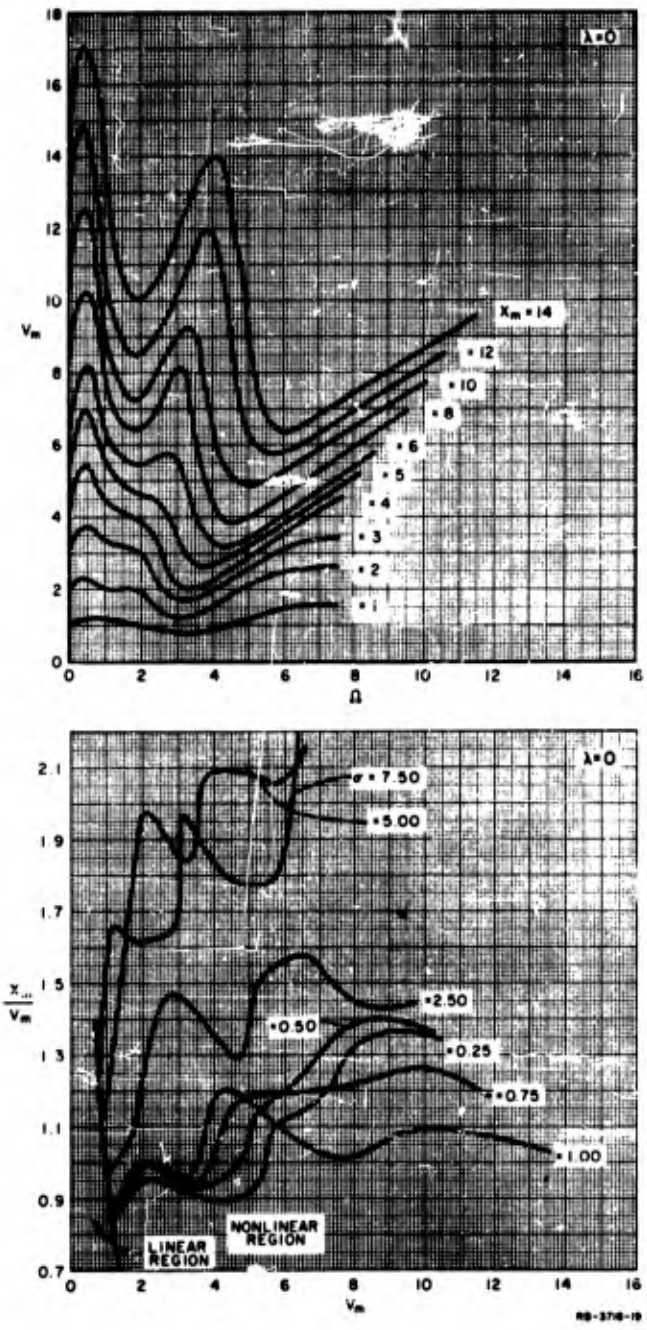

Figure 3.7.7 The Bilinear Case for $\kappa = 0$, $\lambda = 0$; $G_m = \Omega^2$

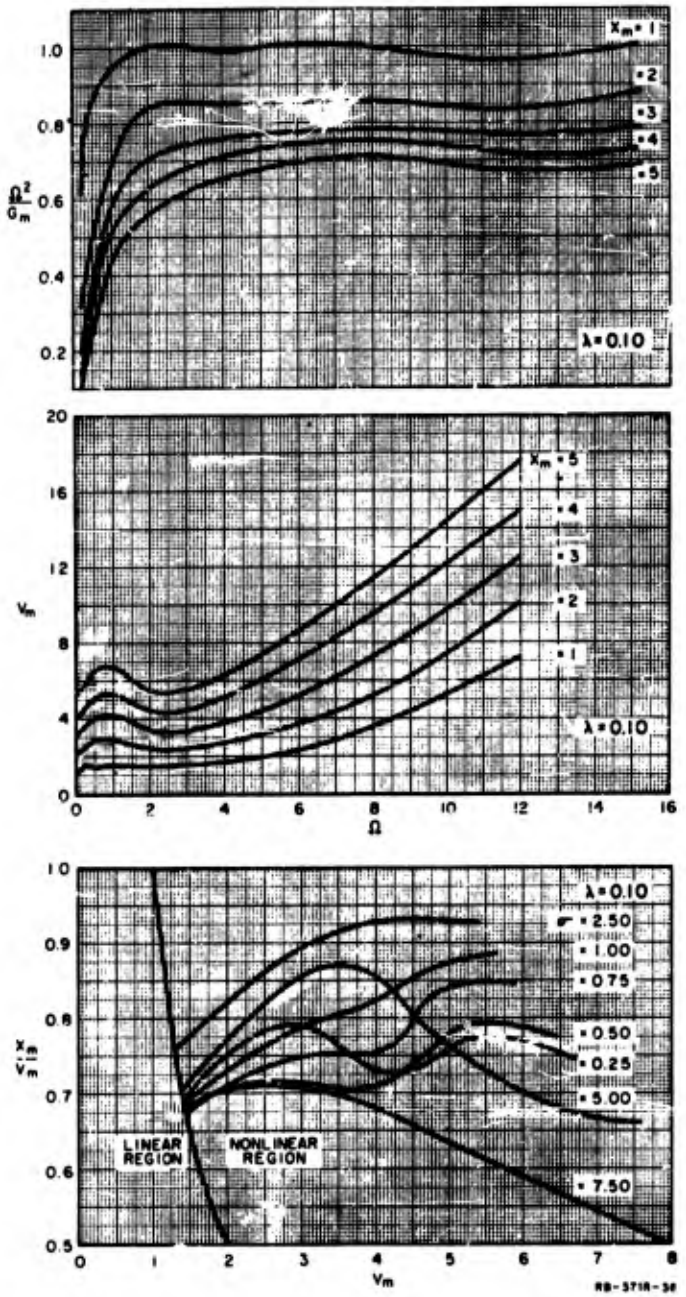

Figure 3.7.8 The Bilinear Case for K = 0, λ = 0.10

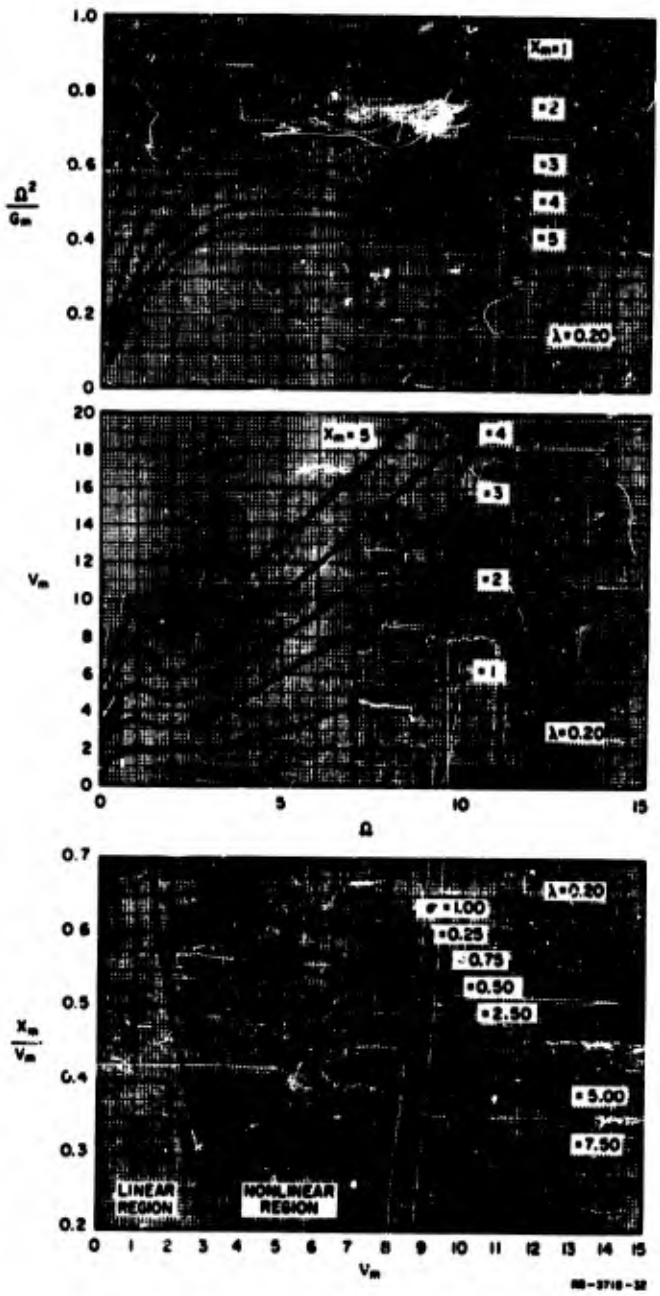

Figure 3.7.9 The Bilinear Case for k = 0, λ = 0.20

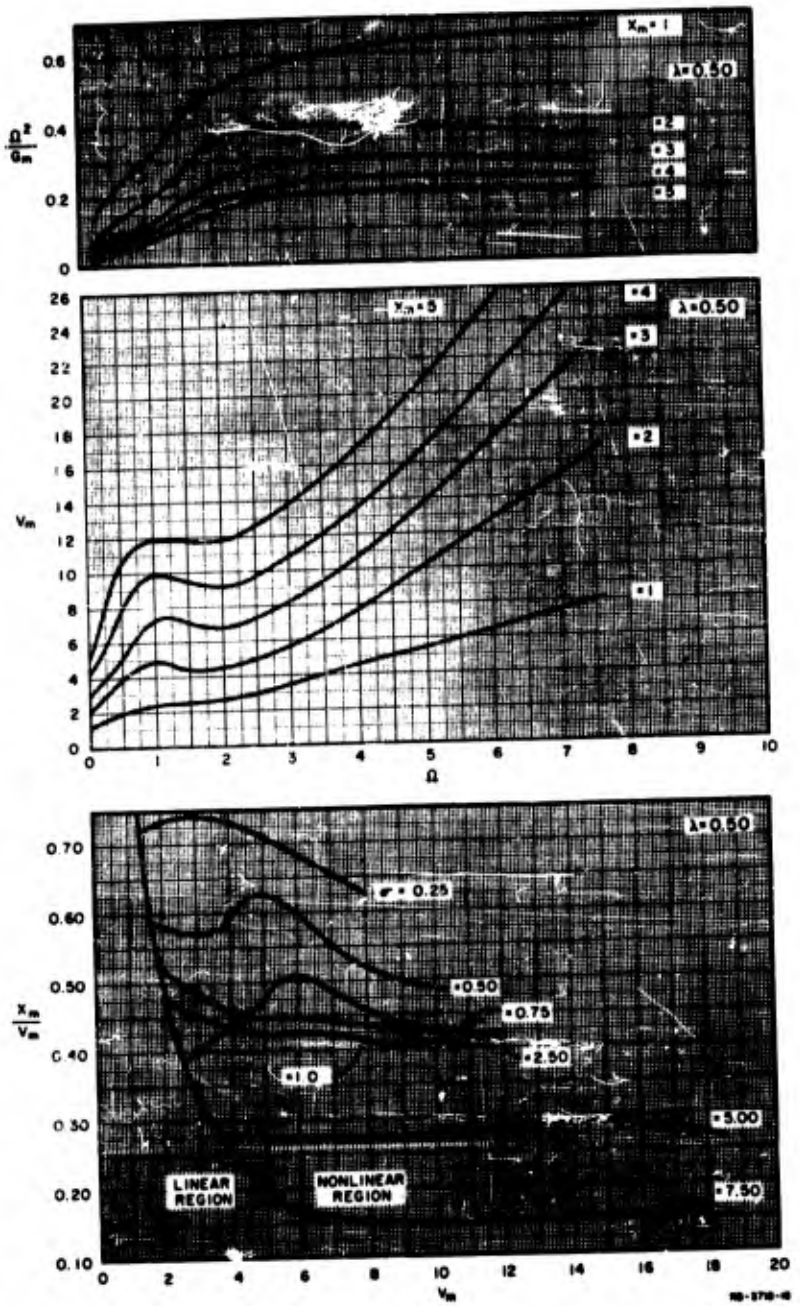

Figure 3.7.10 The Bilinear Case for $\chi = 0$, $\lambda = 0.50$

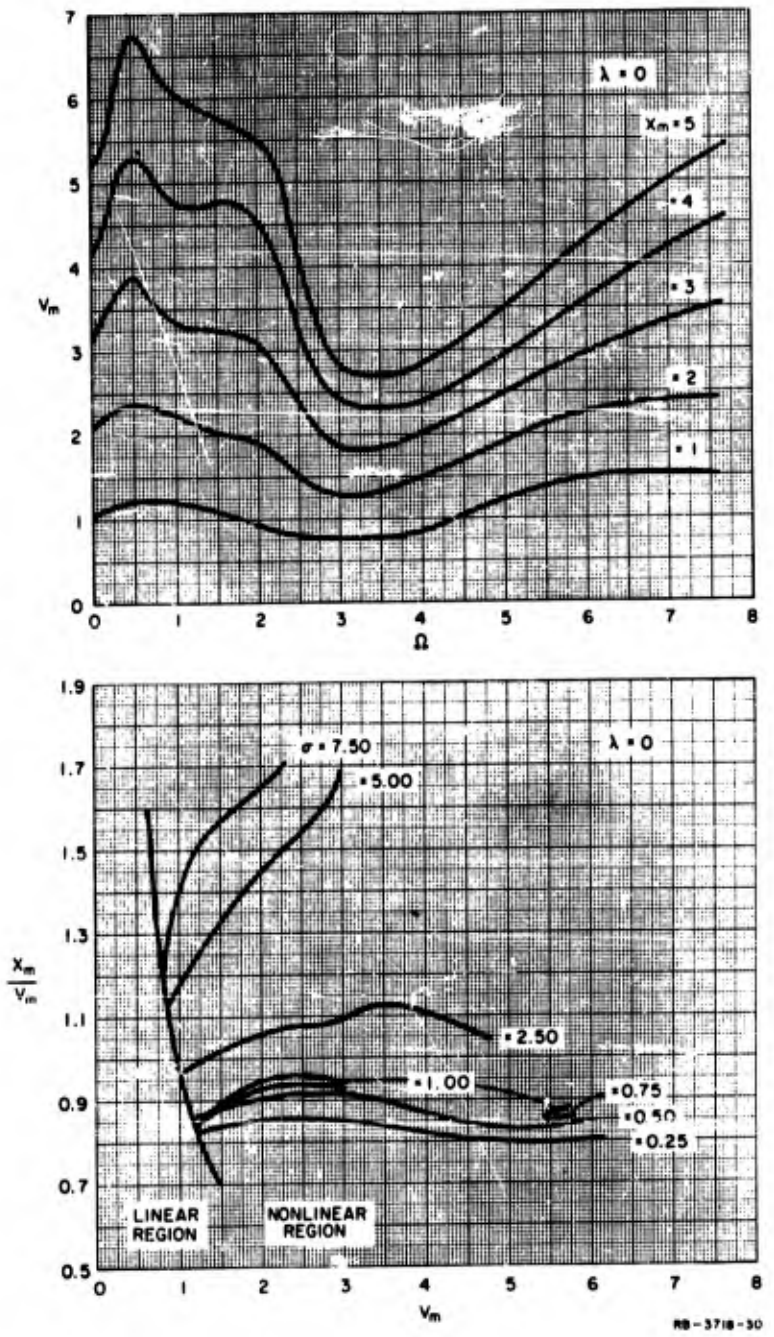

Figure 3.7.11 The Bilinear Case for $k = 0.2, \lambda = 0$; $G_m = \Omega^2(0.8+0.2X_m)$

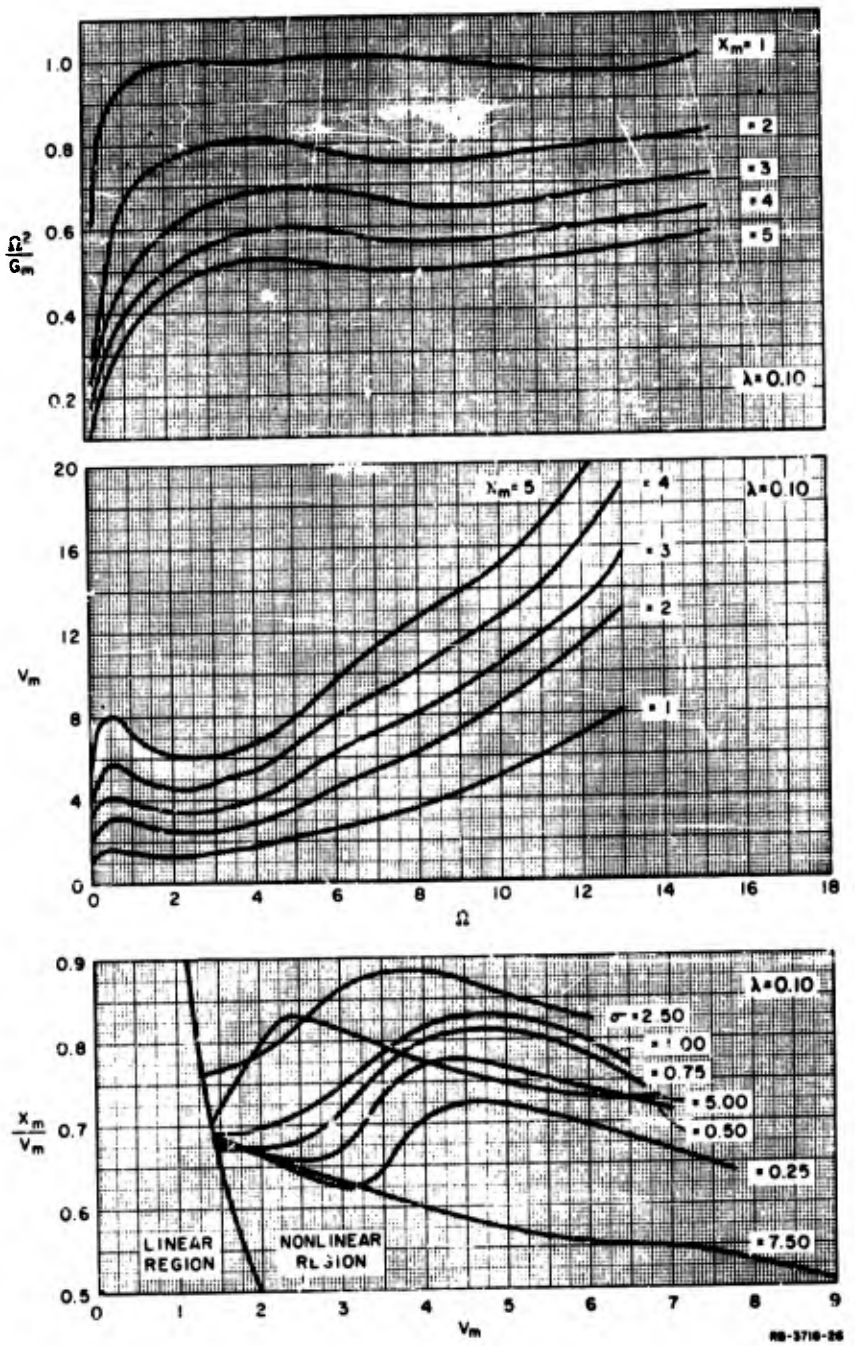

Figure 3.7.12 The Bilinear Case for k = 0.2, λ = 0.10

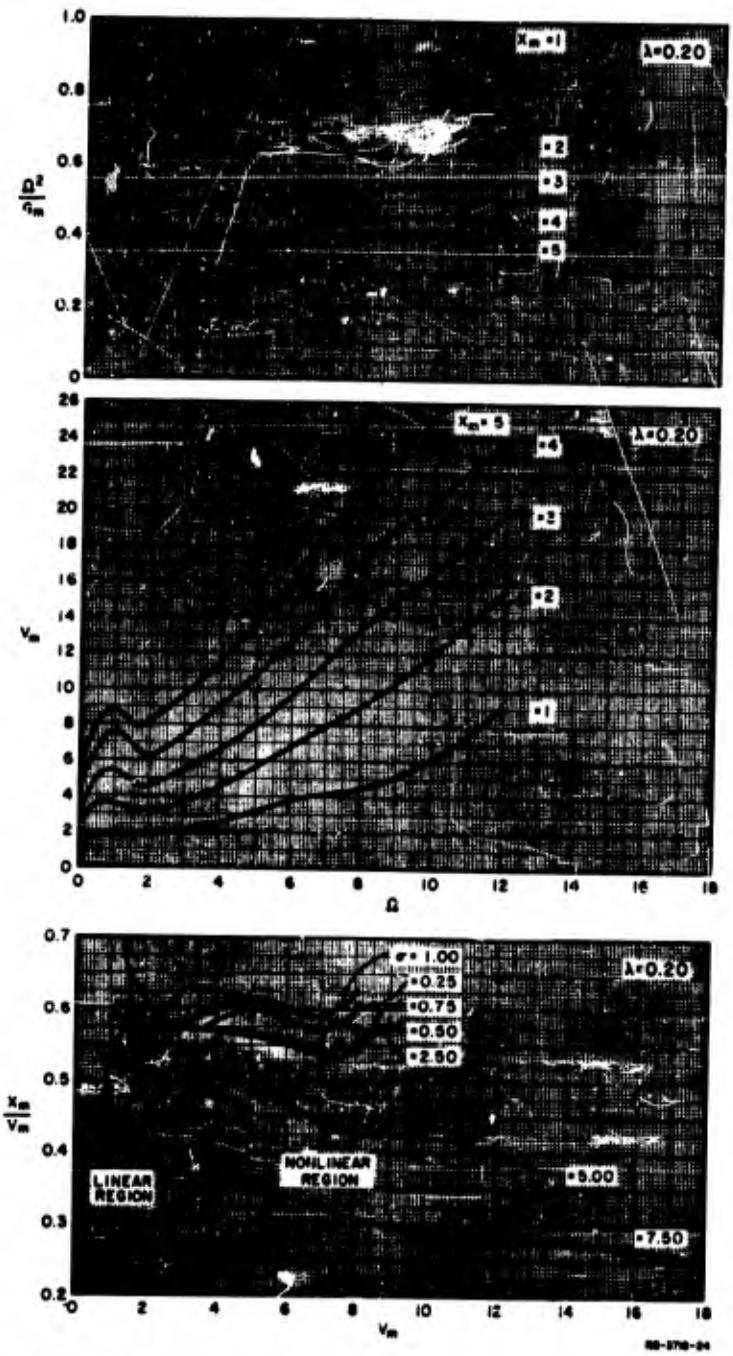

Figure 3.7.13 The Bilinear Case for k = 0.2, λ = 0.20

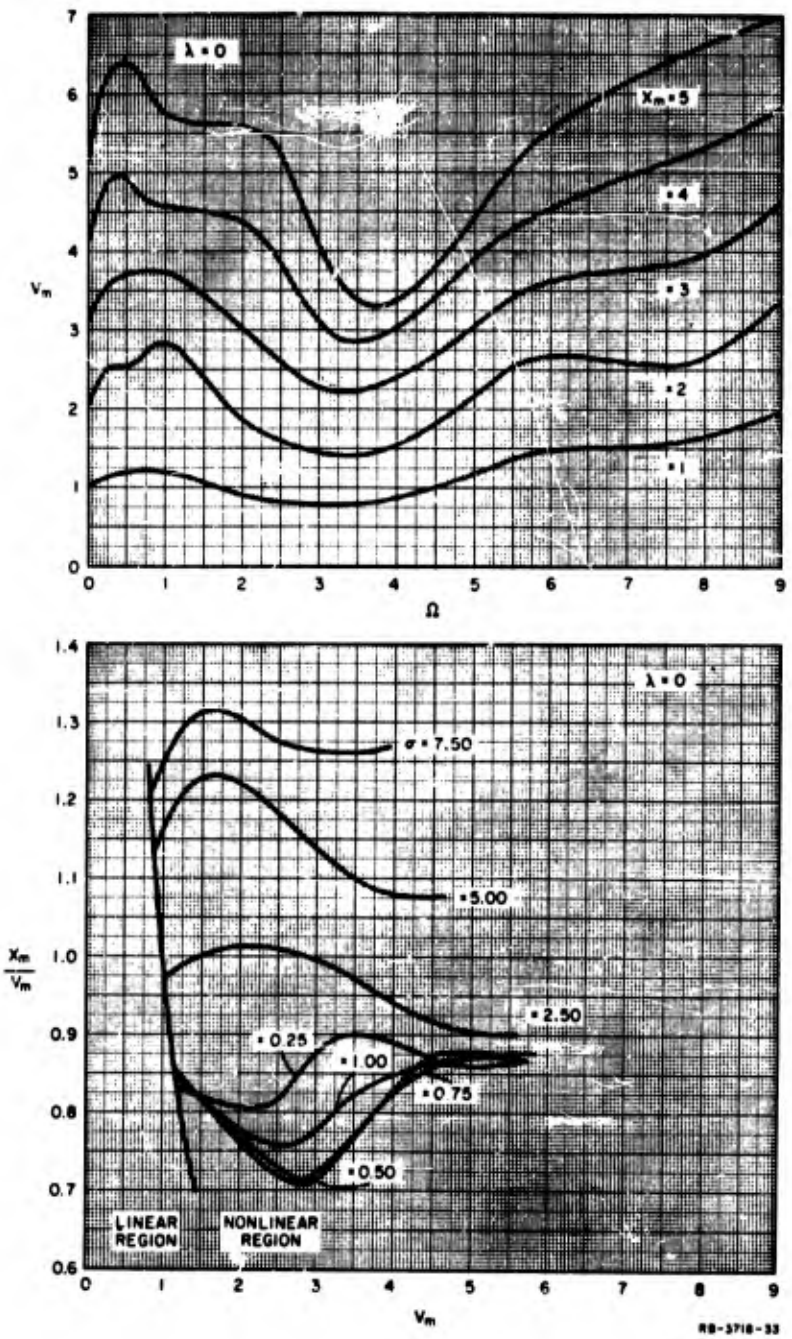

Figure 3.7.14 The Bilinear Case for k = 0.5, λ = 0; $G_m = \Omega^2(0.5+0.5X_m)$

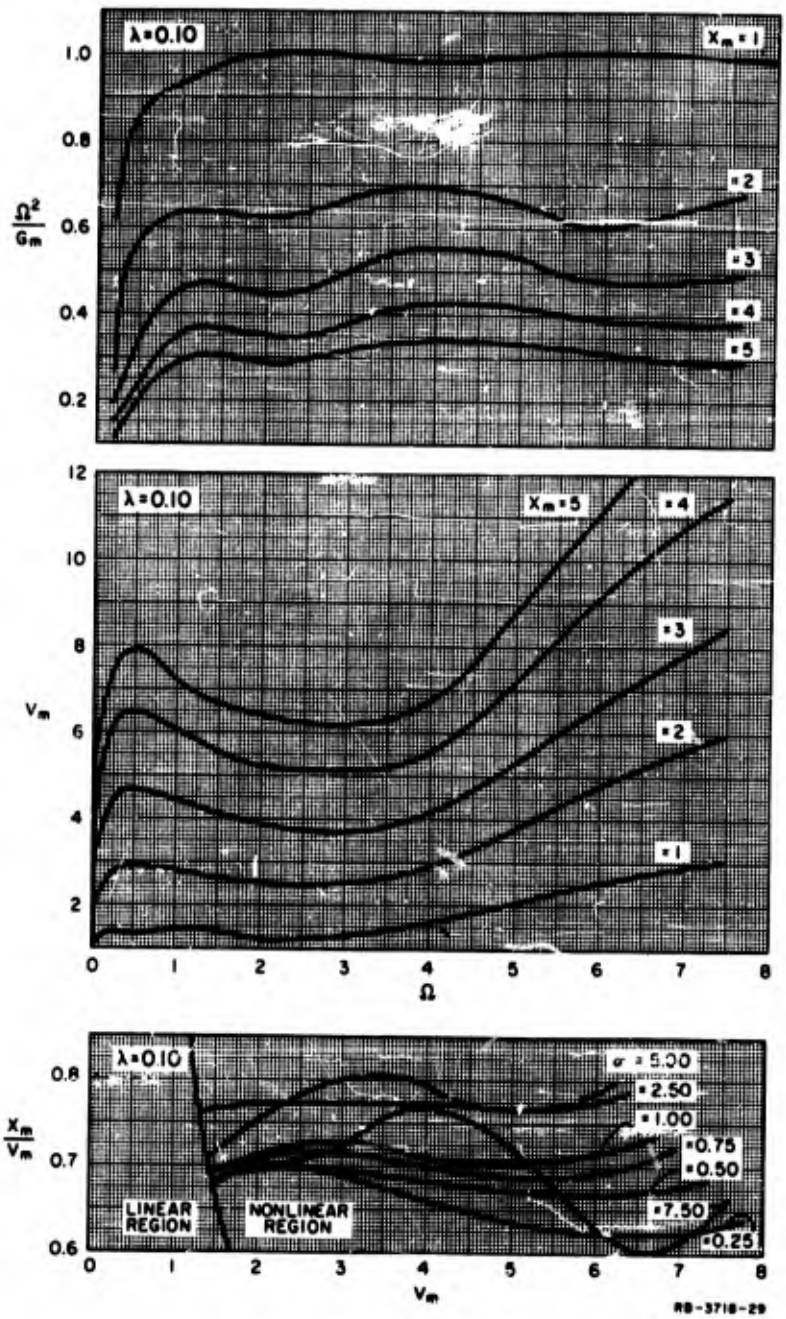

Figure 3.7.15 The Bilinear Case for $k = 0.5, \lambda = 0.10$

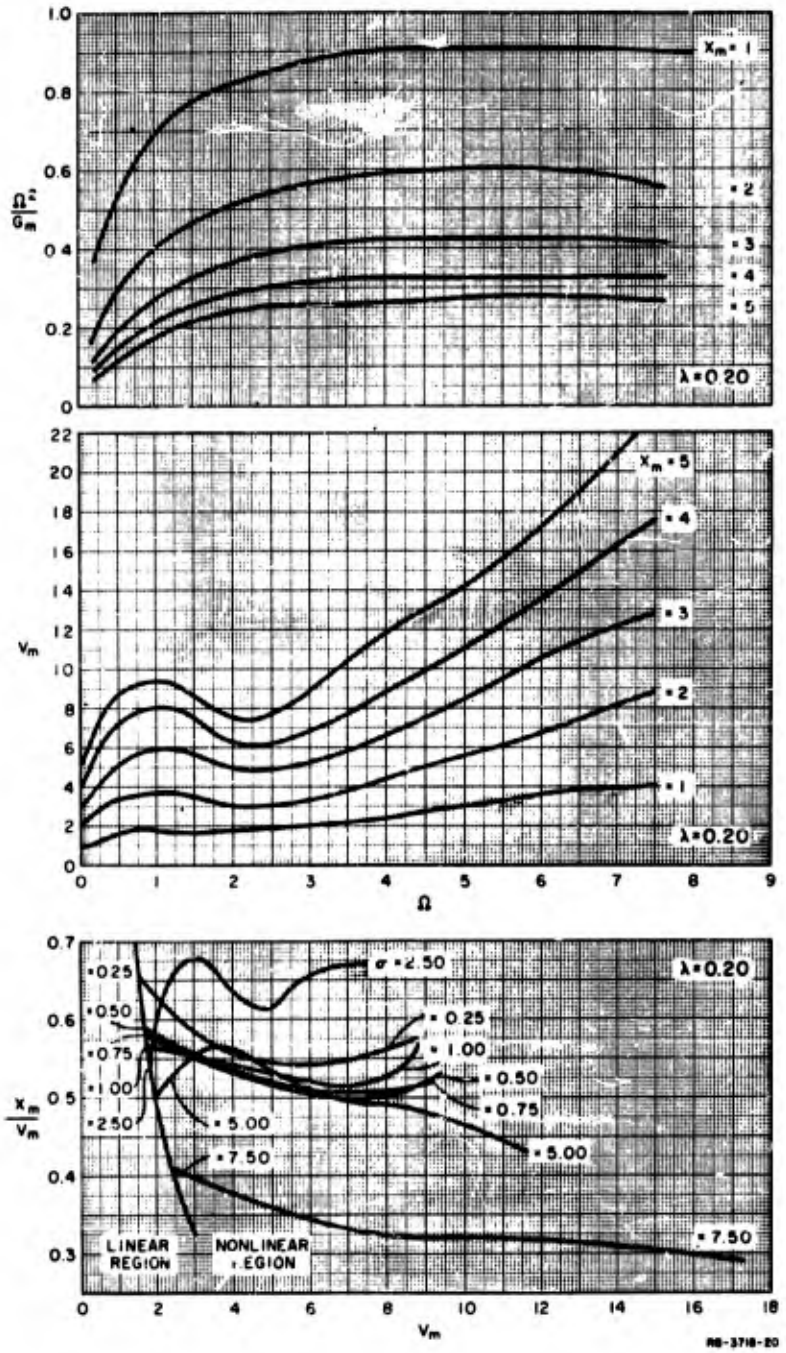

Figure 3.7.16 The Bilinear Case for $k = 0.5, \lambda = 0.20$

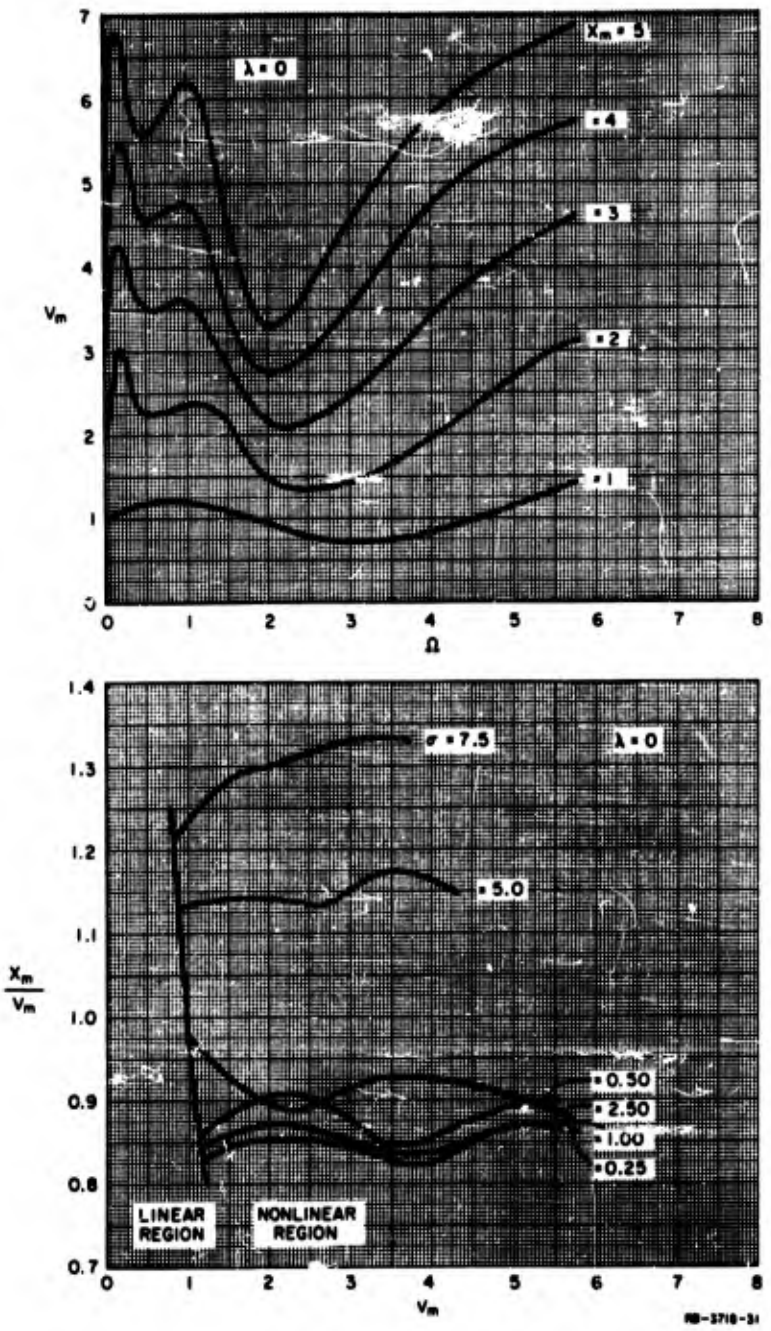

Figure 3.7.17 The Bilinear Case for k = 2.0, λ = 0; $G_m = \Omega^2(2X_m - 1)$

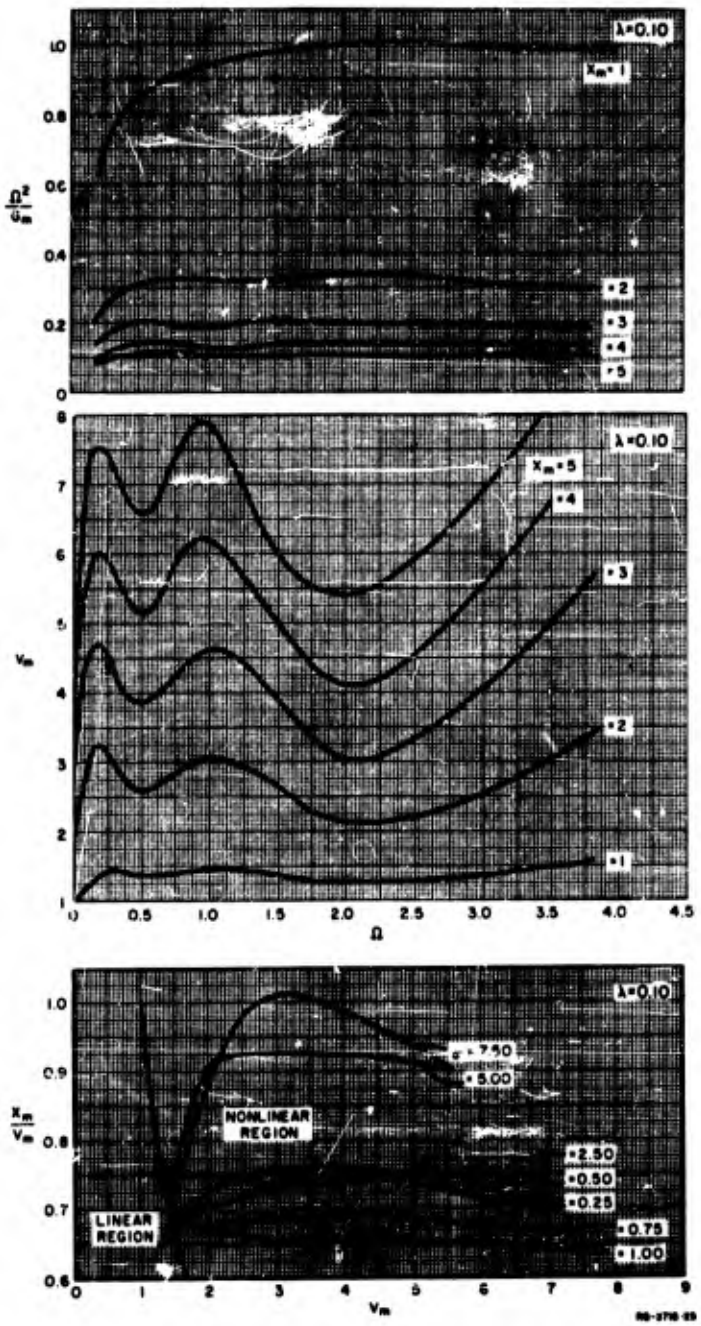

Figure 3.7.18 The Bilinear Case for k = 2.0, λ = 0.10

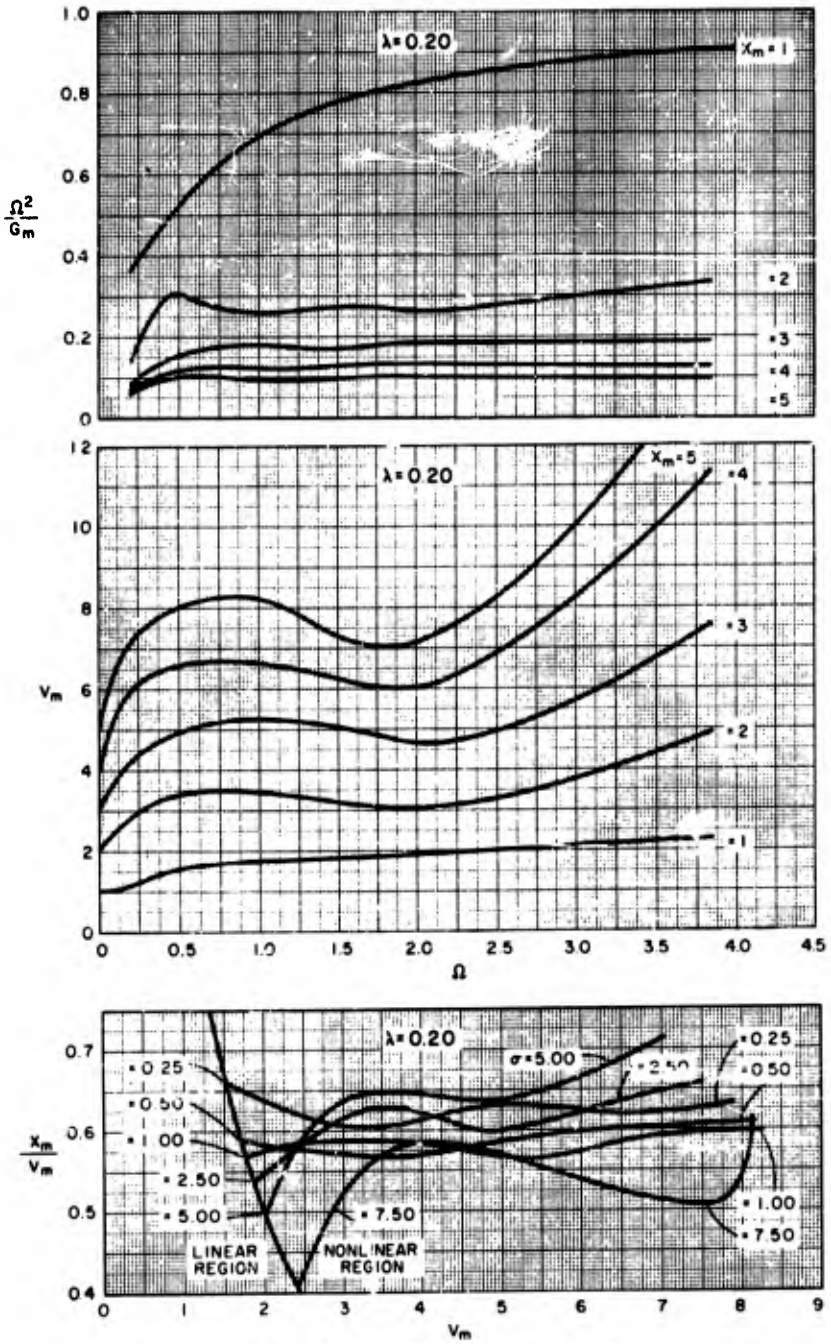

Figure 3.7.19 The Bilinear Case for k = 2.0, λ = 0.20

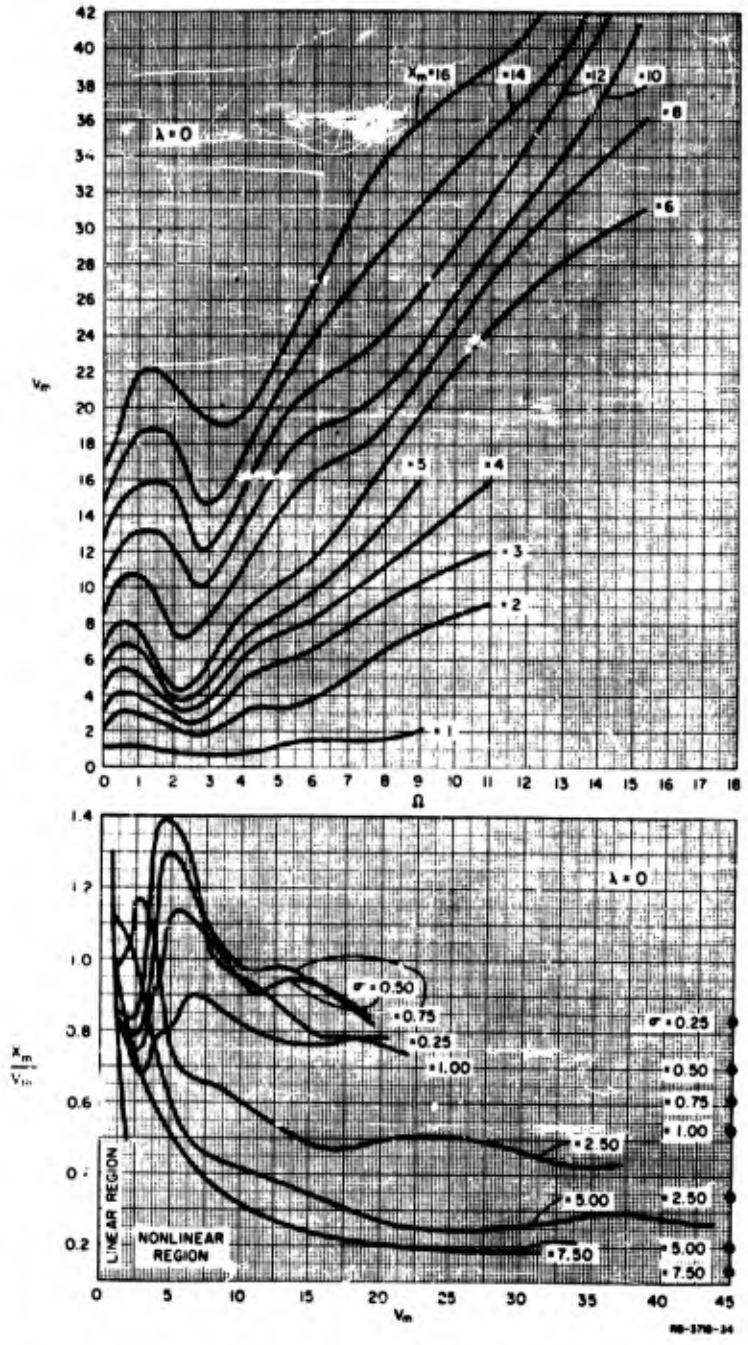

Figure 3.7.20 The Hysteretic Case for $\lambda = 0$; $G_m = \Omega^2$

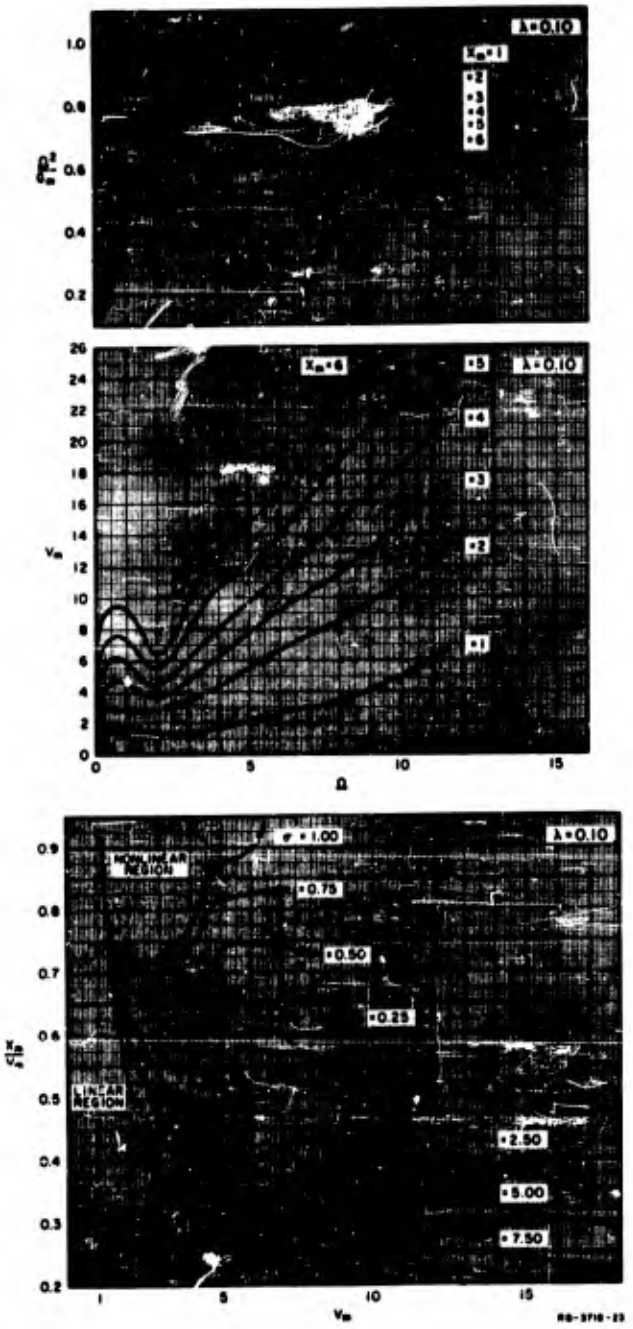

Figure 3.7.21 The Hysteretic Case for $\lambda = 0.10$

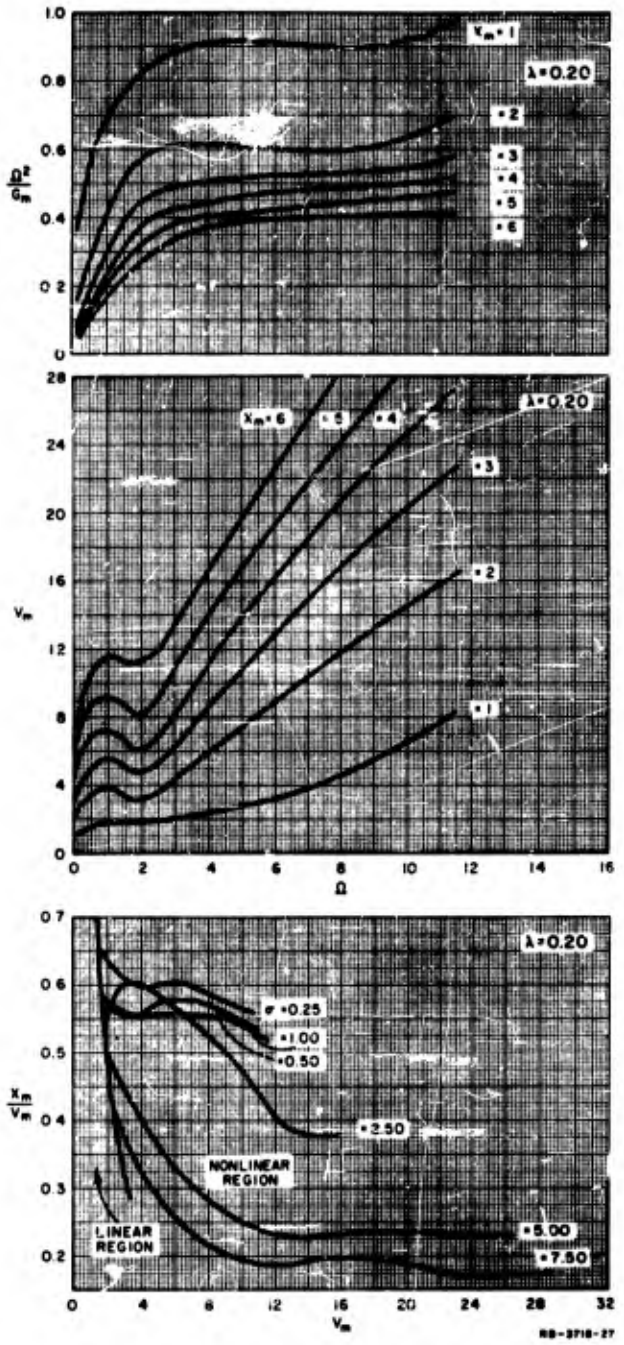

Figure 3.7.22 The Hysteretic Case for $\lambda = 0.20$

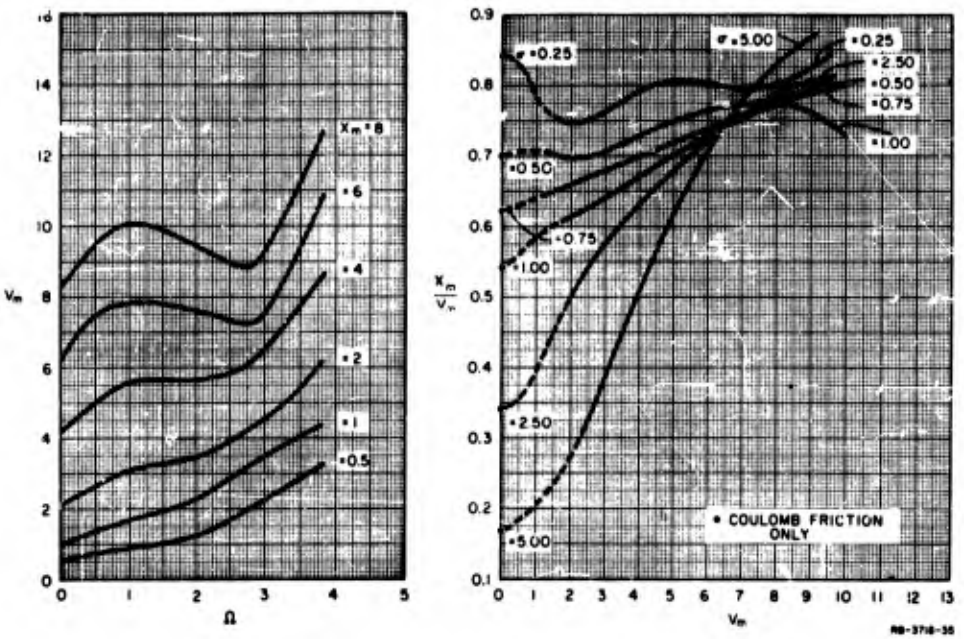

Figure 3.7.23 The Case of the Linear Spring with Coulomb Friction; $G_m = \Omega^2(1+X_m)$

very low value $\sigma = 0.25$. When $V_m = 0$ the situation is that of Coulomb friction only, and the σ curves may be seen to be heading towards these values.

3.7.4.5 Linear Spring with Square-Law Damping

The response and optimization curves for a linear spring with a damping term proportional to the square of the relative velocity are shown in Figure 3.7.24, page 3-132 . The representation of the displacement curves is different from the previous cases because of the necessity of adopting a different form of the nondimensional variables. Here the variable V_m has the value of unity and curves of X_m versus Ω are plotted for various values of the square-law damping coefficient, H. As H tends to zero we approach the undamped linear case, as may be seen by taking the reciprocal of the X_m-versus- Ω curves in Figure 3.7.24.

The optimization curves again show a decrease in relative displacement for increasing damping. However, it is noticed that, depending on the particular value of σ , these optimization curves terminate at various values of H. The points shown in Figure 3.7.24 at which the curves terminate are not the exact points because of the finite steps chosen in the variable H. However, they will be close to the actual termination points. This termination is necessary because with increasing H there must be a point at which the acceleration transmitted by the damper equals the specified acceleration corresponding to the value of σ in question.

Similar remarks apply to a spring with viscous damping but do not appear here because the highest value of λ considered, i.e., $\lambda = 0.5$, is not large enough to reach this point. It will be noted that the lowest values of X_m for any particular σ in Figure 3.7.24 are higher than those associated with the viscously-damped linear spring shown in Figure 3.7.10. As higher values of viscous damping presumably give even lower values of X_m, it appears that viscous damping has an advantage over square-law damping.

3.7.4.6 Linear Spring with Viscous Damping

The case of a linear spring with viscous damping is included in the bilinear case when $X_m = 1$ and has already been discussed. Figure 3.7.25(a), page 3-135, lists the identification number of the input wave form which gives the maximax values of G_m and X_m for the linear viscous-damped case for various values of λ and Ω . Input 17 appears more often than any of the others; but, depending on Ω and λ , over half of the inputs occur at some place in Figure 3.7.25(a).

3.7.4.7 Viscous Damping

If the suspension of the isolated body is of very low stiffness but the motion is viscously damped, the viscous forces predominate. This means a very large value of λ . The acceleration

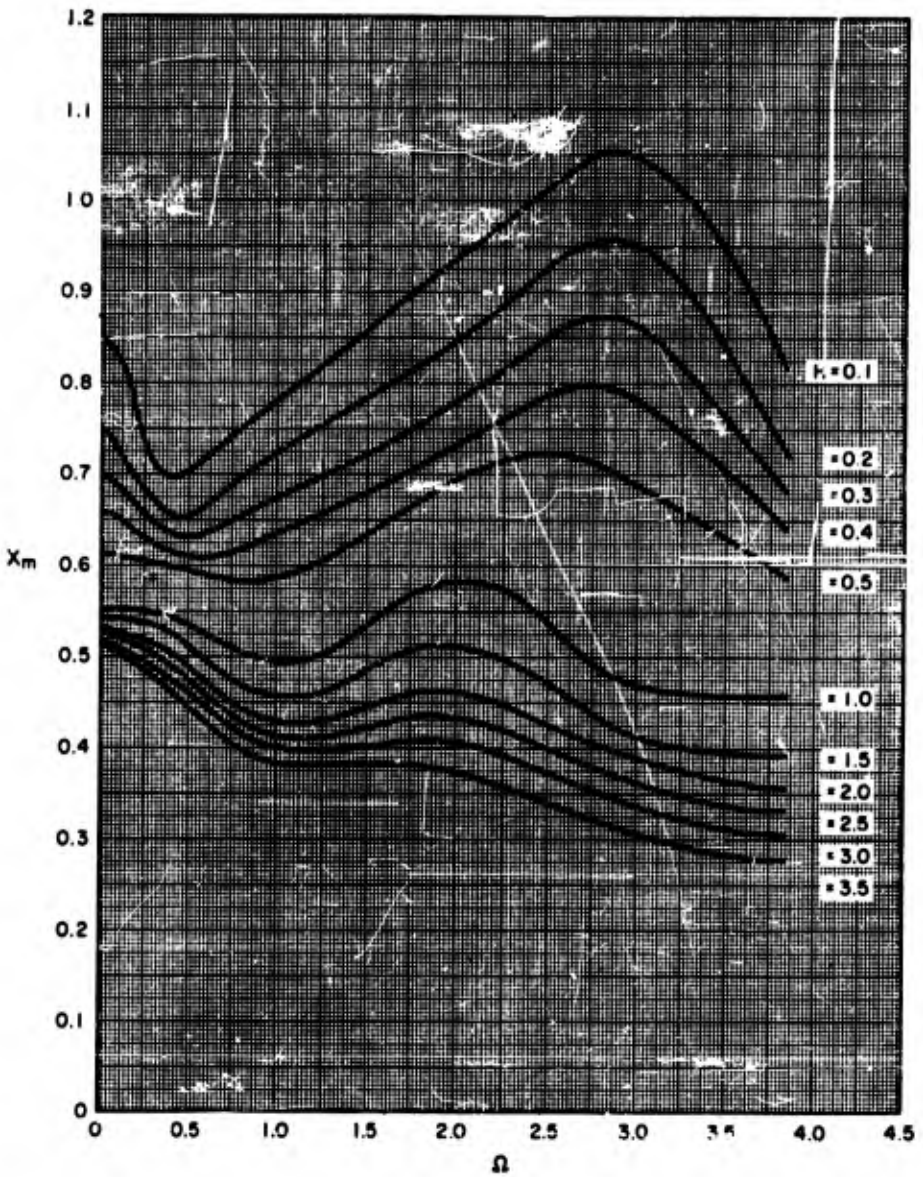

Figure 3.7.24-1 The Case of the Linear Spring with Square-Law Damping; $V_m=1$, $\sigma = G_m$

(Note: This case continued on next two pages)

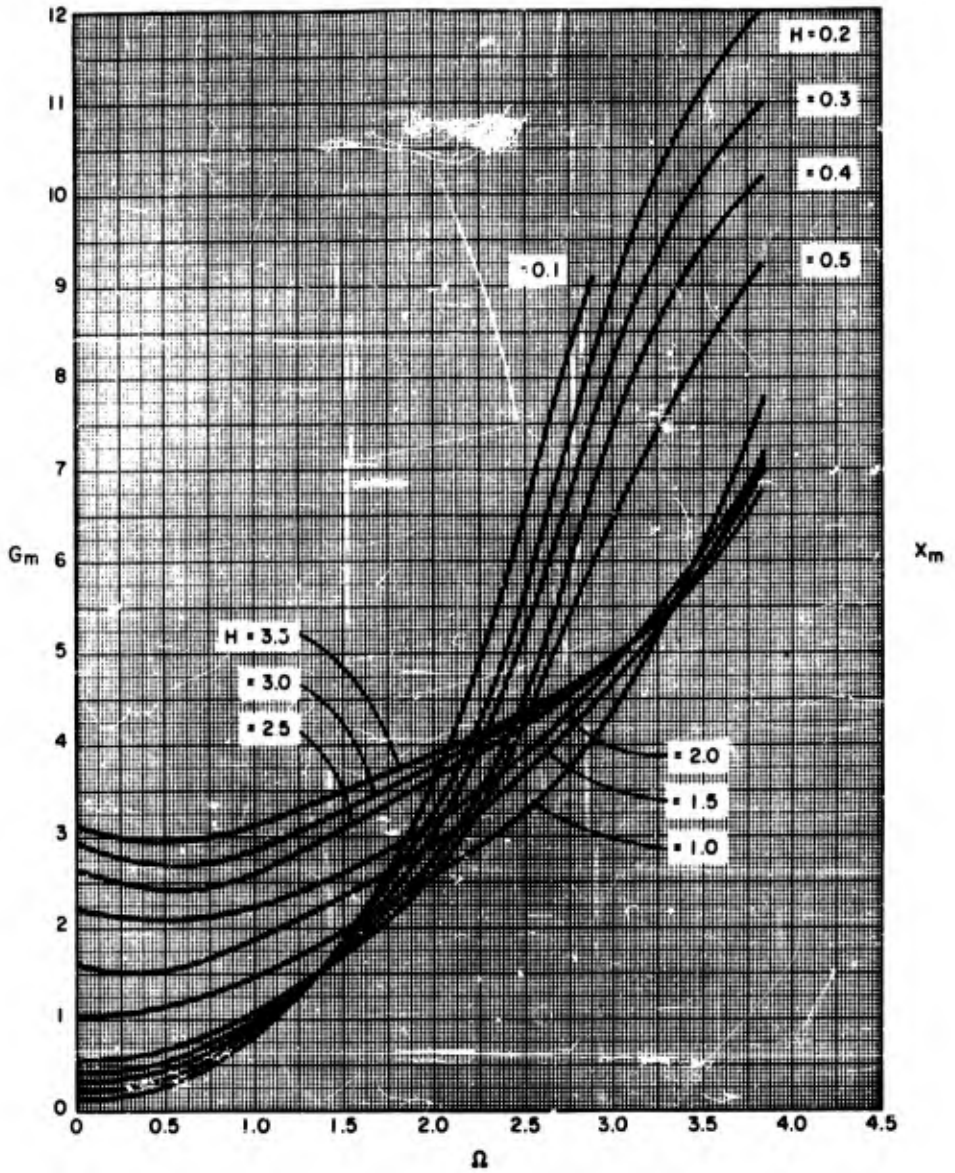

Figure 3.7.24-2 The Case of the Linear Spring with Square-Law Damping; $V_m = 1$, $\mathcal{F} = G_m$

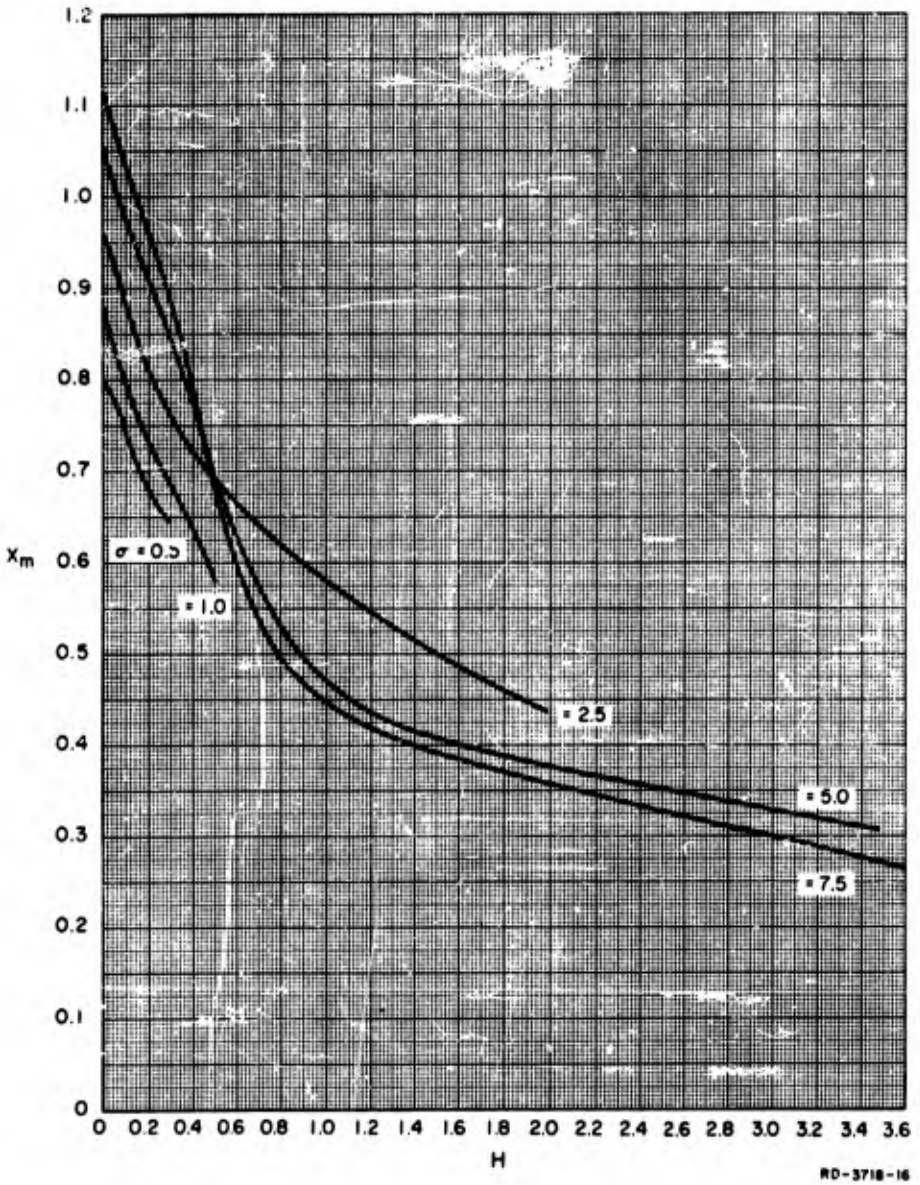

Figure 3.7.24-3 The Case of the Linear Spring with Square-Law Damping; $V_m = 1$, $\sigma = G_m$

curve in Figure 3.7.25(b) G_m versus L, shows that the transmitted force is almost proportional to the damping factor L. This indicates that the maximum relative velocity is little changed by the viscous forces. However, the maximum relative displacement X_m is substantially changed.

Ω	$\lambda = 0$		$\lambda = 0.1$		$\lambda = 0.2$	
	Input No. for G_m	Input No. for X_m	Input No. for G_m	Input No. for X_m	Input No. for G_m	Input No. for X_m
0.2	17	17	17	17	17	17
0.5	14	5	13	14	17	14
1.0	17	17	17	17	14	17
2.0	11	11	14	14	14	14
4.0	18,19	18,19	27	19	17,19	17
6.0	20	20	11,20	24	11,20	11
8.0	6	6	13	13	17	17
10.0	13	13	13,22	13	13	13
12.0	19	19	22	22	13,22	17,22
16.0	11	11	17	17	17	17

Figure 3.7.25(a) Input Giving the Maximax Response for The Linear Case with Viscous Damping

3.7.4.8 Square-Law Damping

Again the situation is considered where the only restraint is one of damping, in this case, square-law damping. The response curves are given in Figure 3.7.24 for $\Omega = 0$. The meaning given to the maximum relative displacement in this situation needs a little explanation. The solution of equation (59) when $\omega = v = 0$ and when the initial conditions are $x = 0$, $t = 0$, and $\dot{x} = v_1$, $t = 0$, is given by

$$x = \frac{1}{C} \log (1 + Cv_1 \ t) \qquad (71)$$

Thus, a body moving freely, except for a square-law damping term, moves an infinite distance. The values of X_m plotted in Figure 3.7.24 for

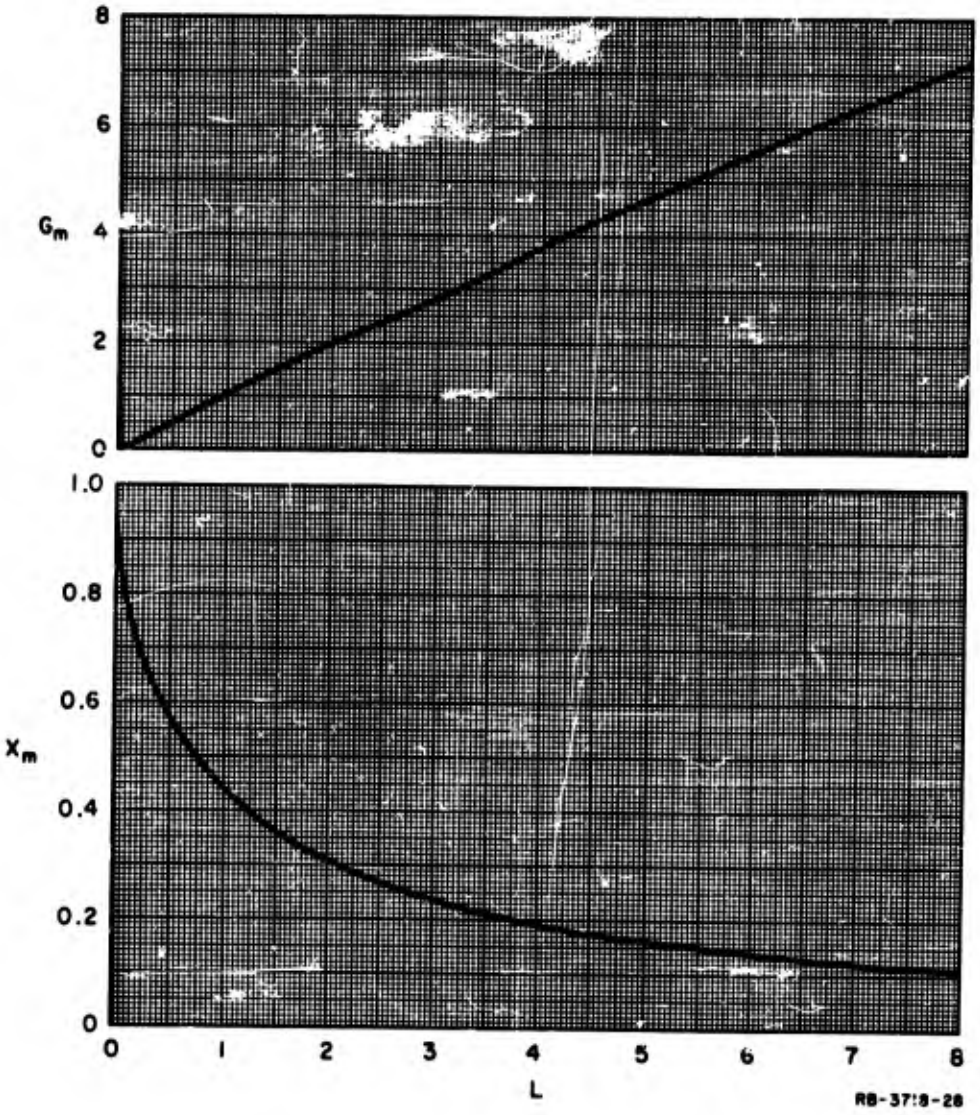

Figure 3.7.25(b) Viscous Damping (No Stiffness)

$\Omega = 0$ are those of the displacements which occur during the passage of the input velocity. When the input has ceased the body will, in general, have a small residual velocity, v_1, and the isolated body will continue to move indefinitely.

3.7.4.9 Coulomb Damping

Reference to equation (65) shows that $G_m \equiv M$, and thus the response and optimization curves coincide. Figure 3.7.26 shows the optimization curves for viscous, square-law, and Coulomb damping, shown together for comparison.

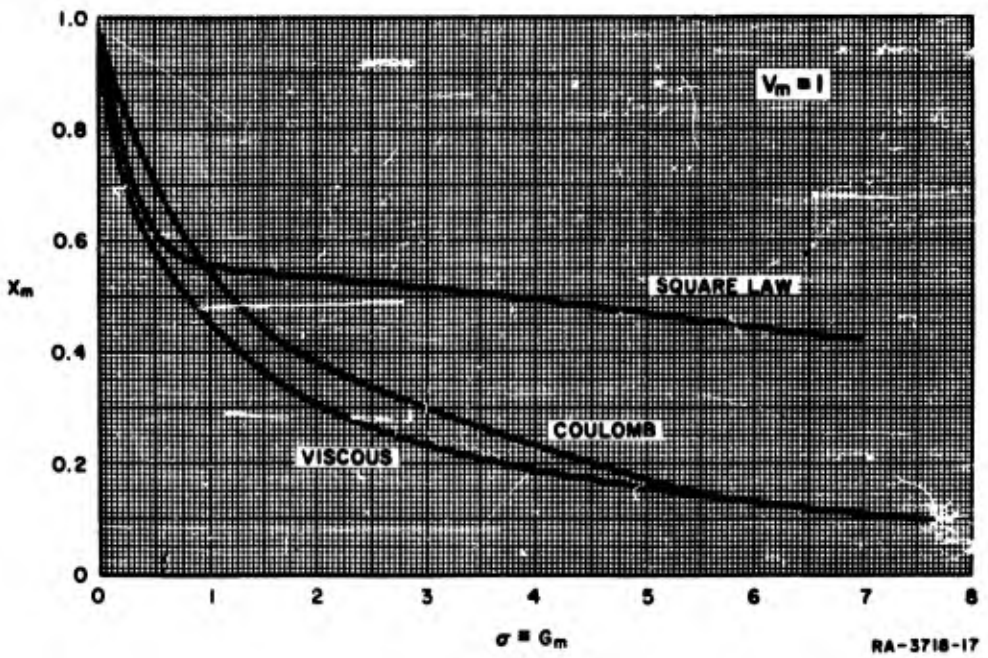

Figure 3.7.26 Comparison of Viscous, Square-Law, Coulomb Damping (No Stiffness); $V_m = 1$, $\sigma \equiv G_m$

At low values of σ the relative displacements are roughly the same in the three cases. However, for higher values of σ viscous and Coulomb damping predominate over that of square-law damping.

3.7.5 Numerical Examples of Design Procedures

The most obvious problem is to determine the response of the isolator when the values of the isolator parameters and input parameters have been specified. This problem arises when one wishes to determine the response of existing or proposed designs. The procedure is now demonstrated by some numerical examples. The notation is as described in Section 3.7.2.

Example #1

Given: Ground motion parameters

$$t_o = 0.2 \text{ sec}, \quad v_m = 12 \text{ ft/sec}$$

Isolator parameters

The isolator has a bilinear characteristic.

$$\omega = 15 \frac{\text{rad}}{\text{sec}}, \quad a = 2 \text{ in.}, \quad k = 2.0, \quad \lambda = 0.10$$

To find: The maximax response of the isolator.

Method: From equations (50), (51), (52) calculate

$$p = \frac{2\pi}{t_o} = \frac{2\pi}{0.2} = 31.4$$

$$\Omega = \frac{\omega}{p} = \frac{15}{31.4} = 0.477$$

$$V_m = \frac{v_m}{ap} = \frac{12 \times 12}{31.4 \times 2} = 2.30$$

Using these values of V_m and Ω we find by interpolation on the V_m versus Ω curves in figure 3.7.10 (see Section 3.7.4) that $X_m = 1.75$. Using $X_m = 1.75$ and $\Omega = 0.477$ we find, by interpolation from the Ω^2/G_m versus Ω curves, that $\Omega^2/G_m = 0.38$.

Using these values and equations (48) and (56) we find

$$x_m = aX_m = 2 \times 1.75 = 3.50 \text{ in.}$$

and

$$Z_m = ap^2G_m = \frac{2 \times (31.4)^2 \times (0.477)^2}{12 \times 0.38} = 99 \text{ ft/sec}^2$$

The above procedure will not always be so straightforward. In general, interpolation between curves will be necessary because the required values of k and λ may not be the particular values used in the curves. Further, as the bilinear characteristic will generally be an approximation to some curved characteristic, care must be exercised in choosing the values of a and k in the bilinear approximation to the curve. This is because, initially, one does not know the value of x_m, i.e., how far along the curved characteristic one is going to move. The procedure in this situation is to guess a value of displacement range, x_m, and then choose values of a and k which will suitably approximate the curved characteristic over this estimated value. The calculation of the actual x_m arising is then made as in Example #1; if it differs so much from the estimated value of x_m as to invalidate the bilinear approximation initially chosen, new values of a and k must be taken and the process repeated. (Also see Section 3.7.8)

Example #2

If the system involves hysteresis the procedure is the same as in the bilinear case as follows:

Given: Ground motion parameters

$$t_o = 0.3 \text{ sec}, \quad v_m = 20 \text{ ft/sec}$$

Isolator parameters

It is assumed that the hysteretic characteristic has been drawn up, approximated by straight lines, and the values of ω and a determined; e.g., $\omega = 50$ rad/sec, a = 1 in. Assume no viscous damping, i.e., $\lambda = 0$.

To find: The maximax response of the isolator.

Method: From equations (50), (51), (52), calculate

$$p = \frac{2\pi}{t_o} = \frac{2\pi}{0.3} = 20.9$$

$$\Omega = \frac{\omega}{p} = \frac{50}{20.9} = 2.39$$

$$V_m = \frac{v_m}{ap} = \frac{20 \times 12}{1 \times 20.9} = 11.5$$

From Figure 3.7.20 (Section 3.7.4) we find by interpolation on the V_m versus Ω curves that $X_m = 10.6$. Then the rattlespace can be found from equation (48) as

$$x_m = aX_m = \frac{10.6}{12} = 0.88 \text{ ft}$$

Because there is no viscous damping the value G_m is given simply by

$$G_m = \Omega^2 = 5.71$$

Then the maximax acceleration is found from equation (56) as

$$Z_m = ap^2 G_m = \frac{(20.9)^2 \times 5.71}{12} = 208 \text{ ft/sec}^2$$

If the isolator is a linear spring with Coulomb friction or square-law damping, then, using the relevant equations, the calculations follow a similar pattern.

In many cases the designer will be given only the values of the input parameters, i.e., v_m and t_o, and will be asked to design an isolator which will minimize the relevant displacement or rattlespace for a specified maximum allowable acceleration of the isolated body, Z_m. If there are no other conditions stated, then the optimization results show that the isolator should be a simple viscous damper because, of all the isolator combinations considered, this gives the lowest rattlespace for any specified maximum acceleration, Z_m.

Example #3

Given: Input parameters

$t_o = 0.4$ sec, $v_m = 10$ ft/sec

Isolator parameters

The isolator is to be a simple viscous damper and the maximum acceleration to be transmitted is 120 ft/sec^2.

To find: The damping coefficient μ in equation (62) and the resulting rattlespace.

Method: From equations (52), (56), (60), calculate

$$p = \frac{2\pi}{t_o} = \frac{2\pi}{0.4} = 15.7$$

$$e = \frac{v_m}{p} = \frac{10}{15.7} = 0.637$$

$$G_m = \frac{Z_m}{ep^2} = \frac{120}{0.637 \times (15.7)^2} = 0.765$$

From Figure 3.7.25

$$L = 0.7$$

and

$$X_m = 0.5$$

and from equations (48), (60), (63), we find

$$x_m = eX_m = 0.637 \times 0.5 \text{ ft} = 0.318 \text{ ft}$$

and

$$\mu = pL = 15.7 \times 0.7 = 11 \text{ sec}^{-1}$$

However, in general, a stiffness term will be necessary in order to determine positioning of the isolated body. The design in this case may specify the input parameters v_m and t_o together with the maximum acceleration of the isolated body, Z_m, and the stiffness of the system in the rest position in terms of the initial angular frequency, ω. Because an isolator functions by acting as a "soft suspension", it is to be expected that a "softening" bilinear characteristic would be useful in the case where the stiffness in the rest position is to be reasonably high.

Example #4

The following example assumes a damped bilinear system where $k = 0$ and $\lambda = 0.10$, i.e., a completely "softening" system.

Given: Input parameters

$$t_o = 0.20 \text{ sec}, \quad v_m = 2 \text{ ft/sec}$$

Isolator parameters

$$Z_m = 200 \text{ ft/sec}^2$$

$$\omega = 90 \text{ rad/sec}$$

To find: The parameter a and the rattlespace

Method: From equations (51) and (52) calculate

$$p = \frac{2\pi}{t_o} = \frac{2\pi}{0.20} = 31.4$$

$$\Omega = \frac{\omega}{p} = \frac{90}{31.4} = 2.87$$

From equations (50) and (56) obtain

$$\frac{G_m}{V_m} = \frac{Z_m}{pv_m} = \frac{200}{31.4 \times 2} = 3.19$$

It is now necessary to construct from Figure 3.7.8 a plot of G_m/V_m versus X_m for the value $\Omega = 2.87$. If this is done, it is found that $G_m/V_m = 3.19$ when $X_m = 3.2$, $V_m = 3.5$, $G_m = 11.2$.

Then from equations (48), (50) we have

$$a = \frac{V_m}{V_m p} = \frac{2}{3.5 \times 31.4} = 0.218 \text{ in.}$$

and

$$x_m = aX_m = 0.218 \times 3.2 \text{ in.} = 0.7 \text{ in.}$$

The optimization curves provide a comparison of all the isolators considered giving the minimum rattlespace for specified maximum accelerations or vice versa. This comparison shows that the effect on the response of nonlinearities in the stiffness characteristic is negligible but that damping is very important. The occasional minimum points noted in the optimization curves are too trivial to be of importance. In the bilinear cases with no damping the optimization curves are substantially horizontal or increasing with V_m.

In the case of $k = 0$, $\lambda = 0$, the value of V_m and hence X_m has been computed to a large value, and there is no evidence of any tendency for X_m/V_m to decrease. However, in certain cases of the "softening" characteristic when there is damping, the optimization curves do show a decreasing value with increasing V_m and X_m. However, as is discussed in Section 3.7.7, this decrease undoubtedly results from the decreasing natural frequency of a "softening" system which means that the over-all damping of the system is effectively increasing.

Consequently, because there does not appear much to distinguish between the various bilinear cases, the optimization charts have limited use in this area. However, they are useful in distinguishing between desirable and undesirable areas to design in.

Example #5

Given: Input parameters

$V_m = 1$ ft/sec, $t_o = 0.2$ sec

Isolator parameters

The isolator has a damped hardening characteristic given by $k = 2.0$, $\lambda = 0.1$, and the maximum acceleration of the isolated body is to be $Z_m = 200$ ft/sec^2.

To find: A suitable design.

Method: Calculate from equations (52) and (68)

$$p = \frac{2\pi}{t_o} = \frac{2\pi}{0.2} = 31.4$$

$$\sigma = \frac{Z_m}{v_m p} = \frac{200}{1 \times 31.4} = 6.4$$

Figure 3.7.18 (Section 3.7.4) shows that for a value of $\sigma = 6.4$, values of V_m greater than 1.5 are to be avoided because of the increased relative displacement. One can actually design for a lower acceleration, e.g., $\sigma = 1.00$, with attendant lower displacement. If, $V_m = 6$, for example, then $X_m/V_m = 0.65$ and $X_m = 3.9$. By interpolation from the V_m versus Ω curves two values of Ω are determined, i.e., $\Omega = 0.90$ and $\Omega = 1.05$.

From equation (68)

$$G_m = \sigma V_m = 1 \times 6 = 6$$

Using the two values of Ω and the associated values of Ω^2/G_m together with the value of X_m, it is found from the Ω^2/G_m curves that $\Omega = 0.90$ is the relevant value of Ω.

Then from equation (51)

$$\omega = p\Omega = 31.4 \times 0.90 = 28.2$$

and from equation (50)

$$a = \frac{v_m}{V_m p} = \frac{1.0}{6 \times 31.4} \text{ ft} = 0.064 \text{ in.}$$

and from equation (48)

$$x_m = aX_m = 0.064 \times 6 \text{ in.} = 0.384 \text{ in.}$$

3.7.6 Effects of Different Inputs

The conclusions arrived at in this project are largely dependent on the nature of the inputs. This may be demonstrated by considering a single impulse applied to a body mounted on a viscously damped linear spring. The equation of motion is the same notation as before is given by

$$\ddot{x} + 2\lambda\omega\dot{x} + \omega^2 x = 0 \qquad (72)$$

The solution to equation (72) which satisfies the conditions that the displacement is zero at time zero but that the velocity at time zero is v_m is given by,

$$x = \frac{v_m e^{-\lambda\omega t}}{\omega\sqrt{1-\lambda^2}} \sin \omega\sqrt{1-\lambda^2}\, t \tag{73}$$

$$\ddot{x} = \frac{\omega v_m e^{-\lambda\omega t}}{\sqrt{1-\lambda^2}} \left\{ \begin{matrix} (2\lambda^2 - 1) \sin \omega\sqrt{1-\lambda^2}\, t \\ -2\lambda\sqrt{1-\lambda^2} \cos \omega\sqrt{1-\lambda^2}\, t \end{matrix} \right\} \tag{74}$$

The maximum values of these two equations may be obtained by differentiating with respect to time and equating to zero and solving for the time at which the displacement x is a maximum and the time for which the acceleration $\ddot{x}$ is a maximum. This gives the maximum value x_m and maximum value $\ddot{x}_m$ in the form

$$x_m = \frac{v_m}{\omega} f_1(\lambda) \tag{75}$$

$$\ddot{x}_m = \omega v_m f_2(\lambda) \tag{76}$$

The optimization procedure follows as before. If a value of $\ddot{x}_m$ is specified, say z_m, then

$$\omega = \frac{z_m}{v_m f_2(\lambda)} \tag{77}$$

and hence

$$x_m = \frac{v_m^2 f_1(\lambda) f_2(\lambda)}{z_m} \tag{78}$$

Now v_m and z_m are fixed and in order to minimize x_m it is necessary to minimize the product $f_1(\lambda) f_2(\lambda)$. This has been calculated and is plotted in Figure 3.7.27. A definite minimum is noted at a value of $\lambda = 0.40$. This is in contrast to the results for our family of inputs which show that λ should be ∞ for minimum rattlespace.

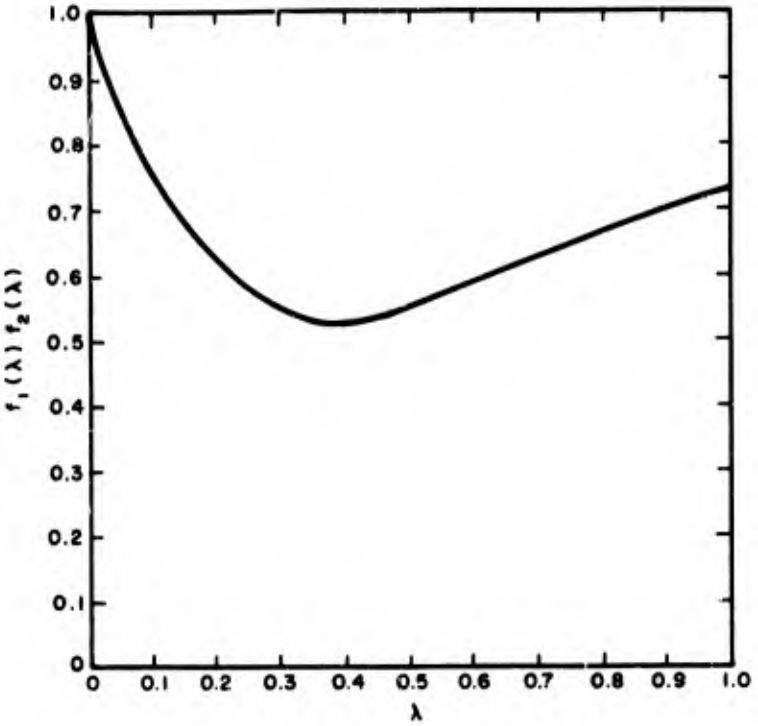

Figure 3.7.27 Single Impulse Applied to Viscous-Damped and Linear Isolator

3.7.7 Discussion and Conclusions

3.7.7.1 Discussion

The responses of the isolators are very much a function of the shape of the input wave forms; and, when reaching conclusions, this fact must be kept in mind. To what extent the results would be changed by, say, the addition of another half cycle of oscillation to the Type II wave form is hard to predict. Similarly, combinations, other than the combinations used here, of the Type I and Type II wave forms will undoubtedly change the results.

The response of the isolators to the five actual vertical ground-motion inputs was always less than the maximax value except for input 32; (Cactus 3V 30) in the case of a very low Ω . When Ω is very low the isolator is acting as a displacement meter, and apparently the

displacement corresponding to input 32 is greater than for any of the others. It will be noticed from Figure 3.7.28, page 3-147 , that inputs 30 and 31 were put on the tape with the wrong time base, i.e., the time at which the first crossover occurs should be about one third the total duration as shown by input 1 instead of the full duration as in inputs 30 and 31. Consequently the phrase that "the response of the isolators to the five actual records is always less that that of the maximax" assumes that the responses to inputs 30 and 31 have been referred to their proper time base.

Only the maximax values have been taken, i.e., for any particular isolator only the largest values of G_m , X_m and V_m for the 29 responses has been recorded. It is hoped in future to read off all the values; but, at the moment, it is assumed that at any given location all combinations of Type 1 and Type II wave forms are possible, and selecting the maximax gives a conservative value.

When there is no damping present in the isolator, there is, in general, a reasonable dispersion between the maximum response values for the different inputs. The addition of damping makes this dispersion considerably less. Further, when there is no damping, small changes in V_m or Ω will make large changes in X_m and hence G_m as may be seen, for example, by consideration of Figure 3.7.7. The addition of damping makes the behavior far less critical.

It was hoped that the preloaded case could be analyzed. Unexplained instability in the circuitry necessary to simulate this situation did not permit this analysis. However, the bilinear case for large X_m approaches the preloaded case and for $X_m = 5$ the bilinear case is probably quite close to the preloaded case. In the case $\lambda = 0$, $k = 0$, values of X_m up to 14 were taken to see if there were any significant changes. This does not appear to be the case. Specification of the damping presents a certain difficulty when X_m becomes large; the damping has been referred to the first part of the bilinear characteristic, and, as the natural period of a "softening" system decreases with amplitude, the effective damping increases with amplitude. For a "hardening" system, the effective damping decreases with amplitude. This may well be part of the explanation of the difference between the optimization curves in the cases $k = 0$, $\lambda = 0.2$ and $k = 2.0$, $\lambda = 0.2$.

3.7.7.2 Conclusions

The main conclusion to this work is that, as far as minimizing relative displacement for a specified maximum acceleration or vice versa is concerned, damping is much more effective than the various nonlinear stiffness characteristics considered. In fact, as far as this optimum criterion is concerned, pure damping, whether viscous or Coulomb, gives a smaller "rattlespace" than when any form of elastic stiffness is included. This is largely true because the oscillatory nature of the Type II input wave form leads to quasi-resonances. However, it was

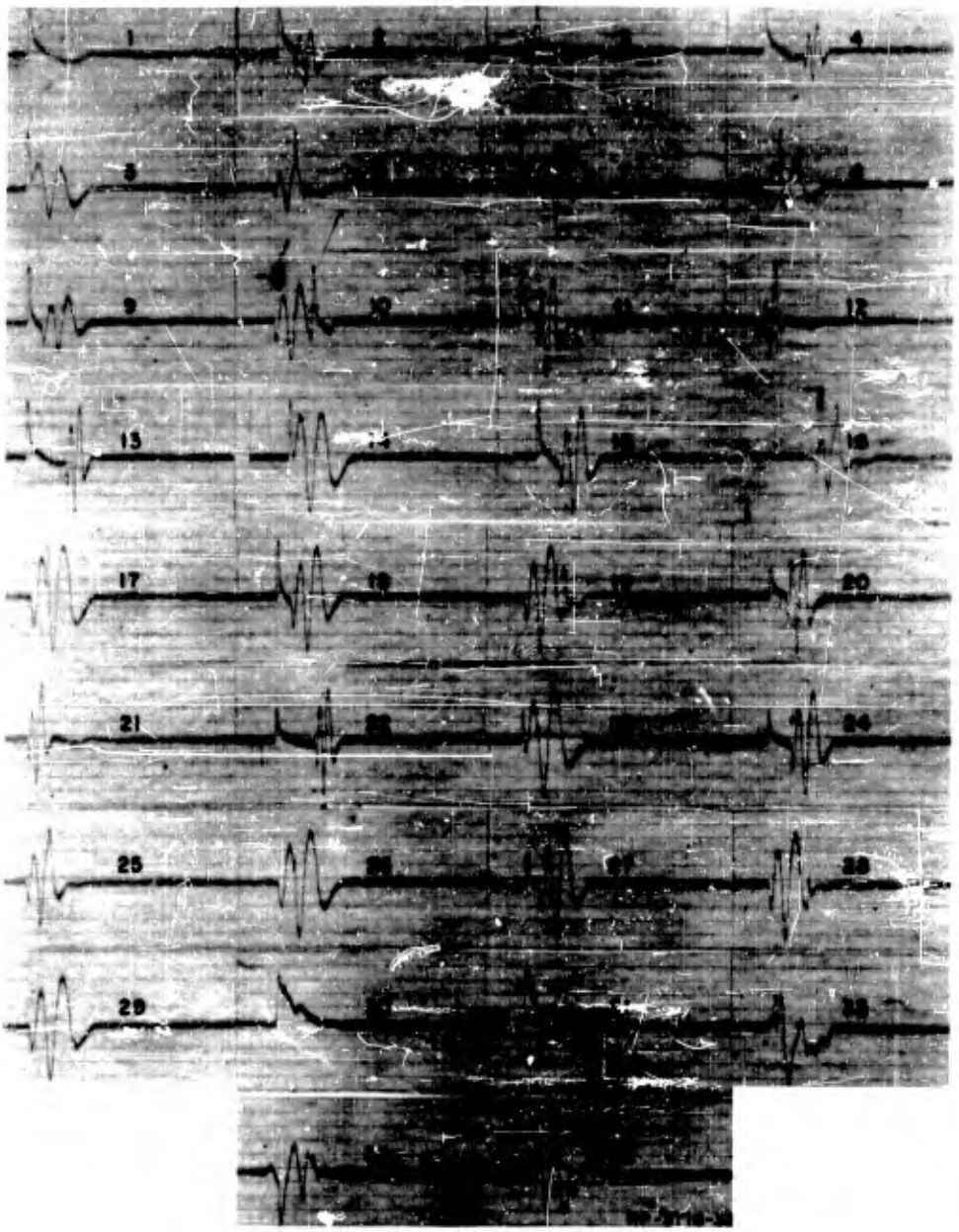

Figure 3.7.28 Velocity Waveforms Used as Inputs in Bilinear Systems Analysis

shown in Section 3.7.6 that if the input consists of a single impulse, the optimum requirements are different from those above. Square-law damping is not as effective as viscous or Coulomb damping except for low values of the parameter C . Of course, in any practical isolator, stiffness must be present to determine positioning of the isolated body. However, there are certain situations such as a vertical cantilever acting both as a beam and an inverted pendulum where the horizontal stiffness could be made extremely small.

The softening bilinear characteristic will be useful where a reasonable amount of rigidity is required in the rest position, i.e., the angular frequency, ω , corresponding to the first part of the characteristic will be considerably higher than that of a comparable linear isolator.

Damping is of further importance in that it makes the response of the isolator far less critical in its behavior when the parameters V_m, are changed. This is very important because the values v_m and p which effectively determine V_m and Ω cannot be accurately estimated beforehand. Further, damping reduces the dispersion between the responses to the various different input wave forms.

The design of any particular isolator will be influenced by many other factors than the criteria discussed so far. A very important factor is the spectrum of the isolator output response. In taking the maximum value G_m as a measure of the acceleration experienced by the components of the isolated body it is tacitly assumed that the natural frequencies of these components are considerably higher than any frequencies present in the output response of the isolator. This will be true in a large number of cases especially for a damped linear isolator where the dominant frequency is that of the natural period of the isolator. However, the introduction of large nonlinearities in either the spring stiffness or its damping will introduce higher frequencies into the isolator output response. This situation is undesirable because these higher frequencies may excite the natural periods of the components of the isolated body and actually magnify the maximum acceleration, G_m, for these components. This situation is very pertinent in the case of an isolator giving a square wave output, either because the stiffness characteristic is flat and preloaded or because the damping is Coulomb.

A square wave contains all frequencies up to infinity, and a component of any natural frequency, no matter how high, will experience an acceleration of 2 G_m if subjected to a single square wave of acceleration of amplitude G_m, and will experience an acceleration of 4 G_m if subjected to a similar double square wave of acceleration. Of course, rounding of the corners of the square wave which will happen in practice will limit the upper frequency content, but there still may well be enough high frequency content to be troublesome.

All these considerations point to the fact that a linear viscously-damped spring appears to be at least as effective as all the nonlinear cases considered. Nonlinearities in the stiffness characteristic appear to be useful only as means of limiting either relative displacement or transmitted acceleration independently.

3.7.8 The Bilinear Approximation

In the preceding paragraphs the restoring forces of certain types of nonlinear elements were approximated by two straight lines of unequal slopes. The responses of systems incorporating these elements were calculated for a variety of ground shock wave forms. The process of selecting the slopes and intersection point of the two lines need not be left to judgment but can be optimized by minimizing the mean square error between the function being approximated and the straight line segments.

To obtain the best accuracy, the error should be minimized over the displacement range of the system, implying that the peak displacement is known. In some cases, therefore, the peak displacement must be estimated and, if the solution indicates a significant error, the process must be repeated. For many types of functions, however, the error in system response due to inaccuracies in estimating the peak displacement is small.

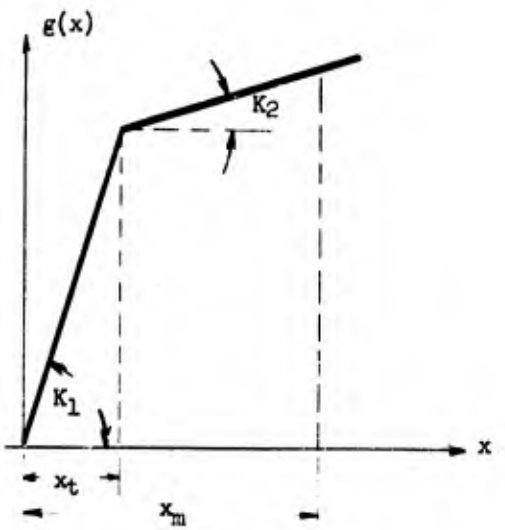

Assume a bilinear approximation of a nonlinear element g(x) of the form (Figure 3.7.29),

$$g_1(x) = K_1 x \qquad x < x_t$$

$$g_2(x) = K_2 x + (K_1 - K_2)\, x_t \qquad x > x_t$$

so that the continuity of the restoring force offered by the nonlinear element is satisfied at the transition point x_t , as yet unknown. That is

$$g_1(x) = \left| g_2(x) \right|_{x = x_t}$$

The mean square error ϵ of the above approximation is expressed by

$$\epsilon^2 = \frac{1}{x_m} \left[\int_0^{x_t} \left(g_1(x) - g(x)\right)^2 dx + \int_{x_t}^{x_m} \left(g_2(x) - g(x)\right)^2 dx \right]$$

where x_m is the maximum displacement and $x_t = a x_m$ is the displacement at the transition point.

The restoring force due to the nonlinear element can always be expressed in the form

$$g(x) = K_1 x \pm h(x)$$

where $K_1 x$ represents the linear restoring force due to the initial stiffness which is inherent to every physical system and coincides with the slope of the nonlinear restoring force at the origin. Substituting the above expression in the equation of the mean square error and minimizing with respect to the variable parameters x_t and K_2, a set of two equations is obtained in the form

$$K_2 - K_1 = \frac{2}{(x_m - x_t)^2} \int_{x_t}^{x_m} h(x) \, dx$$

$$K_2 - K_1 = \frac{6}{(x_m - x_t)^2 (2x_m + x_t)} \int_{x_t}^{x_m} x \, h(x) \, dx$$

which will yield the required values for x_t and K_2. In order to determine x_t and K_2 the maximum displacement x_m must be known. Careful investigation has shown that if the maximum linear displacement

x_m is used in computations instead of the actual maximum nonlinear displacement x_m, the resulting values for the second slope K_2 and transition point x_t are within a satisfactory range of accuracy except for systems with very large nonlinearities. In such cases an iterative procedure must be used.

As an example, consider the element whose force is expressed

$$F = K_1 x + cx^n \tag{79}$$

After performing the required algebra and letting $a = \frac{x_t}{x_m}$, the equation becomes

$$K_2 = K_1 + \frac{2cx_m^{n-1}(1 - a^{n+1})}{(1 - a)^2 (n + 1)}$$

and

$$a + 2 = \frac{3(n + 1)}{n + 2} \qquad \frac{1 - a^{n+2}}{1 - a^{n+1}}$$

Since $a = \frac{x_t}{x_m}$ is always less than 1 and n, the exponent of the deviation from the linear case, will always be greater than 1.0

$$\frac{1 - a^{n+2}}{1 - a^{n+1}} \cong 1$$

and

$$a + 2 = \frac{3(n + 1)}{n + 2} \; ; \quad x_t = \frac{n - 1}{n + 2} x_m$$

then

$$K_2 = K_1 + \frac{2}{9} cx_m^{n-1} \qquad \frac{(n + 2)^2}{n + 1}$$

For nonlinearities in the range $c/K_1 \cong 0.1$ the influence of the selection of the maximum displacement x_m is negligible. For nonlinearities in the range $c/K_1 \cong 1.0$ the influence of the right selection of the maximum displacement becomes significant and iteration procedures may be indicated.

If the difference between the two maximum displacements, that is linear $\overline{x}_m$ and nonlinear x_m, is denoted by Δ so that

$$\overline{x}_m = x_m + \Delta$$

the influence of the correct solutions of the maximum displacement for the purpose of calculating the transition parameters x_t and K_2 is

insignificant as long as

$$\Delta / x_m < 1$$

and in the same range as c/K_1.

3.8 Nonlinearity of the Simple Pendulum

The pendulum suspension system has been used extensively for supporting large loads in underground protective structures. By inserting elastic elements in the pendulum arms to attenuate vertical accelerations and by taking advantage of the low lateral stiffness inherent in long pendulums, simple, economical configurations are obtained. The Atlas, Titan I and II, Minuteman, and Norad facilities all employ a number of systems of this type for isolating manned platforms, missiles, or large assemblies of electronic gear.

In a strict sense, any suspension system is pendular if the moment exerted on the system by the force of gravity varies with the displacement of the body. In underground protective facilities where the direction of the input shock is not known, most, if not all, suspension systems will exhibit some pendular effect. The magnitude of the pendulum action on the dynamic response of the body is a function of the ratio of the gravity moment to the moment exerted by other elements within the system. In many configurations this ratio is negligible, and in any system it can be made small by inserting strong horizontal restoring elements.

While it is well known that the equations of motion for the simple rigid pendulum are nonlinear, the effects of additional nonlinearities introduced by the elasticity of the arm in the pendulum are rarely appreciated. The exact equations of motion for these systems show that the horizontal, x, vertical, z, and rotational, θ, modes are coupled by such terms as products of displacement, velocity, and acceleration. As interest is generally limited to small amplitude oscillations, it is frequently assumed that these nonlinear coupling terms can be neglected.

However, such is not the case for systems in which the uncoupled pendulum frequency is near one-half the uncoupled spring frequency. In these systems an interchange of energy between the pendulum and spring oscillations is possible leading to pendulum motions far exceeding those predicted by the linearized equations.

Approximate solutions to the equations expressing the behavior of elastic pendulums in stable regions were given by Rayleigh (Reference 3.14) and several others during the past half century but the significance of these results and the more serious possibility of instability has been overlooked in the design of many isolation systems.

Sevin (Reference 3.15) was the first to call attention to the seriousness of this omission in the design of systems for underground protective structures. Sevin considered first the influence of floor flexibility on the response of a pendulum supported floor system and showed the details of the energy transfer in free vibration between the pendulum and spring modes for the two-to-one frequency ratio. Later (Reference 3.16) Sevin pointed out that the significance of the energy

transfer lies in the fact that substantial increases in the pendulum amplitude are possible.

The principal concern of the isolation system designer with the problem is not so much with the response of inherently unstable systems as with selecting a basically stable configuration in the first place. To provide the designer with some background on the nature of the responses of pendulum systems, this discussion begins with the simple rigid pendulum and proceeds to the two- and three-degree-of-freedom elastic pendulum.

3.8.1 Simple Pendulum

3.8.1.1 Undamped Pendulum

The motion of a simple pendulum of constant length oscillating in a single vertical plane (Figure 3.8.1) can be represented by the differential equation

$$m \ell \ddot{\phi} + mg \sin \phi = 0$$

Letting $\omega_p^2 = \frac{g}{\ell}$, the above equation reduces to

$$\ddot{\phi} + \omega_p^2 \sin \phi = 0 \qquad (80)$$

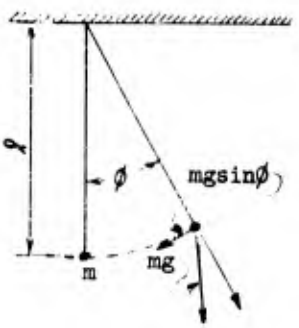

Figure 3.8.1
Simple Pendulum

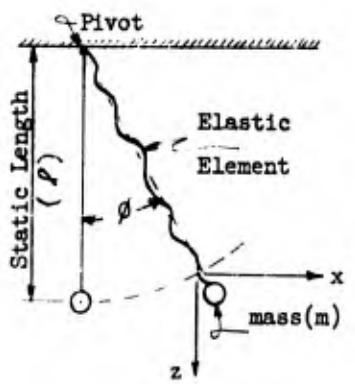

Figure 3.8.2
Elastic Pendulum

The above equation is nonlinear since,

$$\sin \phi = \phi - \frac{\phi^3}{3!} + \frac{\phi^5}{5!} - \frac{\phi^7}{7!} + \cdots\cdots\cdots$$

and (mg sin ϕ) can be interpreted as a kind of variable stiffness, dependent on the pendulum angle ϕ.

Denoting $V = \dot{\phi}$, equation (80) can be expressed in the form

$$V \frac{dV}{d\phi} + \omega_p^2 \sin \phi = 0 \tag{81}$$

Replacing the variable ϕ by a dummy variable θ such that

$$\sin \frac{\phi}{2} = \sin \frac{\phi_o}{2} \sin \theta \qquad \theta = \frac{\pi}{2} \text{ when } \phi = \phi_o$$

$$\theta = 0 \text{ when } \phi = 0$$

Where ϕ_o is the maximum amplitude $|\phi|_{max}$ occuring when $V = 0$, the solution of equation (81) yields

$$\omega_p \, dt = - \frac{d\theta}{\sqrt{1 - \sin^2 \frac{\phi_o}{2} \sin^2 \theta}}$$

Then, if τ is the period of oscillation

$$\tau = \frac{4}{\omega_p} \int_0^{\pi/2} \frac{d\theta}{\sqrt{1 - K^2 \sin^2 \theta}} = \frac{4}{\omega_p} F(K, \frac{\pi}{2})$$

where $K = \sin \frac{\phi_o}{2}$ and $F(K, \frac{\pi}{2})$ is the complete elliptic integral of the first kind, of modulus K, and is readily obtained from standard mathematical tables. By the theory of elliptic functions, F increases with K and therefore, the greater the amplitude, the greater the period τ. It may be noted that τ is a function of the amplitude ϕ_o, as is always the case in nonlinear oscillations. Furthermore, it is apparent that if ϕ is small, so that $\sin \phi \cong \phi$, then $\tau = \frac{2\pi}{\omega_p}$, which is a standard result for small oscillations.

The solution of equation (81) if limited to the first two terms of its Fourier series is

$$\phi = \phi_o \cos \omega t + C \phi_o \cos 3 \omega t \tag{82}$$

where it can be shown that $C \ll 1$, and $\omega^2 \cong \omega_p^2 (1 - \frac{1}{8} \phi_o^2)$.

Hence, for most practical problems, it can be assumed that

$$\phi \cong \phi_o \cos \omega t \tag{83}$$

3.8.1.2 Damped Pendulum

If the pendulum system includes a viscous damper, the nonlinear differential equation of motion (81) becomes

$$\ddot{\phi} + 2\ \delta\ \dot{\phi} + \ \omega_p^2 \sin \phi = 0 \qquad (84)$$

where δ is the ratio of actual damping 'c' to the critical damping c/cr. However, for $\phi < \frac{\pi}{6}$, it is permissible to assume

$$\sin \phi = \phi - \frac{\phi^3}{6}$$

$$\therefore\ \ddot{\phi} + 2\ \delta\ \dot{\phi} + \ \omega_p^2 \left(\phi - \frac{\phi^3}{6} \right) = 0 \qquad (85)$$

Then for initial conditions $t(0) = \phi(\phi_o) = \dot{\phi}\ (0) = \ddot{\phi}(0)$.

The solution of equation (85) is of the form

$$\phi = e^{-\ \delta t}(\phi_o \cos\ \omega t + C \cos 3\ \omega t)$$

where it can be shown that $C << 1$ and

$$\omega^2 = \omega_p^2 \left(1 - \frac{1}{8} \phi_o^2\ e^{-2\ \delta\ t} \right) \qquad (86)$$

Equation (86) shows that after a period of time, the frequency, ω , of the damped nonlinear pendulum approaches that of the simple pendulum, i.e.,

$$\omega \cong \omega_p = \sqrt{\frac{g}{\ell}} \ .$$

3.8.2 The Elastic Pendulum - Two-Degrees-of-Freedom

3.8.2.1 Undamped Pendulum

Consider now a system in which an elastic but massless element is inserted in the pendulum arm, and the system is constrainted to oscillate in the xz plane (Figure 3.8.2, page 3-154). The system contains two-degrees-of-freedom which may be described in terms of z and ϕ, or by the Cartesian reference coordinates x and z. The former coordinates are used here.

The equations of motion of the system in free oscillation are:

$$m\ (z + \ \ell \cos \phi)^{\cdot\cdot} + K_z = 0 \qquad (87)$$

$$\left\{ \left[m(\ell + z \cos \phi)^2 + I_{c.g.} \right] \dot{\phi} \right\}^{\cdot\cdot} = - mg (\ell + z) \phi \qquad (88)$$

For small oscillations, i.e., for $|\phi| < \frac{\pi}{6}$, it may be assumed that

$$\sin \phi \simeq \phi$$

$$\cos \phi \simeq 1 - \frac{\phi^2}{2}$$

Hence, equations (87) and (88) reduce to

$$\ddot{z} + \omega_1^2 z = \ell (\dot{\phi}^2 + \phi \ddot{\phi}) \qquad (89)$$

$$\ddot{\phi} + \omega_o^{*2} \phi = -\frac{1}{\ell^*} (2 \dot{z} \dot{\phi} + 2 z \ddot{\phi} + \omega_2^2 z \phi) \qquad (90)$$

where $\gamma^2 = \frac{I_{c.g.}}{m}$

$\ell^* = \frac{\ell^2 + \gamma^2}{\ell}$ = equivalent pendulum length

$\omega_1^2 = \frac{K}{m}$ = natural frequency of elastic element

$\omega_1^2 = \frac{g}{\ell}$ = natural frequency of simple pendulum

$\omega_o^2 = \frac{g}{\ell^*}$ = natural frequency of equivalent simple pendulum.

As particular cases,

if $\phi = \dot{\phi} = \ddot{\phi} = 0$; $\ddot{z} + \omega_1^2 z = 0$ (oscillation in z-mode only)

o if $z = \dot{z} = \ddot{z} = 0$; $\ddot{\phi} + \omega_1^{*2} \phi = 0$ (Pendulum oscillation only)

In most cases the two modes will be coupled. As can be seen from equations (89) and (90), the coupling between the z and ϕ modes may be linear, as represented by terms such as $\omega_2^2 z \phi$, or may be nonlinear, as represented by terms such as $2 z \dot{\phi}$ and $\phi \ddot{\phi}$. The linear coupling of the modes has the same importance and can be dealt with in a manner similar to that shown for coupled linear systems in Section 3.5. However, the nonlinear coupling cannot always be ignored, as is sometimes done, since certain critical ratios of the elastic element frequency to

the pendulum frequency cause very large amplitude oscillations. The most critical ratio, as shown later, is

$$\frac{\omega_o^{*2}}{\omega_1^2} = \frac{1}{4}$$

and must be avoided under all cases. In general, there will exist two types of nonlinear coupling, viz:

- Nonlinear coupling due to second order effects in translation
- Nonlinear coupling due to second order effects in pendular rotation

Case A: Assume that the pendulum, initially vertical and at rest, is drawn aside and released when

$$|\phi| = |\phi_o| < \frac{\pi}{6} \quad \text{at } t = 0$$

Then, initially $\phi = \phi_o \cos \omega_o^* t$. Substituting this in equation (89),

$$\ddot{z} + \omega_1^2 z = - \ell \phi_o^2 \omega_o^{*2} \cos 2 \omega_o^* t \qquad (91)$$

If $\omega_1 \neq 2 \omega_o^*$, the general solution of equation (91) is of the form

$$z = C_1 \sin \omega_1 t + C_2 \cos \omega_1 t + \frac{\ell \phi_o^2 \omega_o^{*2}}{\omega_1^2 - 4 \omega_o^{*2}} \cos 2 \omega_o^{*2} t \qquad (92)$$

where C_1 and C_2 are constants of integration, to be determined from the initial conditions. The equation shows that the axial motion has two periodic components of frequencies

$$\frac{\omega_1}{2\pi} \quad \text{and} \quad \frac{2 \omega_o^*}{2\pi} .$$

It also shows that an instability condition occurs when $\omega_1 = 2 \omega_o^{*2}$, since for this particular case, the solution of the differential equation includes a particular integral of the aperiodic form ($t \sin 2 \omega_o^* t$). This indicates that the amplitude of oscillation in the z mode will increase with time, leading to an unstable behavior if $\omega_1 = 2 \omega_o^*$. Furthermore, since the energy of the system must remain constant, the amplitude of oscillation in the ϕ mode must decay.

Case B: Assume that the mass m is pulled down by an amount $z_o < \ell^*$ when pendulum is vertical, and then released at the initial time t = 0. The subsequent motion in the z direction will be defined initially by $z = -z_o \cos \omega_1 t$. Substituting this on the right hand side of equation (90)

$$(1 - \frac{2z_o}{\ell^*}\cos \omega t)\ddot{\phi} + (\frac{2z_o}{\ell^*}\omega_1 \sin \omega_1 t)\dot{\phi} + \omega_o^{*2}(1 - \frac{z_o}{\ell}\cos \omega_1 t)\phi = 0 \qquad (93)$$

Approximating $\cos \omega t$ by 1, and since by previous assumption $\frac{z_o}{\ell^*} < 1$, the above equation may be reduced in a first approximation, to

$$\ddot{\phi} + \frac{2z_o}{\ell^*}\omega_1 \sin \omega_1 t\dot{\phi} + \omega_o^{*2}\phi = 0 \qquad (94)$$

Substituting $\omega_1 t = 2\alpha$

$$a = \left(\frac{2\omega_o^*}{\omega_1}\right)^2$$

$$q = \frac{2z_o}{\ell^*}$$

equation (94) becomes

$$\frac{d^2\phi}{d\alpha^2} + 2q \sin 2\alpha \frac{d\phi}{d\alpha} + a\phi = 0 \qquad (95)$$

Further, letting $\phi = e^{1/2q \cos 2\alpha}\, y(\alpha)$, and substituting this in equation (95)

$$\frac{d^2y}{d\alpha^2} + \left[(a - 1/2q^2) - 2q\cos 2\alpha + 1/2q^2 \cos 4\alpha\right] y = 0 \qquad (96)$$

The above equation is a linear differential equation with time variable coefficients of the Hill type, since the coefficients are periodic functions of the variable $\alpha = 1/2\ \omega_1 t$. The solution of Hill's equation can be found in text books on mathematics (Pipes - Reference 3.3).

If the configuration of the system is such that $q = \frac{2z_o}{\ell^*} < 1$, then equation (96) can be reduced in a first approximation to

$$\frac{d^2y}{d\alpha^2} + (a - 2q \cos 2\alpha)\, y = 0 \qquad (97)$$

Note that q can also be written $q = \frac{2\ mg}{K(\ell^2 + \ )}$.

Equation (97) is a linear differential equation, with periodic time varying coefficients of the Mathieu type, with the general solution as explained in Appendix 3-F of the form

$$y = C_1 e^{\mu\alpha} \sum_{\gamma=-\infty}^{+\infty} a_\gamma e^{i\gamma\alpha} + C_2 e^{-\mu\alpha} \sum_{\gamma=-\infty}^{+\infty} b_\gamma e^{i\gamma\alpha} \qquad (98)$$

where C_1 and C_2 are constants of integration, to be determined from the initial condition.

In equation (98) the characteristic exponent μ, as well as the two functions

$$\sum_{\gamma=-\infty}^{+\infty} a_\gamma e^{i\gamma\alpha} \quad \text{and} \quad \sum_{\gamma=-\infty}^{+\infty} b_\gamma e^{i\gamma\alpha}$$

are independent of the initial conditions and depend only on the parameters 'a' and 'q' of the differential equation (97). Depending on the relationship between the two parameters 'a' and 'q', the behavior of the system may be stable or unstable.

For the unstable condition, expression (98) takes the form

$$y = C_1 \, p_3(\alpha) + C_2 \left[\alpha \, p_3(\alpha) + p_4(\alpha)\right] \qquad (99)$$

where $p_3(\alpha)$ and $p_4(\alpha)$ are periodic functions in α, the instability of the system being characterized by the inclusion of α in the configuration. However, it is not necessary to solve the differential equation (97) to determine whether the system is unstable or not. The parameters 'a' and 'q' alone, of the Mathieu differential equation define the stability characteristics of the system as has been shown by Ince and Strutt (References 3.17, 3.18). The results have been graphically represented by curves which constitute the so-called Ince-Strutt diagram, dividing the (a,q) plane into regions of stable and unstable behavior. These diagrams have been transferred by Ince into Tables (Reference 18), describing the properties of the curves. It can be shown that the points for which the system becomes unstable are given by a simple relationship a + q = 1; that is,

$$\frac{4\,\omega_o^{*2}}{\omega_1^{\,2}} + \frac{z_o}{f^*} = 1$$

For small values of $q = \frac{2z_o}{\ell^*} << 1$ the above condition reduces to

$$\frac{{\omega_o^*}^2}{\omega_1^2} = \frac{1}{4}$$

The system is stable if

$$a + q = \frac{4\,{\omega_o^*}^2}{\omega_1^2} + \frac{2z_o}{\ell^*} < 1 \qquad (100)$$

Thus, because of the nonlinearity of the coupling, energy may be transferred between the ϕ and z modes.

3.8.2.2 Design Procedure for a Two-Degree-of-Freedom Elastic Pendulum

Based on the previous discussion, and in conjunction with Appendix 3-F, a design procedure for the elastic pendulum is suggested:

Step #1: Determine the input parameter z_o which is the peak vertical displacement given by the imposed shock spectrum, for a frequency corresponding to the natural frequency of the spring, considered as a single degree-of-freedom spring-mass system.

Step #2: Determine the input parameter ϕ_o which corresponds to the peak horizontal displacement given by the imposed shock spectrum, for a frequency corresponding to the pendulum natural frequency ${\omega_o}^{*2}$.

Step #3: Check the stability of the elastic pendulum. This is accomplished by locating the (a,q) point on the Ince-Strutt diagram (Figure 3.8.3). For most practical cases, only the first V of the Ince-Strutt diagram is needed.

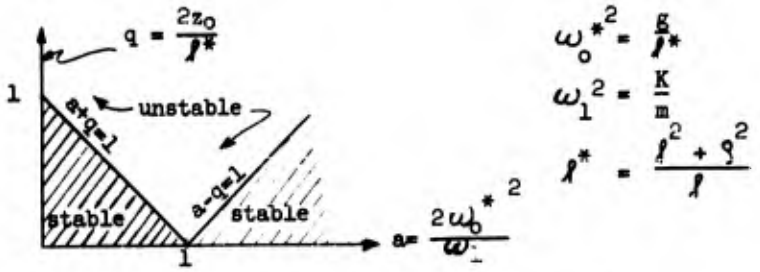

Figure 3.8.3 Ince-Strutt Stability Diagram

For $a < 1$, and if $a + q$ is less than unity, the system is stable; if however $a + q \geq 1$, the system is unstable and the parameters K and/or ρ must be adjusted to stabilize the configuration.

Similarly, for $a > 1$, and if $a - q$ is greater than unity, then the system is stable; but if $a - q \leq 1$, the system is unstable and must be reproportioned.

Step #4: If the system is stable, the response is given by (Appendix 3-F)

$$y = A\left[\cos \nu\alpha - \frac{1}{4}q\left\{\frac{\cos(\nu + 2)\alpha}{\nu + 1} - \frac{\cos(\nu - 2)\alpha}{\nu - 1}\right\}\right] \quad (101)$$

where $\nu^2 \cong a$ as a first approximation

and

$$\nu^2 \cong a - \frac{1}{2(a - 1)} q^2 \text{ as a second approximation}$$

if

$$\frac{1}{2(\nu^2 - 1)} q^2 << \nu^2 .$$

'A' is a constant depending on the initial conditions, it being remembered that $y = y_o$ when $\alpha = 0$, where $2\alpha = \omega_1 t$. However, if

$$\frac{1}{2(\nu^2 - 1)}$$

is not very small with respect to ν^2, equation (101) is not valid and Ince's method of infinite continued fractions must be employed (Reference 3.17). The method is not described in the Design Guide since configuration of these proportions should be avoided if possible.

Step #5: Calculate the pendulum response ϕ from the relationship

$$\phi = e^{1/2q\cos 2\alpha} y.$$

3.8.2.3 Numerical Example: Two-Degrees-of-Freedom Elastic Pendulum

Consider the configuration shown in Figure 3.8.4 exposed to vertical and horizontal shocks whose response spectra are shown in Figure 3.8.5.

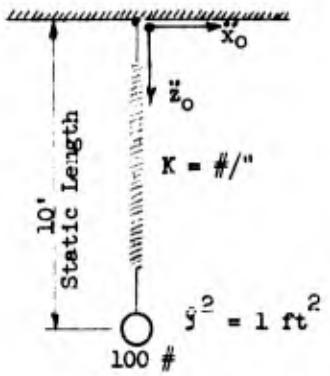

Figure 3.8.4
Elastic Pendulum

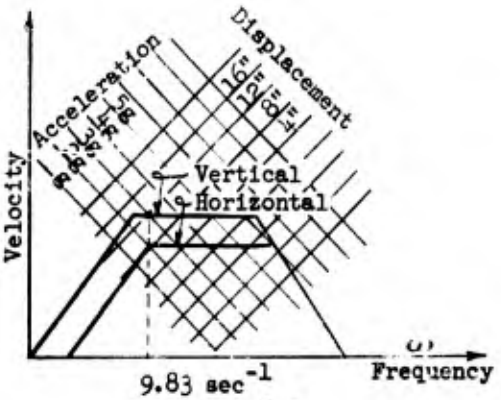

Figure 3.8.5
Response Spectra

The natural frequency of the uncoupled mass spring system is

$$\omega_1^2 = \frac{K}{m} = \frac{(25)(32.2)(12)}{100} = 96.6 \text{ sec}^{-2}, \quad \therefore \omega_1 = 9.83 \text{ sec}^{-1}.$$

$$\omega_2^2 = \frac{g}{\ell} = \frac{32.2}{10} = 3.22 \text{ sec}^{-2}$$

$$\ell^* = \frac{\rho^2 + \ell^2}{\ell} = \frac{10^2 + 1}{10} = 10.1 \text{ ft.}$$

The natural frequency of the uncoupled pendulum is:

$$\omega_o^{*2} = \frac{g}{\ell^*} = \frac{32.2}{10.1} = 3.19 \text{ sec}^{-2}, \quad \therefore \omega_o^* = 1.79$$

From the shock spectrum, for $\omega_1 = 9.83$, $z_o = 12"$

for $\omega_o^* = 1.79$, $\delta_h = 4"$

where δ_h = horizontal displacement: $\phi_o = \frac{\delta_h}{\ell} = \frac{4}{(10)(12)} = 0.033$ ra s

$$\therefore\ q = \frac{2z_o}{\ell^*} = \frac{(2)(12)}{(10.1)(12)} = 0.198$$

$$a = \left(\frac{2\,\omega_o^*}{\omega_1}\right)^2 = \frac{(4)(3.19)}{(96.6)} = 0.132 < 1$$

$\therefore$ for stability, $a + q < 1$

$a + q = 0.132 + 0.198 = 0.33 < 1$

Therefore the system is stable. The location of these system parameters on the Ince-Strutt diagram is shown in Figure 3.8.6.

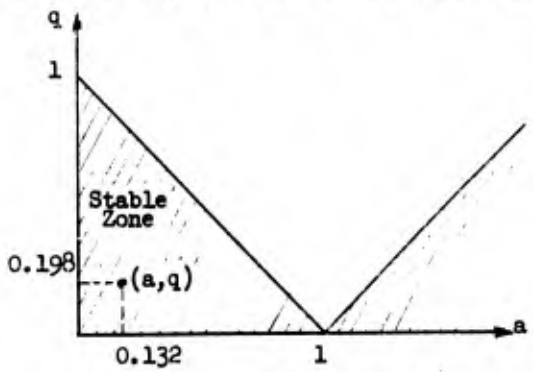

Figure 3.8.6: Ince-Strutt Diagram for Elastic Pendulum

To determine the maximum angular displacement of the pendulum consider as a first approximation,

$$\gamma^2 = a = 0.132 \qquad \therefore\ \gamma = 0.363.$$

As a second approximation,

$$\gamma^2 = a - \frac{1}{2(a-1)}\,q^2 = 0.132 - \frac{1}{2(0.132-1)}\,.(0.196)^2$$

$$= 0.132 + 0.0225 = 0.1545$$

$$\left|\frac{q^2}{2(\gamma^2 - 1)}\right| = \frac{(0.198)^2}{(2)\,(1-0.155)} = 0.023 << \gamma^2$$

Therefore equation (101) for the lateral displacement is valid.

$$\therefore \nu^2 = 0.1545$$

$$\therefore \nu = 0.394$$

$$\text{Then } y = A\left[\cos \nu\alpha - \frac{1}{4} q \left\{\frac{\cos(\nu + 2)}{\nu + 1} - \frac{\cos(\nu - 2)\alpha}{\nu - 1}\right\}\right]$$

$$y = A\left[\cos 0.394\alpha - 0.0355 \cos 2.394\alpha - 0.0818 \cos(-1.606\alpha)\right]$$

$$\therefore \phi = Ae^{\frac{1}{2} q \cos 2\alpha}\left[\cos 0.394\alpha - 0.0355 \cos 2.394\alpha - 0.0818 \cos(-1.606\alpha)\right]$$

When $t = 0$, $\alpha = 0$ and $\phi = \phi_o = 0.03$

$$\therefore \phi_o = Ae^{\frac{1}{2} q}\left[1 - 0.0355 - 0.0818\right]$$

$$\therefore A = \frac{1.135}{e^{1/2\, q}} \phi_o$$

$$y = \frac{1.135}{e^{1/2q}} \phi_o \left[\cos 0.394\alpha - 0.0355 \cos 2.394\alpha - 0.0818 \cos(-1.606\alpha)\right]$$

$$\phi = 1.135e^{\left(\frac{q}{2}\cos 2\alpha - \frac{q}{2}\right)} \phi_o\left[\cos 0.394 - 0.0355\cos 2.394 - 0.0818\cos(-1.606)\right]$$

$$\left(\phi_{max}\right)_{max} = 1.135\, \phi_o \left[1 + 0.0355 + 0.0818\right] = 1.265\, \phi_o$$

$$= (1.265)(0.033)$$

$$= 0.042 \text{ rads}$$

Hence it is seen that in this case with the point (a,q) well within the stable region, the nonlinear coupling of the modes causes an amplification of about 26 per cent.

Next consider a more severe shock spectrum for the same pendulum, so that $z_o = 30"$ and $\phi_o = 0.083$ rad.

$$\text{Then } q = \frac{2z_o}{l^*} = \frac{(2)(30)}{(10.1)(12)} = 0.495$$

$a = 0.132 < 1$, as before

$\therefore a + q = 0.495 + 0.132 = 0.627 < 1$

Therefore the point falls within the stable region of the Ince-Strutt diagram.

As a first approximation $\nu^2 = a = 0.132$

However

$$\frac{q^2}{2(\nu^2 - 1)} = \frac{(0.495)^2}{2(0.132 - 1)} = 0.14$$

Since 0.14 is not very small compared to 0.132, equation (101) is not valid. This problem would necessitate the iterative solution given in Reference 3-17 which will not be dealt with here. However, from a practical viewpoint it should be noted that the amplification factor becomes greater with increasing q, for the same value of a.

Finally, considering a third example, such that

$$a = 0.6$$

$$q = 0.2$$

$$z_o = 12"$$

Then $a + q = 0.2 + 0.6 = 0.8 < 1$ and the system is stable.

The first approximation gives $\nu^2 = a = 0.6$, and the second approximation

$$\nu^2 = a - \frac{q^2}{2(a - 1)} = 0.6 - \frac{(0.2)^2}{2(0.6 - 1)} = 0.65$$

$\therefore \nu = 0.808$

$$\therefore y = A\left[\cos 0.808\alpha - \frac{0.2}{4}\left\{\frac{\cos(2.808\alpha)}{1.808} + \frac{\cos(-1.192\alpha)}{0.192}\right\}\right]$$

$$= A\left[\cos 0.808\alpha - 0.0222 \cos 2.808\alpha - 0.261 \cos(-1.192\alpha)\right]$$

Then, as before, $A = \frac{\phi_o}{1-0.0222 - 0.261} = 1.4\,\phi_o$

$$\therefore \phi = 1.4\phi_o e^{\left(\frac{q}{2}\cos 2\alpha - \frac{q}{2}\right)}\left[\cos 0.808\alpha - 0.0222\cos 2.808\alpha - 0.261\cos(-1.192\alpha)\right]$$

$$\therefore \left(\phi_{max}\right)_{max} = (1.4)\left[1 + 0.0222 + 0.261\right]\phi_o$$

$$= 1.8\,\phi_o$$

This represents an 80 per cent increase over the uncoupled peak pendulum angle. However it must be remembered that the actual maximum will be less than this value and in the event a more accurate answer is needed, the actual maximum may be calculated by standard principles of maxima and minima.

3.8.2.4 The Effect of Damping on the Behavior of the Elastic Pendulum

In the absence of any energy loss, the equation governing the motion of an elastic pendulum given by previous results is

$$\frac{d^2y}{d\alpha^2} + (a - 2q \cos 2\alpha)y = 0; \text{ where } 2\alpha = \omega_1 t \qquad (102)$$

$$\phi = e^{1/2q\cos\alpha} y(\alpha)$$

The amplitude of motion may increase, under conditions described in Appendix 3.9F, exponentially in accordance with one of the solutions of the equation (102) as follows:

$$y = e^{\mu\alpha} \sum_{\gamma=0}^{\infty} \beta_{2\gamma+1} \cos\left[(2\gamma+1)\alpha + \gamma_{2\gamma+1}\right] \qquad \mu_{real} > 0$$

or

$$y = e^{-\mu\alpha} \sum_{\gamma=0}^{\infty} \beta_{2\gamma+1} \cos\left[(2\gamma+1)\alpha + \gamma_{2\gamma+1}\right] \qquad \mu_{real} > 0$$

The second solution may be omitted from the discussion since it vanishes with time. Consequently, the amplitude of motion will be defined by the first solution, and will increase without bounds, unless it is restricted by certain limiting properties of the system.

In case dissipative forces, such as those provided by a viscous damper, are present, then the governing linear differential equation with variable coefficients becomes

$$\frac{d^2y}{d\alpha^2} + 2\delta\frac{dy}{d\alpha} + (a - 2q\cos 2\alpha)y = 0 \qquad (103)$$

where δ is the ratio of critical damping.

Using the transformation

$$y = e^{-\delta\alpha} u(\alpha) \tag{104}$$

equation (103) can be reduced to

$$\frac{d^2u}{d\alpha^2} + (\bar{a} - 2q \cos 2\alpha)u = 0 \tag{105}$$

where $\bar{a} = a - \delta^2$

Equation (105) is again a Mathieu equation, and its significant solution is of the form

$$u = e^{\bar{\mu}\alpha} \sum_{\nu=0}^{\infty} \bar{\vartheta}_{2\nu+1} \cos\left[(2\nu+1)\alpha + \bar{\nu}_{2\nu+1}\right] \tag{106}$$

where $\bar{\mu}$, $\bar{\vartheta}$, $\bar{\nu}$ now have new significance in accordance with the new definition of the parameter $\bar{a}$. As a consequence the solution of equation (103) becomes

$$y = e^{(\bar{\mu} - \delta)\alpha} \sum_{\nu=0}^{\infty} \bar{\vartheta}_{2\nu+1} \cos\left[(2\nu+1)\alpha + \bar{\nu}_{2\nu+1}\right] \tag{107}$$

where $2\alpha = \omega_1 t$.

If $\delta = \bar{\mu}$, the resulting motion is neutral and not influenced by damping.

If $\delta > \bar{\mu}$, the motion is stable for $0 < \alpha < \infty$, since the amplitude will decay exponentially to zero, as $\alpha(t)$ approaches infinity.

If $\delta < \bar{\mu}$, the motion is unstable for $0 < \alpha < \infty$, since the amplitude grows exponentially with time.

The presence of a damping term in the governing equation of motion enlarges the stability region of the Ince-Strutt stability chart, whereas the instability regions are decreased. Instability regions of lower order are less influenced by the damping than the instability regions of higher order, the latter being strongly influenced by the damping in the system. Therefore, because of the residual damping inherent in physical systems, the instability regions of higher order become unimportant form a practical viewpoint.

The Mathieu equation for systems incorporating damping infers the possibility of instability, i.e., solutions that may grow without bounds. Hence, a fundamental difference between damped linear systems with constant coefficients and damped linear systems with variable coefficients lies in the fact that whereas for the former damping always stabilizes the system, in case of the latter, damping may not always stabilize the system (Reference 3.19).

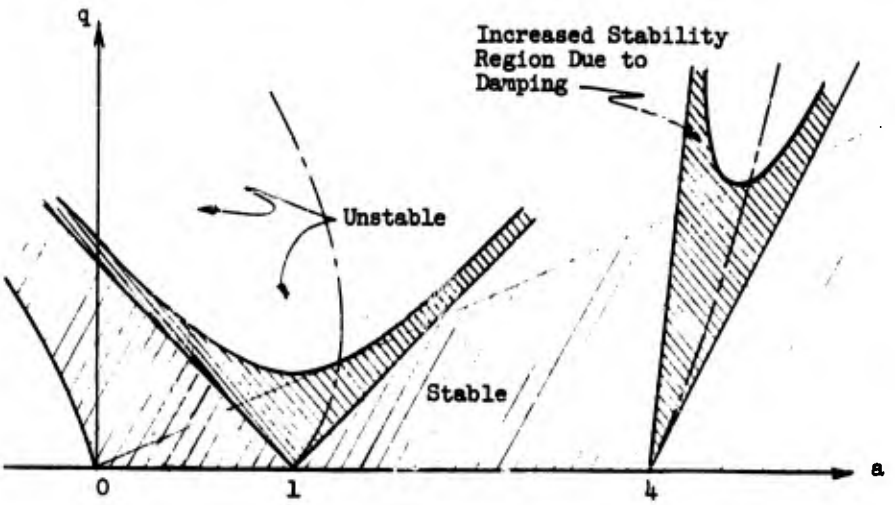

Figure 3.8.7
INCE-Strutt Stability Chart for Damped Systems

Inspection of the Ince-Strutt stability chart for rheolinear systems (Figure 3.8.7) reveals that a large amount of damping is necessary to raise the tip of the first order V-shaped instability curve by a small amount. Accordingly, a damping ratio of 10 per cent may raise the tip of the instability curve from $a = 1$, $q = 0$ to $a = 1$, $q = 0.2$. Comparing these results with those observed for linear systems, it may be concluded that incorporation of viscous damping in the system is far less effective for the performance of rheolinear systems. Other means, such as the incorporation of nonlinear elements in the configuration, may be more effective in stabilizing a rheolinear system.

3.8.3 Three-Degree-of-Freedom Planar Pendulum

3.8.3.1 General Discussion and Equations of Motion

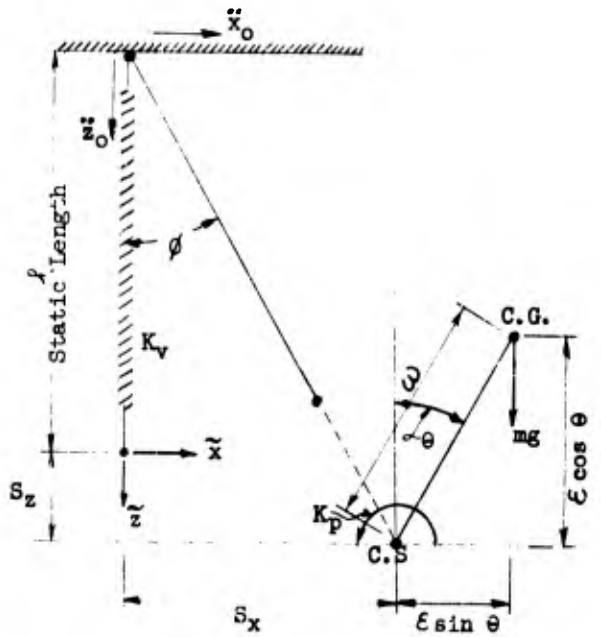

K_v = Axial Spring Stiffness

K_p = Rotational Spring Stiffness

C.S. = Center of Spring

Figure 3.8.8
Three-Degree-of-Freedom Planar Pendulum

The coordinates of the centroid are

$$\tilde{x} = S_x + \varepsilon \sin\theta \cong S_x + \varepsilon\theta$$
$$\tilde{z} = S_z - \varepsilon \cos\theta \cong S_z - \varepsilon \qquad (108)$$

If H and V are defined as the horizontal and vertical spring reactions at the spring center, then the equations of dynamic equilibrium yield

$$-H = m\ddot{\tilde{x}} \cong m\ddot{S}_x + m\varepsilon\ddot{\theta} = -mg\frac{S_x}{\ell}$$
$$-mg - V = m\ddot{\tilde{z}} = m\ddot{S}_z = K_v S_z \qquad (109)$$
$$H\varepsilon\cos\theta - V\varepsilon\sin\theta = H\varepsilon - V\varepsilon\theta = I_{C.G.}\ddot{\theta} + K_p\theta$$

Eliminating H and V between the above equations, there results

$$I_{C.G.}\ddot{\theta} + K_p\theta = -m\varepsilon\ddot{S}_x - m\varepsilon^2\ddot{\theta} + m\ddot{S}_z\varepsilon\theta + mg\varepsilon\theta$$

$$\therefore (I_{C.G.} + m\varepsilon^2)\ddot{\theta} + (K_p - mg\varepsilon)\theta + m\varepsilon(\ddot{S}_x - \ddot{S}_z\theta) = 0$$

However, $I_{C.G.} + m\varepsilon^2 = I_{C.S.}$, therefore the equations of motion in relative coordinates are

$$\begin{aligned} m\ddot{S}_{x_r} + \frac{mg}{\ell} S_{x_r} + m\varepsilon\ddot{\theta} &= -m\ddot{x}_o \\ m\ddot{S}_{z_r} + K_v S_{z_r} &= -m\ddot{z}_o \\ I_{C.S.}\ddot{\theta} + m\varepsilon(\ddot{S}_{x_r} - \ddot{S}_{z_r}\theta) + (K_p - mg\varepsilon)\theta &= m\varepsilon(\ddot{z}_o\theta - \ddot{x}_o) \end{aligned} \qquad (110)$$

where $S_{x_r} = S_x - x_o$

$S_{z_r} = S_z - z_o$

Simplifying the above equations,

$$\ddot{S}_{x_r} = -\varepsilon\ddot{\theta} - \frac{g}{\ell} S_{x_r} - \ddot{x}_o$$

$$\ddot{S}_{z_r} = -\frac{K_v}{m} S_{z_r} - \ddot{z}_o$$

Therefore $\ddot{S}_{x_r} - S_{z_r}\theta = -\varepsilon\theta - \frac{g}{\ell} S_{x_r} - \ddot{x}_o + \frac{K_v}{m} S_{z_r}\theta + \ddot{z}_o\theta$

Substituting this in the third of equations (110)

$$I_{C.S.}\ddot{\theta} + m\varepsilon\left(-\varepsilon\ddot{\theta} - \frac{g}{\ell}S_{x_r} - \ddot{x}_o + \frac{K_v}{m} S_{z_r}\theta + \ddot{z}_o\theta\right)$$

$$+ (K_p - mg\varepsilon)\theta = m\varepsilon(\ddot{z}_o\theta - \ddot{x}_o)$$

Therefore

$$I_{C.G.}\ddot{\theta} - \varepsilon\frac{mg}{\ell} S_{x_r} + \varepsilon K_v S_{z_r}\theta + (K_p - mg\varepsilon)\theta = 0$$

Dropping the index r for convenience, the equations of motion are:

$$\begin{aligned} m(\ddot{S}_x + \varepsilon\ddot{\theta}) + \frac{mg}{\ell} S_x &= -m\ddot{x}_o \\ m\ddot{S}_z + K_v S_z &= -m\ddot{z}_o \\ I_{C.G.}\ddot{\theta} - \varepsilon\frac{mg}{\ell} S_x + \left[K_p + \varepsilon(K_v S_z - mg)\right]\theta &= 0 \end{aligned} \qquad (111)$$

Using the notation $I_{C.G.} = m \rho^2_{C.G.}$, the set of equations (111) reduce to

$$\ddot{S}_x + \varepsilon \ddot{\theta} + \frac{g}{\ell} S_x = -\ddot{x}_o$$

$$\ddot{S}_z + \frac{K_v}{m} S_z = -\ddot{z}_o \qquad (112)$$

$$\ddot{\theta} - \varepsilon \frac{g/\ell}{\rho^2_{C.G.}} x + \frac{\varepsilon}{\rho^2_{C.G.}} \frac{K_v}{m} S_z \theta + \frac{K_p - \varepsilon mg}{m \rho^2_{C.G.}} \theta = 0$$

Further, making the following substitutions,

$$\frac{K_v}{m} = \omega_1^2 \qquad \frac{g}{\ell} = \omega_2^2 \qquad \frac{\rho^2_{C.G.}}{\varepsilon} = \varepsilon^*$$

$$\frac{K_p}{\varepsilon m} - g = g^*$$

$$\frac{K_p - \varepsilon gm}{m \rho^2_{C.G.}} = \frac{g^*}{\varepsilon^*} = \omega_2^{*2}$$

$S_x = x$, and $S_z = z$

The set of equations (112) are reduced to:

$$\ddot{x} + \omega_2^2 x = -\ddot{x}_o - \varepsilon \ddot{\theta}$$

$$\ddot{z} + \omega_1^2 z = -\ddot{z}_o$$

$$\ddot{\theta} - \frac{\omega_2^2}{\varepsilon^*} x = -\frac{\omega_1^2}{\varepsilon^*} \theta z - \omega_2^{*2} \theta$$

The last of equations (111) yields

$$\ddot{\theta} + \omega_1^2 \left(\frac{\omega_2^{*2}}{\omega_1^2} + \frac{1}{\varepsilon^*} z \right) \theta = \frac{\omega_2^2}{\varepsilon^*} x$$

and therefore

$$\ddot{x} + (1 + \frac{\varepsilon}{\varepsilon^*})\,\omega_2^2 x - \varepsilon\omega_1^2 (\frac{\omega^{*2}}{\omega_1^2} + \frac{1}{\varepsilon^*} z)\,\theta = -\ddot{x}_o$$

$$\ddot{z} + \omega_1^2 z = -\ddot{z}_o \qquad (114)$$

$$\ddot{\theta} - \frac{\omega_2^2}{\varepsilon^*} x + \omega_1^2 (\frac{\omega^{*2}}{\omega_1^2} + \frac{1}{\varepsilon^*} z)\,\theta = 0$$

If a periodic solution of the form $z = z_o \cos \omega_1 t$ exists in the z direction, then equation (114) can be written as

$$\ddot{x} + (1 + \frac{\varepsilon}{\varepsilon^*})\,\omega_2^2 x - \varepsilon\omega_1^2 (\frac{\omega_2^{*2}}{\omega_1^2} + \frac{z_o}{\varepsilon^*} \cos \omega_1 t)\theta = 0$$

$$\ddot{\theta} - \frac{\omega_2^2}{\varepsilon^*} x + \omega_1^2 (\frac{\omega_2^{*2}}{\omega_1^2} + \frac{z_o}{\varepsilon^*} \cos \omega_1 t)\,\theta = 0 \qquad (115)$$

Equations (115) clearly indicate that the behavior of the system is controlled by a pair of Mathieu's equations whereby it may be concluded that the system may become unstable under circumstances involving critical relationships between the various parameters defined by the Ince-Strutt charts.

3.8.3.2 Stability of the Motion

The natural frequency ω_n of the system as defined by equations (115) can be obtained from the frequency determinant, as follows:

$$= \begin{vmatrix} -\omega_n^2 + (1 + \frac{\varepsilon}{\varepsilon^*})\,\omega_2^2 & -\varepsilon\omega_2^{*2} \\ -\frac{\omega_2^2}{\varepsilon^*} & (-\omega_n^2 + \omega_2^{*2}) \end{vmatrix} = 0 \qquad (116)$$

$$\therefore \begin{vmatrix} (-\omega_n^2 + \omega_2^2) & -\varepsilon\omega_n^2 \\ -\frac{\omega_2^2}{\varepsilon^*} & -\omega_n^2 + \omega_2^{*2} \end{vmatrix} = 0$$

$$\therefore (\omega_2^2 - \omega_n^2)(\omega_2^{*2} - \omega_n^2) - \frac{\varepsilon}{\varepsilon^*}\,\omega_n^2\,\omega_2^2 = 0$$

or

$$\omega_n^4 - \omega_n^2\left[(1 + \frac{\varepsilon}{\varepsilon^*})\,\omega_2^2 + \omega_2^{*2}\right] + \omega_2^2\,\omega_2^{*2} = 0$$

However, $\frac{\varepsilon}{\varepsilon^*} = \frac{\varepsilon^2}{\rho_{C.G.}^2} << 1$ for small eccentricity

$$\therefore \omega_n^4 - \omega_n^2(\omega_2^2 + \omega_2^{*2}) + \omega_2^2\,\omega_2^{*2} = 0 \qquad (117)$$

In the above equation all elements except ω^2 are completely defined by the geometry of the system. The solution of equation (117) yields the two natural frequencies ω_{n1} and ω_{n2} of the system. For small eccentricity,

$$\omega_{n1} = \omega_2 \quad \text{and} \quad \omega_{n2} = \omega_2^*$$

As the eccentricity increases, the natural frequencies of the system become closer and may yield a resonance condition leading to an unstable behavior of the system.

By the Ljapunov theory (Reference 3-20) the system is stable if

$$a^2 < \left[1/2(q + 2)\right]^2 \qquad (118)$$

where

$$a = 2\left[\cos\frac{2\pi\omega_{n1}}{\omega_1} + \cos\frac{2\pi\omega_{n1}}{\omega_1}\right] - 2\left(\frac{\pi z_o}{e^*}\right)^2$$

$$b = 2\left[\cos\frac{4\pi\omega_{n1}}{\omega_1} + \cos\frac{4\pi\omega_{n2}}{\omega_1}\right] - 2\left(\frac{\pi z_o}{e^*}\right)^2$$

$$q = 1/2(a^2 - b); \quad e^* = \frac{\rho_{C.G.}}{\varepsilon}; \quad \omega_1 = \sqrt{\frac{K_v}{m}}$$

For small eccentricity

$$\omega_{n1} = \omega_2 = \sqrt{\frac{g}{\ell}} \quad \text{and} \quad \omega_{n2} = \omega_2^* = \sqrt{\frac{g}{e^*}}$$

This shows that the natural frequencies of the system are independent of the input z_o and depend only on the geometry of the configuration. As a consequence, the trigonometric quantities in parenthesis become invariant with the input amplitude z_o and the eccentricity $\mathcal{E}$, and depend only on the stiffness characteristic of the dynamic system.

3.8.3.3 Numerical Example of Stability of a Three-Degree-of-Freedom System

Given $\rho = 10$ ft.

$\mathcal{E} = 1$ ft.

$K_v = 25$ lbs/in

$K_p = 300$ ft. lbs/rad

$W = 100$ #

$\varsigma^2 = 1$ ft^2

$$\therefore \omega_1^2 = \frac{K_v}{m} = \frac{(25)(32.2)(12)}{100} = 96.6 \text{ sec}^{-2}; \quad \therefore \omega_1 = 9.84 \text{ sec}^{-1}$$

$$\omega_2^2 = \frac{g}{\rho} = \frac{32.2}{10} = 3.22 \text{ sec}^{-2}$$

$$\mathcal{E}^* = \frac{\varsigma^2}{\mathcal{E}} = \frac{1}{1} = 1 \text{ ft}$$

$$g^* = \frac{K_p}{m} - g = \frac{(300)(32.2)}{(1)(100)} - 32.2 = 64.4 \text{ ft/sec}^2$$

$$\therefore \omega_2^{*2} = \frac{g^*}{\mathcal{E}^*} = \frac{(64.4)}{1} = 64.4 \text{ sec}^{-2}$$

From shock spectrum (Figure 3.8.5, page 3-163) for $\omega = 9.84$ sec^{-1}, $z_o = 1$ ft. Then the frequency equation as given by equation (116) is

$$\omega_n^4 - \omega_n^2 \left[\left(1 + \frac{\mathcal{E}}{\mathcal{E}^*}\right) \omega_2^2 + \omega_2^{*2} \right] + \omega_2^2 \, \omega_2^{*2} = 0$$

$$\therefore \omega_n^4 - \omega_n^2 \left[\left(1 + \frac{1}{1}\right)(3.22) + (64.4) \right] + (3.22)(64.4) = 0$$

$$\therefore \omega_n^4 - 70.84\ \omega_n^2 + 207.368 = 0$$

The roots of this equation are

$$\omega_{n1}^2 = 67.78 \qquad \therefore \omega_{n1} = 8.22$$

$$\omega_{n2}^2 = 3.06 \qquad \therefore \omega_{n2} = 1.75$$

Then from equation (118)

$$a = 2\left[\cos\frac{2\pi\omega_{n1}}{\omega_1} + \cos\frac{2\pi\omega_{n2}}{\omega_2}\right] - 2\left(\frac{z_o}{e^*}\right)^2$$

$$= 2\left[\cos\frac{(2\pi)(1.75)}{(9.84)} + \cos\frac{(2\pi)(8.22)}{(9.84)}\right] - 2\left\{\frac{(\pi)(1)}{(1)}\right\}^2$$

$$= 2\left[0.4384 + 0.5300\right] - 19.719 = 1.937 - 19.719 = -17.782$$

$$b = 2\left[\cos\frac{4\pi\omega_{n1}}{\omega_1} + \cos\frac{4\pi\omega_{n2}}{\omega_1}\right] - 2\left(\frac{\pi z_o}{e^*}\right)^2$$

$$= 2\left[\cos\frac{(4\pi)(1.75)}{(9.84)} + \cos\frac{(4\pi)(8.22)}{(9.84)}\right] - 2\left\{\frac{(\pi)(1)}{(1)}\right\}^2$$

$$= 2\left[-0.6293 - 0.1392\right] - 19.719 = -1.537 - 19.719 = 21.256$$

$$q = \frac{1}{2}(a^2 - b)$$

$$= \frac{1}{2}\left\{(-17.782)^2 - 21.256\right\} = 147.5$$

$$a^2 = (-17.782)^2 = 316.2$$

$$\left\{\frac{1}{2}(q+2)\right\}^2 = \left\{\frac{1}{2}(147.5+2)\right\}^2 = 5587$$

$$a^2 \qquad \left\{\frac{1}{2}(q+2)\right\}^2$$

The system is stable.

3.8.4 Elastic Pendulum - Six-Degrees-of-Freedom

The solution of the general equations describing the behavior of the six-degree-of-freedom pendulum system is considerably more difficult than that of the three-degree-of-freedom system. While an indication of the stability of the system may be obtained by neglecting some of the eccentricities and reducing the problem to one of two- or three-degrees-of-freedom, the complete solution must be undertaken before final design of the isolation system and fixing of rattlespace dimensions.

A rigorous approach to the general problem would require that the pendulum motion be considered as spherical, its position being defined by the two angles ϕ and θ (Figure 3.8.9). Although theoretically feasible, such a solution is extremely complicated and for most applications can be simplified by the following restrictions without sacrificing the needed accuracy.

- The pendulum motion is considered to be planar rather than spherical, i.e., θ is assumed to be zero.
- The pendulum motion is restricted to the xz plane.
- Secondary effects are ignored by letting $\sin \phi = \phi$ and $\cos \phi = 1$.

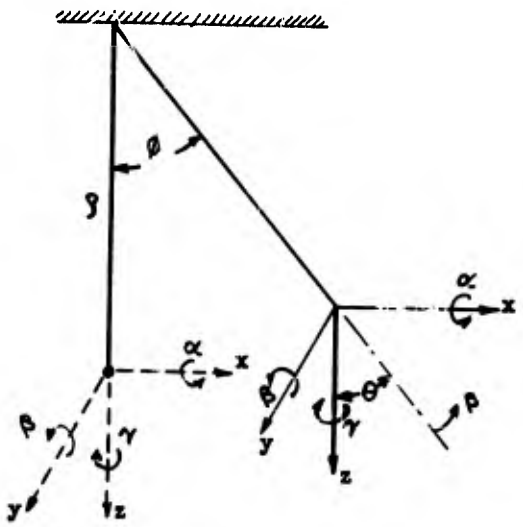

Figure 3.8.9

Coordinate System for Six-Degree-of-Freedom Pendulum

The first two assumptions limit the use of the solution to those cases in which horizontal disturbances occur in the xy plane, implying that the pendulum will swing in the plane of the disturbance. While this is not true, the deviations for strong horizontal shocks are of the second order. It may be noted that the xyz axes need not be the principal axes, so that in any problem the xy plane can be aligned with the direction of the horizontal disturbance.

If there is no horizontal disturbance, or if the horizontal forces due to the shock are small with respect to those due to eccentricities, the direction of the pendulum motion may not be readily apparent. In these cases it is necessary to assume a direction of horizontal motion and check for a maximum response by repeating the calculation for adjacent orientations of the xz plane.

The third assumption implies that the second order coupling effects are negligible. To determine whether or not this will be the case, it is necessary to employ some criterion of stability. The simplest method is to reduce the problem to three-degrees-of-freedom by ignoring eccentricities in the xy plane and to apply the stability criteria given in the previous subsection. If the system configuration exhibits a high degree of stability by this test, it is unlikely that the neglected eccentricities will alter the situation appreciably.

With these approximations, the six general equations of motion in matrix form are as follows, their derivation being given elsewhere in the text.

$$\begin{bmatrix} m & 0 & 0 \\ 0 & m & 0 \\ 0 & 0 & m \end{bmatrix} \begin{bmatrix} \ddot{x} + \ell\ddot{\phi} \\ \ddot{y} \\ \ddot{z} \end{bmatrix} + \left\{ \begin{bmatrix} c_{11} & c_{12} & c_{13} \\ c_{21} & c_{22} & c_{23} \\ c_{31} & c_{32} & c_{33} \end{bmatrix} + \phi \begin{bmatrix} \bar{c}_{11} & \bar{c}_{12} & \bar{c}_{13} \\ \bar{c}_{21} & \bar{c}_{22} & \bar{c}_{23} \\ \bar{c}_{31} & \bar{c}_{32} & \bar{c}_{33} \end{bmatrix} \right\} \begin{bmatrix} x + \ell\phi \\ y \\ z \end{bmatrix} +$$

$$\left\{ \begin{bmatrix} b_{11} & b_{12} & b_{13} \\ b_{21} & b_{22} & b_{23} \\ b_{31} & b_{32} & b_{33} \end{bmatrix} + \phi \begin{bmatrix} \bar{b}_{11} & \bar{b}_{12} & \bar{b}_{13} \\ \bar{b}_{21} & \bar{b}_{22} & \bar{b}_{23} \\ \bar{b}_{31} & \bar{b}_{32} & \bar{b}_{33} \end{bmatrix} \right\} \begin{bmatrix} \alpha \\ \beta \\ \gamma \end{bmatrix} = - \begin{bmatrix} m & 0 & 0 \\ 0 & m & 0 \\ 0 & 0 & m \end{bmatrix} \begin{bmatrix} \ddot{x}_o \\ \ddot{y}_o \\ \ddot{z}_o \end{bmatrix} - \begin{bmatrix} mg\,\phi \\ 0 \\ 0 \end{bmatrix}$$

$$\begin{bmatrix} m & 0 & 0 \\ 0 & m & 0 \\ 0 & 0 & m \end{bmatrix} \begin{bmatrix} \rho^2_{xx} & -\rho^2_{xy} & -\rho^2_{xz} \\ -\rho^2_{yx} & \rho^2_{yy} & -\rho^2_{yz} \\ -\rho^2_{zx} & -\rho^2_{zy} & \rho^2_{zz} \end{bmatrix} \begin{bmatrix} \ddot{\alpha} \\ \ddot{\beta} \\ \ddot{\gamma} \end{bmatrix} + \left\{ \begin{bmatrix} b_{11} & b_{21} & b_{31} \\ b_{12} & b_{22} & b_{32} \\ b_{13} & b_{23} & b_{33} \end{bmatrix} + \phi \begin{bmatrix} \bar{b}_{11} & \bar{b}_{21} & \bar{b}_{31} \\ \bar{b}_{12} & \bar{b}_{22} & \bar{b}_{32} \\ \bar{b}_{13} & \bar{b}_{23} & \bar{b}_{33} \end{bmatrix} \right\} \begin{bmatrix} x + \ell\phi \\ y \\ z \end{bmatrix} +$$

$$\left\{ \begin{bmatrix} e_{11} & e_{12} & e_{13} \\ e_{21} & e_{22} & e_{23} \\ e_{31} & e_{32} & e_{33} \end{bmatrix} + \phi \begin{bmatrix} \bar{e}_{11} & \bar{e}_{12} & \bar{e}_{13} \\ \bar{e}_{21} & \bar{e}_{22} & \bar{e}_{23} \\ \bar{e}_{31} & \bar{e}_{32} & \bar{e}_{33} \end{bmatrix} \right\} \begin{bmatrix} \alpha \\ \beta \\ \gamma \end{bmatrix} = 0$$

The pendulum angle ϕ is defined by kinematic relationship

$$\sin \phi = \frac{x}{\sqrt{x^2 + z^2}}$$

or $$\phi \cong \frac{x}{z} .$$

The [C] , [B] , and [E] matrices have two parts each; a part with coefficients c_{ij}, b_{ij}, and e_{ij}, which is the nonpendulum constant part, and a part with coefficients, $\bar{c}_{ij}$, $\bar{b}_{ij}$, and $\bar{e}_{ij}$, which produce the nonlinear coupling of the six nonpendulum coordinates, with the pendulum angle ϕ. For $\phi = 0$, the second part, i.e., the time-dependent nonlinear part of the [C] , [B] , and [E] matrices vanishes, and further, the equations are then identical with the nonpendulum equations of cases A and B of Section 3.5.5 . Cases C and D incorporate the pendulum terms for the same examples used in cases A and B, respectively. However, this analysis is limited to setting up the equations of nonlinear coupling. For a complete solution, the input must be known in time and numerical or electric analog procedures must be employed.

3.8.4.1 Linear Isolators, No Eccentricities, Pendulum Action Considered (Case C)

The same three arrangements of linear isolators as considered for case A in Section 3.5.5.1 are considered here as a pendulum suspended system, the center of symmetry of the isolators being coincident with the center of gravity of the isolated mass. As previously discussed, there is the pendulum angle ϕ coordinate to be considered in this case. This has the effect of making the [C] , [B] , and [E] matrices time-dependent instead of constant, and introduces the additional problem of solving simultaneous differential equations with time-dependent coefficients, that is, rheolinear equations. As previously mentioned, a simple pendulum oriented to oscillate in the xz plane, contains a nonlinear coupling between the pendulum angle ϕ and some of the nonpendulum coordinates x, y, z, α , β , and γ . Although the eccentricities are zero there may exist a linear coupling between the nonpendulum coordinates, since a finite angle ϕ may destroy the symmetry of the isolator arrangement.

3.8.4.1.1 Example C-1: Horizontal Elastic Elements Omitted

The isolation system is as shown in Figure 3.8.10 .

Let K_a = axial stiffness of each isolator ($\phi = 0$)

$K_{\ell x}$ = lateral stiffness of each isolator in the direction of the x-axis ($\phi = 0$)

$K_{\ell y}$ = lateral stiffness of each isolator in the direction of the y-axis ($\phi = 0$)

Then for any pendulum angle ϕ, the stiffness matrix of each isolator is given by

$$|c|_{\phi} = \begin{bmatrix} K_{\ell x}\cos^2\phi + K_a \sin^2\phi & 0 & -\frac{\sin 2\phi}{2}(K_{\ell x} - K_a) \\ 0 & K_{\ell y} & 0 \\ -\frac{\sin 2\phi}{2}(K_{\ell x} - K_a) & 0 & (K_a\cos^2\phi + K_{\ell x}\sin^2\phi \end{bmatrix}$$

Based on these values for c_{ij}, the [C], [B], and [E] matrices are computed on the following pages. Any approximations are performed at the end in each case. The matrices can be substituted in the general equations on page 3.178 . In this case the [B] matrix is zero, hence the linear coupling of x, y, z, α, β, and γ is not encountered.

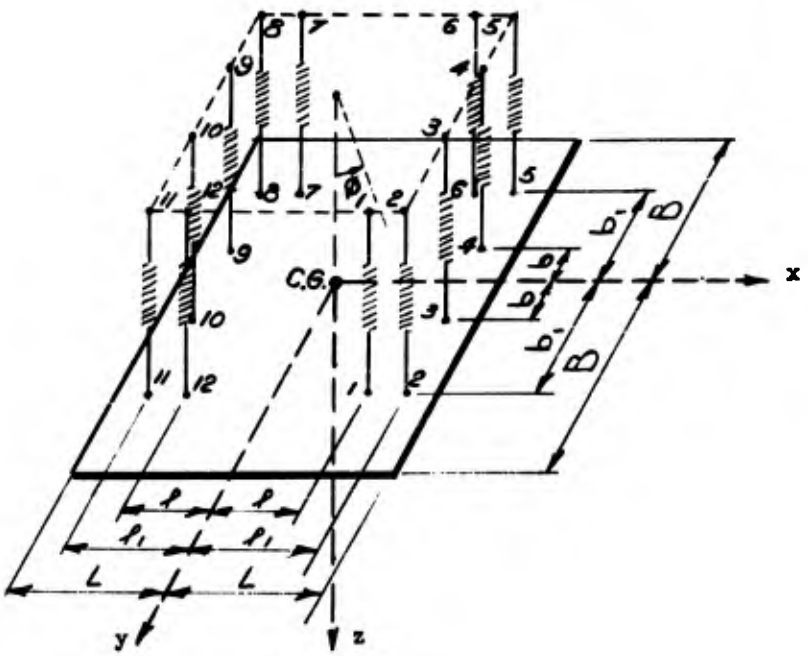

Figure 3.8.10
Symmetrical Elastic Pendulum without Horizontal Elements

Isolator Number	Axial Orientation	r_1	r_2	r_3	c_{11}	c_{22}	c_{33}	$c_{31}=c_{13}$	c_{21}, c_{23} c_{12}, c_{32}
1	Parallel to z-axis	ℓ	b_1	o	$K_{\ell x}\cos^2\phi+K_a\sin^2\phi$	$K_{\ell y}$	$K_a\cos^2\phi+K_{\ell x}\sin^2\phi$	$-\frac{\sin 2\phi}{2}(K_{\ell x}-K_a)$	o
2		ℓ_1	b_1	o	$K_{\ell x}\cos^2\phi+K_a\sin^2\phi$				o
3		ℓ_1	b	o					o
4		ℓ_1	-b	o					o
5		ℓ_1	$-b_1$	o					o
6		ℓ	$-b_1$	o					o
7		$-\ell$	$-b_1$	o					o
8		$-\ell_1$	$-b_1$	o					o
9		$-\ell_1$	-b	o					o
10		$-\ell_1$	b	o					o
11		$-\ell_1$	b_1	o					o
12	Parallel to z-axis	$-\ell$	b_1	o	$K_{\ell x}\cos^2\phi+K_a\sin^2\phi$	$K_{\ell y}$	$K_a\cos^2\phi+K_{\ell x}\sin^2\phi$	$-\frac{\sin 2\phi}{2}(K_{\ell x}-K_a)$	o

$\sum$: $c_{11}=12(K_{\ell x}\cos^2\phi+K_a\sin^2\phi)$; $c_{22}=12K_{\ell y}$; $c_{33}=12(K_a\cos^2\phi+K_{\ell x}\sin^2\phi)$; $c_{31}=-12\frac{\sin 2\phi}{2}(K_{\ell x}-K_a)$; $c_{21}=0$; $c_{23}=0$; $c_{12}=0$; $c_{32}=0$

$$[c]=\begin{bmatrix} 12(K_{\ell x}\cos^2\phi+K_a\sin^2\phi) & o & -12(\frac{\sin 2\phi}{2})(K_{\ell x}-K_a) \\ o & 12K_{\ell y} & o \\ -12(\frac{\sin 2\phi}{2})(K_{\ell x}-K_a) & o & 12(K_{\ell x}\sin^2\phi+K_a\cos^2\phi) \end{bmatrix} + \begin{bmatrix} 12K_{\ell x} & o & o \\ o & 12K_{\ell y} & o \\ o & o & 12K_a \end{bmatrix} + \phi \begin{bmatrix} o & o & -12(K_{\ell x}-K_a) \\ o & o & o \\ -12(K_{\ell x}-K_a) & o & o \end{bmatrix}$$

b_{11} $(r_2c_{13}-r_3c_{12})$	b_{12} $(r_3c_{11}-r_1c_{13})$	b_{13} $(r_1c_{12}-r_2c_{11})$	b_{21} $(r_2c_{23}-r_3c_{22})$	b_{22} $(r_3c_{21}-r_1c_{23})$	b_{23} $(r_1c_{22}-r_2c_{21})$	b_{31} $(r_2c_{33}-r_3c_{32})$	b_{32} $(r_3c_{31}-r_1c_{33})$	b_{33} $(r_1c_{32}-r_2c_{31})$	Isolator No.
$-b_1\frac{\sin 2\beta}{2}(K_{1x}-K_a)$	$l\frac{\sin 2\beta}{2}(K_{1x}-K_a)$	$-b_1(K_{1x}\cos^2\beta+K_a\sin^2\beta)$	0	0	$l K_y$	$b_1(K_a\cos^2\beta+K_{1x}\sin^2\beta)$	$-l(K_a\cos^2\beta+K_{1x}\sin^2\beta)$	$-b_1\frac{\sin 2\beta}{2}(K_{1x}-K_a)$	1
$b_1\frac{\sin 2\beta}{2}(K_{1x}-K_a)$	$l_1\frac{\sin 2\beta}{2}(K_{1x}-K_a)$	$-b_1(K_{1x}\cos^2\beta+K_a\sin^2\beta)$	0	0	l_1K_y	$b_1(K_a\cos^2\beta+K_{1x}\sin^2\beta)$	$-l_1(K_a\cos^2\beta+K_{1x}\sin^2\beta)$	$-b_1\frac{\sin 2\beta}{2}(K_{1x}-K_a)$	2
$-b\frac{\sin 2\beta}{2}(K_{1x}-K_a)$	$l_1\frac{\sin 2\beta}{2}(K_{1x}-K_a)$	$-b(K_{1x}\cos^2\beta+K_a\sin^2\beta)$	0	0	l_1K_y	$b(K_a\cos^2\beta+K_{1x}\sin^2\beta)$	$-l_1(K_a\cos^2\beta+K_{1x}\sin^2\beta)$	$-b\frac{\sin 2\beta}{2}(K_{1x}-K_a)$	3
$b\frac{\sin 2\beta}{2}(K_{1x}-K_a)$	$l_1\frac{\sin 2\beta}{2}(K_{1x}-K_a)$	$b(K_{1x}\cos^2\beta+K_a\sin^2\beta)$	0	0	l_1K_y	$-b(K_a\cos^2\beta+K_{1x}\sin^2\beta)$	$l_1(K_a\cos^2\beta+K_{1x}\sin^2\beta)$	$b\frac{\sin 2\beta}{2}(K_{1x}-K_a)$	4
$b_1\frac{\sin 2\beta}{2}(K_{1x}-K_a)$	$l_1\frac{\sin 2\beta}{2}(K_{1x}-K_a)$	$b_1(K_{1x}\cos^2\beta+K_a\sin^2\beta)$	0	0	l_1K_y	$-b_1(K_a\cos^2\beta+K_{1x}\sin^2\beta)$	$-l_1(K_a\cos^2\beta+K_{1x}\sin^2\beta)$	$-b_1\frac{\sin 2\beta}{2}(K_{1x}-K_a)$	5
$b_1\frac{\sin 2\beta}{2}(K_{1x}-K_a)$	$l\frac{\sin 2\beta}{2}(K_{1x}-K_a)$	$b_1(K_{1x}\cos^2\beta+K_a\sin^2\beta)$	0	0	l_1K_y	$-b(K_a\cos^2\beta+K_{1x}\sin^2\beta)$	$-l(K_a\cos^2\beta+K_{1x}\sin^2\beta)$	$-b_1\frac{\sin 2\beta}{2}(K_{1x}-K_a)$	6
$b_1\frac{\sin 2\beta}{2}(K_{1x}-K_a)$	$-l\frac{\sin 2\beta}{2}(K_{1x}-K_a)$	$b_1(K_{1x}\cos^2\beta+K_a\sin^2\beta)$	0	0	$-l K_y$	$-b_1(K_a\cos^2\beta+K_{1x}\sin^2\beta)$	$l(K_a\cos^2\beta+K_{1x}\sin^2\beta)$	$-b_1\frac{\sin 2\beta}{2}(K_{1x}-K_a)$	7
$b_1\frac{\sin 2\beta}{2}(K_{1x}-K_a)$	$-l_1\frac{\sin 2\beta}{2}(K_{1x}-K_a)$	$b_1(K_{1x}\cos^2\beta+K_a\sin^2\beta)$	0	0	$-l_1K_y$	$-b_1(K_a\cos^2\beta+K_{1x}\sin^2\beta)$	$l_1(K_a\cos^2\beta+K_{1x}\sin^2\beta)$	$-b_1\frac{\sin 2\beta}{2}(K_{1x}-K_a)$	8
$-b\frac{\sin 2\beta}{2}(K_{1x}-K_a)$	$-l_1\frac{\sin 2\beta}{2}(K_{1x}-K_a)$	$b(K_{1x}\cos^2\beta+K_a\sin^2\beta)$	0	0	$-l_1K_y$	$-b(K_a\cos^2\beta+K_{1x}\sin^2\beta)$	$l_1(K_a\cos^2\beta+K_{1x}\sin^2\beta)$	$-b\frac{\sin 2\beta}{2}(K_{1x}-K_a)$	9
$-b\frac{\sin 2\beta}{2}(K_{1x}-K_a)$	$-l_1\frac{\sin 2\beta}{2}(K_{1x}-K_a)$	$-b(K_{1x}\cos^2\beta+K_a\sin^2\beta)$	0	0	$-l_1K_y$	$b(K_a\cos^2\beta+K_{1x}\sin^2\beta)$	$-l_1(K_a\cos^2\beta+K_{1x}\sin^2\beta)$	$b\frac{\sin 2\beta}{2}(K_{1x}-K_a)$	10
$-b_1\frac{\sin 2\beta}{2}(K_{1x}-K_a)$	$-l_1\frac{\sin 2\beta}{2}(K_{1x}-K_a)$	$-b_1(K_{1x}\cos^2\beta+K_a\sin^2\beta)$	0	0	$-l_1K_y$	$b_1(K_a\cos^2\beta+K_{1x}\sin^2\beta)$	$l_1(K_a\cos^2\beta+K_{1x}\sin^2\beta)$	$b_1\frac{\sin 2\beta}{2}(K_{1x}-K_a)$	11
$-b_1\frac{\sin 2\beta}{2}(K_{1x}-K_a)$	$-l\frac{\sin 2\beta}{2}(K_{1x}-K_a)$	$-b_1(K_{1x}\cos^2\beta+K_a\sin^2\beta)$	0	0	$-l_1K_y$	$b_1(K_a\cos^2\beta+K_{1x}\sin^2\beta)$	$l(K_a\cos^2\beta+K_{1x}\sin^2\beta)$	$b_1\frac{\sin 2\beta}{2}(K_{1x}-K_a)$	12
0	0	0	0	0	0	0	0	0	Σ

$[b] = 0$

Isolator Number	$e_{11}=r_2b_{31}-r_3b_{21}$	$e_{12}=r_2b_{32}-r_3b_{22}$	$e_{13}=r_2b_{33}-r_3b_{23}$	$e_{21}=r_3b_{11}-r_1b_{31}$	$e_{22}=r_3b_{12}-r_1b_{32}$
1	$b_1^2(K_a\cos^2\phi+K_{\ell x}\sin^2\phi)$	$-b_1\ell_1(K_a\cos^2\phi+K_{\ell x}\sin^2\phi)$	$b_1\frac{2\sin2\phi}{2}(K_{\ell x}-K_a)$	$-b_1\ell_1(K_a\cos^2\phi+K_{\ell x}\sin^2\phi)$	$\ell_1^2(K_a\cos^2\phi+K_{\ell x}\sin^2\phi)$
2	$b_1^2(K_a\cos^2\phi+K_{\ell x}\sin^2\phi)$	$-b_1\ell_1(K_a\cos^2\phi+K_{\ell x}\sin^2\phi)$	$b_1\frac{2\sin2\phi}{2}(K_{\ell x}-K_a)$	$-b_1\ell_1(K_a\cos^2\phi+K_{\ell x}\sin^2\phi)$	$\ell_1^2(K_a\cos^2\phi+K_{\ell x}\sin^2\phi)$
3	$b^2(K_a\cos^2\phi+K_{\ell x}\sin^2\phi)$	$-b\ell_1(K_a\cos^2\phi+K_{\ell x}\sin^2\phi)$	$b\frac{2\sin2\phi}{2}(K_{\ell x}-K_a)$	$-b\ell_1(K_a\cos^2\phi+K_{\ell x}\sin^2\phi)$	$\ell_1^2(K_a\cos^2\phi+K_{\ell x}\sin^2\phi)$
4	$b^2(K_a\cos^2\phi+K_{\ell x}\sin^2\phi)$	$b\ell_1(K_a\cos^2\phi+K_{\ell x}\sin^2\phi)$	$b\frac{2\sin2\phi}{2}(K_{\ell x}-K_a)$	$b\ell_1(K_a\cos^2\phi+K_{\ell x}\sin^2\phi)$	$\ell_1^2(K_a\cos^2\phi+K_{\ell x}\sin^2\phi)$
5	$b_1^2(K_a\cos^2\phi+K_{\ell x}\sin^2\phi)$	$b_1\ell_1(K_a\cos^2\phi+K_{\ell x}\sin^2\phi)$	$b_1\frac{2\sin2\phi}{2}(K_{\ell x}-K_a)$	$b_1\ell_1(K_a\cos^2\phi+K_{\ell x}\sin^2\phi)$	$\ell_1^2(K_a\cos^2\phi+K_{\ell x}\sin^2\phi)$
6	$b_1^2(K_a\cos^2\phi+K_{\ell x}\sin^2\phi)$	$b_1\ell(K_a\cos^2\phi+K_{\ell x}\sin^2\phi)$	$b_1\frac{2\sin2\phi}{2}(K_{\ell x}-K_a)$	$b_1\ell(K_a\cos^2\phi+K_{\ell x}\sin^2\phi)$	$\ell^2(K_a\cos^2\phi+K_{\ell x}\sin^2\phi)$
7	$b_1^2(K_a\cos^2\phi+K_{\ell x}\sin^2\phi)$	$-b_1\ell(K_a\cos^2\phi+K_{\ell x}\sin^2\phi)$	$b_1\frac{2\sin2\phi}{2}(K_{\ell x}-K_a)$	$-b_1\ell(K_a\cos^2\phi+K_{\ell x}\sin^2\phi)$	$\ell^2(K_a\cos^2\phi+K_{\ell x}\sin^2\phi)$
8	$b_1^2(K_a\cos^2\phi+K_{\ell x}\sin^2\phi)$	$-b_1\ell_1(K_a\cos^2\phi+K_{\ell x}\sin^2\phi)$	$b_1\frac{2\sin2\phi}{2}(K_{\ell x}-K_a)$	$-b_1\ell_1(K_a\cos^2\phi+K_{\ell x}\sin^2\phi)$	$\ell_1^2(K_a\cos^2\phi+K_{\ell x}\sin^2\phi)$
9	$b^2(K_a\cos^2\phi+K_{\ell x}\sin^2\phi)$	$-b\ell_1(K_a\cos^2\phi+K_{\ell x}\sin^2\phi)$	$b\frac{2\sin2\phi}{2}(K_{\ell x}-K_a)$	$-b\ell_1(K_a\cos^2\phi+K_{\ell x}\sin^2\phi)$	$\ell_1^2(K_a\cos^2\phi+K_{\ell x}\sin^2\phi)$
10	$b^2(K_a\cos^2\phi+K_{\ell x}\sin^2\phi)$	$b\ell_1(K_a\cos^2\phi+K_{\ell x}\sin^2\phi)$	$b\frac{2\sin2\phi}{2}(K_{\ell x}-K_a)$	$b\ell_1(K_a\cos^2\phi+K_{\ell x}\sin^2\phi)$	$\ell_1^2(K_a\cos^2\phi+K_{\ell x}\sin^2\phi)$
11	$b_1^2(K_a\cos^2\phi+K_{\ell x}\sin^2\phi)$	$b_1\ell_1(K_a\cos^2\phi+K_{\ell x}\sin^2\phi)$	$b_1\frac{2\sin2\phi}{2}(K_{\ell x}-K_a)$	$b_1\ell_1(K_a\cos^2\phi+K_{\ell x}\sin^2\phi)$	$\ell_1^2(K_a\cos^2\phi+K_{\ell x}\sin^2\phi)$
12	$b_1^2(K_a\cos^2\phi+K_{\ell x}\sin^2\phi)$	$b_1\ell(K_a\cos^2\phi+K_{\ell x}\sin^2\phi)$	$b_1\frac{2\sin2\phi}{2}(K_{\ell x}-K_a)$	$b_1\ell(K_a\cos^2\phi+K_{\ell x}\sin^2\phi)$	$\ell^2(K_a\cos^2\phi+K_{\ell x}\sin^2\phi)$

$\sum$: $e_{11}=4(b^2+2b_1^2)(K_a\cos^2\phi+K_{\ell x}\sin^2\phi)$; $e_{12}=0$; $e_{13}=4(b^2+b_1^2)(\frac{\sin2\phi}{2})(K_{\ell x}-K_a)$; $e_{21}=0$; $e_{22}=4(\ell^2+2\ell_1^2)(K_a\cos^2\phi+K_{\ell x}\sin^2\phi)$

Isolator No.	$\epsilon_{23} = r_3 b_{13} - r_1 b_{33}$	$\epsilon_{31} = r_1 b_{21} - r_2 b_{11}$	$\epsilon_{32} = r_1 b_{22} - r_2 b_{12}$	$\epsilon_{33} = r_1 b_{23} - r_2 b_{13}$
1	$-b_1 l \frac{\sin 2\phi}{2} (K_{fx} - K_a)$	$b_1^2 \frac{\sin 2\phi}{2} (K_{fx} - K_a)$	$-b_1 l \frac{\sin 2\phi}{2} (K_{fx} - K_a)$	$l^2 K_{fy} + b_1^2 (K_{fx}\cos^2\phi + K_a \sin^2\phi)$
2	$-b_1 l_1 \frac{\sin 2\phi}{2} (K_{fx} - K_a)$	$b_1^2 \frac{\sin 2\phi}{2} (K_{fx} - K_a)$	$-b_1 l_1 \frac{\sin 2\phi}{2} (K_{fx} - K_a)$	$l_1^2 K_{fy} + b_1^2 (K_{fx}\cos^2\phi + K_a \sin^2\phi)$
3	$-b l_1 \frac{\sin 2\phi}{2} (K_{fx} - K_a)$	$b^2 \frac{\sin 2\phi}{2} (K_{fx} - K_a)$	$-b l_1 \frac{\sin 2\phi}{2} (K_{fx} - K_a)$	$l_1^2 K_{fy} + b^2 (K_{fx}\cos^2\phi + K_a \sin^2\phi)$
4	$b l_1 \frac{\sin 2\phi}{2} (K_{fx} - K_a)$	$b^2 \frac{\sin 2\phi}{2} (K_{fx} - K_a)$	$b l_1 \frac{\sin 2\phi}{2} (K_{fx} - K_a)$	$l_1^2 K_{fy} + b^2 (K_{fx}\cos^2\phi + K_a \sin^2\phi)$
5	$b_1 l_1 \frac{\sin 2\phi}{2} (K_{fy} - K_a)$	$b_1^2 \frac{\sin 2\phi}{2} (K_{fx} - K_a)$	$b_1 l_1 \frac{\sin 2\phi}{2} (K_{fx} - K_a)$	$l_1^2 K_{fy} + b_1^2 (K_{fx}\cos^2\phi + K_a \sin^2\phi)$
6	$b_1 l \frac{\sin 2\phi}{2} (K_{fx} - K_a)$	$b_1^2 \frac{\sin 2\phi}{2} (K_{fx} - K_a)$	$b_1 l \frac{\sin 2\phi}{2} (K_{fx} - K_a)$	$l^2 K_{fy} + b_1^2 (K_{fx}\cos^2\phi + K_a \sin^2\phi)$
7	$-b_1 l \frac{\sin 2\phi}{2} (K_{fx} - K_a)$	$b_1^2 \frac{\sin 2\phi}{2} (K_{fx} - K_a)$	$-b_1 l \frac{\sin 2\phi}{2} (K_{fx} - K_a)$	$l^2 K_{fy} + b_1^2 (K_{fx}\cos^2\phi + K_a \sin^2\phi)$
8	$-b_1 l_1 \frac{\sin 2\phi}{2} (K_{fx} - K_a)$	$b_1^2 \frac{\sin 2\phi}{2} (K_{fx} - K_a)$	$-b_1 l_1 \frac{\sin 2\phi}{2} (K_{fx} - K_a)$	$l_1^2 K_{fy} + b_1^2 (K_{fx}\cos^2\phi + K_a \sin^2\phi)$
9	$-b l_1 \frac{\sin 2\phi}{2} (K_{fx} - K_a)$	$b^2 \frac{\sin 2\phi}{2} (K_{fx} - K_a)$	$-b l_1 \frac{\sin 2\phi}{2} (K_{fx} - K_a)$	$l_1^2 K_{fy} + b^2 (K_{fx}\cos^2\phi + K_a \sin^2\phi)$
10	$b l_1 \frac{\sin 2\phi}{2} (K_{fx} - K_a)$	$b^2 \frac{\sin 2\phi}{2} (K_{fx} - K_a)$	$b l_1 \frac{\sin 2\phi}{2} (K_{fx} - K_a)$	$l_1^2 K_{fy} + b^2 (K_{fx}\cos^2\phi + K_a \sin^2\phi)$
11	$b_1 l_1 \frac{\sin 2\phi}{2} (K_{fx} - K_a)$	$b_1^2 \frac{\sin 2\phi}{2} (K_{fx} - K_a)$	$b_1 l_1 \frac{\sin 2\phi}{2} (K_{fx} - K_a)$	$l_1^2 K_{fy} + b_1^2 (K_{fx}\cos^2\phi + K_a \sin^2\phi)$
12	$b_1 l \frac{\sin 2\phi}{2} (K_{fx} - K_a)$	$b_1^2 \frac{\sin 2\phi}{2} (K_{fx} - K_a)$	$b_1 l \frac{\sin 2\phi}{2} (K_{fx} - K_a)$	$l^2 K_{fy} + b_1^2 (K_{fx}\cos^2\phi + K_a \sin^2\phi)$
$\sum$	$\epsilon_{23} = 0$	$\epsilon_{31} = -4(b^2+2b_1^2) \frac{\sin 2\phi}{2} (K_{fx} - K_a)$	$\epsilon_{32} = 0$	$\epsilon_{33} = 4\left[(l^2+2l_1^2)K_{fy} + (b^2+b_1^2)(K_{fx}\cos^2\phi + K_a \sin^2\phi)\right]$

$$[E] = \begin{bmatrix} 4(b^2+2b_1^2)(K_a\cos^2\phi + K_{fx}\sin^2\phi) & 0 & 4(b^2+2b_1^2)(\frac{\sin 2\phi}{2})(K_{fx}-K_a) \\ 0 & 4(l^2+2l_1^2)(K_a\cos^2\phi + K_{fx}\sin^2\phi) & 0 \\ +4(b^2+2b_1^2)(\frac{\sin 2\phi}{2})(K_{fx}-K_a) & 0 & 4(l^2+2l_1^2)K_{fy} \\ & & 4(b^2+2b_1^2)(K_{fx}\cos^2\phi + K_a \sin^2\phi) \end{bmatrix} =$$

$$\begin{bmatrix} 4(b^2+2b_1^2)K & 0 & 0 \\ 0 & 4(l^2+2l_1^2)K_a & 0 \\ 0 & 0 & 4(l^2+2l_1^2)K_{fy} \\ & & 4(b^2+2b_1^2)K_{fx} \end{bmatrix} + \phi \begin{bmatrix} 0 & 0 & 4(b^2+2b_1^2) \\ 0 & 0 & (K_{fx}-K_a) \\ 4(b^2+2b_1^2) & 0 & 0 \\ (K_{fx}-K_a) & & \end{bmatrix}$$

3.8.4.1.2 Example C-2: Horizontal Elastic Elements Inclined to Axis

The arrangement of the isolators is as shown in Figure 3.8.11. Let

K_a = axial stiffness of each vertical isolator

$K_{\ell v}$ = lateral stiffness of each vertical isolator

K_{ah} = axial stiffness of each horizontal isolator

$K_{\ell h}$ = lateral stiffness of each horizontal isolator

For the vertical isolators, as in the case of Example C-1, and for a pendulum angle of ϕ, the stiffness matrix of each isolator is given by:

$$[C]_\phi = \begin{bmatrix} (K_{\ell v}\cos^2\phi + K_{av}\sin^2\phi) & 0 & -\frac{\sin 2\phi}{2}(K_{\ell v} - K_{av}) \\ 0 & K_{\ell v} & 0 \\ -\frac{\sin 2\phi}{2}(K_{\ell v} - K_{av}) & 0 & (K_{av}\cos^2\phi + K_{\ell v}\sin^2\phi) \end{bmatrix}$$

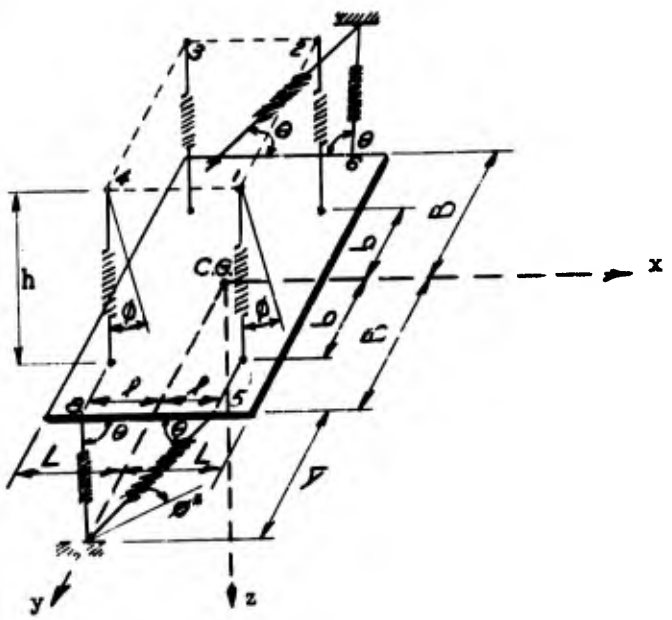

Figure 3.8.11
Symmetrical Elastic Pendulum with Inclined Horizontal Elements

Isolator Number	r_1	r_2	r_3	c_{11}	c_{22}	c_{33}	$c_{12}=c_{21}$	$c_{31}=c_{13}$	$c_{23}=c_{32}$
1	ℓ	b	o	$K_{\ell v}\cos^2\phi+K_{av}\sin^2\phi$	$K_{\ell v}$	$K_{av}\cos^2\phi+K_{\ell v}\sin^2\phi$	o	$-\frac{\sin 2\phi}{2}(K_{\ell v}-K_{av})$	o
2	ℓ	-b	o	$K_{\ell v}\cos^2\phi+K_{av}\sin^2\phi$	$K_{\ell v}$	$K_{av}\cos^2\phi+K_{\ell v}\sin^2\phi$	o	$\frac{\sin 2\phi}{2}(K_{\ell v}-K_{av})$	o
3	$-\ell$	-b	o	$K_{\ell v}\cos^2\phi+K_{av}\sin^2\phi$	$K_{\ell v}$	$K_{av}\cos^2\phi+K_{\ell v}\sin^2\phi$	o	$-\frac{\sin 2\phi}{2}(K_{\ell v}-K_{av})$	o
4	$-\ell$	b	o	$K_{\ell v}\cos^2\phi+K_{av}\sin^2\phi$	$K_{\ell v}$	$K_{av}\cos^2\phi+K_{\ell v}\sin^2\phi$	o	$-\frac{\sin 2\phi}{2}(K_{\ell v}-K_{av})$	o
5	ℓ	B	o	$K_{ah}\cos^2(\theta-\phi^*)+K_{\ell h}\sin^2(\theta-\phi^*)$	$K_{\ell h}\cos^2(\theta-\phi^*)+K_{ah}\sin^2(\theta-\phi^*)$	$K_{\ell h}$	$\frac{\sin 2(\theta-\phi^*)}{2}\left[K_{av}-K_{\ell h}\right]$	o	o
6	ℓ	-B	o	$K_{ah}\cos^2(\theta-\phi^*)+K_{\ell h}\sin^2(\theta-\phi^*)$	$K_{\ell h}\cos^2(\theta-\phi^*)+K_{ah}\sin^2(\theta-\phi^*)$	$K_{\ell h}$	$+\frac{\sin 2(\theta-\phi^*)}{2}\left[K_{ah}-K_{\ell h}\right]$	o	o
7	$-\ell$	-B	o	$K_{ah}\cos^2(\theta+\phi^*)+K_{\ell h}\sin^2(\theta+\phi^*)$	$K_{\ell h}\cos^2(\theta+\phi^*)+K_{ah}\sin^2(\theta+\phi^*)$	$K_{\ell h}$	$\frac{\sin 2(\theta+\phi^*)}{2}\left[K_{ah}-K_{\ell h}\right]$	o	o
8	$-\ell$	B	o	$K_{ah}\cos^2(\theta+\phi^*)+K_{\ell h}\sin^2(\theta+\phi^*)$	$K_{\ell h}\cos^2(\theta+\phi^*)+K_{ah}\sin^2(\theta+\phi^*)$	$K_{\ell h}$	$+\frac{\sin 2(\theta+\phi^*)}{2}\left[K_{ah}-K_{\ell h}\right]$	o	o

$\sum$: $c_{11}=4\left[(K_{\ell v}\cos^2\phi+K_{av}\sin^2\phi)+2\,K_{ah}\cos^2(\theta+\phi^*)+K_{\ell h}\sin^2(\theta-\phi^*)\right]+2\left[K_{ah}\cos^2(\theta+\phi^*)+K_{\ell h}{}^2(\theta+\phi^*)\right]$; $c_{22}=4K_{\ell v}+2\left[K_{\ell h}\cos^2(\theta-\phi^*)+K_{ah}\sin^2(\theta-\phi^*)\right]+2\left[K_{\ell h}\cos^2(\theta+\phi^*)+K_{ah}\sin^2(\theta+\phi^*)\right]$; $c_{33}=4\left[K_{\ell h}+K_{av}\cos^2\phi+K_{\ell v}\sin^2\phi\right]$; $c_{12}=0$; $c_{31}=-4\frac{\sin 2\phi}{2}(K_{\ell v}-K_{av})$; $c_{23}=0$

$$[c]=\begin{bmatrix} 4\left[K_{\ell v}\cos^2\phi+K_{av}\sin^2\phi\right] & & \\ +2\left[K_{ah}\cos^2(\theta-\phi^*)+K_{\ell h}\sin^2(\theta-\phi^*)\right] & o & -4\frac{\sin 2\phi}{2}(K_{\ell v}-K_{av}) \\ +2\left[K_{ah}\cos^2(\theta+\phi^*)+K_{\ell h}\sin^2(\theta+\phi^*)\right] & & \\ & 4\,K_{\ell v}+2K_{\ell h}\cos^2(\theta-\phi^*) & \\ o & +2K_{ah}\sin^2(\theta-\phi^*) & o \\ & +2K_{\ell h}\cos^2(\theta+\phi^*) & \\ & +2K_{ah}\sin^2(\theta+\phi^*) & \\ -4\frac{\sin 2\phi}{2}(K_{\ell h}-K_{av}) & o & 4\left[K_{\ell h}+K_{av}\cos^2\phi \right. \\ & & \left. +K_{\ell v}\sin^2\phi\right] \end{bmatrix} \approx \begin{bmatrix} 4\left[K_{\ell v}+K_{ah}\cos^2\theta \right. & o & o \\ \left. +K_{\ell h}\sin^2\theta\right] & & \\ o & 4\left[K_{\ell v}+K_{\ell h}\cos^2\theta \right. & o \\ & \left. +K_{ah}\sin^2\theta\right] & \\ o & o & 4(K_{\ell h}+K_{av}) \end{bmatrix}$$

$$+\phi\begin{bmatrix} o & o & -4(K_{\ell h}-K_{av}) \\ o & o & o \\ -4(K_{\ell h}-K_{av}) & o & o \end{bmatrix}$$

Isolator No.	b_{11} $(r_2c_{13} - r_3c_{12})$	b_{12} $(r_3c_{11} - r_1c_{13})$	b_{13} $(r_1c_{12} - r_2c_{11})$	b_{21} $(r_2c_{23} - r_3c_{22})$	b_{22} $(r_3c_{21} - r_1c_{23})$
1	$-b\frac{\sin 2\phi}{2}(K_{jv} - K_{av})$	$+j\frac{\sin 2\phi}{2}(K_{jv} - K_{av})$	$-b(K_{jv}\cos^2\phi + K_{av}\sin^2\phi)$	0	0
2	$+b\frac{\sin 2\phi}{2}(K_{jv} - K_{av})$	$+j\frac{\sin 2\phi}{2}(K_{jv} - K_{av})$	$b(K_{jv}\cos^2\phi + K_{av}\sin^2\phi)$	0	0
3	$+b\frac{\sin 2\phi}{2}(K_{jv} - K_{av})$	$-j\frac{\sin 2\phi}{2}(K_{jv} - K_{av})$	$b(K_{jv}\cos^2\phi + K_{av}\sin^2\phi)$	0	0
4	$-b\frac{\sin 2\phi}{2}(K_{jv} - K_{av})$	$-j\frac{\sin 2\phi}{2}(K_{jv} - K_{av})$	$-b(K_{jv}\cos^2\phi + K_{av}\sin^2\phi)$	0	0
5	0	0	$-j\frac{\sin 2(\theta - \phi^*)}{2}(K_{ah} - K_{jh})$ $-B\{K_{ah}\cos^2(\theta - \phi^*) + K_{jh}\sin^2(\theta - \phi^*)\}$	0	0
6	0	0	$j\frac{\sin 2(\theta - \phi^*)}{2}(K_{ah} - K_{jh})$ $B\{K_{ah}\cos^2(\theta - \phi^*) + K_{jh}\sin^2(\theta - \phi^*)\}$	0	0
7	0	0	$j\frac{\sin 2(\theta + \phi^*)}{2}(K_{ah} - K_{jh})$ $B\{K_{ah}\cos^2(\theta - \phi^*) + K_{jh}\sin^2(\theta + \phi^*)\}$	0	0
8	0	0	$-j\frac{\sin 2(\theta + \phi^*)}{2}(K_{ah} - K_{jh})$ $B\{K_{ah}\cos^2(\theta + \phi^*) + K_{jh}\sin^2(\theta + \phi^*)\}$	0	0
$\sum_i$	0	0	0	0	0

Isolator Number	b_{23} $(r_1c_{22}-r_2c_{21})$	b_{31} $(r_2c_{33}-r_3c_{32})$	b_{32} $(r_3c_{31}-r_1c_{33})$	b_{33} $(r_1c_{32}-r_2c_{31})$
1	$\ell K_{\ell v}$	$b(K_{av}\cos^2\phi+K_{\ell v}\sin^2\phi)$	$-\ell(K_{av}\cos^2\phi+K_{\ell v}\sin^2\phi)$	$b\frac{\sin2\phi}{2}(K_{\ell v}-K_{av})$
2	$\ell K_{\ell v}$	$-b(K_{av}\cos^2\phi+K_{\ell v}\sin^2\phi)$	$-\ell(K_{av}\cos^2\phi+K_{\ell v}\sin^2\phi)$	$-b\frac{\sin2\phi}{2}(K_{\ell v}-K_{av})$
3	$-\ell K_{\ell v}$	$-b(K_{av}\cos^2\phi+K_{\ell v}\sin^2\phi)$	$\ell(K_{av}\cos^2\phi+K_{\ell v}\sin^2\phi)$	$-b\frac{\sin2\phi}{2}(K_{\ell v}-K_{av})$
4	$-\ell K_{\ell v}$	$b(K_{av}\cos^2\phi+K_{\ell v}\sin^2\phi)$	$\ell(K_{av}\cos^2\phi+K_{\ell v}\sin^2\phi)$	$b\frac{\sin2\phi}{2}(K_{\ell v}-K_{av})$
5	$\ell K_{\ell h}\cos^2(\theta-\phi^*)+K_{ah}\sin^2(\theta-\phi^*)$ $+B\frac{\sin2(\theta-\phi^*)}{2}(K_{ah}-K_{\ell h})$	$BK_{\ell h}$	$-K_{\ell h}$	o
6	$\ell K_{\ell h}\cos^2(\theta-\phi^*)+K_{ah}\sin^2(\theta-\phi^*)$ $+B\frac{\sin2(\theta-\phi^*)}{2}(K_{ah}-K_{\ell h})$	$-BK_{\ell h}$	$-K_{\ell h}$	o
7	$-\ell K_{\ell h}\cos^2(\theta+\phi^*)+K_{ah}\sin^2(\theta+\phi^*)$ $-B\frac{\sin2(\theta-\phi^*)}{2}(K_{ah}+K_{\ell h})$	$-BK_{\ell h}$	$K_{\ell h}$	o
8	$-\ell K_{\ell h}\cos^2(\theta+\phi^*)+K_{ah}\sin^2(\theta+\phi^*)$ $-B\frac{\sin2(\theta-\phi^*)}{2}(K_{ah}+K_{\ell h})$	$BK_{\ell h}$	$K_{\ell h}$	o
$\sum$:	$b_{23}=0$;	$b_{31}=0$;	$b_{32}=0$;	$b_{33}=0$

$$\therefore \quad [B] = o$$

Isolator Number	e_{11} $(r_2b_{31}-r_3b_{21})$	e_{12} $(r_2b_{32}-r_3b_{22})$	e_{13} $(r_2b_{33}-r_3b_{23})$	e_{21} $(r_3b_{11}-r_1b_{31})$	e_{22} $(r_3b_{12}-r_1b_{32})$	e_{23} $(r_3b_{13}-r_1b_{33})$
1	$b^2(K_{av}\cos^2\phi+K_{\ell v}\sin^2\phi)$	$-b\ell(K_{av}\cos^2\phi+K_{\ell v}\sin^2\phi)$	$b^2\frac{\sin2\phi}{2}(K_{\ell v}-K_{av})$	$-\ell b(K_{av}\cos^2\phi+K_{\ell v}\sin^2\phi)$	$\ell^2(K_{av}\cos^2\phi+K_{\ell v}\sin^2\phi)$	$-b\ell\frac{\sin2\phi}{2}(K_{\ell v}-K_{av})$
2	$b^2(K_{av}\cos^2\phi+K_{\ell v}\sin^2\phi)$	$b\ell(K_{av}\cos^2\phi+K_{\ell v}\sin^2\phi)$	$b^2\frac{\sin2\phi}{2}(K_{\ell v}-K_{av})$	$\ell b(K_{av}\cos^2\phi+K_{\ell v}\sin^2\phi)$	$\ell^2(K_{av}\cos^2\phi+K_{\ell v}\sin^2\phi)$	$b\ell\frac{\sin2\phi}{2}(K_{\ell v}-K_{av})$
3	$b^2(K_{av}\cos^2\phi+K_{\ell v}\sin^2\phi)$	$-b\ell(K_{av}\cos^2\phi+K_{\ell v}\sin^2\phi)$	$b^2\frac{\sin2\phi}{2}(K_{\ell v}-K_{av})$	$-\ell b(K_{av}\cos^2\phi+K_{\ell v}\sin^2\phi)$	$\ell^2(K_{av}\cos^2\phi+K_{\ell v}\sin^2\phi)$	$-b\ell\frac{\sin2\phi}{2}(K_{\ell v}-K_{av})$
4	$b^2(K_{av}\cos^2\phi+K_{\ell v}\sin^2\phi)$	$b\ell(K_{av}\cos^2\phi+K_{\ell v}\sin^2\phi)$	$b^2\frac{\sin2\phi}{2}(K_{\ell v}-K_{av})$	$\ell b(K_{av}\cos^2\phi+K_{\ell v}\sin^2\phi)$	$\ell^2(K_{av}\cos^2\phi+K_{\ell v}\sin^2\phi)$	$b\ell\frac{\sin2\phi}{2}(K_{\ell v}-K_{av})$
5	$B^2K_{\ell h}$	$-\ell BK_{\ell h}$	0	$-B\ell K_{\ell h}$	$\ell^2K_{\ell h}$	0
6	$B^2K_{\ell h}$	$\ell BK_{\ell h}$	0	$B\ell K_{\ell h}$	$\ell^2K_{\ell h}$	0
7	$B^2K_{\ell h}$	$-\ell BK_{\ell h}$	0	$-B\ell K_{\ell h}$	$\ell^2K_{\ell h}$	0
8	$B^2K_{\ell h}$	$\ell BK_{\ell h}$	0	$B\ell K_{\ell h}$	$\ell^2K_{\ell h}$	0

$\sum$ $e_{11}=4\left[b^2(K_{av}\cos^2\phi+K_{\ell v}\sin^2\phi)+B^2K_{\ell h}\right]$; $e_{12}=0$; $e_{13}=4b^2\frac{\sin2\phi}{2}(K_{\ell v}-K_{av})$; $e_{21}=0$; $e_{22}=4\left[\ell^2(K_{av}\cos^2\phi+K_{\ell v}\sin^2\phi)+\ell^2K_{\ell h}\right]$; $e_{23}=0$

Isolator Number	e_{31} $(r_1b_{21}-r_2b_{11})$	e_{32} $(r_1b_{22}-r_2b_{12})$	e_{33} $(r_1b_{23}-r_2b_{13})$
1	$b^2\frac{\sin 2\phi}{2}(K_{\rho v}-K_{av})$	$-b\ell\frac{\sin 2\phi}{2}(K_{\rho v}-K_{av})$	$\ell^2K_{\rho v}+b^2(K_{\rho v}\cos^2\phi+K_{av}\sin^2\phi)$
2	$b^2\frac{\sin 2\phi}{2}(K_{\rho v}-K_{av})$	$b\ell\frac{\sin 2\phi}{2}(K_{\rho v}-K_{av})$	$\ell^2K_{\rho v}+b^2(K_{\rho v}\cos^2\phi+K_{av}\sin^2\phi)$
3	$b^2\frac{\sin 2\phi}{2}(K_{\rho v}-K_{av})$	$-b\ell\frac{\sin 2\phi}{2}(K_{\rho v}-K_{av})$	$\ell^2K_{\rho v}+b^2(K_{\rho v}\cos^2\phi+K_{av}\sin^2\phi)$
4	$b^2\frac{\sin 2\phi}{2}(K_{\rho v}-K_{av})$	$b\ell\frac{\sin 2\phi}{2}(K_{\rho v}-K_{av})$	$\ell^2K_{\rho v}+b^2(K_{\rho v}\cos^2\phi+K_{av}\sin^2\phi)$
5	0	0	$\ell^2\{K_{\rho h}\cos^2(\theta-\phi^*)+K_{ah}\sin^2(\theta-\phi^*)\}+2B\ell\frac{\sin 2(\theta-\phi^*)}{2}(K_{ah}-K_{\rho h})$ $+B^2\{K_{ah}\cos^2(\theta-\phi^*)+K_{\rho h}\sin^2(\theta-\phi^*)\}$
6	0	0	$\ell^2\{K_{\rho h}\cos^2(\theta-\phi^*)+K_{ah}\sin^2(\theta-\phi^*)\}+2B\ell\frac{\sin 2(\theta-\phi^*)}{2}(K_{ah}-K_{\rho h})$ $+B^2\{K_{ah}\cos^2(\theta-\phi^*)+K_{\rho h}\sin^2(\theta-\phi^*)\}$
7	0	0	$\ell^2\{K_{\rho h}\cos^2(\theta+\phi^*)+K_{ah}\sin^2(\theta+\phi^*)\}+2B\ell\frac{\sin 2(\theta+\phi^*)}{2}(K_{ah}-K_{\ell h})$ $+B^2\{K_{ah}\cos^2(\theta+\phi^*)+K_{\ell h}\sin^2(\theta+\phi^*)\}$
8	0	0	$\ell^2\{K_{\rho h}\cos^2(\theta+\phi^*)+K_{ah}\sin^2(\theta+\phi^*)\}+2B\ell\frac{\sin 2(\theta+\phi^*)}{2}(K_{ah}-K_{\ell h})$ $+B^2\{K_{ah}\cos^2(\theta+\phi^*)+K_{\rho h}\sin^2(\theta+\phi^*)\}$

$\sum$: $e_{31}=4b^2\frac{\sin 2\phi}{2}(K_{\rho v}-K_{av})$; $e_{32}=0$; $e_{33}=4\{\ell^2K_{\ell v}+b^2(K_{\rho v}\cos^2\phi+K_{av}\sin^2\phi)\}+2[\ell^2\{K_{\rho h}\cos^2(\theta-\phi^*)+K_{ah}\sin^2(\theta-\phi^*)\}$ $+2B\ell\frac{\sin 2(\theta-\phi^*)}{2}(K_{ah}-K_{\ell h})+B^2\{K_{ah}\cos^2(\theta-\phi^*)+K_{\rho h}\sin^2(\theta-\phi^*)\}]+2[\ell^2\{K_{\rho h}\cos^2(\theta-\phi^*)+K_{ah}\sin^2(\theta-\phi^*)\}$ $+2B\ell\frac{\sin 2(\theta+\phi^*)}{2}(K_{ah}-K_{\rho h})+B^2\{K_{ah}\cos^2(\theta+\phi^*)+K_{\rho h}\sin^2(\theta+\phi^*)\}]$

$$[E]=\begin{bmatrix} 4\{B^2K_{\ell h}+b^2(K_{av}\cos^2\phi+K_{\rho v}\sin^2\phi)\} & 0 & 4b^2\frac{\sin 2\phi}{2}(K_{\rho v}-K_{av}) \\ 0 & 4\{\ell^2K_{\ell h}+\ell^2(K_{av}\cos^2\phi+K_{\ell v}\sin^2\phi)\} & 0 \\ 4b^2\frac{\sin 2\phi}{2}(K_{\rho v}-K_{av}) & 0 & \begin{array}{l}4\{\ell^2K_{\ell v}+b^2(K_{\rho v}\cos^2\phi+K_{av}\sin^2\phi)\} \\ +2[\ell^2\{K_{\rho h}\cos^2(\theta-\phi^*)+K_{ah}\sin^2(\theta-\phi^*)\} \\ +2B\ell\frac{\sin 2(\theta-\phi^*)}{2}(K_{ah}-K_{\ell h}) \\ +B^2\{K_{ah}\cos^2(\theta-\phi^*)+K_{\rho h}\sin^2(\theta-\phi^*)\} \\ +2[\ell^2\{K_{\ell h}\cos^2(\theta+\phi^*)+K_{ah}\sin^2(\theta+\phi^*)\} \\ +2B\ell\frac{\sin 2(\theta+\phi^*)}{2}(K_{ah}-K_{\rho h}) \\ +B^2\{K_{ah}\cos^2(\theta+\phi^*)+K_{\rho h}\sin^2(\theta+\phi^*)\}]\end{array} \end{bmatrix}$$

$$\begin{bmatrix} 4(B^2K_{\ell h}+b^2K_{av}) & 0 & 0 \\ 0 & 4(\ell^2K_{\rho h}+\ell^2K_{av}) & 0 \\ 0 & 0 & \begin{array}{l}4[\ell^2K_{\rho v}+b^2K_{\ell v} \\ +\ell^2(K_{\rho h}\cos^2\theta+K_{ah}\sin^2\theta) \\ +B^2(K_{ah}\cos^2\theta+K_{\ell h}\sin^2\theta) \\ +2B\ell\frac{\sin 2\theta}{2}(K_{ah}-K_{\ell h})]\end{array} \end{bmatrix} + \phi^* \begin{bmatrix} 0 & 0 & 4b^2(K_{\rho v}-K_{av}) \\ 0 & 0 & 0 \\ -4b^2(K_{\rho v}-K_{av}) & 0 & 0 \end{bmatrix}$$

For the horizontal inclined isolators, when $\phi = 0$ the stiffness matrix of each isolator will be identical with the one obtained in Example A-2 (Section 3.5.5.1.1). It is seen that, for a given pendulum motion of the center of gravity of the isolated mass, as defined by ϕ, the angular rotation of the horizontal isolators in the xy plane is given approximately by

$$\phi^* = \left(\frac{h}{2\bar{y}} \sin 2\theta\right) \phi.$$

Hence, for a given pendulum angle ϕ, the stiffness matric for isolator 5 is:

$$[C]_\phi = \begin{bmatrix} K_{ah}\cos^2(\theta - \phi^*) + K_{\ell h}\sin^2(\theta-\phi^*) - \frac{\sin 2(\theta-\phi^*)}{2}(K_{ah}-K_{\ell h}) & 0 \\ -\frac{\sin 2(\theta-\phi^*)}{2}(K_{ah}-K_{\ell h}) & K_{\ell h}\cos^2(\theta-\phi^*) + K_{ah}\sin^2(\theta-\phi^*) \quad 0 \\ 0 \qquad\qquad 0 & K_{\ell h} \end{bmatrix}$$

Similarly, the stiffness matrices for isolators 6, 7, and 8 can be calculated for a given pendulum angle ϕ. The [C], [B], and [E] matrices are tabulated on the following pages, the approximations in this case being:

$$\cos(\theta \pm \phi^*) \cong \cos\theta \; ; \qquad \sin(\theta \pm \phi^*) = \sin\theta$$

Here again the [B] matrix reduces to zero, hence the linear coupling of x, y, z, α, β, and γ is not encountered.

3.8.4.1.3 Example C-3: Horizontal Elastic Elements Parallel to Both Axes

The isolator arrangement consists of elements in the x, y, and z directions, as shown in Figure 3.8.12 . Let:

K_{1a} = axial stiffness of each isolator oriented parallel to the x axis

$K_{1\ell y}$ = lateral stiffness in y direction of each isolator parallel to the x axis

$K_{1\ell z}$ = lateral stiffness in z direction of each isolator parallel to the x axis

K_{2a} = axial stiffness of each isolator oriented parallel to the y axis

$K_{2\ell x}$ = lateral stiffness in x direction of each isolator parallel to the y axis

$K_{2\ell z}$ = lateral stiffness in z direction of each isolator to y axis

K_{3a} = axial stiffness of each isolator oriented parallel to the z axis

K_{3fx} = lateral stiffness in x direction of each isolator parallel to z axis

K_{3fy} = lateral stiffness in y direction of each isolator parallel to z axis.

For a pendulum displacement ϕ, measured to the center of gravity of the isolated mass, isolators 9, 10, 11, and 12 which are oriented parallel to the z axis also move through an angle equal to ϕ. However, isolators 1, 4, 5, and 8 undergo an angular displacement in the xy plane, given by

$$\phi^* = \frac{h}{\bar{y}} \phi.$$

Any rotation of isolators 2, 3, 6, and 7 in the xz plane is assumed to be negligible.

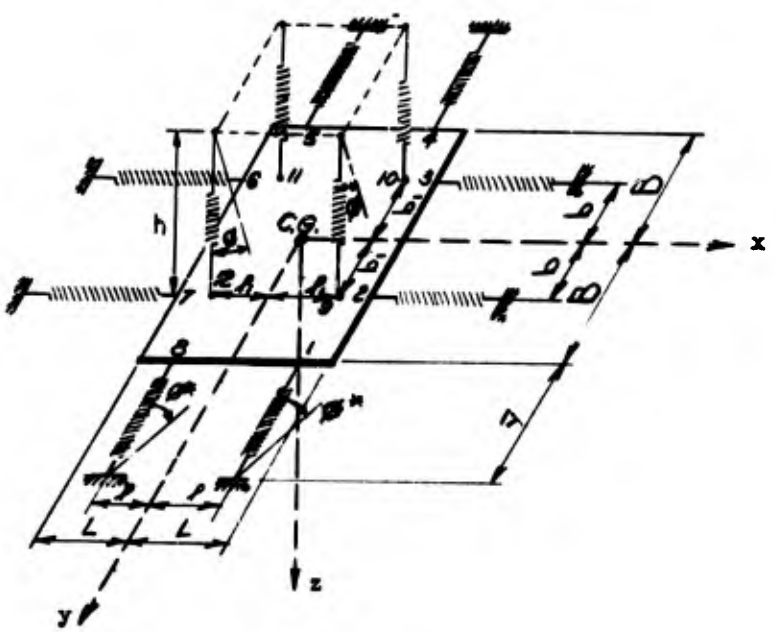

Figure 3.8.12

Symmetrical Elastic Pendulum with Parallel Horizontal Elements

Isolator Number	Axial Orientation	r1	r2	r3	c_{11}	c_{22}	c_{33}	$c_{21}=c_{12}$	$c_{31}=c_{13}$	$c_{23}=c_{32}$
1	Parallel to y-axis	ℓ	B	o	$(K_{2\ell x}\cos^2\phi^* + K_{2a}\sin^2\phi^*)$	$(K_{2\ell x}\sin^2\phi^* + K_{2a}\cos^2\phi^*)$	$K_{2\ell z}$	$-\frac{\sin 2\phi^*}{2}(K_{2a}-K_{2\ell x})$	o	o
4		ℓ	-B	o				$\frac{\sin(2\phi^*)}{2}(K_{2a}-K_{2\ell x})$	o	o
5		$-\ell$	-B	o				$\frac{\sin(2\phi^*)}{2}(K_{2a}-K_{2\ell y})$	o	o
8	Parallel to y-axis	$-\ell$	B	o	$(K_{2\ell x}\cos^2\phi^* + K_{2a}\sin^2\phi^*)$	$(K_{2\ell x}\sin^2\phi^* + K_{2a}\cos^2\phi^*)$	$K_{2\ell z}$	$-\frac{\sin(2\phi^*)}{2}(K_{2a}-K_{2\ell x})$	o	o
2	Parallel to x-axis	L	b	o	K_{1a}	$K_{1\ell y}$	$K_{1\ell z}$	o	o	o
3		L	-b	o				o	o	o
6		-L	-b	o				o	o	o
7	Parallel to x-axis	-	b	o	K_{1a}	$K_{1\ell y}$	$K_{1\ell z}$	o	o	o
9	Parallel to z-axis	ℓ_1	b_1	o	$(K_{3\ell x}\cos^2\phi + K_{3a}\sin^2\phi)$	$K_{3\ell y}$	$(K_{3\ell x}\sin^2\phi + K_{3a}\cos^2\phi)$	o	$-\frac{\sin 2\phi}{2}(K_{3\ell x}-K_{3a})$	o
10		ℓ_1	$-b_1$	o				o		o
11		$-\ell_1$	$-b_1$	o				o		o
12	Parallel to z-axis	$-\ell_1$	b_1	o	$(K_{3\ell x}\cos^2\phi + K_{3a}\sin^2\phi)$	$K_{3\ell y}$	$(K_{3\ell x}\sin^2\phi + K_{3a}\cos^2\phi)$	o	$\frac{\sin 2\phi}{2}(K_{3\ell x}-K_{3a})$	o

$\sum$: $c_{11}=4\{K_{1a}+K_{2\ell x}\cos^2\phi^*+K_{2a}\sin^2\phi^*+K_{3\ell x}\cos^2\phi+K_{3a}\sin^2\phi\}$; $c_{22}=4\{K_{1\ell y}+K_{2\ell x}\sin^2\phi^*+K_{2a}\cos^2\phi^*+K_{3\ell y}\}$; $c_{33}=4\{K_{1\ell z}+K_{2\ell z}+K_{3\ell x}\sin^2\phi+K_{3a}\cos^2\phi\}$; $c_{21}=0$; $c_{31}=-\frac{\sin 2\phi}{2}(K_{3\ell x}-K_{3a})(4)$; $c_{23}=0$

$$[c]=\begin{bmatrix} 4\{K_{1a}+K_{2\ell x}\cos^2\phi^*+K_{2a}\sin^2\phi^* & o & -(4)\frac{\sin(2\phi)}{2}(K_{3\ell x}-K_{3a}) \\ +K_{3\ell x}\cos^2\phi+K_{3a}\sin^2\phi\} & & \\ o & 4\{K_{1\ell y}+K_{2\ell x}\sin^2\phi^* & o \\ & +K_{2a}\cos^2\phi^*+K_{3\ell y}\} & \\ -\left\{(4)\frac{\sin 2\phi}{2}(K_{3\ell x}-K_{3a})\right\} & o & 4\{K_{1\ell z}+K_{3\ell x}\sin^2\phi \\ & & +K_{2\ell z}+K_{3a}\cos^2\phi\} \end{bmatrix} -$$

$$\begin{bmatrix} 4(K_{1a}+K_{2\ell x}+K_{3\ell x}) & o & o \\ o & 4(K_{1\ell y}+K_{3\ell y}+K_{2a}) & o \\ o & o & 4(K_{1\ell z}+K_{2\ell z}+K_{3a}) \end{bmatrix} + \phi \begin{bmatrix} o & o & -4(K_{3\ell x}-K_{3a}) \\ o & o & o \\ -4(K_{3\ell x}-K_{3a}) & o & o \end{bmatrix}$$

Isolator No.	b_{11} $(r_2c_{31}-r_3c_{12})$	b_{12} $(r_3c_{11}-r_1c_{13})$	b_{13} $(r_1c_{12}-r_2c_{11})$	b_{21} $(r_2c_{23}-r_3c_{22})$	b_{22} $(r_3c_{21}-r_1c_{23})$
1	0	0	$-\ell(K_{2a}-K_{2\ell x})\frac{\sin 2\phi_*}{2} - B(K_{2\ell x}\cos^2\phi_* + K_{2a}\sin^2\phi_*)$	0	0
4	0	0	$\ell(K_{2a}-K_{2\ell x})\frac{\sin 2\phi_*}{2} + B(K_{2\ell x}\cos^2\phi_* + K_{2a}\sin^2\phi_*)$	0	0
5	0	0	$-\ell(K_{2a}-K_{2\ell x})\frac{\sin 2\phi_*}{2} + B(K_{2\ell x}\cos^2\phi_* + K_{2a}\sin^2\phi_*)$	0	0
8	0	0	$\ell(K_{2a}-K_{2\ell x})\frac{\sin 2\phi_*}{2} - B(K_{2\ell x}\cos^2\phi_* + K_{2a}\sin^2\phi_*)$	0	0
2	0	0	$-bK_{1a}$	0	0
3	0	0	bK_{1a}	0	0
6	0	0	bK_{1a}	0	0
7	0	0	$-bK_{1a}$	0	0
9	$-b_1(K_{3\ell x}-K_{3a})\frac{\sin 2\phi}{2}$	$1(K_{3\ell x}-K_{3a})\frac{\sin 2\phi}{2}$	$-b_1(K_{3\ell x}\cos^2\phi + K_{3a}\sin^2\phi)$	0	0
10	$+b_1(K_{3\ell x}-K_{3a})\frac{\sin 2\phi}{2}$	$1(K_{3\ell x}-K_{3a})\frac{\sin 2\phi}{2}$	$b_1(K_{3\ell x}\cos^2\phi + K_{3a}\sin^2\phi)$	0	0
11	$+b_1(K_{3\ell x}-K_{3a})\frac{\sin 2\phi}{2}$	$-1(K_{3\ell x}-K_{3a})\frac{\sin 2\phi}{2}$	$b_1(K_{3\ell x}\cos^2\phi + K_{3a}\sin^2\phi)$	0	0
12	$-b_1(K_{3\ell x}-K_{3a})\frac{\sin 2\phi}{2}$	$-1(K_{3\ell x}-K_{3a})\frac{\sin 2\phi}{2}$	$b_1(K_{3\ell x}\cos^2\phi + K_{3a}\sin^2\phi)$	0	0
Σ	0	0	0	0	0

Isolator Number	b_{23} $(r_1c_{22}-r_2c_{21})$	b_{31} $(r_2c_{33}-r_3c_{32})$	b_{32} $(r_3c_{31}-r_1c_{33})$	b_{33} $(r_1c_{32}-r_2c_{31})$
1	$(K_{2\ell x}\sin^2\phi^*+K_{2a}\cos^2\phi^*)+B(K_{2a}-K_{2\ell x})\frac{\sin 2\phi^*}{2}$	$BK_{2\ell z}$	$-\ell K_{2\ell z}$	0
4	$(K_{2\ell x}\sin^2\phi^*+K_{2a}\cos^2\phi^*)+B(K_{2a}-K_{2\ell x})\frac{\sin 2\phi^*}{2}$	$-BK_{2\ell z}$	$-\ell K_{2\ell z}$	0
5	$-(K_{2\ell x}\sin^2\phi^*+K_{2a}\cos^2\phi^*)+B(K_{2a}-K_{2\ell x})\frac{\sin 2\phi^*}{2}$	$-BK_{2\ell z}$	$\ell K_{2\ell z}$	0
8	$-(K_{2\ell x}\sin^2\phi^*+K_{2a}\cos^2\phi^*)+B(K_{2a}-K_{2\ell x})\frac{\sin 2\phi^*}{2}$	$BK_{2\ell z}$	$\ell K_{2\ell z}$	0
2	$LK_{1\ell y}$	$bK_{1\ell z}$	$-LK_{1\ell z}$	0
3	$LK_{1\ell y}$	$-bK_{1\ell z}$	$-LK_{1\ell z}$	0
6	$-LK_{1\ell y}$	$-bK_{1\ell z}$	$LK_{1\ell z}$	0
7	$-LK_{1\ell y}$	$bK_{1\ell z}$	$LK_{1\ell z}$	0
9	$\ell_1 K_{3\ell y}$	$b_1(K_{3\ell x}\sin^2\phi+K_{3a}\cos^2\phi)$	$-\ell_1(K_{3\ell x}\sin^2\phi+K_{3a}\cos^2\phi)$	$b_1(K_{3\ell x}-K_{3a})\frac{\sin 2\phi}{2}$
10	$\ell_1 K_{3\ell y}$	$-b_1(K_{3\ell x}\sin^2\phi+K_{3a}\cos^2\phi)$	$-\ell_1(K_{3\ell x}\sin^2\phi+K_{3a}\cos^2\phi)$	$-b_1(K_{3\ell x}-K_{3a})\frac{\sin 2\phi}{2}$
11	$-\ell_1 K_{3\ell y}$	$-b_1(K_{3\ell x}\sin^2\phi+K_{3a}\cos^2\phi)$	$\ell_1(K_{3\ell x}\sin^2\phi+K_{3a}\cos^2\phi)$	$-b_1(K_{3\ell x}-K_{3a})\frac{\sin 2\phi}{2}$
12	$-\ell_1 K_{3\ell y}$	$b_1(K_{3\ell x}\sin^2\phi+K_{3a}\cos^2\phi)$	$\ell_1(K_{3\ell x}\sin^2\phi+K_{3a}\cos^2\phi)$	$b_1(K_{3\ell x}-K_{3a})\frac{\sin 2\phi}{2}$

$\sum$: $b_{23}=4B(K_{2a}-K_{2\ell x})\frac{\sin 2\phi^*}{2}$; $b_{31}=0$; $b_{32}=0$; $b_{33}=0$

$$[B] = \begin{bmatrix} 0 & 0 & 0 \\ 0 & 0 & +4B(K_{2a}-K_{2\ell x})\frac{\sin 2\phi^*}{2} \\ 0 & 0 & 0 \end{bmatrix} \cong \Phi \begin{bmatrix} 0 & 0 & 0 \\ 0 & 0 & +4B(K_{2a}-K_{2\ell x}) \\ 0 & 0 & 0 \end{bmatrix}$$

Isolator Number	e_{11} $(r_2b_{31}-r_3b_{21})$	e_{12} $(r_2b_{32}-r_3b_{22})$	e_{13} $(r_2b_{33}-r_3b_{23})$	e_{21} $(r_3b_{11}-r_1b_{31})$	e_{22} $(r_3b_{12}-r_1b_{32})$
1	$B^2K_{2\ell z}$	$-B\ell K_{2\ell z}$	0	$-B\ell K_{2\ell z}$	$\ell^2K_{2\ell z}$
4	$B^2K_{2\ell z}$	$B\ell K_{2\ell z}$	0	$B\ell K_{2\ell z}$	$\ell^2K_{2\ell z}$
5	$B^2K_{2\ell z}$	$-L\ell K_{2\ell z}$	0	$-B\ell K_{2\ell z}$	$\ell^2K_{2\ell z}$
8	$B^2K_{2\ell z}$	$B\ell K_{2\ell z}$	0	$B\ell K_{2\ell z}$	$\ell^2K_{2\ell z}$
2	$b^2K_{1\ell z}$	$-bLK_{1\ell z}$	0	$-bLK_{1\ell z}$	$L^2K_{1\ell z}$
3	$b^2K_{1\ell z}$	$bLK_{1\ell z}$	0	$bLK_{1\ell z}$	$L^2K_{1\ell z}$
6	$b^2K_{1\ell z}$	$-bLK_{1\ell z}$	0	$-bLK_{1\ell z}$	$L^2K_{1\ell z}$
7	$b^2K_{1\ell z}$	$bLK_{1\ell z}$	0	$bLK_{1\ell z}$	$L^2K_{1\ell z}$
9	$b_1^2(K_{3\ell x}\sin^2\phi+K_{3a}\cos^2\phi)$	$-b_1\ell_1(K_{3\ell x}\sin^2\phi+K_{3a}\cos^2\phi)$	$b_1^2(K_{3\ell x}-K_{3a})\frac{\sin2\phi}{2}$	$-b_1\ell_1(K_{3\ell x}\sin^2\phi+K_{3a}\cos^2\phi)$	$\ell_1^2(K_{3\ell x}\sin^2\phi+K_{3a}\cos^2\phi)$
10	$b_1^2(K_{3\ell x}\sin^2\phi+K_{3a}\cos^2\phi)$	$b_1\ell_1(K_{3\ell x}\sin^2\phi+K_{3a}\cos^2\phi)$	$b_1^2(K_{3\ell x}-K_{3a})\frac{\sin2\phi}{2}$	$b_1\ell_1(K_{3\ell x}\sin^2\phi+K_{3a}\cos^2\phi)$	$\ell_1^2(K_{3\ell x}\sin^2\phi+K_{3a}\cos2\phi$
11	$b_1^2(K_{3\ell x}\sin^2\phi+K_{3a}\cos^2\phi)$	$-b_1\ell_1(K_{3\ell x}\sin^2\phi+K_{3a}\cos^2\phi)$	$b_1^2(K_{3\ell x}-K_{3a})\frac{\sin2\phi}{2}$	$-b_1\ell_1(K_{3\ell x}\sin^2\phi+K_{3a}\cos^2\phi)$	$\ell_1^2(K_{3\ell x}\sin^2\phi+K_{3a}\cos2\phi$
12	$b_1^2(K_{3\ell x}\sin^2\phi+K_{3a}\cos^2\phi)$	$b_1\ell_1(K_{3\ell x}\sin^2\phi+K_{3a}\cos^2\phi)$	$b_1^2(K_{3\ell x}-K_{3a})\frac{\sin2\phi}{2}$	$b_1\ell_1(K_{3\ell x}\sin^2\phi+K_{3a}\cos^2\phi)$	$\ell_1^2(K_{3\ell x}\sin^2\phi+K_{3a}\cos^2\phi)$

$\sum$: $e_{11}=4\ b_1^2(K_{3\ell x}\sin^2\phi+K_{3a}\cos^2\phi)+B^2K_{2\ell z}+b^2K_{1\ell z}$; $e_{12}=0$; $e_{13}=-4b_1^2(K_{3a}-K_{3\ell x})\frac{\sin2\phi}{2}$; $e_{21}=0$; $e_{22}=4\ \ell^2K_{2\ell z}+L^2K_{1\ell z}+\ell_1^2(K_{3\ell x}\sin^2\phi+K_{3a}\cos^2\phi)$

Isolator Number	e_{23} $(r_3b_{13}-r_1b_{33})$	e_{31} $(r_1b_{21}-r_2b_{11})$	e_{32} $(r_1b_{22}-r_2b_{12})$	e_{33} $(r_1b_{23}-r_2b_{13})$
1	o	o	o	$\ell^2(K_{2\ell x}\sin^2\phi^*+K_{2a}\cos^2\phi^*)+2B\ell(K_{2a}-K_{2\ell x})\frac{\sin2\phi^*}{2}+B^2(K_{2\ell x}\cos^2\phi^*+K_{2a}\sin^2\phi^*)$
4	o	o	o	$\ell^2(K_{2\ell x}\sin^2\phi^*+K_{2a}\cos^2\phi^*)+2B\ell(K_{2a}-K_{2\ell x})\frac{\sin2\phi^*}{2}+B^2(K_{2\ell x}\cos^2\phi^*+K_{2a}\sin^2\phi^*)$
5	o	o	o	$\ell^2(K_{2\ell x}\sin^2\phi^*+K_{2a}\cos^2\phi^*)-2B\ell(K_{2a}-K_{2\ell x})\frac{\sin2\phi^*}{2}+B^2(K_{2\ell x}\cos^2\phi^*+K_{2a}\sin^2\phi^*)$
8	o	o	o	$\ell^2(K_{2\ell x}\sin^2\phi^*+K_{2a}\cos^2\phi^*)-2B\ell(K_{2a}-K_{2\ell x})\frac{\sin2\phi^*}{2}+B^2(K_{2\ell x}\cos^2\phi^*+K_{2a}\sin^2\phi^*)$
2	o	o	o	$L^2K_{1\ell y}+b^2K_{1a}$
3	o	o	o	$L^2K_{1\ell y}+b^2K_{1a}$
6	o	o	o	$L^2K_{1\ell y}+b^2K_{1a}$
7	o	o	o	$L^2K_{1\ell y}+b^2K_{1a}$
9	$-b_1\ell_1(K_{3\ell x}-K_{3a})\frac{\sin2\phi}{2}+b_1^2(K_{3\ell x}-K_{3a})\frac{\sin2\phi}{2}$		$-b_1\ell_1(K_{3\ell x}-K_{3a})\frac{\sin2\phi}{2}$	$\ell_1^2K_{3\ell y}+b_1^2(K_{3\ell x}\cos^2\phi+K_{3a}\sin^2\phi)$
10	$+b_1\ell_1(K_{3\ell x}-K_{3a})\frac{\sin2\phi}{2}+b_1^2(K_{3\ell x}-K_{3a})\frac{\sin2\phi}{2}$		$+b_1\ell_1(K_{3\ell x}-K_{3a})\frac{\sin2\phi}{2}$	$\ell_1^2K_{3\ell y}+b_1^2(K_{3\ell x}\cos^2\phi+K_{3a}\sin^2\phi)$
11	$-b_1\ell_1(K_{3\ell x}-K_{3a})\frac{\sin2\phi}{2}+b_1^2(K_{3\ell x}-K_{3a})\frac{\sin2\phi}{2}$		$-b_1\ell_1(K_{3\ell x}-K_{3a})\frac{\sin2\phi}{2}$	$\ell_1^2K_{3\ell y}+b_1^2(K_{3\ell x}\cos^2\phi+K_{3a}\sin^2\phi)$
12	$+b_1\ell_1(K_{3\ell x}-K_{3a})\frac{\sin2\phi}{2}+b_1^2(K_{3\ell x}-K_{3a})\frac{\sin2\phi}{2}$		$+b_1\ell_1(K_{3\ell x}-K_{3a})\frac{\sin2\phi}{2}$	$\ell_1^2K_{3\ell y}+b_1^2(K_{3\ell x}\cos^2\phi+K_{3a}\sin^2\phi)$

$\sum$: $e_{23}=0$; $e_{31}=+4b_1^2(K_{3\ell x}-K_{3a})\frac{\sin2\phi}{2}$; $e_{32}=0$; $e_{33}=4\left[\ell^2(K_{2\ell x}\sin^2\phi^*+K_{2a}\cos^2\phi^*)+B^2(K_{2\ell x}\cos^2\phi^*+K_{2a}\sin^2\phi^*)+(K_{3\ell x}\cos^2\phi+K_{3a}\sin^2\phi)+L^2K_{1\ell y}+b^2K_{1a}+\ell_1^2K_{3\ell y}\right]$

$$[E] = \begin{bmatrix} 4\left[b_1^2(K_{3\ell x}\sin^2\phi + K_{3a}\cos^2\phi) + B^2K_{2\ell z} + b^2K_{1\ell z}\right] & 0 & 4b_1^2(K_{3\ell x}-K_{3a})\frac{\sin 2\phi}{2} \\ 0 & 4\left[\ell_1^2(K_{3\ell x}\sin^2\phi + K_{3a}\cos^2\phi) + \ell^2K_{2\ell z} + L^2K_{1\ell z}\right] & 0 \\ 4b_1^2(K_{3\ell x}-K_{3a})\frac{\sin 2\phi}{2} & 0 & \begin{matrix} 4\left[\ell^2(K_{2\ell x}\sin^2\phi^* + K_{2a}\cos^2\phi^*)\right. \\ +B^2(K_{2\ell x}\cos^2\phi^* + K_{2a}\sin^2\phi^*) \\ +b_1^2(K_{3\ell x}\cos^2\phi + K_{3a}\sin^2\phi) \\ \left. +L^2K_{1\ell y} + b^2K_{1a} + \ell_1^2K_{3\ell y}\right] \end{matrix} \end{bmatrix}$$

$$\cong \begin{bmatrix} 4(b_1^2K_{3a} + B^2K_{2\ell z} + b^2K_{1\ell z}) & 0 & 0 \\ 0 & 4(\ell_1^2K_{3a} + \ell^2K_{2\ell z} + L^2K_{1\ell z}) & 0 \\ 0 & 0 & \begin{matrix} 4\,(B^2K_{2\ell x} + \ell^2K_{2a} + b_1^2K_{3\ell x} \\ L^2K_{1\ell y} + b^2K_{1a} + \ell_1^2K_{3\ell y}) \end{matrix} \end{bmatrix} + \phi \begin{bmatrix} 0 & 0 & 4b_1^2(K_{3\ell x}-K_{3a}) \\ 0 & 0 & 0 \\ 4b_1^2(K_{3\ell x}-K_{3a}) & 0 & 0 \end{bmatrix}$$

The stiffness matrix for the isolators oriented parallel to the z axis is:

$$[C]_{\phi} = \begin{bmatrix} (K_{3\ell x}\cos^2\phi + K_{3a}\sin^2\phi & 0 & -\frac{\sin 2\phi}{2}(K_{3\ell x} - K_{3a}) \\ 0 & K_{3\ell y} & 0 \\ -\frac{\sin 2\phi}{2}(K_{3\ell x} - K_{3a}) & 0 & (K_{3\ell x}\sin^2\phi + K_{3a}\cos^2\phi) \end{bmatrix}$$

The stiffness matrix for the isolators oriented to the y axis is:

$$[C]_{\phi^*} = \begin{bmatrix} (K_{2\ell x}\cos^2\phi^* + K_{2a}\sin^2\phi^*) & \pm\frac{\sin 2\phi}{2}(K_{2\ell x} - K_{2a}) & 0 \\ \pm\frac{\sin 2\phi^*}{2}(K_{2\ell x} - K_{2a}) & (K_{2\ell x}\sin^2\phi^* + K_{2a}\cos^2\phi^*) & 0 \\ 0 & 0 & K_{2\ell z} \end{bmatrix}$$

The $[C]$, $[B]$, and $[E]$ matrices have been evaluated on the following pages with the following additional approximations:

$$\sin\phi^* = \phi^*$$
$$\cos\phi^* = 1$$

In this example a linear coupling exists between the coordinates y and γ due to the asymmetry introduced by the pendulum angle ϕ.

3.8.4.2 Linear Isolators, Eccentrically Placed, Pendulum Action Considered (Case D)

The same three arrangements of linear isolators as for case B (Section 3.5.5.2) have been considered with the center of symmetry of the isolators being eccentric with respect to the center of gravity of the isolated mass. However, in addition to the nonlinear coupling of the pendulum angle ϕ with the coordinates x, y, z, α, β, and γ, there will exist a linear coupling between the coordinates x, y, z, α, β, and γ themselves due to the eccentricities. The equations obtained in this case are the most general equations for an isolated system behaving as a simple pendulum. The equations of case D can be reduced to those of cases A, B, and C by deleting the appropriate terms.

3.8.4.2.1 Example D-1: Horizontal Elastic Elements Omitted

The isolation system is as shown in Figure 3.8.13. The stiffness matrix is identical with that for Example C-1 (Section 3.8.4.1.1) and hence has not been rewritten here. The values of the $[B]$ and $[E]$ matrices, obtained by the standard formulas, are

derived on the following pages. In this case, in addition to the non-linear coupling of the pendulum angle of ϕ with the coordinates x, y, z, α, β, and γ, there exists a linear coupling of the coordinates x, y, z, α, β, and γ, among themselves. The approximations used in the previous examples have been applied here in setting up the [B] and [E] matrices.

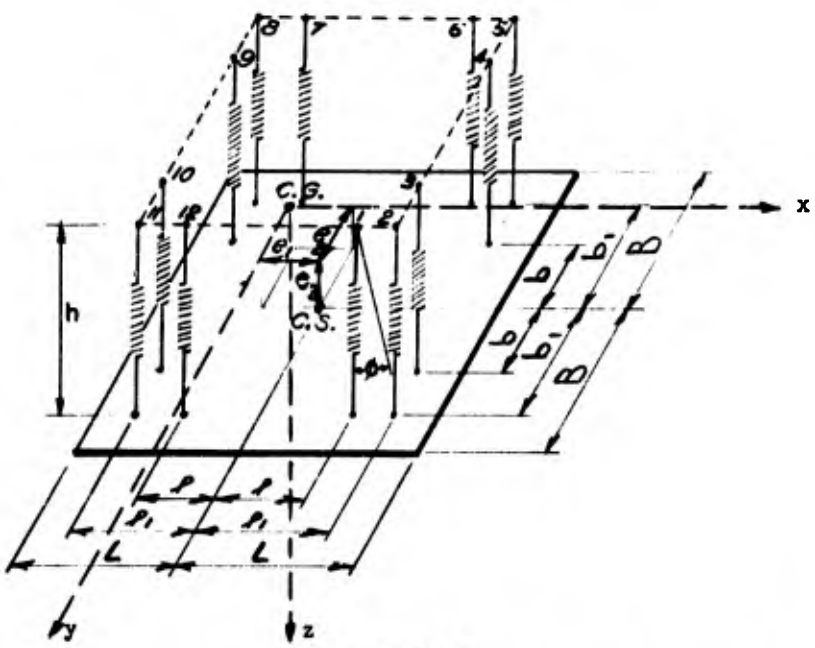

Figure 3.8.13

Unsymmetrical Elastic Pendulum with no Horizontal Elements

3.8.4.2.2 Example D-2: Horizontal Elastic Elements Inclined to Axis

The isolation system is as shown in Figure 3.8.14. The isolator stiffnesses are the same as in Example C-2 (Section 3.8.4.1.2), however the values of r_1, r_2, r_3 are modified to include the eccentricities. Thus, the [B] and [E] matrices are not similar to the [B] and [E] matrices of Example C-2. The evaluation of these [B] and [E] matrices is shown on the following pages. Note the linear and

Isolator Number	Axial Orientation	r_1	r_2	r_3	$b_{11}=r_2c_{13}-r_3c_{12}$	$b_{12}=r_3c_{11}-r_1c_{13}$	$b_{13}=r_1c_{12}-r_2c_{11}$
1	Parallel to z-axis	$\ell-e_1$	b_1+e_2	e_3	$-(b_1+e_2)\frac{\sin 2\phi}{2}(K_{\ell x}-K_a)$	$e_3(K_{\ell x}\cos^2\phi+K_a\sin^2\phi)+(\ell+e_1)\frac{\sin 2\phi}{2}(K_{\ell x}-K_a)$	$-(b_1+e_2)(K_{\ell x}\cos^2\phi+K_a\sin^2\phi)$
2	Parallel to z-axis	ℓ_1+e_1	b_1+e_2	e_3	$-(b_1+e_2)\frac{\sin 2\phi}{2}(K_{\ell x}-K_a)$	$e_3(K_{\ell x}\cos^2\phi+K_a\sin^2\phi)+(\ell_1+e_1)\frac{\sin 2\phi}{2}(K_{\ell x}-K_a)$	$-(b_1+e_2)(K_{\ell x}\cos^2\phi+K_a\sin^2\phi)$
3	Parallel to z-axis	ℓ_1+e_1	$b+e_2$	e_3	$-(b+e_2)\frac{\sin 2\phi}{2}(K_{\ell x}-K_a)$	$e_3(K_{\ell x}\cos^2\phi+K_a\sin^2\phi)+(\ell_1+e_1)\frac{\sin 2\phi}{2}(K_{\ell x}-K_a)$	$-(b+e_2)(K_{\ell x}\cos^2\phi+K_a\sin^2\phi)$
4	Parallel to z-axis	ℓ_1+e_1	e_2-b	e_3	$-(e_2-b)\frac{\sin 2\phi}{2}(K_{\ell x}-K_a)$	$e_3(K_{\ell x}\cos^2\phi+K_a\sin^2\phi)+(\ell_1+e_1)\frac{\sin 2\phi}{2}(K_{\ell x}-K_a)$	$-(e_2-b)(K_{\ell x}\cos^2\phi+K_a\sin^2\phi)$
5	Parallel to z-axis	ℓ_1+e_1	e_2-b_1	e_3	$-(e_2-b_1)\frac{\sin 2\phi}{2}(K_{\ell x}-K_a)$	$e_3(K_{\ell x}\cos^2\phi+K_a\sin^2\phi)+(\ell_1+e_1)\frac{\sin 2\phi}{2}(K_{\ell x}-K_a)$	$-(e_2-b_1)(K_{\ell x}\cos^2\phi+K_a\sin^2\phi)$
6	Parallel to z-axis	$\ell+e_1$	e_2-b_1	e_3	$-(e_2-b_1)\frac{\sin 2\phi}{2}(K_{\ell x}-K_a)$	$e_3(K_{\ell x}\cos^2\phi+K_a\sin^2\phi)+(\ell+e_1)\frac{\sin 2\phi}{2}(K_{\ell x}-K_a)$	$-(e_2-b_1)(K_{\ell x}\cos^2\phi+K_a\sin^2\phi)$
7	Parallel to z-axis	$e_1-\ell$	e_2-b_1	e_3	$-(e_2-b_1)\frac{\sin 2\phi}{2}(K_{\ell x}-K_a)$	$e_3(K_{\ell x}\cos^2\phi+K_a\sin^2\phi)+(e_1-\ell)\frac{\sin 2\phi}{2}(K_{\ell x}-K_a)$	$-(e_2-b_1)(K_{\ell x}\cos^2\phi+K_a\sin^2\phi)$
8	Parallel to z-axis	$e_1-\ell_1$	e_2-b_1	e_3	$-(e_2-b_1)\frac{\sin 2\phi}{2}(K_{\ell x}-K_a)$	$e_3(K_{\ell x}\cos^2\phi+K_a\sin^2\phi)+(e_1-\ell_1)\frac{\sin 2\phi}{2}(K_{\ell x}-K_a)$	$-(e_2-b_1)(K_{\ell x}\cos^2\phi+K_a\sin^2\phi)$
9	Parallel to z-axis	$e_1-\ell_1$	e_2-b	e_3	$-(e_2-b)\frac{\sin 2\phi}{2}(K_{\ell x}-K_a)$	$e_3(K_{\ell x}\cos^2\phi+K_a\sin^2\phi)+(e_1-\ell_1)\frac{\sin 2\phi}{2}(K_{\ell x}-K_a)$	$-(e_2-b)(K_{\ell x}\cos^2\phi+K_a\sin^2\phi)$
10	Parallel to z-axis	$e_1-\ell_1$	$b+e_2$	e_3	$-(b+e_2)\frac{\sin 2\phi}{2}(K_{\ell x}-K_a)$	$e_3(K_{\ell x}\cos^2\phi+K_a\sin^2\phi)+(e_1-\ell_1)\frac{\sin 2\phi}{2}(K_{\ell x}-K_a)$	$-(b+e_2)(K_{\ell x}\cos^2\phi+K_a\sin^2\phi)$
11	Parallel to z-axis	$e_1-\ell_1$	b_1+e_2	e_3	$-(b_1+e_2)\frac{\sin 2\phi}{2}(K_{\ell x}-K_a)$	$e_3(K_{\ell x}\cos^2\phi+K_a\sin^2\phi)+(e_1-\ell_1)\frac{\sin 2\phi}{2}(K_{\ell x}-K_a)$	$-(b_1+e_2)(K_{\ell x}\cos^2\phi+K_a\sin^2\phi)$
12	Parallel to z-axis	$e_1-\ell$	b_1+e_2	e_3	$-(b_1+e_2)\frac{\sin 2\phi}{2}(K_{\ell x}-K_a)$	$e_3(K_{\ell x}\cos^2\phi+K_a\sin^2\phi)+(e_1-\ell)\frac{\sin 2\phi}{2}(K_{\ell x}-K_a)$	$-(b_1+e_2)(K_{\ell x}\cos^2\phi+K_a\sin^2\phi)$
$\sum$:	$b_{11}=12e_2\frac{\sin 2\phi}{2}(K_{\ell x}-K_a)$;	$b_{12}=12e_3(K_{\ell x}\cos^2\phi+K_a\sin^2\phi)+12e_1\frac{\sin 2\phi}{2}(K_{\ell x}-K_a)$;			$b_{13}=-12e_2(K_{\ell x}\cos^2\phi+K_a\sin^2\phi)$		

Isolator Number	b_{21} $(r_2c_{23}-r_3c_{22})$	b_{22} $(r_3c_{21}-r_1c_{23})$	b_{23} $(r_1c_{22}-r_2c_{21})$	b_{31} $(r_2c_{33}-r_3c_{32})$	b_{32} $(r_3c_{31}-r_1c_{33})$	b_{33} $(r_1c_{32}-r_2c_{31})$
1	$-e_3K_{\ell y}$	o	$(\ell-e_1)K_{\ell y}$	$(b_1+e_2)(K_m\cos^2\phi+K_{\ell x}\sin^2\phi)$	$-e_3\frac{\sin2\phi}{2}(K_{\ell x}-K_m)-(\ell+e_1)$ $(K_m\cos^2\phi+K_{\ell x}\sin^2\phi)$	$(b_1+e_2)\frac{\sin2\phi}{2}(K_{\ell x}-K_m)$
2	$-e_3K_{\ell y}$	o	$(\ell_1+e_1)K_{\ell y}$	$(b_1+e_2)(K_m\cos^2\phi+K_{\ell x}\sin^2\phi)$	$-e_3\frac{\sin2\phi}{2}(K_{\ell x}-K_m)-(\ell_1+e_1)$ $(K_m\cos^2\phi+K_{\ell x}\sin^2\phi)$	$(b_1+e_2)\frac{\sin2\phi}{2}(K_{\ell x}-K_m)$
3	$-e_3K_{\ell y}$	o	$(\ell_1+e_1)K_{\ell y}$	$(b+e_2)(K_m\cos^2\phi+K_{\ell x}\sin^2\phi)$	$-e_3\frac{\sin2\phi}{2}(K_{\ell x}-K_m)-(\ell_1+e_1)$ $(K_m\cos^2\phi+K_{\ell x}\sin^2\phi)$	$(b+e_2)\frac{\sin2\phi}{2}(K_{\ell x}-K_m)$
4	$-e_3K_{\ell y}$	o	$(\ell_1+e_1)K_{\ell y}$	$(e_2-b)(K_m\cos^2\phi+K_{\ell x}\sin^2\phi)$	$-e_3\frac{\sin2\phi}{2}(K_{\ell x}-K_m)-(\ell_1+e_1)$ $(K_m\cos^2\phi+K_{\ell x}\sin^2\phi)$	$(e_2-b)\frac{\sin2\phi}{2}(K_{\ell x}-K_m)$
5	$-e_3K_{\ell y}$	o	$(\ell_1+e_1)K_{\ell y}$	$(e_2-b_1)(K_m\cos^2\phi+K_{\ell x}\sin^2\phi)$	$-e_3\frac{\sin2\phi}{2}(K_{\ell x}-K_m)-(\ell_1+e_1)$ $(K_m\cos^2\phi+K_{\ell x}\sin^2\phi)$	$(e_2-b_1)\frac{\sin2\phi}{2}(K_{\ell x}-K_m)$
6	$-e_3K_{\ell y}$	o	$(\ell+e_1)K_{\ell y}$	$(e_2-b_1)(K_m\cos^2\phi+K_{\ell x}\sin^2\phi)$	$-e_3\frac{\sin2\phi}{2}(K_{\ell x}-K_m)-(\ell+e_1)$ $(K_m\cos^2\phi+K_{\ell x}\sin^2\phi)$	$(e_2-b_1)\frac{\sin2\phi}{2}(K_{\ell x}-K_m)$
	$-e_3K_{\ell y}$	o	$(e_1-\ell)K_{\ell y}$	$(e_2-b_1)(K_m\cos^2\phi+K_{\ell x}\sin^2\phi)$	$-e_3\frac{\sin2\phi}{2}(K_{\ell x}-K_m)-(e_1-\ell)$ $(K_m\cos^2\phi+K_{\ell x}\sin^2\phi)$	$(e_2-b_1)\frac{\sin2\phi}{2}(K_{\ell x}-K_m)$
8	$-e_3K_{\ell y}$	o	$(e_1-\ell_1)K_{\ell y}$	$(e_2-b_1)(K_m\cos^2\phi+K_{\ell x}\sin^2\phi)$	$-e_3\frac{\sin2\phi}{2}(K_{\ell x}-K_m)-(e_1-\ell_1)$ $(K_m\cos^2\phi+K_{\ell x}\sin^2\phi)$	$(e_2-b_1)\frac{\sin2\phi}{2}(K_{\ell x}-K_m)$
9	$-e_3K_{\ell y}$	o	$(e_1-\ell_1)K_{\ell y}$	$(e_2-b)(K_m\cos^2\phi+K_{\ell x}\sin^2\phi)$	$-e_3\frac{\sin2\phi}{2}(K_{\ell x}-K_m)-(e_1-\ell_1)$ $(K_m\cos^2\phi+K_{\ell x}\sin^2\phi)$	$(e_2-b)\frac{\sin2\phi}{2}(K_{\ell x}-K_m)$
10	$-e_3K_{\ell y}$	o	$(e_1-\ell_1)(K_{\ell y})$	$(b+e_2)(K_m\cos^2\phi+K_{\ell x}\sin^2\phi)$	$-e_3\frac{\sin2\phi}{2}(K_{\ell x}-K_m)-(e_1-\ell_1)$ $(K_m\cos^2\phi+K_{\ell x}\sin^2\phi)$	$(b+e_2)\frac{\sin2\phi}{2}(K_{\ell x}-K_m)$
11	$-e_3K_{\ell y}$	o	$(e_1-\ell_1)K_{\ell y}$	$(b_1+e_2)(K_m\cos^2\phi+K_{\ell x}\sin^2\phi)$	$-e_3\frac{\sin2\phi}{2}(K_{\ell x}-K_m)-(e_1-\ell_1)$ $(K_m\cos^2\phi+K_{\ell x}\sin^2\phi)$	$(b_1+e_2)\frac{\sin2\phi}{2}(K_{\ell x}-K_m)$
12	$-e_3K_{\ell y}$	o	$(e_1-\ell)K_{\ell y}$	$(b_1+e_2)(K_m\cos^2\phi+K_{\ell x}\sin^2\phi)$	$-e_3\frac{\sin2\phi}{2}(K_{\ell x}-K_m)-(e_1-\ell)$ $(K_m\cos^2\phi+K_{\ell x}\sin^2\phi)$	$(b_1+e_2)\frac{\sin2\phi}{2}(K_{\ell x}-K_m)$

$\sum$: $b_{21}=-12e_3K_{\ell y}$; $b_{22}=0$; $b_{23}=12e_1K_{\ell y}$; $b_{31}=12e_2(K_m\cos^2\phi+K_{\ell x}\sin^2\phi)$; $b_{32}=-12e_3\frac{\sin2\phi}{2}(K_{\ell x}-K_m)-12e_1(K_m\cos^2\phi+K_{\ell x}\sin^2\phi)$; $b_{33}=12e_2\frac{\sin2\phi}{2}(K_{\ell x}-K_m)$

$$[B]=\begin{bmatrix} -12e_2\frac{\sin2\phi}{2}(K_{\ell x}-K_m) & 12e_3(K_{\ell x}\cos^2\phi+K_m\sin^2\phi) & -12e_2(K_{\ell x}\cos^2\phi+K_m\sin^2\phi) \\ & +12e_1\frac{\sin2\phi}{2}(K_{\ell x}-K_m) & \\ -12e_3K_{\ell y} & o & 12e_1K_{\ell y} \\ 12e_2(K_m\cos^2\phi+K_{\ell x}\sin^2\phi) & -12e_3\frac{\sin2\phi}{2}(K_{\ell x}-K_m) & 12e_2\frac{\sin2\phi}{2}(K_{\ell x}-K_m) \\ & -12e_1(K_m\cos^2\phi+K_{\ell x}\sin^2\phi) & \end{bmatrix} = \begin{bmatrix} o & 12e_3K_{\ell x} & -12e_2K_{\ell x} \\ -12e_3K_{\ell y} & & 12e_1K_{\ell y} \\ 12e_2K_m & -12e_1K_m & o \end{bmatrix}$$

$$+\phi\begin{bmatrix} -12e_2(K_{\ell x}-K_m) & +12e_2(K_{\ell x}-K_m) & o \\ o & o & o \\ o & -12e_3(K_{\ell x}-K_m) & +12e_2(K_{\ell x}-K_m) \end{bmatrix}$$

Insulator Number	e_{11} $(r_2b_{11}-r_3b_{21})$	e_{12} $(r_2b_{32}-r_3b_{22})$	e_{13} $(r_2b_{33}-r_3b_{23})$	e_{21} $(r_3b_{11}-r_1b_{31})$
1	$(b_1-e_2)^2(K_m\cos^2\phi+K_{fx}\sin^2\phi)+e_3^2K_{fy}$	$(b_1+e_2)\left[e_3\frac{\sin2\phi}{2}(K_{fx}-K_m)-(l+e_1)(K_m\cos^2\phi+K_{fx}\sin^2\phi)\right]$	$(b_1+e_2)\frac{2\sin2\phi}{2}(K_{fx}-K_m)-e_3(l+e_1)K_{fy}$	$-e_3(b_1+e_2)\frac{\sin2\phi}{2}(K_{fx}-K_m)-(l+e_1)(b_1+e_2)(K_m\cos^2\phi+K_{fx}\sin^2\phi)$
2	$(b_1-e_2)^2(K_m\cos^2\phi+K_{fx}\sin^2\phi)+e_3^2K_{fy}$	$(b_1+e_2)\left[e_3\frac{\sin2\phi}{2}(K_{fx}-K_m)-(l_1+e_1)(K_m\cos^2\phi+K_{fx}\sin^2\phi)\right]$	$(b_1+e_2)\frac{2\sin2\phi}{2}(K_{fx}-K_m)-e_3(l_1+e_1)K_{fy}$	$-e_3(b_1+e_2)\frac{\sin2\phi}{2}(K_{fx}-K_m)-(l_1+e_1)(b_1+e_2)(K_m\cos^2\phi+K_{fx}\sin^2\phi)$
3	$(b+e_2)^2(K_m\cos^2\phi+K_{fx}\sin^2\phi)+e_3^2K_{fy}$	$(b+e_2)\left[e_3\frac{\sin2\phi}{2}(K_{fx}-K_m)-(l_1+e_1)(K_m\cos^2\phi+K_{fx}\sin^2\phi)\right]$	$(b+e_2)\frac{2\sin2\phi}{2}(K_{fx}-K_m)-e_3(l_1+e_1)K_{fy}$	$-e_3(b+e_2)\frac{\sin2\phi}{2}(K_{fx}-K_m)-(l_1+e_1)(b+e_2)(K_m\cos^2\phi+K_{fx}\sin^2\phi)$
4	$(e_2-b)^2(K_m\cos^2\phi+K_{fx}\sin^2\phi)+e_3^2K_{fy}$	$(e_2-b)\left[e_3\frac{\sin2\phi}{2}(K_{fx}-K_m)-(l_1+e_1)(K_m\cos^2\phi+K_{fx}\sin^2\phi)\right]$	$(e_2-b)\frac{2\sin2\phi}{2}(K_{fx}-K_m)-e_3(l_1+e_1)K_{fy}$	$-e_3(e_2-b)\frac{\sin2\phi}{2}(K_{fx}-K_m)-(l_1+e_1)(e_2-b)(K_m\cos^2\phi+K_{fx}\sin^2\phi)$
5	$(e_2-b_1)^2(K_m\cos^2\phi+K_{fx}\sin^2\phi)+e_3^2K_{fy}$	$(e_2-b_1)\left[e_3\frac{\sin2\phi}{2}(K_{fx}-K_m)-(l+e_1)(K_m\cos^2\phi+K_{fx}\sin^2\phi)\right]$	$(e_2-b_1)\frac{2\sin2\phi}{2}(K_{fx}-K_m)-e_3(l+e_1)K_{fy}$	$-e_3(e_2-b_1)\frac{\sin2\phi}{2}(K_{fx}-K_m)-(l+e_1)(e_2-b_1)(K_m\cos^2\phi+K_{fx}\sin^2\phi)$
6	$(e_2-b_1)^2(K_m\cos^2\phi+K_{fx}\sin^2\phi)+e_3^2K_{fy}$	$(e_2-b_1)\left[e_3\frac{\sin2\phi}{2}(K_{fx}-K_m)-(l+e_1)(K_m\cos^2\phi+K_{fx}\sin^2\phi)\right]$	$(e_2-b_1)\frac{2\sin2\phi}{2}(K_{fx}-K_m)-e_3(l+e_1)K_{fy}$	$-e_3(e_2-b_1)\frac{\sin2\phi}{2}(K_{fx}-K_m)-(l+e_1)(e_2-b_1)(K_m\cos^2\phi+K_{fx}\sin^2\phi)$
7	$(e_2-b_1)^2(K_m\cos^2\phi+K_{fx}\sin^2\phi)+e_3^2K_{fy}$	$(e_2-b_1)\left[e_3\frac{\sin2\phi}{2}(K_{fx}-K_m)-(e_1-l)(K_m\cos^2\phi+K_{fx}\sin^2\phi)\right]$	$(e_2-b_1)\frac{2\sin2\phi}{2}(K_{fx}-K_m)-e_3(e_1-l)K_{fy}$	$-e_3(e_2-b_1)\frac{\sin2\phi}{2}(K_{fx}-K_m)-(e_1-l)(e_2-b_1)(K_m\cos^2\phi+K_{fx}\sin^2\phi)$
8	$(e_2-b_2)^2(K_m\cos^2\phi+K_{fx}\sin^2\phi)+e_3^2K_{fy}$	$(e_2-b_2)\left[e_3\frac{\sin2\phi}{2}(K_{fx}-K_m)-(e_1-l_1)(K_m\cos^2\phi+K_{fx}\sin^2\phi)\right]$	$(e_2-b_2)\frac{2\sin2\phi}{2}(K_{fx}-K_m)-e_3(e_1-l_1)K_{fy}$	$-e_3(e_2-b_1)\frac{\sin2\phi}{2}(K_{fx}-K_m)-(e_1-l_1)(e_2-b_1)(K_m\cos^2\phi+K_{fx}\sin^2\phi)$
9	$(e_2-b)^2(K_m\cos^2\phi+K_{fx}\sin^2\phi)+e_3^2K_{fy}$	$(e_2-b)\left[e_3\frac{\sin2\phi}{2}(K_{fx}-K_m)-(e_1-l_1)(K_m\cos^2\phi+K_{fx}\sin^2\phi)\right]$	$(e_2-b)\frac{2\sin2\phi}{2}(K_{fx}-K_m)-e_3^2(e_1-l_1)K_{fy}$	$-e_3(e_2-b)\frac{\sin2\phi}{2}(K_{fx}-K_m)-(e_1-l_1)(e_2-b)(K_m\cos^2\phi+K_{fx}\sin^2\phi)$
10	$(b+e_2)^2(K_m\cos^2\phi+K_{fx}\sin^2\phi)+e_3^2K_{fy}$	$(b+e_2)\left[e_3\frac{\sin2\phi}{2}(K_{fx}-K_m)-(e_1-l_1)(K_m\cos^2\phi+K_{fx}\sin^2\phi)\right]$	$(b+e_2)\frac{2\sin2\phi}{2}(K_{fx}-K_m)-e_3(e_1-l_1)K_{fy}$	$-e_3(b+e_2)\frac{\sin2\phi}{2}(K_{fx}-K_m)-(e_1-l_1)(b+e_2)(K_m\cos^2\phi+K_{fx}\sin^2\phi)$
11	$(b_1+e_2)^2(K_m\cos^2\phi+K_{fx}\sin^2\phi)+e_3^2K_{fy}$	$(b_1+e_2)\left[e_3\frac{\sin2\phi}{2}(K_{fx}-K_m)-(e_1-l_1)(K_m\cos^2\phi+K_{fx}\sin^2\phi)\right]$	$(b_1+e_2)\frac{2\sin2\phi}{2}(K_{fx}-K_m)-e_3(e_1-l_1)K_{fy}$	$-e_3(b_1+e_2)\frac{\sin2\phi}{2}(K_{fx}-K_m)-(e_1-l_1)(b_1+e_2)(K_m\cos^2\phi+K_{fx}\sin^2\phi)$
12	$(b_1+e_2)^2(K_m\cos^2\phi+K_{fx}\sin^2\phi)+e_3^2K_{fy}$	$(b_1+e_2)\left[e_3\frac{\sin2\phi}{2}(K_{fx}-K_m)-(e_1-l)(K_m\cos^2\phi+K_{fx}\sin^2\phi)\right]$	$(b_1+e_2)\frac{2\sin2\phi}{2}(K_{fx}-K_m)-e_3(e_1-l)K_{fy}$	$-e_3(b_1+e_2)\frac{\sin2\phi}{2}(K_{fx}-K_m)-(e_1-l)(b_1+e_2)(K_m\cos^2\phi+K_{fx}\sin^2\phi)$

$\sum$ $e_{11}=4(b^2+2b_1^2+3e_2^2)(K_m\cos^2\phi+K_{fx}\sin^2\phi)+12e_3^2K_{fy}$; $e_{12}=-12e_2e_3\frac{\sin2\phi}{2}(K_{fx}-K_m)-12e_1e_2(K_m\cos^2\phi+K_{fx}\sin^2\phi)$;

$e_{13}=4(b^2+2b_1^2+3e_2^2)\frac{\sin2\phi}{2}(K_{fx}-K_m)-12e_1e_3K_{fy}$; $e_{21}=-12e_2e_3\frac{\sin2\phi}{2}(K_{fx}-K_m)-12e_1e_2(K_m\cos^2\phi+K_{fx}\sin^2\phi)$

Isolator Number	$e_{22} = r_3 b_{12} - r_1 b_{32}$	$e_{23} = r_3 b_{13} - r_1 b_{33}$
1	$e_3\{e_3(K_{fx}\cos^2\phi+K_a\sin^2\phi)+(f+e_1)\frac{\sin2\phi}{2}(K_{fx}-K_a)\}-(f+e_1)\{e_3\frac{\sin2\phi}{2}(K_{fx}-K_a)-(f+e_1)(K_a\cos^2\phi+K_{fx}\sin^2\phi)\}$	$-e_3(b_1+e_2)(K_{fx}\cos^2\phi+K_a\sin^2\phi)-(f+e_1)(b_1+e_2)\frac{\sin2\phi}{2}(K_{fx}-K_a)$
2	$e_3\{e_3(K_{fx}\cos^2\phi+K_a\sin^2\phi)+(f_1+e_1)\frac{\sin2\phi}{2}(K_{fx}-K_a)\}-(f_1+e_1)\{-e_3\frac{\sin2\phi}{2}(K_{fx}-K_a)-(f_1+e_1)(K_a\cos^2\phi+K_{fx}\sin^2\phi)\}$	$-e_3(b_1+e_2)(K_{fx}\cos^2\phi+K_a\sin^2\phi)-(f_1+e_1)(b_1+e_2)\frac{\sin2\phi}{2}(K_{fx}-K_a)$
3	$e_3\{e_3(K_{fx}\cos^2\phi+K_a\sin^2\phi)+(f_1+e_1)\frac{\sin2\phi}{2}(K_{fx}-K_a)\}-(f_1+e_1)\{-e_3\frac{\sin2\phi}{2}(K_{fx}-K_a)-(f_1+e_1)(K_a\cos^2\phi+K_{fx}\sin^2\phi)\}$	$-e_3(b+e_2)(K_{fx}\cos^2\phi+K_a\sin^2\phi)-(f_1+e_1)(b+e_2)\frac{\sin2\phi}{2}(K_{fx}-K_a)$
4	$e_3\{e_3(K_{fx}\cos^2\phi+K_a\sin^2\phi)+(f_1+e_1)\frac{\sin2\phi}{2}(K_{fx}-K_a)\}-(f_1+e_1)\{-e_3\frac{\sin2\phi}{2}(K_{fx}-K_a)-(f_1+e_1)(K_a\cos^2\phi+K_{fx}\sin^2\phi)\}$	$-e_3(e_2-b)(K_{fx}\cos^2\phi+K_a\sin^2\phi)-(f_1+e_1)(e_2-b)\frac{\sin2\phi}{2}(K_{fx}-K_a)$
5	$e_3\{e_3(K_{fx}\cos^2\phi+K_a\sin^2\phi)+(f_1+e_1)\frac{\sin2\phi}{2}(K_{fx}-K_a)\}-(f_1+e_1)\{-e_3\frac{\sin2\phi}{2}(K_{fx}-K_a)-(f_1+e_1)(K_a\cos^2\phi+K_{fx}\sin^2\phi)\}$	$-e_3(e_2-b_1)(K_{fx}\cos^2\phi+K_a\sin^2\phi)-(f_1+e_1)(e_2-b_1)\frac{\sin2\phi}{2}(K_{fx}-K_a)$
6	$e_3\{e_3(K_{fx}\cos^2\phi+K_a\sin^2\phi)+(f+e_1)\frac{\sin2\phi}{2}(K_{fx}-K_a)\}-(f+e_1)\{-e_3\frac{\sin2\phi}{2}(K_{fx}-K_a)-(f+e_1)(K_a\cos^2\phi+K_{fx}\sin^2\phi)\}$	$-e_3(e_2-b_1)(K_{fx}\cos^2\phi+K_a\sin^2\phi)-(f+e_1)(e_2-b_1)\frac{\sin2\phi}{2}(K_{fx}-K_a)$
7	$e_3\{e_3(K_{fx}\cos^2\phi+K_a\sin^2\phi)+(e_1-f)\frac{\sin2\phi}{2}(K_{fx}-K_a)\}-(e_1-f)\{-e_3\frac{\sin2\phi}{2}(K_{fx}-K_a)-(e_1-f)(K_a\cos^2\phi+K_{fx}\sin^2\phi)\}$	$-e_3(e_2-b_1)(K_{fx}\cos^2\phi+K_a\sin^2\phi)-(e_1-f)(e_2-b_1)\frac{\sin2\phi}{2}(K_{fx}-K_a)$
8	$e_3\{e_3(K_{fx}\cos^2\phi+K_a\sin^2\phi)+(e_1-f_1)\frac{\sin2\phi}{2}(K_{fx}-K_a)\}-(e_1-f_1)\{-e_3\frac{\sin2\phi}{2}(K_{fx}-K_a)-(e_1-f_1)(K_a\cos^2\phi+K_{fx}\sin^2\phi)\}$	$-e_3(e_2-b_1)(K_{fx}\cos^2\phi+K_a\sin^2\phi)-(e_1-f_1)(e_2-b_1)\frac{\sin2\phi}{2}(K_{fx}-K_a)$
9	$e_3\{e_3(K_{fx}\cos^2\phi+K_a\sin^2\phi)+(e_1-f_1)\frac{\sin2\phi}{2}(K_{fx}-K_a)\}-(e_1-f_1)\{-e_3\frac{\sin2\phi}{2}(K_{fx}-K_a)-(e_1-f_1)(K_a\cos^2\phi+K_{fx}\sin^2\phi)\}$	$-e_3(e_2-b)(K_{fx}\cos^2\phi+K_a\sin^2\phi)-(e_1-f_1)(e_2-b)\frac{\sin2\phi}{2}(K_{fx}-K_a)$
10	$e_3\{e_3(K_{fx}\cos^2\phi+K_a\sin^2\phi)+(e_1-f_1)\frac{\sin2\phi}{2}(K_{fx}-K_a)\}-(e_1-f_1)\{-e_3\frac{\sin2\phi}{2}(K_{fx}-K_a)-(e_1-f_1)(K_a\cos^2\phi+K_{fx}\sin^2\phi)\}$	$-e_3(b+e_2)(K_{fx}\cos^2\phi+K_a\sin^2\phi)-(e_1-f_1)(b+e_2)\frac{\sin2\phi}{2}(K_{fx}-K_a)$
11	$e_3\{e_3(K_{fx}\cos^2\phi+K_a\sin^2\phi)+(e_1-f_1)\frac{\sin2\phi}{2}(K_{fx}-K_a)\}-(e_1-f_1)\{-e_3\frac{\sin2\phi}{2}(K_{fx}-K_a)-(e_1-f_1)(K_a\cos^2\phi+K_{fx}\sin^2\phi)\}$	$-e_3(b_1+e_2)(K_{fx}\cos^2\phi+K_a\sin^2\phi)-(e_1-f_1)(b_1+e_2)\frac{\sin2\phi}{2}(K_{fx}-K_a)$
12	$e_3\{e_3(K_{fx}\cos^2\phi+K_a\sin^2\phi)+(e_1-f)\frac{\sin2\phi}{2}(K_{fx}-K_a)\}-(e_1-f)\{-e_3\frac{\sin2\phi}{2}(K_{fx}-K_a)-(e_1-f)(K_a\cos^2\phi+K_{fx}\sin^2\phi)\}$	$-e_3(b_1+e_2)(K_{fx}\cos^2\phi+K_a\sin^2\phi)-(e_1-f)(b_1+e_2)\frac{\sin2\phi}{2}(K_{fx}-K_a)$

$$\sum: e_{22}=\left\{12e_3^2(K_{fx}\cos^2\phi+K_a\sin^2\phi)+24e_1e_3\frac{\sin2\phi}{2}(K_{fx}-K_a)+4(f^2+2f_1^2+3e_1^2)(K_a\cos^2\phi+K_{fx}\sin^2\phi)\right\};$$

$$e_{23}=-12e_2e_3(K_{fx}\cos^2\phi+K_a\sin^2\phi)-12e_1e_2\frac{\sin2\phi}{2}(K_{fx}-K_a)$$

Isolator Number	$e_{31}=r_1b_{21}-r_2b_{11}$	$e_{32}=r_1b_{22}-r_2b_{12}$	$e_{33}=r_1b_{23}-r_2b_{13}$
1	$-(\ell+e_1)\,e_3K_{\ell y}+(b_1+e_2)\frac{2\sin2\phi}{2}(K_{\ell x}-K_a)$	$-(b_1+e_2)\left[e_3(K_{\ell x}\cos^2\phi+K_a\sin^2\phi)+(\ell+e_1)\frac{\sin2\phi}{2}(K_{\ell x}-K_a)\right]$	$(\ell+e_1)^2K_{\ell y}+(b_1+e_2)^2(K_{\ell x}\cos^2\phi+K_a\sin^2\phi)$
2	$-(\ell_1+e_1)e_3K_{\ell y}+(b_1+e_2)\frac{2\sin2\phi}{2}(K_{\ell x}-K_a)$	$-(b_1+e_2)\left[e_3(K_{\ell x}\cos^2\phi+K_a\sin^2\phi)+(\ell_1+e_1)\frac{\sin2\phi}{2}(K_{\ell x}-K_a)\right]$	$(\ell_1+e_1)^2K_{\ell y}+(b_1+e_2)^2(K_{\ell x}\cos^2\phi+K_a\sin^2\phi)$
3	$-(\ell_1+e_1)e_3K_{\ell y}+(b+e_2)\frac{2\sin2\phi}{2}(K_{\ell x}-K_a)$	$-(b+e_2)\left[e_3(K_{\ell x}\cos^2\phi+K_a\sin^2\phi)+(\ell_1+e_1)\frac{\sin2\phi}{2}(K_{\ell x}-K_a)\right]$	$(\ell_1+e_1)^2K_{\ell y}+(b+e_2)^2(K_{\ell x}\cos^2\phi+K_a\sin^2\phi)$
4	$-(\ell_1+e_1)e_3K_{\ell y}+(e_2-b)\frac{2\sin2\phi}{2}(K_{\ell x}-K_a)$	$-(e_2-b)\left[e_3(K_{\ell x}\cos^2\phi+K_a\sin^2\phi)+(\ell_1+e_1)\frac{\sin2\phi}{2}(K_{\ell x}-K_a)\right]$	$(\ell_1+e_1)^2K_{\ell y}+(e_2-b)^2(K_{\ell x}\cos^2\phi+K_a\sin^2\phi)$
5	$-(\ell_1+e_1)e_3K_{\ell y}+(e_2-b_1)\frac{2\sin2\phi}{2}(K_{\ell x}-K_a)$	$-(e_2-b_1)\left[e_3(K_{\ell x}\cos^2\phi+K_a\sin^2\phi)+(\ell_1+e_1)\frac{\sin2\phi}{2}(K_{\ell x}-K_a)\right]$	$(\ell_1+e_1)^2K_{\ell y}+(e_2-b_1)^2(K_{\ell x}\cos^2\phi+K_a\sin^2\phi)$
6	$-(\ell+e_1)e_3K_{\ell y}+(e_2-b_1)\frac{2\sin2\phi}{2}(K_{\ell x}-K_a)$	$-(e_2-b_1)\left[e_3(K_{\ell x}\cos^2\phi+K_a\sin^2\phi)+(\ell+e_1)\frac{\sin2\phi}{2}(K_{\ell x}-K_a)\right]$	$(\ell+e_1)^2K_{\ell y}+(e_2-b_1)^2(K_{\ell x}\cos^2\phi+K_a\sin^2\phi)$
7	$-(e_1-\ell)e_3K_{\ell y}+(e_2-b_1)\frac{2\sin2\phi}{2}(K_{\ell x}-K_a)$	$-(e_2-b_1)\left[e_3(K_{\ell x}\cos^2\phi+K_a\sin^2\phi)+(e_1-\ell)\frac{\sin2\phi}{2}(K_{\ell x}-K_a)\right]$	$(e_1-\ell)^2K_{\ell y}+(e_2-b_1)^2(K_{\ell x}\cos^2\phi+K_a\sin^2\phi)$
8	$-(e_1-\ell_1)e_3K_{\ell y}+(e_2-b_1)\frac{2\sin2\phi}{2}(K_{\ell x}-K_a)$	$-(e_2-b_1)\left[e_3(K_{\ell x}\cos^2\phi+K_a\sin^2\phi)+(e_1-\ell_1)\frac{\sin2\phi}{2}(K_{\ell x}-K_a)\right]$	$(e_1-\ell_1)^2K_{\ell y}+(e_2-b_1)^2(K_{\ell x}\cos^2\phi+K_a\sin^2\phi)$
9	$-(e_1-\ell_1)e_3K_{\ell y}+(e_2-b)\frac{2\sin2\phi}{2}(K_{\ell x}-K_a)$	$-(e_2-b)\left[e_3(K_{\ell x}\cos^2\phi+K_a\sin^2\phi)+(e_1-\ell_1)\frac{\sin2\phi}{2}(K_{\ell x}-K_a)\right]$	$(e_1-\ell_1)^2K_{\ell y}+(e_2-b)^2(K_{\ell x}\cos^2\phi+K_a\sin^2\phi)$
10	$(e_1-\ell_1)e_3K_{\ell y}+(b+e_2)\frac{2\sin2\phi}{2}(K_{\ell x}-K_a)$	$-(b+e_2)\left[e_3(K_{\ell x}\cos^2\phi+K_a\sin^2\phi)+(e_1-\ell_1)\frac{\sin2\phi}{2}(K_{\ell x}-K_a)\right]$	$(e_1-\ell_1)^2K_{\ell y}+(b+e_2)^2(K_{\ell x}\cos^2\phi+K_a\sin^2\phi)$
11	$-(e_1-\ell_1)e_3K_{\ell y}+(b_1+e_2)\frac{2\sin2\phi}{2}(K_{\ell x}-K_a)$	$-(b_1+e_2)\left[e_3(K_{\ell x}\cos^2\phi+K_a\sin^2\phi)+(e_1-\ell_1)\frac{\sin2\phi}{2}(K_{\ell x}-K_a)\right]$	$(e_1-\ell_1)^2K_{\ell y}+(b_1+e_2)^2K_{\ell x}\cos^2\phi+K_a\sin^2\phi)$
12	$-(e_1-\ell)e_3K_{\ell y}+(b_1+e_2)\frac{2\sin2\phi}{2}(K_{\ell x}-K_a)$	$-(b_1+e_2)\left[e_3(K_{\ell x}\cos^2\phi+K_a\sin^2\phi)+(e_1-\ell)\frac{\sin2\phi}{2}(K_{\ell x}-K_a)\right]$	$(e_1-\ell)^2K_{\ell y}+(b_1+e_2)^2(K_{\ell x}\cos^2\phi+K_a\sin^2\phi)$

$\sum$: $e_{31}=-12e_1e_3K_{\ell y}+4(b^2+2b_1^2+3e_2^2)\frac{\sin2\phi}{2}(K_{\ell x}-K_a)$; $e_{32}=-12e_2e_3(K_{\ell x}\cos^2\phi+K_a\sin^2\phi)-12e_1e_2\frac{\sin2\phi}{2}(K_{\ell x}-K_a)$;

$e_{33}=4(\ell^2+2\ell_1+3e_1^2)K_{\ell y}+4(b^2+2b_1^2+3e_2^2)(K_{\ell x}\cos^2\phi+K_a\sin^2\phi)$

$$
\begin{bmatrix}
4(b^2+2b_1^2+3e_2^2)(K_a\cos^2\phi + K_{fx}\sin^2\phi) & -12\, e_2e_3\frac{\sin 2\phi}{2}\,(K_{fx}-K_a) & 4(b^2+2b_1^2+3e_2^2)\frac{\sin 2\phi}{2}\,(K_{fx}-K_a) \\
\quad + 12\, e_3^2 K_{fy} & \quad - 12\, e_1e_2(K_a\cos^2\phi + K_{fx}\sin^2\phi) & \quad - 12\, e_1e_3K_{fy} \\
-12\, e_2e_3\frac{\sin 2\phi}{2}\,(K_{fx}-K_a) & 4(f^2+2f_1^2+3e_1^2)\,(K_a\cos^2\phi + K_{fx}\sin^2\phi) & -12\, e_2e_3(K_{fx}\cos^2\phi + K_a\sin^2\phi) \\
\quad - 12\, e_1e_2\,(K_a\cos^2\phi + K_{fx}\sin^2\phi) & \quad + 12\, e_3^2\,(K_{fx}\cos^2\phi + K_a\sin^2\phi) & \quad - 12\, e_1e_2\frac{\sin 2\phi}{2}\,(K_{fx}-K_a) \\
 & \quad + 24\, e_1e_3\frac{\sin 2\phi}{2}\,(K_{fx}-K_a) & \\
4(b^2+2b_1^2+3e_2^2)\frac{\sin 2\phi}{2}\,(K_{fx}-K_a) & -12\, e_2e_3(K_{fx}\cos^2\phi + K_a\sin^2\phi) & 4(b^2+2b_1^2+3e_2^2)\,(K_{fx}\cos^2\phi+K_a\sin^2\phi) \\
\quad - 12\, e_1e_3K_{fy} & \quad - 12\, e_1e_2\frac{\sin 2\phi}{2}\,(K_{fx}-K_a) & \quad + 4(f^2+2f_1^2+3e_1^2)\,K_{fy}
\end{bmatrix}
$$

$$
+\phi
\begin{bmatrix}
4(b^2+2b_1^2+3e_2^2)\,K_a & -12\, e_1e_2K_a & -12\, e_1e_3K_{fy} \\
\quad + 12\, e_3^2 K_{fy} & & \\
-12\, e_1e_2K_a & 4(f^2+2f_1^2+3e_1^2)\,K_a & -12\, e_2e_3K_{fx} \\
 & \quad + 12\, e_3^2 K_{fx} & \\
-12\, e_1e_2K_{fy} & -12\, e_2e_3K_{fx} & 4(f^2+2f_1^2+3e_1^2)K_{fy} \\
 & & \quad +4(b^2+2b_1^2+3e_2^2)K_{fx}
\end{bmatrix}
\begin{bmatrix}
0 & -12\, e_2e_3(K_{fx}-K_a) & 4(b^2+2b_1^2+3e_2^2) \\
 & & (K_{fx}-K_a) \\
-12\, e_2e_3(K_{fx}-K_a) & 24\, e_1e_3(K_{fx}K_a) & -12\, e_1e_2 \\
 & & (K_{fx}-K_a) \\
4(b^2+2b_1^2+3e_2^2) & -12\, e_1e_2(K_{fx}-K_a) & 0 \\
(K_{fx}-K_a) & &
\end{bmatrix}
$$

nonlinear coupling after the additional approximation:

$$\sin(\theta - \phi^*) = \sin\theta$$

$$\cos(\theta - \phi^*) = \cos\theta$$

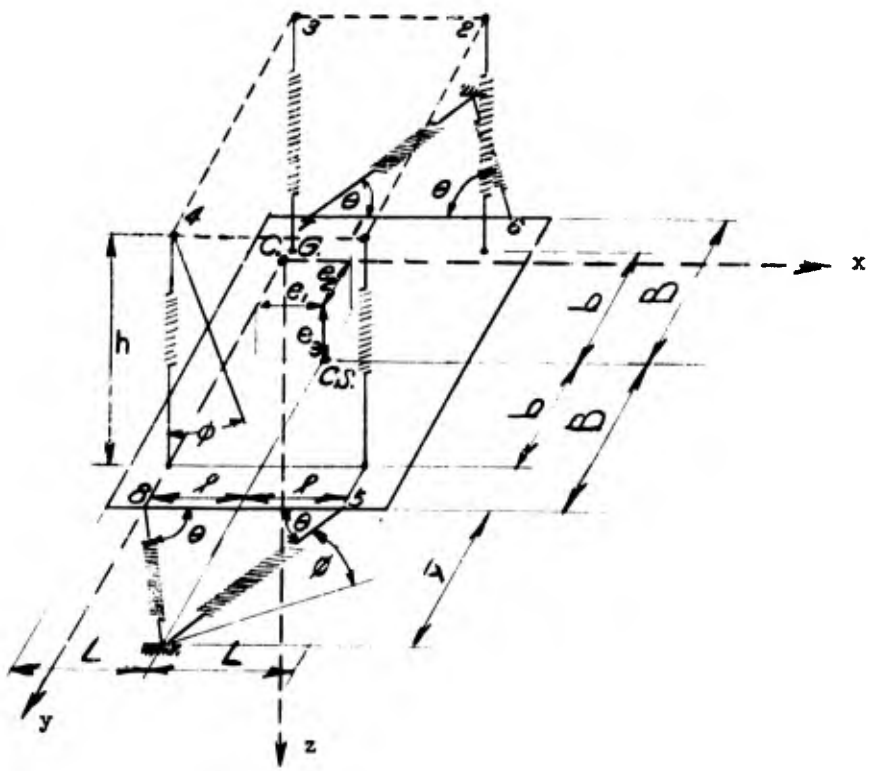

Figure 3.8.14

Unsymmetrical Elastic Pendulum with Inclined Horizontal Elements

Isolator Number	Axial Orientation	r_1	r_2	r_3	b_{11} $(r_2c_{13}-r_3c_{12})$	b_{12} $(r_3c_{11}-r_1c_{13})$	b_{13} $(r_1c_{12}-r_2c_{11})$
1	Parallel to z-axis	$\ell+e_1$	$b+e_2$	e_3	$-(b+e_2)\frac{\sin 2\phi}{2}(K_{\ell v}-K_{av})$	$e_3(K_{\ell v}\cos^2\phi+K_{av}\sin^2\phi)$ $+(\ell+e_1)\frac{\sin 2\phi}{2}(K_{\ell v}-K_{av})$	$-(b+e_2)(K_{\ell v}\cos^2\phi+K_{av}\sin^2\phi)$
2	Parallel to z-axis	$\ell+e_1$	e_2-b	e_3	$-(e_2-b)\frac{\sin 2\phi}{2}(K_{\ell v}-K_{av})$	$e_3(K_{\ell v}\cos^2\phi+K_{av}\sin^2\phi)$ $+(\ell+e_1)\frac{\sin 2\phi}{2}(K_{\ell v}-K_{av})$	$-(e_2-b)(K_{\ell v}\cos^2\phi+K_{av}\sin^2\phi)$
3	Parallel to z-axis	$e_1-\ell$	e_2-b	e_3	$-(e_2-b)\frac{\sin 2\phi}{2}(K_{\ell v}-K_{av})$	$e_3(K_{\ell v}\cos^2\phi+K_{av}\sin^2\phi)$ $+(e_1-\ell)\frac{\sin 2\phi}{2}(K_{\ell v}-K_{av})$	$-(e_2-b)(K_{\ell v}\cos^2\phi+K_{av}\sin^2\phi)$
4	Parallel to z-axis	$e_1-\ell$	$b+e_2$	e_3	$-(b+e_2)\frac{\sin 2\phi}{2}(K_{\ell v}-K_{av})$	$e_3(K_{\ell v}\cos^2\phi+K_{av}\sin^2\phi)$ $+(e_1-\ell)\frac{\sin 2\phi}{2}(K_{\ell v}-K_{av})$	$-(b+e_2)(K_{\ell v}\cos^2\phi+K_{av}\sin^2\phi)$
5	$(180-\theta)^\circ$ to x-axis	$\ell+e_1$	$B-e_2$	e_3	$e_3\frac{\sin 2(\theta-\phi^*)}{2}(K_{ah}-K_{\ell h})$	$e_3\{K_{ah}\cos^2(\theta-\phi^*)$ $+K_{\ell h}\sin^2(\theta-\phi^*)\}$	$-(\ell+e_1)\frac{\sin 2(\theta-\phi^*)}{2}(K_{ah}-K_{\ell h})$ $-(B+e_2)\{K_{ah}\cos^2(\theta-\phi^*)+K_{\ell h}\sin^2(\theta-\phi^*)\}$
6	$(180+\theta)^\circ$ to x-axis	$\ell+e_1$	e_2-B	e_3	$-e_3\frac{\sin 2(\theta-\phi^*)}{2}(K_{ah}-K_{\ell h})$	$e_3\{K_{ah}\cos^2(\theta-\phi^*)$ $+K_{\ell h}\sin^2(\theta-\phi^*)\}$	$(\ell+e_1)\frac{\sin 2(\theta-\phi^*)}{2}(K_{ah}-K_{\ell h})$ $-(e_2-B)\{K_{ah}\cos^2(\theta-\phi^*)+K_{\ell h}\sin^2(\theta-\phi^*)\}$
7	$-\theta^\circ$ to x-axis	$e_1-\ell$	e_2-B	e_3	$e_3\frac{\sin 2(\theta+\phi^*)}{2}(K_{ah}-K_{\ell h})$	$e_3\{K_{ah}\cos^2(\theta+\phi^*)$ $+K_{\ell h}\sin^2(\theta+\phi^*)\}$	$-(e_1-\ell)\frac{\sin 2(\theta+\phi^*)}{2}(K_{ah}-K_{\ell h})$ $-(e_2-B)\{K_{ah}\cos^2(\theta+\phi^*)+K_{\ell h}\sin^2(\theta+\phi^*)\}$
8	$+\theta^\circ$ to x-axis	$e_1-\ell$	$B+e_2$	e_3	$-e_3\frac{\sin 2(\theta+\phi^*)}{2}(K_{ah}-K_{\ell h})$	$e_3\{K_{ah}\cos^2(\theta+\phi^*)$ $+K_{\ell h}\sin^2(\theta+\phi^*)\}$	$(e_1-\ell)\frac{\sin 2(\theta+\phi^*)}{2}(K_{ah}-K_{\ell h})$ $-(B+e_2)\{K_{ah}\cos^2(\theta+\phi^*)+K_{\ell h}\sin^2(\theta+\phi^*)\}$

$\sum$: $b_{11}=-4e_2\frac{\sin 2\phi}{2}(K_{\ell v}-K_{av})$; $b_{12}=4e_3\{K_{\ell v}\cos^2\phi+K_{av}\sin^2\phi\}+2e_3\{K_{ah}\cos^2(\theta-\phi^*)+K_{\ell h}\sin^2(\theta-\phi^*)\}+4e_1\frac{\sin 2\phi}{2}(K_{\ell v}-K_{av})$ $+2e_3\{K_{ah}\cos^2(\theta+\phi^*)+K_{\ell h}\sin^2(\theta+\phi^*)\}$; $b_{13}=-4e_2(K_{\ell v}\cos^2\phi+K_{av}\sin^2\phi)-2e_2(K_{ah}\cos^2(\theta-\phi^*)+K_{\ell h}\sin^2(\theta-\phi^*)$ $-2e_2\{K_{ah}\cos^2(\theta+\phi^*)+K_{\ell h}\sin^2(\theta+\phi^*)\}$

Isolator Number	b_{21} $(r_2c_{23}-r_3c_{22})$	b_{22} $(r_3c_{21}-r_1c_{23})$	b_{23} $(r_1c_{22}-r_2c_{21})$	b_{31} $(r_2c_{33}-r_3c_{32})$	b_{32} $(r_3c_{31}-r_1c_{33})$	b_{33} $(r_1c_{32}-r_2c_{31})$
1	$-e_3K_{fv}$	0	$(1+e_1)K_{fv}$	$(1+e_2)\left[K_{av}\cos^2\beta + K_{fv}\sin^2\beta\right]$	$-e_3\frac{\sin 2\beta}{2}(K_{fv}-K_{av})$ $-(1+e_1)(K_{av}\cos^2\beta+K_{fv}\sin^2\beta$	$(1+e_2)\frac{\sin 2\beta}{2}(K_{fv}-K_{av})$
2	$-e_3K_{fv}$	0	$(1+e_1)K_{fv}$	$(e_2-1)\left[K_{av}\cos^2\beta + K_{fv}\sin^2\beta\right]$	$-e_3\frac{\sin 2\beta}{2}(K_{fv}-K_{av})$ $-(1+e_1)(K_{av}\cos^2\beta+K_{fv}\sin^2\beta$	$(e_2-1)\frac{\sin 2\beta}{2}(K_{fv}-K_{av})$
3	$-e_3K_{fv}$	0	$(e_1-1)K_{fv}$	$(e_2-1)\left[K_{av}\cos^2\beta + K_{fv}\sin^2\beta\right]$	$-e_3\frac{\sin 2\beta}{2}(K_{fv}-K_{av})$ $-(e_1-1)(K_{av}\cos^2\beta+K_{fv}\sin^2\beta$	$(e_2-1)\frac{\sin 2\beta}{2}(K_{fv}-K_{av})$
4	$-e_3K_{fv}$	0	$(e_1-1)K_{fv}$	$(1+e_2)\left[K_{av}\cos^2\beta + K_{fv}\sin^2\beta\right]$	$-e_3\frac{\sin 2\beta}{2}(K_{fv}-K_{av})$ $-(e_1-1)(K_{av}\cos^2\beta+K_{fv}\sin^2\beta$	$(1+e_2)\frac{\sin 2\beta}{2}(K_{fv}-K_{av})$
5	$-e_3\left[K_{fh}\cos^2(\theta-\beta^*) + K_{ah}\sin^2(\theta-\beta^*)\right]$	$-e_3\frac{\sin 2(\theta-\beta^*)}{2}(K_{ah}-K_{fh})$	$(1+e_1)\left[K_{fh}\cos^2(\theta-\beta^*)+K_{ah}\sin^2(\theta-\beta^*)\right]$ $-(1+e_2)\frac{\sin 2(\theta-\beta^*)}{2}(K_{ah}-K_{fh})$	$(1+e_2)K_{fh}$	$-(1+e_1)K_{fh}$	0
6	$-e_3\left[K_{fh}\cos^2(\theta-\beta^*) - K_{ah}\sin^2(\theta-\beta^*)\right]$	$e_3\frac{\sin 2(\theta-\beta^*)}{2}(K_{ah}-K_{fh})$	$(1+e_1)\left[K_{fh}\cos^2(\theta-\beta^*)+K_{ah}\sin^2(\theta-\beta^*)\right]$ $-(e_2-1)\frac{\sin 2(\theta-\beta^*)}{2}(K_{ah}-K_{fh})$	$(e_2-1)K_{fh}$	$-(1+e_1)K_{fh}$	0
7	$-e_3\left[K_{fh}\cos^2(\theta-\beta^*) - K_{ah}\sin^2(\theta-\beta^*)\right]$	$-e_3\frac{\sin 2(\theta-\beta^*)}{2}(K_{ah}-K_{fh})$	$(e_1-1)\left[K_{fh}\cos^2(\theta-\beta^*)+K_{ah}\sin^2(\theta-\beta^*)\right]$ $+(e_2-1)\frac{\sin 2(\theta-\beta^*)}{2}(K_{ah}-K_{fh})$	$(e_2-1)K_{fh}$	$-(e_1-1)K_{fh}$	0
8	$-e_3\left[K_{fh}\cos^2(\theta-\beta^*) - K_{ah}\sin^2(\theta-\beta^*)\right]$	$e_3\frac{\sin 2(\theta-\beta^*)}{2}(K_{ah}-K_{fh})$	$(e_1-1)\left[K_{fh}\cos^2(\theta-\beta^*)+K_{ah}\sin^2(\theta-\beta^*)\right]$ $-(1+e_2)\frac{\sin 2(\theta-\beta^*)}{2}(K_{ah}-K_{fh})$	$(1+e_2)K_{fh}$	$-(e_1-1)K_{fh}$	0

$b_{21}=-2e_3\left[K_{fh}\cos^2(\theta-\beta^*)+K_{ah}\sin^2(\theta-\beta^*)+2K_{fv}\right]-2e_3\left[K_{fh}\cos^2(\theta+\beta^*)+K_{ah}\sin^2(\theta+\beta^*)\right]$; $b_{22}=0$; $b_{23}=2e_1\left[K_{fh}\cos^2(\theta-\beta^*)+K_{ah}\sin^2(\theta-\beta^*)+2K_{fv}\right]+2e_1\left[K_{fh}\cos^2(\theta+\beta^*)+K_{ah}\sin^2(\theta+\beta^*)\right]$; $b_{31}=4e_2\left[K_{fh}+K_{av}\cos^2\beta+K_{fv}\sin^2\beta\right]$; $b_{32}=-4e_1\left[K_{fh}+K_{av}\cos^2\beta+K_{fv}\sin^2\beta\right]+4e_3\frac{\sin 2\beta}{2}(K_{fv}-K_{av})$; $b_{33}=4e_2\frac{\sin 2\beta}{2}(K_{fv}-K_{av})$

$$[B] = \begin{bmatrix} -4e_2\frac{\sin 2\beta}{2}(K_{fv}-K_{av}) & 4e_3\left[K_{fv}\cos^2\beta+K_{av}\sin^2\beta\right] & -4e_2\left[K_{fv}\cos^2\beta+K_{av}\sin^2\beta\right] \\ & +2e_3\left[K_{ah}\cos^2(\theta+\beta^*)+K_{fh}\sin^2(\theta+\beta^*)\right] & -2e_2\left[K_{ah}\cos^2(\theta+\beta^*)-K_{fh}\sin^2(\theta+\beta^*)\right] \\ -2e_3\left[K_{fh}\cos^2(\theta-\beta^*)\right. & +2e_3\left[K_{ah}\cos^2(\theta+\beta^*)+K_{fh}\sin^2(\theta+\beta^*)\right] & -2e_2\left[K_{ah}\cos^2(\theta+\beta^*)-K_{fh}\sin^2(\theta+\beta^*)\right] \\ \left.+K_{ah}\sin^2(\theta-\beta^*)+2K_{fv}\right] & +4e_1\frac{\sin 2\beta}{2}(K_{fv}-K_{av}) & 2e_1\left[K_{fh}\cos^2(\theta-\beta^*)\right. \\ -2e_3\left[K_{fh}\cos^2(\theta-\beta^*)+K_{ah}\sin^2(\theta-\beta^*)\right] & 0 & \left.+K_{ah}\sin^2(\theta-\beta^*)+2K_{fv}\right] \\ & & +2e_1\left[K_{fh}\cos^2(\theta+\beta^*)+K_{ah}\sin^2(\theta+\beta^*)\right] \\ 4e_2\left[K_{fh}+K_{av}\cos^2\beta+K_{fv}\sin^2\beta\right] & -4e_1\left[K_{fh}+K_{av}\cos^2\beta+K_{fv}\sin^2\beta\right] & +4e_2\frac{\sin 2\beta}{2}(K_{fv}-K_{av}) \\ & -4e_3\frac{\sin 2\beta}{2}(K_{fv}-K_{av}) & \end{bmatrix} \times$$

$$\begin{bmatrix} 0 & 4e_3\left[K_{fv}+K_{ah}\cos^2\theta\right. & -4e_2\left[K_{fv}+K_{ah}\cos^2\theta\right. \\ & \left.+K_{fh}\sin^2\theta\right] & \left.+K_{fh}\sin^2\theta\right] \\ -4e_3\left[K_{fh}\cos^2\theta\right. & 0 & 4e_1\left[K_{fv}+K_{fh}\cos^2\theta\right. \\ \left.+K_{ah}\sin^2\theta+K_{fv}\right] & & \left.+K_{ah}\sin^2\theta\right] \\ 4e_2(K_{fh}+K_{fv}) & -4e_1(K_{fh}+K_{av}) & 0 \end{bmatrix} \cdot \beta \begin{bmatrix} -4e_2(K_{fv}-K_{av}) & -4e_1(K_{fv}-K_{av}) & 0 \\ 0 & 0 & 0 \\ 0 & -4e_3(K_{fv}-K_{av}) & +4e_2(K_{fv}-K_{av} \end{bmatrix}$$

Isolator Number	e_{11} $(r_2b_{31}-r_3b_{21})$	e_{12} $(r_2b_{32}-r_3b_{22})$	e_{13} $r_2b_{33}-r_3b_{23}$
1	$(b+e_2)^2(K_{av}\cos^2\phi+K_{\ell v}\sin^2\phi)$ $+e_3^2K_{\ell v}$	$(b+e_2)\left\{-e_3\frac{\sin2\phi}{2}(K_{\ell v}-K_{av})-(\ell+e_1)\right.$ $\left.(K_{av}\cos^2\phi+K_{\ell v}\sin^2\phi)\right\}$	$+(b+e_2)^2\frac{\sin2\phi}{2}(K_{\ell v}-K_{av})-e_3(\ell+e_1)K_{\ell v}$
2	$(e_2-b)^2(K_{av}\cos^2\phi+K_{\ell v}\sin^2\phi)$ $+e_3^2K_{\ell v}$	$(e_2-b)\left\{-e_3\frac{\sin2\phi}{2}(K_{\ell v}-K_{av})-(\ell+e_1)\right.$ $\left.(K_{av}\cos^2\phi+K_{\ell v}\sin^2\phi)\right\}$	$+(e_2-b)^2\frac{\sin2\phi}{2}(K_{\ell v}-K_{av})-e_3(\ell+e_1)K_{\ell v}$
3	$(e_2-b)^2(K_{av}\cos^2\phi+K_{\ell v}\sin^2\phi)$ $+e_3^2K_{\ell v}$	$(e_2-b)\left\{-e_3\frac{\sin2\phi}{2}(K_{\ell v}-K_{av})-(e_1-\ell)\right.$ $\left.(K_{av}\cos^2\phi+K_{\ell v}\sin^2\phi)\right\}$	$+(e_2-b)^2\frac{\sin2\phi}{2}(K_{\ell v}-K_{av})-e_3(e_1-\ell)K_{\ell v}$
4	$(b+e_2)^2(K_{av}\cos^2\phi+K_{\ell v}\sin^2\phi)$ $+e_3^2K_{\ell v}$	$(b+e_2)\left\{-e_3\frac{\sin2\phi}{2}(K_{\ell v}-K_{av})-(e_1-\ell)\right.$ $\left.(K_{av}\cos^2\phi+K_{\ell v}\sin^2\phi)\right\}$	$+(b+e_2)^2\frac{\sin2\phi}{2}(K_{\ell v}-K_{av})-e_3(e_1-\ell)K_{\ell v}$
5	$(B+e_2)^2K_{\ell h}+e_3^2\left\{K_{\ell h}\cos^2(\theta-\phi^*)\right.$ $\left.+K_{ah}\sin^2(\theta-\phi^*)\right\}$	$-(B+e_2)(\ell+e_1)K_{\ell h}+e_3^2\frac{\sin2(\theta-\phi^*)}{2}(K_{ah}-K_{\ell h})$	$-e_3\left[(\ell+e_1)\left\{K_{\ell h}\cos^2(\theta-\phi^*)+K_{ah}\sin^2(\theta-\phi^*)\right\}\right.$ $\left.+(B+e_2)\frac{\sin2(\theta-\phi^*)}{2}(K_{ah}-K_{\ell h})\right]$
6	$(e_2-B)^2K_{\ell h}+e_3^2\left\{K_{\ell h}\cos^2(\theta-\phi^*)\right.$ $\left.+K_{ah}\sin^2(\theta-\phi^*)\right\}$	$-(e_2-B)(\ell+e_1)K_{\ell h}-e_3^2\frac{\sin2(\theta-\phi^*)}{2}(K_{ah}-K_{\ell h})$	$-e_3\left[(\ell+e_1)\left\{K_{\ell h}\cos^2(\theta-\phi^*)+K_{ah}\sin^2(\theta-\phi^*)\right\}\right.$ $\left.-(e_2-B)\frac{\sin2(\theta-\phi^*)}{2}(K_{ah}-K_{\ell h})\right]$
7	$(e_2-B)^2K_{\ell h}+e_3^2\left\{K_{\ell h}\cos^2(\theta+\phi^*)\right.$ $\left.+K_{ah}\sin^2(\theta+\phi^*)\right\}$	$-(e_2-B)(e_1-\ell)K_{\ell h}+e_3^2\frac{\sin2(\theta+\phi^*)}{2}(K_{ah}-K_{\ell h})$	$-e_3\left[(e_1-\ell)\left\{K_{\ell h}\cos^2(\theta+\phi^*)+K_{ah}\sin^2(\theta+\phi^*)\right\}\right.$ $\left.+(e_2-B)\frac{\sin2(\theta+\phi^*)}{2}(K_{ah}-K_{\ell h})\right]$
8	$(B+e_2)^2K_{\ell h}+e_3^2\left\{K_{\ell h}\cos^2(\theta+\phi^*)\right.$ $\left.+K_{ah}\sin^2(\theta+\phi^*)\right\}$	$-(B+e_2)(e_1-\ell)K_{\ell h}-e_3^2\frac{\sin2(\theta+\phi^*)}{2}(K_{ah}-K_{\ell h})$	$-e_3\left[(e_1-\ell)\left\{K_{\ell h}\cos^2(\theta+\phi^*)+K_{ah}\sin^2(\theta+\phi^*)\right\}\right.$ $\left.-(B+e_2)\frac{\sin2(\theta+\phi^*)}{2}(K_{ah}-K_{\ell h})\right]$

$\sum$: $e_{11}=+2e_3^2\left[2K_{\ell v}+\left\{K_{\ell h}\cos^2(\theta-\phi^*)+K_{ah}\sin^2(\theta-\phi^*)\right\}\right]+4e_2^2\left[(K_{av}\cos^2\phi+K_{\ell v}\sin^2\phi)+K_{\ell h}\right]+4B^2K_{\ell h}+4b^2(K_{av}\cos^2\phi+K_{\ell v}\sin^2\phi)$
$+2e_3^2\left[K_{\ell h}\cos^2(\theta+\phi^*)+K_{ah}\sin^2(\theta+\phi^*)\right]$; $e_{12}=-4e_1e_2\left[(K_{av}\cos^2\phi+K_{\ell v}\sin^2\phi)+K_{\ell h}\right]-4e_2e_3\frac{\sin2\phi}{2}(K_{\ell v}-K_{av})$;
$e_{13}=-2e_1e_3\left[2K_{\ell v}+\left\{K_{\ell h}\cos^2(\theta-\phi^*)+K_{ah}\sin^2(\theta-\phi^*)\right\}\right]+4(b^2+e_2^2)\frac{\sin2\phi}{2}(K_{\ell v}-K_{av})-2e_1e_3\left[K_{\ell h}\cos^2(\theta+\phi^*)+K_{ah}\sin^2(\theta+\phi^*)\right]$

Isolator Number	e_{21} $(r_3b_{11}-r_1b_{31})$	e_{22} $(r_3b_{12}-r_1b_{32})$	e_{23} $(r_3b_{13}-r_1b_{33})$
1	$-e_3(b+e_2)\frac{\sin2\phi}{2}(K_{\ell v}-K_{av})-(\ell-e_1)$ $(b+e_2)(K_{av}\cos^2\phi+K_{\ell v}\sin^2\phi)$	$e_3(\ell+e_1)\frac{\sin2\phi}{2}(K_{\ell v}-K_{av})+e_3^2(K_{\ell v}\cos^2\phi+K_{av}\sin^2\phi)-(\ell+e_1)$ $\left\{-e_3\frac{\sin2\phi}{2}(K_{\ell v}-K_{av})-(\ell+e_1)(K_{av}\cos^2\phi+K_{\ell v}\sin^2\phi)\right\}$	$-e_3(b+e_2)(K_{\ell v}\cos^2\phi+K_{av}\sin^2\phi)$ $-(\ell+e_1)(b+e_2)\frac{\sin2\phi}{2}(K_{\ell v}-K_{av})$
2	$-e_3(e_2-b)\frac{\sin2\phi}{2}(K_{\ell v}-K_{av})-(\ell+e_1)$ $(e_2-b)(K_{av}\cos^2\phi+K_{\ell v}\sin^2\phi)$	$e_3(\ell+e_1)\frac{\sin2\phi}{2}(K_{\ell v}-K_{av})+e_3^2(K_{\ell v}\cos^2\phi+K_{av}\sin^2\phi)-(\ell+e_1)$ $\left\{-e_3\frac{\sin2\phi}{2}(K_{\ell v}-K_{av})-(\ell+e_1)(K_{av}\cos^2\phi+K_{\ell v}\sin^2\phi)\right\}$	$-e_3(e_2-b)(K_{\ell v}\cos^2\phi+K_{av}\sin^2\phi)$ $-(\ell+e_1)(e_2-b)\frac{\sin2\phi}{2}(K_{\ell v}-K_{av})$
3	$-e_3(e_1-b)\frac{\sin2\phi}{2}(K_{\ell v}-K_{av})-(e_1-\ell)$ $(e_2-b)(K_{av}\cos^2\phi+K_{\ell v}\sin^2\phi)$	$e_3(e_1-\ell)\frac{\sin2\phi}{2}(K_{\ell v}-K_{av})+e_3^2(K_{\ell v}\cos^2\phi+K_{av}\sin^2\phi)-(e_1-\ell)$ $\left\{-e_3\frac{\sin2\phi}{2}(K_{\ell v}-K_{av})-(e_1-\ell)(K_{av}\cos^2\phi+K_{\ell v}\sin^2\phi)\right\}$	$-e_3(e_2-b)(K_{\ell v}\cos^2\phi+K_{av}\sin^2\phi)$ $-(e_1-\ell)(e_2-b)\frac{\sin2\phi}{2}(K_{\ell v}-K_{av})$
4	$-e_3(b+e_2)\frac{\sin2\phi}{2}(K_{\ell v}-K_{av})-(e_1-\ell)$ $(b+e_2)(K_{av}\cos^2\phi+K_{\ell v}\sin^2\phi)$	$e_3(e_1-\ell)\frac{\sin2\phi}{2}(K_{\ell v}-K_{av})+e_3^2(K_{\ell v}\cos^2\phi+K_{av}\sin^2\phi)-(e_1-\ell)$ $\left\{-e_3\frac{\sin2\phi}{2}(K_{\ell v}-K_{av})-(e_1-\ell)(K_{av}\cos^2\phi+K_{\ell v}\sin^2\phi)\right\}$	$-e_3(b+e_2)(K_{\ell v}\cos^2\phi+K_{av}\sin^2\phi)$ $-(e_1-\ell)(b+e_2)\frac{\sin2\phi}{2}(K_{\ell v}-K_{av})$
5	$e_3\frac{\sin2(\theta-\phi^*)}{2}(K_{ah}-K_{\ell h})-(\ell+e_1)$ $(B+e_2)K_{\ell h}$	$e_3^2\left\{K_{ah}\cos^2(\theta-\phi^*)+K_{\ell h}\sin^2(\theta-\phi^*)\right\}+(\ell+e_1)^2K_{\ell h}$	$e_3\left[-(\ell+e_1)\frac{\sin2(\theta-\phi^*)}{2}(K_{ah}-K_{\ell h})\right.$ $\left.-(B+e_2)\left\{K_{ah}\cos^2(\theta-\phi^*)+K_{\ell h}\sin^2(\theta-\phi^*)\right\}\right]$
6	$-e_3\frac{\sin2(\theta-\phi^*)}{2}(K_{ah}-K_{\ell h})-(\ell+e_1)$ $(e_2-B)K_{\ell h}$	$e_3^2\left\{K_{ah}\cos^2(\theta-\phi^*)+K_{\ell h}\sin^2(\theta-\phi^*)\right\}+(\ell+e_1)^2K_{\ell h}$	$e_3\left[+(\ell+e_1)\frac{\sin2(\theta-\phi^*)}{2}(K_{ah}-K_{\ell h})\right.$ $\left.-(e_2-B)\left\{K_{ah}\cos^2(\theta-\phi^*)+K_{\ell h}\sin^2(\theta-\phi^*)\right\}\right]$
7	$-e_3\frac{\sin2(\theta-\phi^*)}{2}(K_{ah}-K_{\ell h})-(e_1-\ell)$ $(e_2-B)K_{\ell h}$	$e_3^2\left\{K_{ah}\cos^2(\theta-\phi^*)+K_{\ell h}\sin^2(\theta-\phi^*)\right\}+(e_1-\ell)^2K_{\ell h}$	$e_3\left[-(e_1-\ell)\frac{\sin2(\theta-\phi^*)}{2}(K_{ah}-K_{\ell h})\right.$ $\left.-(e_2-B)\left\{K_{ah}\cos^2(\theta-\phi^*)+K_{\ell h}\sin^2(\theta-\phi^*)\right\}\right]$
8	$-e_3\frac{\sin2(\theta-\phi^*)}{2}(K_{ah}-K_{\ell h})-(e_1-\ell)$ $(e_2+B)K_{\ell h}$	$e_3^2\left\{K_{ah}\cos^2(\theta+\phi^*)+K_{\ell h}\sin^2(\theta+\phi^*)\right\}+(e_1-\ell)^2K_{\ell h}$	$e_3\left[+(e_1-\ell)\frac{\sin2(\theta+\phi^*)}{2}(K_{ah}-K_{\ell h})\right.$ $\left.-(B+e_2)\left\{K_{ah}\cos^2(\theta+\phi^*)+K_{\ell h}\sin^2(\theta+\phi^*)\right\}\right]$

$\sum$: $e_{21}=-4e_1e_2\left\{(K_{av}\cos^2\phi+K_{\ell v}\sin^2\phi)+K_{\ell h}\right\}-4e_2e_3\frac{\sin2\phi}{2}(K_{\ell v}-K_{av})$; $e_{22}=2e_3^2\left[2(K_{\ell v}\cos^2\phi+K_{av}\sin^2\phi)+K_{ah}\cos^2(\theta-\phi^*)+K_{\ell h}\sin^2(\theta-\phi^*)\right]$
$+4(\ell^2+e_1^2)\left\{K_{av}\cos^2\phi+K_{\ell v}\sin^2\phi+K_{\ell h}\right\}+8e_1e_3\frac{\sin2\phi}{2}(K_{\ell v}-K_{av})+2e_3^2\left[K_{ah}\cos^2(\theta+\phi^*)-K_{\ell h}\sin^2(\theta+\phi^*)\right]$; $e_{23}=2e_2e_3\left\{2K_{\ell v}\cos^2\phi\right.$
$\left.+\sin^2\phi+K_{ah}\cos^2(\theta-\phi^*)+K_{\ell h}\sin^2(\theta-\phi^*)\right\}-4e_1e_2\frac{\sin2\phi}{2}(K_{\ell v}-K_{av})-2e_2e_3\left[K_{ah}\cos^2(\theta+\phi^*)+K_{\ell h}\sin^2(\theta+\phi^*)\right]$

Isolator Number	e_{31} $(r_1b_{21}-r_2b_{11})$	e_{32} $(r_1b_{22}-r_2b_{12})$	e_{33} $(r_1b_{23}-r_2b_{13})$
1	$-(\ell+e_1)e_3K_{\ell v}+(b+e_2)\frac{2\sin2\phi}{2}(K_{\ell v}-K_{av})$	$-(b+e_2)(\ell+e_1)\frac{\sin2\phi}{2}(K_{\ell v}-K_{av})$ $-e_3(b+e_2)(K_{\ell v}\cos^2\phi+K_{av}\sin^2\phi)$	$(\ell+e_1)^2K_{\ell v}+(b+e_2)^2(K_{\ell v}\cos^2\phi+K_{av}\sin^2\phi)$
2	$-(\ell+e_1)e_3K_{\ell v}+(e_2-b)\frac{2\sin2\phi}{2}(K_{\ell v}-K_{av})$	$-(e_2-b)(\ell+e_1)\frac{\sin2\phi}{2}(K_{\ell v}-K_{av})$ $-e_3(e_2-b)(K_{\ell v}\cos^2\phi+K_{av}\sin^2\phi)$	$(\ell+e_1)^2K_{\ell v}+(e_2-b)^2(K_{\ell v}\cos^2\phi+K_{av}\sin^2\phi)$
3	$-(e_1-\ell)e_3K_{\ell v}+(e_2-b)\frac{2\sin2\phi}{2}(K_{\ell v}-K_{av})$	$-(e_2-b)(e_1-\ell)\frac{\sin2\phi}{2}(K_{\ell v}-K_{av})$ $-e_3(e_2-b)(K_{\ell v}\cos^2\phi+K_{av}\sin^2\phi)$	$(e_1-\ell)^2K_{\ell v}+(e_2-b)^2(K_{\ell v}\cos^2\phi+K_{av}\sin^2\phi)$
4	$-(e_1-\ell)e_3K_{\ell v}+(b+e_2)\frac{2\sin2\phi}{2}(K_{\ell v}-K_{av})$	$-(b+e_2)(e_1-\ell)\frac{\sin2\phi}{2}(K_{\ell v}-K_{av})$ $-e_3(b+e_2)(K_{\ell v}\cos^2\phi+K_{av}\sin^2\phi)$	$(e_1-\ell)^2K_{\ell v}+(b+e_2)^2(K_{\ell v}\cos^2\phi+K_{av}\sin^2\phi)$
5	$-(\ell+e_1)e_3\left\{K_{\ell h}\cos^2(\theta-\phi^*)+K_{ah}\sin^2(\theta-\phi^*)\right\}$ $-(B+e_2)\frac{\sin2(\theta-\phi^*)}{2}(K_{ah}-K_{\ell h})(e_3)$	$(\ell+e_1)e_3\frac{\sin2(\theta-\phi^*)}{2}(K_{ah}-K_{\ell h})$ $-e_3(B+e_2)\left\{K_{ah}\cos^2(\theta-\phi^*)+K_{\ell h}\sin^2(\theta-\phi^*)\right\}$	$(\ell+e_1)\left[(\ell+e_1)\left\{K_{\ell h}\cos^2(\theta-\phi^*)+K_{ah}\sin^2(\theta-\phi^*)\right\}\right.$ $\left.+(B+e_2)\frac{\sin2(\theta-\phi^*)}{2}(K_{ah}-K_{\ell h})\right]-(B+e_2)$ $\left[(\ell+e_1)\frac{\sin2(\theta-\phi^*)}{2}(K_{ah}-K_{\ell h})-(B+e_2)\right.$ $\left.\left\{K_{ah}\cos^2(\theta-\phi^*)+K_{\ell h}\sin^2(\theta-\phi^*)\right\}\right]$
6	$-(\ell+e_1)e_3\left\{K_{\ell h}\cos^2(\theta-\phi^*)+K_{ah}\sin^2(\theta-\phi^*)\right\}$ $+(e_2-B)\frac{\sin2(\theta-\phi^*)}{2}(K_{ah}-K_{\ell h})(e_3)$	$-(\ell+e_1)(-e_3)\frac{\sin2(\theta-\phi^*)}{2}(K_{ah}-K_{\ell h})$ $-e_3(e_2-B)\left\{K_{ah}\cos^2(\theta-\phi^*)+K_{\ell h}\sin^2(\theta-\phi^*)\right\}$	$(\ell+e_1)\left[(\ell+e_1)\left\{K_{\ell h}\cos^2(\theta-\phi^*)+K_{ah}\sin^2(\theta-\phi^*)\right\}\right.$ $\left.-(e_2-B)\frac{\sin2(\theta-\phi^*)}{2}(K_{ah}-K_{\ell h})\right]-(e_2-B)$ $\left[(\ell+e_1)\frac{\sin2(\theta-\phi^*)}{2}(K_{ah}-K_{\ell h})-(e_2-B)\right.$ $\left.\left\{K_{ah}\cos^2(\theta-\phi^*)+K_{\ell h}\sin^2(\theta-\phi^*)\right\}\right]$
7	$-(e_1-\ell)e_3\left\{K_{\ell h}\cos^2(\theta+\phi^*)+K_{ah}\sin^2(\theta+\phi^*)\right\}$ $-(e_2-B)\frac{\sin2(\theta+\phi^*)}{2}(K_{ah}-K_{\ell h})(e_3)$	$-(e_1-\ell)(e_3)\frac{\sin2(\theta+\phi^*)}{2}(K_{ah}-K_{\ell h})$ $-e_3(e_2-B)\left\{K_{ah}\cos^2(\theta+\phi^*)+K_{\ell h}\sin^2(\theta+\phi^*)\right\}$	$(e_1-\ell)\left[(e_1-\ell)\left\{K_{\ell h}\cos^2(\theta+\phi^*)+K_{ah}\sin^2(\theta+\phi^*)\right\}\right.$ $\left.+(e_2-B)\frac{\sin2(\theta+\phi^*)}{2}(K_{ah}-K_{\ell h})\right]-(e_2-B)$ $\left[(e_1-\ell)\frac{\sin2(\theta+\phi^*)}{2}(K_{ah}-K_{\ell h})-(e_2-B)\right.$ $\left.\left\{K_{ah}\cos^2(\theta+\phi^*)+K_{\ell h}\sin^2(\theta+\phi^*)\right\}\right]$
8	$-(e_1-\ell)e_3\left\{K_{\ell h}\cos^2(\theta+\phi^*)+K_{ah}\sin^2(\theta+\phi^*)\right\}$ $+(B+e_2)\frac{\sin2(\theta+\phi^*)}{2}(K_{ah}-K_{\ell h})(e_3)$	$-(e_1-\ell)(-e_3)\frac{\sin2(\theta+\phi^*)}{2}$ $(K_{ah}-K_{\ell h})-e_3(B+e_2)$ $\left\{K_{ah}\cos^2(\theta+\phi^*)+K_{\ell h}\sin^2(\theta+\phi^*)\right\}$	$(e_1-\ell)\left[(e_1-\ell)\left\{K_{\ell h}\cos^2(\theta+\phi^*)+K_{ah}\sin^2(\theta+\phi^*)\right\}\right.$ $\left.-(B+e_2)\frac{\sin2(\theta+\phi^*)}{2}(K_{ah}-K_{\ell h})\right]-(B+e_2)$ $\left[(e_1-\ell)\frac{\sin2(\theta+\phi^*)}{2}(K_{ah}-K_{\ell h})-(B+e_2)\right.$ $\left.\left\{K_{ah}\cos^2(\theta+\phi^*)+K_{\ell h}\sin^2(\theta+\phi^*)\right\}\right]$

$\sum$: $e_{31}=-2e_1e_3\left\{2K_{\ell v}+K_{\ell h}\cos^2(\theta-\phi^*)+K_{ah}\sin^2(\theta-\phi^*)\right\}+4(b^2+e_2^2)\frac{\sin2\phi}{2}(K_{\ell v}-K_{av})-2e_1e_3\left\{K_{ah}\cos^2(\theta+\phi^*)+K_{ah}\sin^2(\theta+\phi^*)\right\}$;
$e_{32}=-2e_2e_3\left\{2K_{\ell v}\cos^2\phi+2K_{av}\sin^2\phi+K_{ah}\cos^2(\theta-\phi^*)+K_{\ell h}\sin^2(\theta-\phi^*)\right\}-4e_1e_2\frac{\sin2\phi}{2}(K_{\ell v}-K_{av})-2e_2e_3\left[K_{ah}\cos^2(\theta+\phi^*)\right.$
$\left.+K_{\ell h}\sin^2(\theta+\phi^*)\right]$; $e_{33}=2(\ell^2+e_1^2)\left\{2K_{\ell v}+K_{\ell h}\cos^2(\theta-\phi^*)+K_{ah}\sin^2(\theta-\phi^*)\right\}+4(b^2+e_2^2)(K_{\ell v}\cos^2\phi+K_{av}\sin^2\phi)+2(B^2+e_2^2)$
$\left\{K_{ah}\cos^2(\theta-\phi^*)+K_{\ell h}\sin^2(\theta-\phi^*)\right\}+4B\ell\frac{\sin2(\theta-\phi^*)}{2}(K_{ah}-K_{\ell h})+4B\ell\frac{\sin2(\theta+\phi^*)}{2}(K_{ah}-K_{\ell h})+2(\ell^2+e_1^2)\left[K_{\ell h}\cos^2(\theta+\phi^*)\right.$
$\left.+K_{ah}\sin^2(\theta+\phi^*)\right]+2(B^2+e_2^2)\left[K_{ah}\cos^2(\theta+\phi^*)+K_{\ell h}\sin^2(\theta+\phi^*)\right]$

$$[E] = \begin{bmatrix} 2e_3^2\left[2K_{fv}+\left\{K_{fh}\cos^2(\theta-\phi^*)+K_{ah}\sin^2(\theta-\phi^*)\right\}\right]+4e_2^2\left[(K_{av}\cos^2\phi+K_{fv}\sin^2\phi)+K_{fh}\right]+4b^2(K_{av}\cos^2\phi+K_{fv}\sin^2\phi)+4B^2K_{fh}+2e_3^2\left[K_{fh}\cos^2(\theta+\phi^*)+K_{ah}\sin^2(\theta+\phi^*)\right] & \left\{-4e_1e_2\left[(K_{av}\cos^2\phi+K_{fv}\sin^2\phi)+K_{fh}\right]-4e_2e_3\frac{\sin2\phi}{2}(K_{fv}-K_{av})\right\} & -2e_1e_3\left[2K_{fv}+\left\{K_{fh}\cos^2(\theta-\phi^*)+K_{ah}\sin^2(\theta-\phi^*)\right\}\right]+4(b^2+e_2^2)\frac{\sin2\phi}{2}(K_{fv}-K_{av})-2e_1e_3\left[K_{fh}\cos^2(\theta+\phi^*)+K_{ah}\sin^2(\theta+\phi^*)\right] \\ \left[-4e_1e_2\left\{(K_{av}\cos^2\phi+K_{fv}\sin^2\phi)+K_{fh}\right\}-4e_2e_3\frac{\sin2\phi}{2}(K_{fv}-K_{av})\right] & \left\{2e_3^2\left[2(K_{fv}\cos^2\phi+K_{av}\sin^2\phi)+K_{ah}\cos^2(\theta-\phi^*)+K_{fh}\sin^2(\theta-\phi^*)\right]-8e_1e_3\frac{\sin2\phi}{2}(K_{fv}-K_{av})+4(f^2+e_1^2)(K_{av}\cos^2\phi+K_{fv}\sin^2\phi)+2e_3^2\left[K_{ah}\cos^2(\theta+\phi^*)+K_{fh}\sin^2(\theta+\phi^*)\right]\right\} & \left[-2e_2e_3\left\{2K_{fv}\cos^2\phi+2K_{av}\sin^2\phi+K_{fh}\cos^2(\theta-\phi^*)+K_{ah}\sin^2(\theta-\phi^*)\right\}+4e_1e_2\frac{\sin2\phi}{2}(K_{fv}-K_{av})\right] \\ \left[-2+e_1e_3\left\{2K_{fv}+K_{fh}\cos^2(\theta-\phi^*)\right\}+4(b^2+e_2^2)\frac{\sin2\phi}{2}(K_{fv}-K_{av})\right]-2e_1e_3\left[K_{fh}\cos^2(\theta+\phi^*)+K_{ah}\sin^2(\theta+\phi^*)\right] & \left[-2e_2e_3\left\{2K_{fv}\cos^2\phi+2K_{av}\sin^2\phi+K_{fh}\cos^2(\theta-\phi^*)+K_{ah}\sin^2(\theta-\phi^*)\right\}+4e_1e_2\frac{\sin2\phi}{2}(K_{fv}-K_{av})\right]-2e_2e_3 & \left[2(f^2+e_1^2)\left\{2K_{fv}+K_{fh}\cos^2(\theta-\phi^*)+K_{ah}\sin^2(\theta-\phi^*)\right\}+4B(b^2+e_2^2)(K_{fv}\cos^2\phi+K_{av}\sin^2\phi)+4B\frac{\sin2\phi}{2}(K_{ah}-K_{fv})+2(B^2+e_2^2)\left\{K_{ah}\cos^2(\theta-\phi^*)+K_{fh}\sin^2(\theta-\phi^*)\right\}+4B\frac{\sin2(\theta+\phi^*)}{2}(K_{ah}-K_{fh})+2(f^2+e_1^2)\left[K_{fh}\cos^2(\theta+\phi^*)+K_{ah}\sin^2(\theta+\phi^*)\right]+2(B^2+e_2^2)\left[K_{ah}\cos^2(\theta+\phi^*)+K_{fh}\sin^2(\theta+\phi^*)\right] \end{bmatrix}$$

$$
\therefore [E] = \begin{bmatrix}
4e_3^2(K_{\rho v}+K_{\rho h}\cos^2\theta+K_{ah}\sin^2\theta) & -4e_1e_2(K_{av}+K_{\rho h}) & -4e_1e_3(K_{\rho v}+K_{\rho h}\cos^2\theta+K_{ah}\sin^2\theta) \\
+4e_2^2(K_{av}+K_{\eta h})+4b^2K_{zv} & & \\
+4B^2K_{\rho h} & & \\
-4e_1e_2(K_{av}+K_{\rho h}) & 4e_3^2(K_{\rho v}+K_{ah}\cos^2\theta+K_{\rho h}\sin^2\theta) & -4e_2e_3(K_{\rho v}+K_{ah}\cos^2\theta+K_{\rho h}\sin^2\theta) \\
 & +4(\rho^2+e_1^2)(K_{av}+K_{\rho h}) & \left[4(\rho^2+e_1^2)\{(K_{\rho v}+K_{\rho h}\cos^2\theta+K_{ah}\sin^2\theta\right. \\
-4e_1e_3(K_{\rho v}+K_{\rho h}\cos^2\theta & -4e_2e_3(K_{\rho v}+K_{ah}\cos^2\theta+K_{\rho h}\sin^2\theta) & +4(b^2+e_2^2)K_{\rho v}+4(B^2+e_2^2)(K_{ah}\cos^2\theta-K_{\rho h}\sin^2\theta) \\
+K_{ah}\sin^2\theta) & & -8B\rho\frac{\sin 2\theta}{2}(K_{ah}-K_{\rho h})
\end{bmatrix}
$$

$$
+ \begin{bmatrix}
0 & -4e_2e_3(K_{\rho v}-K_{av}) & 4(b^2+e_2^2)(K_{\rho v}-K_{av}) \\
-4e_2e_3(K_{\rho v}-K_{av}) & 8e_1e_3(K_{\rho v}-K_{av}) & -4e_1e_2(K_{\rho v}-K_{av}) \\
4(b^2+e_2^2)(K_{\rho v}-K_{av}) & -4e_1e_2(K_{\rho v}-K_{av}) & 0
\end{bmatrix}
$$

3.8.4.2.3 Example D-3: Horizontal Elastic Elements Parallel to Both Axes

The isolation system is as shown in Figure 3.8.15. The isolator stiffnesses are similar to the stiffnesses of Example C-3 (Section 3.8.4.1.3). The presence of eccentricities changes the [B] and [E] matrices which are tabulated on the following pages.

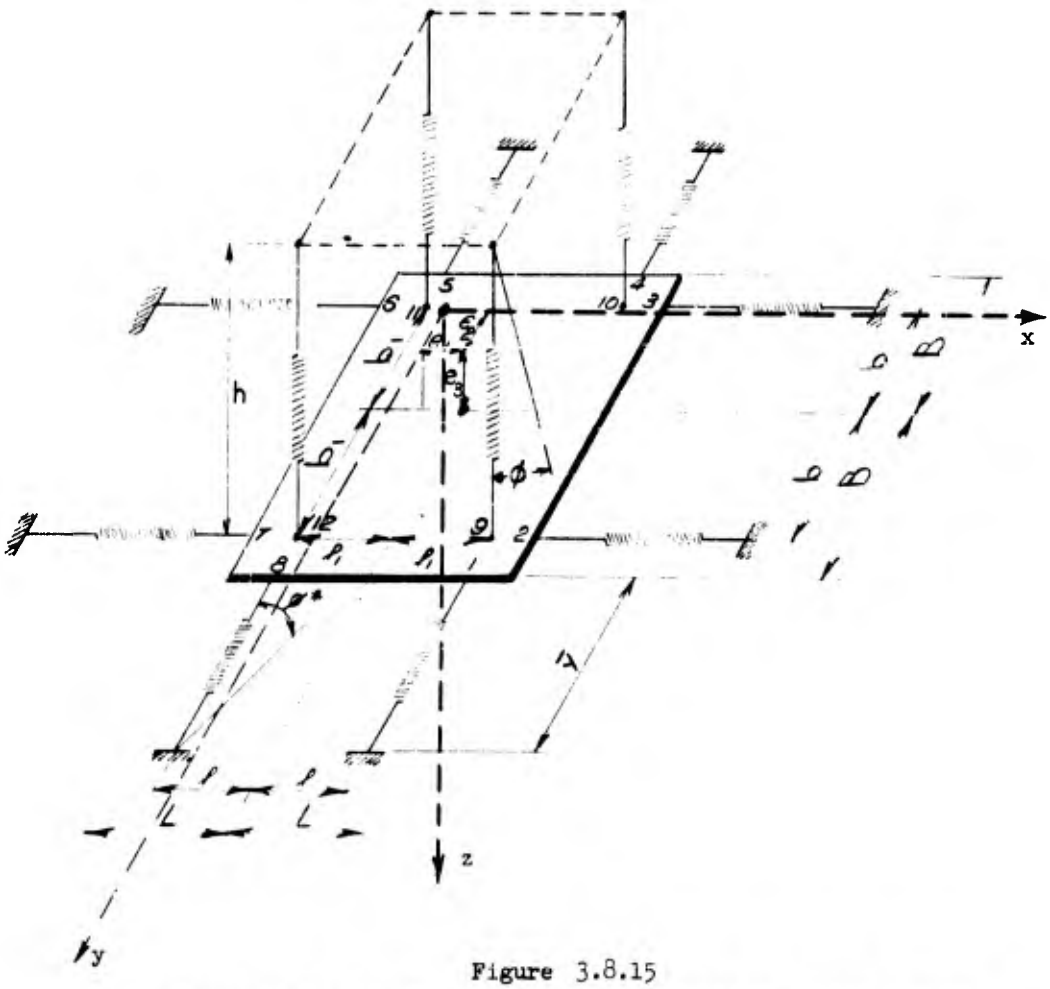

Figure 3.8.15

Unsymmetrical Elastic Pendulum with Parallel Horizontal Elements

Isolator Number	Axial Orientation	r_1	r_2	r_3	b_{11} $(r_2c_{13}-r_3c_{12})$	b_{12} $(r_3c_{11}-r_1c_{13})$	b_{13} $(r_1c_{12}-r_2c_{11})$
1	Parallel to y-axis	$\ell+e_1$	$B+e_2$	e_3	$e_3\frac{\sin2\phi^*}{2}(K_{2a}-K_{2\ell x})$	$e_3(K_{2\ell x}\cos^2\phi^*+K_{3a}\sin^2\phi^*)$	$\left[-(\ell+e_1)\frac{\sin2\phi^*}{2}(K_{2a}-K_{2\ell x})\right.$ $\left.-(B+e_2)(K_{2\ell x}\cos^2\phi^*+K_{2a}\sin^2\phi^*)\right]$
4	Parallel to y-axis	$\ell+e_1$	e_2-B	e_3	$-e_3\frac{\sin2\phi^*}{2}(K_{2a}-K_{2\ell x})$	$e_3(K_{2\ell x}\cos^2\phi^*+K_{2a}\sin^2\phi^*)$	$\left[-(\ell+e_1)\frac{\sin2\phi^*}{2}(K_{2\ell x}-K_{2a})\right.$ $\left.-(e_2-B)(K_{2\ell x}\cos^2\phi^*+K_{2a}\sin^2\phi^*)\right]$
5	Parallel to y-axis	$e_1-\ell$	e_2-B	e_3	$-e_3\frac{\sin2\phi^*}{2}(K_{2a}-K_{2\ell x})$	$e_3(K_{2\ell x}\cos^2\phi^*+K_{2a}\sin^2\phi^*)$	$\left[-(e_1-\ell)\frac{\sin2\phi^*}{2}(K_{2\ell x}-K_{2a})\right.$ $\left.-(e_2-B)(K_{2\ell x}\cos^2\phi^*+K_{2a}\sin^2\phi^*)\right]$
8	Parallel to y-axis	$e_1-\ell$	$B+e_2$	e_3	$e_3\frac{\sin2\phi^*}{2}(K_{2a}-K_{2\ell x})$	$e_3(K_{2\ell x}\cos^2\phi^*+K_{2a}\sin^2\phi^*)$	$\left[-(e_1-\ell)\frac{\sin2\phi^*}{2}(K_{2a}-K_{2\ell x})\right.$ $\left.-(B+e_2)(K_{2\ell x}\cos^2\phi^*+K_{2a}\sin^2\phi^*)\right]$
2	Parallel to x-axis	$L+e_1$	$b+e_2$	e_3	o	e_3K_{1a}	$-(b+e_2)K_{1a}$
3	Parallel to x-axis	$L+e_1$	e_2-b	e_3	o	e_3K_{1a}	$-(e_2-b)K_{1a}$
6	Parallel to x-axis	e_1-L	e_2-b	e_3	o	e_3K_{1a}	$-(e_2-b)K_{1a}$
7	Parallel to x-axis	e_1-L	$b+e_2$	e_3	o	e_3K_{1a}	$-(b+e_2)K_{1a}$
9	Parallel to z-axis	ℓ_1+e_1	b_1+e_2	e_3	$-(b_1+e_2)\frac{\sin2\phi}{2}(K_{3\ell x}-K_{3a})$	$\left\{e_3(K_{3\ell x}\cos^2\phi+K_{3a}\sin^2\phi)\right.$ $\left.+(\ell_1+e_1)\frac{\sin2\phi}{2}(K_{3\ell x}-K_{3a})\right\}$	$-(b_1+e_2)(K_{3\ell x}\cos^2\phi+K_{3a}\sin^2\phi)$
10	Parallel to z-axis	ℓ_1+e_1	e_2-b_1	e_3	$-(e_2-b_1)\frac{\sin2\phi}{2}(K_{3\ell x}-K_{3a})$	$\left\{e_3(K_{3\ell x}\cos^2\phi+K_{3a}\sin2\phi)\right.$ $\left.+(\ell_1+e_1)\frac{\sin2\phi}{2}(K_{3\ell x}-K_{3a})\right\}$	$-(e_2-b_1)(K_{3\ell x}\cos^2\phi+K_{3a}\sin^2\phi)$
11	Parallel to z-axis	$e_1-\ell_1$	e_2-b_1	e_3	$-(e_2-b_1)\frac{\sin2\phi}{2}(K_{3\ell x}-K_{3a})$	$\left\{e_3(K_{3\ell x}\cos^2\phi+K_{3a}\sin2\phi)\right.$ $\left.+(e_1-\ell_1)\frac{\sin2\phi}{2}(K_{3\ell x}-K_{3a})\right\}$	$-(e_2-b_1)(K_{3\ell x}\cos^2\phi+K_{3a}\sin^2\phi)$
12	Parallel to z-axis	$e_1-\ell_1$	b_1+e_2	e_3	$-(b_1-e_2)\frac{\sin2\phi}{2}(K_{3\ell x}-K_{3a})$	$\left\{e_3(K_{3\ell x}\cos^2\phi+K_{3a}\sin2\phi)\right.$ $\left.+(e_1-\ell_1)\frac{\sin2\phi}{2}(K_{3\ell x}-K_{3a})\right\}$	$-(b_1+e_2)(K_{3\ell x}\cos^2\phi+K_{3a}\sin^2\phi)$

$\sum$: $b_{11}=4e_2\frac{\sin2\phi}{2}(K_{3\ell x}-K_{3a})$; $b_{12}=\left[4e_3\left\{(K_{2\ell x}\cos^2\phi^*+K_{2a}\sin^2\phi^*)+K_{1a}+(K_{3\ell x}\cos^2\phi+K_{3a}\sin^2\phi)\right\}+4e_1\frac{\sin2\phi}{2}(K_{3\ell x}-K_{3a})\right]$;

$b_{13}=-4e_2\left[(K_{2\ell x}\cos^2\phi^*+K_{2a}\sin^2\phi^*)+K_{1a}+(K_{3\ell x}\cos^2\phi+K_{3a}\sin^2\phi)\right]$

Isolator Number	b_{21} $(r_2c_{23}-r_3c_{22})$	b_{22} $(r_3c_{21}-r_1c_{23})$	b_{23} $(r_1c_{22}-r_2c_{21})$	b_{31} $(r_2c_{33}-r_3c_{32})$	b_{32} $(r_3c_{31}-r_1c_{33})$	b_{33} $(r_1c_{32}-r_2c_{31})$
1	$-e_3(K_{21x}\sin^2\phi^*+K_{2a}\cos^2\phi^*)$	$-e_3\frac{\sin2\phi}{2}(K_{2a}-K_{21x})$	$(f+e_1)(K_{21x}\sin^2\phi^*+K_{2a}\cos^2\phi^*)$ $(b+e_2)\frac{\sin2\phi}{2}(K_{2a}-K_{21x})$	$(b+e_2)K_{21x}$	$-(f+e_1)K_{21x}$	0
4	$-e_3(K_{21x}\sin^2\phi^*+K_{2a}\cos^2\phi^*)$	$-e_3\frac{\sin2\phi}{2}(K_{21x}-K_{2a})$	$(f+e_1)(K_{21x}\sin^2\phi^*+K_{2a}\cos^2\phi^*)$ $+(e_2-b)\frac{\sin2\phi}{2}(K_{21x}-K_{2a})$	$(e_2-b)K_{21x}$	$-(f+e_1\ K_{21x}$	0
5	$-e_3(K_{21x}\sin^2\phi^*+K_{2a}\cos^2\phi^*)$	$-e_3\frac{\sin2\phi}{2}(K_{21x}-K_{2a})$	$(e_1-f)(K_{21x}\sin^2\phi^*+K_{2a}\cos^2\phi^*)$ $+(e_2-b)\frac{\sin2\phi}{2}(K_{21x}-K_{2a})$	$(e_2-b)K_{21x}$	$-(e_1-f)K_{21x}$	0
8	$-e_3(K_{21x}\sin^2\phi^*+K_{2a}\cos^2\phi^*)$	$-e_3\frac{\sin2\phi}{2}(K_{2a}-K_{21x})$	$(e_1-f)(K_{21x}\sin^2\phi^*+K_{2a}\cos^2\phi^*)$ $+(b+e_2)\frac{\sin2\phi}{2}(K_{2a}-K_{21x})$	$(b+e_2)K_{21x}$	$-(e_1-f)K_{21x}$	0
2	$-e_3K_{11y}$	0	$(L+e_1)K_{11y}$	$(b+e_2)K_{11x}$	$-(L+e_1)K_{11x}$	0
3	$-e_3K_{11y}$	0	$(L+e_1)K_{11y}$	$(e_2-b)K_{11x}$	$-(L+e_1)K_{11x}$	0
6	$-e_3K_{11y}$	0	$(e_1-L)K_{11y}$	$(e_2-b)K_{11x}$	$-(e_1-L)K_{11x}$	0
7	$-e_3K_{11y}$	0	$(e_1-L)K_{11y}$	$(b+e_2)K_{11x}$	$-(e_1-L)K_{11x}$	0
9	$-e_3K_{31y}$	0	$(f_1+e_1)K_{31y}$	$(b_1+e_2)(K_{31x}\sin^2\phi-K_{3a}\cos^2\phi)$	$-(f_1+e_1)(K_{31x}\sin^2\phi+K_{3a}\cos^2\phi$ $-e\frac{\sin2\phi}{2}(K_{31x}-K_{3a})$	$(b_1+e_2\frac{\sin2\phi}{2}(K_{31x}-K_{3a})$
10	$-e_3K_{31y}$	0	$(f_1+e_1)K_{31y}$	$(e_2-b_1)(K_{31x}\sin^2\phi+K_{3a}\cos^2\phi)$	$-(f_1+e_1)(K_{31x}\sin^2\phi+K_{3a}\cos^2\phi$ $-e_3\frac{\sin2\phi}{2}(K_{31x}-K_{3a})$	$(e_2-b_1\frac{\sin2\phi}{2}(K_{31x}-K_{3a})$
11	$-e_3K_{31y}$	0	$(e_1-f_1)K_{31y}$	$(e_2-b_1)(K_{31x}\sin^2\phi+K_{3a}\cos^2\phi)$	$-(e_1-f_1)(K_{31x}\sin^2\phi+K_{3a}\cos^2\phi)$ $-e_3\frac{\sin2\phi}{2}(K_{31x}-K_{3a})$	$(e_2-b_1\frac{\sin2\phi}{2}(K_{31x}-K_{3a})$
12	$-e_3K_{31y}$	0	$(e_1-f_1)K_{31y}$	$(b_1+e_2)(K_{31x}\sin^2\phi+K_{3a}\cos^2\phi)$	$+(e_1-f_1)(K_{31x}\sin^2\phi+K_{3a}\cos^2\phi)$ $-e_3\frac{\sin2\phi}{2}(K_{31x}-K_{3a})$	$(b_1+e_2\frac{\sin2\phi}{2}(K_{31x}-K_{3a})$

$$\sum: \quad b_{21}=-e_3\left[K_{11y}\cdot K_{31y}\cdot(K_{21x}\sin^2\phi+K_{2a}\cos^2\phi)\right];\ b_{22}=0;\ b_{23}=e_1\left[K_{21x}\sin^2\phi^*+K_{2a}\cos^2\phi^*+K_{11y}\cdot K_{31y}\right]+b\frac{\sin2\phi}{2}(K_{2a}-K_{21x});\ b_{31}=e_2\left[K_{21x}\cdot K_{11x}\cdot(K_{31x}\sin^2\phi+K_{3a}\cos^2\phi)\right];$$
$$b_{32}=-e_1\left[K_{21x}\cdot K_{11x}\cdot K_{31x}\sin^2\phi+K_{3a}\cos^2\phi\right]-e_3\frac{\sin2\phi}{2}(K_{31x}\cdot K_{3a});\ b_{33}=e_2\frac{\sin2\phi}{2}(K_{31x}-K_{3a})$$

$$[B]=\begin{bmatrix} -e_2\frac{\sin2\phi}{2}(K_{31x}-K_{3a}) & \left[e_3\left\{(K_{21x}\cos^2\phi^*+K_{2a}\sin^2\phi^*)\right.\right. & -e_2\left[K_{21x}\cos^2\phi^*+K_{2a}\sin^2\phi^*\right. \\ & \left.\left.-K_{11x}\cdot(K_{31x}\cos^2\phi+K_{3a}\sin^2\phi)\right\}\right. & \left.+K_{31x}\cos^2\phi+K_{3a}\sin^2\phi+K_{11x}\right] \\ & \left.+e_1\frac{\sin2\phi}{2}(K_{31x}-K_{3a})\right] & \\ -e_3\left[K_{11y}\cdot K_{31y}\right. & 0 & e_1\left[K_{21x}\sin^2\phi^*+K_{2a}\cos^2\phi^*\right. \\ \left.\cdot K_{21x}\sin^2\phi+K_{2a}\cos^2\phi\right] & & \left.+K_{11y}\cdot K_{31y}\right]+b\frac{\sin2\phi}{2}(K_{2a}-K_{21x}) \\ \left[e_2\left[K_{21x}+K_{11x}\right.\right. & -e_1\left[K_{21x}+K_{11x}\cdot K_{31x}\sin^2\phi\right. & +e_2\frac{\sin2\phi}{2}(K_{31x}-K_{3a}) \\ \left.\left.+K_{31x}\sin^2\phi\ K_{3a}\cos^2\phi\right]\right. & \left.+K_{3a}\cos^2\phi\right]-e_3\frac{\sin2\phi}{2}(K_{31x}\cdot K_{3a}) & \end{bmatrix} \cdot \begin{bmatrix} 0 & e_3(K_{21x}+K_{1a}+K_{31x}) & -e_2(K_{21x}+K_{1a}+K_{31x}) \\ -e_3(K_{11y}+K_{31y}+K_{2a}) & 0 & e_1(K_{2a}+K_{11y}+K_{31y}) \\ e_2(K_{21x}+K_{11x}+K_{3a}) & -e_1(K_{21x}+K_{11x}+K_{3a}) & 0 \end{bmatrix}$$

$$\cdot \begin{bmatrix} -e_2(K_{31x}-K_{3a}) & e_1(K_{31x}-K_{3a}) & 0 \\ 0 & 0 & -b\ (K_{21x}-K_{1a}) \\ 0 & -e_3(K_{31x}-K_{3a}) & -e_2(K_{31x}-K_{3a}) \end{bmatrix}$$

Isolator Number	e_{11} $(r_2b_{31}-r_3b_{21})$	e_{12} $(r_2b_{32}-r_3b_{22})$	e_{13} $(r_2b_{33}-r_3b_{23})$
1	$(B+e_2)^2K_{2fz}+e_3^2(K_{2fx}\sin^2\phi^*+K_{2a}\cos^2\phi^*)$	$-(B+e_2)(l+e_1)K_{2fz}+e_3\frac{2\sin2\phi^*}{2}(K_{2a}-K_{2fx})$	$-e_3\{(l-e_1)(K_{2fx}\sin^2\phi^*+K_{2a}\cos^2\phi^*)$ $+(B+e_2)\frac{\sin2\phi^*}{2}(K_{2a}-K_{2fx})\}$
4	$(e_2-B)^2K_{2fz}+e_3^2(K_{2fx}\sin^2\phi^*+K_{2a}\cos^2\phi^*)$	$-(e_2-B)(l+e_1)K_{2fz}+e_3\frac{2\sin2\phi^*}{2}(K_{2fx}-K_{2a})$	$-e_3\{(l+e_1)(K_{2fx}\sin^2\phi^*+K_{2a}\cos^2\phi^*)$ $-(e_2-B)\frac{\sin2\phi^*}{2}(K_{2a}-K_{2fx})$
5	$(e_2-B)^2K_{2fz}+e_3^2(K_{2fx}\sin^2\phi^*+K_{2a}\cos^2\phi^*)$	$-(e_2-B)(e_1-l)K_{2fz}+e_3\frac{2\sin2\phi^*}{2}(K_{2fx}-K_{2a})$	$-e_3\{(e_1-l)(K_{2fx}\sin^2\phi^*+K_{2a}\cos^2\phi^*)$ $-(e_2-B)\frac{\sin2\phi^*}{2}(K_{2a}-K_{2fx})$
8	$(B+e_2)^2K_{2fz}+e_3^2(K_{2fx}\sin^2\phi^*+K_{2a}\cos^2\phi^*)$	$-(B+e_2)(e_1-l)K_{2fz}+e_3\frac{2\sin2\phi^*}{2}(K_{2fx}-K_{2a})$	$-e_3\{(e_1-l)(K_{2fx}\sin^2\phi^*+K_{2a}\cos^2\phi^*)$ $+(B+e_2)\frac{\sin2\phi^*}{2}(K_{2a}-K_{2fx})\}$
2	$(b+e_2)^2K_{1fz}+e_3^2K_{1fy}$	$-(b+e_2)(L+e_1)K_{1fz}$	$-e_3(L+e_1)K_{1fy}$
3	$(e_2-b)^2K_{1fz}+e_3^2K_{1fy}$	$-(e_2-b)(L+e_1)K_{1fz}$	$-e_3(L+e_1)K_{1fy}$
6	$(e_2-b)^2K_{1fz}+e_3^2K_{1fy}$	$-(e_2-b)(e_1-L)K_{1fz}$	$-e_3(e_1-L)K_{1fy}$
7	$(b+e_2)^2K_{1fz}+e_3^2K_{1fy}$	$-(b+e_2)(e_1-L)K_{1fz}$	$-e_3(e_1-L)K_{1fy}$
9	$(b_1-e_2)^2(K_{3fx}\sin^2\phi+K_{3a}\cos^2\phi)+e_3^2K_{3fy}$	$(b_1-e_2)\{-(l+e_1)(K_{3fx}\sin^2\phi+K_{3a}\cos^2\phi)$ $-e_3\frac{\sin2\phi}{2}(K_{3fx}-K_{3a})\}$	$+(b_1+e_2)\frac{2\sin2\phi}{2}(K_{3fx}-K_{3a})-e_3(l+e_1)$ K_{3fy}
10	$(e_2-b_1)^2(K_{3fx}\sin^2\phi+K_{3a}\cos^2\phi)+e_3^2K_{3fy}$	$(e_2-b_1)\{-(l+e_1)(K_{3fx}\sin^2\phi+K_{3a}\cos^2\phi)$ $-e_3\frac{\sin2\phi}{2}(K_{3fx}-K_{3a})\}$	$+(e_2-b_1)\frac{2\sin2\phi}{2}(K_{3fx}-K_{3a})-e_3(l+e_1)$ K_{3fy}
11	$(e_2-b_1)^2(K_{3fx}\sin^2\phi+K_{3a}\cos^2\phi)+e_3^2K_{3fy}$	$(e_2-b_1)\{-(e_1-l)(K_{3fx}\sin^2\phi+K_{3a}\cos^2\phi)$ $-e_3\frac{\sin2\phi}{2}(K_{3fx}-K_{3a})\}$	$+(e_2-b_1)\frac{2\sin2\phi}{2}(K_{3fx}-K_{3a})-e_3(e_1-l)$ K_{3fy}
12	$(b_1+e_2)^2(K_{3fx}\sin^2\phi+K_{3a}\cos^2\phi)+e_3^2K_{3fy}$	$(b_1+e_2)\{-(e_1-l)(K_{3fx}\sin^2\phi+K_{3a}\cos^2\phi)$ $-e_3\frac{\sin2\phi}{2}(K_{3fx}-K_{3a})\}$	$+(b_1+e_2)\frac{2\sin2\phi}{2}(K_{3fx}-K_{3a})-e_3(e_1-l)$ K_{3fy}

$\sum$: $e_{11}=4(B^2+e_2^2)K_{2fz}+4(b^2+b_2^2)K_{1fz}+4e_3^2(K_{1fy}+K_{3fy})+4e_3^2(K_{2fx}\sin^2\phi^*+K_{2a}\cos^2\phi^*)+4(b_1^2+e_2^2)(K_{3fx}\sin^2\phi+K_{3a}\cos^2\phi)$;
$e_{12}=4e_1e_2(K_{2fz}+K_{1fz}+K_{3fz}\sin^2\phi+K_{3a}\cos^2\phi)-4e_2e_3\frac{\sin2\phi}{2}(K_{3fx}-K_{3a})$; $e_{13}=-4e_1e_3\{K_{2fx}\sin^2\phi^*+K_{2a}\cos^2\phi^*$
$+K_{1fy}+K_{3fy}\}+4(b_1^2+e_2^2)\frac{\sin2\phi}{2}(K_{3fx}-K_{3a})-8e_3\frac{\sin2\phi^*}{2}(K_{2a}-K_{2fx})$

Isolation Number	e_{21} $(r_3b_{11} - r_1b_{31})$	e_{22} $(r_3b_{12} - r_1b_{32})$	e_{23} $(r_3b_{13} - r_1b_{33})$
1	$e_3\frac{2\sin2\phi^*}{2}(K_{2a}-K_{2\ell x})$ $-(\ell+e_1)(B+e_2)K_{2\ell z}$	$e_3{}^2(K_{2\ell x}\cos^2\phi^*+K_{2a}\sin^2\phi^2)+(\ell+e_1)^2K_{2\ell z}$	$e_3\left\{-(\ell+e_1)\frac{\sin2\phi^*}{2}(K_{2a}-K_{2\ell x})\right.$ $\left.-(B+e_2)(K_{2\ell x}\cos^2\phi^*+K_{2a}\sin^2\phi^*)\right\}$
4	$e_3\frac{2\sin(-2\phi^*)}{2}(K_{2a}-K_{2\ell x})$ $-(\ell+e_1)(e_2-B)K_{2\ell z}$	$e_3{}^2(K_{2\ell x}\cos^2\phi^*+K_{2a}\sin^2\phi^*)+(\ell+e_1)^2K_{2\ell z}$	$e_3\left\{-(\ell+e_1)\frac{\sin2\phi^*}{2}(-K_{2a}+K_{2\ell x})\right.$ $\left.-(e_2-B)(K_{2\ell x}\cos^2\phi^*+K_{2a}\sin^2\phi^*)\right\}$
5	$e_3\frac{2\sin(-2\phi^*)}{2}(K_{2a}-K_{2\ell x})$ $-(e_1-\ell)(e_2-B)K_{2\ell z}$	$e_3{}^2(K_{2\ell x}\cos^2\phi^*+K_{2a}\sin^2\phi^*)+(e_1-\ell)^2K_{2\ell z}$	$e_3\left\{-(e_1-\ell)\frac{\sin2\phi^*}{2}(-K_{2a}+K_{2\ell x})\right.$ $\left.-(e_2-B)(K_{2\ell x}\cos^2\phi^*+K_{2a}\sin^2\phi^*)\right\}$
8	$e_3\frac{2\sin(2\phi^*)}{2}(K_{2a}-K_{2\ell x})$ $-(e_1-\ell)(B+e_2)K_{2\ell z}$	$e_3{}^2(K_{2\ell x}\cos^2\phi^*+K_{2a}\sin^2\phi^*)+(e_1-\ell)^2K_{2\ell z}$	$e_3\left\{-(e_1-\ell)\frac{\sin2\phi^*}{2}(K_{2a}-K_{2\ell x})\right.$ $\left.-(B+e_2)(K_{2\ell x}\cos^2\phi^*+K_{2a}\sin^2\phi^*)\right\}$
2	$-(L+e_1)(b+e_2)K_{1\ell z}$	$e_3{}^2K_{1a}+(L+e_1)^2K_{1\ell z}$	$-e_3(b+e_2)K_{1a}$
3	$-(L+e_1)(e_2-b)K_{1\ell z}$	$e_3{}^2K_{1a}+(L+e_1)^2K_{1\ell z}$	$-e_3(e_2-b)K_{1a}$
6	$-(e_1-L)(e_2-b)K_{1\ell z}$	$e_3{}^2K_{1a}+(e_1-L)^2K_{1\ell z}$	$-e_3(e_2-b)K_{1a}$
7	$-(e_1-L)(b+e_2)K_{1\ell z}$	$e_3{}^2K_{1a}+(e_1-L)^2K_{1\ell z}$	$-e_3(b+e_2)K_{1a}$
9	$-e_3(b_1+e_2)\frac{\sin2\phi}{2}$ $(K_{3\ell x}-K_{3a})-(\ell_1+e_1)$ (b_1+e_2) $(K_{3\ell x}\sin^2\phi+K_{3a}\cos^2\phi)$	$e_3\left\{e_3(K_{3\ell x}\cos^2\phi+K_{3a}\sin^2\phi)+(\ell_1+e_1)\frac{\sin2\phi}{2}(K_{3\ell x}-K_{3a})\right\}+$ $(\ell_1+e_1)\left\{(\ell_1+e_1)(K_{3\ell x}\sin^2\phi+K_{3a}\cos^2\phi)+e_3\frac{\sin2\phi}{2}\right.$ $\left.(K_{3\ell x}-K_{3a})\right\}$	$-e_3(b_1+e_2)(K_{3\ell x}\cos^2\phi+K_{3a}\sin^2\phi)$ $-(\ell_1+e_1)(b_1+e_2)\frac{\sin2\phi}{2}(K_{3\ell x}-K_{3a})$
10	$-e_3(e_2-b_1)\frac{\sin2\phi}{2}$ $(K_{3\ell x}-K_{3a})-(\ell_1+e_1)$ (e_2-b_1) $(K_{3\ell x}\sin^2\phi+K_{3a}\cos^2\phi)$	$e_3\left\{e_3(K_{3\ell x}\cos^2\phi+K_{3a}\sin^2\phi)+(\ell_1+e_1\frac{\sin2\phi}{2}(K_{3\ell x}-K_{3a})\right\}+$ $(\ell_1+e_1)\left\{(\ell_1+e_1)(K_{3\ell x}\sin^2\phi+K_{3a}\cos^2\phi)+e_3\frac{\sin2\phi}{2}(K_{3\ell x}-K_{3a})\right\}$	$-e_3(e_2-b_1)(K_{3\ell x}\cos^2\phi+K_{3a}\sin^2\phi)$ $-(\ell_1+e_1)(e_2-b_1)\frac{\sin2\phi}{2}(K_{3\ell x}-K_{3a})$
11	$-e_3(e_2-b_1)\frac{\sin2\phi}{2}$ $(K_{3\ell x}-K_{3a})-(e_1-\ell_1)$ (e_2-b_1) $(K_{3\ell x}\sin^2\phi+K_{3a}\cos^2\phi)$	$e_3\left\{e_3(K_{3\ell x}\cos^2\phi+K_{3a}\sin^2\phi)+(e_1-\ell_1)\frac{\sin2\phi}{2}(K_{3\ell x}-K_{3a})\right\}$ $+(e_1-\ell_1)\left\{(e_1-\ell_1)(K_{3\ell x}\sin^2\phi+K_{3a}\cos^2\phi)+e_3\frac{\sin2\phi}{2}(K_{3\ell x}-K_{3a})\right\}$	$-e_3(e_2-b_1)(K_{3\ell x}\cos^2\phi+K_{3a}\sin^2\phi)$ $-(e_1-\ell_1)(e_2-b_1)\frac{\sin2\phi}{2}(K_{3\ell x}-K_{3a})$
12	$-e_3(b_1+e_2)\frac{\sin2\phi}{2}$ $(K_{3\ell x}-K_{3a})-(e_1-\ell_1)$ (b_1+e_2) $(K_{3\ell x}\sin^2\phi+K_{3a}\cos^2\phi)$	$e_3\left\{e_3(K_{3\ell x}\cos^2\phi+K_{3a}\sin^2\phi)+(e_1-\ell_1)\frac{\sin2\phi}{2}(K_{3\ell x}-K_{3a})\right\}$ $+(e_1-\ell_1)\left\{(e_1-\ell_1)(K_{3\ell x}\sin^2\phi+K_{3a}\cos^2\phi)+e_3\frac{\sin2\phi}{2}(K_{3\ell x}-K_{3a})\right\}$	$-e_3(b_1+e_2)(K_{3\ell x}\cos^2\phi+K_{3a}\sin^2\phi)$ $-(e_1-\ell_1)(b_1+e_2)\frac{\sin2\phi}{2}(K_{3\ell x}-K_{3a})$

$\sum$: $e_{21}=-4e_1e_2(K_{2\ell z}+K_{1\ell z}+K_{3\ell x}\sin^2\phi+K_{3a}\cos^2\phi)-4e_2e_3\frac{\sin2\phi}{2}(K_{3\ell x}-K_{3a})$; $e_{22}=4e_3{}^2\left\{K_{2\ell x}\cos^2\phi^*+K_{2a}\sin^2\phi^*+K_{1a}\right.$ $\left.+(K_{3\ell x}\cos^2\phi+K_{3a}\sin^2\phi)\right\}+4e_1{}^2\left\{K_{2\ell z}+K_{1\ell z}+K_{3\ell x}\sin^2\phi+K_{3a}\cos^2\phi\right\}+4\ell^2K_{2\ell z}+4\ell^2K_{1\ell z}+4\ell_1{}^2(K_{3\ell x}\sin^2\phi+K_{3a}\cos^2\phi)+8e_1e_3\frac{\sin2\phi}{2}$ $(K_{3\ell x}-K_{3a})$; $e_{23}=-4e_2e_3\left\{(K_{2\ell x}\cos^2\phi^*+K_{2a}\sin^2\phi^*)+K_{1a}+(K_{3\ell x}\cos^2\phi+K_{3a}\sin^2\phi)\right\}-4e_1e_2\frac{\sin2\phi}{2}(K_{3\ell x}-K_{3a})$

Isolator Number	e_{31} $(r_1b_{21}-r_2b_{11})$	e_{32} $(r_1b_{22}-r_2b_{12})$	e_{33} $(r_1b_{23}-r_2b_{13})$
1	$-(l+e_1)(e_3)(K_{2fx}\sin^2\phi^*+K_{2a}\cos^2\phi^*)$ $-e_3(B+e_2)\frac{\sin2\phi^*}{2}(K_{2a}-K_{2fx})$	$-e_3(l+e_1)\frac{\sin2\phi^*}{2}(K_{2a}-K_{2fx})-$ $e_3(+e_2)(K_{2fx}\cos^2\phi^*+K_{2a}\sin^2\phi^*)$	$(l+e_1)\{(l+e_1)(K_{2fx}\sin^2\phi^*+K_{2a}\cos^2\phi^*)$ $+(B+e_2)\frac{\sin2\phi^*}{2}(K_{2a}-K_{2fx})\}+(B+e_2)\{(l+e_1)\frac{\sin2\phi^*}{2}$ $(K_{2a}-K_{2fx})-(B+e_2)(K_{2fx}\cos^2\phi^*+K_{2a}\sin^2\phi^*)\}$
4	$-(l+e_1)(e_3)(K_{2fx}\sin^2\phi^*+K_{2a}\cos^2\phi^*)$ $-e_3(e_2-B)\frac{\sin2\phi^*}{2}(K_{2fx}-K_{2a})$	$-e_3(l+e_1)\frac{\sin2\phi^*}{2}(K_{2fx}-K_{2a})-$ $e_3(e_2-B)(K_{2fx}\cos^2\phi^*+K_{2a}\sin^2\phi^*)$	$(l+e_1)\{(l+e_1)(K_{2fx}\sin^2\phi^*+K_{2a}\cos^2\phi^*)$ $+(e_2-B)\frac{\sin2\phi^*}{2}(K_{2fx}-K_{2a})\}+(e_2-B)\{(l+e_1)\frac{\sin2\phi^*}{2}$ $(K_{2fx}-K_{2a})-(e_2-B)(K_{2fx}\cos^2\phi^*+K_{2a}\sin^2\phi^*)\}$
5	$-(e_1-l)(e_3)(K_{2fx}\sin^2\phi^*+K_{2a}\cos^2\phi^*)$ $-e_3(e_2-B)\frac{\sin2\phi^*}{2}(K_{2fx}-K_{2a})$	$-e_3(e_1-l)\frac{\sin2\phi^*}{2}(K_{2fx}-K_{2a})-$ $e_3(e_2-B)(K_{2fx}\cos^2\phi^*+K_{2a}\sin^2\phi^*)$	$(e_1-l)\{(e_1-l)(K_{2fx}\sin^2\phi^*+K_{2a}\cos^2\phi^*)$ $+(e_2-B)\frac{\sin2\phi^*}{2}(K_{2fx}-K_{2a})\}+(e_2-B)\{(e_1-l)\frac{\sin2\phi^*}{2}$ $(K_{2fx}-K_{2a})-(e_2-B)(K_{2fx}\cos^2\phi^*+K_{2a}\sin^2\phi^*)\}$
8	$-(e_1-l)(e_3)(K_{2fx}\sin^2\phi^*+K_{2a}\cos^2\phi^*)$ $-e_3(B+e_2)\frac{\sin2\phi^*}{2}(K_{2a}-K_{2fx})$	$-e_3(e_1-l)\frac{\sin2\phi^*}{2}(K_{2a}-K_{2fx})-$ $e_3(B+e_2)(K_{2fx}\cos^2\phi^*+K_{2a}\sin^2\phi^*)$	$(e_1-l)\{(e_1-l)(K_{2fx}\sin^2\phi^*+K_{2a}\cos^2\phi^*)$ $+(B+e_2)\frac{\sin2\phi^*}{2}(K_{2a}-K_{2fx})\}+(e_2+B)\{(e_1-l)\frac{\sin2\phi^*}{2}$ $(K_{2a}-K_{2fx})-(B+e_2)(K_{2fx}\cos^2\phi^*+K_{2a}\sin^2\phi^*)\}$
2	$-e_3(L+e_1)K_{1fy}$	$-e_3(b+e_2)K_{1a}$	$(L+e_1)^2K_{1fy}+(b+e_2)^2K_{1a}$
3	$-e_3(L+e_1)K_{1fy}$	$-e_3(e_2-b)K_{1a}$	$(L+e_1)^2K_{1fy}+(e_2-b)^2K_{1a}$
6	$-e_3(e_1-L)K_{1fy}$	$-e_3(e_2-b)K_{1a}$	$(e_1-L)^2K_{1fy}+(e_2-b)^2K_{1a}$
7	$-e_3(e_1-L)K_{1fy}$	$-e_3(b+e_2)K_{1a}$	$(e_1-L)^2K_{1fy}+(b+e_2)^2K_{1a}$
9	$-e_3(l_1+e_1)K_{3fy}+(b_1+e_2)\frac{\sin2\phi}{2}$ $(K_{3fx}-K_{3a})$	$-(b_1+e_2)\{e_3(K_{3fx}\cos^2\phi+K_{3a}\sin^2\phi)$ $+(l_1+e_1)\frac{\sin2\phi}{2}(K_{3fx}-K_{3a})\}$	$(l_1+e_1)^2K_{3fy}+(b_1+e_2)^2(K_{3fx}\cos^2\phi+K_{3a}\sin^2\phi)$
10	$-e_3(l_1+e_1)K_{3fy}(e_2-b_1)^2\frac{\sin2\phi}{2}$ $(K_{3fx}-K_{3a})$	$-(e_2-b_1)\{e_3(K_{3fx}\cos^2\phi+K_{3a}\sin^2\phi)$ $+(e_1+e_1)\frac{\sin2\phi}{2}(K_{3fx}-K_{3a})\}$	$(l_1+e_1)^2K_{3fy}+(e_2-b_1)^2(K_{3fx}\cos^2\phi+K_{3a}\sin^2\phi)$
11	$-e_3(e_1-l_1)K_{3fy}+(e_2-b_1)^2\frac{\sin2\phi}{2}$ $(K_{3fx}-K_{3a})$	$-(e_2-b_1)\{e_3(K_{3fx}\cos^2\phi+K_{3a}\sin^2\phi)$ $+(e_1-l_1)\frac{\sin2\phi}{2}(K_{3fx}-K_{3a})\}$	$(e_1-l_1)^2K_{3fy}+(e_2-b_1)^2(K_{3fx}\cos^2\phi+K_{3a}\sin^2\phi)$
12	$-e_3(e_1-l_1)K_{3fy}+(e_2+e_2)^2\frac{\sin2\phi}{2}$ $(K_{3fx}-K_{3a})$	$-(b_1+e_2)\{e_3(K_{3fx}\cos^2\phi+K_{3a}\sin^2\phi)$ $+(e_1-l_1)\frac{\sin2\phi}{2}(K_{3fx}-K_{3a})\}$	$(e_1-l_1)^2K_{3fy}+(b_1+e_2)^2(K_{3fx}\cos^2\phi+K_{3a}\sin^2\phi)$

$\sum$: $e_{31}=4e_1e_3\{K_{2fx}\sin^2\phi^*+K_{2a}\cos^2\phi^*+K_{1fy}+K_{3fy}\}+4(e_2^2+b_1^2)\frac{\sin2\phi^*}{2}(K_{3fx}-K_{3a})+4b_1e_3\frac{\sin2\phi^*}{2}(K_{2fx}-K_{2a})$; $e_{32}=4e_2e_3\{K_{2fx}\cos^2\phi^*+K_{2a}\sin^2\phi^*+K_{1a}+K_{3fx}\cos^2\phi+K_{3a}\sin^2\phi\}+4e_1e_2\frac{\sin2\phi^*}{2}(K_{3fx}-K_{3a})$; $e_{33}=4e_1^2\{K_{2fx}\sin^2\phi^*+K_{2a}\cos^2\phi^*)+K_{1fy}+K_{3fy}\}+4l^2(K_{2fx}\sin^2\phi^*+K_{2a}\cos^2\phi^*)$ $+4e_2^2\{(K_{2fx}\cos^2\phi+K_{2a}\sin^2\phi^*)K_{1a}+(K_{3fx}\cos^2\phi+K_{3a}\sin^2\phi)\}+4L^2K_{1fy}+4l_1^2K_{3fy}+4B^2(K_{2fx}\cos^2\phi^*+K_{2a}\sin^2\phi^*)+4b^2K_{1a}+4b_1^2$ $(K_{3fx}\cos^2\phi+K_{3a}\sin^2\phi)+4e_1b\frac{\sin2\phi^*}{2}(K_{2a}-K_{2fx})$

$$
[E] = \begin{bmatrix}
\begin{bmatrix} 4(b^2+e_2^2)K_{2fz} + 4(b^2+e_2^2)K_{1fz} \\ + 4e_3^2(K_{1fy}+K_{3fy}) \\ + 4e_3^2(K_{2fx}\sin^2\phi + K_{2m}\cos^2\phi) \\ + 4(b_1^2+e_2^2)(K_{3fx}\sin^2\phi + K_{3m}\cos^2\phi) \end{bmatrix}
&
\begin{bmatrix} -4e_1e_2(K_{2fz}+K_{1fz}+K_{3fx}\sin^2\phi + K_{3m}\cos^2\phi) \\ -4e_2e_3\frac{\sin 2\phi}{2}(K_{3fx}-K_{3m}) \end{bmatrix}
&
\begin{bmatrix} -4e_1e_3\{K_{2fx}\sin^2\phi + K_{2m}\cos^2\phi + K_{1fy} + K_{3fy}\} \\ + 4(b_1^2+e_2^2)\frac{\sin 2\phi}{2}(K_{3fx}-K_{3m}) \\ - 8e_3\frac{\sin 2\phi}{2}(K_{2m}-K_{2fx}) \end{bmatrix}
\\
\begin{bmatrix} -4e_1e_2(K_{2fz}+K_{1fz}+K_{3fx}\sin^2\phi + K_{3m}\cos^2\phi) \\ -4e_2e_3\frac{\sin 2\phi}{2}(K_{3fx}-K_{3m}) \end{bmatrix}
&
\begin{bmatrix} 4e_3^2\{K_{2fx}\cos^2\phi + K_{2m}\sin^2\phi + K_{1m} + K_{3fx}\cos^2\phi + K_{3m}\sin^2\phi\} \\ + 4e_1^2\{K_{2fz} + K_{1fz} + K_{3fx}\sin^2\phi + K_{3m}\cos^2\phi\} \\ + 4l^2K_{2fz} + 4l^2K_{1fz} + 4e_1^2(K_{3fx}\sin^2\phi + K_{3m}\cos^2\phi) \\ + 8e_1e_3\frac{\sin 2\phi}{2}(K_{3fx}-K_{3m}) \end{bmatrix}
&
\begin{bmatrix} -4e_2e_3(K_{2fx}\cos^2\phi + K_{2m}\sin^2\phi + K_{1m} \\ + K_{3fx}\cos^2\phi + K_{3m}\sin^2\phi) \\ -4e_1e_2\frac{\sin 2\phi}{2}(K_{3fx}-K_{3m}) \end{bmatrix}
\\
\begin{bmatrix} -4e_1e_3\{K_{2fx}\sin\phi + K_{2m}\cos\phi + K_{1fy} + K_{3fy}\} \\ + 4(e_2^2+e_1^2)\frac{\sin 2\phi}{2}(K_{3fx}-K_{3m}) + 48e_3\frac{\sin 2\phi}{2}(K_{2fx}-K_{2m}) \end{bmatrix}
&
\begin{bmatrix} -4e_2e_3\{K_{2fx}\cos^2\phi + K_{2m}\sin^2\phi + K_{1m} + K_{3fx}\cos^2\phi \\ + K_{3m}\sin^2\phi\} + 4e_1e_2\frac{\sin 2\phi}{2}(K_{3fx}-K_{3m}) \end{bmatrix}
&
\begin{bmatrix} 4e_1^2\{K_{2fx}\sin^2\phi + K_{2m}\cos^2\phi + K_{1fy} + K_{3fy}\} + 4l^2K_{1fy} \\ + 4e_2^2\{K_{2fx}\cos^2\phi + K_{2m}\sin^2\phi + K_{1m} + K_{3fx}\cos^2\phi + K_{3m}\sin^2\phi\} \\ + 4f^2(K_{2fx}\sin^2\phi + K_{2m}\cos^2\phi) + 4f_1^2K_{3fy} + 4b^2K_{1m} \\ + 4B^2(K_{2fx}\cos^2\phi + K_{2m}\sin^2\phi) + 4b_1^2(K_{3fx}\cos^2\phi + K_{3m}\sin^2\phi) \\ + 8e_1B\frac{\sin 2\phi}{2}(K_{2m}-K_{2fx}) \end{bmatrix}
\end{bmatrix}
$$

$$
[E] \cong \begin{bmatrix}
\begin{bmatrix} 4(b^2+e_2^2)K_{2fz} + 4(b^2+e_2^2)K_{1fz} \\ + 4e_3^2(K_{1fy}+K_{3fy}+K_{2m}) \\ + 4(b_1^2+e_2^2)K_{3m} \end{bmatrix}
& -4e_1e_2(K_{2fz}+K_{1fz}+K_{3m}) & -4e_1e_3(K_{1fy}+K_{3fy}+K_{2m})
\\
-4e_1e_2(K_{2fz}+K_{1fz}+K_{3m})
&
\begin{bmatrix} 4e_3^2\{K_{2fx}+K_{1m}+K_{3fx}\} + 4l^2K_{2fz} \\ + 4e_1^2\{K_{2fz}+K_{1fz}+K_{3m}\} + 4l^2K_{1fz} \\ + 4l_1^2K_{3m} \end{bmatrix}
& -4e_2e_3(K_{1m}+K_{3fx}+K_{2fx})
\\
-4e_1e_3(K_{1fy}+K_{3fy}+K_{2m})
& 4e_2e_3(K_{1m}+K_{3fx}+K_{2fx})
&
\begin{bmatrix} 4e_1^2\{K_{2m}+K_{1fy}+K_{3fy}\} + \\ 4e_2^2\{K_{2fx}+K_{1m}+K_{3fx}\} + \\ 4l^2K_{1fy} + 4f^2K_{2m} + \\ 4f_1^2K_{3fy} + 4b^2K_{1m} + \\ 4B^2K_{2fx} + 4b_1^2K_{3fx} \end{bmatrix}
\end{bmatrix}
+ \phi
\begin{bmatrix}
0 & -4e_2e_3(K_{3fx}-K_{3m}) & \begin{matrix} + 4(b_1^2+e_2^2)(K_{3fx}-K_{3m}) \\ + 8e_3\beta(K_{2fx}-K_{2m}) \end{matrix}
\\
-4e_2e_3(K_{3fx}-K_{3m}) & + 8e_1e_3(K_{3fx}-K_{3m}) & -4e_1e_2(K_{3fx}-K_{3m})
\\
\begin{matrix} \{4(e_2^2+b_1^2)(K_{3fx}-K_{3m}) \\ + 48e_3\beta(K_{2fx}-K_{2m}) \end{matrix} & -4e_1e_2(K_{3fx}-K_{3m}) & -88e_1\beta(K_{2m}-K_{2fx})
\end{bmatrix}
$$

Where $\beta = \frac{h}{\phi}$

SECTION 3.0 NOTATION

a	Relative displacement at which the elastic stiffness characteristic changes slope
A	Voltage of the biasing batteries.
b_{ij}	Restoring force in isolator, in direction i, due to unit rotation of isolated mass about an axis through the mass centroid in direction j. Or, element of first moment stiffness matrix (constant).
$\bar{b}_{ij}$	That part of b_{ij} which creates non-linear coupling with the pendulum mode.
$[\,]$	First moment stiffness matrix.
$[b]$	$=\sum[\,]$
	Characteristic length
c	Coefficient of damping.
	Coefficient of critical damping
c_{ij}	Restoring force in isolator in direction i due to a unit deformation of the isolator, in direction j. Or, elements of stiffness matrix (constant)
$\bar{c}_{ij}$	That part of c_{ij} which creates non-linear coupling with the pendulum mode.
$[c]$	Stiffness matrix of an isolator.
$[c]$	$=\sum[c]$
	Square-law damping coefficient.
D_n	Required rattlespace.
D_{ij}	The peak displacement indicated by a given shock spectrum, in direction j, at the mode frequency ωi.
$\{D\}$	Peak displacement matrix.
$[\,]$	Transformation matrix for rotation of cartesian coordinate reference system.
	$=c/p$. A characteristic length.
e_{ij}	Resultant moment of restoring forces in isolator about an axis through the mass centroid in direction i, due to a unit rotation of isolated mass about an axis through the mass centroid in direction j. (constant)
$\bar{e}_{ij}$	That part of e_{ij} which creates non-linear coupling with the pendulum mode
$[e]$	Second moment of stiffness matrix.
$[\,]$	$=\sum[e]$
$\vec{F}$	Resultant of external force acting on a body.
F_x	Component of restoring force in direction x.
F_y	Component of restoring force in direction y.
F_z	Component of restoring force in direction z.
f	Acceleration corresponding to the Coulomb friction force.
F_o	Resultant restoring force through the C.G. of a constrained rigid body.
F_1	Force applied through the C.G. of a constrained rigid body.
g	Acceleration due to gravity.
g'	$=(p/\omega_n)^2 g$
G	Nondimensionalized acceleration of isolated body.
G_i	Maximum value of G
$\dot{\vec{H}}_o$	Time rate of change of moment of momentum of mass centre about a fixed point O.
$\dot{\vec{H}}_c$	Time rate of change of moment of momentum of mass about mass centre.
$h=c/c_c$	Nondimensionalized square-law damping coefficient.

$(I_{xx})_1; I_{xx}$	Moment of inertia about x_1x_1 and xx axis respectively.
$(I_{yy})_1; I_{yy}$	Moment of inertia about y_1y_1 and yy axis respectively.
$(I_{zz})_1; I_{zz}$	Moment of inertia about z_1z_1 and zz axis respectively.
$I_{c.g.}$	Mass moment of inertia about centre of gravity.
$I_{s.a.}$	Mass moment of inertia about spring attachment point on the mass.
$[I]$	Mass moment of inertia matrix.
k	Ratio of the square of the angular frequencies corresponding to the final and initial values of stiffness of bilinear system.
K	Stiffness of spring.
K_v	Axial spring stiffness.
K_ϕ	Rotational spring stiffness.
l	Static length of pendulum.
l'	Equivalent length of simple pendulum.
$L=\frac{\mu}{p}$	Nondimensional viscous damping coefficient.
m	Mass of rigid body.
$M=C_m=\frac{F}{pv_m}$	Nondimensional coulomb friction coefficient.
$\vec{M}_O$	Moment of the resultant of all external forces acting on the body about any fixed point O.
$\vec{M}_c$	Moment of the resultant of all external forces acting on the body, about mass centre.
$M'x, M'y, M'z$	Moment of the resultant of all external forces acting on the body about x,y,z axis respectively.
M_α, M_ϕ, M_ψ	Components of the restoring moments in directions α, ϕ and ψ respectively.
$[M_o]$	Matrix of constraint moments developed by the isolators because of shock transmitted to the system.
$p=\sqrt{\frac{k}{m}}$	Angular frequency.
$p=\frac{2\pi}{t_p}$	Angular frequency.
q_i	Normal coordinates.
$\{\ddot{q}\}$	Acceleration matrix in normal coordinates.
$\{q\}$	Displacement matrix in normal coordinates.
r_1, r_2, r_3	Coordinates of isolator attachment point.
$\vec{\bar{r}}$	Position vector of centroid in an inertial system of reference.
$\vec{r}$	Position vector of centroid in a moving reference system.
s	Largest expected value of x for scaling purposes.
$s=j\omega$	Complex frequency in Laplace form.
$\ddot{\vec{s}}$	Acceleration of the centre of mass in a fixed coordinate system.
$\{s\}$	Displacement matrix
$\{\bar{s}\}$	Displacement matrix referred to inertial reference system.
$\{\bar{s}_o\}$	Matrix of ground motion displacement.
$\{\ddot{s}\}$	Acceleration matrix.
t	Time
t_o	Duration of the input waveform.
$t'=tp$	Nondimensionalized time.
T_o	Resultant restoring moment about the C.G.
T_1	Externally applied moment

SECTION 3.0 LIST OF SYMBOLS

u	Algebraic sum of all "yield" displacements up to time considered.
v	Displacement in relative coordinates.
$\tilde{v}$	Displacement in absolute coordinates.
u_0	Ground motion displacement.
$\ddot{v}$	Acceleration in relative coordinates.
$\ddot{\tilde{v}}$	Acceleration in absolute coordinates.
$\ddot{v}_0$	Ground motion acceleration.
u_a	Absolute displacement of mass.
$\ddot{u}_a$	Absolute acceleration of mass.
$v (= u_a - a)$	Relative displacement of mass.
$\ddot{v}$	Relative acceleration of mass.
V	Input velocity.
V_{max}	Maximum value of V.
V_{sp}	Nondimensionalized velocity input.
V_m	Largest value of V.
$W = mg$	Weight of the body
x	Relative displacement between table or platform and ground.
x_m	Largest value of x.
x	Relative displacement of mass in x direction.
$\tilde{x}$	Absolute displacement of mass in x direction
x_0	Ground motion displacement in x direction.
$\ddot{x}$	Relative acceleration of mass in x direction.
$\ddot{\tilde{x}}$	Absolute acceleration of mass in x direction.
$\ddot{x}_0$	Ground motion acceleration in x direction.
x_{max}	Shock spectrum displacement corresponding to Wn.
$X = \frac{x}{a}$	Nondimensionalized displacement.
X_m	Largest value of X.
y	Relative displacement of mass in y-direction.
$\tilde{y}$	Absolute displacement of mass in y-direction.
y_0	Ground motion displacement in y-direction.
$\ddot{y}$	Relative acceleration of mass in y direction.
$\ddot{\tilde{y}}$	Absolute acceleration of mass in y direction.
$\ddot{y}_0$	Ground motion acceleration in y direction.
Y	Voltage corresponding to displacement X.
z	Relative displacement of mass in z direction
$\tilde{z}$	Absolute displacement of mass in z direction.
z_0	Ground motion displacement in z direction.
$\ddot{z}$	Relative acceleration of mass in z direction.
$\ddot{\tilde{z}}$	Absolute acceleration of mass in z direction.
$\ddot{z}_0$	Ground motion acceleration in z direction.
$\ddot{z}_m$	Maximum permissible absolute acceleration of body.
a	Acceleration of isolated body.
α	Angular rotation about x-axis.
β	Angular rotation about y-axis
γ	Angular rotation about z-axis.
$[\gamma]$	Modal participation factor matrix
$\delta = \frac{c}{c_r}$	Critical damping ratio.
δ_x δ_y δ_z	Deformation of isolator in x,y,z, directions respectively
δ_x, δ_y, δ_z	Displacement of mass centroid along x,y,z axes respectively.
δ_α, δ_β, δ_γ	Angular rotation of mass centroid about x,y,z axes respectively.
ε	Eccentricity defined as the distance between the C.G. of a pendulum mass and spring attachment point on the mass.
ε^*	$\delta_{C.G.}/\varepsilon$
θ	Inclination of isolator with x-axis.
ψ	Inclination of the line joining the C.G. of a pendulum mass and spring attachment point on the mass at any time (t).
λ	Coefficient of viscous damping referred to the first part of the stiffness characteristic.
μ	Viscous damping coefficient.
$\sigma = \frac{I_G}{mR^2}$	Radius of gyration of rigid body about ...
$\sigma = \frac{k_m}{V_m D}$	"Optimization" variable.
ϕ	Angular rotation of base
ϕ	Pendulum angle.
ϕ	Pendulum angle in x2 plane for six-degree of freedom system.
$\dot{\phi}$	Angular velocity of pendulum.
$\ddot{\phi}$	Angular acceleration of pendulum.
$\dot{\beta}$	Angular velocity of mass.
$\ddot{\beta}$	Angular acceleration of mass.
β_0	Angular displacement of base.
$\overset{r}{\beta}$	Relative angular rotation of mass.
$\overset{a}{\beta}$	Absolute angular rotation of mass.
$\overset{a}{\beta}_0$	Absolute angular rotation of base
$\ddot{\overset{a}{\beta}}$	Absolute angular acceleration.
$\ddot{\beta}_0$	Angular acceleration of base motion
$[\beta]$	Modal matrix.
$\Omega = \frac{\omega}{p}$	Nondimensional angular frequency.
ω	Natural angular frequency of isolated mass, oscillating on the first part of the characteristic rad/sec.
ω	Frequency of pendulum system.
$\omega_1 = \sqrt{\frac{K}{m}}$	Natural frequency of elastic element.
$\omega_2 = \sqrt{\frac{g}{l}}$	Natural frequency of simple pendulum (elastic pendulum problem).
ω_n	Natural frequency of system.
$[\omega_n^2]$	Diagonal frequency matrix.
$\omega_p = \sqrt{\frac{g}{l}}$	Angular frequency of simple pendulum.
$\omega_o^* = \sqrt{\frac{g}{l}}$,	Natural frequency of equivalent simple pendulum.
τ	Period of oscillation.

SECTION 3.0 REFERENCES

3.1 Housner, G. W., and Hudson, D. E.
Applied Mechanics - Dynamics
McGraw-Hill Book Company Inc., New York. 1959

3.2 Karman, Th. von, and Biot, M. A.
Mathematical Methods in Engineering
McGraw-Hill Book Company, Inc., New York. 1940

3.3 Pipes, L. A.
Applied Mathematics for Engineers and Physicists
McGraw-Hill Book Company, Inc., New York. 1958

3.4 Timoshenko, S. P.
Vibration Problems in Engineering
D. Van Nostrand Company, Inc., New York. 1955

3.5 Crandall, S. H.
Random Vibrations
John Wiley & Sons, Inc., New York. 1959

3.6 Den Hartog, J. P.
Mechanical Vibrations
McGraw-Hill Book Company, Inc., New York. 1956

3.7 Jacobsen, L. S., and Ayre, R. S.
Engineering Vibrations
McGraw-Hill Book Company, Inc., New York. 1958

3.8 Myklestad, N. O.
Fundamentals of Vibration Analysis
McGraw-Hill Book Company, Inc., New York. 1956

3.9 Norris, C. H., Hansen, R. J., et al.
Structural Design for Dynamic Loads
McGraw-Hill Book Company, Inc., New York. 1959

3.10 Timoshenko, S. P., and Young, D. H.
Advanced Dynamics
McGraw-Hill Book Company, Inc., New York. 1948

3.11 Flügge, W.
Handbook of Engineering Mechanics
McGraw-Hill Book Company, Inc., New York. 1962

3.12 Fung, Y. C.
Shock Loading and Response Spectra
Colloquium on Shock and Structural Response, Mechanics Division, ASME. November 1960

3.13 Young, D.
Response of Structural Members to Ground Shock
Colloquium on Shock and Structural Response, Mechanics Division, ASME. November 1960

3.14 Rayleigh, Lord
Theory of Sound
2nd Ed., Volume I, Dover Publications, New York. 1945

3.15 Sevin, E.
On the Design of Shock Isolated Floor Systems
Proceedings of the 29th Annual Shock and Vibration Symposium. March 1960

3.16 Sevin, E.
On the Parametric Excitation of a Pendulum Type Vibration Absorber
Journal of Applied Mechanics, Volume 28, Series E, No. 3. September 1961

3.17 Ince, E. L.
Proceedings of the Royal Society of Edinburgh
Volume 52, pp. 355-433. 1931/1932

3.18 Strutt, M. J. O.
Lamésche, Mathieuche und Verwandte Funktionen in Physik und Technik
Springer, Berlin. 1932

3.19 Kotowski, G.
Zeitschrift der Angewandte Mathematik und Mechanik
Volume 23, pp. 226. 1943

3.20 Malkin, I. G.
Theorie der Stabilitat der Bemegung
Oldenburg, München, West Germany

APPENDIX 3-A

INVERSION OF A MATRIX COMPOSED OF POLYNOMIALS BY ELECTRONIC DIGITAL COMPUTER

Electronic digital computers are capable of handling numerical coefficients only. Hence the elements of the matrix to be inverted must be numbers if the inversion is to be accomplished on an electronic digital computer. But, as often happens in practice, the matrix to be inverted has as its elements polynomials of some unknown variable quantity, say 'x'. Then the inverted matrix will also contain polynomials of some power of 'x', depending on the size of the matrix. It is desired, then, to evaluate the coefficients of the polynomials of the inverted matrix. If the coefficients of the polynomials of the original matrix are numbers, then it is possible to obtain the coefficients of the inverted matrix, also as numbers. Since this operation is entirely numerical, it can be handled by an electronic digital computer as is shown by considering two specific examples below:

1. A 3 x 3 Matrix Composed of First Order Polynomials

Given a matrix

$$[x] = \begin{bmatrix} a_{11}x + b_{11} & a_{12}x + b_{12} & a_{13}x + b_{13} \\ a_{21}x + b_{21} & a_{22}x + b_{22} & a_{23}x + b_{23} \\ a_{31}x + b_{31} & a_{32}x + b_{32} & a_{33}x + b_{33} \end{bmatrix}$$

Where a_{ij} and b_{ij} are numerical coefficients, and x is an unknown variable. Each element of the inverted matrix consists of a co-factor of the matrix $[x]$ divided by the determinant of the matrix $|x|$. For this particular case the determinant will be a third order polynomial in x and the co-factors will be second order polynomials in x. Hence, we can write

$$[x]^{-1} = \begin{bmatrix} a_{11}x+b_{11} & a_{12}x+b_{12} & a_{13}x+b_{13} \\ a_{21}x+b_{21} & a_{22}x+b_{22} & a_{23}x+b_{23} \\ a_{31}x+b_{31} & a_{32}x+b_{32} & a_{33}x+b_{33} \end{bmatrix}^{-1} = \begin{bmatrix} \frac{c_{11}x^2+d_{11}x+e_{11}}{\alpha x^3+\beta x^2+\gamma x+\delta} & \frac{c_{12}x^2+d_{12}x+e_{12}}{\alpha x^3+\beta x^2+\gamma x+\delta} & \frac{c_{13}x^2+d_{13}x+e_{13}}{\alpha x^3+\beta x^2+\gamma x+\delta} \\ \frac{c_{21}x^2+d_{21}x+e_{21}}{\alpha x^3+\beta x^2+\gamma x+\delta} & \frac{c_{22}x^2+d_{22}x+e_{22}}{\alpha x^3+\beta x^2+\gamma x+\delta} & \frac{c_{23}x^2+d_{23}x+e_{23}}{\alpha x^3+\beta x^2+\gamma x+\delta} \\ \frac{c_{31}x^2+d_{31}x+e_{31}}{\alpha x^3+\beta x^2+\gamma x+\delta} & \frac{c_{32}x^2+d_{32}x+e_{32}}{\alpha x^3+\beta x^2+\gamma x+\delta} & \frac{c_{33}x^2+d_{33}x+e_{33}}{\alpha x^3+\beta x^2+\gamma x+\delta} \end{bmatrix}$$

Where c_{ij}, d_{ij}, α, β, γ, and δ are numerical coefficients. The above relationship can be rewritten as follows:

$$\left[x\right]^{-1} = \left\{\begin{bmatrix} a_{11} & a_{12} & a_{13} \\ a_{21} & a_{22} & a_{23} \\ a_{31} & a_{32} & a_{33} \end{bmatrix} x + \begin{bmatrix} b_{11} & b_{12} & b_{13} \\ b_{21} & b_{22} & b_{23} \\ b_{31} & b_{32} & b_{33} \end{bmatrix}\right\}^{-1} =$$

$$\frac{1}{\alpha x^3+\beta x^2+\gamma x+\delta} \left\{\begin{bmatrix} c_{11} & c_{12} & c_{13} \\ c_{21} & c_{22} & c_{23} \\ c_{31} & c_{32} & c_{33} \end{bmatrix} x^2 + \begin{bmatrix} d_{11} & d_{12} & d_{13} \\ d_{21} & d_{22} & d_{23} \\ d_{31} & d_{32} & d_{33} \end{bmatrix} x + \begin{bmatrix} e_{11} & e_{12} & e_{13} \\ e_{21} & e_{22} & e_{23} \\ e_{31} & e_{32} & e_{33} \end{bmatrix}\right\}$$

Or

$$\left[x\right]^{-1} = \left\{\left[A\right] x + \left[B\right]\right\}^{-1} = \frac{1}{\alpha x^3+\beta x^2+\gamma x+\delta} \left\{\left[C\right] x^2 + \left[D\right] x + \left[E\right]\right\}$$

The problem then is to evaluate $[C]$, $[D]$ and $[E]$ in terms of the numerical matrices $[A]$ and $[B]$ and the coefficients α, β, γ and δ.

By the definition of an inverse matrix

$$\left\{\left[A\right] x + \left[B\right]\right\} \left\{\frac{1}{\alpha x^3+\beta x^2+\gamma x+\delta} \left(\left[C\right] x^2 + \left[D\right] x + \left[E\right]\right)\right\} = \left[I\right]$$

Or

$$\left[A\right]\left[C\right] x^3 + \left(\left[A\right]\left[D\right] + \left[B\right]\left[C\right]\right) x^2 + \left(\left[A\right]\left[E\right] + \left[B\right]\left[D\right]\right) x + \left[B\right]\left[E\right] = \left\{\alpha x^3+\beta x^2+\gamma x+\delta\right\} \left[I\right]$$

Equating the coefficients of similar powers of x.

$$\left[A\right]\left[C\right] = \alpha\left[I\right]; \quad \left[A\right]\left[D\right] + \left[B\right]\left[C\right] = \beta\left[I\right]; \quad \left[B\right]\left[D\right] + \left[A\right]\left[E\right] = \gamma\left[I\right]; \quad \left[B\right]\left[E\right] = \delta\left[I\right]$$

Using the first three of these equations, since the fourth one is linearly dependent on the first three, we obtain

$$\begin{bmatrix} [A] & o & o \\ [B] & [A] & o \\ [o] & [B] & [A] \end{bmatrix} \begin{bmatrix} [C] \\ [D] \\ [E] \end{bmatrix} = \begin{bmatrix} \alpha[I] \\ \beta[I] \\ \gamma[I] \end{bmatrix}$$

Then

$$\begin{bmatrix} [C] \\ [D] \\ [E] \end{bmatrix} = \begin{bmatrix} [A] & o & o \\ [B] & [A] & o \\ o & [B] & [A] \end{bmatrix}^{-1} \begin{bmatrix} \alpha[I] \\ \beta[I] \\ \gamma[I] \end{bmatrix}$$

This last equation is entirely numerical and enables the computer to evaluate $[C]$, $[D]$, and $[E]$; the numerical coefficients α, β, γ and δ of the polynomial derived from the determinant of $[x]$ have to be evaluated beforehand. This may be done either conventionally or on a computer depending on the size of the problem. A method for determining these coefficients on an electronic digital computer is discussed in Appendix 3.9B.

2. A 6 x 6 Matrix Composed of First Order Polynomials

In basic theory, this example is exactly similar to the previous one, except that it involves a greater amount of arithmetic. Thus, given a matrix

$$[x] = \begin{bmatrix} a_{11}x+b_{11} & a_{12}x+b_{12} & a_{13}x+b_{13} & a_{14}x+b_{14} & a_{15}x+b_{15} & a_{16}x+b_{16} \\ a_{21}x+b_{21} & a_{22}x+b_{22} & a_{23}x+b_{23} & a_{24}x+b_{24} & a_{25}x+b_{25} & a_{26}x+b_{26} \\ a_{31}x+b_{31} & a_{32}x+b_{32} & a_{33}x+b_{33} & a_{34}x+b_{34} & a_{35}x+b_{35} & a_{36}x+b_{36} \\ a_{41}x+b_{41} & a_{42}x+b_{42} & a_{43}x+b_{43} & a_{44}x+b_{44} & a_{45}x+b_{45} & a_{46}x+b_{46} \\ a_{51}x+b_{51} & a_{52}x+b_{52} & a_{53}x+b_{53} & a_{54}x+b_{54} & a_{55}x+b_{55} & a_{56}x+b_{56} \\ a_{61}x+b_{61} & a_{62}x+b_{62} & a_{63}x+b_{63} & a_{64}x+b_{64} & a_{65}x+b_{65} & a_{66}x+b_{66} \end{bmatrix}$$

where a_{ij} and b_{ij} are numerical coefficients and x is an unknown variable. In this case the determinant of $[x]$ will be a sixth order polynomial in x, and the co-factors of $[x]$ will be firth order polynomials in x. Hence, writing in matrix form,

$$[x]^{-1} = \left\{[A]\ x + [B]\right\}^{-1} = \frac{1}{\alpha x^6+\beta x^5+\gamma x^4+\delta x^3+\varepsilon x^2+\lambda x+\psi} \left\{\begin{matrix}[C]\ x^5 + [D]\ x^4 + [E]\ x^3 + \\ [F]\ x^2 + [G]\ x + [H]\end{matrix}\right\}$$

where $[A]$, $[B]$, $[C]$, $[D]$, $[E]$, $[F]$, $[G]$, and $[H]$ are 6 x 6 numerical matrices. Then,

$$\left\{[A]\ x + [B]\right\} \frac{\left\{[C]\ x^5 + [D]\ x^4 + [E]\ x^3 + [F]\ x^2 + [G]\ x + [H]\right\}}{\alpha x^6+\beta x^5+\gamma x^4+\delta x^3+\varepsilon x^2+\lambda x+\psi} = [I]$$

Or:

$$[A][C]x^6 + ([A][D] + [B][C])x^5 + ([A][E] + [B][D])x^4 + ([A][F] + [B][E])x^3 + ([A][G] + [B][F])x^2 + ([A][H]x + [B][G])x + [B][H] = (\alpha x^6 + \beta x^5 + \gamma x^4 + \delta x^3 + \varepsilon x^2 + \lambda x + \psi)[I]$$

Then comparing the coefficients of similar powers of x,

$$\begin{aligned}
[A][C] &= \alpha[I] \\
[A][D] + [B][C] &= \beta[I] \\
[A][E] + [B][D] &= \gamma[I] \\
[A][F] + [B][E] &= \delta[I] \\
[A][G] + [B][F] &= \varepsilon[I] \\
[A][H] + [B][G] &= \lambda[I] \\
[B][H] &= \psi[I]
\end{aligned}$$

Taking the first six of these seven equations,

$$\begin{bmatrix} [A] & 0 & 0 & 0 & 0 & 0 \\ [B] & [A] & 0 & 0 & 0 & 0 \\ 0 & [B] & [A] & 0 & 0 & 0 \\ 0 & 0 & [B] & [A] & 0 & 0 \\ 0 & 0 & 0 & [B] & [A] & 0 \\ 0 & 0 & 0 & 0 & [B] & [A] \end{bmatrix} \begin{bmatrix} [C] \\ [D] \\ [E] \\ [F] \\ [G] \\ [H] \end{bmatrix} = \begin{bmatrix} \alpha[I] \\ \beta[I] \\ \gamma[I] \\ \delta[I] \\ \varepsilon[I] \\ \lambda[I] \end{bmatrix}$$

From the above equation we can obtain C , D , E , F , G and H if α , β , γ , δ , ε , and λ are known.

Or, considering the first three and the last three equations,

$$\begin{bmatrix} [A] & 0 & 0 & 0 & 0 & 0 \\ [B] & [A] & 0 & 0 & 0 & 0 \\ 0 & [B] & [A] & 0 & 0 & 0 \\ 0 & 0 & 0 & [B] & [A] & 0 \\ 0 & 0 & 0 & 0 & [B] & [A] \\ 0 & 0 & 0 & 0 & 0 & [B] \end{bmatrix} \begin{bmatrix} [C] \\ [D] \\ [E] \\ [F] \\ [G] \\ [H] \end{bmatrix} = \begin{bmatrix} \alpha[I] \\ \beta[I] \\ \gamma[I] \\ \delta[I] \\ \varepsilon[I] \\ \lambda[I] \end{bmatrix}$$

The choice of equations should be such as to make the large square matrix nonsingular.

APPENDIX 3-B

EVALUATION OF A DETERMINANT COMPOSED OF POLYNOMIALS BY ELECTRONIC DIGITAL COMPUTER

A computer program for handling a polynomial determinant can accept numerical data only. Thus, a polynomial determinant is solved by the evaluation of several numerical determinants. For example, a determinant composed of polynomials, as follows:

$$\begin{bmatrix} a_{11}s^2+b_{11} & a_{12}s^2+b_{12} & a_{13}s^2+b_{13} & a_{14}s^2+b_{14} & a_{15}s^2+b_{15} & a_{16}s^2+b_{16} \\ a_{21}s^2+b_{21} & a_{22}s^2+b_{22} & a_{23}s^2+b_{23} & a_{24}s^2+b_{24} & a_{25}s^2+b_{25} & a_{26}s^2+b_{26} \\ a_{31}s^2+b_{31} & a_{32}s^2+b_{32} & a_{33}s^2+b_{33} & a_{34}s^2+b_{34} & a_{35}s^2+b_{35} & a_{36}s^2+b_{36} \\ a_{41}s^2+b_{41} & a_{42}s^2+b_{42} & a_{43}s^2+b_{43} & a_{44}s^2+b_{44} & a_{45}s^2+b_{45} & a_{46}s^2+b_{46} \\ a_{51}s^2+b_{51} & a_{52}s^2+b_{52} & a_{53}s^2+b_{53} & a_{54}s^2+b_{54} & a_{55}s^2+b_{55} & a_{56}s^2+b_{56} \\ a_{61}s^2+b_{61} & a_{62}s^2+b_{62} & a_{63}s^2+b_{63} & a_{64}s^2+b_{64} & a_{65}s^2+b_{65} & a_{66}s^2+b_{66} \end{bmatrix}$$

which in the expanded form reduces to

$$As^{12}+Bs^{10}+Cs^8+Ds^6+Es^4+Fs^2+G$$

requires for its solution, the evaluation of the coefficients A, B, C, D, E, F and G. Making the following designations:

1 = row a_{11} a_{12} a_{13} a_{14} a_{15} a_{16}

2 = row a_{21} a_{22} a_{23} a_{24} a_{25} a_{26}

3 = row a_{31} a_{32} a_{33} a_{34} a_{35} a_{36}

4 = row a_{41} a_{42} a_{43} a_{44} a_{45} a_{46}

5 = row a_{51} a_{52} a_{53} a_{54} a_{55} a_{56}

6 = row a_{61} a_{62} a_{63} a_{64} a_{65} a_{66}

7 = row b_{11} b_{12} b_{13} b_{14} b_{15} b_{16}

8 = row b_{21} b_{22} b_{23} b_{24} b_{25} b_{26}

9 = row b_{31} b_{32} b_{33} b_{34} b_{35} b_{36}

10 = row b_{41} b_{42} b_{43} b_{44} b_{45} b_{46}

11 = row b_{51} b_{52} b_{53} b_{54} b_{55} b_{56}

12 = row b_{61} b_{62} b_{63} b_{64} b_{65} b_{66}

Then A = 1, 2, 3, 4, 5, 6, i.e., the numerical value of A is given by the value of the numerical determinant composed of rows 1, 2, 3, 4, 5 and 6, taken in that order.

Similarly, B = (1,2,3,4,5,12) + (1,2,3,4,11,6) + (1,2,3,10,5,6)
+ (1,2,9,4,5,6) + (1,8,3,4,5,6) + (7,2,3,4,5,6)

i.e., the numerical value of B is given by the sum of the values of six numerical determinants, formed by the combination of 6 rows, numbered and taken in the order given above.

Similarly, C = (1,2,3,4,11,12) + (1,2,3,10,11,6) + (12,9,10,5,6)
+ (1,8,9,4,5,6) + (7,8,3,4,5,6) + (7,2,3,4,5,12)
+ (1,2,3,10,5,12) + (1,2,9,4,11,6) + (1,8,3,10,5,6)
+ (7,2,9,4,5,6) + (1,8,3,4,5,12) + (7,2,3,4,11,6)
+ (1,2,9,4,5,12) + (1,8,3,4,11,6) + (7,2,3,10,5,6)

D = (1,2,3,10,11,12) + (1,2,9,10,11,6) + (1,8,9,10,5,6)
+ (7,8,9,4,5,6) + (7,8,3,4,5,12) + (7,2,3,4,11,12)
+ (1,2,9,4,11,12) + (1,8,3,4,11,12) + (1,2,9,10,5,12)
+ (1,8,3,10,5,12) + (7,2,3,10,5,12) + (1,8,3,10,11,6)
+ (7,2,3,10,11,6) + (1,8,9,4,5,12) + (1,8,9,4,11,6)
+ (7,8,3,4,11,6) + (7,8,3,10,5,6) + (7,2,9,4,5,12)
+ (7,2,9,4,11,6) + (7,2,9,10,5,6)

E = (7,8,9,10,5,6) + (7,8,9,4,5,12) + (7,8,3,4,11,12)
+ (7,2,3,10,11,12) + (1,2,9,10,11,12) + (1,8,9,10,11,6)
+ (7,8,9,4,11,6) + (7,8,3,10,5,12) + (7,2,9,4,11,12)
+ (1,8,3,10,11,12) + (7,2,9,10,11,6) + (1,8,9,10,5,12)
+ (7,8,3,10,11,6) + (7,2,9,10,5,12) + (1,8,9,4,11,12)

F = (7,8,9,10,11,6) + (7,8,9,10,5,12) + (7,8,9,4,11,12)
+ (7,8,3,10,11,12) + (1,8,9,10,11,12) + (7,2,9,10,11,12)

G = (7,8,9,10,11,12)

The evaluation of a 6th order numerical determinant by computer can be achieved by the following formula. (Aitken)*

$$A = \sum_{j=1}^{6} a_{ij} (-1)^{1+j} \left[\sum_{K=1}^{6} a_{2K} (\alpha) \left\{ \sum_{\ell=1}^{6} a_{3\ell} (\beta) \left[\sum_{m=1}^{6} a_{4m} (\gamma) \left(\sum_{n=1}^{6} a_{5n} (\delta) a_{6p} \right) \right] \right\} \right]$$

where

$\alpha = (-1)^{1+K}$ when $K < j$

$\alpha = (-1)^{K}$ $K > j$

$\alpha = 0$ $K = j$

$\beta = (-1)^{1+\ell}$ $\ell > K$, $\ell > j$

$= (-1)^{1+\ell}$ $\ell < K$, $\ell < j$

$= (-1)^{\ell}$ $\ell > K$, $\ell < j$

$= (-1)^{\ell}$ $\ell < K$, $\ell > j$

$= 0$ $\ell = K$

$\beta = 0$ $\ell = j$

$\gamma = (-1)^{1+m}$ $m > \ell$, $m < K$, $m > j$

$= (-1)^{1+m}$ $m < \ell$, $m > K$, $m > j$

$= (-1)^{1+m}$ $m < \ell$, $m < K$, $m < j$

$= (-1)^{1+m}$ $m > \ell$, $m > K$, $m < j$

$= (-1)^{m}$ $m > \ell$, $m > K$, $m > j$

$= (-1)^{m}$ $m > \ell$, $m < K$, $m < j$

$= (-1)^{m}$ $m < \ell$, $m > K$, $m < j$

$= (-1)^{m}$ $m < \ell$, $m < K$, $m > j$

$= 0$ $m = \ell$

$= 0$ $m = K$

$\gamma = 0$ $m = j$

$\delta = -1$ $n > p$

$\delta = +1$ $n < p$

$\delta = 0$ $n = p$

$p = 1,2,3,4,5$ or 6 but $\neq j,k,\ell,m,$ or n.

*Aitken, A.C., Determinants and Matrices, Oliver and Boyd, London, 1959

APPENDIX 3-C

CONVERSION OF A POLYNOMIAL EXPRESSION TO PARTIAL FRACTIONS

One of the problems which arises in the solution of the equation of motion of a coupled six-degree-of-freedom isolation system is the conversion to partial fractions of each of the 36 elements of the inverted 6 by 6 frequency matrix. A typical element of this inverted frequency matrix is in the form

$$\frac{As^{10} + Bs^{8} + Cs^{6} + Ds^{4} + Es^{2} + F}{(s^2+\alpha)(s^2+\beta)(s^2+\gamma)(s^2+\delta)(s^2+\Sigma)(s^2+\lambda)}$$

where α, β, γ, δ, Σ, and λ are the six previously determined squares of the natural frequencies of the coupled system. It is desired to convert the above expression, for reasons explained elsewhere in the text, to the following form:

$$\frac{a}{s^2+\alpha} + \frac{b}{s^2+\beta} + \frac{c}{s^2+\gamma} + \frac{d}{s^2+\delta} + \frac{e}{s^2+\Sigma} + \frac{f}{s^2+\lambda}$$

Equating these two expressions, we are left with the relationship

$$\begin{aligned}
&a(s^2+\beta)(s^2+\gamma)(s^2+\delta)(s^2+\Sigma)(s^2+\lambda)\\
&+b(s^2+\alpha)(s^2+\gamma)(s^2+\delta)(s^2+\Sigma)(s^2+\lambda)\\
&+c(s^2+\alpha)(s^2+\beta)(s^2+\delta)(s^2+\Sigma)(s^2+\lambda)\\
&+d(s^2+\alpha)(s^2+\beta)(s^2+\gamma)(s^2+\Sigma)(s^2+\lambda)\\
&+e(s^2+\alpha)(s^2+\beta)(s^2+\gamma)(s^2+\delta)(s^2+\lambda)\\
&+f(s^2+\alpha)(s^2+\beta)(s^2+\gamma)(s^2+\delta)(s^2+\Sigma)\\
&= As^{10} + Bs^{8} + Cs^{6} + Ds^{4} + Es^{2} + F
\end{aligned}$$

Equating the coefficients of similar powers of s^2 on the right hand side and the left hand side of the above equation, we obtain six equations, which express the six unknows a, b, c, d, e and f in terms of the known coefficients A, B, C, D, E and F, and the known squares of the frequencies, α, β, γ, δ, Σ and λ. These equations can be written in matrix form, as follows, and can be conveniently solved on an electronic digital computer.

$$\frac{As^{10}+Bs^{8}+Cs^{6}+Ds^{4}+Es^{2}+F}{(s^2+\alpha)(s^2+\beta)(s^2+\gamma)(s^2+\delta)(s^2+\epsilon)(s^2+\lambda)} = \frac{a}{(s^2+\alpha)} + \frac{b}{(s^2+\beta)} + \frac{c}{(s^2+\gamma)} + \frac{d}{(s^2+\delta)} + \frac{e}{(s^2+\epsilon)} + \frac{f}{(s^2+\lambda)}$$

$$\begin{bmatrix} 1 & 1 & 1 & 1 & 1 & 1 \\ (\beta+\gamma+\delta+\epsilon+\lambda) & (\alpha+\gamma+\delta+\epsilon+\lambda) & (\alpha+\beta+\delta+\epsilon+\lambda) & (\alpha+\beta+\gamma+\epsilon+\lambda) & (\alpha+\beta+\gamma+\delta+\lambda) & (\alpha+\beta+\gamma+\delta+\epsilon) \\ \begin{matrix}(\beta\gamma+\beta\delta+\beta\epsilon+\beta\lambda\\ +\gamma\delta+\gamma\epsilon+\gamma\lambda\\ +\delta\epsilon+\delta\lambda+\epsilon\lambda)\end{matrix} & \begin{matrix}(\alpha\gamma+\alpha\delta+\alpha\epsilon+\alpha\lambda\\ +\gamma\delta+\gamma\epsilon+\gamma\lambda\\ +\delta\epsilon+\delta\lambda+\epsilon\lambda)\end{matrix} & \begin{matrix}(\alpha\beta+\alpha\delta+\alpha\epsilon+\alpha\lambda\\ +\beta\delta+\beta\epsilon+\beta\lambda\\ +\delta\epsilon+\delta\lambda+\epsilon\lambda)\end{matrix} & \begin{matrix}(\alpha\beta+\alpha\gamma+\alpha\epsilon+\alpha\lambda\\ +\beta\gamma+\beta\epsilon+\beta\lambda\\ +\gamma\epsilon+\gamma\lambda+\epsilon\lambda)\end{matrix} & \begin{matrix}(\alpha\beta+\alpha\gamma+\alpha\delta+\alpha\lambda\\ +\beta\gamma+\beta\delta+\beta\lambda\\ +\gamma\delta+\gamma\lambda+\delta\lambda)\end{matrix} & \begin{matrix}(\alpha\beta+\alpha\gamma+\alpha\delta+\alpha\epsilon\\ +\beta\gamma+\beta\delta+\beta\epsilon\\ +\gamma\delta+\gamma\epsilon+\delta\epsilon)\end{matrix} \\ \begin{matrix}(\beta\gamma\delta+\beta\gamma\epsilon+\beta\gamma\lambda\\ +\beta\delta\epsilon+\beta\delta\lambda+\beta\epsilon\lambda\\ +\gamma\delta\epsilon+\gamma\delta\lambda+\gamma\epsilon\lambda\\ +\delta\epsilon\lambda)\end{matrix} & \begin{matrix}(\alpha\gamma\delta+\alpha\gamma\epsilon+\alpha\gamma\lambda\\ +\alpha\delta\epsilon+\alpha\delta\lambda+\alpha\epsilon\lambda\\ +\gamma\delta\epsilon+\gamma\delta\lambda+\gamma\epsilon\lambda\\ +\delta\epsilon\lambda)\end{matrix} & \begin{matrix}(\alpha\beta\delta+\alpha\beta\epsilon+\alpha\beta\lambda\\ +\alpha\delta\epsilon+\alpha\delta\lambda+\alpha\epsilon\lambda\\ +\beta\delta\epsilon+\beta\delta\lambda+\beta\epsilon\lambda\\ +\delta\epsilon\lambda)\end{matrix} & \begin{matrix}(\alpha\beta\gamma+\alpha\beta\epsilon+\alpha\beta\lambda\\ +\alpha\gamma\epsilon+\alpha\gamma\lambda+\alpha\epsilon\lambda\\ +\beta\gamma\epsilon+\beta\gamma\lambda+\beta\epsilon\lambda\\ +\gamma\epsilon\lambda)\end{matrix} & \begin{matrix}(\alpha\beta\gamma+\alpha\beta\delta+\alpha\beta\lambda\\ +\alpha\gamma\delta+\alpha\gamma\lambda+\alpha\delta\lambda\\ \beta\gamma\delta+\beta\gamma\lambda+\beta\delta\lambda\\ +\gamma\delta\lambda)\end{matrix} & \begin{matrix}(\alpha\beta\gamma+\alpha\beta\delta+\alpha\beta\epsilon\\ +\alpha\gamma\delta+\alpha\gamma\epsilon+\alpha\delta\epsilon\\ +\beta\gamma\delta+\beta\gamma\epsilon+\beta\gamma\epsilon\\ +\gamma\delta\epsilon)\end{matrix} \\ \begin{matrix}(\beta\gamma\delta\epsilon+\beta\gamma\delta\lambda\\ +\beta\gamma\epsilon\lambda+\beta\delta\epsilon\lambda\\ +\gamma\delta\epsilon\lambda)\end{matrix} & \begin{matrix}(\alpha\gamma\delta\epsilon+\alpha\gamma\delta\lambda\\ +\alpha\gamma\epsilon\lambda+\alpha\delta\epsilon\lambda\\ +\gamma\delta\epsilon\lambda)\end{matrix} & \begin{matrix}(\alpha\beta\delta\epsilon+\alpha\beta\delta\lambda\\ +\alpha\beta\epsilon\lambda+\alpha\beta\epsilon\lambda\\ +\beta\delta\epsilon\lambda)\end{matrix} & \begin{matrix}(\alpha\beta\gamma\epsilon+\alpha\beta\gamma\lambda\\ +\alpha\beta\epsilon\lambda+\alpha\gamma\epsilon\lambda\\ +\beta\gamma\epsilon\lambda)\end{matrix} & \begin{matrix}(\alpha\beta\gamma\delta+\alpha\beta\gamma\lambda\\ +\alpha\beta\delta\lambda+\alpha\gamma\delta\lambda\\ +\beta\gamma\delta\lambda)\end{matrix} & \begin{matrix}(\alpha\beta\gamma\delta+\alpha\beta\gamma\epsilon\\ +\alpha\beta\delta\epsilon+\alpha\gamma\delta\epsilon\\ +\beta\gamma\delta\epsilon)\end{matrix} \\ \beta\gamma\delta\epsilon\lambda & \alpha\gamma\delta\epsilon\lambda & \alpha\beta\delta\epsilon\lambda & \alpha\beta\gamma\epsilon\lambda & \alpha\beta\gamma\delta\lambda & \alpha\beta\gamma\delta\epsilon \end{bmatrix} \begin{bmatrix} a \\ b \\ c \\ d \\ e \\ f \end{bmatrix} \begin{bmatrix} A \\ B \\ C \\ D \\ E \\ F \end{bmatrix}$$

APPENDIX 3-D

INVERSION OF A MATRIX CONSISTED OF BLOCK MATRICES

Several conventional methods of inverting a matrix consisting of scalar elements, have been developed recently with a view towards shortening the computational time. One of the methods frequently used, involves the inversion of a matrix by blocks: This reduces the operation of inverting a very large matrix, to that of inverting several smaller order matrices. In this case, the elements of the matrix are themselves matrices of lower orders. Hence, extreme care must be taken in operating with the partitioned blocks, since these cannot be treated like scalar quantities, and must conform with the laws of operation of matrices. One of the advantages of this method is its ability to retain the physical significance of each partitioned block, even in the inverted form. The partitioned blocks may be all of equal order or not, depending on the nature of the problem.

Below are discussed the inversion procedures for two cases viz., 1) a matrix consisting of four block matrices, and b) a matrix consisting of nine block matrices. In these examples, it is assumed that the blocks are all of equal order. The same principles illustrated here, can be extended to the inversion of matrices consisting of blocks of dissimilar order, or a larger number of blocks.

1. Inversion of a Four Block Matrix

Let it be required to solve the following set of equations:

$$a_{11}x_1 + a_{12}x_2 + a_{13}x_3 + b_{11}y_1 + b_{12}y_2 + b_{13}y_3 = p_1$$

$$a_{21}x_1 + a_{22}x_2 + a_{23}x_3 + b_{21}y_1 + b_{22}y_2 + b_{23}y_3 = p_2$$

$$a_{31}x_1 + a_{32}x_2 + a_{33}x_3 + b_{31}y_1 + b_{32}y_2 + b_{33}y_3 = p_3$$

$$c_{11}x_1 + c_{12}x_2 + c_{13}x_3 + d_{11}y_1 + d_{12}y_2 + d_{13}y_3 = q_1$$

$$c_{21}x_1 + c_{22}x_2 + c_{23}x_3 + d_{21}y_1 + d_{22}y_2 + d_{23}y_3 = q_2$$

$$c_{31}x_1 + c_{32}x_2 + c_{33}x_3 + d_{31}y_1 + d_{32}y_2 + d_{33}y_3 = q_3$$

In matrix form,

$$[A]\ \{x\} + [B]\ \{y\} = \{p\}$$

$$[C]\ \{x\} + [D]\ \{y\} = \{q\}$$

Or,

$$\begin{bmatrix} [A] & [B] \\ [C] & [D] \end{bmatrix} \begin{bmatrix} \{x\} \\ \{y\} \end{bmatrix} = \begin{bmatrix} \{p\} \\ \{q\} \end{bmatrix}$$

Required to find:

$$\begin{bmatrix} [A] & [B] \\ [C] & [D] \end{bmatrix}^{-1}$$

Let

$$\begin{bmatrix} [A_1] & [B_1] \\ [C_1] & [D_1] \end{bmatrix} = \begin{bmatrix} [A] & [B] \\ [C] & [D] \end{bmatrix}^{-1}$$

Then

$$\begin{aligned} [A_1][A] + [B_1][C] &= [I] \\ [A_1][B] + [B_1][D] &= 0 \\ [C_1][A] + [D_1][C] &= 0 \\ [C_1][B] + [D_1][D] &= [I] \end{aligned}$$

Solving the above four equations, bearing in mind that we are dealing with matrices and not scalar quantities, we obtain,

$$\begin{aligned} [A_1] &= [A]^{-1} + [A]^{-1}[I][\Delta]^{-1}[C][A]^{-1} \\ [B_1] &= -[A]^{-1}[B][\Delta]^{-1} \\ [C_1] &= -[\Delta]^{-1}[C][A]^{-1} \\ [D_1] &= [\Delta]^{-1} \end{aligned}$$

Where $[\Delta] = \{[D] - [C][A]^{-1}[B]\}$ which is the determinant of the original matrix, in matrix form. It may be noticed here that it deviates from the accepted scalar form of (AD-BC). It must be pointed out here that the inverse exists only if $[A]^{-1}$ and $[A]^{-1}$ exist. Then,

$$\begin{bmatrix} [A] & [B] \\ [C] & [D] \end{bmatrix}^{-1} = \begin{bmatrix} [A]^{-1} + [A]^{-1}[B][\Delta]^{-1}[C][A]^{-1} & -[A]^{-1}[B][\Delta]^{-1} \\ -[\Delta]^{-1}[C][A]^{-1} & [\Delta]^{-1} \end{bmatrix}$$

2. Inversion of a Nine Block Matrix

Given:

$$[K]\{x\} + [L]\{y\} + [M]\{z\} = \{u\}$$
$$[N]\{x\} + [P]\{y\} + [Q]\{z\} = \{v\}$$
$$[R]\{x\} + [S]\{y\} + [T]\{z\} = \{w\}$$

Or:

$$\begin{bmatrix} [K] & [L] & [M] \\ [N] & [P] & [Q] \\ [R] & [S] & [T] \end{bmatrix} \begin{bmatrix} \{x\} \\ \{y\} \\ \{z\} \end{bmatrix} = \begin{bmatrix} \{u\} \\ \{v\} \\ \{w\} \end{bmatrix}$$

Required to find

$$\begin{bmatrix} [K] & [L] & [M] \\ [N] & [P] & [Q] \\ [R] & [S] & [T] \end{bmatrix}^{-1}$$

Let:

$$\begin{bmatrix} [A] & [B] & [C] \\ [D] & [E] & [F] \\ [G] & [H] & [J] \end{bmatrix} = \begin{bmatrix} [K] & [L] & [M] \\ [N] & [P] & [Q] \\ [R] & [S] & [T] \end{bmatrix}^{-1}$$

Then:

$$[A][K] + [B][N] + [C][R] = [I]$$
$$[A][L] + [B][P] + [C][S] = 0$$
$$[A][M] + [B][Q] + [C][T] = 0$$

$$[D][K] + [E][N] + [F][R] = 0$$
$$[D][L] + [E][P] + [F][S] = [I]$$
$$[D][M] + [E][Q] + [F][T] = 0$$

$$[G][K] + [H][N] + [J][R] = 0$$
$$[G][L] + [H][P] + [J][S] = 0$$
$$[G][M] + [H][Q] + [J][T] = [I]$$

Solving the above nine equations, and bearing in mind that the operations involve matrices and not scalar quantities,

$$[A] = [K]^{-1}\left[[I] + \left\{[L][\alpha][N] + \left([L][\beta] - [M]\right)[\Delta]^{-1}\left([\gamma][N] - [R]\right)\right\}[K]^{-1}\right]$$

$$[B] = -[K]^{-1}\left[[L][\alpha] + \left\{[L][\beta] - [M]\right\}[\Delta]^{-1}[\gamma]\right]$$

$$[C] = [K]^{-1}\left\{[L][\beta] - [M]\right\}[\Delta]^{-1}$$

$$[D] = -\left[[\beta][\Delta]^{-1}\left\{[\gamma][N] - [R]\right\} + [\alpha][N]\right][K]^{-1}$$

$$[E] = [\beta][\Delta]^{-1}[\gamma] + [\alpha]$$

$$[F] = -[\beta][\Delta]^{-1}$$

$$[G] = [\Delta]^{-1}\left\{[\gamma][N] - [R]\right\}[K]^{-1}$$

$$[H] = -[\Delta]^{-1}[\gamma]$$

$$[J] = [\Delta]^{-1}$$

Where,

$$[\Delta] = \left[\left\{[T] - [R][K]^{-1}[M]\right\} - \left\{[S] - [R][K]^{-1}[L]\right\}\left\{[P] - [N][K]^{-1}[L]\right\}^{-1}\left\{[Q] - [N][K]^{-1}[M]\right\}\right]$$

$$[\alpha] = \left\{[P] - [N][K]^{-1}[L]\right\}^{-1}$$

$$[\beta] = [\alpha]\left\{[Q] - [N][K]^{-1}[M]\right\}$$

$$[\gamma] = \left\{[S] - [R][K]^{-1}[L]\right\}[\gamma]$$

The solution exists if, and only if, $[\Delta]^{-1}$, $[\alpha]$, and $[K]^{-1}$ exist.

APPENDIX 3-E

THE ROUTH-HURWITZ STABILITY CRITERION FOR A SIX DEGREE OF FREEDOM LINEAR SYSTEM

The frequency determinant in Laplace form, for a six-degree-of-freedom linear system can be written as follows:

$$D(s^2) = a_o s^{12} + a_1 s^{10} + a_2 s^8 + a_3 s^6 + a_4 s^4 + a_5 s^2 + a_6$$

Then the conditions that all the roots of $D(s^2)$ have negative real parts (which signifies dynamic stability) are as follows*:

1. All the a's in the above equations have the same sign (a necessary but not a sufficient condition for stability).

2. The following test functions T_i are all positive when the equation $(D(s^2)=o$ is put in such a form that a_o is positive (a necessary and sufficient condition for stability).

$$T_1 = a_o > o; \quad T_2 = \begin{vmatrix} a_1 & a_o \\ a_3 & a_2 \end{vmatrix} > o; \quad T_3 = \begin{vmatrix} a_1 & a_o & o \\ a_3 & a_2 & a_1 \\ a_5 & a_4 & a_3 \end{vmatrix} > o;$$

$$T_4 = \begin{vmatrix} a_1 & a_o & o & o \\ a_3 & a_2 & a_1 & a_o \\ a_5 & a_4 & a_3 & a_2 \\ o & a_6 & a_5 & a_4 \end{vmatrix} > o; \quad T_5 = \begin{vmatrix} a_1 & a_o & o & o & o \\ a_3 & a_2 & a_1 & a_o & o \\ a_5 & a_4 & a_3 & a_2 & a_1 \\ o & a_6 & a_5 & a_4 & a_3 \\ o & o & o & a_6 & a_5 \end{vmatrix} > o$$

The above conditions when grouped together give the following complete criterion for the stability of a sixth order system.

1. All the a's are positive
2. $a_5\left[a_1a_2a_3a_4 - a_1^2a_4^2 - a_3^2a_4 + 2a_1a_4a_5 - a_1^2a_2a_5 + a_2a_3a_5 + a_5^2\right]$
$$> a_6\left[a_1^2a_2a_3^2 - 2a_1^2a_2a_5 - a_1^2a_3a_4 + a_1^3a_6 + 3a_1a_3a_5 - a_3^3\right]$$

when $D(s^2) = 0$ is such that $a_o = 1$

*Pipes, Louis A., Applied Mathematics for Engineers and Physicists, McGraw-Hill Book Company, New York, 1958

APPENDIX 3-F

THE MATHIEU DIFFERENTIAL EQUATION

AND THE MATHIEU FUNCTIONS

The general Mathieu equation is represented as follows:

$$\ddot{y} + (a - 2q \cos 2\alpha)\, y = 0 \qquad (1)$$

where y is the dependent variable, α is a function of the independent variable with respect to which y is differentiated, and q and a are the constant parameters defining the system configuration.

The general solution of the Mathieu equation may be one of the following three types, depending on the relationship between the parameters a and q.

1. A periodic solution with period $2\pi S$ where S is an integral number greater than or equal to 2.

2. An aperiodic solution, but bounded as $\alpha \longrightarrow \infty$

3. An aperiodic solution, unbounded as $\alpha \longrightarrow \infty$

The solutions of the Mathieu differential equation having a period π or 2π consist entirely of sine or cosine terms, but not a combination of the two. Furthermore, if one of the solutions is even then the other solution is odd, and as such two independent even solutions or two independent odd solutions cannot occur.

The coefficient $(a - 2q \cos 2\alpha)$ of y is a single valued periodic function of α, having a period π. With $\omega t = 2\alpha$, the above equation may be regarded as the representative equation of motion of a conservative dynamical system having a variable spring stiffness $(a - 2q \cos 2\alpha)$, the variation being caused by a driving agent.

Standard solutions of the three general types for equation (1), as explained previously, exist and have been set up by Ince* and Strutt, whereby the entire (a,q) plane has been divided into zones of stability and instability.

*Ince, E.L., Proceedings of the Royal Society, Edinburgh, Volume 52, pp. 355-433, 1931/1932

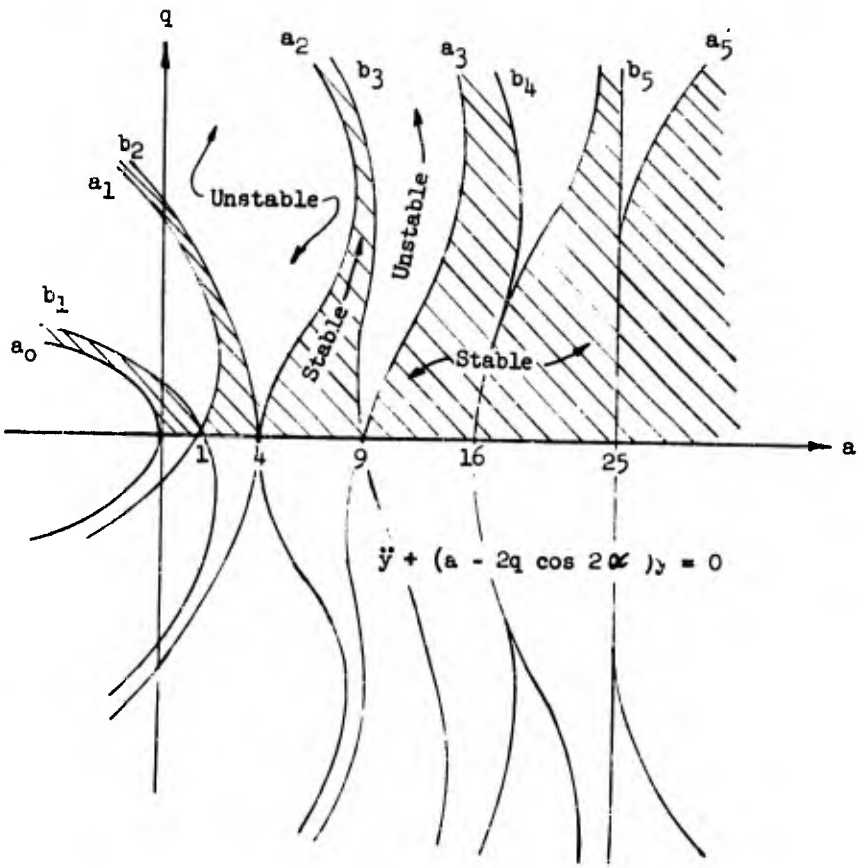

Figure 3-F-1 Ince-Strutt Stability Chart

The Ince-Strutt chart (Figure 3-F-1) is symmetrical about the a axis in the range q). The significant results of the Ince-Strutt study may be summarized as follows:

1. If the operating point (a,q) lies within a stable region, the two linearly independent solutions of equation (1) are:

$$y_1 = \sum_{r=-\infty}^{\infty} C_M \cos(M + \gamma)\alpha$$

$$y_2 = \sum_{r=-\infty}^{\infty} C_M \sin(M + \gamma)\alpha \qquad (2)$$

where $M = 2r$ or $2r + 1$, depending on whether the point (a,q) lies on the a_{2n} or a_{2n+1} curve; C_m is a real quantity and depends on a and q. All solutions of the above type are bounded and therefore if (a,q) lies in a stable region, the resulting oscillations are almost periodic and quasi-harmonic, as shown in Figure 3-F-2.

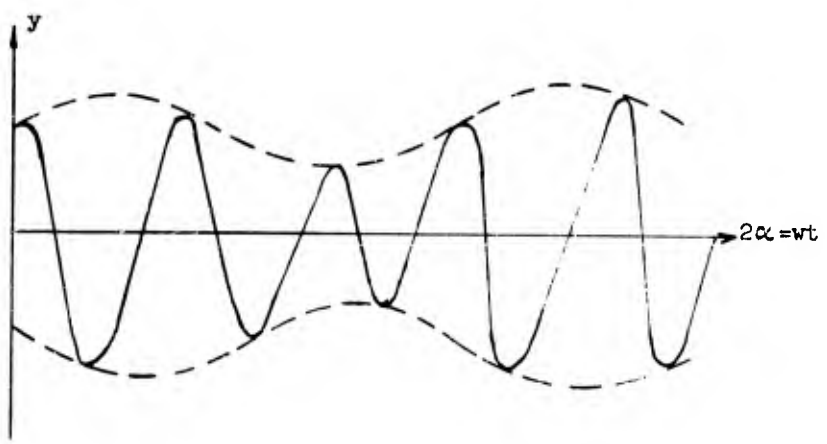

Figure 3-F-2
A Stable Mathieu-Type Oscillation

2. If (a,q) lies within an unstable region, then the two linearly independent solutions of equation (1) have the nonperiodic form:

$$y_1 = e^{\mu\alpha} \sum_{r=0}^{\infty} \rho_M \cos(M\alpha + \nu_M) \qquad (3)$$

$$y_2 = e^{-\mu\alpha} \sum_{r=0}^{\infty} \rho_M \cos(M\alpha - \nu_M)$$

where ρ_M and ν_M are real constants depending on a and q, and M = 2r or 2 r + 1 as before. The quantity M is a real and positive number, independent of the initial conditions and depending only on the parameters a and q of differential equation (1).

All solutions of the above type are unbounded and therefore if a,q lies in an unstable region, the resulting oscillations will be almost periodic and quasi-harmonic, but unstable, as shown in Figure 3-F-3.

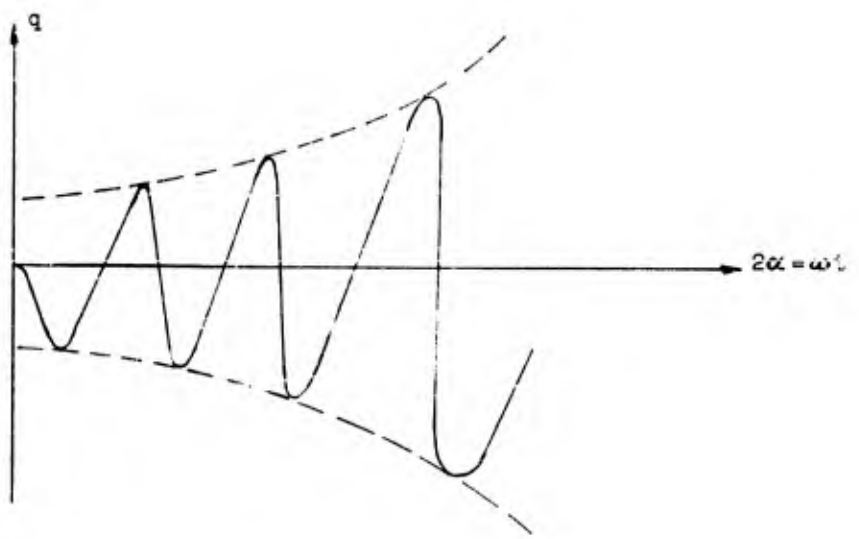

Figure 3-F-3
An Unstable Mathieu-Type Oscillation

3. If (a,q) lies on one of the bordering instability curves, then the linearly independent solutions of equation (1) may have one of the following forms depending on the order of the curve on which it is located.

$$y_1 = \sum_{r=0}^{\infty} A_M \cos M\alpha \qquad (4)$$

$$y_2 = C(q)\,\alpha\, y_1 + f(\alpha)$$

in which case $M = 2r$ or $2r + 1$ depending on whether point (a,q) lies on curve a_{2n} or a_{2n+1}; C(q) is a function of q.

$$y_1 = \sum_{r=0}^{\infty} B_M \sin M\alpha \qquad (5)$$

$$y_2 = S(q)\,\alpha\, y_1 + g(\alpha)$$

in which case $M = 2r + 1$ or $2r + 2$ depending on whether point (a,q) lies on curve b_{2n+1} or b_{2n+2}; S(q) is a function of q.

In expressions (4) and (5) the quantities A_M and B_M are real constants depending on a and q, and $f(\alpha)$ and $g(\alpha)$ are periodic functions of α, having the same period as y_1. The period of y_1 is π if the representative point (a,q) lies on curves a_{2n} or b_{2n+2} and 2π if it lies on curves a_{2n+1} or b_{2n+1}. Neither of these solutions of y_1 are either stable or unstable, and as such are classified as neutral. However, both solutions for y_2 are unstable and nonperiodic.

For small values of q, the points for which the Mathieu equation has unstable solutions lie in the neighborhood of the abscissa values of a, given by

$$a = (m)^2 \qquad (6)$$

where m is an integer number.

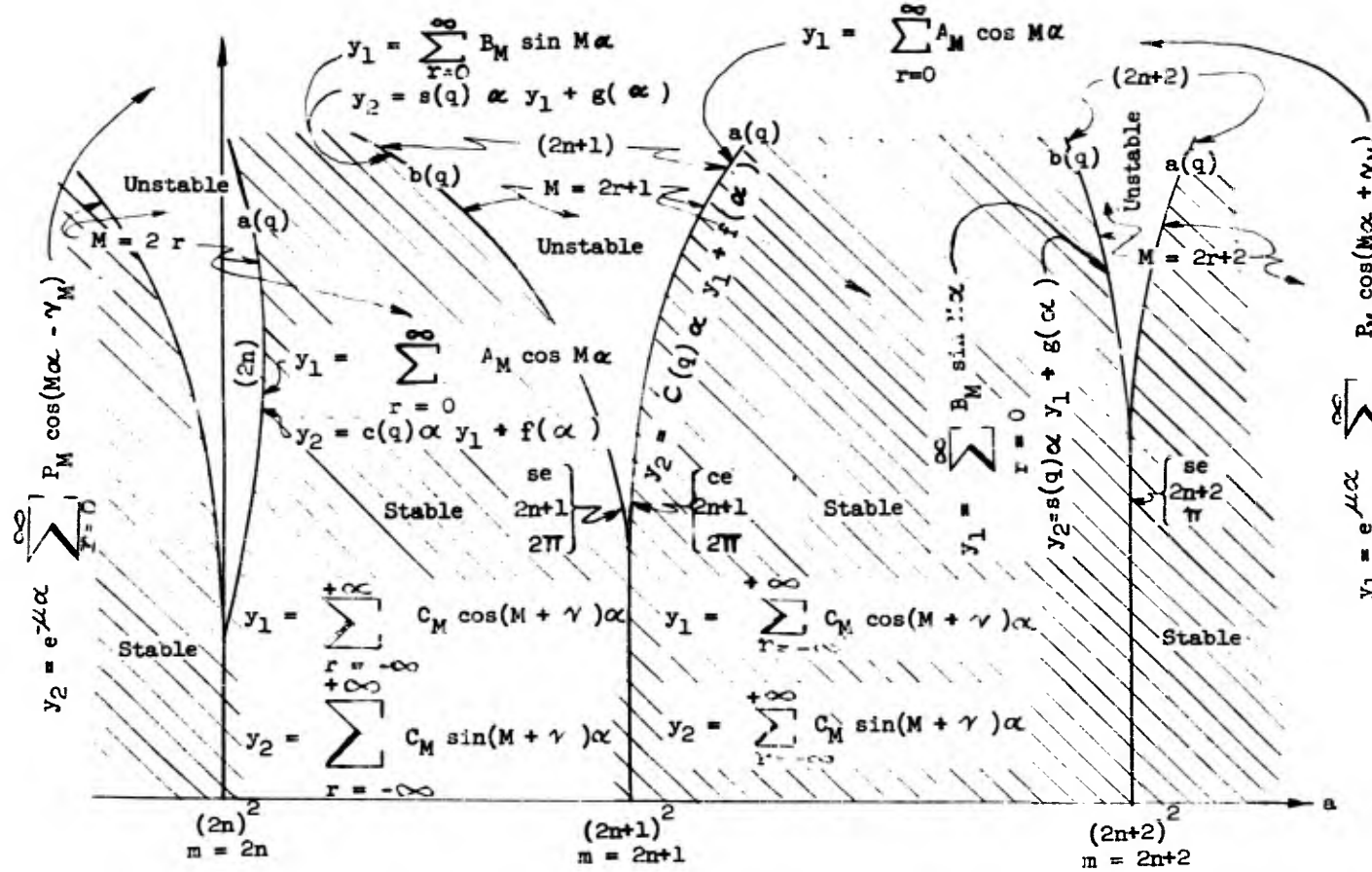

Figure 3. Ince-Strutt Stability Diagram
Expanded Diagram

$$\left(\frac{2\omega_o}{\omega_1}\right)^2 = a = (m)^2$$

or $$\omega_1 = \frac{2\omega_o}{m} \qquad (7)$$

Therefore, these values do not lie at multiples of the natural frequency, but at submultiples of the natural frequency, and lead to the phenomenon of subharmonic resonance.

An inspection of the Ince-Strutt stability chart reveals that

1. The stability curves are symmetrical about the abscissa, i.e., the a-axis.

2. The crossover points of the stability curves lie in the neighborhood of the abscissa at intervals given by $a = m^2$, $m = 0, 1, 2, 3, \ldots\ldots$, for small values of q.

3. The area of instability decreases with increasing a, for small values of q.

It may further be mentioned here that the curves a_n are even functions of q whereas the curves b_n are odd functions of q. Hence

$$2a_n(q) = 2a_n(-q)$$

$$a_{2n+1}(q) = b_{2n+1}(-q)$$

$$b_{2n}(q) = b_{2n}(-q)$$

On an enlarged scale the area in the neighborhood of an instability region will appear as shown in Figure 3-F-4, where the three types of solutions of the Mathieu differential equation have been included. The behavior of the solutions in terms of the parameters a and q is clearly indicated.

The periodic solutions of the Mathieu Equation at the borderline between stability and instability regions are the Mathieu functions and have been designated by a special nomenclature related to the boundary curves a(q) and b(q).

Thus, associated with the boundary curve $a_{2n}(q)$ there corresponds a Mathieu function

$$Ce_{2n} = \sum_{r=o}^{\infty} A_{2n},\ 2r \cos 2r\ t$$

for curve $a_{2n+1}(q)$ there corresponds a Mathieu function

$$Ce_{2n+1} = \sum_{r=o}^{\infty} A_{2n+1},\ 2r+1 \cos (2r+1)\ t$$

for curve $b_{2n}(q)$ there corresponds a Mathieu function

$$Se_{2n} = \sum_{r=o}^{\infty} B_{2n}\ 2r \sin (2r+1)$$

for curve $b_{2n+1}(q)$ there corresponds a Mathieu function

$$Se_{2n+1} = \sum_{r=o}^{\infty} B_{2n+1},\ 2r+1 \sin (2r+1)\ t$$

The functions Ce_{2n} and Se_{2n} are of period π, whereas Ce_{2n+1} and Se_{2n+1} are of period 2π

Since the presence of a damping term in the Mathieu Equation strongly influences and greatly reduces the extent of instability regions of higher order, it is usually sufficient to investigate only the region bounded by the curves $a_o(q)$, $b_1(q)$, and $a_1(q)$ of the Ince-Strutt diagram. These expressions have been computed by McLachlan* and given as

$$a_1(q) = 1 + q - \frac{1}{8}q^2 - \frac{1}{64}q^3 - \frac{1}{1536}q^4 + \frac{11}{36864}q^5 + \Sigma(q^6)$$

$$b_1(q) = 1 - q - \frac{1}{8}q^2 + \frac{1}{64}q^3 - \frac{1}{1536}q^4 - \frac{11}{36864}q^5 + \Sigma(q^6)$$

The curve for $a_o(q)$ is unimportant for practical considerations. Furthermore, if q is a small quantity

$$a_1(q) \cong a - q = 1$$

$$b_1(q) \cong a + q = 1 \qquad (8)$$

*McLachlan, N.W., Theory and Application of Mathieu Functions, Oxford University Press, London, 1946

$$b_2(q) \cong a + 1/12\, q^2 = 4$$
$$a_o(q) \cong a + 1/2\, q^2 = 0 \qquad (8\text{-a})$$

On an enlarged scale, the above region has been shown in Figure 3-F-5. Returning to the original Mathieu Equation (1) it is obvious that if q = 0 the equation reduces to a standard second order differential equation

$$\ddot{y} + ay = 0$$

in which case the Ince-Strutt diagram reduces to the a-axis, i.e., the entire region along the abscissa is stable.

By the foregoing discussion, if q is increased from 0 to a finite value by keeping a constant, the system may go from a stable condition to an unstable condition, stability being defined by

$$a \pm q \leq 1.$$

Thus the inclusion of a q term in the equation of motion of the system may result in an unstable behavior before a stable condition is reached, or conversely in a stable behavior before an unstable condition is reached, depending on the initial location of the operating point. A similar condition arises in keeping q constant and varying a, as shown in Figure 3-F-6.

Of practical importance is the solution of the Mathieu equation in the stable region bounded by the stability curve b_1 and the positive a,q quadrant. The complete solution of Mathieu's equation in this region is given by

$$y = A\, Ce_\gamma(\alpha, q) + B\, Se_\gamma(\alpha, q) \qquad (9)$$

However, in practical problems dealing with shock isolation sy tems, the initial conditions are such as to disallow a solution of the type $B\, Se_\gamma(\alpha, q)$ which is a sine series. Hence, the complete solution in such cases reduces to

$$y = A\, Ce_\gamma(\alpha, q) \qquad (10)$$

where

$$Ce_\gamma(\alpha, q) = \cos\gamma\alpha - \frac{1}{4} q \left[\frac{\cos(\gamma + 2)}{\gamma + 1} - \frac{\cos(\gamma - 2)}{\gamma - 1}\right]$$
$$+ \frac{1}{32} q^2 \left[\frac{\cos(\gamma + 4)\alpha}{(\gamma + 1)(\gamma + 2)} + \frac{\cos(\gamma - 4)\alpha}{(\gamma - 1)(\gamma - 2)}\right] - \cdots\cdots \qquad (11)$$

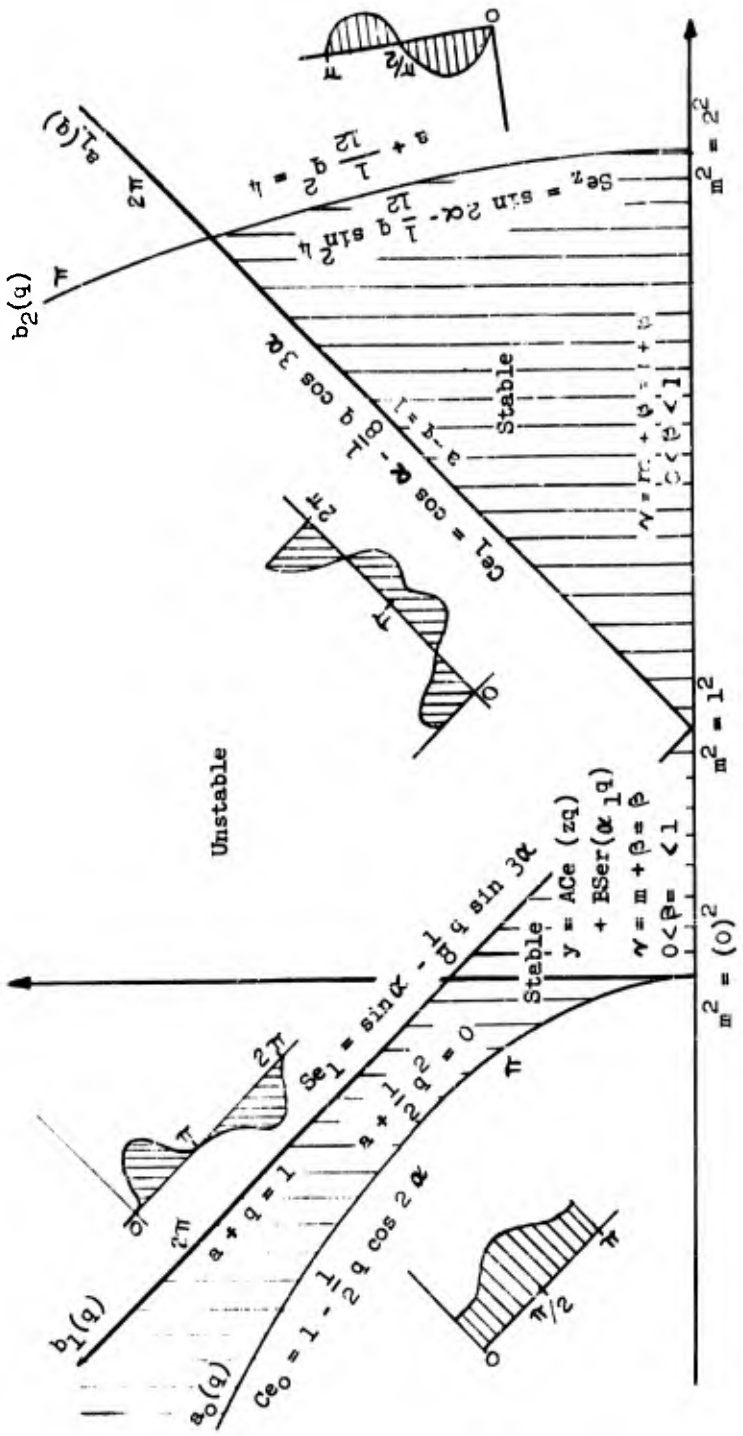

Figure 3-F-5 Ince-Strutt Stability Chart
Expended Diagram at the Origin

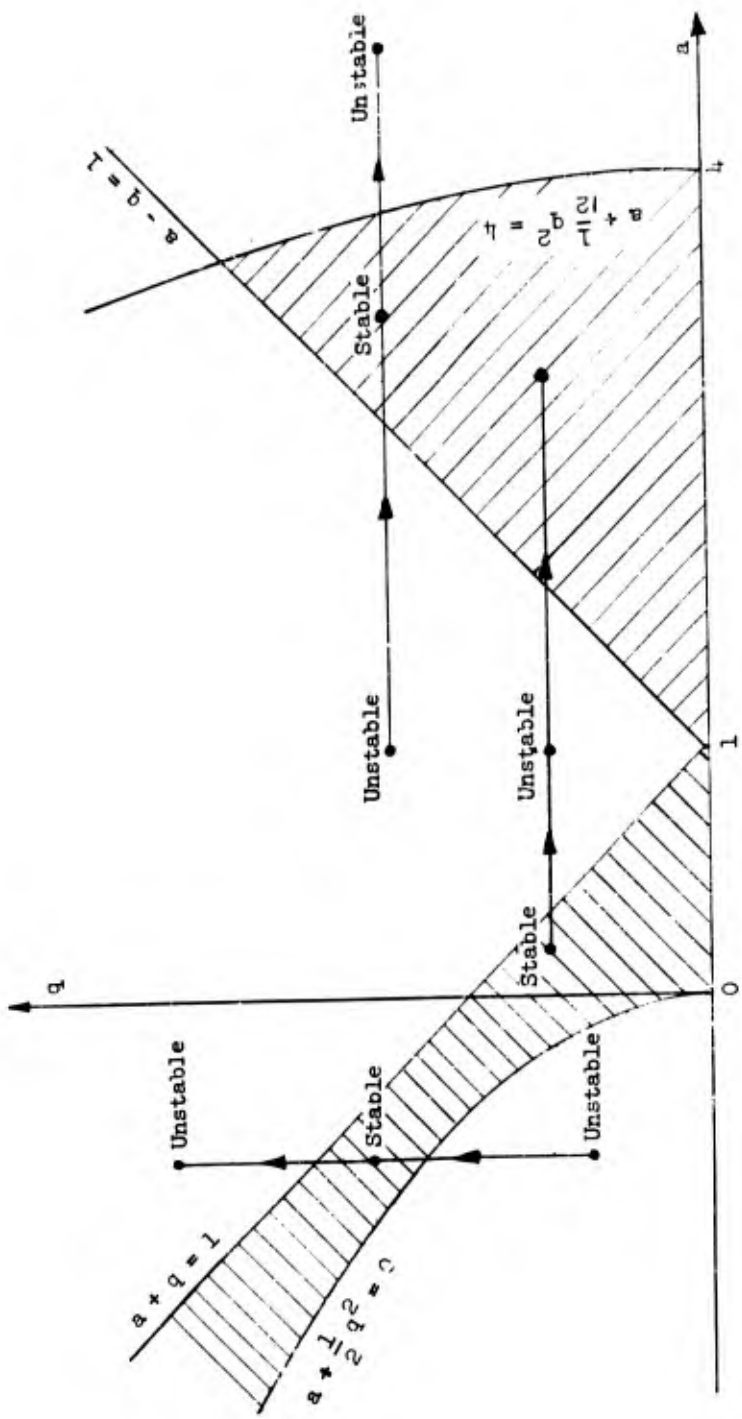

Figure 3-F-6 Transient Stability and/or Instability of a Rheolinear System

A is a constant depending on the initial conditions, and

$$a = \gamma^2 + \frac{1}{2(\gamma^2 - 1)} q^2 + \frac{5\gamma^2 + 1}{(\gamma^2 - 1)^3 (\gamma^2 - 4)} q^4 + \cdots \quad (12)$$

Equation (11) is valid only when

$$\frac{q^2}{2(\gamma^2 - 1)} << \gamma^2, \qquad \gamma > 0 \quad (13)$$

and $\gamma = m + \beta$ as shown in Figure 3-F-7

m = a positive integer, which may also be zero

β = a rational fraction.

Thus for a point (a,q) in the stable region where $a < 1$, $q < 1$, it is seen that $m = 0$.

$$\therefore \gamma = \beta$$

γ can then be determined from equation (12) if the condition stipulated in equation (13) is valid. It may be mentioned that γ, as given by equation (12) is single valued, and the value that is obtained gives the solution of the representative Mathieu's equation by equation (11).

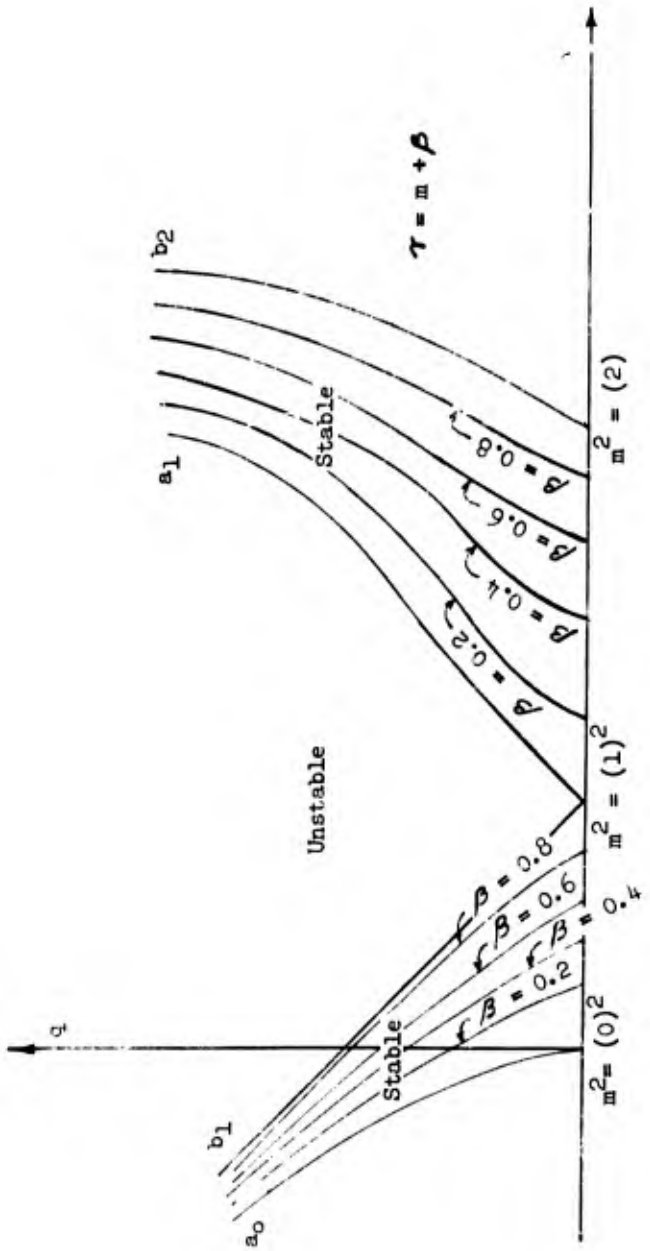

Figure 3-F-7 Stability Chart for Fractional

SECTION 4. SHOCK TOLERANCES

4.1 Introduction

The fundamental objective of shock isolation is to convert the motion of an intolerable shock to a form which the isolated equipment or personnel can survive. In Section 2.0 of the Design Guide, the nature of the ground shock and its distortion by interactions with the underground structure were reviewed and the environment to which unisolated equipment might be exposed was partially defined. In Section 3.0, the motion conversion characteristics of isolation systems were studied, leading to methods for calculating the shock environment of isolated equipment. It would appear to be a simple matter then to assess the tolerable motion of a particular item of equipment, to compare it with the unattenuated motion of the underground structure, and if isolation was needed, to rigorously establish the required motion conversion characteristics of the isolation system.

The use of a purely analytical approach as a practical design procedure however is rendered virtually impossible by the mechanical complexity of most equipment, by a lack of understanding of damage phenomena, and by the limited information available on the nature of the input shock. While these problems are of genuine concern to the isolation system designer, they are not unique to systems for protection from nuclear blast. In few problems involving shock isolation is an exact definition of the input or the precise requirements of the output known. Thus, many of the techniques developed in other fields of shock isolation can be applied to this problem.

By far the most common method of assigning a quantitative value to the limiting level of shock an item of equipment will tolerate, is by exposing it to an environment simulating the field conditions. The need for the simulation in the design of almost all military equipment is based largely upon two factors which are almost unique (Reference 4.1). First, it is difficult to test military equipment under the most severe conditions it must survive in service. For underground facilities, designed to resist high yield nuclear weapons, full-scale testing is out of the question. Second, equipment is designed or selected concurrently with design of the facility in which it will be installed. Thus the decision as to whether or not the equipment is to be shock mounted, and the design of any isolators required, must be completed before tests of even the larger subassemblies are possible.

In principle (Reference 4.2), the simulation of a shock environment, or shock testing, is concerned with the reproduction in the laboratory of equipment damage analogous to that occurring in the field. The effect of a shock motion on equipment depends not only upon the characteristics of the motion, but also on the properties of the equipment. The shock motion occurring as a result of a nuclear blast is affected by many variables, and the characteristics of the motion vary

significantly from one occurrence to another. Thus, a laboratory test is required to simulate not a single defined motion, but rather any one arbitrarily selected from a group of shock motions. The test must be applicable over a wide range of equipment properties as well as a wide range of shock characteristics. The nature and severity of the test must be such that any possible failure that would occur in the field should have first occurred in the laboratory shock test.

Two factors complicate the simulation of shock environments in the laboratory. First, only the gross features of the wave form can be deduced, since a detailed time history of the shock rarely exists. Second, a test machine designed to reproduce faithfully the waveform of a complex, high-intensity shock would be very expensive to construct. Thus, to define the environment to be reproduced in the laboratory, parameters directly relating damage to shock characteristics must be identified. However, there has not been formulated a rigorous universal criterion of damage nor do the standards now employed satisfy all of the requirements imposed even by simple theory. Nonetheless, the designer of isolation systems for underground protective structures has no recourse but to utilize laboratory results to guide him in establishing isolation system output requirements.

It is suggested in Section 4.0 that the response spectrum be accepted as a criterion of damage for equipment with one stipulation. Thus, the damage potential of the input shock can also be represented quantitatively by its response spectrum. This concept is not a new one, having been described frequently in the literature (References 4.2 and 4.3), and employed occasionally in establishing shock testing requirements for equipment intended for use in underground protective structures. Its lack of general usage may be due in part to the fact that cases can be postulated where it will not indicate damage potential, and that in these cases its prediction will be nonconservative. Despite its shortcomings, the selection of the response spectrum as a criterion of damage appears to offer optimum simplicity, meaningfulness, and accuracy within the limits of the present state of knowledge of the phenomena and capabilities of testing facilities.

Once the response spectrum is accepted as a criterion of damage, a ready means is provided for establishing the need for shock isolation, for determining the required output characteristics of the isolation system, and for selecting a test machine for verifying the tolerance of the equipment. Each of these aspects of the design problem is discussed in detail in this section.

4.2 Damage Criteria

Despite the large number of equipment shock tests which have been conducted in laboratories in the United States, there are very few experimental data available of the type which gives an insight into the damaging characteristics of shock (Reference 4.1). The large majority of laboratory tests are conducted to determine whether the equipment is constructed in conformance with the applicable specification, that is, it is a "go no-go" type of test. Either the equipment survives the specified tests or it fails to do so. Very few tests are conducted with a systematic variation of parameters where the test is continued to failure and the duration of the test is correlated with the severity of the testing conditions. As a consequence, little is known about the laws governing the failure of equipment subjected to shock. Until a better understanding is gained of the basic phenomena, the results of laboratory tests in their present form will remain somewhat less than convincing.

With the lack of a complete picture of the damage mechanisms, it is necessary to formulate some hypothesis of failure in order to provide a rational basis for establishing test procedures. For example, one possible assumption is that the probability of equipment sustaining damage as a result of shock is directly related to the maximum stress experienced by the equipment during shock. Of course, this criterion disregards any cumulative damage resulting from several shocks. Even so, the correlation between peak stress and shock parameters is not a simple one, and with the acceptance of stress as the critical damage mechanism, the shock test procedure is still not completely defined.

It is an established principle of mechanics that two single-degree-of-freedom systems having the same natural frequency and damping capacity will respond in an identical manner to a given steady-state, or transient, excitation (Reference 4.1). If the excitation is of a nonoscillatory nature, the damping tends to be of secondary importance so that systems with the same natural frequency but different damping characteristics tend to exhibit approximately the same response. A given item of equipment thus might be represented as an array of simple systems, the natural frequency of each system being equal to the natural frequency of the element which it portrays. If the peak stress, and therefore the peak acceleration, which each simple element can survive, is plotted as a function of the natural frequency of that element, the resulting curve is simply the response spectrum of the greatest shock that can be tolerated by the equipment. Any shock whose spectrum at any frequency exceeds the survival spectrum of the equipment will cause failure in one or more of the simple elements. For equipment which can be represented in this manner, then, the response spectrum constitutes a criterion of damage.

The limitations of this approach stem from the fact that few pieces of equipment can be represented as an array of simple elements in parallel. Most structures contain a large number of elements in series or elements which contain more than one mode of vibration. In these cases, as was seen in discussing the responses of coupled linear systems in Section 3.0, the response spectrum does not contain sufficient information to define the peak acceleration in any coupled mode. Further, some equipment contains elements whose elastic properties are nonlinear, thus two shocks with identical response spectra may produce different stresses in some types of equipment. Therefore, characteristics of the shock, other than those described by the response spectrum, must also be reproduced in the test if true damage potential is to be simulated.

The most significant information omitted from a response spectrum is the phasing of the responses. Since the relative time of occurrence of each spectral component of the shock fixes the phase relationship of vibrations in the various modes of the responding element, some simulation of the phasing must be reproduced in the shock test. Of course, this implies that the shape of the wave form produced in the test must be similar to that expected in service. As noted earlier, however, the exact wave form cannot be reproduced, due to a lack of knowledge of the wave form, and to the large expense of constructing special test machines. If a general type of wave form is reproduced in the test machine which not only has the gross characteristics of the expected shock, but also produces the same response spectrum, the arguments against the use of the spectrum alone as a criterion of damage can be reduced in relative importance, if not in number.

In summary, to base equipment ruggedness levels solely on spectral representation of the shock input is to assume that the equipment responds as a system of uncoupled, undamped linear oscillators. It is also to assume that the mechanism of damage may be expressed in terms of the maximum oscillator response. When the response spectrum is coupled with a wave form of the general shape of that expected in service, the above assumption is not invalidated, but only becomes less important as the test wave form approaches that of the service shock.

4.3 Shock Testing Machines

Since it is necessary to simulate in the laboratory the conditions to which equipment may be exposed in the field, it is essential that the shock isolation system designer be familiar with laboratory equipment and techniques. First, if he accepts the response spectrum as a criterion of damage, he must have available to him spectral representations of the outputs of various testing machines under different loading and operating conditions. Second, as the response spectrum alone is not sufficient to define the damage potential of the shock, the general type of wave form which the test machine produces must also be known. And, third, the interaction between most simulation machines and the items being tested makes it necessary that the designer have a clear picture of the construction of each machine he intends to use.

The following discussion of shock testing machines is intended to acquaint the isolation system designer with some of the available equipment. The discussion will emphasize those machine characteristics of primary importance in assuring that the service environment is simulated properly. The three significant features of the output of shock testing machines which will be presented are wave form type, spectral distribution, and acceleration impulse.

4.3.1 Wave Form Type

Several wave forms generated by different shock testing machines are shown in Figure 4.3.1, page 4 - 8. Each of the wave forms may be classified as being one of three general types: velocity shock (a), simple pulse (b through e), and single complex (f). An extensive list of machines which produce each type of wave form is given in Reference 4.3; a few examples are listed below:

Velocity Shock

- Drop Tester for Shipping Containers (Reference 4.4)
- Drop Tester for Airdrop Delivery (Reference 4.5)
- Inclined Plane Test (Reference 4.6)

Simple Shock Pulse

- Shock Testing Mechanism for Indicating Instruments (Reference 4.6)
- Medium Impact Shock Machine (Sand Drop Table) (References 4.7, 4.8)
- Hyge Shock Tester (Reference 4.9)
- Barry Drop Table (Reference 4.10)

Single Complex

Navy High Impact Shock Machine for Lightweight Devices (References 4.11, 4.12)

Navy High Impact Shock Machine for Medium Weight Equipment (References 4.12, 4.13)

Shock Machine for Electronic Devices (Reference 4.14)

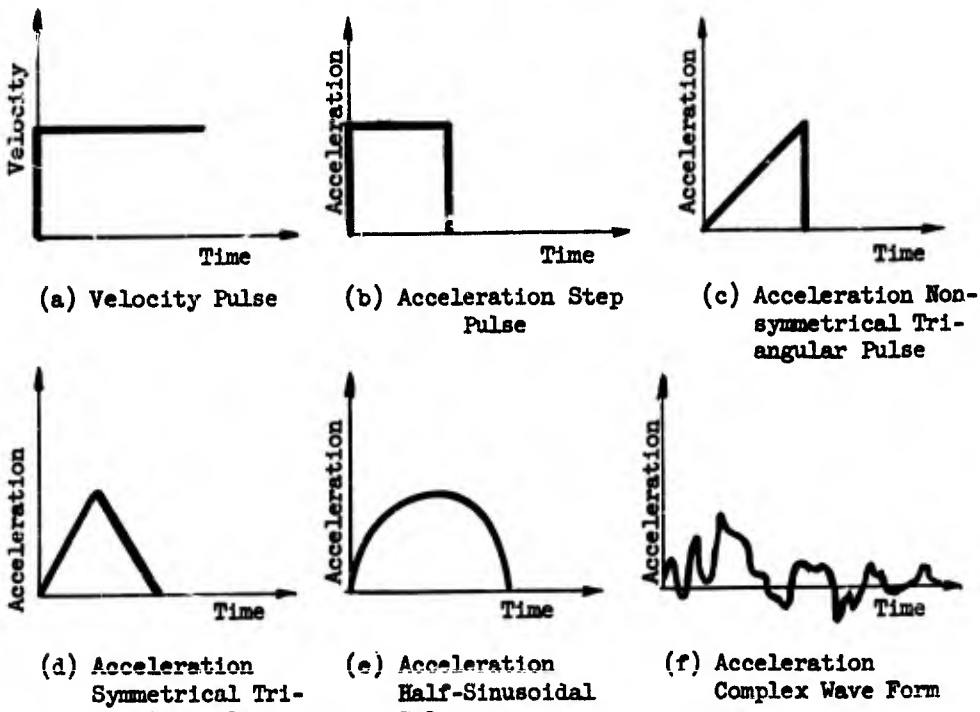

(a) Velocity Pulse

(b) Acceleration Step Pulse

(c) Acceleration Non-symmetrical Triangular Pulse

(d) Acceleration Symmetrical Triangular Pulse

(e) Acceleration Half-Sinusoidal Pulse

(f) Acceleration Complex Wave Form

Figure 4.3.1
Characteristic Types of Shocks

Note that except for the acceleration complex wave form (f), all of the wave forms shown yield velocities only in one direction, that is, they indicate the time-history of a positive velocity change but do not show details of how the velocity returns to its initial value. This result is inevitable with machines in which the test item is set into motion and the shock produced by bringing it to an abrupt stop. Although the complex acceleration wave form shows negative accelerations, its time integral, or residual velocity, is still positive. Machines which produce this type of shock can therefore be classed with those above.

4.3.1.1 Wave Form Distribution Introduced by Test Item

The wave form generated by a shock machine is influenced by frequencies characteristic of the item being tested. The effect of the equipment may be appreciable, particularly if the weight of the item is near the upper limit of the machine capacity. The test item may act as a dynamic vibration absorber (Reference 4.3), and if it is relatively heavy may reduce the response spectrum to a minimum at the antiresonance frequencies. If the test shock is increased to raise the low points of the spectrum, the part may be easily overstressed. Considerable judgement is thus required in interpreting the test results.

4.3.1.2 Wave Form Distortions Introduced by Testing Machine

The wave form of a shock produced by a testing machine may be modified significantly at frequencies characteristic of the machine itself. This effect is reduced as the rigidity of the machine itself increases but, in nearly all testing equipment, some frequency ranges will be amplified. It is essential that the critical frequencies for each machine are known and that care is taken to avoid using machines whose frequencies are near the natural frequency of the test item. In this respect, it is important that the method of attaching the equipment to the test machine is given special attention to ensure that resonances, with either the machine or the equipment, are avoided in the mounting structure.

4.3.2 Response Spectra

In view of these extraneous vibrations imposed on the basic motion of the test machine, it is evident that the wave form actually produced in a test will differ from the relatively simple shapes shown in Figure 4.3.1, page 4 - 8 . In most cases the differences will be even more evident if the response spectra of the two wave forms are compared. Resonances in the machine elements can usually be detected by peaks in the response spectrum of the shock; the spectrum will show dips at the natural frequencies of the test item.

Calibrations of testing machines are generally performed with rigidly attached, deadweight loads. Thus, the vibrations of the machine elements will be evident in the calibration spectra. Modification to the spectra due to the reaction of the test item may be evaluated by comparing the calibration spectrum with that of an actual test of the item.

4.3.3 Acceleration Pulse

The total duration of shock produced by most standard testing machines is much shorter than those generated in the ground by a nuclear explosion. For example, the total duration of the motion of a soil particle at the ground surface due to a 1000 psi overpressure from

a 10-megaton weapon is about 2.5 seconds (Figure 2.2.4, page 2-8). The duration of shocks produced by test machines, on the other hand, rarely exceeds a few hundred milliseconds.

It is evident from the wave forms of Figure 4.3.1 that test machines of this type produce only a change of velocity and do not reproduce the section of the wave form where the velocity is returned to its initial value. The initial high-acceleration portion of the ground shock, however, can be reproduced in real time by the machine with good accuracy. As far as is known, there is no standard testing machine which will generate a complete wave form such as a Type I or Type II, but only that portion which includes the velocity rise.

In this Section, several of the standard shock testing machines used most frequently in validating equipment for underground protective structures are described in some detail. Many other machines are available however, and each isolation system designer should prepare and maintain a comprehensive list of such machines and their significant characteristics.

4.3.4 Navy High Impact Machines

A number of shock-testing machines are in current use, their characteristics varying widely in accordance with the requirements of particular applications. These testing machines have been devised in a variety of ways. Some machines have been developed entirely on an empirical basis, others by a rather superficial interpretation of field data, and others by a fairly elaborate interpretation of field data.

Modern concepts of shock testing began with World War II. The earliest of modern shock-testing machines was the direct outcome of excessive damage in British ships as a result of shock created by German mines. This was a critical problem and a solution was urgently demanded. As a consequence of this experience with German mines, the British had a relatively large quantity of damaged equipment available for study. This was the only available measurement of shock severity. Because of wartime conditions and the urgency of the problem, there was no time available to make measurements of the nature and severity of the shock. As a solution to the problem, the British developed in a purely empirical manner a shock-testing machine that was capable of causing damage substantially similar to that resulting from German mines. This machine, designated the High Impact Shock Testing Machine, was subsequently adopted by the Bureau of Ships of the United States Navy and is still in extensive use, with only minor changes, to test equipment intended for ultimate application aboard ships. More recently, the machines have been used to simulate other environments which can be described by a single shock of complex shape.

4.3.4.1 High Impact Shock Testing Machine for Lightweight Equipment

The High Impact Shock Testing Machine for Lightweight Equipment (LWHI) (Reference 4.4), illustrated in Figure 4.3.2, has an anvil A which is struck on the back side by the pendulum hammer C; alternately, the anvil is rotated 90 degrees about the vertical axis and struck on the end by the pendulum hammer. The drop-hammer B can be made to strike the top of the anvil, thus providing principal shock motions in the third orthogonal direction. The weight of equipment tested on this machine is limited to 250 pounds, although weights up to 400 pounds may be authorized in some instances.

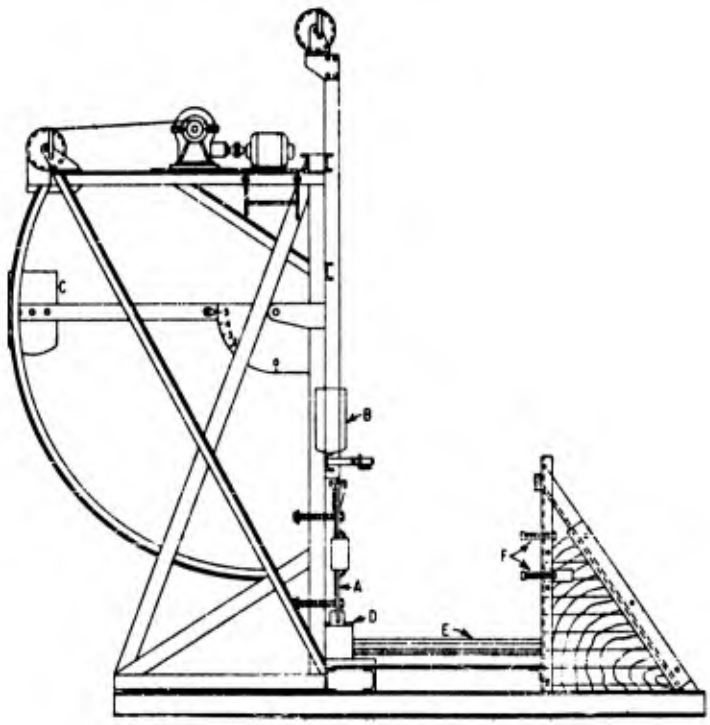

Figure 4.3.2

High Impact Shock Testing Machine for Lightweight Equipment, Intended Primarily for Testing Naval Ship-Borne Equipment. (Reproduced from Reference 4.4)

In the conventional method of conducting a test (Reference 4.16), the equipment is attached to the anvil plate by means of a mounting adapter specified for the particular equipment. The impact of the hammer on the anvil plate excites transient vibrations in the anvil plate and mounting adapter which are then superimposed on the over-all motion. As the natural frequency of the adapter plate-equipment

assembly is a function of the weight of the equipment, the transient vibrations introduced into the equipment will vary with the equipment weight. The variation in natural frequency of one of the mounting adapters is shown in Figure 4.3.3 as a function of supported load. Note that the natural frequency of the mounting adapter decreases as the equipment weight increases since its stiffness remains substantially constant. The data shown in the Figure are for hammer impacts to the anvil plate in the back direction. Similar results should be expected from hammer impacts in other directions.

The four mounting adapters used with the LWHI machine are:

Mounting Adapter Type	Type of Equipment
4A	Bulkhead mounted equipment
4C	Deck or platform mounted equipment
6D	Electrical indicating switchboard instruments and other panel mounted equipment
6E	Electrical controller components (contactors, resistors, relays, et cetera)

A typical time-displacement record for the LWHI machine is shown in Figure 4.3.4.

Shock spectra for the 5-foot hammer drops with 4A and 4C mountings have been measured by Dick (Reference 4.15) for various equipment weights and are presented in Figures 4.3.5 through 4.3.12. Although the spectra for hammer drops of less than five feet were not given, an indication of the magnitude of their effect is given in Figure 4.3.13. The spectrum for the 3-foot drop overlays the spectra for greater drops at the higher frequencies. The author reports that this series is typical.

The experimentally determined average velocities of the anvil plate under various conditions of operation have been taken from wave form records such as that of Figure 4.3.4 and are shown in Figures 4.3.14 through 4.3.16, page 4-19, for hammer impacts applied at the back, side, and top directions, respectively (Reference 4.16). Each Figure shows the average velocity expressed in inches per second as a function of height of hammer drop. The average velocity decreases as the weight of the equipment under test increases, and increases as the height of hammer drop increases.

The maximum acceleration measured at the center of the Type 4A mounting adapter under various conditions of operation is shown in Figures 4.3.17 through 4.3.19. These data have also been reproduced from Reference 4.16. The impacts were from the back, side, and top directions, respectively. Each Figure indicates the maximum acceleration expressed as a multiple of the acceleration due to gravity, as a function

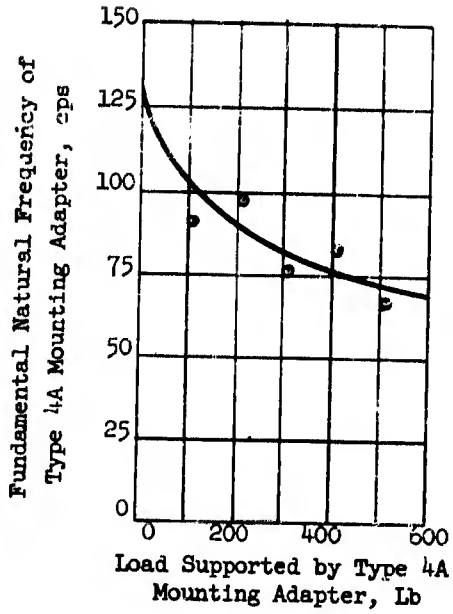

Figure 4.3.3

Fundamental Natural Frequency of Type 4A Mounting Adapter in Front-to-Back Direction; High Impact Shock Testing Machine for Lightweight Equipment

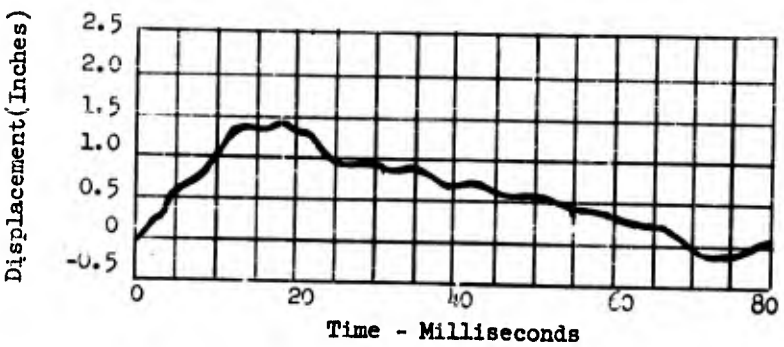

Figure 4.3.4

Typical Time-Displacement Record for Type 4A Mounting Adapter: High Impact Shock Testing Machine for Lightweight Equipment, Hammer Impact from Back (Height of Hammer Drop = 5 Ft., No Load on Mounting Adapter)

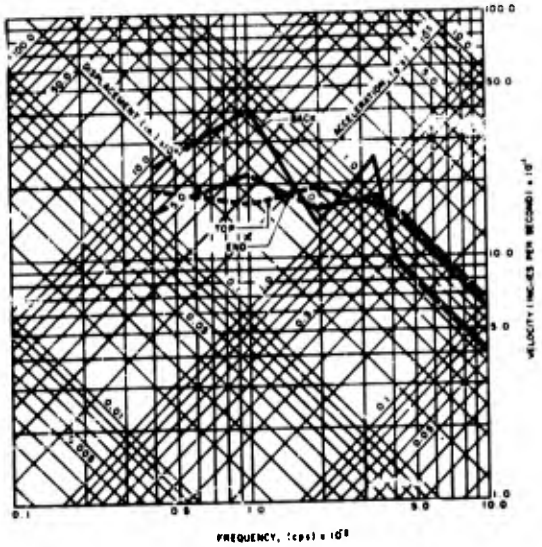

Mounting: 4A Plate
Specimen Weight: 57 lbs
Drop Height: 5 ft

Figure 4.3.5
Shock Spectra for Navy Lightweight High Impact Machine

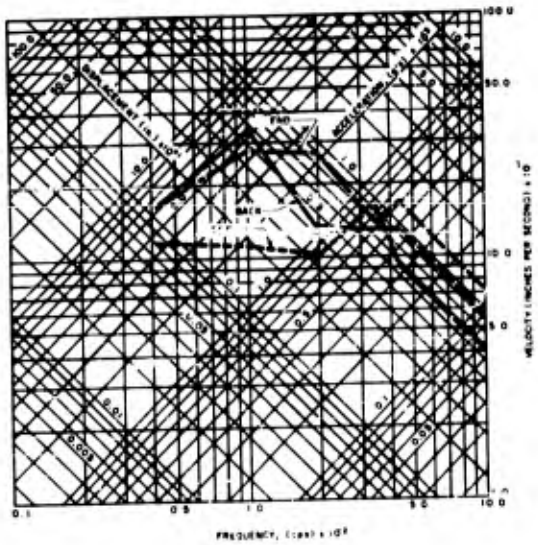

Mounting: 4A Plate
Speciment Weight: 121 lbs
Drop Height: 5 ft

Figure 4.3.6
Shock Spectra for Navy Lightweight High Impact Machine

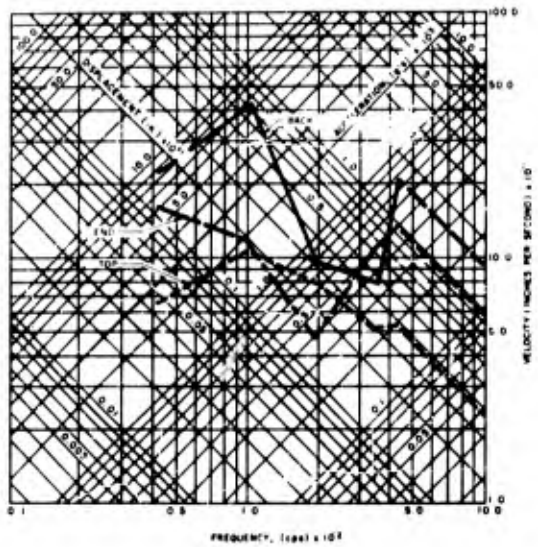

Mounting: 4A Plate
Specimen Weight: 261 lbs
Drop Height: 5 ft

Figure 4.3.7
Shock Spectra for Navy Lightweight High Impact Machine

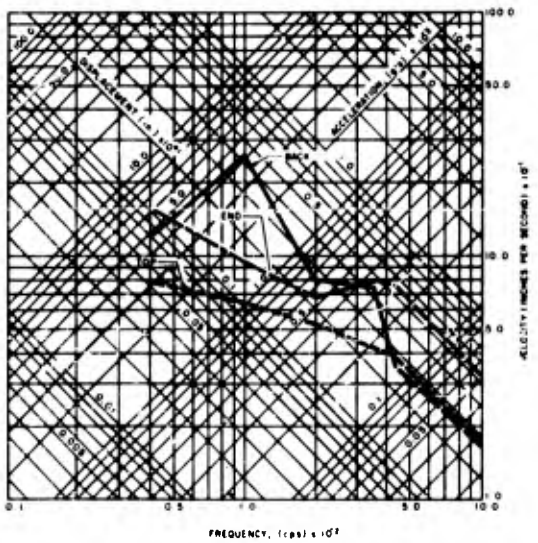

Mounting: 4A Plate
Specimen Weight: 389 lbs
Drop Height: 5 ft

Figure 4.3.8
Shock Spectra for Na y Lightweight High Impact Machine

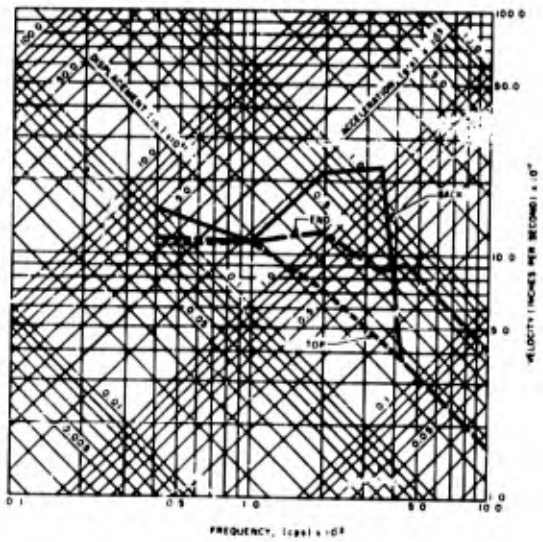

Mounting: 4A Plate
Specimen Weight: 57 lt
Drop Height: 5 ft

Figure 4.3.9
Shock Spectra for Navy Lightweight High Impact Machine

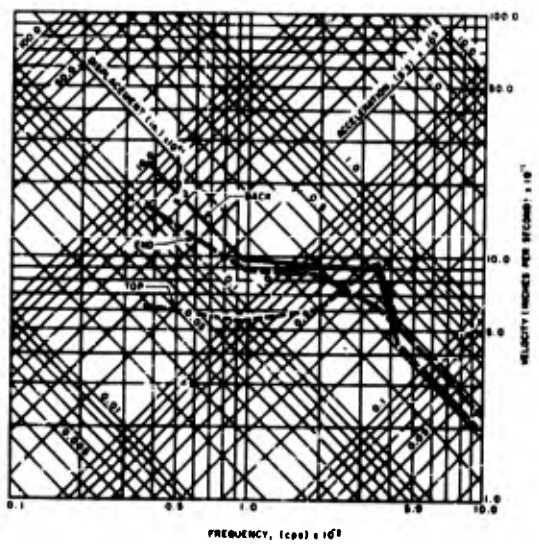

Mounting: 4C Plate
Specimen Weight: 121 lbs
Drop Height: 5 ft

Figure 4.3.10
Shock Spectra for Navy Lightweight High Impact Machine

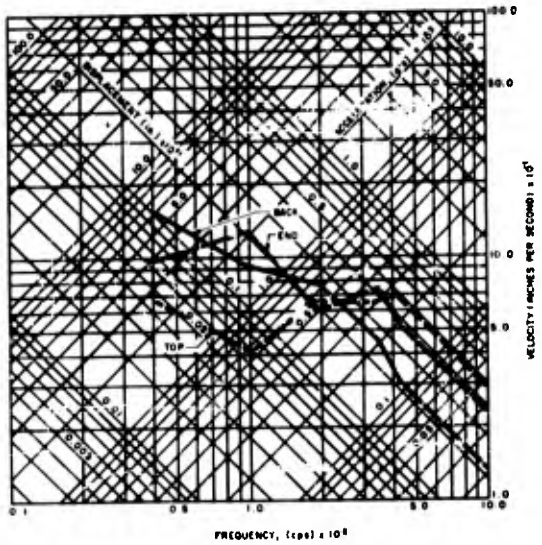

Mounting: 4C Plate
Specimen Weight: 261 lbs
Drop Height: 5 ft

Figure 4.3.11
Shock Spectra for Navy Lightweight High Impact Machine

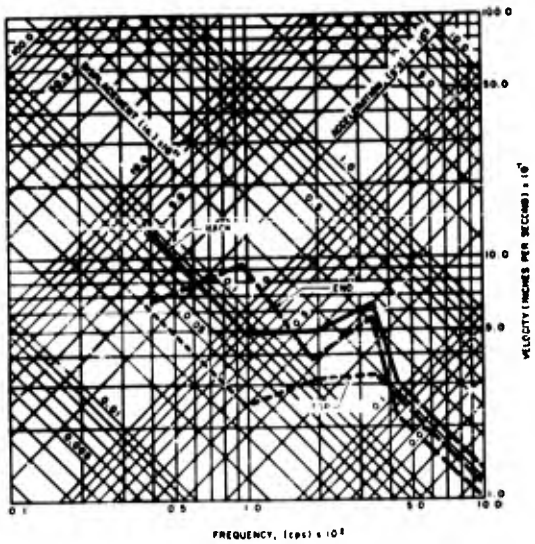

Mounting: 4C Plate
Specimen Weight: 389 lbs.
Drop Height: 5 ft

Figure 4.3.12
Shock Spectra for Navy Lightweight High Impact Machine

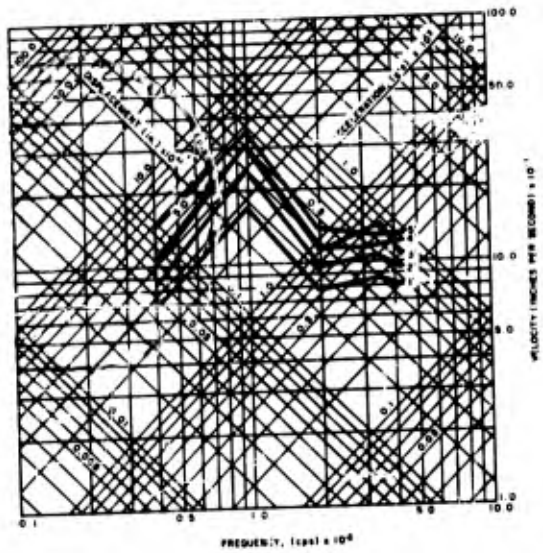

Position: Back

Specimen Weight: 121 lbs

Drop Height: 1 - 5 ft

Figure 4.3.13

Shock Spectra for Navy Lightweight High Impact Machine

of the height of hammer drop. The maximum acceleration decreases as the weight of the equipment increases and increases as the height of hammer drop increases.

The maximum acceleration experienced by the Type 4A mounting adapter decreases at a greater rate than the average velocity when the weight of equipment under test is increased. The average velocity reflects the motion of the anvil plate while the maximum acceleration is measured on the Type 4A mounting adapter. As the weight of the equipment increases, the natural frequency of the mounting adapter decreases, as shown in Figure 4.3.3 , and the acceleration experienced by the equipment tends to decrease. The decrease in acceleration shown in Figures 4.3.17 through 4.3.19 therefore reflects both the decrease in average velocity and the decrease in natural frequency of the mounting adapter.

4.3.4.2 High Impact Shock Testing Machine for Medium Weight Equipment

The High Impact Shock Testing Machine for Medium Weight Equipment (Figure 4.3.20, page 4 - 21), similar to that previously described, is used to test equipment, together with its supporting structures, weighing up to 5600 pounds. This machine consists principally of a 3000-lb hammer and a 4000-lb anvil. Loads are not

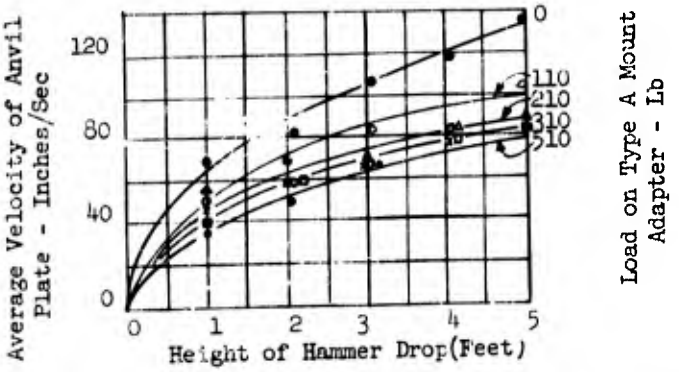

Figure 4.3.14: Average Velocity of Anvil Plate: High Impact Shock Testing Machine for Lightweight Equipment; Hammer Impact at Back

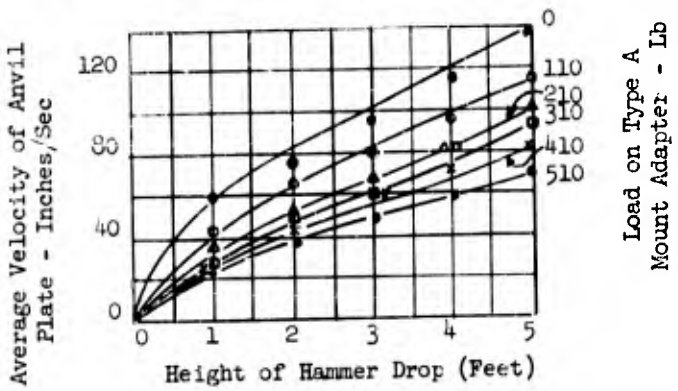

Figure 4.3.15: Average Velocity of Anvil Plate: High Impact Shock Testing Machine for Lightweight Equipment; Hammer Impact from Side

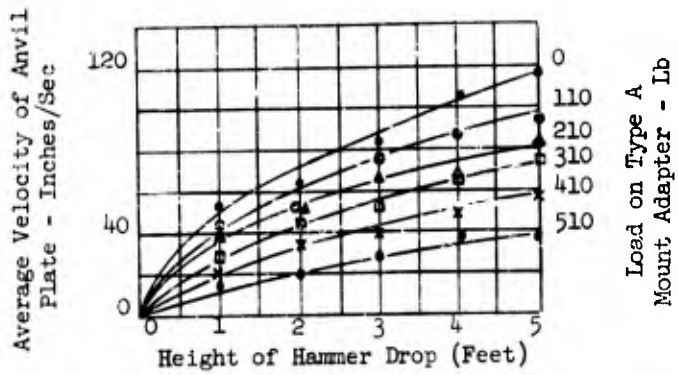

Figure 4.3.16: Average Velocity of Anvil Plate: High Impact Shock Testing Machine for Lightweight Equipment; Hammer Impact from Top

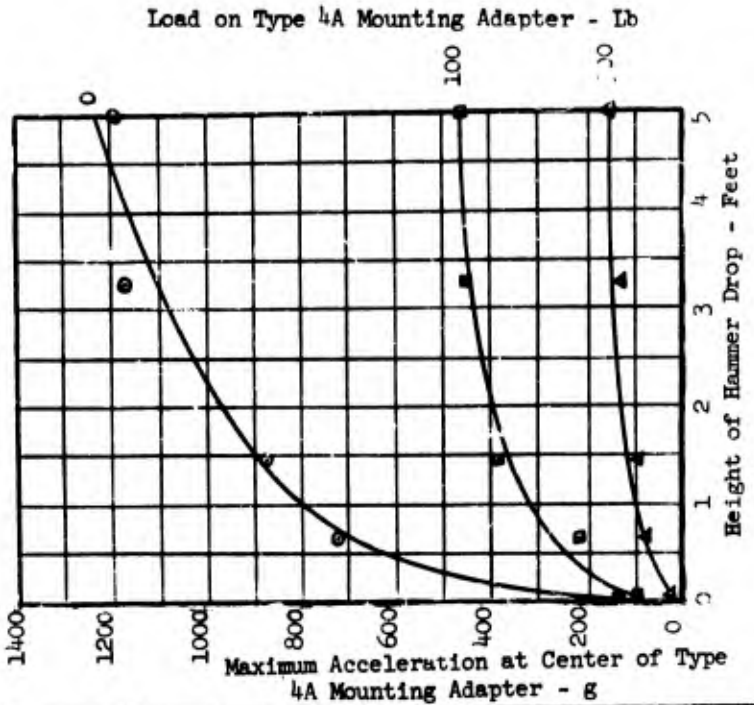

Figure 4.3.16: Maximum Acceleration at Center of Type 4A Mounting Adapter; High Impact Shock Testing Machine for Lightweight Equipment; Hammer Impact at Side

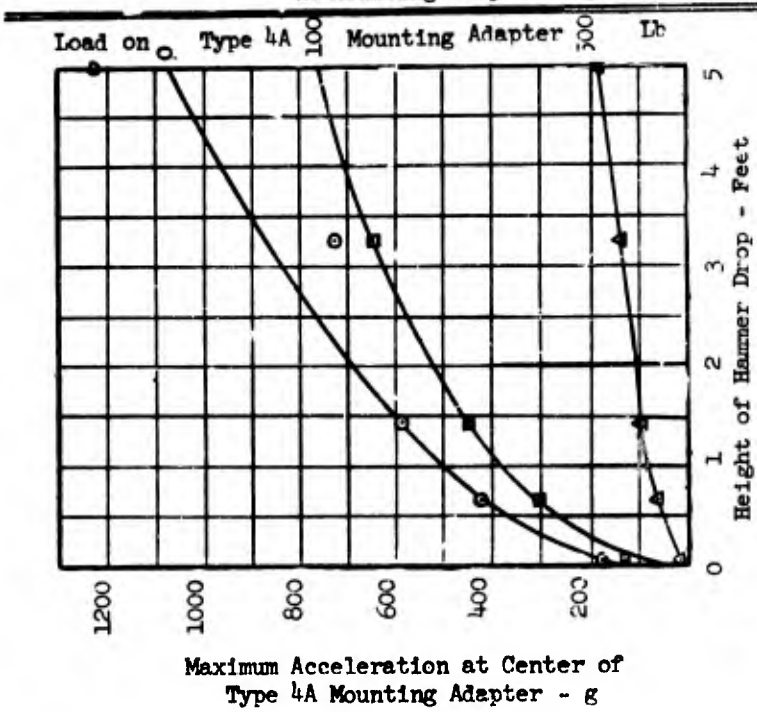

Figure 4.3.17: Maximum Acceleration at Center of Type 4A Mounting Adapter; High Impact Shock Testing Machine for Lightweight Equipment; Hammer Impact at Back

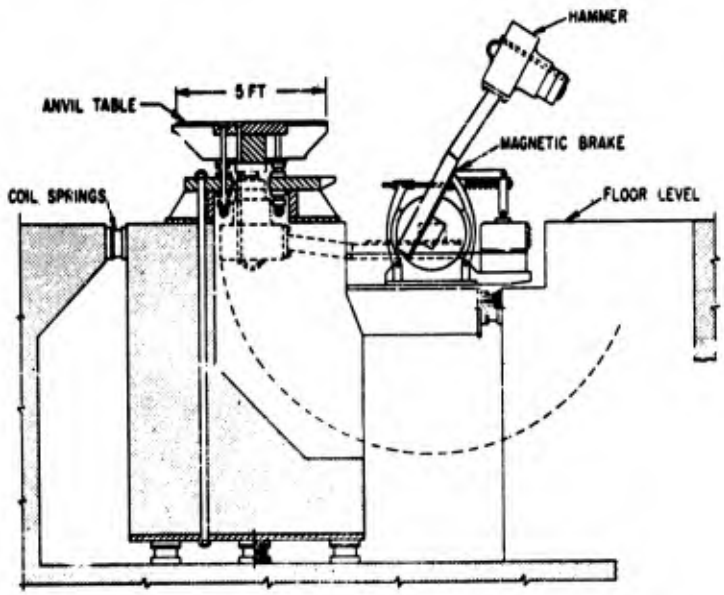

Figure 4.3.20

High Impact Shock Testing Machine
for Medium Weight Equipment
(Reference 4.4)

attached directly to the rigid anvil structure. They are attached to a group of steel channel beams which are supported at their ends by steel members, which in turn are attached to the anvil table. The number of channels employed is dependent upon the weight of the load and is such as to cause the natural frequency of the load on these channels to be about 60 cps. The hammer can be dropped from a maximum effective height of 5.5 feet. It swings around on its axle so as to strike the anvil on the bottom, giving it an upward velocity. The anvil is permitted to travel a distance up to 3 inches before being stopped by a ring of retaining bolts. The machine is secured to a large block of concrete which is mounted on springs to isolate the surrounding area from shock motions.

The displacement-time diagram shown in Figure 4.3.21 was obtained from measurements made directly on the anvil plate and does not include the superimposed vibration of the type shown in Figure 4.3.3 for a mounting adapter of the High Impact Testing Machine for Lightweight Equipment.

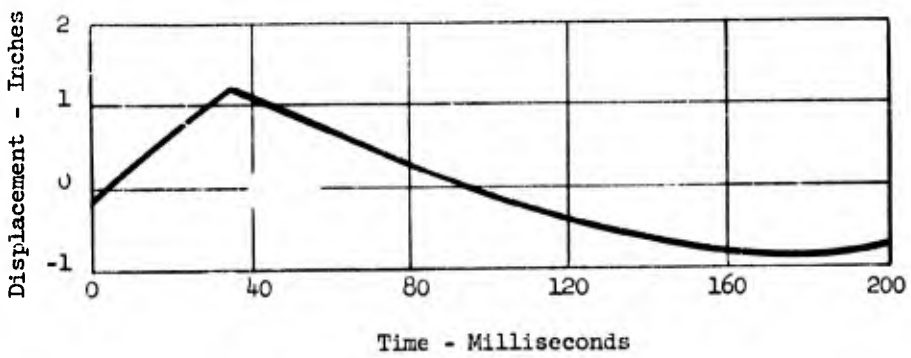

Figure 4.3.21

Typical Displacement-Time Record for Anvil Plate;
High Impact Testing Machine for Medium Weight Equipment.
Maximum Upward Travel = 1 1/2 inches
(Height of Hammer Drop = 1 foot;
1680 lb. Load on Anvil Plate)

The required length of the hammer drop and initial up travel of the anvil table for the MWHI machine is shown in Figure 4.3.22.

Group Number	I	II	III
Number of Blows	2	2	2
Anvil Table Travel, Inches	3	3	1-1/2
Total Weight on Anvil Table, Pounds:	Height of Hammer Drop (Feet)		
250 - 1,000	0.75	1.75	1.75
1,000 - 2,000 *	1.0	2.0	2.0
2,000 - 3,000	1.25	2.25	2.25
3,000 - 3,500 *	1.5	2.5	2.5
3,500 - 4,000	1.75	2.75	2.75
4,000 - 4,200	2.0	3.0	3.0
4,200 - 4,400	2.0	3.25	3.25
4,400 - 4,600 *	2.0	3.5	3.5
4,600 - 4,800	2.25	3.75	3.75
4,800 - 5,000	2.25	4.0	4.0
5,000 - 5,200	2.5	4.5	4.5
5,200 - 5,400	2.5	5.0	5.0
5,400 - 5,600 *	2.5	5.5	5.5

Note 1: Total weight on anvil table is the sum of equipment weight plus weight of mounting.

Note 2: The height of hammer drop shall be measured by means of the existing markings on the scale of the machine, no corrections being made for the added anvil table travel for the blows of groups I and II.

Figure 4.3.22

Required Hammer Drop and Anvil Table Travel for MWHI Machine

Response spectra of the shock motions generated during the test have been measured by Dick and Blake (Reference 4.17) and are given in Figures 4.3.23 through 4.3.26 for equipment whose total weight is indicated thus (*) in Figure 4.3.22.

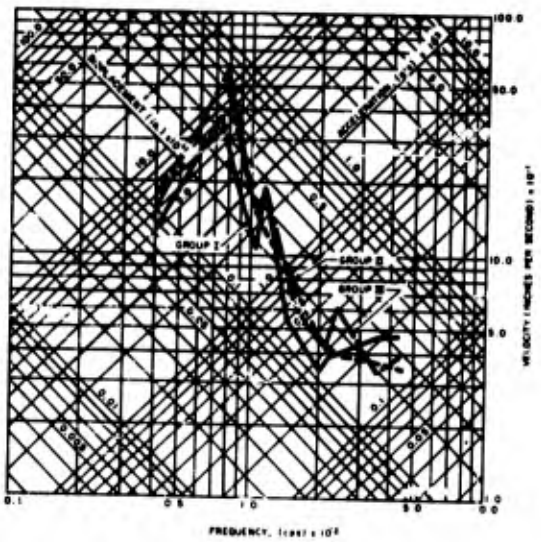

Group:	I	II	III	
Drop Height:	1.0	2.0	2.0	ft
Table Travel:	3.0	3.0	1.5	in.
Specimen Weight:	1115 lbs.			
Total Weight on Anvil Table:	1858 lbs.			

Figure 4.3.23

Class A Test Spectra for Navy Medium Weight High Impact Shock Machine

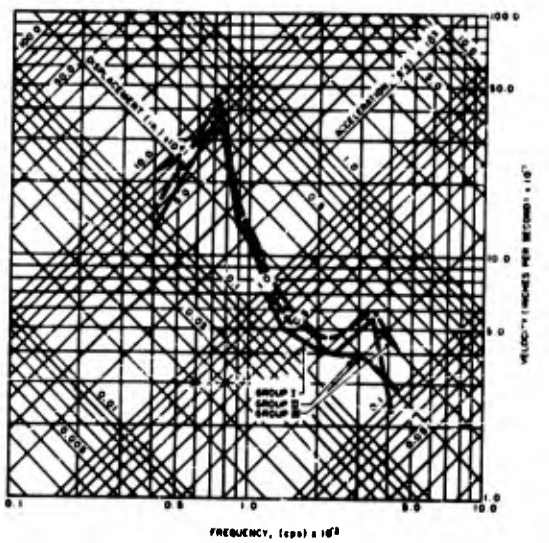

Group:	I	II	III	
Drop Height:	2.0	3.5	3.5	ft.
Table Travel:	3.0	3.0	1.5	in.
Specimen Weight:	3386 lbs.			
Total Weight on Anvil Table:	4424 lbs.			

Figure 4.3.24

Class A Test Spectra for Navy Medium Weight High Impact Shock Machine

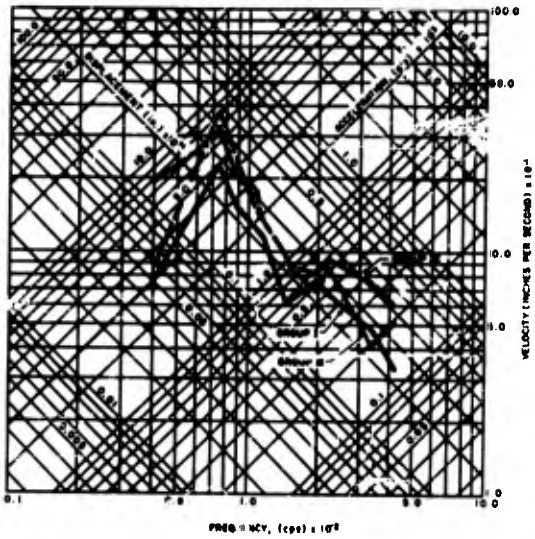

Group:	I	II	III	
Drop Height:	2.5	5.5	5.5	ft.
Table Travel:	3.0	3.0	1.5	in.
Specimen Weight:	4423 lbs.			
Total Weight on Anvil Table:	5391 lbs.			

Figure 4.3.25

Class A Test Spectra for Navy Medium Weight High Impact Shock Machine

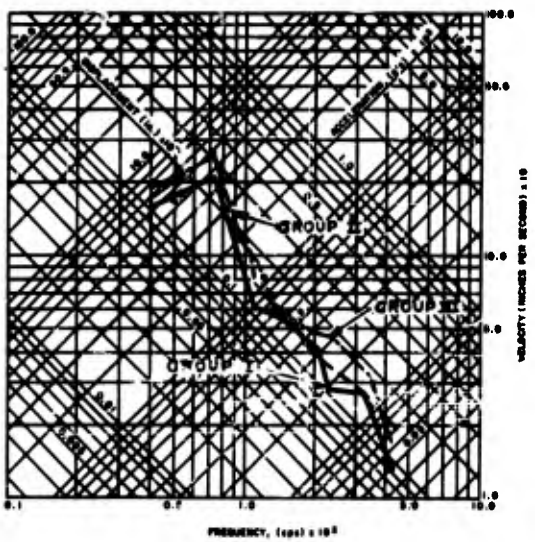

Group:	I	II	III	
Drop Height:	1.5	2.5	2.5	ft.
Table Travel:	3.0	3.0	1.5	in.
Specimen Weight:	2051 lbs.			
Total Weight on Anvil Table:	3026 lbs.			

Figure 4.3.26

Class A Test Spectra for Navy Medium Weight High Impact Shock Machine

The performance of the Shock Testing Machine for Medium Weight Equipment is further indicated by these parameters (Reference 4.16).

- Average velocity, measured from the wave form records such as given in Figure 4.3.20.
- Maximum acceleration, occurring approximately at the moment of hammer impact and also obtained from the wave form record.

The average velocity expressed in inches per second is shown as a function of the height of hammer drop in Figure 4.3.27 for various weights of equipment mounted on the anvil plate. The average velocity decreases as the weight of the equipment decreases, and increases as the height of the hammer drop increases.

The maximum acceleration, measured at the moment of hammer impact, is shown in Figure 4.3.28 for one particular test item weight of 2400 pounds. The maximum acceleration is seen to increase as the height of hammer drop increases.

4.3.5 Medium Impact, Variable Duration Shock Testing Machine

Shortly after the end of World War II, it became evident that the effects of mechanical shock are important to air-borne equipment. Consequently, a machine for conducting shock tests on air-borne equipment was devised. The maximum acceleration and fundamental period of the shock produced by this machine were based upon an inspection of the time-histories of acceleration measured on certain aircraft during rough landings. The acceleration values thus determined were increased arbitrarily to a higher value to represent the maximum acceleration anticipated during the most severe landing for which equipment protection was desirable. From the acceleration and frequencies found on the landing records, an acceleration pulse for shock-testing purposes was specified. This is the familiar pulse defined by maximum acceleration of 30 g and duration of 0.011 second which is recognized by essentially all designers of air-borne equipment. One testing machine commonly used to create such a shock is the sand drop table shown in Figure 4.3.29. It consists of a drop-table whose fall is arrested by dropping into a sandbox which forms the base of the machine. An adjustable number of blocks, attached to the underside of the table, penetrate the sand and determine the magnitude and duration of the stopping acceleration. A refined 30-40 grit sand is used which must be carefully maintained as to depth, packing, and surface condition if consistent results are to be obtained.

The machines are made of several different sizes so that different load ranges can be accommodated.

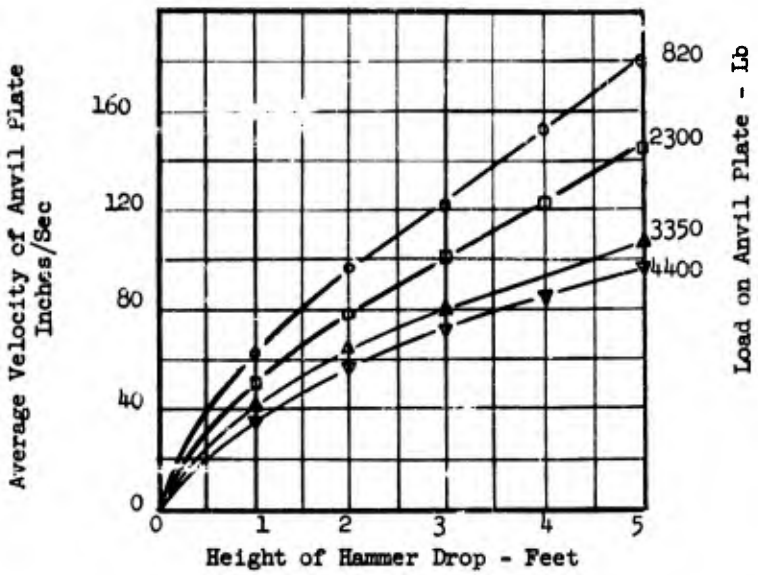

Figure 4.3.27: Average Velocity of Anvil Plate: High Impact Shock Testing Machine for Medium Weight Equipment

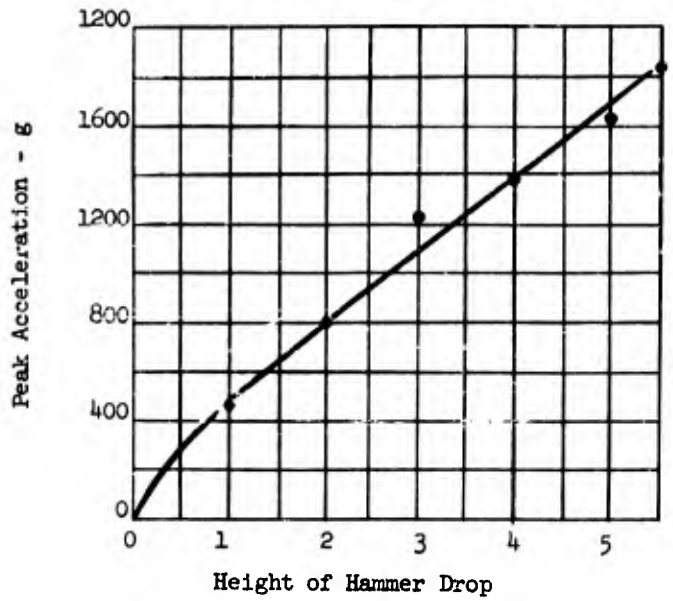

Figure 4.3.28: Peak Acceleration of Anvil Plate; High Impact Shock Testing Machine for Medium Weight Equipment. Load on Anvil Plate: 2400 lbs.

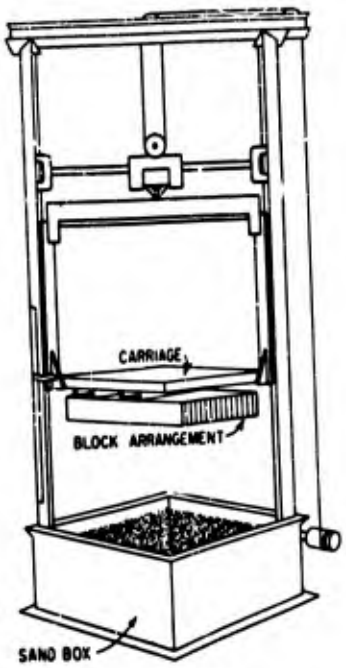

Figure 4.3.29

Medium Impact, Variable Duration Shock-Testing Machine, Intended Primarily for Testing Air-Borne Equipment. A Box of Sand Arrests Downward Motion of the Carriage. (Reproduced from Reference 4.2).

The three sizes described in MIL-S-4456 (USAF) are the 20-pound, the 150-pound, and the 1200-pound machines. When performing shock tests with these machines, the weight of the equipment load and dead weight is kept constant at 20, 150, and 1200 pounds, respectively. Shock tests of equipment weighing less than 20 pounds where the pulse duration is 8 milliseconds or less are performed on a machine using lead rather than sand as an arresting material.

The three principal variables which determine the maximum amplitude of the acceleration and the duration of the pulse are:

. Combined weight of elevator, dead load, and equipment being tested.

. Number and arrangement of blocks.

. Height of drop.

Response spectra for the motions of the 150-400 pound and 1200- pound machines have been computed from test data by Crede (Reference 4.18) and are presented here as Figures 4.3.30 through 4.3.33. The shaded areas indicate a band which includes 95 per cent of the data points obtained from tests on eleven machines using 10-, 11-, and 12-block configurations and 13- and 25-inch drop heights.

Calibration curves taken from Reference 4.8 for the three machines are shown in Figures 4.3.34 through 4.3.36. The accuracy of the curves is estimated in the Reference as being within plus or minus 15 per cent. In Figure 4.3.33 the maximum acceleration in gravities is given as a function of height of drop in inches for various block configurations. The duration of the shock in milliseconds is indicated in the Table presenting the block data. It may be noted that for a given height of drop, the impulse in inch-seconds increases slightly as the peak acceleration is decreased.

The calibration curves for the 150-pound machine are shown in Figure 4.3.34, also for several block configurations. Here the total impulse decreases with decreasing acceleration at the high drops, but increases with decreasing acceleration for the low drops.

4.3.6 Plastic Pellet Drop Tables

A close control of simple pulse shapes can be obtained by the use of drop testing machines employing shaped lead pellets instead of sand as the means of arresting the downward motion of the carriage. A typical machine (Figure 4.3.37, page 4 - 35) embodies a freely falling table similar to that of the Variable Duration Sand Drop Table described in Section 4.3.2. The platform to which the equipment is attached is cast from aluminum and designed to have the greatest possible natural frequencies consistent with the over-all dimensions. The impacting surfaces are of hardened steel.

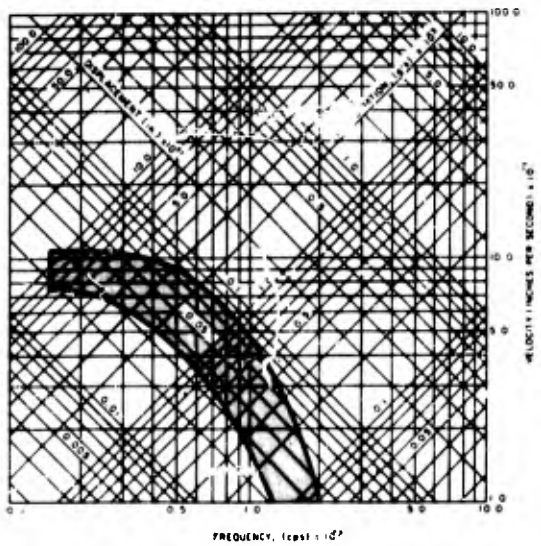

Figure 4.3.30
Range of Response Spectra for 13-Inch Free Fall
of 150 - 400 VD Machine

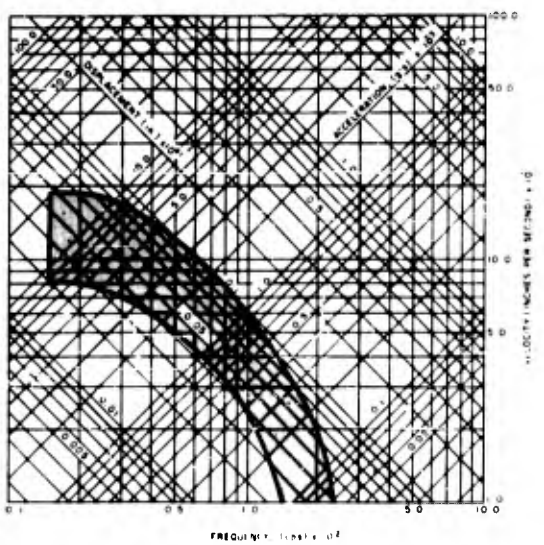

Figure 4.3.31
Range of Response Spectra for 25-Inch Free Fall
of 150 - 400 VD Machine

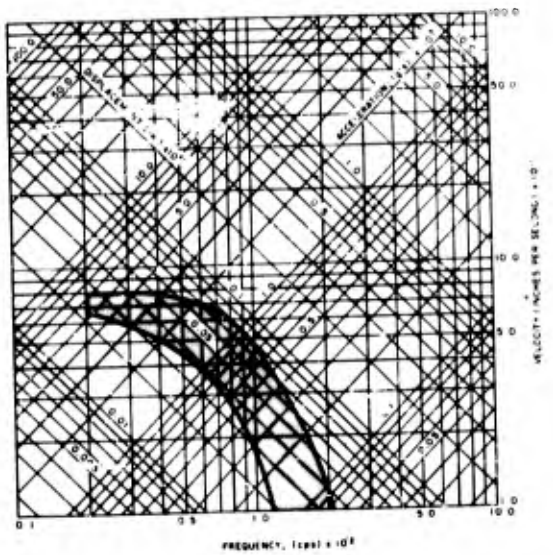

Figure 4.3.32
Range of Response Spectra for 13-Inch Free Fall of 1200 VD Machine

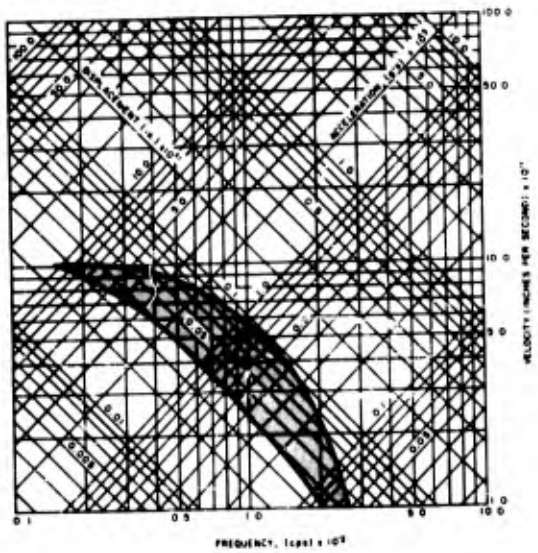

Figure 4.3.33
Range of Response Spectra for 25-Inch Free Fall of 1200 VD Machine

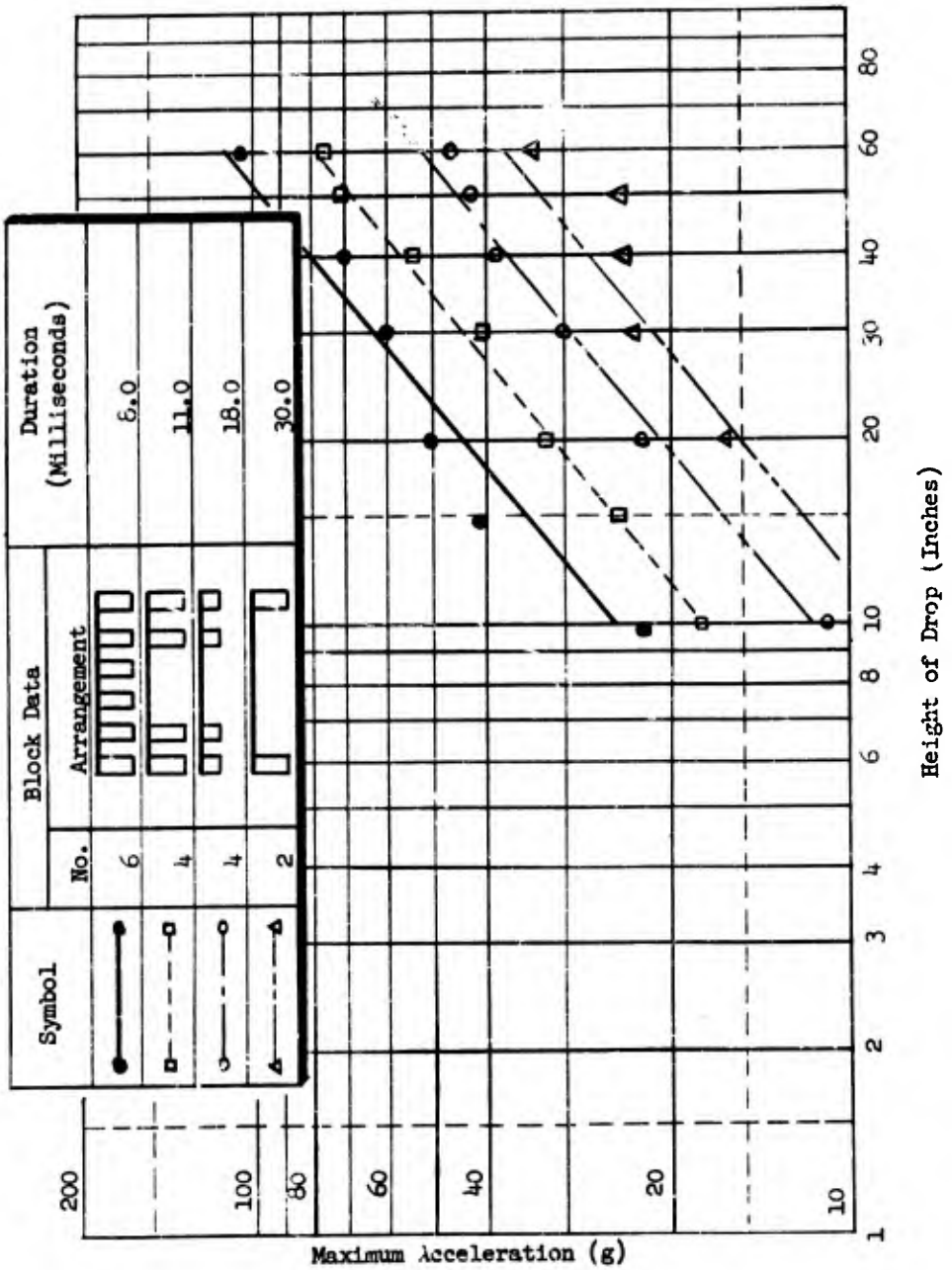

Figure 4.3.34

Sand Calibration Curves for 20 lb.
High Impact Variable Duration Shock Machine
(Reference 4.8)

Symbol	Block Data		Nominal Duration (Milliseconds)
	No.	Arrangement	
□——□	12		6.5
●— — —●	10		11
○- - - - -○	9		16
▲—·—▲	8		24
△— - -△	6		32

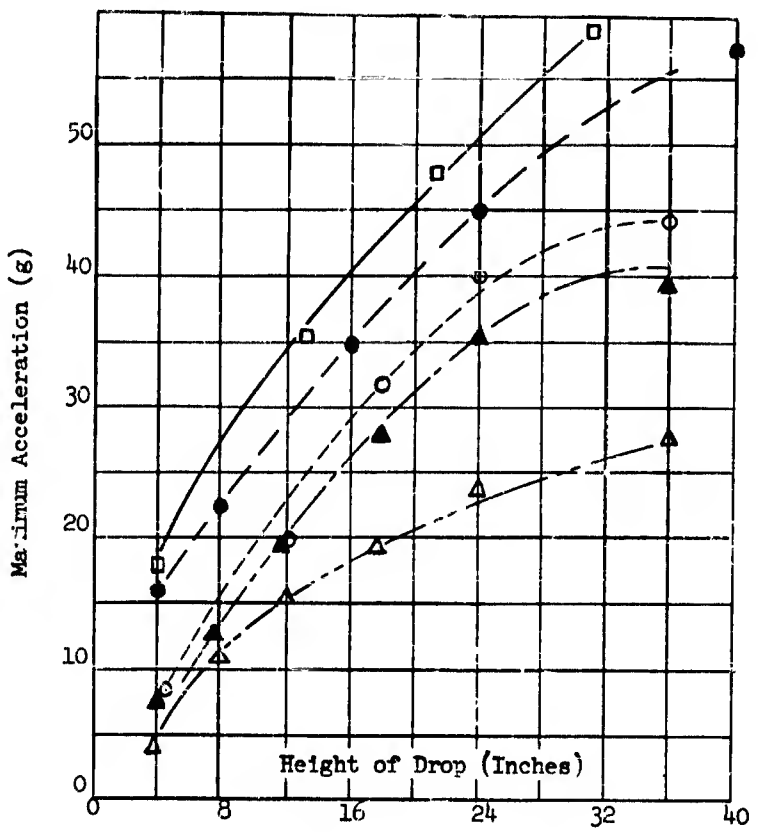

Figure 4.3.35

Calibration Curves for 150 Lb
Medium Impact Variable Duration Shock Machine
(Reference 4.8)

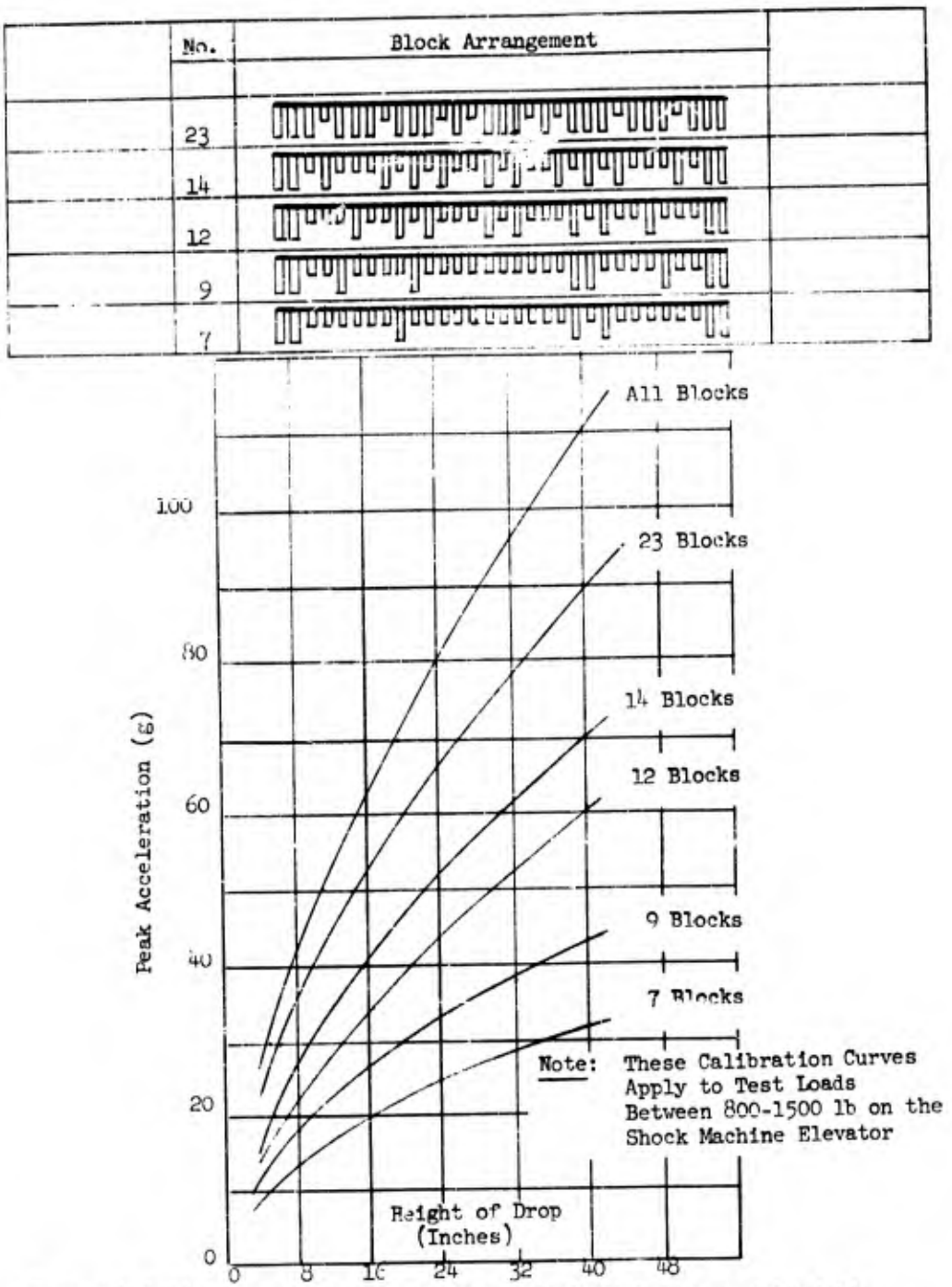

Figure 4.3.36: Calibration Curves for 1200-Lb Medium Impact Variable Duration Shock Machine (Reference 4.8)

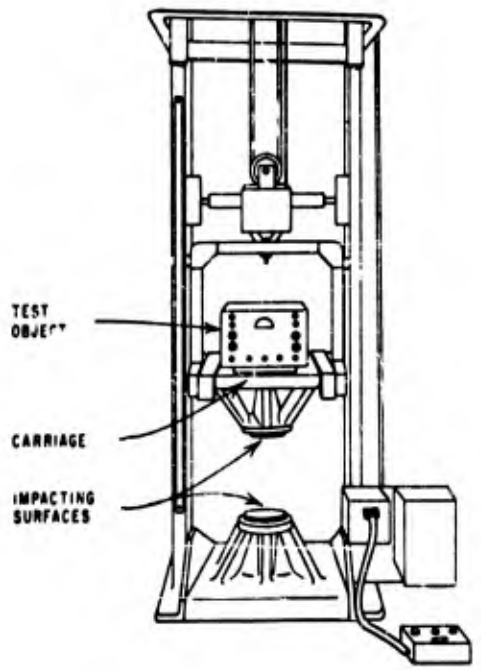

Figure 4.3.37

Shock Testing Machine for Applying the Pulse
Shown in Figure
A Lead Pellet Arrests Downward Motion of the Carriage.

The gross characteristics of a wave form typical of that produced by the machine of Figure 4.3.37 is shown in Figure 4.3.36

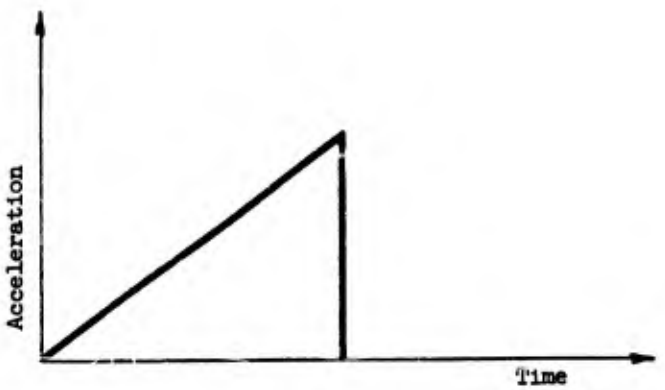

Figure 4.3.38

Sawtooth Time-History of Acceleration
Produced by Lead Pellet Drop Table
of Figure 4.3.37

The use of a test shock with a sawtooth wave form has an advantage in that its response spectrum is relatively uniform over a wide frequency range with no extreme values which would discriminate for or against equipment with certain natural frequencies (Reference 4.3). This form of excitation provides a satisfactory test for many types of shock environments where it is required that the shock spectrum rise to a maximum value within the first 100 cps and remain constant thereafter. The amplitude and duration of the pulse may be modified by changing the dimensions of the pellet.

When velocity changes larger than can be achieved by a free-falling carriage are required, some machines are constructed so that the carriage may be accelerated downward by other means than gravity.

4.3.7 Inclined Plane Testing Machine

A shock-testing machine involving a freely falling table inherently produces only an upward acceleration pulse when the motion of the table is arrested. It is common practice to orient the equipment in several different positions on the table to attain several directions of shock. There are certain limitations and inconveniences to such a

procedure if the equipment is large or if it contains components which are sensitive to the direction of gravity forces. A more feasible method of obtaining horizontal shock is to attach the equipment to a carriage that is adapted to move horizontally with a predetermined velocity, and to be arrested by impact with a fixed structure. For example, the package-testing machine illustrated in Figure 4.3.39 embodies a carriage adapted to run down an inclined track under the influence of gravity forces and impact an abutment. A similar result could be obtained by suspending the platform as a multifilar pendulum and swinging it against a wall.

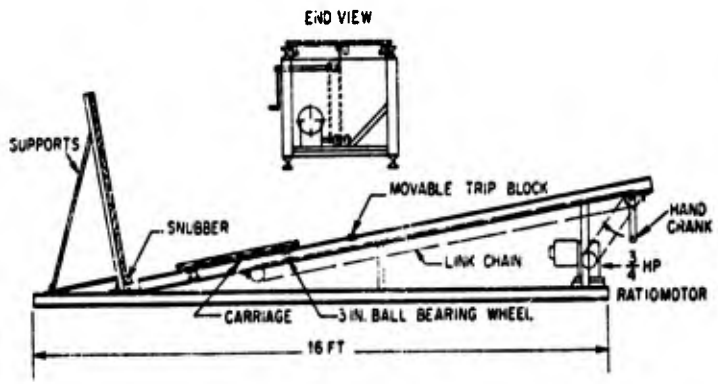

Figure 4.3.39

Conbur Shock-Testing Machine
Intended Primarily for Testing Packages Items

4.3.8 Hyge Shock Tester

A machine developed within recent years (Reference 4.9) employs the energy of a compressed gas to create a force whose magnitude as a function of displacement can be predetermined. A typical device of this kind is shown in Figure 4.3.40, page 4 - 38 . The pressure in the lower chamber is greater than that in the upper chamber, but prior to operation the upward force exerted on the thrust column is less than the downward force because of the smaller area exposed in the lower chamber. As the pressure difference is increased, the upward

force becomes greater than the downward force and the ring seal, which prevents the pressure of the lower chamber from acting over the entire bottom area of the piston, breaks. There is then a sudden increase in the upward thrust. The shape of the acceleration pulse experienced by the thrust column and its load is determined principally by orifice sizes and metering-pin shapes. A liquid usually is used, as shown, in the region surrounding the metering pins; the liquid is forced through the orifices by the gas pressure of the accumulator and is involved in the pulse-shaping mechanism. Acceleration pulses of many shapes can be made by proper design of the metering pins, consideration being taken of the mass of the load. Some models have a maximum thrust output of 10,000 lbs., and for small loads can provide sustaining accelerations up to 300 g for a stroke of about 6 inches. The nature of the metering pin inherently limits a testing machine of this type to shock motions having relatively long strokes.

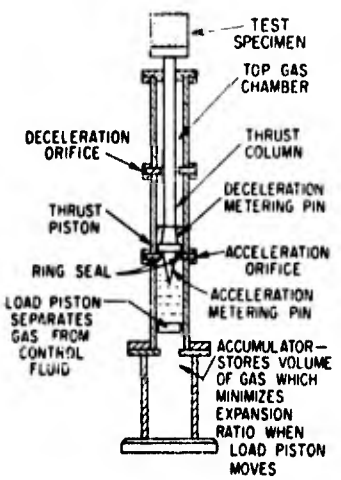

Figure 4.3.40
Hyge Shock-Testing Machine
(Reference 4.9)

4.3.9 Improvised Tests

All currently used shock-testing machines have capacity to test equipment of quite limited weight and size. For example, the maximum weight of equipment that can be tested on the machine previously described is 5600 pounds. This weight limitation naturally raises the question of methods for testing heavier equipment. A suitable test may be devised provided proper attention is given to an adequate velocity change sustained by the equipment under test; properly designed means to arrest motion of the equipment; and precautions to ensure repeatability of the test. The last requirement is most likely to be found troublesome. A convenient means for applying a horizontally oriented shock motion is illustrated in Figure 4.3.41(a); it consists of a multifilar pendulum which constitutes a platform upon which the equipment (phantom outline) is mounted. The platform is displaced as indicated by the dotted lines and permitted to swing against a rigid wall, a cushioning element A being interposed to control the nature of the deceleration. A method for achieving an analogous result for a vertically oriented shock motion, used by the Naval Ordnance Laboratory, is illustrated in Figure 4.3.41(b). It consists of two platforms and an interposed linkage B with light springs for maintaining the platforms parallel and normally separated. The equipment (phantom outline) is attached to the upper platform; the entire assembly is lifted by an overhead crane and dropped from a predetermined height. Cushioning elements C are interposed between the platforms and the linkage ensures that such cushioning elements engage the upper platform in a repeatable manner.

The requirements for improvised tests may be determined by plotting the spectrum for the field service condition. Then the height of drop should be selected so that the free-fall velocity at time of impact is approximately the greatest value of the spectrum as read on the velocity scale. The characteristics of the arresting means must then be chosen so that the maximum acceleration experienced by the equipment is equal to the acceleration asymptote of the spectrum at its high frequency end. To meet both of these requirements simultaneously necessitates that the tests be carefully controlled.

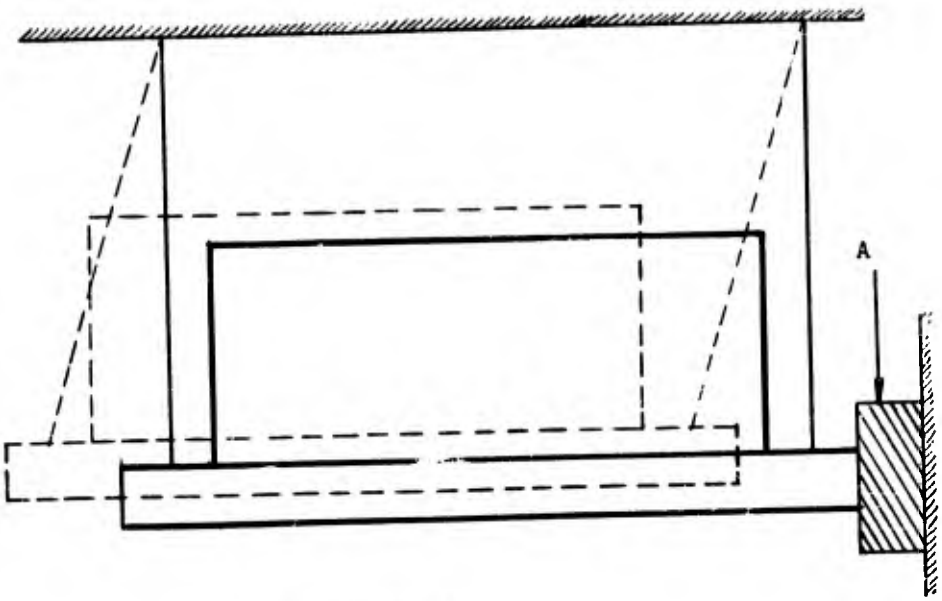

(a) Multifilar Pendulum

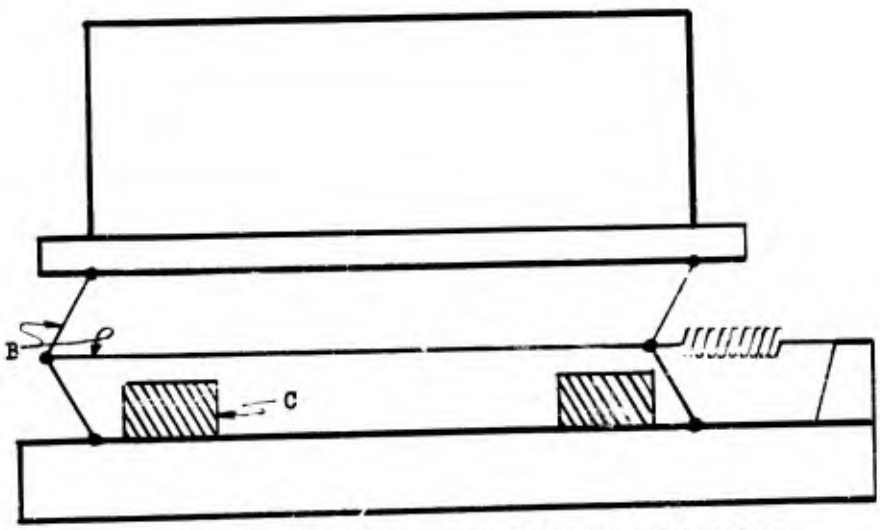

(b) Machine Used by Naval Ordnance Laboratory

Figure 4.3.41
Improvised Test Machines

4.4 Equipment Shock Tolerances

If the shock response spectrum is employed as the primary criterion of damage potential, the selection of equipment, or the decision to provide shock isolation, can be made on the basis of a comparison of the spectrum of the service shock with that of a test shock which the equipment has survived. If the test spectrum envelopes the service spectrum at all frequencies, presumably the equipment will withstand the service shock successfully. If not, isolation must be provided.

Rarely has the model and make of the equipment been determined at the stage in the design where the decision whether or not to isolate the equipment must be made. In the usual procurement procedure, the entire facility design is completed before the final selection of equipment. In the interest of economy it is desirable to utilize commercial grade equipment wherever possible. To specify arbitrarily that the equipment withstand the service shock without regard for commercial standards may require that a specially designed unit be constructed.

A further complication arises from the lack of a comprehensive body of shock test data on commercial grade equipment. Ample test data would provide the isolation system designer with a basis for forming a reasonable estimate of the shock tolerance level of equipment in which he is interested. Many important items have never been tested; in those instances where tests have been made, the strength of the test shock is rarely defined by its response spectrum. In any case, the data are widely scattered.

As an initial step in assembling shock test data on the type of equipment regularly employed in underground protective structures, a large number of shock test reports have been abstracted and the results tabulated in this Section. Each Table presents the results of a single shock test and lists:

- the general description of the equipment
- the test machine employed
- the test conditions
- the number of items tested
- the test specification
- the test report designation or issuing agency
- the results of the test.

The spectrum of the shock which the equipment survived or failed can then be determined by relating the shock machine and test conditions to the spectra appearing earlier in this Section.

The Tables are far from complete in considering all classes, types, and sizes of equipment the facility engineer might use. Further, the variations in tolerance level of the same type of equipment produced by different manufacturers may be sizable. Nevertheless it is hoped that

the tabulation will be of assistance to the isolation system designer: illustrating how such test information may be interpreted and applied to his specific problem; and providing him with a gross indication of the tolerance level of equipment in those cases where the various manufacturers have not conducted shock tests.

4.4.1 Index to Equipment Test Tables

ELECTRONIC EQUIPMENT

[illegible]AB

GENERAL DESCRIPTION: NCN antennas, 2 type AS-391, 2 types AT-693, and type 994 were reported on.

Type	Approximate Weight (lb)	Test Environment	Test Machine	Number Tested	Test Specification	Report Designation	Result	Type of Failure
Antennas	30	1, 3 and 5 Ft. drops	Navy LWHI Shock Machine	5	MIL-S-901B 4C Mounting	Mare Island NavShipYd 405h-61	Passed	

FREQUENCY STANDARD

GENERAL DESCRIPTION: Model 103AR frequency standard

Model 103AR	65.5	1, 3 and 5 ft. side 1 and 3 ft. top blow	Navy LWHI Shock Machine	1	MIL-E-16400	Mare Island NavShipYd 5569-59	Failed (3 ft.top)	Crystal Assembly was damaged

OSCILLOSCOPE

GENERAL DESCRIPTION: 1. Type AN/USN-105 oscilloscope with plug-in units.

2. Model 160AN oscilloscope with dual trace amplifier.

3. Type AMT/USN-105 oscilloscope.

1	98	1,2, 4 ft. and 2, 3, and 4 ft. blows from back and side and from top	Navy LWHI Shock Machine	1	MIL-S-901B 4C Mounting	Mare Island NavShipYd 1806-60	Passed	
2	72	1,2, 3 ft. and 2, 3, and 4 ft. blows from back and side and from top	Navy LWHI Shock	1	MIL-T-945 4C Mounting	Mare Island NavShipYd 2365-59	Passed	
3	90	1,2, and 3 2, 3, and 4 1, 2 and 3 ft. blows	Navy LWHI Shock Machine	1	MIL-S-901B 4C Mounting	Mare Island NavShipYd 8103-59	Passed	

OSCILLOSCOPE COMPONENTS

GENERAL DESCRIPTION: The components consisted of one transformer and four chokes.

Components	30	1, 3 and 5 ft. drops	Navy LWHI Shock Machine	5	MIL-S-901B 4A Mounting	Mare Island NavShipYd 7810-59	Passed	

TIME COMPARATOR SYSTEM

GENERAL DESCRIPTION: 1. Time comparator system AN-K-17-999B with frequency divider model 116AR.

2. Time comparator AN/UP-K-17-999 A/B component with Model 116AR scope and 725 AR power supply.

3. Frequency divider and clock model [illegible].

Type	Approximate Weight (lb)	Test Environment	Test Machine	Number Tested	Test Specification	Report Designation	Result	Type of Failure
1	144	1, 2 and 3 ft. drops	Navy [illegible] Shock Machine	2	MIL-S-901B 4C Mounting	Mare Island NavShipYd 6987-61	Passed	
2	180	1, 2 and 3 ft. drops	Navy LWHI Shock Machine	1	MIL-S-901B 4C Mounting	Mare Island NavShipYd 4296-61	Failed (1 ft. Back)	Cathode Ray Tube Broke Away From Base
3	40	1, 2 and 3 ft. drops	Navy LWHI Shock Machine	1	MIL-S-901B 4C Mounting	Mare Island NavShipYd 1027-59	Passed	

TUBE TRAVELING WAVE

GENERAL DESCRIPTION: Traveling wave tube No. X 29

Tube	35	1, 3 and 5 ft. drops	Navy LWHI Shock Machine	1	MIL-S-901B 4C Mounting	Mare Island NavShipYd 4055-61	Failed (3 ft. Back)	Broken Cathode

MECHANICAL EQUIPMENT

COMPRESSORS

GENERAL DESCRIPTION: The compressor was a two stage, horizontally opposed, type AS150-300 CFM Air compressor. The compressor was driven by a gasoline engine, incorporated into the same unit as was the compressor. The Compressor was tested with power on.

150-300 CFM	210	1, 3 and 5 ft. drop	Navy LWHI Shock Machine	1	MIL-S-901	ASTIA-AD 201782	Passed	

FANS

GENERAL DESCRIPTION: Two reports were reviewed both fans were of 8-inch diameter. One used a 115V DC motor. The second used a 115-V AC motor. Both fans were made for refrigeration and both were tested with power on.

115-V AC	60	1, 3, and 5 ft. drops	Navy LWHI Shock Machine	1	JAN-F-151B	ASTIA-AD43519	Failed	Base Plate Buckled
115-V DC	60*	1, 3 and 5 ft. drops	Navy LWHI Shock Machine	1	JAN-F-151B	ASTIA-AD42119	Failed	Fan Blade Locked Against Guard

* Estimated

FASTENERS, ANCHOR

GENERAL DESCRIPTION: The anchor fasteners consisted of an assembly of cable hangers and lengths of cable attached to a steel plate by means of a perforated surface plate and adhesive.

Type	Approximate Weight (lb)	Test Environment	Test Machine	Number Tested	Test Specification	Report Designation	Result	Type of Failure
Anchor	10	1, 3 and 5 ft. drops	Navy LWHI Shock Machine	1	MIL-S-901B Mounting Not Mentioned	Mare Island Report 1202-60	Failed on 5 ft. drop back	(See Note)

NOTES: Separation of 3/4-inch cable at the point of the "V".

FRAME DIESEL ENGINE

GENERAL DESCRIPTION: The equipment consisted of a diesel engine frame with two cylindrical castings and bearing cap assemblies. A bar of rolled steel was inserted into the crank shaft position to simulate the mass of the crankshaft. This was a single throw, type FV-9A diesel engine frame made of Modular Iron.

FV-9A	4565	2.0, 3.5, and 3.5 ft. blows	MWKI Shock Machine	1	MIL-S-901	EES 5C101782	Passed	

GAGES

GENERAL DESCRIPTION: The filter gage model MGD gives a signal when air filters should be serviced, and was being considered for use by the Navy. The Navy also considered using a Magnehelic gage to indicate when a filter required cleaning. The pointer gage has slack diaphragms for sensing elements, the pointers are attached to the diaphragm by linkages. Two brass based pressure controls for air conditioning control equipment were also in the available reports.

Filter	1.9	1 and 3 ft drop	Navy LWHI Shock Machine	1	MIL-S-901B 6D Mounting	ASTIA-AD 160612	Failed 5th Blow (Back)	(1)
Magne-helic	1.1	1 and 3 ft drop	Navy LWHI Shock Machine	1	MIL-S-901B 6D Mounting	ASTIA-AD 160458	Failed 6th Blow (Back)	(2)
Pointer	6.8	1, 3 and 5 ft. drop	Navy LWHI Shock Machine	1	MIL-S-9018 6D Mounting	Material Lab NY NavShipYd 5956-3	Failed 1st Blow Fixed Then Passed	(3)
Control Sample A	4.6	1 and 3 ft drop	Navy LWHI Shock Machine	2	N.D. 6683 4A Mounting	Material Lab NY NavShipYd 4429-C-22B	Failed	Cover Slip Loosened Lost Adjusting Knob
Sample B	4.4	1, 3 and 5 ft. drop						

NOTES: (1) Entire front housing of the gage flew off and fell to the floor.
(2) Indicator needle broke off, helical bar supporting needle jumped its bearings, and the magnet broke.
(3) On the first blow, the indicator failed to indicate properly.
On the fifth blow, the frame arrestor pointer failed to indicate properly.
After calibration and repair of a crack in hose, the equipment passed.

HEAT EXCHANGER

GENERAL DESCRIPTION: A laboratory-developed, water-cooled, heat exchanger was made to alleviate the problem of maintaining satisfactory ambient temperatures for electronic equipment aboard Naval vessels. The heat exchangers were filled with water during shock test.

Type	Approximate Weight (lb)	Test Environment	Test Machine	Number Tested	Test Specification	Report Designation	Result	Type of Failure
Heat Exchanger	75	1, 3 and 5 ft. drops	Navy MANI Shock Machine	1	Mil-S-901D 4A Mounting	Material Lab NY NavShipYd 5441-3	Passed	

MOTORS AND PUMPS

GENERAL DESCRIPTION: Eleven reports were reviewed on motors and pumps. It is most convenient for the equipment to be broken down into three classifications by weight. The equipment was tested running and at a standstill during alternate blows. The first of these: 0-300 lb. and takes in the following equipment:

I
1. 1 hp 30 rpm close-coupled centrifugal M and P
2. 3 hp 250 gpm close-coupled centrifugal M and P
3. 5 hp 50 gpm close-coupled centrifugal M and P
4. 2 hp 2 gpm close-coupled centrifugal M and P

The next were in the 300-600 class:

II
1. 3 hp 100 gpm close-coupled centrifugal M and P
2. 15 hp 185 gpm close-coupled centrifugal M and P
3. 5 hp 400 gpm close-coupled centrifugal M and P
4. 10 hp 125 gpm close-coupled centrifugal M and P
5. 7.5 hp 600 gpm close-coupled centrifugal M and P

The final group consisted of those reports reviewed in the above 600 lb. class:

III
1. 15 hp 100 gpm close-coupled centrifugal M and P
2. 25 hp 250 gpm close-coupled centrifugal M and P

I	0-300	1, 3 and 5 ft. drops	Navy MANI Shock Machine	4	N.D. 6653	ASTIA-AD 201017 201031 201015 201016	4 Passed	(1)
II	300-600	1, 3 and 5 ft. drops	Navy MANI Shock Machine	5	N.D. 6653	200977 201019 ATI205436 AD 201020 201018	4 Passed 1 Failed	(2)
III	600	.75, 1.75, and 1.75 ft. blows	Navy MANI Shock Machine	2	N.D. 6653	AD 201076 201077	Passed	

NOTES: (1) On the 3-foot-back blow, the 5 hp 50 gpm motor and pump sustained permanent deformation of the shaft to bind during rotation.
(2) On the 1-feet front blow, the motor of the 5 hp 400 gpm motor and pump sustained electrical damage. All of the above pumps had to be modified for whipping action of the overhanging mass at the pump housing.

PUMPS

GENERAL DESCRIPTION: 1. A positive displacement, constant delivery, vane type, hydraulic pump with a maximum fluid delivery rate of 8.4 GPM at 1200 rpm.

2. A 100 HP Motor and suitable reduction gear as the prime mover. It too was a hydraulic pump, and was used as a power pump with a delivery rate of 192 GPM at 1100 psi.

The equipment was running and at a standstill during alternate blows.

Vane	29	1 and 3 ft drops	Navy MANI Shock Machine	1	MIL-P-17869 4C Mounting	ASTIA-AD 97814	Failed	Mounting Base Fractured on 3 ft. Vertical Blow
Power	2575	1.25, 2.25 and 2.25 ft. drops	Navy MANI Shock Machine	1	MIL-S-901D	ASTIA-AD 159766	Passed	

LEAD SHIELDING

GENERAL DESCRIPTION: Two types or methods of shielding surfaces with lead were reviewed the first was by spraying the lead and the second method was by burning in the lead.

Type	Approximate Weight (lb)	Test Environment	Test Machine	Number Tested	Test Specification	Report Designation	Result	Type of Failure
Sprayed	13.85	1,3, and 5 ft. drops	Navy LWHI Shock Machine	1	MIL-S-901B 4A Mounting	Mare Island NavShipYd 1635-59	Failed	Hairline Crack of Bond
Burned	14.0	1, 3 and 5 ft. drops		1	MIL-S-901B 4A Mounting		Passed	

VALVES

GENERAL DESCRIPTION:
1. Two ball valves.
2. A rotor valve.
3. Two 1/2 inch packless valves in closed position.
4. A pressure control, diaphragm operated external air pilot actuated type I valve - corresponds to a Navy type I, Series 150, Class B valve

Ball Valves 2-1/2 inch	80	1, 3 and 5 ft. drops	Navy LWHI Shock Machine	2	MIL-S-901B 4A Mounting	Mare Island NavShipYd 4035-61	Passed
6 inch	30						
Rotor Valve	75	1, 3 and 5 ft. drops	Navy LWHI Shock Machine	1	MIL-S-901B 4A Mounting	Mare Island NavShipYd 3188-61	Passed
Packless No. 1 and No. 2	3.5	1, 3 and 5 ft.	Navy LWHI Shock Machine	2	Norman Browning Co. (Pipe and Metal Blocks Mounting)	Mare Island NavShipYd 1478-60	Passed
Pilot Valves Alum Steel	10*	1, 3 and 5 ft.	Navy LWHI Shock Machine	2	MIL-S-901B (Mounted in Piping)	ASTIA-AD 106139	Passed

* Estimated

ELECTRICAL EQUIPMENT

GENERAL DESCRIPTION:
1. Three samples of the Mark 47 Mod. 0 silver oxide - zinc-alkaline secondary type.
2. Two samples of the Mark 39 Mod. 0 silver oxide-zinc-alkaline secondary type in the dry charge condition.
3. Two preproduction samples of battery 39 Mark 0.
4. Two preproduction samples of battery Mark 42 Mod. 0 of the silver oxide-zinc alkaline secondary type.
5. Two production samples of torpedo propulsion battery Mark 41 Mod. 1.

Type	Approximate Weight (lb)	Test Environment	Test Machine	Number Tested	Test Specification	Report Designation	Result	Type of Failure
Mark 47	210	1550	21-inch Air Gun	3	MIL-B-16955	ASTIA-AD 101822	Failed	Top Cover Seal Failed
Mark 39	29.4	50 G for 0.05-sec Duration	21-inch Air Gun	2	MIL-B-16955	ASTIA-AD 99715	Passed	
Mark 39 Preproduction	30.75 0	500 for 0.05 sec Duration	21-inch Air Gun	2	MIL-B-16955	ASTIA-AD 96344	Passed	
Mark 42	64.0	100 G 200 G For 0.04-sec Duration	Torpedo Cylinder	2	MIL-B-17348A	ASTIA-AD 108996	Passed	
Mark 41	18.5	50 G for 0.05 sec. Duration Not Mentioned	Bush-Clevite Torpedo Battery Mount	2	MIL-B-17348A	ASTIA-AD 151664	Passed	

GENERAL DESCRIPTION:
1. Two laminated hard rubber jars with type HRX-47 elements.
2. Four laminated hard rubber jars with concave exterior bottom and with type WRK-45 oxide type elements.
3. Two permali (laminated plywood) jars with oxide type 5350 I elements.

Laminated Hard Rubber	92	1, 2, 3, 4 and 5 ft drops	Navy MWHI Shock Machine	2	RRC-5B17 X0609	RRB-5B 066832	Passed	
Concave	90	1, 2, 3, 4 and 5 ft. drops	Navy MWHI Shock Machine	4	RRB-5B17 X0699	RRB-5C 066032	Passed	
Permali Jars	79	1, 2, 3, 4 and 5 ft. drops	Navy MWHI Shock Machine	2	RRC-5B17 X0609	RRB-5D 066832	Failed	Sustained Slight Cracks

BRUSH HOLDERS

GENERAL DESCRIPTION: The DC Brushholder is of the reaction die cast holder type. The material is aluminum bronze.

DC Brush-holder	2	5-2000 Ft.-lb. shocks	Navy LWHI Shock Machine	1	1707	ASTIA-AD59694	Passed

BUS TRANSFER UNIT

GENERAL DESCRIPTION: 1. Type ABT-A2 [illegible] designed for automatic or manual operation (A 150/150 AMP, 440 volts AC, 3 phase, 60 cycle.
2. Type ABT-A3 unit rated at 150 AMP, 440 volts, 3 phase, 60 cycles, designed for automatic or manual operation.

Type	Approximate Weight (lb)	Test Environment	Test Machine	Number Tested	Test Specification	Report Designation	Result	Type of Failure
ABT-A2 [illegible]	100*	1, 3 and 5 ft. drops	Navy LWHI - Shock Machine	1	MIL-S-901B 4A Mounting	ASTIA-AD-205142	Passed	
ABT-A3	150*	1, 3 and 5 ft. drops	Navy LWHI Shock Machine	1	MIL-S-901B 4A Mounting	ASTIA-AD 161434	Passed	

*Estimated

CIRCUITY BREAKERS

GENERAL DESCRIPTION: 1. Navy Type AQB, 3 pole, 400 ampere frame, 500 volt AC, 250 volt DC units
2. A type AQB-A250 breaker with a 160 ampere trip unit.
3. A 1600 ampere frame size with a 2 pole, 250 V. DC breaker.
4. A 2000 ampere frame size type ACB.
5. Type ALB-1 circuit breakers-single pole, 50 ampere frame size, 125 volt AC-DC units.

400 AMP	49.5	1, 3 and 5 ft. drops	Navy LWHI Shock Machine	1	MIL-S-901 Special Mounting	ASTIA-AD 207199	Failed 5 ft. Rear	The Breaker Tripped
160 AMP	25*	1, 3 and 5 Ft. drops	Navy LWHI Shock	1	MIL-S-901	ASTIA-AD 141256	Failed 5 Ft. Vert.	Handle Moved From Closed Position to Open Pos.
1600 AMP	323	1, 3 and 5 ft. drops	Navy LWHI	1	1791(INT)	ASTIA-AD 435115	Passed	
2000 AMP	400*	0.75, 1.75 and 1.75 ft. drops	Navy LWHI Shock Machine	1	MIL-S-901	ASTIA-AD 206127	Failed (5 ft. Rear)	The Breaker Tripped
50 AMP	0.5	1, 3 and 5 ft. drops	Navy LWHI Shock Machine	1	MIL-S-901 4A Mounting	ASTIA-AD 67250	Passed	

* Estimated

CONTACTOR

GENERAL DESCRIPTION: 1. Type IFN-630 contactor unit, 3 pole, 600 ampere, 440-volt, AC, 3 phase, 60 cycle, size 6 contactor.
2. Two temperature actuated units of the integral bulb type provided with 3/4-inch male pipe fittings for insertion into pipe fittings in service.

IFN-630	105	1, 3 and 5 ft. drops	Navy LWHI Shock Machine	1	MIL-S-901 4A Mounting	ASTIA-AD 139914	Passed	
Bulb Type	100*	1, 3 and 5 ft drops	Navy LWHI Shock Machine	1	MIL-S-901 4A Mounting	ASTIA-AD20710	Failed 5 ft. Rear	(1)

NOTES: (1) Bending of the sensitive element of the bulb type temperature switch.

*Estimated

CONTROLLER

GENERAL DESCRIPTION:
1. Two speed motor controller at 25 HP, 50 AMP, 440 volt, 3 phase, 60 cps [illegible], double throw contactor, one relay, 2 overload [illegible], start and stop buttons, speed selector, and control switch.
2. Magnetic, size 1, across the line starter designed for 2 or 3 wire control.
3. Manually-operated, across the line motor starter rated at 7-1/2 HP, 440 volts, 3 phase, 60 cps AC.

Type	Approximate Weight (lb)	Test Environment	Test Machine	Number Tested	Test Specification	Report Designation	Result	Type of Failure
25 HP	90	1, 3 and 5 ft. drops	Navy LWHI Shock Machine	1	MIL-S-901 4A Mount	ASWIA-AD 45071	Passed	
7-1/2 HP	29	1, 3 and 5 ft. drops	Navy LWHI Shock Machine	1	MIL-S-901 4A Mount	ASWIA-AD 67242	Passed	
Manually Operated	12	1, 3 and 5 ft. drops	Navy LWHI Shock Machine	1	MIL-S-901 4A Mount	ASWIA-AD 56169	Passed	

DIESEL GENERATORS

GENERAL DESCRIPTION:
1. Two cycle 6 cycle diesel engine and a direct driven, 60 KW generator.
2. Four stroke 1 cycle diesel engine and a 2.5 KW. 115 volt, AC, 60 cycle generator.
3. An air cooled cast aluminum diesel engine directly connected to a 5KW, 28 volt, DC generator.

60KW	3777	1 and 3 ft. drops	Navy MWHI	1	MIL-S-901	ASWIA-AD 204925	Failed (3 ft. up)	(1)
2.5KW	434	1 and 3 ft. drops	Navy MWHI Shock Machine	1	MIL-S-901	ASWIA-AD 201051	Failed (3 ft up)	(2)
5KW	663	1 and 3 ft. drops	Navy MWHI Shock Machine	1	MIL-S-901	AVT-204807	Failed (3 ft. up)	Crack in Flywheel Housing

NOTES: (1) Cracked flywheel housing and severe structural damage to the front support of the engine.
(2) Extreme damage to the mounting pad and front support.

FITTINGS, ENCAPSULATED

GENERAL DESCRIPTION:
1. RG 14A/U encapsulated pressure barrier designated for halibut (SSGN 587).
2. Type 14 AU encapsulated potted fittings for the halibut (SSGN 587).

RG14A/U	6	1, 3 and 5 ft. drops	Navy LWHI Shock Machine	1	MIL-S-901B 4A Mount	Mare Island NavShipYd 5931-59	Passed
14AU	31	1, 3 and 5 ft. drops	Navy LWHI Shock Machine	2	MIL-S-901B 4C Mount	Mare Island NavyShipYd 4317-59	Passed

FUSEBOX

GENERAL DESCRIPTION: A tank indicator fusebox (BSCH 587)

Type	Approximate Weight (lb)	Test Environment	Test Machine	Number Tested	Test Specification	Report Designation	Result	Type of Failure
Tank Indicator	30	1, 3 and 5 ft. drops	Navy LWHI Shock Machine	1	MIL-S-901B 4A Mount	Mare Island NavShipYd 2715-59	Passed	

GEAR MOTOR

GENERAL DESCRIPTION: Gear motor for helicopter lift.

Type	Approximate Weight (lb)	Test Environment	Test Machine	Number Tested	Test Specification	Report Designation	Result	Type of Failure
Gear Motor	232 motor 100 foundation	1, 3 and 5 ft. drops	Navy LWHI Shock Machine	1	MIL-S-901B 4A Mount	Mare Island NavShipYd 04[illegible]-60	Passed	

MOTORS

GENERAL DESCRIPTION: Several reports were reviewed and then grouped into one of two power classes.

0-25HP Class
1. 6HP, 245 V DC Navy A type motor.
2. 15/10 HP, 440V AC motor.
3. 15 HP, 230V DC, Navy A service type motor.
4. 17.5 HP, 440V AC, air conditioning compressor motor.
5. 25 HP 500 V DC, hydraulic power plant on SS563 submarine motor.

25-50 HP Class
1. 30 HP, 250V DC, high pressure air compressor.
2. 30 HP, 355/250V DC, high pressure air compressor motor. SSK1, SSK2, SSK3 motors.
3. 55 HP, 500V DC motor for a trim pump on SS563 submarines.

Type	Approximate Weight (lb)	Test Environment	Test Machine	Number Tested	Test Specification	Report Designation	Result	Type of Failure
0-25 HP	302-625	0.75, 1.75 and 1.75 ft. drops	Navy MWHI Shock Machine *	5	N.D. 6683	EES 5W70001 AD 200998 EES 3A(2) 51832 ADP01042 EES 5UX 1609	1 Failure	(1)
26-55HP	1169-1727	1, 2, and 2 ft. drops	Navy MWHI Shock Machine *	3	N.D. 6683	AD 205025 AD 201028 EES 5AA1 X1609	Passed	

NOTES: (1) The 15HP motor failed one 0.75 foot-back blow. The brush rigging supports broke loose from the insulating ring on the housing of the motor.

* All motor types tested on Navy MWHI shock machines.

GENERATORS

GENERAL DESCRIPTION:
1. 60 KW 240/120 volts, DC, turbine driven generator.
2. 250KW, AC 3 phase 60 cps ship's service generator with 3.5 exciter.

Type	Approximate Weight (lb)	Test Environment	Test Machine	Number Tested	Test Specification	Report Designation	Result	Type of Failure
60KW	2100	1.25, 2.25 and 2.25 ft. blows	Navy MWHI Shock Machine	1	N.D. 6683	EES C-2526-2	Passed	
250KW	3965	1.75, 2.75 and 2.75 ft. blows	Navy MWHI Shock Machine	1	N.D. 6683	EES C-2593	Failed	End Bracket Fractured

MOTOR GENERATORS

GENERAL DESCRIPTION. 1. 1.4KW, [illegible] ator and 1 HP-440 volts AC motor for batte[illegible]ging in ships service dial telephone equipment.
2. 2.8 KW, 56 volt DC generator and 5 HP 440 volt AC motor also for ships service dial telephone equipment.
3. 25KVA, 120 volt generator and 30 HP 220 volt battery.

Type	Approximate Weight (lb)	Test Environment	Test Machine	Number Tested	Test Specification	Report Designation	Result	Type of Failure
1.4KW	315	0.75, 1.75 and 1.75 blows	Navy MWKI Shock Machine	1	M.D. 6663	NRH 5QX 1609	Passed	
2.8KW	501	0.75, 1.75 and 1.75 blows	Navy MWKI Shock Machine	1	M.D. 6683	NRH 5KX 1603	Passed	
25KVA	1320	1, 2 and 2 ft. blows	Navy MWKI Shock	1	MIL-S-901	NRH 5AKX 1609 AD 201040	Passed	

PANELS

GENERAL DESCRIPTION: 1. Air sampler alarm system relay panel.
2. Type B-52 alarm panel.
3. Aft remote control panel for main hydraulic pumps and accum No. 1 and 2.

B-52 Air Sampler, Alarm Sampler	10	1, 3 and 5 ft. blows	Navy LWKI Shock Machine	1	MIL-S-901B 4A Mount	Mare Island NavShipYd 2751-59	Passed	
Type B-52 Alarm	11	1, 3 and 5 ft. blows	Navy LWKI- Shock Machine	1	MIL-S-901B 4A Mount	ASTIA AD206035	Passed	
Control	120	1, 3 and 5 ft. blows	Navy LWKI Shock Machine	1	MIL-S-901B 4A Mount	Mare Island NavShipYd 2750-59	Passed	

PLUG AND RECEPTACLE

GENERAL DESCRIPTION: 1. 3-contact plugs with 3-contact receptacles with triple conductor cable and rated at 15 amps.
2. 3-ten amp plugs and 3-ten amp receptacles. Receptacles are in water tight drawn brass enclosure.
3. Two 40 amp plugs and receptacles in water tight drawn brass enclosures.

15 AMP	2*	1, 3 and 5 ft. drops	Navy LWKI Shock Machine	1	MIL-S-901B 4A Mount	ASTIA-AD 86539	Passed	
10AMP	2.25	1, 3 and 5 ft. drops	Navy LWKI Shock Machine	3	MIL-S-901B 4A Mount	ASTIA AD 86534	Passed	
40 AMP	3.6	1 and 3 ft. drops	Navy LWKI Shock Machine	2	MIL-S-904B 4A Mount	ASTIA-AD 86534	Failed (3 ft. back)	(1)

NOTES: (1) The plug became wedged against the receptacle in such a way that removal was very difficult.

* Estimated

RECTIFIERS

GENERAL DESCRIPTION: Type A selenium rectifier panel for battery charging, designed for 50° C. ambient temperature and is rated at 440V, 3 phase, 60 cycle input with 2-6 Amp DC output.

Type	Approximate Weight (lb)	Test Environment	Test Machine	Number Tested	Test Specification	Report Designation	Result	Type of Failure
Selenium Rectifier	180	1, 3 and 5 ft. drops	Navy LWHI Shock Machine	1	MIL-R-15736 (Bulkhead Mounted)	ASTIA-AD 37551	Passed	

RELAYS

GENERAL DESCRIPTION: Many reports on relays were reviewed. The following is only a brief description.

1. The type IAC time overcurrent relay consists of an induction disk operating mechanism, a set of single-pole contacts and a dust tight sheet steel enclosure. It is used to trip a circuit breaker when over-current conditions occur.
2. The auxiliary relays consisted of a solenoid operating magnet and plunger which is cross-connected to the contact assemblies.
3. Five bulletin 130 auxiliary control relays from 150-440 volts AC coil voltage.

IAC	11.5	1, 3 and 5 ft. drops	Navy LWHI Shock Machine	1	MIL-S-901 6D Mounting	ASTIA-AD 111803	Passed	
Auxiliary	About 4	1, 3 and 5 ft. drops	Navy LWHI Shock Machine	8	MIL-S-901 6E Mounting	ASTIA-AD 139798	2 Failed (Back and top 3 and 5 ft.)	Normally Closed Contacts Opened
Control	1.3 to 4.3	1, 3 and 5 ft. drops	Navy LWHI Shock Machine	5	6683 6E Mounting	Material Lab NY NavShipYd 5225-1	Failed (All Blows)	(1)

NOTES: (1) Malfunction of the electrical contacts.

* Estimated

RESISTORS

GENERAL DESCRIPTION: 1. Fixed, accurate, wire wound resistors from 10-3750 K ohms.
2. Variable subminiature resistors from 100-5,000,000 ohms.

Wire	3*	30 impacts at 50 G's with 0.012 sec. duration	Navy LWHI Shock Machine	1152	Battelle Memorial Institute	Signal Corps Project 2006-A	Passed
Miniature	2*	30 impacts at 50 G's with 0.012 sec. duration	Navy LWHI Shock Machine	40	Battelle Memorial Institute	Signal Corps Project 2006-A	Passed

* Estimated

SWITCHBOARDS

GENERAL DESCRIPTION:

1. The [illegible] sprinkling-alarm switchboard is a [illegible] unit that visually and audibly indicates conditions in remote compartments as reported by sensing elements.
2. The magazine sprinkling alarm switchboard is designed to automatically monitor the operation of the fire fighting sprinkling system installed in the ship's magazines 10 lines.

Type	Approximate Weight (lb)	Test Environment	Test Machine	Number Tested	Test Specification	Report Designation	Result	Type of Failure
Alarm Magazine Sprinkling	100*	1, 3 and 5 ft. drops	Navy MWHI Shock Machine	1	MIL-A-17196A	ASTIA-AD 77815	Passed	
10 Line Alarm	109	1, 3 and 5 ft. drops	Navy MWHI Shock Machine	2	MIL-S-901 4A Mounting **	ASTIA-AD 27734	Failed	False Alarms

* Estimated

** As detected in photograph

SWITCHES, LIMIT

GENERAL DESCRIPTION:

1. Micro limit switch type ML-X[illegible] for the [illegible] guided missile launching system.
2. The D1450 trackway limit switch is rated to carry 20 Amps at 440 volts AC or 230 volts DC.
3. Type A mark 6 limit switches.

Type	Approximate Weight (lb)	Test Environment	Test Machine	Number Tested	Test Specification	Report Designation	Result	Type of Failure
Micro Switch	20*	1, 3 and 5 ft. blows	Navy LWHI Shock Machine	5	MIL-S-901B 6E Mounting	ASTIA-AD 48707	Passed	
Trackway	22	1, 3 and 5 ft. blows	Navy LWHI Shock Machine	3	MIL-S-901 4A Mounting	ASTIA-AD 145797	Passed	
Mark 6	20*	1, 3 and 5 ft. blows	Navy LWHI Shock Machine	6	MIL-S-901B 6E Mounting	ASTIA-AD 139696	Failed	Fluttering and opening of the normally closed circuit

*Estimated

[illegible] ROTARY

GENERAL DESCRIPTION:
1. Six miniature rotary switches. Three contained bushings and shaft seals and the other three were equipped with boots to provide water-tightness.
2. Three type 2JL5 and three type 2JL10 rotary selector switch.
3. Three each of the following: S-2JF1, S2JF3, and S2JF5 rotary switches.
4. One each of rotary switches, type S2JR10 and S2JR25.

Type	Approximate Weight (lb)	Test Environment	Test Machine	Number Tested	Test Specification	Report Designation	Result	Type of Failure
Miniature	5	1, 3 and 5 ft. blows	Navy LWRI Shock Machine	6	MIL-S-901B 4A Mounting	ASTIA-AD 214276	Failed	(1)
Selector 2JL5 and	0.5	1, 3 and 5 ft. blows	Navy LWRI Shock Machine	6	MIL-S-901B 6D Mounting	ASTIA-AD 207729	3 type 2JL5 Failed (5 ft. test) 3 type 2JL10 passed	Shaft Ejected Completely From the Switch
2JL10	1.125							
S2JF1	3.3*	1, 3 and 5 ft. blows	Navy LWRI Shock Machine	9	MIL-S-901B 6D Mounting	ASTIA-AD 207741	Failed (5ft. Test)	Distortion of Components
S2JF3 S2JF5	3.7** 4.25*							
S2JR10	2.3	1, 3 and 5 ft. blows	Navy LWRI Shock Machine	2	MIL-S-901B 7C Mounting	ASTIA-AD 207788	Passed	
S2JR25	4.6							

NOTES: (1) The shaft was ejected from the sample with the bushing and shaft seal.

* Weight in ounces.

SWITCHES, ROTARY SNAP

GENERAL DESCRIPTION:
1. Seven 60 AMP, 450V AC, 250V DC, Type 6SR3A1 Base Mounted rotary snap switches.
2. Seven 60 AMP, 450V AC, 250V DC, Type 6SR3A1 Panel Mounted rotary snap switches.
3. Seven 10 AMP, 120V AC rotary snap switch type 1SR3A1. TPST.
4. Seven 30 AMP, 500V AC, 250V DC, Type 3SR3B4 Base Mounted rotary snap switches.
5. Seven 10 AMP, 120V AC, Type 1SR3B1. TPDT, front mounted for panels with handles.
6. Three each of types 20SR3B1 and 20SR6F1 200 AMP, rotary snap switches that are panel mounted.
7. One type 91740-A5 switch and one type 91741-A5 switch. Both are miniature rotary switches for interior communication equipment
8. Models CA-54, CA-55 and CA-56 rotary solenoid switches for high altitude use.
9. Ten rotary switches of non-magnetic construction were reviewed. "O" ring groove.
10. Four 8 position, 25 section, multipole rotary switches.

Type	Approximate Weight (lb)	Test Environment	Test Machine	Number Tested	Test Specification	Report Designation	Result	Type of Failure
6SR3A1 (Base Mounted)	7.6	1, 3 and 5 ft. blows	Navy LWHI Shock Machine	7	MIL-S-901B 4A Mounting	ASTIA-AD 129390	Passed	
6SR3A1 (Panel Mounted)	5.9	1, 3 and 5 ft. blows	Navy LWHI Shock Machine	7	MIL-S-901B 4A Mounting	ASTIA-AD 129389	Passed	
1SR3A1	0.75	1, 3 and 5 ft. blows	Navy LWHI Shock Machine	7	MIL-S-901B 4A Mounting	ASTIA-AD 129388	Passed	
1SR3B1	0.5							
3SR3B4	2.1	1, 3 and 5 ft. blows	Navy LWHI Shock Machine	7	MIL-S-901B 4A Mounting	ASTIA-AD 129386	Passed	
1SR3B1		1, 3 and 5 ft. blows	Navy LWHI Shock Machine	7	MIL-S-901B 4A Mounting	ASTIA-AD 206102	Passed	
20SR3B1	1*	1, 3 and 5 ft. blows	Navy LWHI Shock Machine	2	MIL-S-901 4C Mounting	ETL-1367 Electrical Testing Lab Portsmouth, N.H.	Passed	
20SR6F1								
91740-A5	1.5	1, 3 and 5 ft. blows	Navy LWHI Shock Machine	2	MIL-S-901B 4A Mounting	ASTIA-AD 214227	Failed	Porcelain Spacer Fractured
91741-A5								
CA-54	2	200	Navy LWHI Shock Machine	3	JAN-S-44	ASTIA-AD	Passed	
CA-55	2							
CA-56	5							
Non-Magnetic	7*	1, 3 and 5 ft. blows	Navy LWHI Shock Machine	10	MIL-S-901B 6D Mounting	ASTIA-AD 209987	Failed	Mounting Plate Buckled
A-384-5WA	7*	1, 3 and 5 ft. blows	Navy LWHI Shock Machine	2	MIL-S-901B 6D Mounting	ATI-195747	Passed	
Multipole	7*	1, 3 and 5 ft. blows	Navy LWHI Shock Machine	4	MIL-S-901B 6D Mounting	ATI-210276	Passed	

* Estimated

SWITCHES, TOGGLE

* GENERAL DESCRIPTION: 1. Eighteen basic toggle switches, type T2104, are miniaturized two circuit switches designed for use in applications where panel space is at a premium.

2. Environmental-proof multipole, multiposition, toggle switch.

* 3. 20 different types of toggle switches.

Type	Approximate Weight (lb)	Test Environment	Test Machine	Number Tested	Test Specification	Report Designation	Result	Type of Failure
T2104	0.5*	75G	Navy LWHI Shock Machine	18	JAN-S-23	ASTIA-AD 111723	Passed	
Environment Toggle Switch	0.24	500 for 0.5-9.7 sec Duration	Navy LWHI Shock Machine	1	AER-EL-62 XE-126 AN-5-200	ASTI-96739	Failed	Momentary Opening of Contacts
Toggle Switches	0.5 ea.	1, 3 and 5 ft. blows	Navy LWHI Shock Machine	20	MIL-S-901B 6D Mounting	ASTIA-AD 214225	Failed	

* Estimated

SWITCHES MISCELLANEOUS

GENERAL DESCRIPTION: 1. Five temperature-operated master switches and six pressure-operated automatic master switches.
2. 1 - stepping switch, 20 VAC, Type 58-2.
3. 8 switches each of types D8-4 (15 AMP at 125/250 VAC) B3-204, B1-4 (10A at 125/250 VAC) E3-4 (2.5A and 5A at 125/250 VAC, and 7 type B2-104 switches (10A at 125/250 VAC).
4. 40 hinge roller leaf type sensitive switches SSO7A10, SSO7A20, SSO7B40, and SSO7B70.
5. Two sample pressure proof IMC-7MC switches were accomplished by use of a phosphor bronze diaphragm. They were pierced ant 50 ft. soldered to a brass actuator rod.

Temperature and Pressure Operated Switches	2.2	1, 3 and 5 ft. blows	Navy LWHI Shock Machine	11	MIL-S-901 6E Mounting	ASTIA-AD 36805	Passed	
Stepping Switch	5*	1, 3 and 5 ft. blows	Navy LWHI Shock Machine	1	MIL-S-901B 6E Mounting	ASTIA-AD 59337	Failed	Cam Forced Out of Position
B3-204	1* each	1, 3 and 5 ft. blows	Navy LWHI Shock Machine	8	MIL-S-901B 6E Mounting	ASTIA-AD 48789	Failed	(1)
B2-104								
Roller Leaf	3 each	1, 3 and 5 ft. blows	Navy LWHI shock Machine	32	MIL-S-901A 6 E Mounting	ASTIA-AD 2,60[illegible]	Passed	
Pressure-Proof	9.8	1, 3 and 5 ft. blows	Navy LWHI Shock Machine	2	MIL-S-901B 4A Mounting	ASTIA-AD [illegible]	Failed	Diaphragm Revealed Leakage

NOTE: (1) Transfer contacts of each switch made contact with the normally open contact of its respective switch.

*Estimated

[illegible]

GENERAL DESCRIPTION: The elements were the disk, bead, or rod shape type.

Type	Approximate Weight (lb)	Test Environment	Test Machine	Number Tested	Test Specification	Report Designation	Result	Type of Failure
Elements	½*	30 impacts at 50 G's for 8 to 12 millisec duration	Navy LWKI Shock Machine	102	FR ser C No. 59-FLB/ D-3431	Signal Corps Project 2006-A	Passed	

* Estimated

VOLTAGE SENSITIVE ELEMENTS

GENERAL DESCRIPTION: 80 specimens were tested. The specimens differed from one another in material (plastic, glass, or metal), shape (tubular or disk), and mounting (by soldering, clamping, or bolting).

Elements	Below 1 *	30 impacts at 50 G's each impact applied for 8 to 12 millisec.	Navy LWKI Shock Machine	80	Battelle Memorial Institute	Signal Corps Project No. 2006-A	Passed	

* Estimated

4.5 Human Shock Tolerances

4.5.1 Introduction

In the operation of most underground protective structures, there are some functions which demand the presence of human beings. Thus, the tolerance of human beings to shock becomes a subject of importance to the isolation system designer in determining the attenuation requirement of areas housing personnel. For this application, human shock tolerance is defined broadly as the level of shock which a person may withstand without impairing his ability to perform essential duties. In some cases, the critical level of shock may be that which produces injury directly, and in others that which causes the man to fall down, indirectly exposing him to injury. Implicit in the shock tolerance, then, is the "mode-of-failure".

Most of the later underground protective structures are designed to withstand ground shocks of sufficient strength to necessitate shock protection for all personnel. Thus, the personnel are exposed most frequently, not to the complex motion of the ground, but to the nearly sinusoidal damped oscillation of the isolated platform or other supporting device. Further, the basic design criteria for many facilities specify that the personnel shall be assumed to receive no warning of attack and, therefore, may be occupied by any of their normal functions at the instant the shock occurs.

The environments to which the tolerance of human beings is of primary interest to the isolation system designer, then, are:

- Tolerance to motion typical of ground (shock)
- Tolerance to motion typical of soft shock isolated platforms (low frequency vibration)

In each case significant parameters are the degree of support provided the personnel, the direction of motion and the warning time.

To date there have been no tests of human subjects designed specifically to determine their tolerance to shock in environments typical of those encountered in underground protective structures. It is necessary therefore to draw heavily on results obtained for other applications. The principal limitations of the experimental data presently available are:

The conditions of restraint used in obtaining the data were generally more extensive than those permitted by USAF for personnel in underground protective structures.

- The characteristics, including direction, of the applied acceleration usually deviated considerably from those expected in underground protective structures.
- The subjects were prepared to resist shock.
- The definitions of tolerance used by different investigators varied from perception, through anxiety to unbearable pain. None reviewed considered incapacity as the survival criterion.

4.5.2 Basis for Design in Existing USAF Facilities.

Both experimental and analytical data on which to base human shock tolerances for existing underground protective structures were and still remain extremely limited. Although the operating command may define qualitatively the mode of failure, the translation of this criterion to peak permissible accelerations, frequencies and other significant parameters of the motion must rely heavily on opinion.

In the Figure 4.5.1, the maximum accelerations for personnel areas are shown for several weapon system facilities.

Weapon System	Maximum Acceleration in Personnel Areas, g	
	Vertical	Horizontal
Atlas Silo	1.5	0.125
Atlas Control Center	"...mounted to reduce ground shock without impairing operational ability"	
Titan II (Criteria)	3.0	3.0
(Initial Design)	2.4	0.5
(Revision)	0.5	0.5
Minuteman (Criteria)	1.0 (down) 3.0 (up)	1.0
(Design)	0.5	0.15

Figure No. 4.5.1

Although the natural frequencies of the personnel support systems are not indicated in the table, in all cases they are less than one cycle per second. Similarly, the mode of failure in all cases is based on impairment of operational capability of all personnel, some of whom may be standing unsupported and may be unprepared. The downward trend in peak accelerations believed to be necessary to achieve the desired protection is clearly indicated by the differences between those specified by early design criteria and those used in final design of the Titan II and Minuteman facilities.

It should be noted that all the suspension systems indicated are pendular and that the maximum horizontal acceleration is fixed more by the practical aspects of the pendulum design than by a human shock tolerance.

In this subsection some of the studies on which the final design values for the Minuteman facility were based are discussed briefly.

4.5.3 Summary of Applicable Human Tolerance Studies

Murfin (Ref. 4-19) at Space Technology Laboratories was one of the first to attempt to apply the results of existing work in human shock tolerances to the special environments encountered in underground protective structures. He found the most pertinent data to be those of Ziegenruecker and Magid (Ref. 4 - 20), who determined the tolerance of seated subjects to vertical harmonic vibrations, and of Eiband (Ref. 4 - 21), who reported the results of similar tests where the shock input was a trapezoidal acceleration pulse.

The significance of Eiband's work to this application is that it establishes tolerance limits to shocks which might be considered as representative of the ground motion. In all tests the seated subject was well supported with lap and shoulder straps. For tests in which the direction of the acceleration was headward, the subject was further protected by a soft leather cushion and for tailward accelerations he was given a lap belt tie-down strap. The chair in which the subject was seated was structurally rigid and was attached firmly to the floor. The subject was given a warning 20 to 30 seconds prior to the test. The acceleration pulse was roughly trapezoidal and was described by three parameters: rate of onset, duration, and magnitude.

A few of Eiband's results are presented in Figures 4.5.2 through 4.5.5. In Figure 4.5.2 tolerance to headward acceleration is shown as a function of the magnitude and duration of the acceleration pulse. It may be noted that the limiting acceleration to avoid any injury is only about 16 g's even though the subject is well supported. If the personnel are seated upright, ground shock accelerations in this direction can result either from a Type II wave or from the acceleration portion of the airblast- or cratering-induced (Type I) waves.

Figure 4.5.3 shows the tolerance to tailward acceleration as a function of magnitude and duration of the acceleration pulse. Here the peak tolerable acceleration is reduced to about 10 g's in the area of interest.

Similar data were obtained by Eiband for spineward and sternumward shocks and are shown in Figures 4.5.4 and 4.5.5. For these cases the peak accelerations were increased to about 45 and 35 g's respectively. Thus, by facing the subject in the direction from which the strongest ground shock is expected, some increase in tolerance can be achieved.

Tolerance curves for conditions of less than optimum restraint will most certainly be well below those shown in the Figures. The accelerations reported were those measured on the test seat, not at the body location which determined tolerance. The effect of rate of onset of acceleration was not clear-cut.

For spineward accelerations, Eiband noted that the absence of thigh straps lowered the tolerance level shown in Figure 4.5.4 by a factor of about 2.5 to 3.0, and all exposures above 18 g's were intolerable. The benefits of thigh straps were attributed to their preventing headward rotation of the lap strap, which if held on the pelvis will apply the major portion of the accelerating force to the pelvic-girdle instead of the soft abdominal region. Shoulder straps were used in both instances.

Voluntary tolerance to sternumward acceleration is believed to equal that for spineward acceleration, although sternumward test exposures were not as severe in magnitude or duration as for the spineward tests. Again, maximum restraint was applied. Were the head and neck not restrained, "whiplash" would likely be a limiting factor for tolerance to rapidly applied sternumward acceleration. The feet and thighs should be restrained to prevent the feet from flying up or back behind the seat, causing the subject to rotate toward a slouching position and the acceleration force to be applied to the spine instead of the pelvis.

No tests were recorded for acceleration applied from either sideward direction.

For the Minuteman facilities in which Murfin was principally interested, Eiband's results were not applicable, since not only were the tolerable accelerations exceeded, but also Minuteman criteria did not permit artificial supports to be used. The data of Ziegenruecker and Magid were then examined, since the harmonic oscillations they employed in their tests approximated more closely the motion of a shock isolated platform. However, here again, the subjects were seated, given warning of the shock, and provided varying degrees of support.

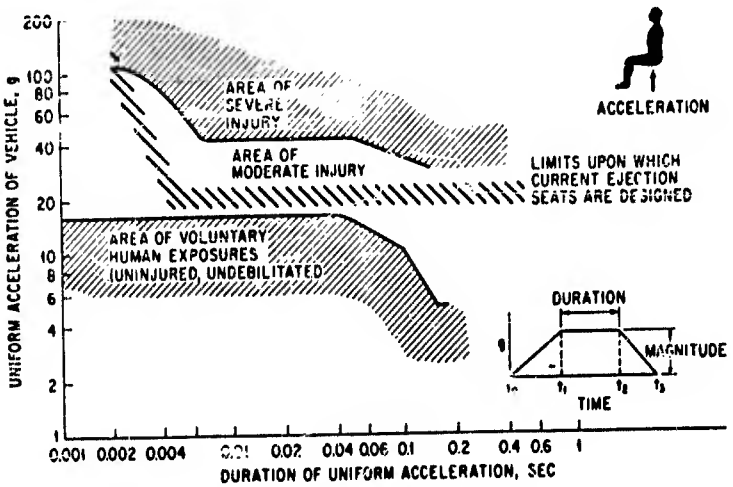

Figure 4.5.2

Tolerance to Headward Acceleration
as a Function of Magnitude and Duration
(Reference 4.22)

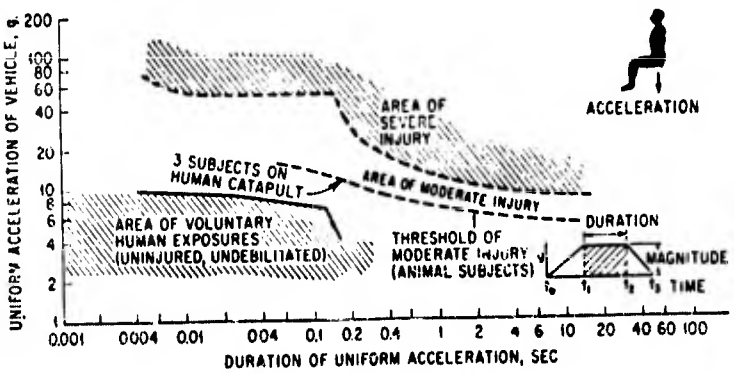

Figure 4.5.3

Tolerance to Tailward Acceleration
as a Function of Magnitude and Duration of
Impulse (Reference 4.22)

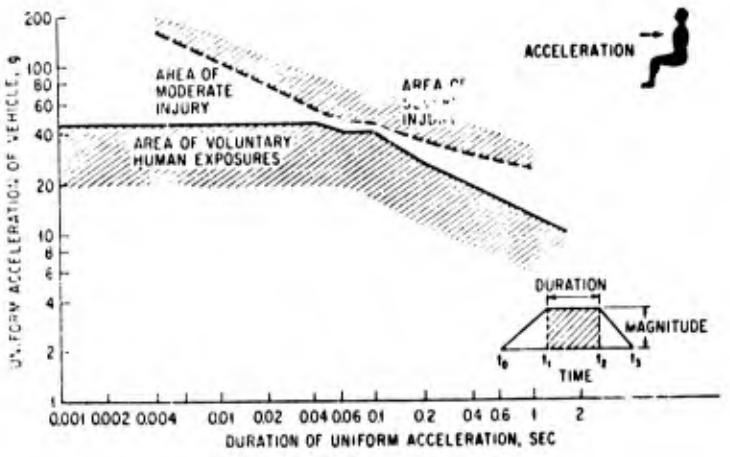

Figure 4.5.4

Tolerance to Spineward Acceleration
as a Function of Magnitude and Duration of Impulse
(Reference 4.22)

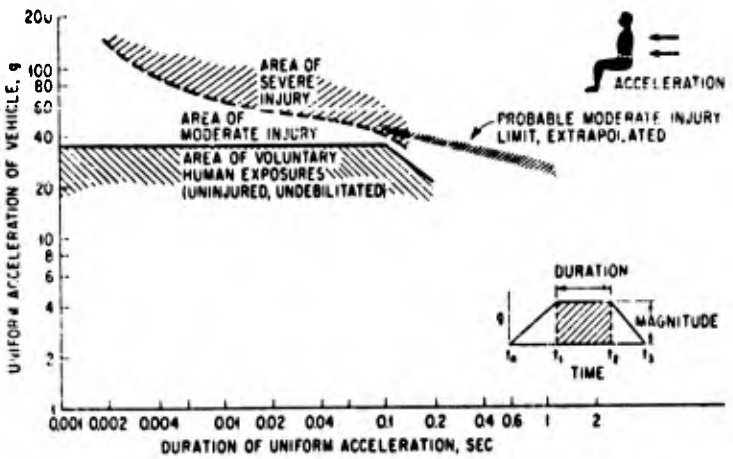

Figure 4.5.5

Tolerance to Sternumward Acceleration
as a Function of Magnitude and Duration of Impulse
(Reference 4. 22)

The tolerance limits of a seated human being to short duration vertical harmonic vibration are shown in Figure 4.5.6 as a function of frequency. The indicated accelerations are those which the subjects refused to tolerate further, although reference 4 - 22 suggests that the curve must be considered the borderline beyond which physical tissue damage occurs in a relatively short time. Also shown in the figure are the exposure times in seconds at the corresponding frequency. The subjects were strapped in an airplane seat with seat belt and shoulder harness.

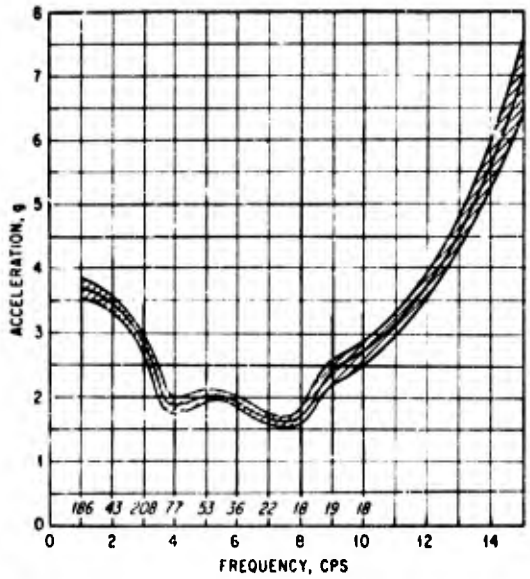

Figure 4.5.6: Peak acceleration at various frequencies at which subjects refuse to tolerate further a short exposure (less than 5 minutes) to vertical vibration. The figures above the abscissa indicate the exposure time in seconds at the corresponding frequency. The shaded area has a width of one standard deviation on either side of the mean (10 subjects). (Ref 4 - 20).

The accelerations given in Figure 4.5.6 must be used with caution, for even though the subjects were partially supported, their extremities were still free to flail. Williams (Ref. 4 - 23) points to the danger of not providing enough restraint for the extremities and notes that injuries in aircraft and car accidents frequently stem from whiplash, flailing of extremities, dislodgment, crushing, falling and impact against sharp objects, rather than high acceleration.

Despite the value of these investigations in providing tolerance data on seated and restrained subjects, these conditions cannot be accepted in some protective structures, for example, those of the Minuteman. Insofar

as the magnitude of accelerations transmitted to the various parts of the body are concerned, some very qualitative indications may be obtained from transmission curves such as those obtained by Dieckmann and by Radke (Ref. 4.24 and 4.25) and shown here in Figures 4.5.7 through 4.5.9. These figures indicate the ratio of acceleration transmitted from an oscillation table to various parts of the subjects body. Data are given both for seated and standing subjects and for horizontal and vertical oscillations.

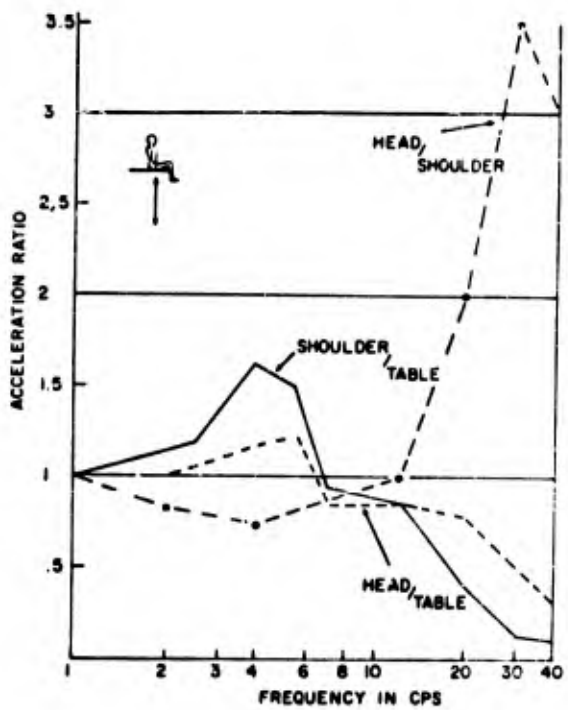

Figure 4.5.7: Transmission of longitudinal vertical vibration from table to various parts of body of seated human subject (after Dieckmann).

In an effort to establish some broad guidelines which might be used as a basis for design in the Minuteman project, Crede (Ref. 4 - 26) considered analytically a highly simplified model. The problem is an extremely difficult one to formulate mathematically. Injury to the subject is most likely to occur as a result of his losing balance and falling rather than from excessive axial strain. Further, falling itself may not produce injury unless a critical part of the subject strikes a rigid or sharp object.

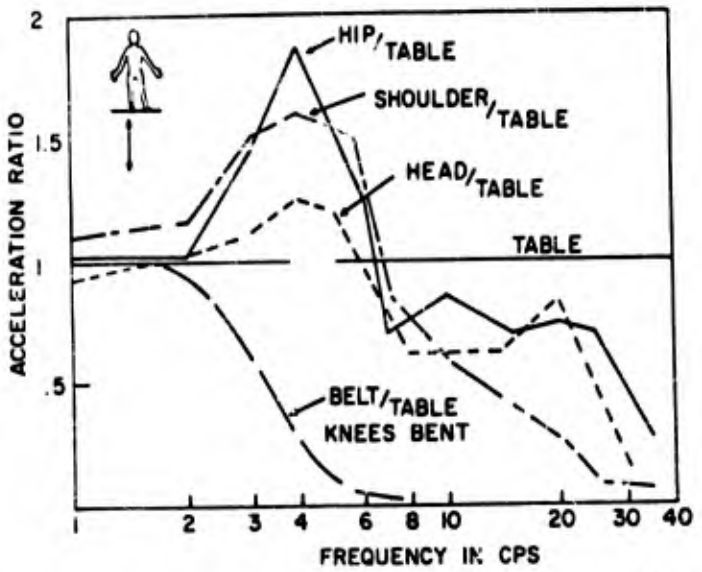

Figure 4.5.8: Transmission of vertical vibration from table to various parts of the body of a standing humar subject (Reference 4.24), data for transmission to belt from Reference 4.25.

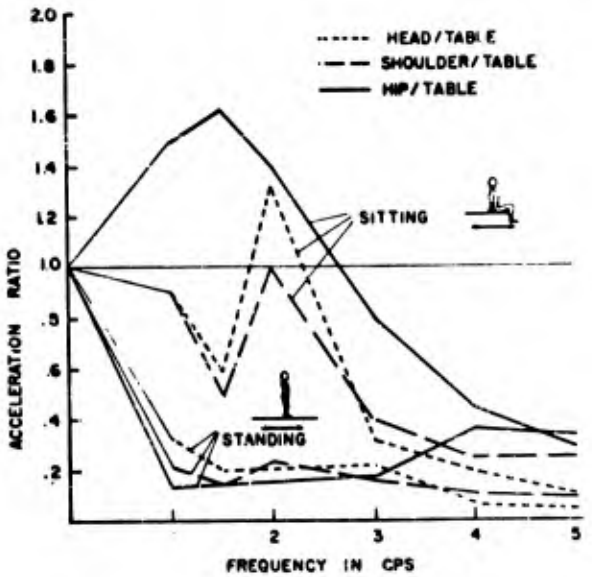

Figure 4.5.9: Transmission of transverse, horizontal vibration from table to various parts of sitting and standing human subject (Reference 4.24).

Other factors whose effects are equally difficult to evaluate are the feedback through both voluntary and involuntary muscular reaction, the direction of line of action of the acceleration force through the subject's center of gravity, and the initial position and motion of the subject.

Despite these formidable obstacles to analysis, design data were needed urgently. Crede portrayed the subject as a simple undamped mass-spring system supported by a platform. He then postulated that injury would be sustained by the subject if he lost contact with the platform. Crede first considered a case where the platform was accelerated suddenly downward at some constant value less than one gravity. He then showed that if the downward acceleration exceeded one-half gravity, the peak amplitude of the relative motion of the subject and the platform would exceed the static displacement of the subject; ergo, the subject would fall down.

As a second case, Crede assumed the platform was supported by an elastic element from a roof which was accelerated suddenly downward. He then calculated the relative motion of the subject and the platform and, assuming the natural frequency of the subject to be in the order of or larger than 10 π radians the second (ref. 4 . 22), showed that the natural frequency of the platform is limited by the following relationship if the subject is to remain in contact with it:

$$\omega_p \leq \frac{g}{v_o}$$

where ω_p = natural circular frequency of platform, rad/sec.

g = acceleration due to gravity, feet/sec^2

v_o = initial downward velocity of the roof, fps.

It is evident that the natural frequency of the platform, as computed by the above equation, will be very low for many practical installations, and in the Minuteman facilities a slightly higher value was used in design. It would be remarkable indeed in view of the many simplifying assumptions, if either of Crede's results yielded accurate predictions of the limits of stability of a human being. Even if they were accurate, there is no assurance that simple loss of stability would result in physical damage. Nonetheless they are and should continue to be useful in indicating the order of magnitude of tolerance until more appropriate experimental data become available.

4.5.4 Design Procedure

Except for those cases where all essential personnel are well-restrained and seated, there is little quantitative information on which to base design recommendations. In general, however, it can be assumed

that in almost all installations some shock protection for personnel will be necessary. Thus, the motion to which the personnel will be subjected can be defined broadly as a nearly harmonic oscillation, damped to negligible amplitude in not more than about 60 seconds. The specification of harmonic motion, of course, implies that the peak upward acceleration is equal to the peak downward acceleration and that the peak horizontal acceleration will be equal from all radial directions.

One significant difference in the service environment from that of most tests is that in practice the supporting platform usually oscillates vertically and horizontally simultaneously. The extent to which a concurrent lateral oscillation would influence the human tolerances shown in Figure 4.5.6 , for example, is not known. For estimating the tolerance of human beings to combined vertical and horizontal accelerations for aircraft conditions, reference 4. 27 recommends the use of an "elliptic g-function". The function is shown in Figure 4.5.10 where the maximum tolerable vertical and radial accelerations are represented by the major and minor semi-axes of the ellipse. The ellipse, then, represents the maximum tolerance of the human being to any combination of vertical and radial acceleration.

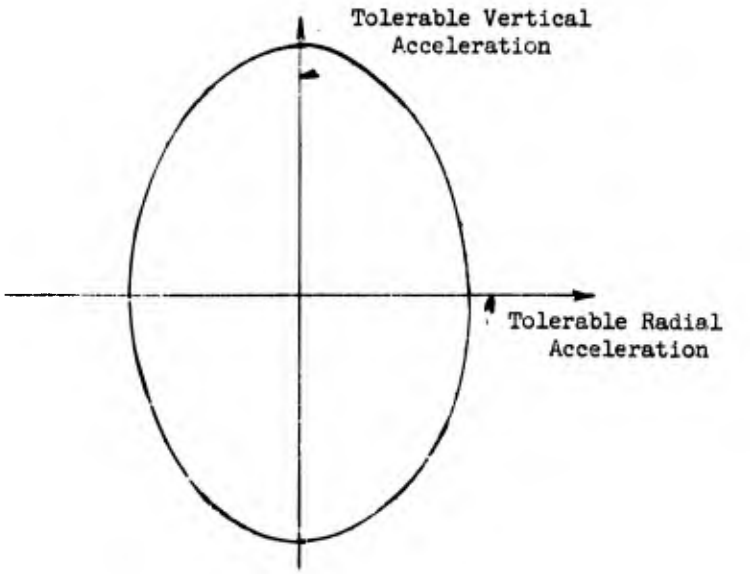

Figure 4.5.10: Elliptic g-Function for Human Acceleration Tolerances

The elliptic g-function probably predicts with acceptable accuracy the interaction effects on seated and restrained subjects. It is equally probable, however, that it does not truly represent the highly nonlinear interactions one would expect to occur in the case of a standing, unsupported subject.

While in each design case the entire problem of protection for personnel must be considered from the viewpoints of facility mission, shock environment, and modes of failure, the peak accelerations shown in Figure 4.5.11 are suggested tentatively as guidelines.

Direction	Maximum Acceleration (g)	
	Seated and Well-Restrained	Standing Without Support
Vertical	1.75	0.75
Radial	1.75	0.50

Figure 4.5.11

The values finally selected for vertical acceleration with the subject standing without support should also be compared with those given by Crede's analysis.

4.6 Selection of Low Frequency Isolator System Characteristics

The decision regarding the need for shock isolation to prevent equipment damage can be based on a simple comparison of the spectrum of the greatest shock survived by the equipment during test with the spectrum of the service environment. The equipment can be considered as being sufficiently strong to withstand the service environment without shock protection if the test spectrum envelopes the service spectrum at all frequencies. Conversely, if the test spectrum does not envelop the service spectrum at all frequencies, the equipment will require added protection.

If the test spectrum is not known directly but the tests have been conducted on a standard machine for which the test conditions can be determined, information relating the machine and the response spectrum it produces can be obtained from Section 3.2 or from the machine's manufacturer. As noted earlier, the general type of wave form produced by the machine should also be compared with that expected in service.

In many cases the make and model of the equipment will not be known at the time the isolation system is being designed. Test information on the general type of equipment, such as that given in Section 4.4, must then be relied on to indicate the level of tolerable shock. The error introduced by this approximation may be sizeable. However, the risk is not in the failure of the equipment in service, but in establishing a shock tolerance which is so high that commercial grade equipment is not acceptable, and special, more expensive equipment must be procured.

The environment to which the equipment needing shock isolation will be exposed is defined by the spectrum of the motion of the equipment-isolator assembly rather than by the spectrum of the ground shock. Since the isolator has not been selected at this phase of the design, the motion of the assembly is not known. It therefore becomes necessary to formulate a procedure by which a reasonable approximation can be made.

A procedure is recommended here for determining the isolator characteristics necessary to yield a response spectrum of the motion of the isolated mass such that the spectrum will be lower for all frequencies than that of a given test spectrum. The assumption is made that the natural period of the isolator-platform system is large relative to the time interval during which the ground motion occurs. This assumption is necessary only to maintain the rigor of the analysis. For practical purposes the natural period of the isolator could be substantially smaller.

Consider a motion of the ground, or hard-mounted structure, as defined by: the velocity time-history shown in Figure 4.6.1, the displacement time-history shown as curve (a) of Figure 4.6.2, and the response spectrum shown in Figure 4.6.3. The motion of the shock-mounted equipment package then will be approximately as shown by

curve (b) of Figure 4.6.2. The maximum displacement, x_{max}, indicated in the Figure corresponds to a point on the response spectrum at a frequency equal to the natural frequency of the isolator.

Figure 4.6.1

Velocity-Time History of Hard Supporting Structure

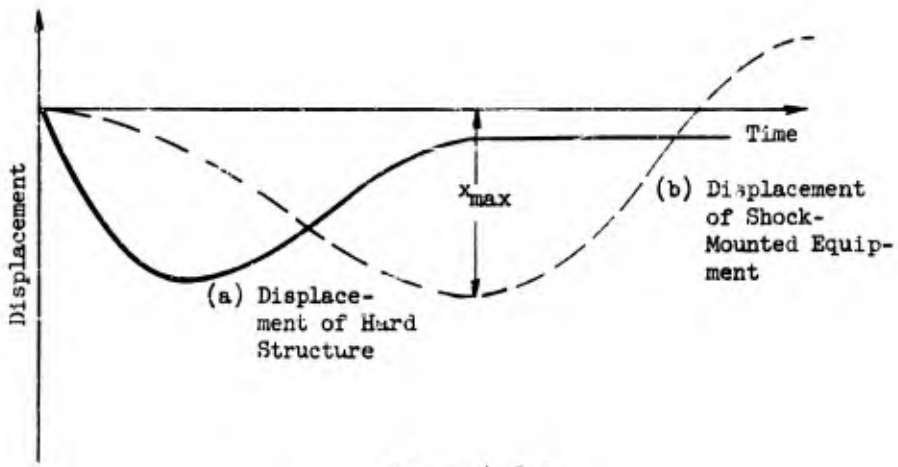

Figure 4.6.2

Displacement-Time History
of
Hard Supporting Structure and Shock-Mounted Equipment

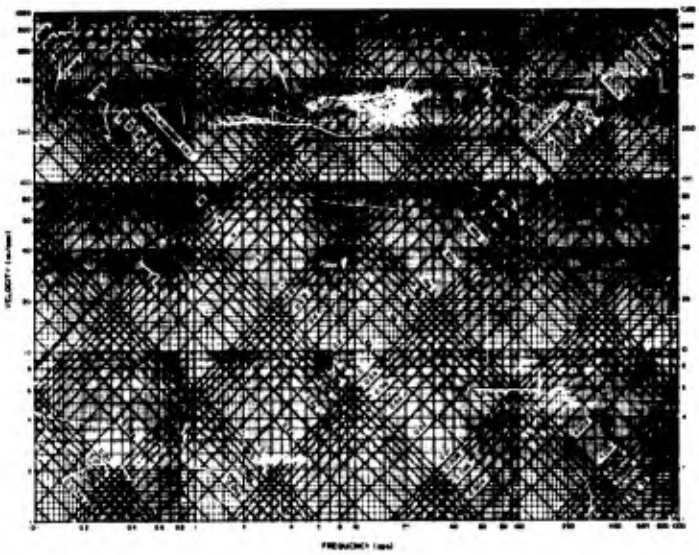

Figure 4.6.3
Undamped Response Spectrum for Shock Motion
of
Hard Supporting Structure

To obtain a response spectrum of the platform motion indicated by curve (b) in Figure 4.6.2, the work of Mindlin (Reference 4.28) may be used. The system investigated by Mindlin is shown in Figure 4.6.4, page 4-76 . The entire assembly was assumed to approach the ground at a known velocity and the large mass, m_3, to impact inelastically with the ground.

For this application, the mass m_3 is considered as the hard structure supporting the isolated equipment; the m_2k_2 system as the isolated equipment; and by varying k_1 the m_1k_1 system as an analyzer of the spectrum of the motion of m_2.

This displacement-time history of the mass m_2 is shown in Figure 4.6.5. The time history of acceleration of m_2 is quite similar to the acceleration-time history associated with the curve (b) in Figure 4.6.2. Therefore their spectra are similar.

If the natural frequency of the m_2k_2 system of Figure 4.6.4 is taken equal to the natural frequency of the isolator, and conditions are adjusted so that the maximum displacements, x_{max}, of Figures 4.6.5

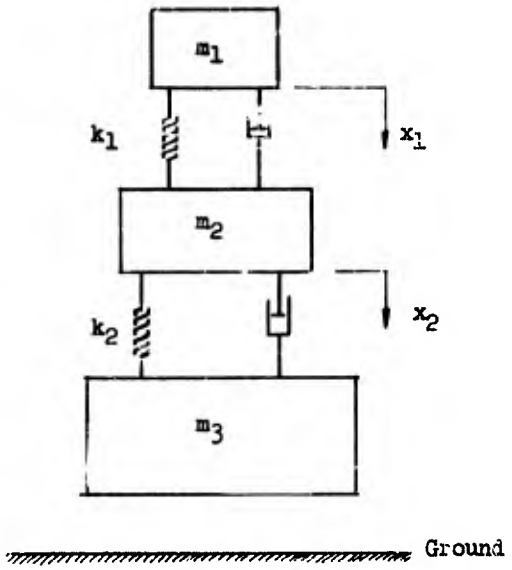

Figure 4.6.4
System Investigated by Mindlin

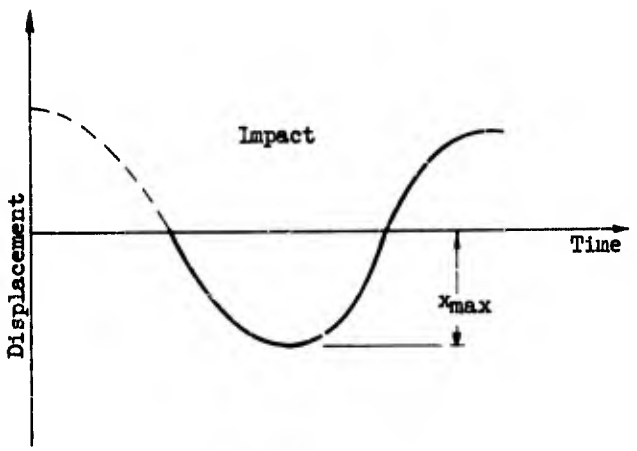

Figure 4.6.5
Displacement-Time History of Mass, m_2

and 4.6.2 are equal, then the ratios of $\ddot{x}_1/\ddot{x}_2$ given by Mindlin can be used to obtain a response spectrum for the output motion of m_2. Curves of Mindlin's results are shown in Figures 4.6.6 through 4.6.11, page 4-78 through 4-80.

As an example, assume the isolator to have a natural frequency ω_2 of one cycle per second where

$$\omega_2 = \sqrt{\frac{k_2}{m_2 + m_1}}$$

But since $m_2 >> m_1$,

$$\omega_2 \cong \sqrt{\frac{k_2}{m_2}}$$

From the response spectrum of the motion of the hard supporting structure (Figure 4.6.3) the maximum acceleration is seen to be 1.0 g. The response spectrum of the motion of m_2 is then obtained by plotting $\ddot{x}_1$ as a function of ω_1 where

$$\omega_1 = \sqrt{\frac{k_1}{m_1}}$$

In Mindlin's curves, the acceleration amplification ratio $\ddot{x}_1/\ddot{x}_2$ is plotted as a function of the frequency ratio ω_1/ω_2 and the independent parameters β_1 and β_2 used.

The damping ratio β_1 is that of the m_1k_1 "spectrum analyzer" system and should be set to match the damping ratio of the test spectrum. Frequently the test spectra do not indicate the damping ratios used, but since almost all these spectra are computed using very small or zero damping ratios, a value of $\beta_1 = 0.005$ should be satisfactory. The damping ratio for the m_2k_2 isolation system can be set at will by the designer inasmuch as it is the amount of damping he has built, or intends to build, into his system.

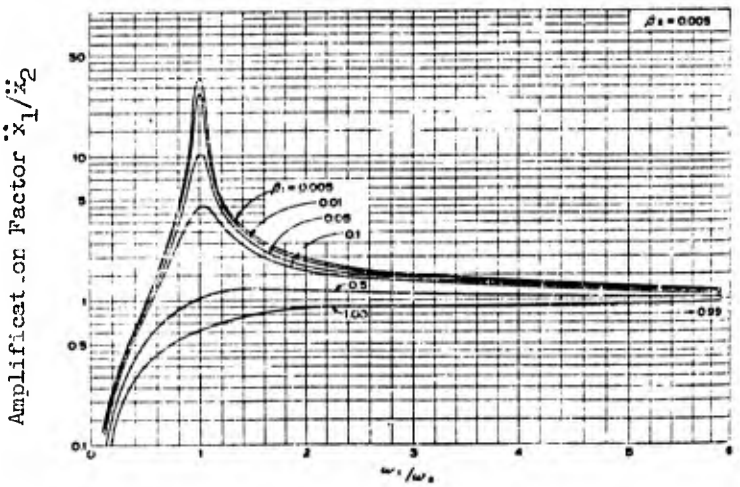

Figure 4.6.6
Amplification Factors for Linear Damped Cushioning with no Rebound. $\beta_2 = 0.005$

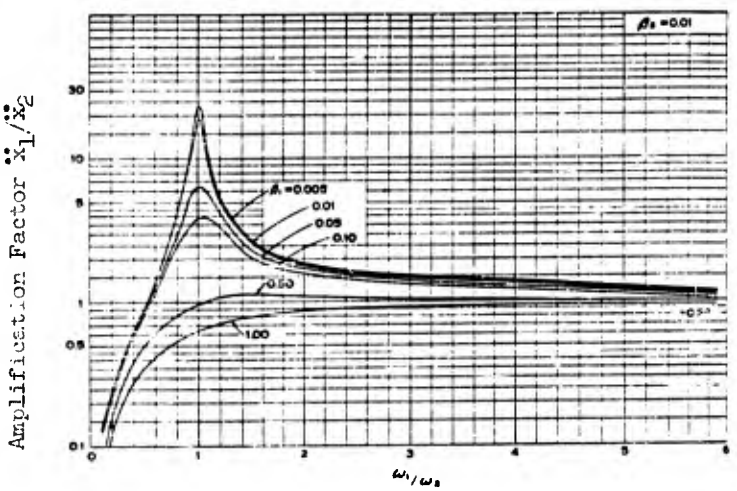

Figure 4.6.7
Amplification Factors for Linear Damped Cushioning with no Rebound. $\beta_2 = 0.01$

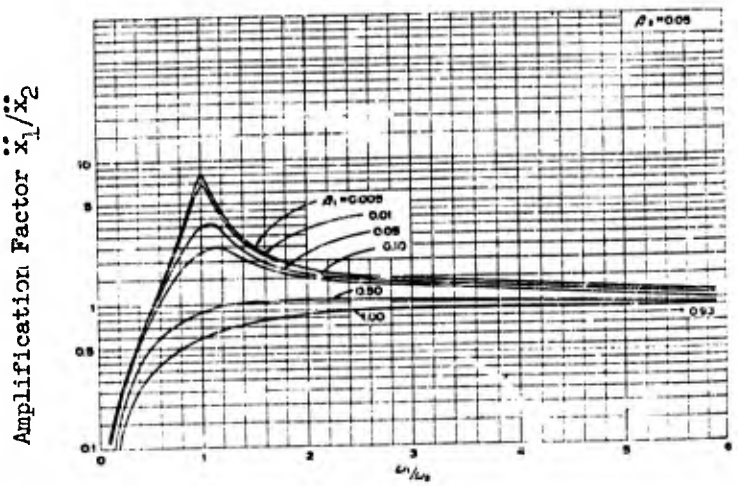

Figure 4.6.8

Amplification Factors for Linear Damped Cushioning with no Rebound. $\beta_2 = 0.05$

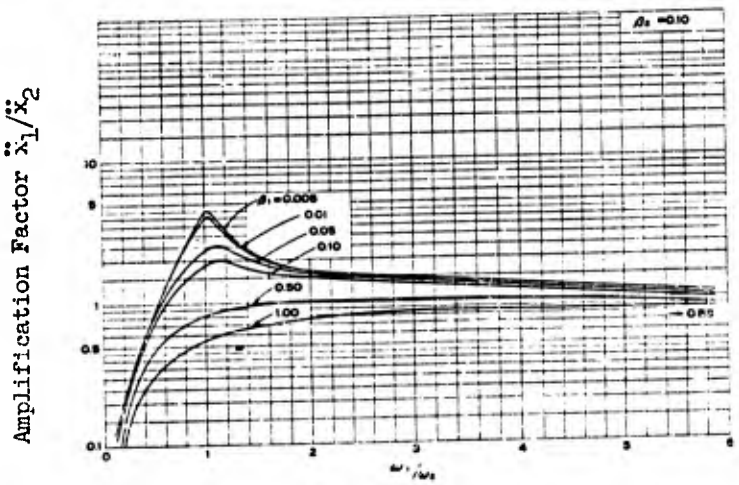

Figure 4.6.9

Amplification Factors for Linear Damped Cushioning with no Rebound. $\beta_2 = 0.10$

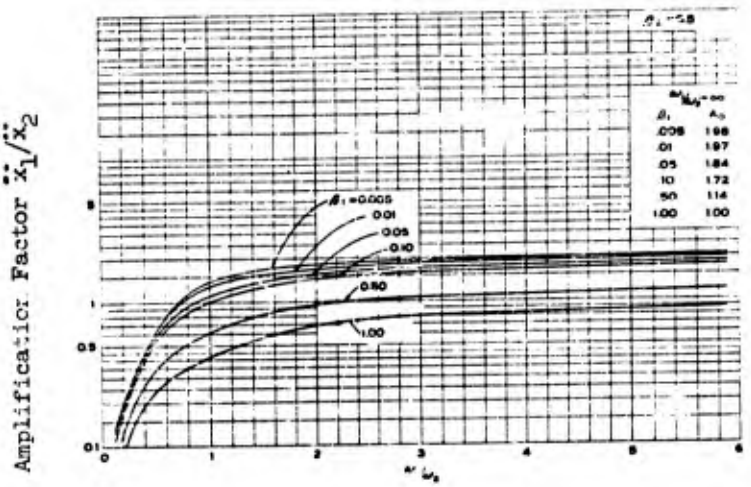

Figure 4.6.10

Amplification Factors for Linear Damped Cushioning with no Rebound. $\beta_2 = 0.50$

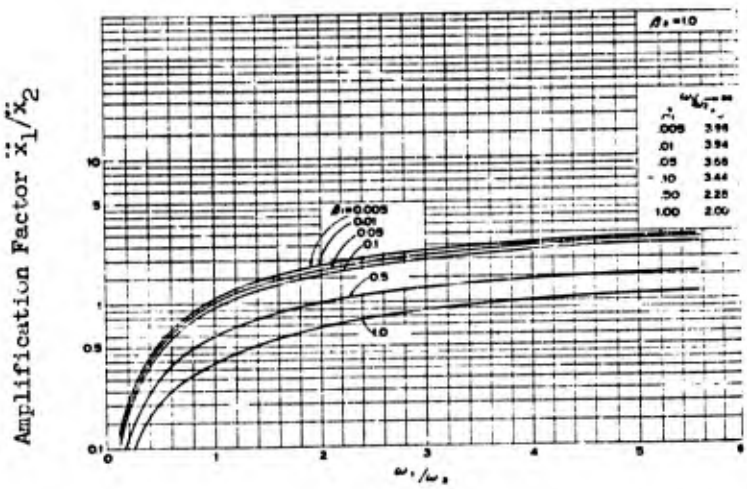

Figure 4.6.11

Amplification Factors for Linear Damped Cushioning with no Rebound. $\beta_2 = 1.0$

For the example, assume $\beta_1 = 0.005$ and $\beta_2 = 0.10$. Then, varying the "spectrum analyzer" frequency ω_1, the following values are obtained for $\ddot{x}_1$ from Figure 4.6.9:

	ω_1 (cps)							
	.4	.6	.8	1	2	3	4	5
ω_1/ω_2	.4	.6	.8	1	2	3	4	5
$\ddot{x}_1/\ddot{x}_2$	.6	1.35	2.5	4.5	1.6	1.5	1.35	1.20
$\ddot{x}_1$ (g)	.6	1.35	2.5	4.5	1.6	1.5	1.35	1.20

These values of $\ddot{x}_1$ are plotted as curve (a) in Figure 4.6.12, (see below), giving the response spectrum of the isolated equipment motion. This spectrum then must be enveloped by the test spectrum of the equipment if survival is to be ensured. If the equipment response is not enveloped by the test spectrum, or if it is too conservative, a new value of ω_2 is selected and a new response spectrum calculated in the same manner. For example, curve (b) of Figure 4.6.12 shows the response spectrum for $\omega_2 = 5.0$ cps.

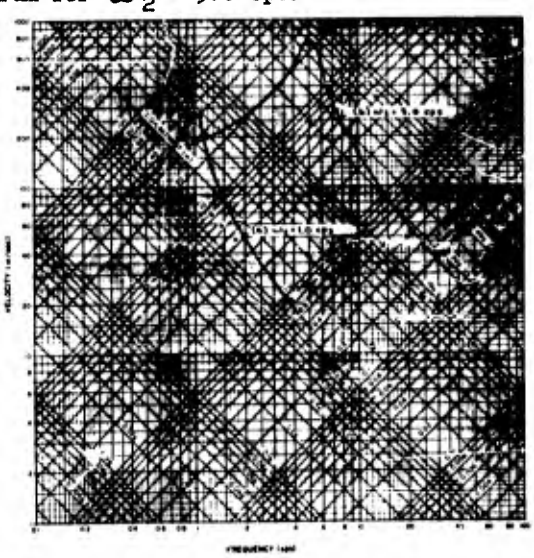

Figure 4.6.12
Response Spectra of the Motion of the Mass m_2 where $\omega_2 = 1.0$ cps and 5.0 cps, and $\ddot{x}_2 = 1.0$ g

SECTION 4.0 REFERENCES

4.1 Crede, C. E.
The Simulation of Shock and Vibration Environments
Proceedings, Society for Experimental Stress Analysis, Vol. XVII No. 1. 1957

4.2 Crede, C. E.
Concepts in Shock Testing Equipment
Colloquium on Shock and Structural Response, ASME. August 1960

4.3 Vigness, I.
Shock Testing Machines
Shock and Vibration Handbook, Vol. 2, Ch. 26. McGraw-Hill Book Company, Inc., New York. 1961

4.4 ASTM Standards
Part 7, page 1087. 1955

4.5 Matlock, H., Ripperberger, E. A., Turnbow, J., and Thompson, J. N.
Drop-Test Facilities and Instrumentation
Shock and Vibration Bulletin No. 25, Part II, page 144, Office of the Secretary of Defense R and D. December 1957

4.6 ASTM Standards
Shock Testing Mechanism for Electrical Indicating Instruments
ASA Publication C39.3-1948, Part 7, page 1101. 1955

4.7 American Standard Specification for
Design, Construction and Operation of a Variable Duration, Medium Import Shock Testing Machine for Lightweight Equipment
ASA Publication S2.1. 1961

4.8 U. S. Military Specification MIL-S-4456 or
U. S. Air Force Specification 7201

4.9 The Hyge Shock Tester
Bulletin 4-70, Consolidated Electrodynamics Corp., Rochester, New York. February 1957

4.10 Lowe, R.
Barry Shock and Vibration Control Notes No. 7
Barry Controls, Inc., Watertown, Mass. August 1957

4.11 The American Standard Specification for Design, Construction and Operation of Class H1 (High Impact) Shock Testing Machines for Lightweight Equipment ASA Publication [illegible].17. 1955

4.12 Military Specification for Shock Proof Equipment MIL-S-901B (Navy) of 9 April 1954, or Interim Military Specification Tests, Shock, Vibration, and Inclination, MIL-T-17[illegible] (Ships) 25 July 1952.

4.13 MacDuff, J. N, and Curreri, S. R. Vibration Control, Chapter 7 McGraw-Hill Book Company, Inc., New York. 1958

4.14 Military Specifications for Electron Tubes, MIL-E-1B (Sec. 4.9.20.5) Armed Services Electro Standards Agency, Fort Monmouth, New Jersey. 2 May 1952

4.15 Dick, A. F. Reed-Gage Shock-Spectrum Characteristics of Navy Light-weight High Impact Shock Machine NRL Report 4749.

4.16 Crede, C. E. and Junger, M. C. A Guide for Design of Shock Resistant Naval Equipment U. S. Bureau of Ships, NAVSHIPS 250-660-30. 1949

4.17 Dick, A. F. and Black, R. E. Reed-Gage Shock-Spectrum Characteristics of Navy Medium-Weight High Impact Shock Machine NRL Report 4750.

4.18 Crede, C. E. Unpublished Data from Tests Conducted at the California Institute of Technology. 1962

4.19 Murfin, T. L. LCC Design Criteria, Human Tolerance to Shock and Vibration Unpublished Memorandum, Space Technology Laboratories. March 1960

4.20 Ziegenruecker, G. H. and Magid, E. B. Short Time Tolerance to Sinusoidal Vibrations WADC TR 59-391. July 1959

4.21 Eiband, M. A. Human Tolerances to Rapidly Applied Accelerations: A Summary of the Literature NASA Memorandum 1959E. June 1959

4.22 Goldman, D. E., and Von Gierke, N. E.
The Effects of Shock and Vibration on Man
Lecture and Review Series No. 60-3,
Naval Medical Research Institute. January, 1960

4.23 Williams, D. W.
Human Survivability: Human Tolerance to Ground Shock and Low Frequency Vibrations in Command and Control Facilities
MITRE Corporation TM-3057, Contract AF 33(600)-39852.
April 1961

4.24 Dieckmann, D.,
Intern. Z. angew. Physiol. einschl. Arbeitsphysiol.
Vol. 16, page 519. 1957

4.25 Radke, A. O.
Proceedings ASME. December 1957

4.26 Crede, C. E.
Relative Motion of a Man Supported by an Accelerating Floor
Unpublished Report, Roberts and Schaefer, New York.
April 1960

4.27 Anon
Elliptic g-Function for Estimating Tolerance to Combined Accelerations
WADD, Aircraft Laboratory, WCLSJ-1. September 1958

4.28 Mindlin, R. D.
Dynamics of Package Cushioning
Bell System Technical Journal, Vol. XXIV, Nos. 3-4.
July - October 1945

SECTION 5.0 INTRODUCTION

TABLE OF CONTENTS

5.1 Introduction

The design of shock isolation systems for underground protective structures must be approached from the broad viewpoint of the complete ground-structure-equipment system. The known parameters are the maximum weapon size, the nearest location of the burst, the general conditions at the site, and the type of equipment to be protected. The design requirement is that the equipment or personnel survive the shock. Between these end points lie the problems of ground motion, soil-structure interaction, response of secondary structures, isolation system performance, and, finally, the reaction of the items to be protected.

The large number of indeterminate influences between the weapon and the equipment precludes a rigorous statement of the input and output requirements of the shock isolation system. To be truly indicative of the degree of confidence which can be placed in the survival of the equipment, an evaluation of the performance of the isolation system must include the possible effect on the system of all unknown factors between it and the weapon on one side, and the equipment on the other side. To accept criteria defining the interfaces between elements of the system where they have been established without regard for the dynamic properties characteristic of the particular isolation system, is to accept a risk of undetermined magnitude and to foster false confidence in the ability of the system to respond as predicted.

Thus the shock isolator designer cannot accept a simple response spectrum of the ground motion at the point of interest, a maximum "permissible" rattlespace, and a maximum "allowable" acceleration as sufficient criteria for the design of his system. Rather, he must know something of the types of ground waves which generate the response spectrum, their phasing, and the possible error in them. He must know something of the structure which will support his system and its response to the ground motion. He must know something of the modes of failure of the equipment to be protected and the types of motion to which they are sensitive. And he must know intimately the behavior of his isolation system to all types of input motions.

The design process then consists of devising an isolation system which is compatible not only with the environment which is most likely to exist, but also with any environment which cannot be shown conclusively not to exist.

5.2 Isolation System Environment

A method for estimating the wave form of the free-field ground motion was described in Section 2.C and summarized in Figure 2.6.2 (page 2-58). The method employs existing ground shock prediction procedures to estimate the significant parameters of the Type I and Type II wave forms, uses a wave front diagram to indicate the direction of motion, and presents equations which yield the approximate durations of each wave form. The high frequencies observed in the test data from which these waves were synthesized have been deleted so that their use to determine the responses of high frequency systems is invalid.

The general shape of both the air-blast induced and cratering-induced Type I wave forms can be explained on a rational basis as resulting from the pressure loadings on the soil. No simple explanation can be offered for the Type II wave form. The Type II wave form has simply been observed to occur in test data from layered sites where reflections and refractions were unquestionably present. There is no positive assurance that the Type II wave form exists as a separate and distinct phenomenon. Yet the regularity of the oscillations which were observed appears to support the premise that they are not merely the result of random interactions of several waves of the Type I form impinging on a point. In any case, the strong influence of an oscillatory wave on the response of an isolation system is of vital concern to the designer and the fact that the oscillations, whatever their source, have been observed, is sufficient cause for concern.

If the site is such that only a Type I wave form can occur, i.e., the geological formation is homogeneous, the critical condition for the shock isolation system may be either of the following:

- For systems in which the vertical or horizontal modes are coupled with each other or to the same rotational mode, the weapon yielding the greatest vertical ground velocity will be critical for the vertical mode, while the one yielding the greatest horizontal velocity will be critical for the horizontal mode.

- For systems in which the vertical and horizontal modes are intercoupled or coupled to the same rotational mode, several weapon sizes and locations must be considered to find the critical condition. The phasing of the vertical and horizontal components of the ground shock also becomes a parameter in this case.

At sites where the Type II wave form can occur at the point of interest, the number of conditions to which the response of the isolation system may be critical are increased. Since a Type II wave form cannot exist alone, all the conditions mentioned above in connection with the Type I wave form must be examined. In addition, the following possibilities must be considered:

- The Type II wave, being the result of reflections and/or refractions, first increases in strength with distance from ground zero and then decreases. The Type I wave, either airblast or cratering-induced, always decreases in strength with increasing range. Thus the relative strengths of the two waves and their phasing are continually changing as they recede from the point of burst. Since the response of the isolation system is sensitive both to the relative strengths and phasing, the range at which maximum response will occur is not immediately evident and usually must be found by trial and error.

- The horizontal component of the Type II wave form has been observed only in a very few test records. In all cases the wave form is a gentle outward-moving velocity pulse rather than an oscillation. The data are insufficient to serve as a basis for general conclusions however, and it is suggested that the horizontal vector of the Type II wave be used in the system analysis as a horizontal input.

An indication of the effect of the wave forms of different ratios of Type I to Type II can be obtained by an inspection of Figure 3.7.5(a). If the periods of the waves are taken as their durations, assuming the durations to be equal, and taking the phase angle as positive for a leading Type I wave, the variation of the maximum undamped velocity amplification ratios are shown in the following Table as a function of the phase angle ϕ.

Amplitude of Type I / Amplitude of Type II	Maximum Velocity Amplification Ratio		
	$\phi = +\pi$	$\phi = 0$	$\phi = -\pi$
2.0	1.65	3.50	2.20
1.0	2.30	3.75	2.85
0.5	2.70	2.75	2.50

The sensitivity of velocity amplification ratio to change in phase angle would probably be even more apparent if the ratios had been calculated for intermediate values of Ø.

Another factor which may be of great importance in the design of some underground facilities is the necessity for surviving multiple attack. The criteria for many facilities specify that the isolation systems be capable of withstanding repeated shocks, although the expected frequency of the attacks is rarely established. If the attacks were to occur at short, reasonably regular intervals, the resulting ground motion would be quasiperiodic regardless of the shape of the waves generated by the individual bursts. Further, if the intervals were near the natural periods of the isolation system, the response of the system would be amplified appreciably.

If the possibility of sustaining damage through multiple attack appears to be remote, it should be remembered that the periods of many isolation systems fall in the range from 2 to 5 seconds; that there are usually many critical isolation systems in a facility, each containing several modes of oscillation; that many systems are only lightly damped; and that several small bursts may cause a greater system response than a single large one. It would appear therefore that damage from the accumulative effects of multiple attack is quite possible and that systems intended to survive in this environment must be designed to resist quasiresonances excited by the periodic inputs.

Distortion of the wave form introduced by the interaction of the soil with the structure is almost impossible to evaluate quantitatively at the present time. If the structure is rigid, the isolation system designer is probably justified in neglecting any interaction effect and in using the free-field ground motion. For highly deformable linings and for unlined cavities, studies of simple models have indicated that amplification of the motion can occur. While service conditions differ appreciably from those considered in the analyses, the designer is cautioned to review the results of these works carefully before assigning quantitative values to the interaction effect.

In addition to the large number of possible ground motions which must be considered in the design of the isolation system, the accuracy with which the parameters of each wave can be predicted is so uncertain that it is desirable to consider each parameter as a range of values rather than a discrete number. Sauer (Reference 5-1) notes that the possible error in his prediction equations for near surface vertical velocities is plus or minus 20 per cent for the superseismic case and plus 60 to minus 40 per cent for the subseismic case. While Newmark (Reference 5-2) does not estimate the possible error, his equations were derived from essentially the same data as those of Sauer and they give comparable results. It would be expected therefore that the errors could be of the same magnitude.

The method used for predicting phase angle between the Type I and Type II waves is based on the assumptions that the soil is elastic and that reflections and refractions take place at abrupt discontinuities between the layered media. As noted in Section 2.0, the validity of these assumptions is dependent on the local site conditions and in some cases may be grossly in error.

Further, in the Design Guide the periods and relative amplitudes of the Type II wave form have been fixed, based on averages of those values observed in the test data. It is highly improbable that these values are independent of site and weapon conditions.

In summary, the large number of wave-form patterns which may be critical to the response of the isolation system, the many parameters needed to define each pattern, and the broad range of uncertainty surrounding the specific values given by the various prediction methods all emphasize an essential need for thoroughness in isolation system design. Even the simple shock spectrum, as usually formulated, should be viewed with suspicion by the isolation system designer, until the conditions of shock which it represents have been clearly defined.

Does the spectrum account properly for the oscillatory ground motion? Has the phasing of the Type I and Type II waves been considered so as to give peak response? What damping was used in obtaining the spectrum? Were multiple attacks considered? These are only a few of the points the designer must verify before he accepts the spectrum as a valid indication of response to the shock.

5.3 Variations in Isolation System Design Parameters

In the previous section, the isolation system parameters were considered as single valued, and the effects of variations in external conditions were discussed. In service, however, many of the parameters of the isolation system itself may change through wear, aging, up-dating, or even during normal operation. These changes may alter significantly the behavior of the system.

5.3.1 Load Changes

As indicated earlier in the Design Guide, rarely is the make and model number of the equipment to be isolated known at the time the facility is being designed. Thus the center of gravity location and the total weight of many items can only be estimated roughly. It is evident that a complete uncoupling of the six possible modes of oscillation is essentially impossible under these conditions without corresponding changes being made in the system configuration. Whenever the equipment is to be provided by a single supplier, it is highly desirable to specify that he furnish the isolators with the unit. In this way the need for the facility designer to allow for adjustments in the mounting provisions is obviated. Further, shock testing, if required, can be accomplished at one time on the complete shock-mounted unit. Care must be taken, however, to ensure that flexible lines, cables, or other connections added later do not influence seriously the dynamic response of the unit. Here again, the provision of these accessories by the equipment supplier and their inclusion in the shock-test unit is desirable.

In many instances, however, it is not possible to employ this procedure. The isolated mass may comprise an assembly of units of different kinds ranging in number from two or three to the myriad required to house and equip a large operations crew. In these instances the facility designer must anticipate the possible variations in total suspended weight and in center of gravity location and to ensure that the system performance is satisfactory throughout the range of loading conditions.

In the very large shock-isolated systems which support power plants, liquid storage tanks, personnel areas including living quarters and items of this nature, load changes occurring during normal operation must be given careful attention. The flow and consumption of water, fuel, and solids, the disposal of wastes, and the movement of personnel must be studied to ensure that under no possible condition can the load sizes and arrangement exceed the safe operating limits of the isolation system.

Changes in the magnitude of the load or position of its center of gravity can have profound effects on the system response. A change of weight on any isolator, for example, will be reflected by a corresponding change in its natural frequency. The resulting motion of that isolator will, therefore, be altered. If the center of gravity is changed from

its original location, the resulting change of weight due to the redistribution of load on each isolator will introduce coupling between the translational and rotational modes even though the system was uncoupled initially. In large systems rotation is particularly undesirable since even small angles of rotation result in large linear displacements at points remote from the axis of rotation. Further, since most isolation systems are relatively "soft", small center of gravity shifts can produce sizable static inclinations from the horizontal position, a particularly undesirable occurrence in those installations housing personnel.

It is evident then that in many instances provisions must be made to adjust the system to accommodate load changes. If large changes occur frequently or rapidly, this requirement may necessitate the use of partially or fully automatic systems for maintaining a well balanced load.

Balancing can be accomplished by several means. The simplest in concept, and frequently the easiest, is by means of ballasting the assembly to maintain a constant total weight and center of gravity position. If the degree of coupling initially in the system is not to be altered when the unit is reballasted to correct for a load change, the directions of the principal axes of the reballasted mass should be identical with their initial directions. However, within the range of normal load changes, this requirement is probably not essential.

In small installations, simple lead or iron weights may be sufficient to provide the needed ballasting. In larger shock-isolated systems and where the complexity is warranted, liquid may be distributed among several tanks by a cross-feed pumping system. Frequently liquid is needed for other purposes and while extra liquid must be added for this purpose, some tankage and liquid-handling equipment may already be available. Care must be taken with all liquid storage systems, however, to ensure that the forces introduced by sloshing are considered in evaluating the dynamic response of the isolation system.

A second means for balancing the system to account for changes in load is by providing the proper adjustments within the isolators themselves. First, the force exerted by the isolator must be adjustable so that the position and equilibrium of the suspended mass can be kept constant throughout weight or center of gravity changes. Second, the stiffness of the isolator must be adjustable so that the natural frequency of the isolator does not change with changing load.

Variable stiffness can be achieved in practical isolator elements by a variety of means. For example, the effective length of beams and torsion members, or the volume of liquid and air springs can be adjusted. For nonlinear elements, however, it should be remembered that it is not sufficient that the stiffness of all isolators be equal in the static position, but that their force-displacement curves be coincident

throughout the entire stroke.

If the system contains only velocity damping, no adjustment need be made to the damping when correcting for isolator characteristics to accommodate changes in load.

5.3.2 Damping Requirements

The provision of damping in isolation system in underground protective structures is rarely given the attention it deserves. It frequently has been the practice to damp those systems supporting personnel and to rely on friction and the internal hysteresis of the materials to damp those systems supporting equipment. This design approach overlooks completely the possibility of quasi-resonances being excited by oscillating components of the shock wave and periodic disturbances due to multiple attack.

The effectiveness of damping in reducing oscillations due to an impulsive input similar to the Type I wave form is slight. For example, Figure 5.3.1 shows the ratio of the damped to the undamped response as a function of damping ratio for a single degree of freedom linear system subjected to a half-sine acceleration pulse. For a damping ratio as high as 50 per cent of the critical value, it may be noted that the peak response is reduced only by 50 per cent.

However damping has an appreciable influence on the response of systems exposed to oscillating motion such as the Type II wave. For example, the attenuation due to damping for an input consisting of a decaying sinusoid is also shown in Figure 5.3.1. Here a 50 per cent decrease in peak response can be achieved with only 5 per cent critical damping. Since the response to an oscillating motion is greater than to a pulse however, the Type II waveform still produces the critical response.

In Figure 5.3.2 the acceleration amplification ratios for the half-sine pulse and the decaying sinusoid are compared. For the case considered here it can be noted that a damping ratio of 0.15 is needed to reduce the response to the decaying sinusoid to a value of 2.0, the figure recommended by Newmark (Ref. 5-2) as a correction for a "complex" wave form. While the decaying sinusoid is not strictly comparable to the Type II wave form, the zero damping case matches closely the velocity amplification factors given for the Type II wave form in Figure 3.7.5(b) (Page 3-110).

The effect of repeated pulses due to multiple attack on the peak response of the system is dependent largely on the number of pulses and their spacing. Thus the extent of the safeguards which must be incorporated in the isolation system to resist failure from this cause is

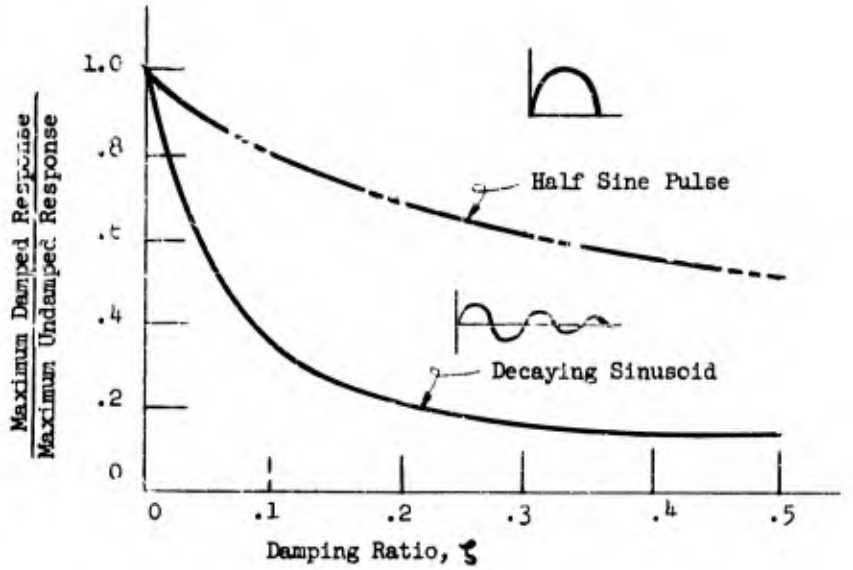

Figure 5.3.1
Effect of Damping Ration on Peak Respouse of Single-Degree-of-Freedom Linear System ot a Half Sine Pulse and a Decaying Sinusoid

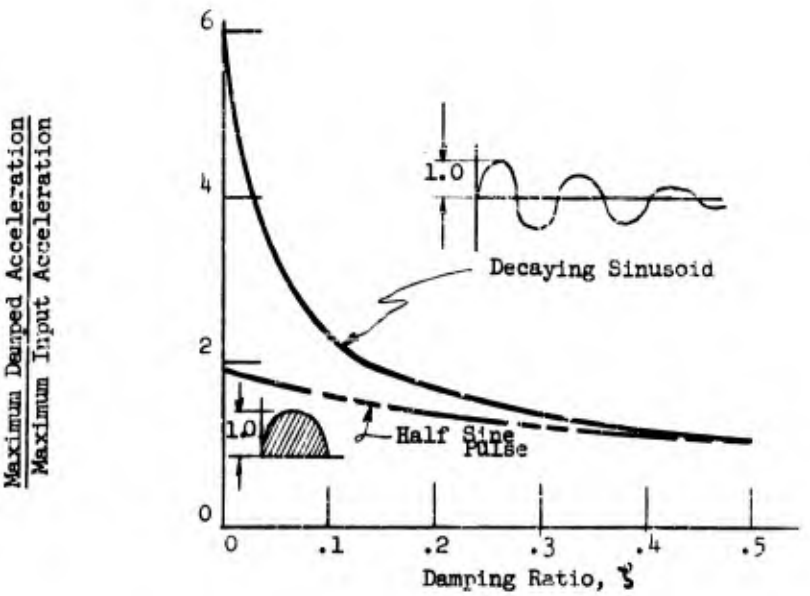

Figure 5.3.2
Amplification Factor as a Function of Damping Ratio for Half Sine Pulse and Decaying Sinusoid

closely related to the basic philosophy of the facility. In almost all installations a sequence of nuclear bursts can be postulated which will destroy some of the isolation system. In this instance, then, the probability of the occurrence of such a sequence must be weighed against added cost of the protective measures. It should be noted, however, that the critical attack can be determined only after the gross characteristics of the isolation system are known.

In addition to minimizing the peak response of the primary isolation system, damping is also beneficial in reducing the exposure time of the supported equipment and personnel to the oscillatory motion. The tolerance of both equipment and personnel to a short duration oscillation is significantly greater than to a steady vibration of the same peak amplitude and acceleration because of the lesser energy transferred.

From these considerations, it is seen that the amount of damping needed in almost, if not all, isolation systems for underground protective structures is appreciably greater than that inherent in moving joints and the internal hysteresis of the materials. Auxiliary damping devices must then be provided. Coulomb damping, because of its deleterious effect on the static positioning of the system and the high frequencies which it introduces in the output motion, is generally undesirable and velocity damping should be used.

In most cases, some tradeoff between damping and rattlespace can be made. That is, provision for oscillatory and/or periodic inputs can be made by adjusting the damping and rattlespace to achieve the most economical over-all installation. However, as the damping is decreased, the sensitivity of the system to oscillations is increased and a greater confidence in the reliability of the ground motion predictions is implied.

5.3.3 Output Requirements

A procedure for selecting the output requirements of shock isolation systems to match a spectral representation of the tolerance level of the equipment is described in Section 4.6. "Tolerance level" however is associated intimately with the mode of failure and before quantitative values can be established, the function of the equipment and its duties during and following attack must be clearly defined.

The spectrum of the motion of the isolated system is governed by the natural frequency of the system, the isolator force-displacement characteristic and the kinematic arrangement. The natural frequency usually fixes the peak acceleration of the response while the latter two items control the breadth of the band of frequencies over which significant accelerations occur. The minimum spectrum is obtained by employing linear elastic elements and arranging the suspension system so that all modes of acceleration are uncoupled.

It may be noted that the procedure of Section 4.6 is based on just these assumptions. Systems containing nonlinear elements or coupled modes then will yield broader spectra and appropriate allowances must be made in comparing the simplified output spectra with the equipment tolerance data.

Most shock tests are conducted with the force applied along axes normal or parallel to the mounting base. In service, the force may be applied from any one of many directions and may vary during the shock. It is probable that the elliptic g function method described in Section 4.5.4 in connection with human acceleration tolerances could be applied here as well.

5.4 Summary

The two most important safeguards the isolation system designer can build into his system are rattlespace and damping. The details of the attack and the resulting ground shock cannot be defined explicitly; only the gross characteristics of the site geology are usually known; the interactions between the soil and the structure cannot be determined quantitatively and, in fact, probably vary considerably with construction technique; and the mechanism of damage in a particular item of equipment can only be based on broad generalizations. Faced with these many uncertainties, the designer must provide his system with a capability for surviving any and all conditions which cannot be proven to be outside the realm of possibility. Any lesser capability should be accepted only on the basis of calculated risk and not on optimism.

While in most underground structures, space is at a minimum, rattlespace should be recognized for what it is, a part of the factor of safety of the isolation system. Reducing it to a marginal value is comparable to reducing the strength of the structure to a bare minimum.

Similarly, damping should be considered more as a factor of safety than simply as a means for reducing response to an assumed input. All of these systems are sensitive to oscillatory motions, and in view of the little known of the oscillatory components of the ground motion, damping acts as a governor in minimizing the effect of such motion on the isolation system.

The designer is entreated to extend his zone of inquiry to the weapon system extending from the methods of attack to the functioning of the protected equipment and to regard his isolation system as an essential part of a weapon. For only by assuming this broad viewpoint can he hope to attain an integrated, reliable design.

SECTION 5.0 REFERENCES

5.1 Sauer, F. M.
Ground Motions Produced by Above-Ground Nuclear Explosions
Air Force Special Weapons Center SWC-TN-59-71
April 1959 (s)

5.2 Newmark, N.M., et.al.
Protective Construction Review Guide-Ha[illegible]ning
Volume I, Department of Defense, June 1961.

DISTRIBUTION

No. Cys.

HEADQUARTERS USAF

3 Hq USAF (AFOCE), Wash 25, DC

1 Hq USAF (AFRDR), Wash 25, DC

1 USAF Dep IG for Insp (AFCDI-B-3), Norton AFB, Calif

1 USAF Dep IG for Safety (AFINS), Kirtland AFB, NM

1 AFOAR, Bldg T-D, Wash 25, DC

1 AFOSR, Bldg T-D, Wash 25, DC

MAJOR AIR COMMANDS

1 AFSC (SCT), Andrews AFB, Wash 25, DC

SAC, Offutt AFB, Nebr

1 (OA)

1 (OAWS)

1 AUL, Maxwell AFB, Ala

AFSC ORGANIZATIONS

ASD (Aeronautical Systems Division), Wright-Patterson AFB, Ohio

1 (ASAPRL, Technical Doc Library)

2 (ASTEVD)

2 (ASMCE)

1 (ASBMA)

BSD (Ballistic Systems Division), AF Unit Post Office, Los Angeles 45, Calif

1 (BST)

1 (BSQ)

1 (BSR)

3 (BSSCF-R)

2 SSD (Space Systems Division), AF Unit Post Office, Los Angeles 45, Calif

ESD, Hanscom Fld, Bedford, Mass

1 (ESAT)

1 (ESFE)

2 ESD, Murphy Institute, (Mr. Anthony Minichiello), 424 Trapelo Road, Waltham, Mass

DISTRIBUTION (cont'd)

No. Cys

RADC, Griffiss AFB, NY

1 (Document Library)

2 (RCSGM)

KIRTLAND AFB ORGANIZATIONS

AFSWC, Kirtland AFB, NM

1 (SWEH)

50 (SWOI)

8 (SWR)

1 (SWV)

2 (SWT)

2 (SWTTL)

1 AFSWC Shock Tube Facility, Research Directorate,(AFSWC, Dr. Eugene Zwoyer), Kirtland AFB, NM

1 US Naval Weapons Evaluation Facility (NWEF) (Code 404), Kirtland AFB, NM

OTHER AIR FORCE AGENCIES

1 Director, USAF Project RAND, (RAND Library), via: Air Force Liaison Office, The RAND Corporation, 1700 Main Street, Santa Monica, Calif

ARMY ACTIVITIES

1 Director, Ballistic Research Laboratories (Library), Aberdeen Proving Ground, Md

1 Commanding Officer, US Army Engineers, Research & Development Laboratories, Ft. Belvoir, Va

1 Commanding General, White Sands Missile Range (Technical Library), White Sands, NM

1 Chief of Engineers, Department of the Army (ENGEB), Wash 25, DC

2 Office of the Chief, Corps of Engineers, US Army (Protective Construction Branch), Wash 25, DC

1 Director, Army Research Office, Arlington Hall Sta, Arlington

3 Director, US Army Waterways Experiment Sta (WESRL), P. O. Box 60. Vicksburg, Miss

DISTRIBUTION (cont'd)

No. Cys

NAVY ACTIVITIES

1	Chief of Naval Research, Wash 25, DC
1	Chief, Bureau of Naval Weapons, Department of the Navy, Wash 25, DC
3	Chief, Bureau of Yards and Docks (Code E-220), Department of the Navy, Wash 25, DC
1	Chief, Bureau of Ships, Department of the Navy, Wash 25, DC
1	Commanding Officer, Naval Research Laboratory, Wash 25, DC
3	Commanding Officer and Director, Naval Civil Engineering Laboratory, Port Hueneme, Calif
1	Commander, Naval Ordnance Laboratory, White Oak, Silver Spring, Md
1	Officer-in-Charge, Civil Engineering Corps Officers, US Naval School, Naval Construction Battalion Center, Port Hueneme, Calif
1	Office of Naval Research, Wash 25, DC
1	Superintendent, US Naval Postgraduate School, Monterey, Calif

OTHER DOD ACTIVITIES

1	Chief, Defense Atomic Support Agency (Document Library), Wash 25, DC
1	Commander, Field Command, Defense Atomic Support Agency, (FCAG3, Special Weapons Publication Distribution), Sandia Base NM
1	Director, Weapon Systems Evaluation Group, Room 2E1006, The Pentagon, Wash 25, DC
1	Director, Advanced Research Projects Agency, Department of Defense, The Pentagon, Wash 25, DC
2	Chief, Defense Atomic Support Agency, (Blast and Shock Div), Wash 25, DC
1	Director, Defense Research & Engineering, The Pentagon, Wash 25, DC
20	ASTIA (TIPDR), Arlington Hall Sta, Arlington 12, Va

AEC ACTIVITIES

1	President, Sandia Corporation (Document Control Division), Sandia Base, NM

DISTRIBUTION (cont'd)

No. Cys	OTHER
3	Office of Civil Defense Mobilization (OCDM), Battle Creek, Mich
20	OTS, Department of Commerce, Wash 25, DC
5	The Ralph M. Parsons Company, (Dr. M S Agbabian), 617 West Seventh St., Los Angeles 17, Calif
1	The National Engineering Science Company, (Dr. Lars Skjelbreia, Director of Engineering), 711 Fair Oaks Avenue, Pasadena, Calif
1	American Machine and Foundry Company, Mechanics Research Div, (Mr. Tom Morrison), 7501 N. Natchez Ave., Niles, Ill
5	Stanford Research Institute, (Ernie Chilton), 333 Ravens Wood, Menlo Park, Calif
1	Paul Weidlinger Associates, (Mr. Paul Weidlinger), 770 Lexington Ave, New York 21, NY
5	Armour Research Foundation, Mechanics Research Division, (Dr. Eugene Sevin), 3422 South Dearborn Street, Chicago 15, Ill
1	California Institute of Technology, Division of Engineering, (Prof. Charles E. Crede), 1201 East California Blvd, Pasadena, Calif
1	Stanford University, School of Mechanical Engineering, (Dr. Lydik S. Jacobsen), Stanford, Calif
1	Shannon and Wilson, (Mr. Stanley D. Wilson), 1105 North 38th Street, Seattle 3, Wash
1	Massachusetts Institute of Technology, Dept of Civil & Sanitary Engineering, (Dr. Robert V. Whitman), 77 Massachusetts Avenue, Cambridge 39, Mass
2	The MITRE Corporation, (Mr. Warren McCabe), P. O. Box 208, Bedford, Mass
1	University of Notre Dame, (Harry C. Saxe, Professor & Head Dept of Civil Engineering), Notre Dame, Ind
1	Space Technology Labs, Inc., (Dr. Millard V. Barton, Eng. Mech. Dept), P. O. Box 95001, Los Angeles 45, Calif
1	Allied Research Associates, (Mr. David C. Knoell), 43 Leon Street, Boston, Mass
1	MITRON Research and Development Corp, (Dr. Maurice Gertel), 899 Main Street, Waltham, Mass
1	Barry Controls, Inc., (Richard Cavanaugh), 1400 Flower Street, Glendale, Calif
1	United Research Services, (Mr. Harold Mason), 1811 Trousdale Dr, Burlingame, Calif
1	Southwest Research Institute, (Dr. Dana Young), 8500 Culebra Rd., San Antonio 6, Tex

DISTRIBUTION (cont'd)

No. Cys	
12	National Academy of Sciences, National Research Council, Advisory Committee on Civil Defense, Subcommittee on Protective Structures, (Mr. Richard Parks, Secretary), 2101 Constitution Avenue, Wash 25, DC
1	University of Illinois. (Dr. Nathan M. Newmark), 207 Talbot Laboratory, Urbana, Ill
1	St. Louis University, Institute of Technology, (Dr. Carl Kisslinger), 3621 Olive St., St. Louis 8, Mo
1	University of Florida, Dept of Civil Engineering, (Frank E. Richardt), Gainesville, Fla
1	University of California, (Prof Martin Duke, Assistant Dean), College of Engineering, Los Angeles, Calif
1	Portland Cement Assoc, (Eivind Hognestad, Manager, Structural Development Section), 33 W. Grand Avenue, Chicago, Ill
1	Michigan College of Mining & Technology, (Dean Frank Kerecke), Houghton, Mich
1	University of Illinois, Theoretical and Applied Mechanics Dept., (A. P. Boresi), Urbana, Ill
1	North Carolina State, (Ralph Fadum, Head, Dept of Civil Engineering), Raleigh, NC
1	Official Record Copy (SWRS, Lt Merkle)

Air Force Special Weapons Center, Kirtland AF Base, N.M.
Rpt. No. AFSWC-TDR-62-64. A GUIDE FOR THE DESIGN OF SHOCK ISOLATION SYSTEMS FOR UNDERGROUND PROTECTIVE STRUCTURES. Dec 62, 447 p, incl illus., tables, 85 refs.
Unclassified Report

This report reviews the major considerations relating to the design of Shock Isolation Systems for use in underground protective structures, emphasizing in particular those areas where special guidance is needed by the facility engineer. The motion of the ground due to nuclear blast, the interaction of the ground motion with buried structures, and the tolerances of typical facility equipment to shock are described and employed to establish the input and output requirements for isolation systems. Analytical

1. Blast damage
2. Ground motion
3. Shock phenomena
4. Shock waves
5. Structural materials--effects of blast
6. Underground structures--effects of blast
7. Wave mechanics
I. AFSC Project 1080, Task 10803
II. Contract AF 29(601)4551
III. Parsons (Ralph M.) Co., Los Angeles, Calif
IV. In ASTIA collection

Air Force Special Weapons Center, Kirtland AF Base, N.M.
Rpt. No. AFSWC-TDR-62-64. A GUIDE FOR THE DESIGN OF SHOCK ISOLATION SYSTEMS FOR UNDERGROUND PROTECTIVE STRUCTURES. Dec 62, 447 p, incl illus., tables, 85 refs.
Unclassified Report

This report reviews the major considerations relating to the design of Shock Isolation Systems for use in underground protective structures, emphasizing in particular those areas where special guidance is needed by the facility engineer. The motion of the ground due to nuclear blast, the interaction of the ground motion with buried structures, and the tolerances of typical facility equipment to shock are described and employed to establish the input and output requirements for isolation systems. Analytical

1. Blast damage
2. Ground motion
3. Shock phenomena
4. Shock waves
5. Structural materials--effects of blast
6. Underground structures--effects of blast
7. Wave mechanics
I. AFSC Project 1080, Task 10803
II. Contract AF 29(601)4551
III. Parsons (Ralph M.) Co., Los Angeles, Calif
IV. In ASTIA collection

Air Force Special Weapons Center, Kirtland AF Base, N.M.
Rpt. No. AFSWC-TDR-62-64. A GUIDE FOR THE DESIGN OF SHOCK ISOLATION SYSTEMS FOR UNDERGROUND PROTECTIVE STRUCTURES. Dec 62, 447p, incl illus., tables, 85 refs.
Unclassified Report

This report reviews the major considerations relating to the design of Shock Isolation Systems for use in underground protective structures, emphasizing in particular those areas where special guidance is needed by the facility engineer. The motion of the ground due to nuclear blast, the interaction of the ground motion with buried structures, and the tolerances of typical facility equipment to shock are described and employed to establish the input and output requirements for isolation systems. Analytical

1. Blast damage
2. Ground motion
3. Shock phenomena
4. Shock waves
5. Structural materials--effects of blast
6. Underground structures--effects of blast
7. Wave mechanics
I. AFSC Project 1080, Task 10803
II. Contract AF 29(601)4551
III. Parsons (Ralph M.) Co., Los Angeles, Calif
IV. In ASTIA collection

Air Force Special Weapons Center, Kirtland AF Base, N.M.
Rpt. No. AFSWC-TDR-62-64. A GUIDE FOR THE DESIGN OF SHOCK ISOLATION SYSTEMS FOR UNDERGROUND PROTECTIVE STRUCTURES. Dec 62, 447 p, incl illus., tables, 85 refs.
Unclassified Report

This report reviews the major considerations relating to the design of Shock Isolation Systems for use in underground protective structures, emphasizing in particular those areas where special guidance is needed by the facility engineer. The motion of the ground due to nuclear blast, the interaction of the ground motion with buried structures, and the tolerances of typical facility equipment to shock are described and employed to establish the input and output requirements for isolation systems. Analytical

1. Blast damage
2. Ground motion
3. Shock phenomena
4. Shock waves
5. Structural materials--effects of blast
6. Underground structures--effects of blast
7. Wave mechanics
I. AFSC Project 1080, Task 10803
II. Contract AF 29(601)4551
III. Parsons (Ralph M.) Co., Los Angeles, Calif
IV. In ASTIA collection

methods for determining the dynamic responses of both linear and nonlinear isolation systems are summarized and, for several of the more commonly used configurations, the equations are reduced to simple form. The report suggests the use of the shock response spectrum in a unified approach to the specification of attenuation requirements, equipment shock tolerances and shock test machine selection.		methods for determining the dynamic responses of both linear and nonlinear isolation systems are summarized and, for several of the more commonly used configurations, the equations are reduced to simple form. The report suggests the use of the shock response spectrum in a unified approach to the specification of attenuation requirements, equipment shock tolerances and shock test machine selection.	
methods for determining the dynamic responses of both linear and nonlinear isolation systems are summarized and, for several of the more commonly used configurations, the equations are reduced to simple form. The report suggests the use of the shock response spectrum in a unified approach to the specification of attenuation requirements, equipment shock tolerances and shock test machine selection.		methods for determining the dynamic responses of both linear and nonlinear isolation systems are summarized and, for several of the more commonly used configurations, the equations are reduced to simple form. The report suggests the use of the shock response spectrum in a unified approach to the specification of attenuation requirements, equipment shock tolerances and shock test machine selection.	

Air Force Special Weapons Center, Kirtland AF Base, N.M.
Rpt. No. AFSWC-TDR-62-64. A GUIDE FOR THE DESIGN OF SHOCK ISOLATION SYSTEMS FOR UNDERGROUND PROTECTIVE STRUCTURES. Dec 62, 447 p, incl illus., tables, 85 refs.

Unclassified Report

This report reviews the major considerations relating to the design of Shock Isolation Systems for use in underground protective structures, emphasizing in particular those areas where special guidance is needed by the facility engineer. The motion of the ground due to nuclear blast, the interaction of the ground motion with buried structures, and the tolerances of typical facility equipment to shock are described and employed to establish the input and output requirements for isolation systems. Analytical

1. Blast damage
2. Ground motion
3. Shock phenomena
4. Shock waves
5. Structural materials--effects of blast
6. Underground structures--effects of blast
7. Wave mechanics

I. AFSC Project 1080, Task 10803
II. Contract AF 29(601)4551
III. Parsons (Ralph M.) Co., Los Angeles, Calif
IV. In ASTIA collection

Air Force Special Weapons Center, Kirtland AF Base, N.M.
Rpt. No. AFSWC-TDR-62-64. A GUIDE FOR THE DESIGN OF SHOCK ISOLATION SYSTEMS FOR UNDERGROUND PROTECTIVE STRUCTURES. Dec 62, 447 p, incl illus., tables, 85 refs.

Unclassified Report

This report reviews the major considerations relating to the design of Shock Isolation Systems for use in underground protective structures, emphasizing in particular those areas where special guidance is needed by the facility engineer. The motion of the ground due to nuclear blast, the interaction of the ground motion with buried structures, and the tolerances of typical facility equipment to shock are described and employed to establish the input and output requirements for isolation systems. Analytical

1. Blast damage
2. Ground motion
3. Shock phenomena
4. Shock waves
5. Structural materials--effects of blast
6. Underground structures--effects of blast
7. Wave mechanics

I. AFSC Project 1080, Task 10803
II. Contract AF 29(601)4551
III. Parsons (Ralph M.) Co., Los Angeles, Calif
IV. In ASTIA collection

Air Force Special Weapons Center, Kirtland AF Base, N.M.
Rpt. No. AFSWC-TDR-62-64. A GUIDE FOR THE DESIGN OF SHOCK ISOLATION SYSTEMS FOR UNDERGROUND PROTECTIVE STRUCTURES. Dec 62, 447 p, incl illus., tables, 85 refs.

Unclassified Report

This report reviews the major considerations relating to the design of Shock Isolation Systems for use in underground protective structures, emphasizing in particular those areas where special guidance is needed by the facility engineer. The motion of the ground due to nuclear blast, the interaction of the ground motion with buried structures, and the tolerances of typical facility equipment to shock are described and employed to establish the input and output requirements for isolation systems. Analytical

1. Blast damage
2. Ground motion
3. Shock phenomena
4. Shock waves
5. Structural materials--effects of blast
6. Underground structures--effects of blast
7. Wave mechanics

I. AFSC Project 1080, Task 10803
II. Contract AF 29(601)4551
III. Parsons (Ralph M.) Co., Los Angeles, Calif
IV. In ASTIA collection

Air Force Special Weapons Center, Kirtland AF Base, N.M.
Rpt. No. AFSWC-TDR-62-64. A GUIDE FOR THE DESIGN OF SHOCK ISOLATION SYSTEMS FOR UNDERGROUND PROTECTIVE STRUCTURES. Dec 62, 447 p, incl illus., tables, 85 refs.

Unclassified Report

This report reviews the major considerations relating to the design of Shock Isolation Systems for use in underground protective structures, emphasizing in particular those areas where special guidance is needed by the facility engineer. The motion of the ground due to nuclear blast, the interaction of the ground motion with buried structures, and the tolerances of typical facility equipment to shock are described and employed to establish the input and output requirements for isolation systems. Analytical

1. Blast damage
2. Ground motion
3. Shock phenomena
4. Shock waves
5. Structural materials--effects of blast
6. Underground structures--effects of blast
7. Wave mechanics

I. AFSC Project 1080, Task 10803
II. Contract AF 29(601)4551
III. Parsons (Ralph M.) Co., Los Angeles, Calif
IV. In ASTIA collection

methods for determining the dynamic responses of both linear and nonlinear isolation systems are summarized and, for several of the more commonly used configurations, the equations are reduced to simple form. The report suggests the use of the shock response spectrum in a unified approach to the specification of attenuation requirements, equipment shock tolerances and shock test machine selection.		methods for determining the dynamic responses of both linear and nonlinear isolation systems are summarized and, for several of the more commonly used configurations, the equations are reduced to simple form. The report suggests the use of the shock response spectrum in a unified approach to the specification of attenuation requirements, equipment shock tolerances and shock test machine selection.	
methods for determining the dynamic responses of both linear and nonlinear isolation systems are summarized and, for several of the more commonly used configurations, the equations are reduced to simple form. The report suggests the use of the shock response spectrum in a unified approach to the specification of attenuation requirements, equipment shock tolerances and shock test machine selection.		methods for determining the dynamic responses of both linear and nonlinear isolation systems are summarized and, for several of the more commonly used configurations, the equations are reduced to simple form. The report suggests the use of the shock response spectrum in a unified approach to the specification of attenuation requirements, equipment shock tolerances and shock test machine selection.	